FUEL CELL

1990 Fuel Cell Seminar

Program and Abstracts

RECEIVED

November 25–28, 1990
Phoenix, Arizona

In Cooperation with:

UNITED STATES
Department of Energy
Electric Power Research Institute
Gas Research Institute
National Aeronautics and Space Administration

EUROPE
Commission of the European Communities

JAPAN
Fuel Cell Development Information Center

Sponsored by
Fuel Cell
Seminar
Organizing
Committee

DISTRIBUTION OF THIS DOCUMENT IS UNLIMITED

Neither the U.S. Government nor any of its employees makes any warranty expressed or implied or assumes any legal liability or responsibility for the accuracy, completeness, or usefulness of any information, apparatus, product, or process disclosed or represents that its use does not infringe upon privately owned rights.

CONF-901106- —

FUEL CELL

Program and Abstracts

1990 Fuel Cell Seminar

November 25–28, 1990
Phoenix, Arizona

DISCLAIMER

This report was prepared as an account of work sponsored by an agency of the United States Government. Neither the United States Government nor any agency thereof, nor any of their employees, makes any warranty, express or implied, or assumes any legal liability or responsibility for the accuracy, completeness, or usefulness of any information, apparatus, product, or process disclosed, or represents that its use would not infringe privately owned rights. Reference herein to any specific commercial product, process, or service by trade name, trademark, manufacturer, or otherwise does not necessarily constitute or imply its endorsement, recommendation, or favoring by the United States Government or any agency thereof. The views and opinions of authors expressed herein do not necessarily state or reflect those of the United States Government or any agency thereof.

DISTRIBUTION OF THIS DOCUMENT IS UNLIMITED

Seminar Coordinated by
Courtesy Associates, Inc.
Washington, D.C.

MASTER

DISCLAIMER

Portions of this document may be illegible in electronic image products. Images are produced from the best available original document.

PREFACE

The members of the Fuel Cell Seminar Organizing Committee welcome you to this, the twelfth in the series of Fuel Cell Seminars. This year's theme, "Fuel Cells – An Answer to a Cleaner Environment" is most appropriate as we move into the 1990s. The Opening Session – "An Environmental Overview" brings together an international perspective on environmental issues and strategic directions for fuel cell research, development, and demonstration (RD&D).

During the 1990s, fuel cells will come of age. Not only have past RD&D efforts achieved successful field demonstrations, but also developers are establishing the manufacturing facilities for the commercial introduction of fuel cell systems. This decade will bring to the international energy community a greatly increased awareness and concern for the quality of our environment. Fuel cells are the cleanest, fossil-fueled power generation technology available.

Although the objective of the Seminar has evolved over the years, it has not fundamentally changed. Today, the objective is to bring together participants in the major fuel cell research, development, demonstration and commercialization programs and to provide a forum in which to exchange information within the international community interested in fuel cell technologies. The Seminar provides both the developers and users opportunities to learn more about the various activities, to make contacts with others working toward similar objectives, and to help establish an integrated international program which brings the benefits of fuel cell technologies to fruition.

The interest in fuel cells has increased significantly. The 1990 Fuel Cell Seminar continues the strong international flavor that has typified the last two sessions. With forceful and vibrant RD&D efforts around the globe, this year's program brings together more than 130 authors representing over 14 countries.

The committee hopes that you find this years program informative and stimulating. We invite you to actively participate in both the oral and poster sessions. The receptions also provide a relaxed environment in which to meet other participants in the growing international fuel cell community.

Richard Root Woods
Chairman
Fuel Cell Seminar Organizing Committee

ACKNOWLEDGEMENTS

The organizers of the 1990 Fuel Cell Seminar express their gratitude for the generous support received from the following organizations:

ABB Combustion Engineering
1000 Prospect Hill Road
Windsor, Connecticut 06095

Allied-Signal Aerospace Company
AiResearch Los Angeles Division
P.O. Box 2960
2525 West 190th Street
Torrance, California 90509-2960

Ballard Power Systems Inc.
980 West 1st Street, Unit 107
North Vancouver, British Columbia
Canada V7P 3N4

Energy Research Corporation
3 Great Pasture Road
Danbury, Connecticut 06813

Fuji Electric Company, Ltd.
12-1 Yurakucho 1-chome, Chiyoda-ku
Tokyo 100
Japan

Haldor Topsoe A/S
Nymollevej 55, DK-2800 Lyngby
Denmark

Hitachi, Ltd.
Molten Carbonate Fuel Cell
Development Center
1-1, Saiwaicho 3-chome
Hitachi-shi, Ibaraki-ken 317
Japan

International Fuel Cells
P.O. Box 739
195 Governors Highway
South Windsor, Connecticut 06074

IHI
Ishikawajima-Harima Heavy Industries, Co., Ltd.
1-15, Toyosu 3-chome Koto-ku
Tokyo 135
Japan

M-C Power Corporation
8040 South Madison Street
Burr Ridge, Illinois 60521-5808

Mitsubishi Electric Corporation
2-2-3, Marunouchi, Chiyoda-ku Tokyo 100
Japan

Toshiba Corporation
Fuel Cell Systems Division
1-6, Uchisaiwaicho 1-chome
Chiyoda-ku, Tokyo 100
Japan

Westinghouse Electric Corporation
Advanced Energy Conversion Department
Science & Technology Center
1310 Beulah Road
Pittsburgh, Pennsylvania 15235

Ztek Corporation
460 Totten Pond Road
Waltham, Massachusetts 20154

AGENDA

SUNDAY, NOVEMBER 25, 1990

3:00 pm - 6:00 pm **Registration** - *Conference Center Registration Area*

5:00 pm - 7:00 pm **Welcoming Reception** - *Poolside*

MONDAY, NOVEMBER 26, 1990

7:30 am - 8:30 am **Speakers' Breakfast** - *Sedona Room*
(Monday Speakers only)

8:00 am - 5:00 pm **Registration** - *Conference Center Registration Area*

8:00 am **Continental Breakfast** - *Main Foyer*

9:00 am - 11:45 am OPENING SESSION - "AN ENVIRONMENTAL OVERVIEW"
Chairman: Root Woods - *Arizona Biltmore Ballroom*
Gas Research Institute

"Keynote Address"
Dr. James Lents, Executive Officer, South Coast
Air Quality Management District

10:00 am - 10:15 am **Break** - *Main Foyer*

"ENVIRONMENTAL ASPECTS PUSH FUEL CELL TECHNOLOGY R&D PROGRAM AHEAD IN JAPAN" 1
Dr. Takeshi Sugimoto
New Energy and Industrial Technology Development
Organization (NEDO)

"HIGHLIGHTS OF FUEL CELL ACTIVITIES IN THE NETHERLANDS" 3
Dr. Klaas Joon
Netherlands Energy Research Foundation (ECN)

"ENVIRONMENTAL IMPACTS OF ENERGY FACILITIES BASED ON FUEL CELLS" 7
Dr. Kunt L. Seip
Senter for Industriforskning

12 Noon - 1:45 pm **Luncheon** - *Grand Ballroom*

2:00 pm - 5:00 pm TRANSPORTATION APPLICATIONS I (2A) - *Casa Grande Room*
Chairman: Pandit Patil
U.S. Department of Energy

MONDAY, NOVEMBER 26

"THE PHOSPHORIC ACID FUEL CELL/BATTERY BUS PROJECT" 10
Russ J. Kevala
Booz, Allen & Hamilton, Inc.

"LIQUID-COOLED PHOSPHORIC ACID FUEL CELL SUBSYSTEM FOR THE BUS" 14
Kazukiyo Okano
Fuji Electric Co., Ltd.

"ALKALINE H2-AIR FUEL CELLS FOR CITY BUS APPLICATION" 18
Hugo Van den Broeck
Elenco N.V.

3:30 pm - 3:45 pm Break - *Main Foyer*

"MERITS OF AFC-SYSTEMS FOR FORK LIFT TRUCKS" 20
Olle Lindstrom
Royal Institute of Technology

"DEACTIVATION OF METHANOL STEAM REFORMING CATALYST UNDER SIMULATED CONDITIONS OF TRANSPORTATION FUEL CELL SYSTEMS" 24
Akitoshi Seya
Fuji Electric Corporate R&D, Ltd.

"AIR-COOLED FUEL CELL POWER SOURCE FOR BUS" 28
S. Abens
Energy Research Corporation

2:00 pm - 5:30 pm TECHNOLOGY ADVANCEMENTS FOR MOLTEN CARBONATE FUEL CELLS I (2B) - *Flagstaff Room*
Chairman: Tom George
Department of Energy, Morgantown Energy Technology Center

"MCFC STACK DEVELOPMENT THE NETHERLANDS ENERGY RESEARCH FOUNDATION ECN" . . . . . *
L. A. H. Machielse
Netherlands Energy Research Foundation (ECN)

"SCALE-UP OF CARBONATE FUEL CELL STACK TECHNOLOGY" 32
Larry Pactsch
Energy Research Corporation

"100 kW CARBONATE FUEL CELL DEMO PLANT" 36
Douglas J. Herman
Pacific Gas and Electric Company

* Abstract not available at time of publication.

MONDAY, NOVEMBER 26

3:30 pm - 3:45 pm **Break** - *Main Foyer*

"COMPARISON OF DIRECT AND INDIRECT INTERNAL REFORMING MCFC STACKS" 40
Kazunao Sato
Mitsubishi Electric Corporation

"ADVANCES IN REFORMING TECHNOLOGY FOR FUEL CELL APPLICATIONS" 44
Carsten Lau Laursen
Haldor Topsoe A/S

"SUBSCALE IMHEX MCFC STACK TESTING AT IGT" 48
R. J. Petri
Institute of Gas Technology

"MCFC DEVELOPMENTAL ISSUES" 53
Tom J. George
Department of Energy,
Morgantown Energy Technology Center

6:00 pm - 8:00 pm **Manufacturers' Reception** - *Poolside*

TUESDAY, NOVEMBER 27, 1990

7:30 am - 8:30 am **Speakers' Breakfast** - *Sedona Room*
(Tuesday Speakers only)

7:30 am - 8:30 am **Poster Speakers' Breakfast** - *Grand Ballroom*
(Tuesday Speakers' only)

8:00 am - 5:00 pm **Registration** - *Conference Center and Registration Area*

8:00 am - **Continental Breakfast** - *Main Foyer*

9:00 am - 12 Noon TRANSPORTATION APPLICATIONS II (3A) - *Mesa Room*
Chairman: Alan Lloyd
South Coast Air Quality
Management District

"RESEARCH AND DEVELOPMENT OF A PROTON - EXCHANGE - MEMBRANE (PEM) FUEL CELL SYSTEM FOR TRANSPORTATION APPLICATIONS" 57
H. F. Creveling
General Motors Corp.

TUESDAY, NOVEMBER 27

"ADVANCED SYSTEM ANALYSIS FOR
INDIRECT METHANOL FUEL CELL POWER PLANTS
FOR TRANSPORTATION APPLICATIONS" 61
N. E. Vanderborgh
Los Alamos National Laboratory

"STATUS OF SOLID POLYMER FUEL CELL
DEVELOPMENT AT BALLARD" 65
D. S. Watkins
Ballard Power Systems

10:30 am - 10:45 am Break - *Main Foyer*

"STATUS OF SOLID OXIDE FUEL CELLS
FOR TRANSPORTATION" 71
Dennis W. Dees
Argonne National Laboratory

"METHANOL REFORMERS FOR FUEL CELL
POWERED VEHICLES: SOME DESIGN CONSIDERATIONS" 76
Romesh Kumar
Argonne National Laboratory

"STATUS OF ONTARIO MINISTRY OF ENERGY PROJECTS
RELATED TO FUEL CELLS AND TRANSPORTATION" 80
Robert G. Greven
Ontario Ministry of Energy

9:00 am - 12 Noon **TECHNOLOGY ADVANCEMENTS FOR MOLTEN CARBONATE FUEL CELLS II (3B)** - *Casa Grande Room*
Chairman: Rocky Goldstein
Electric Power Research Institute

"ECONOMIC FEASIBILITY STUDY OF 5-mW FUEL CELL
POWER GENERATION SYSTEM AND RESEARCH FOR THE
1000-kW CLASS MCFC PILOT PLANT IN JAPAN" 83
K. Doi
MCFC Research Association

"OPERATING TEST OF 2kW MCFC PLANT" 87
Kazunori Kobayashi
Ishikawajima-Harima Heavy Industries Co., Ltd.

"MCFC TECHNOLOGY DEVELOPMENT IN TOSHIBA" 91
Toshiro Terayama
Toshiba Corporation

TUESDAY, NOVEMBER 27

10:30 am - 10:45 am **Break** - *Main Foyer*

"STATUS OF LARGE SIZED MCFC CELL & STACK TECHNOLOGY DEVELOPMENT AT HITACHI" 95
Toshiki Kahara
Hitachi, Ltd.

"IHI LARGE SIZE MOLTEN CARBONATE FUEL CELL ADVANCEMENTS" 99
Minoru Hasaka
Ishikawajima-Harima Heavy Industries, Co., Ltd.

"6kW CLASS MCFC TEST WITH GAS RECYCLING" 103
Yoshihiro Mugikura
Central Research Institute of Electric
Power Industry (CRIEPI)

9:00 am - 12 Noon TECHNOLOGY ADVANCEMENTS FOR SOLID OXIDE FUEL CELLS I (3C) - *Flagstaff Room*
Chairman: Pieter Zegers
Commission of the European Communities

"SOLID OXIDE FUEL CELL DEVELOPMENT AT FUJI ELECTRIC" 107
Kazuo Koseki
Fuji Electric Corporate R&D, Ltd.

"SOLID OXIDE FUEL CELLS: CFP DESIGN AND CELL PERFORMANCE" 111
Robert F. Singer
ABB Corporate Research

"PLANAR SOLID OXIDE FUEL CELL TECHNOLOGY DEVELOPMENT" 115
Michael Hsu
Ztek Corporation

10:30 am - 10:45 am **Break** - *Main Foyer*

"PEROVSKITE SOLID ELECTROLYTES FOR INTERMEDIATE TEMPERATURE SOLID OXIDE FUEL CELLS" 119
Anthony F. Sammells
Eltron Research, Inc.

"OPTIMISATION OF PLANAR CONFIGURATION SOFC STRUCTURAL COMPONENTS" 123
B. C. H. Steele
Centre for Technical Ceramics, Imperial College

TUESDAY, NOVEMBER 27

"RESEARCH AND DEVELOPMENT OF SOFC" 127
F. Umemura
Tokyo Electric Power Co., Inc.

12 Noon - 2:00 pm **Luncheon/Session #4 - Posters - *Grand Ballroom***
Authors will be available to discuss their papers.

COMPONENT TECHNOLOGIES AND SYSTEMS ANALYSIS I (#4)
Chairmen:
Dan Scarpiello, Gas Research Institute
Charlie Pax, Department of Energy

4A "THIN ELECTROLYTE LAYERS FOR SOLID OXIDE FUEL CELLS BY ELECTROCHEMICAL VAPOR DEPOSITION (EVD)" 131
L. G. J. de Haart
Laboratory of Inorganic Chemistry
University of Twente

4B "CHARACTERIZATION OF HIGH TEMPERATURE FUEL CELLS BASED ON ELECTROCHEMICAL IMPEDANCE MEASUREMENTS" 135
H. Landes
Siemens AG

4C "MULTILAYER ELECTRODES FOR PLANAR SOFC" 137
E. Ivers-Tiffe
Siemens AG

4D "AIR SINTERABLE SOLID OXIDE FUEL CELL INTERCONNECTS" 141
Harlan U. Anderson
University of Missouri-Rolla

4E "IMPROVED CERAMICS - THE KEY TO ECONOMIC FUEL CELLS" 145
Dr. K. Kendall
ICI Advanced Ceramics

4F "THE USE OF MOLTEN CARBONATE FUEL CELLS IN AN INTEGRATED COAL TO TRANSPORTATION LIQUIDS FACILITY" 148
John H. Hirschenhofer
Gilbert/Commonwealth, Inc.

4G "THERMODYNAMIC ANALYSIS ON REACTIONS BETWEEN MOLTEN CARBONATES AND ALLOYS" 152
Harumi Yokokawa
Tsukuba Research Center

TUESDAY, NOVEMBER 27

4H "CHEMICAL STABILITY OF INTERFACE BETWEEN AIR ELECTRODE AND ELECTROLYTE IN SOLID OXIDE FUEL CELL" 156
Harumi Yokokawa
Tsukuba Research Center

4I "DEFINITION OF PROCESS STEPS FOR MCFC COMPONENTS AND CELLS OF LABORATORY SCALE" 160
Hartmut Wendt
Institut fur Chemische Technologie

4J "VOLATILITY OF ALKALI CARBONATE MELTS - BASIC ENGINEERING DATA FOR MOLTEN CARBONATE FUEL CELLS" 164
Holger Mohn
Institut fur Chemische Technologie

4K "NEW PROCESS DESIGN FOR A SOLID OXIDE FUEL CELL POWER PLANT" 168
Masamichi Ippommatsu
Osaka Gas Company, Ltd.

4L "DEVELOPMENT OF NEW MATERIAL FOR MCFC SEPARATOR" 171
Toru Shimada
NKK Corporation

4M "INTERNAL REFORMING - MCFC SYSTEM PERFORMANCE STUDY UNDER FULL- AND PARTIAL-LOAD CONDITIONS" 175
Peter C. van der Laag
Netherlands Energy Research Foundation (ECN)

4N "MATERIAL STUDIES ON MOLTEN CARBONATE FUEL CELL" 179
Yoshinori Miyazaki
Government Industrial Research Institute

4O "DEVELOPMENT OF PETROLEUM NAPHTHA FUELED MCFC SYSTEM" 183
Yoshikazu Aoyagi
Tonen Corporation

4P "STUDY OF THE HYDROGEN OXIDATION AT GOLD IN MOLTEN LI+K (68/32) CARBONATE USING IMPEDANCE MEASUREMENTS AND CHRONOAMPEROMETRY" .. 187
R. Weewer
Delft University of Technology

TUESDAY, NOVEMBER 27

4Q "TEMPERATURE INFLUENCE ON THE MCFC LIFE TIME" 191
S. Freni
Institute C.N.R.-T.A.E.

4R "ON THE PROSPECTS OF OPERATING AN SOFC ON DRY NATURAL GAS" 195
Mogens Mogensen
Riso National Laboratory

4S "HYBRID COMBUSTION OF MCFC ANODE EXHAUST GAS FOR HEAT EXCHANGE STEAM REFORMER" 199
Osamu Togari
Chiyoda Corporation

4T "DEVELOPMENT OF A 25 kW SOFC COGENERATION SYSTEM UNIT" 205
Kenichi Shinozaki
Osaka Gas Company, Ltd.

4U "RECENT PROGRESS ON A FUEL CELL R&D PROJECT OF NEDO" 209
Hiroshi Ayada
New Energy & Industrial Technology Development Organization (NEDO)

4V "MONOLITHIC SOLID OXIDE FUEL CELLS FOR DIESEL BASED SYSTEMS" 213
Gorik Hossepian
Allied-Signal Aerospace Company

4W "ELECTROLYTE CHEMISTRY AND WETTING EFFECTS ON MCFC CATHODE KINETICS AND PERFORMANCE" 214
J. Robert Selman
Illinois Institute of Technology (I.I.T.)

4X "THERMOCHEMICAL CONSIDERATIONS AND PERFORMANCE OF SOLID OXIDE FUEL CELLS" 218
Christopher Milliken
Ceramatec, Inc.

4Y "DEVELOPMENT OF ALTERNATE CERAMIC CATHODE MATERIAL FOR MOLTEN CARBONATE FUEL CELLS" 222
S. Elangovan
Ceramatec, Inc.

TUESDAY, NOVEMBER 27

4Z "HALF-CELL ELECTROCHEMICAL CHARACTERIZATION OF MATERIALS FOR MCFC CATHODES" 226
L. Bigoni
CISE Tecnologie Innovative SpA

4AA "DEVELOPMENT AND CHARACTERIZATION OF MOLTEN CARBONATE FUEL CELL ANODES" 231
M. Takeuchi
Hitachi Research Laboratory, Hitachi, Ltd.

4BB "IMPEDANCE MEASUREMENTS OF THE OXYGEN REDUCTION IN MOLTEN CARBONATES AT 650 DEGREES C" 235
R. C. Makkus
Delft University of Technology

4CC "PERFORMANCE PREDICTIONS FOR MONOLITHIC SOLID OXIDE ELECTROLYZER ARRAYS" 239
Thomas M. Maloney
NASA Lewis Research Center

4DD "MATHEMATICAL ANALYSIS OF THE THERMAL CHARACTERISTICS OF A 25kWe REGENERATIVE FUEL CELL ENERGY STORAGE SYSTEM" 244
Thomas M. Maloney
NASA Lewis Research Center

2:00 pm - 5:00 pm **STATIONARY POWER APPLICATIONS I (5A)** - *Mesa Room*
Chairman: Dan Rastler
Electric Power Research Institute

"A PRACTICAL REVIEW OF COMPOSITE UTILITY GENERATION OPTIONS" 250
Martin Fry
WS Atkins Energy

"TECHNOLOGY ADVANCEMENTS IN THE WESTINGHOUSE AIR-COOLED PHOSPHORIC ACID FUEL CELL PROGRAM" 254
Maynard K. Wright
Westinghouse Electric Corporation

"FIELD TEST RESULTS OF 50kW PRESSURIZED PHOSPHORIC ACID FUEL CELL PILOT PLANT FOR ELECTRIC UTILITY" 256
T. Saito
Touhoku Electric Power Co., Inc.

TUESDAY, NOVEMBER 27

3:30 pm - 3:45 pm — Break - *Main Foyer*

"PRODE PROJECT: 1 MW PAFC EUROPEAN DEMONSTRATOR DESIGN PROGRESS AND LICENSING ASPECTS" 260
Bartolomeo G. Marcenaro
Ansaldo Ricerche

"PAC TEST OPERATION OF 11 MW PAFC POWER PLANT AT TEPCO GOI THERMAL POWER STATION" 264
Naoshi Kato
Toshiba Corporation

"NATURAL GAS/DIRECT FUEL CELL POWER PLANTS: DEVELOPMENT AND COMMERCIALIZATION ACTIVITIES" 267
Hans C. Maru
Energy Research Corporation

2:00 pm - 5:30 pm — MARINE AND SPACE APPLICATIONS (5B) - *Flagstaff Room*
Chairman: Paul Prokopius
NASA Lewis Research Center

"MARINE APPLICATIONS OF FUEL CELLS" 273
V. W. Adams
Procurement Executive Ministry of Defense

"FUEL CELLS IN NAVAL APPLICATIONS" 278
David P. Bloomfield
Analytic Power Corporation

"SOLID POLYMER FUEL CELL POWER SYSTEMS FOR AIR-INDEPENDENT SUPPLY OF SUBMARINE AUXILIARY POWER" . . . . . *
Alfred P. Meyer
International Fuel Cells Corporation

3:30 pm - 3:45 pm — Break - *Main Foyer*

"REGENERATIVE FUEL CELL ENERGY STORAGE SYSTEMS FOR FUTURE MANNED SPACE MISSIONS" . . . . . *
Paul R. Prokopius
NASA Lewis Research Center

* Abstract not available at time of publication.

TUESDAY, NOVEMBER 27

"SPE REGENERATIVE HYDROGEN/OXYGEN FUEL CELLS FOR SPACE AND MARINE APPLICATIONS" 282
James F. McElroy
United Technologies Corporation
Hamilton Standard Division

"POTENTIAL APPLICATIONS FOR SDI-DEVELOPED ALKALINE FUEL CELL TECHNOLOGY" . . . . . *
Joseph P. Fellner
Wright Research and Development Center

"REGENERATIVE FUEL CELL SYSTEMS TRADE-OFF ANALYSIS" 286
James R. Huff
Los Alamos National Laboratory

2:00 pm - 5:30 pm TECHNOLOGY ADVANCEMENTS FOR MOLTEN CARBONATE FUEL CELLS III (5C) - *Casa Grande Room*
Chairman: Karen Trimble
Gas Research Institute

"PHYSICAL PROPERTY OPTIMIZATION OF LITHIUM ALUMINATES FOR FABRICATION OF MOLTEN CARBONATE FUEL CELL MATRICES" 289
Patrick M. Brown
Cyprus Foote Mineral Company

"DEGRADATION OF NiO CATHODES: MODELING AND EXPERIMENTAL STUDIES" 294
David A. Shores
University of Minnesota, Corrosion Research Center

"TECHNOLOGY BASE RESEARCH FOR THE MCFC: STATUS AND NEEDS" 298
J. Robert Selman
Illinois Institute of Technology (I.I.T.)

3:30 pm - 3:45 pm Break - *Main Foyer*

"DURABILITY STUDY OF A MOLTEN CARBONATE FUEL CELL AT ELEVATED PRESSURE" 302
Isamu Sone
Hitachi Research Laboratory, Hitachi, Ltd.

* Abstract not available at time of publication.

TUESDAY, NOVEMBER 27

"OVERVIEW OF THE DOE-FUNDED FUEL CELL CONTAMINANTS R&D PROGRAM" 306
Mark Williams
Department of Energy,
Morgantown Energy Technology Center

"MCFC MATERIALS RESEARCH AT THE NETHERLANDS ENERGY RESEARCH FOUNDATION ECN" 310
L. Plomp
Netherlands Energy Research Foundation (ECN)

"COPPER-BASED ANODE" 314
E. T. Ong
Institute of Gas Technology

6:00 pm - 8:00 pm **Reception** - *Poolside*

WEDNESDAY, NOVEMBER 28, 1990

7:30 am - 8:30 am **Speakers' Breakfast** - *Sedona Room*
(Wednesday Speakers only)

7:30 am - 8:30 am **Poster Speakers' Breakfast** - *Grand Ballroom*
(Wednesday Speakers only)

8:00 am - 2:00 pm **Registration** - *Conference Center Registration Area*

8:00 am **Continental Breakfast** - *Main Foyer*

9:00 am - 12 Noon STATIONARY POWER APPLICATIONS II (6A) - *Flagstaff Room*
Chairman: Noboru Itoh
Fuel Cell Development Information Center

"RESULTS OF 100kW METHANOL FUELED PAFC PILOT PLANT AND RECENT CELL TECHNOLOGY" 318
Hideaki Miyoshi
Mitsubishi Electric Corporation

"DEVELOPMENT OF 200kW PHOSPHORIC ACID FUEL CELL SYSTEM FOR DETACHED ISLANDS" 322
Toshihide Nogi
Fuji Electric Company, Ltd.

"DEVELOPMENT OF ON-SITE PAFC BASED ON NAPHTHA AND KEROSENE" 326
Shigeru Yanagida
Nippon Petroleum Refining Co., Ltd.

WEDNESDAY, NOVEMBER 28, 1990

10:30 am - 10:45 am **Break** - *Main Foyer*

"DEVELOPMENT OF ON-SITE PAFC FOR COGENERATION IN TOKYO GAS" 330
Masanori Kaizaki
Research & Development Institute of Tokyo Gas

"DEVELOPMENT OF FUEL CELLS FOR COMMERCIAL USE UNDER THE MOONLIGHT PROJECT" 334
Toshitaka Omoto
Osaka Gas Company, Ltd.

"DEMONSTRATION TEST OF 200kW WATER-COOLED TYPE PHOSPHORIC ACID FUEL CELL PLANT" 338
T. Makabe
The Tokyo Electric Power Co., Inc. (TEPCO)

9:00 am - 12 Noon **TECHNOLOGY ADVANCEMENTS FOR ACID TYPE FUEL CELLS (6B)** - *Casa Grande Room*
Chairman: Al Landgrebe
Department of Energy

"STABILITY OF PHOSPHORIC ACID FUEL CELL ELECTROCATALYSTS" 342
K. Tsurumi
Tanaka Kikinzoku Kogyo Technical Center

"OPERATIONAL EXPERIENCE OF A 100 W PHOSPHORIC ACID FUEL CELL STACK" 347
V. Recupero
Institute C.N.R.-T.A.E.

"EVOLUTION OF THE STRUCTURAL PROPERTIES OF PTFE BOUND GAS DIFFUSION ELECTRODES" 351
V. Alderucci
Institute C.N.R.-T.A.E.

10:30 am - 10:45 am **Break** - *Main Foyer*

"INFLUENCE OF PARTICLE SIZE OF PLATINUM CATALYSTS SUPPORTED ON CARBON UPON ELECTROCHEMICAL O_2 REDUCTION IN PAFC" 355
E. Passalacqua
Institute CNR-TAE

WEDNESDAY, NOVEMBER 28

"DEVELOPMENTAL STATUS OF A 34kW FUEL CELL MODULE IN PEM TECHNOLOGY AS AN AIR-INDEPENDENT POWER SOURCE" 359
W. Bette
Siemens AG

"METHODS TO ATTAIN HIGH ENERGY EFFICIENCIES AND HIGH POWER DENSITIES IN SOLID POLYMER ELECTROLYTE FUEL CELLS WITH LOW OR HIGH PLATINUM LOADING ELECTRODES" 364
Supramaniam Srinivasan
Texas A&M University

12 Noon - 2:00 pm **Luncheon/Session #7 - Posters - *Grand Ballroom***
Authors will be available to discuss their papers.

COMPONENT TECHNOLOGIES AND SYSTEMS ANALYSIS II (#7)
Chairmen:
Ed Beyma, Department of Energy, Morgantown Energy Technology Center
Patricia O'Donnell, NASA Lewis Research Center

7A "SUBMERGED APPLICATIONS FOR FUEL CELLS: THE GENERAL EVALUATION APPROACH" ..... *
William H. Kumm
Arctic Energies, Ltd.

7B "ONSITE FUEL CELLS AND A PACKAGED COGENERATOR AT THE SAME SITE" 368
Thomas Naples
Brooklyn Union Gas Company

7C "STABILITY OF ELECTROCATALYSTS AND EVALUATION OF FUEL GAS COMPOSITION IN AIR-COOLED PAFC" ..... *
Aurelio Ascoli
CISE Tecnologie Innovative, S.p.A.;

7D "CORROSION-RESISTANT CATALYST SUPPORTS FOR PHOSPHORIC ACID FUEL CELLS" 371
J.A. Kosek
Giner, Inc.

7E "WORK ON THE LARGE SCALE ADVANCED TYPE PAFC" 375
Masanori Yamaguchi
Hitachi Research Laboratory

* Abstract not available at time of publication.

WEDNESDAY, NOVEMBER 28

7F "A WORLDWIDE PERSPECTIVE ON FUEL CELL MARKETS" 378
Diane Traub Hooie
NORA Management, Inc.

7G "THE DEVELOPMENT OF AN SPFC POWER GENERATION SYSTEM DEMONSTRATOR" 379
Clive M. Seymour
Vickers Shipbuilding & Engineering, Ltd.

7H "DEMONSTRATION TEST OF A 200kW PAFC POWER PLANT AT AN OFFICE BUILDING" 383
Masatsune Harada
Osaka Gas Company, Ltd.

7I "A STUDY ON THE COSTS OF ELECTRICITY GENERATED BY FUEL CELLS AND CONVENTIONAL POWER PLANTS IN TAIWAN" 387
Moses L. Ng
Industrial Technology Research Institute

7J "ELECTROCHEMICAL EVALUATION OF THE EFFECT OF PTFE CONTENT ON THE PERFORMANCE OF FUEL CELL ELECTRODES" 391
D. Rocco de Sena
Instituto de Fisica e Quimica de Sao Carlos/USP

7K "OPTIMIZATION OF PLATINUM LOADING AMOUNT OF CARBON-SUPPORTED ALLOY CATHODE CATALYST FOR ADVANCED PHOSPHORIC ACID FUEL CELL" 395
Takashi Ito
N.E. CHEMCAT Corporation

7L "THE METHANOL PERMEABILITY ISSUE FOR THE DIRECT METHANOL AIR PEM CELL" 399
Liu Jingsong
Royal Institute of Technology

7M "PYROLYZED MACROCYCLES ON HIGH SURFACE AREA CARBONS FOR THE REDUCTION OF OXYGEN IN ALKALINE FUEL CELLS" 403
Yohannes Kiros
Royal Institute of Technology

WEDNESDAY, NOVEMBER 28

7N "AFC CO-GENERATION SYSTEMS" 407
Timo Kivisaari
Royal Institute of Technology

7O "FUEL PROCESSORS FOR RURAL FUEL CELL POWER PLANTS" 411
Sara Thyberg
Royal Institute of Technology

7P "PREPARATION AND MEASUREMENT OF AIR ELECTRODES FOR ALKALINE FUEL CELLS" 415
Juhani Kivisaari
Royal Institute of Technology

7Q "ELECTROCHEMICAL INVESTIGATION OF MICROAGGLOMERATES FROM FC-CATHODES" 419
Martin Bursell
Royal Institute of Technology

7R "REDUCING DOWNTIME USING POINTER: AN INTELLIGENT MAINTENANCE AID" 422
ARINC Research Corporation

7S "FUEL CELL COGENERATION PLANT - A TECHNICAL AND ECONOMICAL FEASIBILITY STUDY FOR A PETROCHEMICAL PLANT IN FINLAND" 429
J. P. Nieminen
Neste Oy

7T "COMPARATIVE ANALYSIS OF POWER GENERATION OPPORTUNITIES" 433
Richard Root Woods
Gas Research Institute

7U "POLYMER ELECTROLYTE FUEL CELL RESEARCH" 437
C. Derouin
Los Alamos National Laboratory

7V "THE TREATMENT OF CO POISONING IN LOW TEMPERATURE FUEL CELLS BY THE INJECTION OF OXYGEN OR AIR INTO THE ANODE FEED STREAM" 441
M. T. Paffett
Los Alamos National Laboratory

WEDNESDAY, NOVEMBER 28

7W "MEASUREMENTS OF WATER TRANSPORT PROPERTIES AND IMAGING WATER PROFILES IN IONOMERIC MEMBRANES EMPLOYED IN POLYMER ELECTROLYTE FUEL CELLS" 445
Tom Zawodzinski
Los Alamos National Laboratory

7X "CATALYTIC RECOMBINER FOR ELIMINATION OF FUEL CELL PURGE GASES" 449
K. Ledjeff
Fraunhofer-Institute for Solar Energy Systems

7Y "THE SOUTH COAST AIR QUALITY MANAGEMENT DISTRICTS PERSPECTIVE ON THE USE OF FUEL CELLS FOR TRANSPORTATION AND STATIONARY APPLICATIONS" ..... *
Lawrence S. Watkins
South Coast Air Quality Management District

7Z "PREPARATION AND CHARACTERIZATION OF GAS DIFFUSION ELECTRODES FOR ALKALINE FUEL CELLS" 453
E. Gulzow
DLR-Institute for Technical Thermodynamics

7AA "THE FUEL CELL BUS PROGRAM AND ITS APPLICATION TO TRANSIT MISSIONS" 457
Samuel Romano
Georgetown University

7BB "ELECTROCHEMICAL ENERGY CONVERSION FOR STORAGE OF SOLAR ENERGY" 462
K. Ledjeff
Fraunhofer-Institute for Solar Energy Systems

7CC "EFFECT OF DIFFERENT COOLANT AIR FLOW DIRECTIONS ON PHOSPHORIC ACID FUEL CELL PERFORMANCE" 467
M. T. Le
Westinghouse Electric Corporation

* Abstract not available at time of publication.

7DD "CARBON DIOXIDE TOLERANT HYDROGEN AND METHANOL FUEL CELL WITH AN AQUEOUS CARBONATE ELECTROLYTE" 471
Peter Kalal
ASTRIS, Inc.

7EE "CORROSION SCREENING OF CANDIDATES FOR THE ALKALINE FUEL CELL CATHODE" 475
Richard S. Baldwin
NASA Lewis Research Center

7FF "THE GRI ELECTROLYTE PROGRAM TETRAFLUOROETHYLENE-1, 2-BIS-PHOSPHORIC ACID" 480
D. L. Maricle
International Fuel Cells

2:00 pm - 5:00 pm **STATIONARY POWER APPLICATIONS III (8A)** - *Flagstaff Room*
Chairman: Ed Gillis
Electric Power Research Institute

"FUEL CELL COMMERCIALIZATION THROUGH A PARTIAL ENERGY SERVICE" 484
David M. Moard
Southern California Gas Company

"PAFC - APPROACH TO COMMERCIALIZATION" 486
Rioji Anahara
Fuji Electric Company, Ltd.

"TOSHIBA'S STRATEGY FOR FUEL CELL POWER PLANT COMMERCIALIZATION" 491
Haruo Kawahara
Toshiba Corporation

3:30 pm - 3:45 pm Break - *Main Foyer*

"HIGH-TEMPERATURE FUEL CELL POWER SYSTEM STUDIES FOR SMALL AND MEDIUM SIZED POWER PLANTS" 495
W. Drenckhahn
Siemens AG KWU

"RESULTS FROM APPA'S 'NOTICE OF MARKET OPPORTUNITY' FOR FUEL CELLS (NOMO): A NEW COMMERCIALIZATION PARTNERSHIP" 499
M. K. Bergman
Instar Community Systems, Inc.

"POTENTIAL FOR USE OF FUEL CELL POWER PLANTS IN TRANSIT BUSES" 503
Thomas J. Ross
Phoenix Transit System

2:00 pm - 5:00 pm TECHNOLOGY ADVANCEMENTS FOR SOLID OXIDE FUEL CELLS II (8B) - *Casa Grande Room*
Chairman: Manville Mayfield
Department of Energy, Morgantown Energy Technology Center

"SOFC TECHNOLOGY STATUS AT WESTINGHOUSE" 506
Emerson R. Ray
Westinghouse Electric Corporation

"PLANAR SOFC DEVELOPMENT AT THE NETHERLANDS ENERGY RESEARCH FOUNDATION ECN" 512
J. P. P. Huijsmans
Netherlands Energy Research Foundation (ECN)

"TONEN TEST OF PLANAR SOFC" 516
Takayuki Hoshina
Tonen Corporation

3:30 pm - 3:45 pm Break - *Main Foyer*

"DEVELOPMENT OF MOLB TYPE SOLID OXIDE FUEL CELL" 520
Toshio Inoue
Chubu Electric Power Company, Inc.

"MONOLITHIC SOLID OXIDE FUEL CELL TECHNOLOGICAL STATUS" 524
Nguyen Q. Minh
Allied-Signal Aerospace Company

"PLANAR SOLID OXIDE FUEL CELL DESIGN, CHARACTERIZATION, AND INVESTIGATION" 527
Meilin Liu
Ceramatec, Inc.

5:00 pm - Conclusion of the 1990 Fuel Cell Seminar

ENVIRONMENTAL ASPECTS PUSH FUEL CELL TECHNOLOGY R&D PROGRAM AHEAD IN JAPAN

Takeshi Sugimoto
Vice Chairman of Fuel Cell Development Information Center (FCDIC)
Executive Director of New Energy and Industrial Technology Development Organization (NEDO)
Sunshine 60 3-1-1, Higashi-Ikebukuro, Toshima-ku, Tokyo, Japan

Introduction

A fuel cell can directly generate electric power at high efficiency by a chemical reaction of hydrogen and oxygen. Because it has basically no combustion or dynamo, a fuel cell power generation system is very quite and clean.

Thus, in Japan, recently growing concern regarding environmental problems has been responsible for accelerating a R&D program on the promising generation and co-generation technologies offered by the fuel cell.

1. Long-Term Energy Supply and Demand Prospects

MITI recently has published a report on Japan's long-term energy supply and demand prospects until 2010. According to the report, though energy consumption in Japan is exepected to increase steadily in the future, by considering restrictive factors such as the shortage of energy sources and environmental problems, it is much more important to promote the development of energy saving and highly efficient energy generation technology.

In addition, this report shows concrete target values for energy supply in 2000 and 2010. Among them, a great amount of fuel cells is expected to be utilized in various fields, as follows:

	Year:2000	Year:2010
For electric utilities:	1.05 million kW	5.50 million kW
For private use :	0.85 million kW	2.70 million kW

2. National Project of Fuel Cell Technology

In Japan, a systematic national project on fuel cells started in 1981 as part of a R&D project on large-scale energy saving technology (Moonlight Project). NEDO has been promoting the 15-year R&D project as an implementing agency.

(1) Phosphoric acid fuel cell

The PAFC project is in the final stage towards commercialization.

NEDO is now conducting field tests of the two types of 200 kW on-site power generation systems, one of which is a methanol fueled type for generation on a detached island and the other is a city gas fueled type for co-generation use in hotels, hospitals and so on. For the purpose of dispersed power generation use, NEDO is about to start a 5 MW demonstration plant project with 9 power utilities.

(2) Molten carbonate fuel cell

NEDO has been carrying out the second phase of the MCFC project in order to develop a 1000kW class pilot plant by FY 1995. Recently, the electrode area could be extended to the $1m^2$ class, and by using th e world largest cells, two types of cell stacks, a 25 kW class stack for atmospheric pressure operation and a 10 kW class stack for pressurized operation, were developed and operated in 1990.

A 3 kW class cell stack with directly internal reforming was also developed and operated successfully this year.

The system design study and the development of BOP are also being carried out by the Technology Research Association for MCFC Power Generation System.

The development of 100 kW class stacks is to be started next year.

(3) Solid oxide fuel cell

NEDO started a three-year R&D project in 1989 in order to develop the basic fabrication technology for large sized cells and stacks through five different approaches and to study the overall generating system.

3. R&D Activities in private sector

In addition to the Moonlight Project, research and development of various fuel cells has been actively promoted by the private sector. In the area of PAFC for example, Tokyo Electric Power Company is presently constructing an 11 MW plant and Tokyo Gas, Osaka Gas and Toho Gas have started a commercialization program for 50kW and 100kW package type system, where products will be put on the market in 1993.

CONCLUSION

Rising concern regarding global environmental problems and successes in the Moonlight Project and others have led to further efforts to commercialize fuel cell generation technology in Japan. The Fuel Cell Development Information Center, which was founded for supporting the commercialization of fuel cell technology by exchanging information, now has 108 members and is expected to play an important role inthis undertaking.

HIGHLIGHTS OF FUEL CELL ACTIVITIES IN THE NETHERLANDS

K. Joon, J.P.T. Vossen
Netherlands Energy Research Foundation ECN,
Petten, The Netherlands

P.H. van Dijkum
NOVEM B.V.
Utrecht, The Netherlands

INTRODUCTION

The Dutch Fuel Cell Programme was initiated by NOVEM in 1986. It is sponsored by the government (Ministry of Economic Affairs). From the beginning ECN has been the main contractor. The program has been described on several occasions (1, 2, 10). There is interest in fuel cells because:

- fuel cells are environmentally benign;
- natural gas and other fossil fuels can be converted efficiently;
- development of fuel cells requires a high level of technological research in which electrochemistry and materials technology play an important role;
- fuel cell development forms a solid basis for commercial activities.

The MCFC research activities at ECN can be divided into 5 main groups:

- basic electrochemical research;
- development of porous materials;
- fabrication of components;
- separator plate/stack technology;
- system studies.

BASIC ELECTROCHEMICAL RESEARCH

The fundamental research is performed in cooperation with Delft University of Technology. Electrochemical techniques (e.g. impedance measurements) have been used in order to obtain information about the reaction kinetics at the anode and the cathode. For these experiments a pot cel type set-up is being used. The main results are that the cathode behaviour is under control of a chemical reaction. The wetting characteristics of the anode material seem to depend on the substrate composition. For more details see (3, 4).

DEVELOPMENT OF MATERIALS

Materials development follows two lines, i.e. modification of existing materials and development of new materials. The development of the anode material mainly concentrates on modification of nickel chromium. Attention is being paid to deformation and creep phenomena. Recently, nickel aluminum has succesfully been investigated as a more creep resistant alternative. In addition, a new method has been developed for producing nickel aluminum (5).

Two ways are being investigated to improve the cathode lifetime. One is to reduce the solubility of the nickel oxide by changing the melt

basicity by means of additives. A model on nickel transport through the electrolyte matrix has been presented (6). On the other hand, physico-chemical research on alternative materials has been performed. Initially, this was concentrated on lithium ferrite (LiFeO2). The performance characteristics of this material were inferior to those of nickel oxide. Recently, a new material, lithium cobaltate ($LiCoO_2$), has been developed succesfully. The performance of this material is competitive to that of nickel oxide (5, 7).

In order to avoid gas cross-over an anode bubble barrier has been used up till now. Because the production of this component is costly, ways are being developed to avoid its application. For this reason research has been carried out to make the matrix less prone to cracking. To this end alumina fibres are used. The alumina is in situ converted to alfa aluminate and improves the strenght of the matrix.

FABRICATION OF POROUS COMPONENTS

For production of all porous components the tape casting technique was chosen. Extensive research and development efforts have been spent on powder optimization, stability and optimization of suspensions, the tape casting procedure, the drying conditions and the sintering process. These aimed at optimization of the component characteristics, cell performance and upscaling. At present, single components of 240*80 cm^2 can be produced with uniform pore characteristics and a thickness tolerance of < 0.02 mm. Further research aims at (semi-)continuous production.

STACK/SEPARATOR PLATE TECHNOLOGY

The basic separator plate design concept developed at ECN includes an internal gas manifolding incorporated in the sealing rail. This rail is realized as a soft rail in order to be able to follow (long term) deformations of the porous components. This concept has proven to be leak tight for pressure differences between anode and cathode and between anode/cathode and environment of 70 cm water column in short-stack tests of 1000 cm^2 cells. Further design improvements are related to gas distribution in order to obtain a more uniform loading pattern. This design concept was chosen also with a view to the possibilities for scaling up the production.

An important field of research is the separator plate corrosion. In this respect a large number of exposure tests has been performed on a range of candidate materials. In addition, post-test analyses of separator plates from stack tests have generated a better understanding of the relevant hot corrosion processes. Based on these results Ph.D. research has started to elucidate the influence of material composition and operational parameters on the corrosion behaviour. Research into different protection techniques has resulted in a nickel coating process for the anode gas chamber and aluminization of the wet-seal area.

Present efforts concentrate on upscaling to 4000 cm^2. Evaluations have started to adapt the design for internal reforming purposes.

SYSTEM STUDIES

Several systems studies have been carried out at ECN. The first one was a study on the use of basic oxygen furnace gas in a MCFC power plant (8). Also, a comparative study on internal and external reforming MCFC systems has been carried out. Internal reforming appears to be superior to external reforming, provided some problems involved in internal reforming can be solved. Another study is performed on the efficiency of fuel cells under partial and full load conditions (9). A study carried out by KTI was titled: "Fuel Cell Systems", May 1988. A study on a pressurized external reforming system was carried out by ESTS entitled "Process Design of a Pilot Plant for MCFC", March 1989. Both studies focussed on optimal component configuration for producing electricity with high efficiencies and were reported in (10).

FUTURE MCFC ACTIVITIES AT ECN

A new phase in the MCFC programme started on January 1, this year, with participation of the industry and probably important financial contributions from the electric utilities. The aim of this phase is to demonstrate that a technology concept including production techniques has been developed as a solid basis for further commercial application. To reach this aim, a pressurized 10 kW unit of 4000 cm^2 cell area will be operated by the end of 1992.

A parallel program on basic and applied research aims at developing further design improvements for implementation at about the same time.
In addition, also in 1992, a proof of principle test of a 1 kW internal reforming unit is envisaged.

PAFC AND SOFC ACTIVITIES

Apart from ECN's activities in the area of MCFC, also activities with respect to PAFC and SOFC are performed in The Netherlands. As far as the PAFC activities are concerned, these are concentrated on the demonstration program for 25 kW and 300 kW units of KTI with financial support from NOVEM and the CEC (11).

SOFC activities take place at ECN, University of Twente, Delft University of Technology and the Netherlands Organization for Applied Scientific Research TNO. These are mainly carried out in cooperation with foreign partners, like Siemens and ABB, as part of the CEC fuel cell programme. Recently, discussions have started to coordinate these activities on a national scale, focussing at the flat-plate thin-layer concept.

References

1. D. van der Giessen, K. Joon, The ESTS/ECN-program for industrial MCFC Development. Paper presented in Scheveningen, the Netherlands, 26-29 1 October 987.

2. K. Joon, MCFC-developments in The Netherlands; Progress and Plans. Paper presented in Tokyo, 7-8 June 1988.

3. R. Weewer, K. Hemmes, J.H.W. de Wit, Study of the hydrogen oxidation at various electrode materials in molten carbonates using impedance measurements and chronoamperometry. Paper presented at this Seminar.

4. R.C. Makkus, K. Hemmes, J.H.W. de Wit, Impedance measurements of the oxygen reduction in molten carbonates at 650 °C. Paper presented at this Seminar.

5. L. Plomp, F.P.F. van Berkel, J.B.J. Veldhuis, S.B. van der Molen, MCFC Materials Research at The Netherlands Energy Research Foundation ECN. Paper presented at this Seminar.

6. J.B.J. Veldhuis, R.C. Makkus, S.B. van der Molen, G.H.J. Broers, NiO Cathode Dissolution and Long Term MCFC Operation. April 1990, submitted to "Berichte der Bunsengesellschaft fur Physikalische Chemie".

7. L. Plomp, E.F. Sitters, J.P.P. Huijsmans, S.B. van der Molen, Research on Alternative MCFC Cathode Materials. Paper presented at 178th ECS Meeting, Seattle, 14-19 October 1990.

8. P.E. Lugten, U. Stikker, Basic Oxygen Furnace Gas Fueled MCFC Power Plant. Paper presented in Scheveningen, the Netherlands, 26-29 October 1987.

9. P.C. van der Laag, Internal Reforming - MCFC System Performance Study, under Full- and Partial-load Conditions. Paper presented at this Seminar.

10. P.H. van Dijkum, K. Joon, The Molten Carbonate Fuel Cell Programme in The Netherlands, J. Power Sources, 29 (1990), 77-83.

11. L.J.M.J. Blomen, M. Mugerwa Technology Development and Market Introduction of PAFC Systems, J. Power Sources 29 (1990) 71-76.

ENVIRONMENTAL IMPACTS OF ENERGY FACILITIES BASED ON FUEL CELLS

Knut L. Seip (1) , Bernt Thorstensen (1), and Hagbarth Wang (2)
(1) Center for Industrial Research, Forskningsvn. 1, P. O. Box 124, 0134 Blindern, Oslo 3, NORWAY
(2) Saga Petroleum A/S, Kjørbovn 16, P.O. Box 16,1301 Sandvika, NORWAY

We compare the environmental side effects of power plants based on Fuel Cell technology to the side effects of conventional electric power plants based on coal and natural gas. The side effects are emission products, e.g., CO , particulates, heat and noise. Figure 1 indicates how these side effects impact the environment.

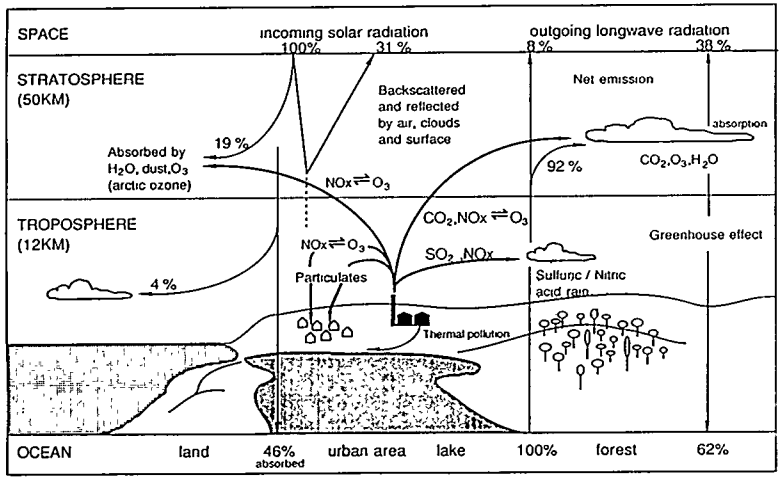

Figure 1
Emission products from power plants and their interaction with the environment and with processes responsible for the greenhouse effect. Figure based on [1, 3, 5].

We have assessed the impacts by constructing a general objectives' hierarchy which divides the objectives into three levels. The overall objective is to identify the energy source which has the smallest side effects. We first group the side effects into four subgroups: Environmental impacts, impacts on materials and buildings, socioeconomic impacts and impacts on health and safety. The lowest level objectives are the primary attributes. The full objective hierarchy is shown in Figure 2.

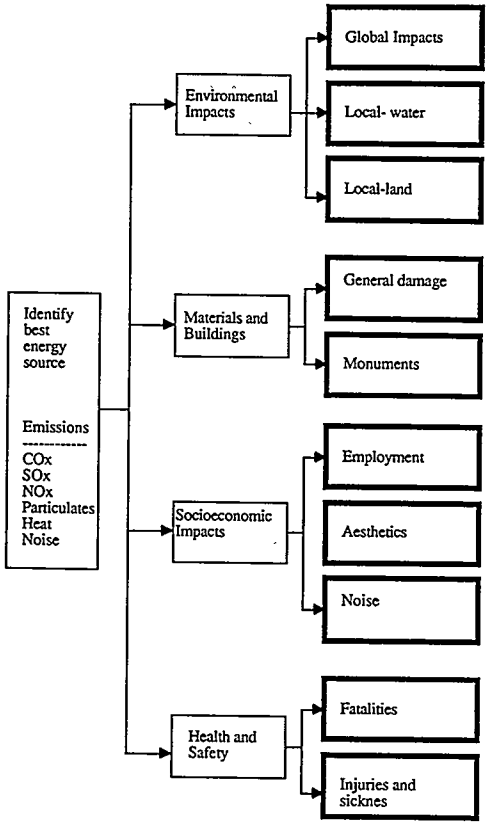

Figure 2
General objectives' hierarchy for energy facilities. Partly after [2].

The results of the study showed that the environmental impact from a Solid Oxide Fuel cell plant is very much less than for a coal or oil fired plant. For air pollution we got a factor of 1/ 1000 and for water pollution we got a factor of 1/ 3. Damages are reduced between 50 % and 80% compared to conventional gas plant. Damages to cultural monuments and buildings are negligible for a Fuel Cell plant. Socioeconomic negative impacts are reduced about 30 % relative to conventional gas plants (aesthetics and noise), whereas employment is unaltered. Damages to health and safety are greatly reduced compared to coal fired plants, and about 70 % compared to conventional gas plants.

Preliminary results suggest that the society's willingness to pay (WTP) for clean air, and thereby better health, matches the cost of installing emission reducing equipment on conventional power plants. There probably is an additional WTP for other benefits (e.g., decreased risk for global warming). Thus, the utility of very small emissions, lower CO_2 discharges, and other benefits from these generators, may compensate for an increased cost of producing electricity by SOFC generators. Seip et al. [4] give a full documentation of this study.

Literature

1. Cortese, A. D. "Clearing the air." Environ. Sci. Technol. 24: 442-448, 1990.

2. Keeney, R. L. "Siting of energy facilities." 1984 Academic Press. New York.

3. Mitchell, J. F. B. "The "Greenhouse" effect and climate change." Rew.Geophysics. 27: 115-139, 1989.

4. Seip, K. L., B. Thorstensen and H. Wang. Environmental impacts of energy facilities based on fuel cells. 1990.

5. Singh, H. B. "Reactive nitrogen in the troposphere." Environ. Sci. Technol. 21: 320-327, 1987.

THE PHOSPHORIC ACID FUEL CELL/BATTERY BUS PROJECT

Russ J. Kevala

Booz, Allen & Hamilton, Inc
4330 East-West Highway
Bethesda, Maryland 20814

This paper presents the status and plans for the fuel cell/battery bus project. Under the first phase, completed in February 1990, the feasibility of using a liquid-cooled phosphoric acid fuel cell (L-PAFC) for powering a small transit bus was demonstrated by means of a half-scale brassboard system. During the second phase, three test-bed buses will be designed, fabricated and tested to further evaluate the concept and demonstrate the practicality of fuel cell/battery systems to power transit buses.

Design Considerations

Major considerations in the design of the fuel cell/battery bus are:

- Bus performance should be equivalent to that of a standard diesel bus,
- Operation should be demonstrated over the standard DOT urban bus cycle as well as over specified GUTS Arlington Loop route,
- All bus, fuel cell and battery components should be readily available.

The electric drivetrain provides superior traction capabilities to the bus. It offers high initial acceleration and system efficiencies. Added energy saving benefits are offered by regenerative braking. Regenerative braking also reduces brake wear, a major maintenance item for current transit buses.

The fuel cell bus will meet all present and future environmental standards. Particulate emissions are absent. Operation of the fuel cell stack and reformer is silent.

The L-PAFC system was selected for its higher overall efficiency and ease of passenger heating compared to air-cooled PAFC systems. Performance trade-offs, availability, and cost considerations resulted in the specification of a power source consisting of a 50 kW (net) fuel cell, a 132 Amp-hour lead-acid battery, and a 120 kW (peak) dc traction motor.

System Feasibility

To demonstrate feasibility, a fully functioning brassboard power source was fabricated and tested in the laboratory. A photograph of the brassboard fuel cell subsystem is shown in Figure 1.

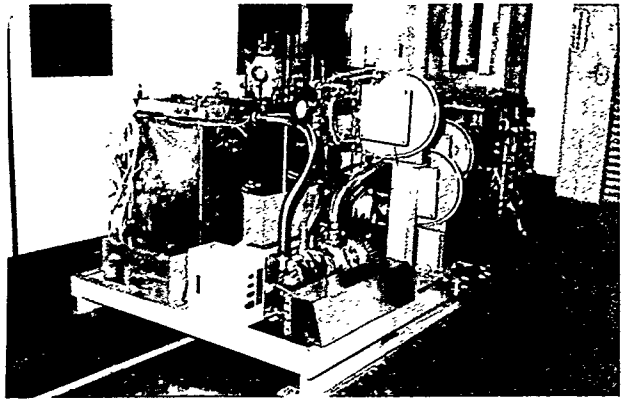

Figure 1
Photograph of the Brassboard L-PAFC System

The brassboard tests showed that fuel cell subsystem efficiency at full power was 36.5% with auxiliaries. The L-PAFC auxiliaries (cooling pumps, air and fuel supply pumps, etc.) consumed only 2.3% of the gross output of the fuel cell. Subsystem efficiencies exceeding 41% are projected for the full size fuel cell through improvements in stack design during the next phase.

The bus fuel economy projections from the brassboard measurements were in excellent agreement with the simulation results. Good correlation was also obtained between the measured and projected system response, bus acceleration times, battery conditions during the runs, and the system power output under route conditions. These results provided the proof of feasibility of the fuel cell/ battery system as a potential power source for urban transit buses.

Test-Bed Bus System

An Artist's concept for the proposed test-bed bus (TBB) is shown in Figure 2. The bus will utilize a 27 ft length low floor chassis and a two-speed axle. Standard bus accessories that are normally driven directly by the diesel engine (air compressor, air conditioner compressor and hydraulic power steering pump) will be driven by standard 120 V ac motors powered through invertors. The interior and exterior lights and other accessories requiring 24 V dc will be powered from the traction battery through a dc to dc converter. Conventional passenger heating and windshield defrosting ducts will be retained since the L-PAFC system permits the use of efficient liquid-to-air heat exchangers.

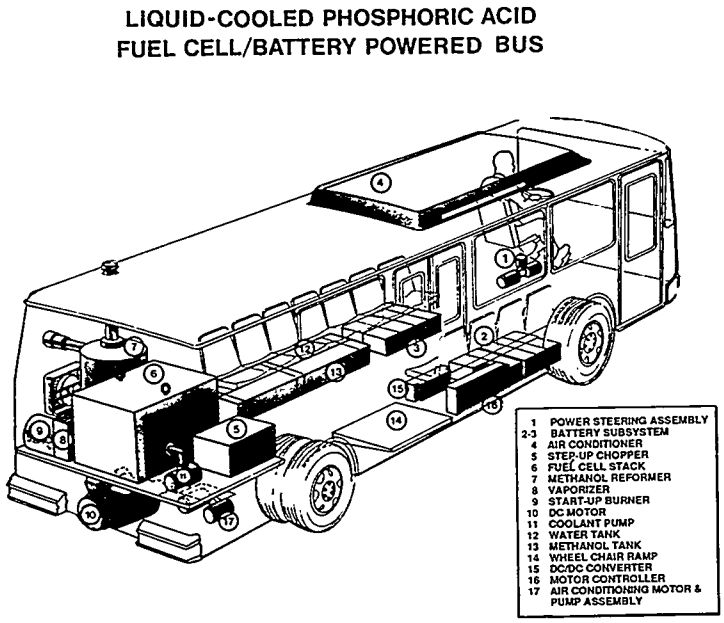

Figure 2
Artist's Concept for the Test-Bed Bus

The fuel cell/battery bus is expected to exhibit at least a 10 percent improvement in efficiency over diesel and methanol fueled buses on a Btu basis over comparable routes. Regenerative braking will provide additional energy savings, which could amount to 15 to 18 percent, depending on the route gradients. The TBB will have a curb weight of 7,937 kg (17,500 lb) and a gross weight of (9,570 kg (21,100 lb) with 24 passengers.

Maturity of Technology

L-PAFC technology has been under development at Engelhard Corporation and Fuji Electric since 1975. The technology has undergone several generations of improvement and thousands of hours of testing for the development of a commercial forklift truck power system and during the design and development of the brassboard fuel cell for Phase I. Fuji Electric recently completed 10,000 hours of continuous testing of a 21-cell stack at a current density of 240 mA/sq cm, which showed less than 1.5 percent drop in the 0.66 V/cell design voltage.

Capital and Life Cycle Costs

Based on a production volume of 10,000 fuel cell units/year, the sale price of a fuel cell/battery powered TBB-size bus is estimated to be $153,000, compared to $140,000 for an equivalent diesel engine powered bus. The life cycle cost, assuming a methanol price of $0.50 per gallon, a 10 % discount rate, and a 15 year bus life, would be $0.41 per mile. This compares favorably with an equivalent diesel engine bus if the diesel fuel cost (excluding taxes) is assumed to be $1.00 per gallon.

Design of 35-40 Ft Bus

One of the tasks in the project is to develop a detailed design by a large transit bus manufacturer, Transportation Manufacturing Corporation, for a full size 35-40 ft transit bus. A 40 Ft RTS bus body/chassis will the basis for the conceptual design, trade-offs and system specifications for the full-size transit bus. Advances in fuel cell technology including on-board water recovery and increased stack power density, advanced batteries, and ac power trains will be included in the trade-off analysis. A design layout of the bus will be developed and an economic assessment will be performed. The findings of this task, along with the test results for the 27 ft TBB will provide the information needed by bus industry to make decisions for the commercialization potential of fuel cell powered buses.

Commercialization of Fuel Cell Buses

Production volumes of the order of 10,000 units of fuel cell systems per year may be needed to justify the major investment needed for a new fuel cell manufacturing facility and to achieve costs competitive with diesel and other alternate fuel engine buses. Since the current U.S. transit bus market is not adequate to absorb this volume of production, bus fuel cell designs must be adaptable to other applications.

Commercial production of fuel cell powered buses will require industry acceptable performance, reliability and life cycle costs. These need to be demonstrated before bus manufacturers and operators will begin to accept the new technology. Compliance with emission regulations, efficient conversion of methanol fuel, and the energy savings due to regenerative braking are important areas in which the fuel cell powered bus will offer advantages over other internal combustion engine powered buses.

LIQUID-COOLED PHOSPHORIC ACID FUEL CELL SUBSYSTEM FOR THE BUS

Kazukiyo Okano
Fuel Cell Division. Fuji Electric Co.,Ltd.
7 Yawatakaigan-Dori, Ichihara-City,
Chiba, 290 Japan

Fuji Electric has been developing Phosphoric Acid Fuel Cell (PAFC) since 1973, and manufactured a number of water, air, liquid-cooled power plants ranging from 4 kW to 1 MW. A liquid-cooled fuel cell/battery hybrid system was constructed and demonstrated successfully for forklift truck application. Fuji Electric is also an active participant of the DOE Fuel Cell/Battery Bus Program.

This report summarizes the results obtained from a 25 kW brassboard fuel cell subsystem during Phase 1 of the DOE Bus Program. The design of a 50 kW PAFC fuel cell subsystem suitable for a test bed bus will also be discussed.

Brassboard Fuel Cell Subsystem

The 25kW PAFC fuel cell subsystem consists of a PAFC stack, a methanol steam reformer, a step-up chopper, and auxiliary equipments such as heat exchangers, start-up burner, tanks, pumps, blowers, etc.. An internal controller controls all operations.

Figure 1 depicts a block diagram of the fuel cell/battery hybrid power system which was adopted for the 25 kW brassboard system. Batteries with high peak power capabilities are connected in parallel with the fuel cell to provide peak power for vehicle acceleration and slope driving.

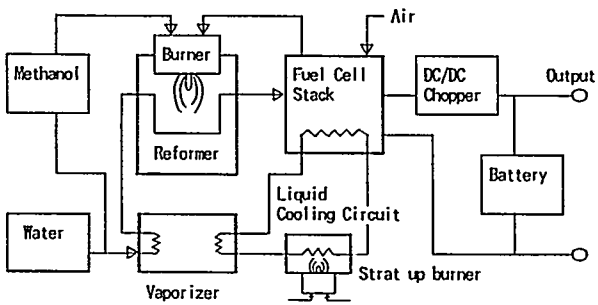

Fig.1. Block Diagram of FC/Battery Hybrid Power System

The system is based on dielectric liquid cooling which provides excellent characteristics listed in Figure 2. A liquid-cooled system is most suitable for vehicles which require a compact and high efficiency power source.

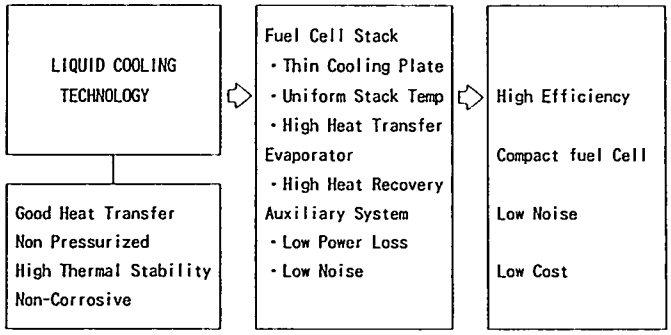

Fig.2. Features of Fuji's Liquid Cooling Fuel Cell System

Test Results of the Brassboard Fuel Cell Subsystem

Comprehensive test runs were conducted at Fuji Electric to verify the system performance with respect to design goals. The PAFC fuel cell subsystem was operated automatically by the internal controller. Test results are shown in Table 1. The brassboard fuel cell subsystem exceeded the power and efficiency specifications.

Table 1. Test Results of Brassboard Fuel Cell Subsystem

1.	Fuel Cell Output Power	25 kW
2.	System Efficiency	38 % (LHV. Excl. Aux.)
3.	Fuel Consumption	
	Methanol	10.8 kg/hour
	Water	9.3 kg/hour
4.	Start up time	40 min.
5.	Emission	NOx: 0.5 ppm, HC: Nil CO: 30 ppm, SOx: Nil

The emission levels were measured at the exhaust and the maximum emissions recorded from the fuel cell subsystem are well below that of an internal combustion engines.

The fuel cell/battery characterization tests were conducted at Pentastar Electronic Inc. in the United States. Excellent results were confirmed.

The 50 kW Fuel Cell Subsystem Design

Fuji's approach to the 50 kW fuel cell subsystem design for the test bed bus stresses the following.

- Compact and light weight
- Simplicity
- Safe and reliable
- Low cost

The liquid-cooled high power density PAFC system offers the possibility of a highly compact and light weight design. Specifications of the 50 kW PAFC fuel cell subsystem are shown in Table 2.

Table 2. Specifications of 50 kW Fuel Cell Subsystem

1.	Fuel Cell	Liquid Cooled PAFC
2.	Rated Output Power	
	Fuel Cell Stack	55.2 kW One Stack
	Chopper	47.5 kW
	Reformer	47.1 Nm^3/hour
3.	Fuel Consumption	
	Methanol	22.4 kg/hour
	Water	18.9 kg/hour
4.	System Efficiency	38 % (LHV)
5.	Total Weight of Subsystem	1,180 kg (2,600 lb)

1) Fuel Cell Stack Design Considerations

The PAFC stack has an active cell electrode area of 2000 cm^2, which is based on size, weight and cost trade-offs. The one-stack design has a power density of 0.18 W/cm^2 and an output of 55.2 kW. Dimension of the stack is 700 mm (2.3 ft) width x 700 mm (2.3 ft) length x 1,450 mm (4.7 ft) height. Weight is 560 kg (1,234 lb).

In addition to having the advantage of liquid-cooling, Fuji Electric achieves the compact and light weight design goal by utilizing special and proprietary stack architecture.

2) Methanol Reformer Design Considerations

The methanol reformer vessel adopts a concentric double tubes catalyst bed and a superheater. Copper oxide/zinc oxide reforming catalysts are used in order to achieve high conversion efficiencies.

Typical methanol conversion rate is over 99 % with a hydrogen flow rate of about 47 Nm^3/hour. Dimension of the reformer is 700 mm (2.3 ft) in diameter and 1,000 mm (3.6 ft) in height. Total weight is 200 kg (440 lb).

3) Plant Design Considerations

Based on earlier 25 kW brassboard experience, a number of considerations are taken into for hardware design. For examples:

- Waste heat is recovered and used for the vaporization of methanol/water fuel mixture via a heat exchanger in the liquid-cooling loop.
- High frequency (20 kHz) chopper is adopted for weight, size and cost reduction.
- Process blowers and flammable gas detectors will be installed inside the power package for safety.
- Standard AC motors and commercial parts will be utilized providing AC power to auxiliary equipments.

The entire system is in one package which can be installed at the rear compartment of a bus body and has a dimension of 2,100 mm (6.9 ft) width x 1,300 mm (4.3 ft) length x 1,450 mm (4.8 ft) height. Total weight is 1,180 kg (2,600 Ib).

Conclusion

Both hardware verification tests and the design of a fuel cell/battery subsystem for a test bed bus have confirmed that the liquid-cooled PAFC system is fully capable for powering a standard urban transit bus.

The fuel cell offers an attractive and a non-polluting power source for mobile applications. Multi-discipline cooperations are necessary in order to make this a commercial reality.

Acknowledgment

The 25 kW brassboard work was performed under the contract to the U.S. Department of Energy, Washington D.C..The author acknowledges the valuable guidance and assistance provided by Dr. P. Patil of DOE, Dr. C. Christiansen of Argonne National Lab., Mr. S. Romano of Georgetown University and Dr.R. Kevala of Booz, Allen & Hamilton Inc..

References

R. J. Kevala and Daryl M. Marinetti, " Fuel Cell Power Plants for Public Transport Vehicles," The Future Transportation Technology Conference and Exposition, August 1989, SAE Paper No.891658.

ALKALINE H_2-AIR FUEL CELLS FOR CITY BUS APPLICATION

H. Van den Broeck
Elenco N.V.
Gravenstraat 73 bis
B-2480 Dessel, Belgium

At earlier seminars the technical work of the Belgian company Elenco N.V. on the development of alkaline hydrogen-air fuel cells has already been presented.

In recent years Elenco's technology of the fuel cell stacks and of the ancillary equipment has been improved on the basis of the implementation of feedback results from tests. These tests have on the one hand consisted of stack endurance tests on laboratory test benches, and on the other hand of tests of complete systems incorporating such stacks. These systems have been of different power levels (1 kW stationary, 15 kW in an electric van, and 40 kW stationary).

The general experience with respect to system testing has turned out to be rather similar to that accumulated for phosphoric acid fuel cell systems : at the start, the importance of the ancillary equipment is underestimated, and practically all problems and operating failures of the fuel cell system have appeared to be related to that ancillary equipment. As a consequence, a "second generation" approach is required, incorporating a few new components and adapting the engineering of the whole system.

This experience is of course of great importance as part of the basis for setting up further demonstration projects.

From the start of its activities, Elenco has considered electric vehicles, and especially electric city buses, as very interesting application areas for its fuel cells. Therefore a few years ago efforts have been started to set up industrial consortia for designing, building and testing city buses equiped with fuel cells. Economic studies were made, showing that already with the present fuel cell technology in most cases a fuel cell bus would be more attractive operationally and economically than other electric buses, such as battery or trolley buses, and that the penalty with respect to present diesel buses is relatively limited and should be acceptable with a view to the associated advantages in terms of environment and energy conservation.

In 1988 Elenco started a feasibility and pre-engineering study with two Dutch companies with a view to the development of a fuel cell city bus for the city of Amsterdam. The results of this study indicated the best basic choices for the bus system :

- a hybrid system, with the fuel cell for the baseload, and an energy buffer for the acceleration peaks;
- for this energy buffer, a flywheel seemed to be the most attractive solution : less weight and better braking energy recovery than the alternative solution, consisting of secundary batteries;

- for the hydrogen storage, the use of liquid hydrogen is preferred.

Consequently, it was decided to prepare for the construction phase and to address the practical choice of the main components. The original partnership was extended with a fourth partner, so that a collaboration was set up between HOLEC (for electrotechnical and electronic equipment and for the flywheel), Den Oudsten (for bus construction), Air Products Nederland (for H_2 storage and supply), all of the Netherlands, and Elenco (for the fuel cell system).

At the moment of writing this abstract, this phase is nearing its end. Actually, it turned out to be quite longer than anticipated, the reason being the difficulty to identify and procure a suitable and payable flywheel. It is expected that at the time of the seminar the situation will have become clear with respect to the exact timing, and that it will be possible to make available some more detailed information about the intended city bus build-up and the construction of the bus.

Furthermore, Elenco also pursues other possibilities to set up similar projects in other countries. There should be no doubt that the present general concern about pollution, especially in cities in Europe, North America and the Far East, calls for initiatives. In such a frame, a city bus using a hydrogen fuel cell offers the ideal solution in terms of the environment, without putting a burden on the operational flexibility of the bus in the city traffic.

MERITS OF AFC-SYSTEMS FOR FORK LIFT TRUCKS

Olle Lindström
Department of Chemical Technology
The Royal Institute of Technology
S-100 44 Stockholm, Sweden

Fuel cell systems may detronize ICE-systems for all vehicular applications the next century. The present study has a more limited scope: fuel cell generators and other electro-chemical power sources are assessed for a 2 ton fork lift truck. Market introduction is set at 1995 and the fixed cost should be < $ 0.20/kWh. Candidate plants have to fit into 480 dm^3 of available space and should produce a minimum of 45 kWh during a shift, with 75 % delivered at 1C.

Five candidates remained after intitial screening, i.e. the lead acid battery, the nickel/iron batteri, the sodium/sulphur battery, the second generation iron/air battery and the AFC-generator for hydrogen. Twenty different electrode combinations were considered initially. Space and cost aspects eliminated all fuel cell concepts except the AFC-option.

The AFC-generators are of state of art design with bipolar collectors in nickel plated steel, teflon bonded nickel electrodes catalyzed by macro-cycle black for the cathode and a noble metal formulation for the anode. The electrolyte is contained in a chrysotile matrix. The stack is built up of sevencell modules, separated by end-plates also serving as coolant plates.

Product water is removed by the circulating anode gas and by the cathode gas, when air is used as cathode reactant. This generator design is also used for large power and co-generation plants which are at present under study at this department.

This design involves no exotic materials or unconventional production methods. No such fuel cell generators have yet been built in full size, however. Estimates of cost, life and performance should be taken seriously, however, in view of the experience in this field, which has been gained since the early sixties and also more recently in Europe. The 1995 requirement should be met provided the R&D work is being carried out.

The second generation iron/air battery is much related to the design of the AFC stack. The major difference is that hydrogen electrodes and hydrogen plenums have been substituted for the porous iron electrodes. The bipolar design of the second generation increases the energy density considerably compared to the monopolar first generation, which was produced and tested on a fairly large scale in Sweden during the early seventies.

Hydrogen and oxygen were produced by electrolysis and stored in steel cylinders, accomodated in the space allocated to the power source. Comparison between hydrogen/oxygen and hydrogen/air as well as iron/oxygen and iron/air shows much better performance for the air embodiments, since the equipment for CO_2-removal from air takes much less space than the oxygen cylinders. The oxygen produced either in the electrolyzer for the AFC-system or during charge of the iron systems gives a most considerable credit. This oxygen can be used in the very same plant using the trucks. Figure 1 shows schematically the arrangement of nine hydrogen cylinders and two AFC-stacks with space for auxiliaries.

Fig. 1. Truck system with 2 AFC-generators and 9 H_2 cylinders.

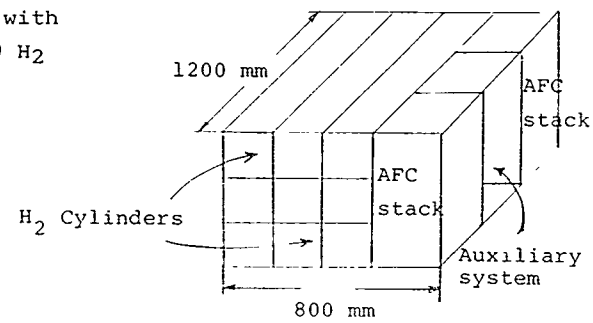

This particular arrangement with hydrogen stored at 30 Mpa gives a nominal energy content of 73.2 kWh. The operating point for the AFC-generators is 0.86 V at 325 mA/cm^2. Table 1 summarizes key-data for the five candidate systems. For comparison data is also included for an electric car application, the IDSEP van, run according to the simplified federal urban driving schedule (SFUDS).

Table 1. Performance of selected power sources matching the requirements of the reference truck

	kWh, nominal	kWh, at max.power	kWh, *) SFUDS	Wh/dm^3, nominal	Comments
Lead acid, tubular plates, standard	38 (5 h)	23 (1 h)	-	80	Proven,long life
Lead acid, flat plates (KTH)	58 (5 h)	36 (1 h)	-	120	Proven,short life
Lead acid, flow through (DOE goal)	-	-	57	(120) *)	Life ?
Nickel/iron, NIFE	44 (5 h)	31 (1 h)	-	92	Proven, long life
Nickel/iron (DOE goal)	-	-	54	(110) *)	
Sodium/sulphur, ASB	58	46		120	Reliability ?
Sodium/sulphur (DOE goal)	-	-	64	130	
Iron/air, ML-IIB (KTH)	97	78		200	50 % cap.reserve, O_2 sales
Iron/oxygen, ML-IIB with external O_2	-	-	-	160	No reserve, no O_2 sales
Iron/air (DOE goal)	-	-	53-72	(110-150) *)	
AFC, H_2/O_2	73	63	-	150	No O_2 sales
AFC, H_2/air	98	74	-	200	O_2 sales

*) IDSEP Van tested according to SFUDS, Simplified Federal Urban Driving Schedule

The table shows that the alkaline hydrogen and iron systems are in a class of their own.

Comparison between the much related iron and hydrogen systems gives a competitive edge for the true fuel cell approach. Two fuel cell stacks produce about the same power as six similar iron/air generators. The fuel cell truck is "charged" with

filled up bottles. The generators of the iron/air truck may be removed for charging in the same way as is practiced with present lead acid batteries, which calls for investment in several battery packs in case the fork lift truck is used during two shifts or three shifts.

The fuel cell system evidently requires a facility for electrolysis and gas cylinder fill up, whereas the iron/air truck requires only a charger in case the oxygen is used for other purposes. These two embodiments of AFC-technology are, therefore, complementary. A special advantage with the iron/air option is that the second discharge step of the iron electrode gives a capacity reserve of 50 % on an Ah basis.

It is interesting to note that the economic requirements on these power sources for the truck application coincide with the goals specified for power sources for electric vehicles. This means roughly 100 /kWh and say 500 deep cycles for the battery options. The second generation iron/air battery as well as the AFC-generator are capable of meeting these goals in mass production.

It is an open question whether the vehicular applications of AFC-technology will pave the way for utility applications or vice versa. For economic reasons utility would be first and vehicles second. The fuel cell community seems, however, to have earmarked the AFC for tractionary applications disregarding the utility market due to the CO_2 syndrome (the misconception that CO_2 cannot be removed from reactant gases for use in AFC generators in a cost effective way).

DEACTIVATION OF METHANOL STEAM REFORMING CATALYST UNDER SIMULATED CONDITIONS OF TRANSPORTATION FUEL CELL SYSTEMS

A.Seya, K.Harashima, and I.Osawa
Fuji Electric Corporate Research and Development,Ltd.
7 Yawatakaigan-dori Ichihara-shi 290, Japan

Introduction

Liquid methanol is a suitable fuel for transportation fuel cell systems. In order to design a methanol steam reformer and to determine the operating conditions for transportation fuel cell systems, we must estimate the activity of methanol steam reforming catalysts, and estimate deactivation under operating conditions. Especially in transportation systems, a methanol reforming catalyst is exposed to frequent and rapid heating and cooling. Furthermore, a layer of methanol reforming catalyst has a wide temperature distribution. We obtained the reaction rate equation for a methanol steam reforming catalyst, and studied the influence of operating temperature and heat cycles on deactivation rate.

1. Methanol-steam reforming reaction rate equation

We used a screening test to chose a commercial catalyst. The methanol-steam reforming reaction is illustrated in Eq.(1)

$$CH_3OH+H_2O \rightarrow CO_2+3H_2 \quad \cdots\cdots (1)$$

We defined the reaction rate equation in the simplest form as shown in Eqs. (2) and (3).

$$r=k \times P_M \quad \cdots\cdots (2)$$

$$k=A \times \exp(-E/RT) \quad \cdots\cdots (3)$$

The k value (Reaction rate constant) shows catalytic activity, and was obtained from the conversion of methanol to hydrogen with a chemical reaction engineering method using Eqs.(2) and (3). The degree of conversion of initial conversion components was measured at various temperatures with a micro reactor. This allowed us to study the temperature dependance of k, and obtain an E value (Activation energy) of about 20 kcal/mol. The reaction rate and degree of conversion can be estimated quantitatively with Eqs.(2) and (3).

r;Reaction rate
k;Reaction rate constant
P_M ;Partial pressure of methanol
A;Frequency factor
E;Activation energy
R;Gas constant
T;Absolute temperature

2. Influence of temperature on deactivation rate

In order to study the influence of temperature on deactivation rate, we carried out a series of catalyst lifetime tests over the temperature range 220℃ to 350 ℃. Reactor operation was at a set temperature. In order to measure the degree of conversion, the reactor was frequently cooled to 220℃. The results of the measurements made at various temperatures were used to calculate k values. The k value dependance on temperature over time is shown in Fig.1. In the figure, the deactivation rate at 220℃ is almost equal to that at 260 ℃. However, at higher temperatures, the deactivation rate is larger than at either of those temperatures. The deactivation rate dependance on temperature is shown in Fig.2. Sintering of Cu particles may cause the large deactivation rate above 300 ℃. The deactivation rate at various temperatures can be estimated from Fig.2.

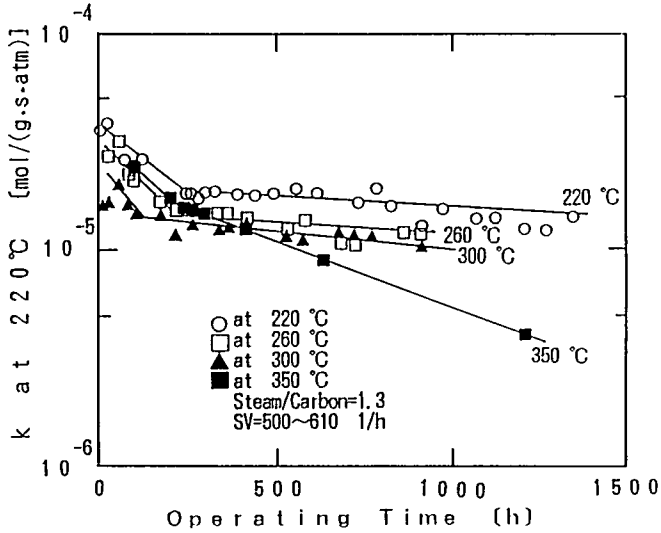

Fig.1 Deactivation of catalyst

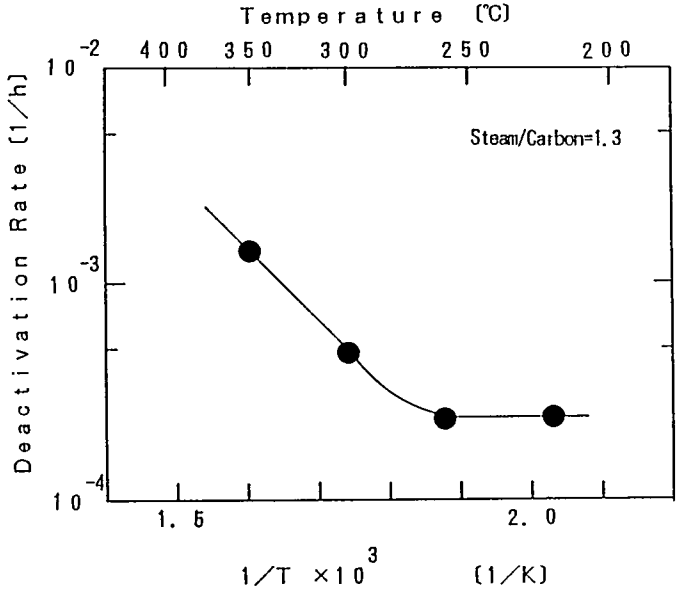

Fig.2 Influence of temperature on deactivation rate

3. Influence of heat cycles on deactivation rate

In order to study the influence of heat cycles on deactivation rate, we carried out heat cycle lifetime tests. The heat cycle patterns which simulate the heating conditions of a transportation fuel cell reformer are shown in Fig.3. Figure 4 shows changes in k values under various heat cycle conditions. At the same point on the time scale, the deactivation rate for pattern 1 is largest. That is, pattern 1 has the largest number of heat cycles. The deactivation rate is a little smaller at lower temperatures. The k value dependance on the number of heat cycles is the same whether cycles are shorter or longer after 100 heat cycles. These results led us to conclude that the number of heat cycles is another cause of deactivation. However, after 100 heat cycles, the number of heat cycles may not affect deactivation.

4. Reformer performance estimation

The results we obtained in the above temperature and heat cycle experiments allowed us to define the reaction rate constant k as shown in Eq. (4).

$$k = A_0 \exp(at + \alpha n) \times \exp(-E/RT) \quad \cdots (4)$$

A_0;Intial frequency factor
a;Rate of temperature caused deactivation
t;Operation time
α;Rate of heat cycle caused deactivation
n;Number of heat cycles

Parameters such as "a" (rate of temperature caused deactivation) are correlated with Fig.2, and "α" (rate of heat cycle caused deactivation) is correlated by comparing the deactivation rate of Fig.4 with that of Fig.1. Using this equation, we estimated the degree of conversion at various temperatures and space velocities. The results we obtained are shown in Fig.5. For example, it can be seen that at a space velocity of 260 1/h, and an operating temperature of 260 ℃, the degree of conversion will be about 90% after 8000 hours. Furthermore, when a catalyst layer is exposed to heat cycles, and has a wide temperature distribution, we can also estimate reformer performance by dividing the catalyst layer into segments, estimating the degree of conversion for each segment and then estimating the degree of conversion for the catalyst layer from the values obtained for the segments. The measured degree of conversion obtained for a 5kw class methanol steam reformer was about 89.5% after 1400hrs and 400 heat cycles. The estimated degree of conversion that we obtained under the same conditions was 93.0%. This value agreed well with the measured one. In this way, we can estimate reformer performance in a simulated transportation fuel cell system and, so, can more precisely design reformers.

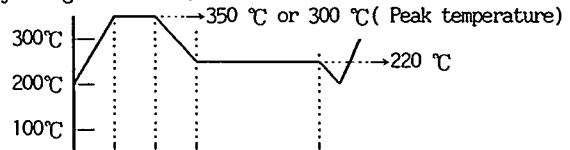

Pattern 1	15	15	15	120 (min)	Total 2.75 hours;Peak 350 ℃
Pattern 2	15	30	15	270 (min)	Total 5.50 hours;Peak 350 ℃
Pattern 3	15	15	15	120 (min)	Total 2.75 hours;Peak 300 ℃

Fig.3 Simulated heat cycle patterns

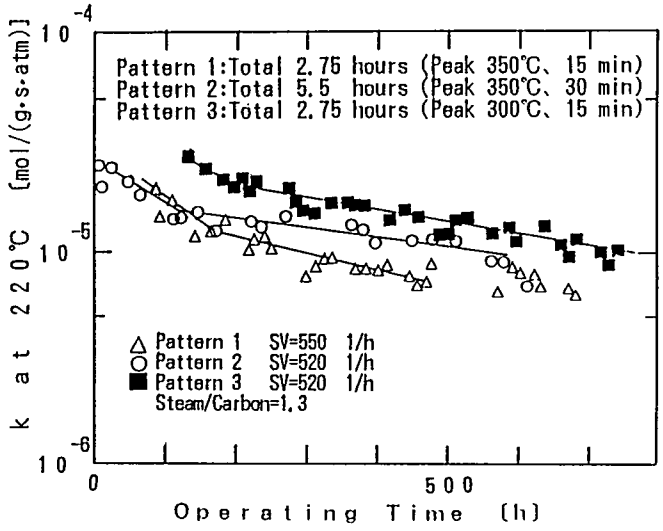

Fig.4 Influence of heat cycles on deactivation

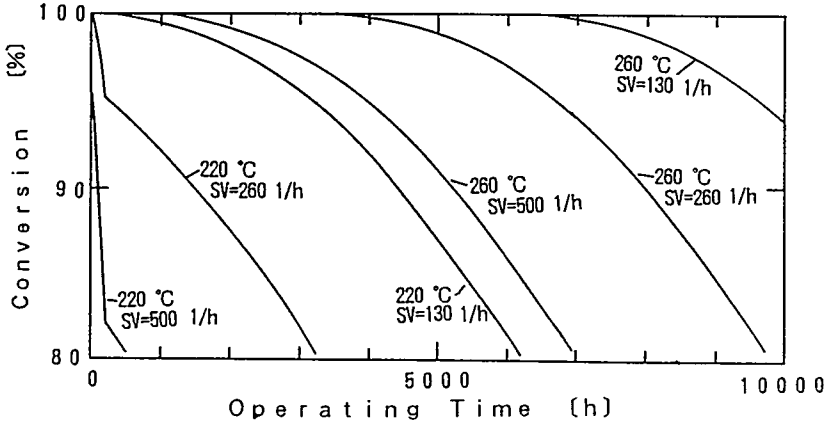

Fig.5 Estimation of reformer performance

AIR-COOLED FUEL CELL POWER SOURCE FOR BUS

S. Abens, C. Chi, D. Glenn
Energy Research Corporation
3 Great Pasture Road
Danbury, CT 06813

INTRODUCTION

In 1986, Los Alamos National Laboratory concluded a study for the Department of Transportation on the feasibility of powering buses with fuel cells operating on methanol fuel[1]. The study concluded that the phosphoric acid fuel cell is the only technology available with demonstrated performance (in full-scale stacks) on reformed methanol fuel. The study showed that a hybrid fuel cell/battery powered bus can be built with available technology to meet typical inner city service requirements.

A city bus development program was initiated in 1987 as a joint DOE/DOT initiative. As part of the first phase of this program, Energy Research Corporation (ERC) constructed and tested a half-scale brassboard hybrid bus power source and conducted design trade-off studies and economic evaluation of the power source concept. This paper presents the results of this work.

POWER SOURCE DESIGN

The hybrid power source concept is based on a phosphoric acid fuel cell in parallel connection with a storage battery. The fuel cell provides the prime source of energy, while the battery provides instant power boost for meeting heavy load requirements. Fuel cell and battery operating characteristics for the hybrid fuel cell/battery power source for a city bus are shown in Figure 1. The battery augments fuel cell current during heavy load and is recharged during light load periods. The fuel cell maximum current is limited electronically to a predetermined value. An overall system schematic for an air cooled, methanol fired, phosphoric acid fuel cell power source is shown in Figure 2. Air cooling provides lightweight, highly reliable, simple power plant design. Hydrogen for the anode is derived by steam reforming of methanol. Water required for steam reforming is obtained by condensing the product water. This concept has already been demonstrated[2]. Stack waste heat used for vaporization can be extracted from the air cooling loop[3].

For the Phase I brassboard power source built and tested by ERC, the methanol was premixed with water, and both vaporization and reforming heat load was provided solely by stack tailgas combustion. This approach allowed the use of available hardware designs while achieving the major objective of demonstrating operation of an automatic hybrid fuel cell/battery power source under the city bus cyclic load conditions.

BRASSBOARD POWER SOURCE

The 60 kW power source was designed to deliver about one-half of the power projected for the Test Bed Bus (TBB). A 240-cell, air-cooled, phosphoric acid fuel cell stack; and an annular bed, integral vaporizer methanol reformer were used. The lightweight air cooling system provides a stack startup capability of under 15 minutes[4,5,6,7]. The fuel cell operated in parallel with a 100 Ah polymer bonded electrode nickel cadmium battery. The battery utilized electrode process technology developed by ERC for electric vehicle and other battery applications which require high rate performance in combination with reduced cost. This battery is considerably lighter than the lead acid battery and was recharged at high rates from the fuel cell without the use of a step up voltage transformer.

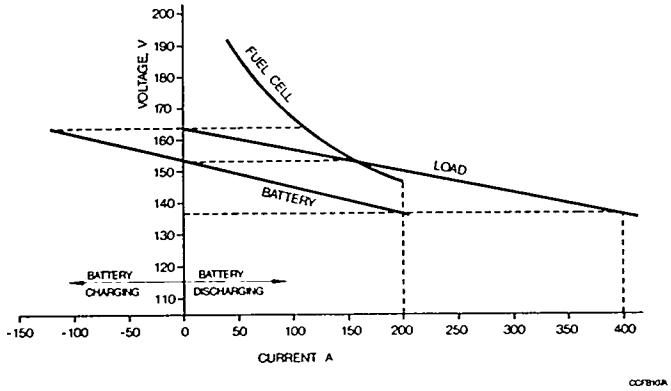

Figure 1 Hybrid Operation of Fuel Cell/Battery Power Source

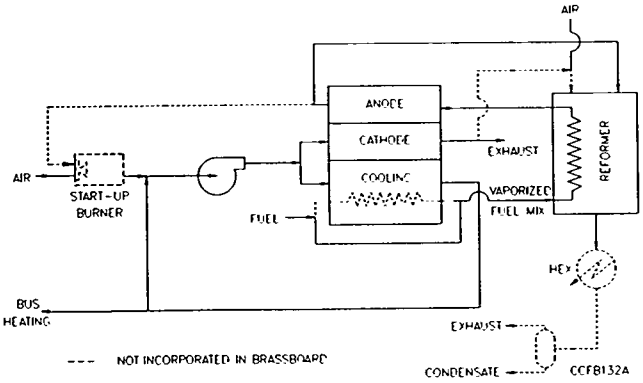

Figure 2 Schematic of Air Cooled Fuel Cell System

The brassboard power source was tested with automatic control under simulated DOT White Book Duty Cycle conditions. A computer controlled load was used to simulate the bus load cycle. Figure 3 shows battery and fuel cell current recorded during brassboard testing. The battery state of charge (SOC) reduction during the 47 minute, 14 mile White Book Cycle was from about 92% to about 85%. The original SOC can be restored after about 10 minutes of charging at the depot (a 13 minute rest is available).

Hydrocarbons and carbon monoxide in the exhaust were undetectable, with instrument sensitivity of 10 ppm, during operation of the brassboard. No nitrogen oxides were found with a test sensitivity of 0.1 ppm.

TEST BED BUS DESIGN

Performance parameters for the TBB predicted on the basis of brassboard power source design, shown in Table I, exceed the DOT "Alternative Power" requirements. The 23,000 lb., 29 seat TBB with power source and electrical drive is shown in Figure 4.

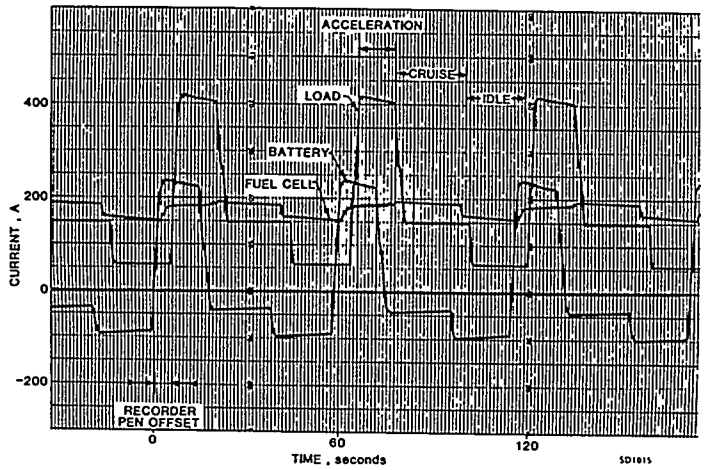

Figure 3 Phase I Brassboard Response to DOT White Book Duty Composite Cycles

Table 1 Projected Test Bed Bus Performance

	FC/B Baseline TBB	DOT Alternative Power
0-20 mph	10 sec	12 sec
0-50 mph	70 sec	90 sec
Acceleration, 0-15 mph	0.115 g	0.06 g
Top Speed, Level Ground	55 mph	50 mph
Top Speed, 2.5% Grade	38 mph	34 mph
Top Speed, 12% Grade	13 mph	7 mph

With recovery of heat from the stack, the average fuel consumption for the bus would decrease from the brassboard figure of 0.94 lb. MeOH/kWh to 0.80 lb. MeOH/kWh (40% thermal efficiency based on the HHV of methanol). Cost sensitivity studies showed that the resulting 15% decrease in fuel consumption would reduce life cycle cost for the fuel cell bus by about 3% (from $1.72/mile to $1.67/mile at $0.74/gal CH_3OH).

CONCLUSIONS

The engineering analyses and hardware verification testing demonstrated the feasibility of an air cooled PAFC/battery hybrid power source for a city bus. The power source is competitive with conventional diesel engines both on the basis of performance and life cycle cost, with real benefits arising from the reduction of noise and pollutant emission, and the use of a nonpetroleum fuel.

ACKNOWLEDGMENT

The work was performed under DOE Contract DE-AC08-87NV10714 with technical direction by Argonne National Laboratory. The authors wish to thank Messrs. Robert Davis and Ferenc Pavlics of BMI and Dr. Hugh Murray of LANL for their contributions.

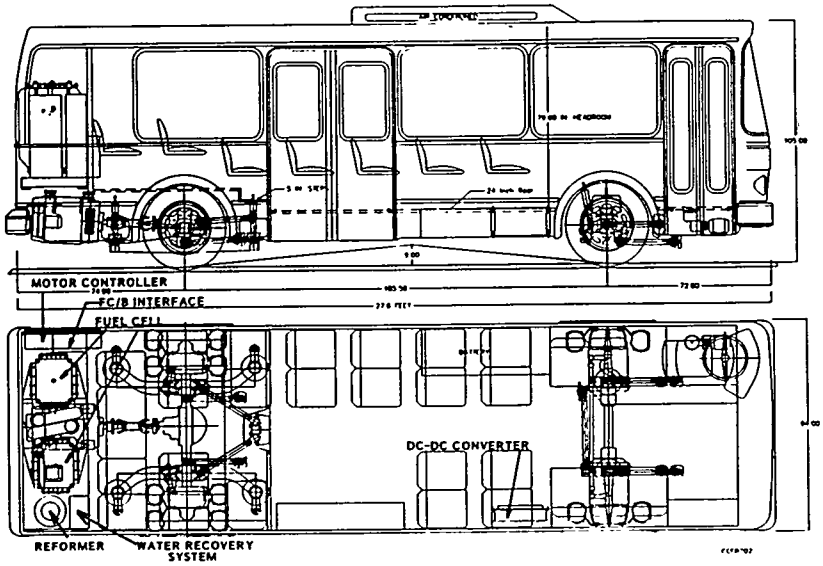

Figure 4 Test Bed Bus Layout

REFERENCES

[1] DOT Fuel Cell Powered Bus Feasibility Study, Final Report, DOE Contract W-7405-ENG-36, Los Alamos National Laboratory, Dec. 1986.

[2] S. Abens and M. Farooque, "Development of 3 and 5 kW Fuel Cell Power Plants", Final Technical Report, Contract DAAK70-79-C-0249, Dec. 1985.

[3] D.Q. Hoover and S.G. Abens, "Application of Air-Cooled Phosphoric Acid Fuel Cells to OS/IES", National Fuel Cell Seminar Proceedings, 1979, p. 95-98.

[4] S.N. Simons, R.B. King, P.R. Prokopius, "Phosphoric Acid Fuel Cell Technology Status", Institute of Gas Technology Symposium on Fuel Cells Technical Status and Application, Chicago, IL, Nov. 1981.

[5] C. Chi, J. Fan, L. Richards, S. Abens, "Low Cost Methanol-Phosphoric Acid Fuel Cell Power Plants", National Fuel Cell Seminar Proceedings, 1986, p. 186-189.

[6] S. Abens and M. Farooque, "Development of 3 and 5 kW Fuel Cell Power Plants", Final Technical Report, Contract DAAK70-79-C-0249, Dec. 1985.

[7] S. Abens, R. Hayes, W. Keil, "3 and 5 kW Methanol Power Program", National Fuel Cell Seminar Proceedings, 1982, p. 55-58.

SCALE-UP OF CARBONATE FUEL CELL STACK TECHNOLOGY

L. Paetsch, R. Bernard, M. Farooque, P. Patel
Energy Reseach Corporation
3 Great Pasture Road
Danbury, CT 06813

Introduction

Carbonate Fuel Cell Technology at Energy Research Corporation (ERC) has been scaled up from one square foot area short stacks (1kW) to large area (four square foot) 20kW stacks, built with approximately sixty cells. The stack is externally manifolded and capable of operating on either a direct methane or a coal gas fuel. Methane fuel is internally reformed within the stack either directly in the anode chamber (DIR design) or in inter-cell reforming units (IIR design). The internal reforming approach eliminates the need for external fuel processing equipment and the endothermic methane reforming reaction reduces the cooling load required to maintain the carbonate fuel cell (CFC) stack temperature.

ERC's 100kW full size stack design is based on further area scale-up to a six square foot cell size. The full size 100kW stack will be an externally manifolded assembly of approximately 200 six square foot size cells. Megawatt-size CFC power plants would be based on truck transportable pallet mounted assemblies of 100kW stacks. The 100kW full size stack design will be presented. Test results of stacks scaled up to the 20kW size will also be reviewed.

Stack Technology and Design

Technology for the carbonate fuel cell has advanced significantly at ERC over the past few years. Figure 1 illustrates that ERC's CFC stack has been scaled up from 1 kW (1 ft^2 subscale size) in 1987 to a 20kW (4 ft^2 size) within 3 years. The design of a 100kW full size stack is based on further cell area scale up. The major design features of the full size 100 kW stack are shown in Table 1. The stack will have internal methane reforming capability and therefore will be able to operate on different fuels. The external manifolds and cross-flow design are based on previous ERC stack design experience. Each 100kW stack contains around 200 cells with one reforming unit for every six cells with a nominal cell area of 6 square foot.

The full size 100kW stack has its own manifold and header systems and the assembly is contained within one external compression system. The design of megawatt size power plants is based on the concept of using the 100kW stack as the basic repeating unit.

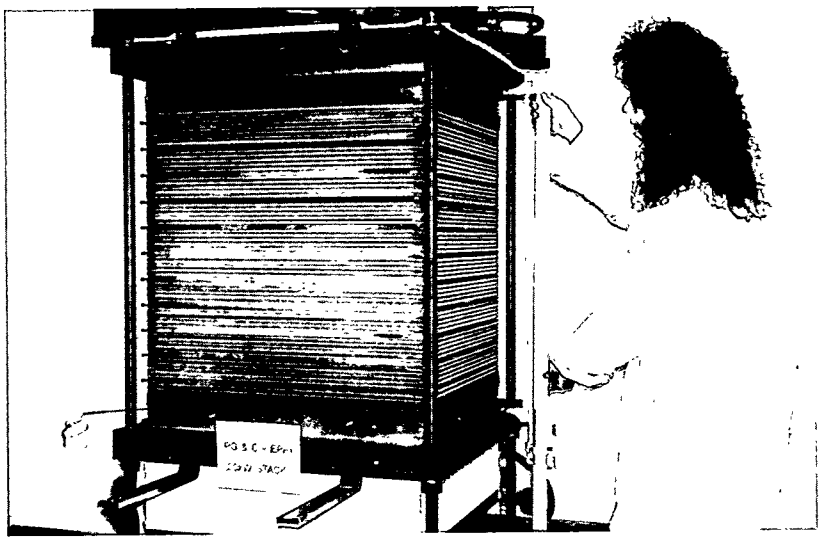

FIGURE 1

20kW, CFC STACK PREPARED FOR TEST

Stack Scale Up Results

ERC has aggressively pursued a stack technology development path leading to the 100kW full size stack. Twelve large area (4 ft^2) stacks have been constructed and tested since 1988. Eight of these were 2kW short stacks tested for design iterations of repeat and non-repeat hardware. Components under recent evaluation include improved current collector designs, compliant end-cells, manifold retention systems and electrolyte management approaches.

Scale-up to a 5-8kW size stack was done with both large area (4 ft^2) and subscale size cells. A large area 5kW stack AF-5-1 was an indirect internal reforming design (IIR) which operated on a methane fuel. This stack was successfully endurance tested for 5,000 hours including three thermal cycles. A subscale 5kW stack AS-5-1 contained 60, 1 ft^2 size cells. This is the tallest CFC stack built to date and was tested to examine height related issues.

Two 8kW stacks have recently been tested. These stacks contain 19-20 4 ft^2 cells. Stack AF-8-1 was a direct internal reforming (DIR) stack which operated on a CH_4 containing coal gas fuel (KRW/O_2). The other test combined the DIR and IIR concept and is on test in a fully integrated system. The fuel for this test is pipeline natural gas which is combusted in the anode exhaust stream, mixed with air and fed to the cathode inlet.

TABLE 1

100kW STACK MAJOR DESIGN FEATURES

- Stack Major Specifications
  - Cell Area 6 ft^2 Nominal
  - ~200 Cells
  - Reforming Unit Every 6 Cells
- External Manifolds with Cross-Flow Geometry
- Truck Transportable
- Dual Fuel (coal gas, natural gas)

A 20kW, 4 ft^2, 60 cell stack (AF-20-1) is assembled and final test preparation is underway. This stack provides the stepping stone for the full-size 100kW, whose demonstration is planned for next year. Stack performance results illustrating the effect of both area and height scale-up are shown in Figure 2.

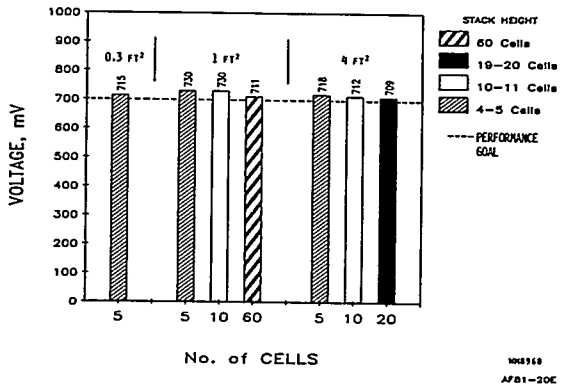

FIGURE 2

STACK PERFORMANCE COMPARISON AT 160 mA/cm^2

Scale up Issues Resolved

Technical issues were examined during both area and height scale-up. The stack area was increased from 1 to 4 ft^2 in the 1987-8 time frame. Problems encountered and resolved included manufacturing of components to close dimensional tolerance, mechanical and thermal distortion of auxiliary hardware during transients and thermal gradients. Manufacturing issues were resolved by appropriate selection of fabrication techniques such as tape casting for cell components. Thermal distortion was overcome by reducing mass and thermal conductivity in large area auxiliary components. Special attention to mechanical strength was

found to be critical in handling force concentration and providing uniformly distributed loads. Increased thermal gradients are a direct consequence of area scale up, however with a internal reforming stack design the endothermic reforming reaction can be utilized to adsorb excessive heat generation. Design of the flow configuration in inter-cell reforming units was particularly successful in uniformly distributing heat and electrical current.

Height scale-up results in accumulation of voltage, because the cells are electrically connected in series. Dielectric isolation of external manifolds and voltage-driven electrolyte migration are the recent focus of development efforts. In an externally manifolded stack the electrolyte migration problem is isolated to narrow (<1/2 in.) vertical edges of the stack where engineering solutions can be implemented. Gaskets are currently used to form the gas seal between the surface of the stack and the gas manifold. Off-the-shelf ceramic products exhibit good gas sealing properties but provide a low resistance path through which the electrolyte will migrate to the negative end of the stack. A variety of promising approaches have been identified to increase the resistance of this path and mitigate the problem. An out-of-cell rig has been utilized to screen improved gaskets.

Dielectric isolation between metallic manifold and stack face is accomplished with dense non-conductive ceramics. These ceramics are typically brittle and possess lower coefficients of thermal expansion than the surrounding metallic components. Scale up of the stack height imposes fabrication and functional requirements which include: dielectric isolation to >200 volts, flexibility to conform to the thermally distorted shape of the operating stack, and sufficient mechanical strength to avoid cracking caused by differential thermal expansion during transient operation.

Ceramic coatings applied by thermal spray process have been evaluated in out-of-cell testing. Selection of the substrate material, coating thickness and composition is in progress. Tall stack verification of selected coating is scheduled in upcoming technology stacks.

Acknowledgement

Work was performed under DOE Contract DE-AC21-87MC23274, Electric Power Research Contract RP3058-1, Pacific Gas and Electric Co., as well as in-house R&D.

100 kW CARBONATE FUEL CELL DEMO PLANT

Doug Herman and Charlie Middleton

Pacific Gas & Electric Company
San Francisco, CA 94106

Introduction

Pacific Gas and Electric Company (PG&E) is currently designing and building a complete, carbonate fuel cell power plant. The 100 kW fuel cell plant will operate off pipeline natural gas and deliver AC power to the utility grid. We plan to start operating the plant in late 1991. The projected conversion efficiency is 50 percent (LHV). We expect that the plant will not emit any NO_x, CO, particulates, or sulfur compounds.

Objectives of the project are to demonstrate the high efficiency and environmental cleanliness of carbonate fuel cell technology, serve as a prototype for development of future larger-scale commercial units, test the performance and durability of large fuel cell stacks, serve as a test vehicle for alternative system concepts, and to help focus research and development to meet the needs of the ultimate users of the technology. PG&E, U.S. Dept. of Energy, Electric Power Research Institute, California Energy Commission, and Energy Research Corporation are sponsoring the project.

Stack Description

The heart of the plant is Energy Research Corporation's indirect internal-reforming, 100 kW carbonate fuel cell stack. The stack consists of 300 cells, divided into five modules of 60 cells each. Sixty reformer units sandwiched between the cells reform the natural gas fed directly to the stack into hydrogen-rich fuel, which is internally routed to the anodes.

100 kW Stack Characteristics

Power	100 kW DC
Current Density	140 mA/cm^2
Cell Area	4 ft^2
Cell Number	300
Reforming Units	60

Process Description

Figure 1 is a block flow diagram of the PG&E 100 kW carbonate fuel cell plant. The process begins with pipeline natural gas passing through a cold gas desulfurization system to remove the mercaptan odorants and other sulfur impurities from the gas. The desulfurized natural gas is mixed with demineralized water, then heated in the fuel heater, which recuperates waste heat from the fuel cell cathode exhaust. The heated steam and natural gas mixture is fed to the reforming units in the fuel cell stack. The reforming units convert the hot fuel mixture into a hydrogen-rich fuel for the fuel cell anodes. The anode off-gas burner oxidizes the residual fuel in the anode exhaust. The burner exhaust is quenched with air and returned to the fuel cell cathode, to complete the electrochemical circuit. The cathode exhaust heats the incoming fuel mixture.

The DC power produced by the stack is converted to AC power, which is then delivered to the PG&E grid. A distributed control system supervises the entire plant.

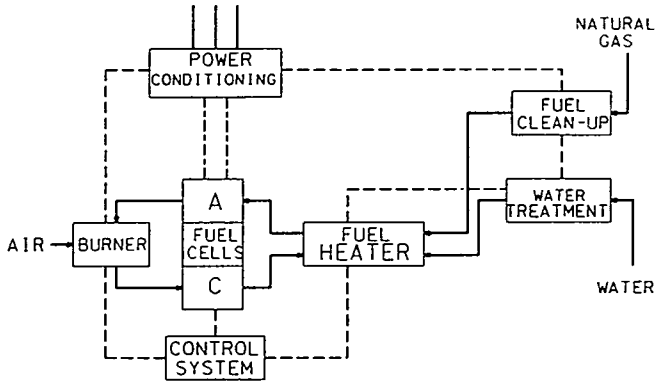

FIGURE 1: **BLOCK FLOW DIAGRAM**

Fuel Clean-Up System

The desulfurizer is a simple, passive, room temperature system consisting of four adsorbers arranged in series. The first two adsorbers contain activated aluminum with 4% potassium permanganate. The potassium permanganate removes carbonyl sulfide, hydrogen sulfide, methyl mercaptan, tertrary butyl mercaptan, and other reactive sulfur compounds. The first adsorber provides bulk separation, while the second downstream vessel provides residual separation. The third and fourth vessels contain molecular sieves. The sieves remove non-reactive sulfur compounds, such as the troublesome dimethyl sulfide.

An operator takes a chromatograph reading of the outlet gases every two weeks to determine when to replace the adsorbent. By opening and closing valves, the operator can replace adsorbent while the plant is operating, and place the freshest adsorbent downstream of the previously freshest adsorbent.

PG&E has tested over eleven different adsorbent materials. In almost all cases dimethyl sulfide was the first sulfur component to "break through" the adsorbent, although sometimes it was hydrogen sulfide. None of the adsorbents worked well enough to qualify them for usage in larger plants, but performance of the selected ones is adequate for the 100 kW plant.

Water Treatment System

Impurities in the water could foul the fuel heater, or worse, deactivate the reforming catalyst or electrodes in the fuel cell stack. Due to the very high cost of the fuel cell stack, we decided to provide a water treatment system that would make ultra-high purity water.

The system consists of filters and demineralizers, followed by a vapor compression evaporator. The water passes through a pair of feedwater filters and flow deionizers, then a pair of effluent filters. The water is continuously recirculated through this loop to prevent stagnation and channeling. The demineralizers are one cation bed, one anion bed, followed by two mixed beds. A conductivity analyzer with alarm is placed at each bed's outlet. If any impurities should happen to leak through the demineralizer system, they would soon be captured in the vapor compression evaporator downstream.

Fuel Heater

The fuel heater consists of three separate cylindrical shells, each containing 100 feet of one-inch diameter tube wrapped in a spiral coil. Water and methane flow inside the tube, and hot cathode exhaust flows across the tubes in two passes within each shell. The water and natural gas are mixed directly before entering the first heat exchanger.

We have assembled and tested the heat exchangers at PG&E's San Ramon plant site. Performance meets all the requirements for full load fuel cell operation. The methane/steam outlet temperature is above 1050° F. The shell side pressure drop is negligible. Evaporation of the water seems to be smooth and steady. Performance at part-load is somewhat unsatisfactory. The heat losses due to the high operating temperature are so great that the outlet methane temperature at part load drops below 800° F, which is too cold for inlet to the fuel cell stack and reformer. We plan to re-insulate the heat exchangers before the operating the system with the fuel cell stack.

Burner System

The burner is a straight tube with anode exhaust flowing in one end and quenched combustion products out the other end. Air flows through nozzles spaced around the perimeter of the tube. Combustion air enters through one ring of nozzles near the burner inlet, and quench air enters through a second ring of nozzles near the burner exit. We chose this tunnel-tube design for its very low pressure drop and its demonstrated high performance in combusting the dilute anode exhaust fuel.

The burner has been tested at nearly full-scale, and was able to completely combust simulated anode off gas without supplementary fuel. The vendor will perform additional computer modeling, testing, and optimization before using the burner with the fuel cell. NO_x measurements on the prototype burner are very low, near the lower detectable limit of the analyzer.

Power Conditioner

A 6-pulse, line commutated silicon controlled rectifier will convert the DC power generated by the fuel cell stack to AC power. We chose SCR technology for its proven reliability and high conversion efficiency. We expect the unit to have a DC to AC conversion efficiency of 96%, including transformer. Other more recently developed power electronic devices that offer faster switching and cleaner power are being demonstrated in many other projects. Demonstrating the fuel cell system is more important to us than demonstrating the power converter technology.

Control System

A distributed control system, similar to what is used in large power and chemical process plants, will control the plant. Plant control is fairly simple, with only five control parameters: fuel feed, water feed, burner combustion air, burner quench air, and stack power output. The operator selects the desired plant output and the fuel, steam, and combustion air feed rates are adjusted (feed forward control) to maintain a fixed fuel utilization. The control system adjusts burner quench air to maintain the desired stack temperature.

Plant start-up will be manually sequenced from the control computer terminal. Load changes will be operator initiated, but flow changes will be sequenced automatically. The burner will be fired with auxiliary fuel during rapid load changes to minimize likelihood of burner flame-out.

We have designed the plant for unattended operation. It will have automatic shut down, isolation, and safety features, and an operator will monitor the plant remotely. When a trip occurs, an operator will visit the plant to correct any problem and re-start the plant.

COMPARISON OF DIRECT AND INDIRECT INTERNAL REFORMING MCFC STACKS

K.Sato, T.Tanaka, and T.Murahashi
Mitsubishi Electric Corporation
Central Research Laboratory
1-1, Tsukaguchi-Honmachi 8-Chome
Amagasaki, Hyogo 661, Japan

INTRODUCTION

Molten carbonate fuel cell (MCFC) has conspicuous features and high potential in being used as an energy converter of various kinds of fuel to electricity and heat. MCFC yields ignorant environmental emissions, and especially it gives a good solution for the recent topical global greenhouse effect problem. The MCFC's features become particularly outstanding with Internal Reforming (IR) scheme. This concept realizes much higher plant efficiency and compact system than conventional systems. Aiming at these superior features, Mitsubishi Electric has taken up the IR concept system as the goal of the MCFC development.

At present, two types of IR-MCFC are being developed in parallel, e.g., Direct Internal Reforming (DIR) and Indirect Internal Reforming (IIR).

3 kW DIR STACK

Several DIR stacks have been built and tested since 1986. Recently, a nominal 3 kW DIR stack (code name : DIR50-1) has been tested. The main objectives of the stack are to investigate the thermal balance in the stack as well as full scale size cell technology. The key specifications are listed in Table 1 and the whole view of DIR50-1 is shown in Photo 1.

TABLE 1
KEY SPECIFICATIONS OF DIR50-1

Output Power	3 kW
Cell Number	5 cells
Effective Area	5,016 cm^2
Temperature	650 °C
Pressure	1 atm
Active Component	
Anode	Ni-Al
Cathode	NiO
Matrix	$LiAlO_2$
IR Catalyst	Ni/MgO

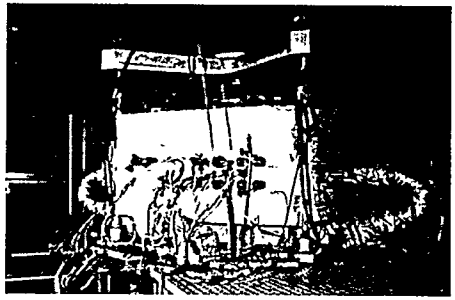

PHOTO 1
WHOLE VIEW OF DIR50-1

(1) Stack Performance

The stack performance was examined at DIR mode with methane (CH_4, S/C = 2.0) and RG mode with standard gas (H_2/CO_2 /H_2O= 72/18/10) feed, respectively. A typical flow rate of the fuel is selected at 80 % of fuel utilization (U_F) at 200 mA/cm^2 of current density, which is equivalent to U_F = 60 % at 150 mA/cm^2, while oxidant utilization is 20 % in both cases. The voltage - current density (V - i) curves at DIR mode and RG mode show almost the same characteristics. It implies that the internal reforming reaction is well taken place in the stack. The average cell voltage attains 0.8 V at 150 mA/cm^2 and it keeps more than 0.7 V even at 200 mA/cm^2.

(2) Steam-to-Carbon Ratio (S/C) Dependence

An effect of the S/C in the methane fuel on the average cell voltage was examined. The average cell voltage was improved about 7 mV as the S/C decreases from 4.0 to 2.0. This phenomena is caused by the increase of hydrogen partial pressure due to the decrease of the amount of steam in the anode gas. This improvement of the cell voltage at low S/C operation leads higher efficiency of DIR-MCFC systems. Actually, DIR50-1 can be operated with as low as 1.5 of S/C.

(3) Endurance

An operating record of DIR50-1 is shown in Figure 1. After the achievement of the initial performance test with RG mode for about 100 hours, the stack has been operated continuously with methane under the load of 150 mA/cm^2. The fuel utilization is 60 %, or 70 % while the cathode gas composition is Air/CO_2 = 88/12 which simulates for actual system operation condition. The stack is being operated as long as 4,000 hours with stable performance.

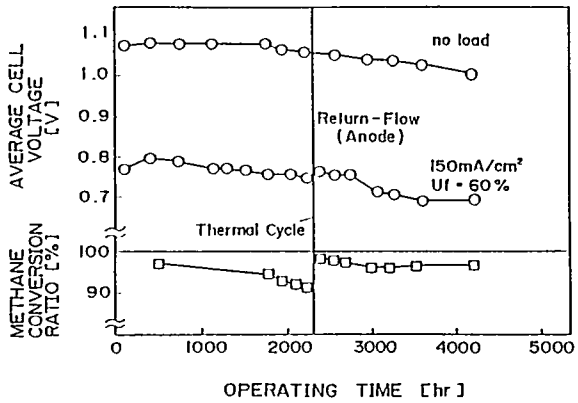

FIGURE 1 OPERATING RECORD OF DIR50-1

10 kW IIR STACK

IIR stacks are expected to attain a longer life than DIR stacks due to less electrolyte contamination of reforming catalysts. Aiming at this prominent feature, two stacks have been built and tested so far.

The first IIR stack (code name : IIR50-1) was tested to verify the IIR stack functions in 1989. The nominal output capacity is 3.6 kW and the key specifications are listed in Table 2. The stack was operated stably for 2,185 hours, while some technical issues to be overcome were cleared. For example, the temperature difference between maximum and minimum in cell plane was so high as 120 °C. In order to get a wide range operability as well as high performance of stacks, it is important to minimize the temperature distribution in cell plane and stacking direction.

After the achievement of investigation on the effect of the fuel gas flow in the reforming unit on the temperature distribution in the cell plane, the second IIR stack (code name : IIR50-2) was designed. The nominal output capacity is 10 kW and the key specifications are listed in Table 2. A whole view of IIR50-2 testing is shown in Photo 2. The test was started in March of this year and terminated after the achievement of 2,052 hour operation.

The stack performance was examined at both IIR mode and RG mode. In the case of IIR mode, S/C was selected at 4.0. At the initial stage, the average cell voltage attained 0.742 V in IIR mode at 150 mA/cm^2 and 60 % of fuel utilization. The average cell voltage in IIR mode is 27 mV lower than that in RG mode. It is because that the stack temperature at IIR mode is 20 - 30 °C lower compared with that at RG mode.

As far as the temperature distribution, the difference between maximum and minimum in the cell plane was improved from 120 °C to 90 °C.

TABLE 2 KEY SPECIFICATIONS OF IIR STACKS

	IIR50-1	IIR50-2
Output Power	3.6 kW	10 kW
Effective Area	5,016 cm^2	5,016 cm^2
Cell Number	3 cells	20 cells
Reforming Unit	1 unit	3 units
Active Components	same as DIR50-1	

As shown in Figure 2, the performance of IIR50-2 was stable. The decay rate of average cell voltage was as low as 5 mV/1000h. At about 1,200 operating hours, the stack was cooled down once and heated up again. This thermal cycle gave little effect on the stack performance.

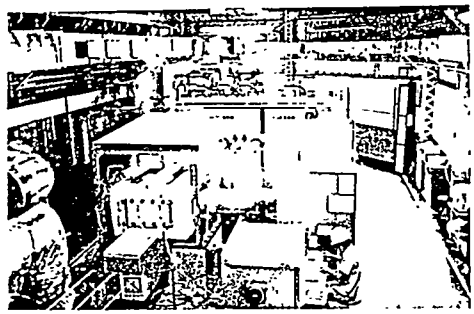

PHOTO 2 WHOLE VIEW OF IIR50-2 TESTING

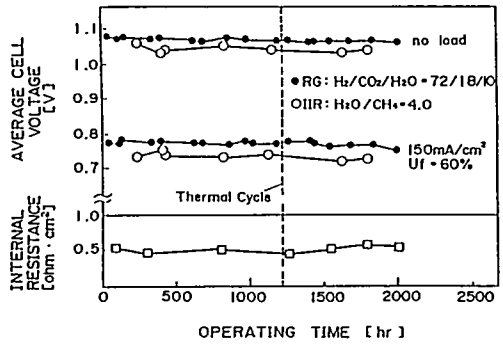

FIGURE 2 OPERATING RECORD OF IIR50-1

CONCLUDING REMARKS

The test results obtained so far with DIR and IIR stacks are all encouraging for possibility of realization of IR-MCFC systems. Therefore, further development for hundreds kW class stacks are scheduled in a few years, including the technical issues to be overcome such as thermal control in stacks, tall stack technology and so on. In order to realize IR-MCFC systems, the development of process control technology as well as of system consisting equipments are also being conducted.

ACKNOWLEDGEMENT

The development of the DIR stack has conducted under a contract from NEDO (New Energy and Industrial Technology Development Organization), and the development of the IIR stacks has conducted as a collaboration with The Kansai Electric Power Company, Inc..

ADVANCES IN REFORMING TECHNOLOGY FOR FUEL CELL APPLICATIONS

Carsten Lau Laursen and Lars J. Christiansen
Haldor Topsøe A/S
Copenhagen, Denmark

Niels R. Udengaard
Haldor Topsoe, Inc.
Houston, Texas 77058

It is well-known that next to the Fuel Cell stack, the reformer is the most critical piece of equipment in Fuel Cell plants.

Depending on the feedstock and the type of Fuel Cell stack, different requirements are imposed on the Fuel Processing System and thus on the reformer system.

The layout, performance, efficiency, and reliability of the Fuel Processing System are critical items for the overall Fuel Cell power plant.

For more than 30 years, Haldor Topsøe A/S (HTAS) has supplied fuel processing technology for the chemical industry. More than 150 reforming systems have been supplied. These systems are based on engineering design, processes, and catalysts developed by HTAS.

The R & D efforts within these fields have been intensified in relation to Fuel Cell power plants, and major advances have been achieved by strong interaction between development and pilot plant testing.

The main activities within Fuel Processing Systems for Fuel Cell power plant application are related to

PAFC
MCFC-ER
MCFC-IR.

Feedstocks have been natural gas, naphtha, and kerosene.

The first Heat Exchange Reformer (HER) designed for Fuel Cell power plant application was the 1.25 MW full-scale demonstration unit installed in Houston, Texas. This program was co-sponsored by Electric Power Research Institute and HTAS in connection with the Westinghouse 7.5 MW PAFC plant.

The unit has been operated for 4200 hours under a two-year test program which proved the correctness of the design as well as the performance.

The principle of the HER is shown on Figure 1. The reformer consists of 7 concentric tubes containing a burner in the centre and two downflow annular catalyst beds. The heat exchange takes place by means of countercurrent flow in 1st catalyst bed and co-current flow in 2nd catalyst bed.

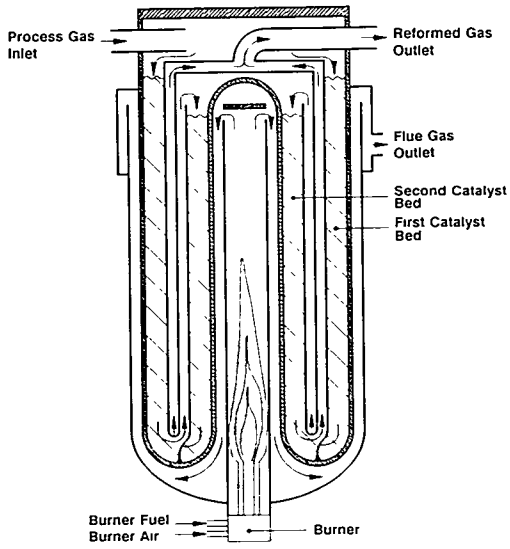

Figure 1
Heat Exchange Reformer Principle

The main advantages of the design described above are

- high thermal efficiency
- low maximum metal temperatures
- compactness
- quick response.

By means of HTAS design simulation program, the HER can be designed for a variety of process conditions, feedstocks, and capacities.

For PAFC power plants, the HER has been installed in a 200 kW kerosene-based Fuel Processing System (FPS) at Nippon Oil Company, Ltd. in 1988. This unit has operated successfully for nearly 5000 hours.

A complete FPS unit, including the HER, will be supplied this year for the Ansaldo 1 MW PAFC project for ENEA/AEM, Milan.

A single HER unit has been selected for the 5 MW PAFC project jointly planned by Japanese electric power companies and scheduled to start operation mid-1993.

As to MCFC power plants with external reformer, the HER will be supplied this year for a 100 kW unit under IHI's MCFC program.

An extensive demonstration program for MCFC technology has been initiated by the Danish electrical utility company, ELKRAFT, including tests of HTAS catalyst systems for internal reforming. The first phase of the program comprises a 7 kW MCFC plant to be put into operation in September 1990. The next step is foreseen to include a larger unit.

The operation of the 7 kW MCFC plant is fully automatic. The plant runs on pipeline gas and is installed in a separate building at the Danish power plant, Kyndbyværket, and connected to the public grid. HTAS has performed the engineering and supplied the catalysts for this unit. Energy Research Corporation has supplied the stack.

A block process diagram of this unit is shown on Figure 2.

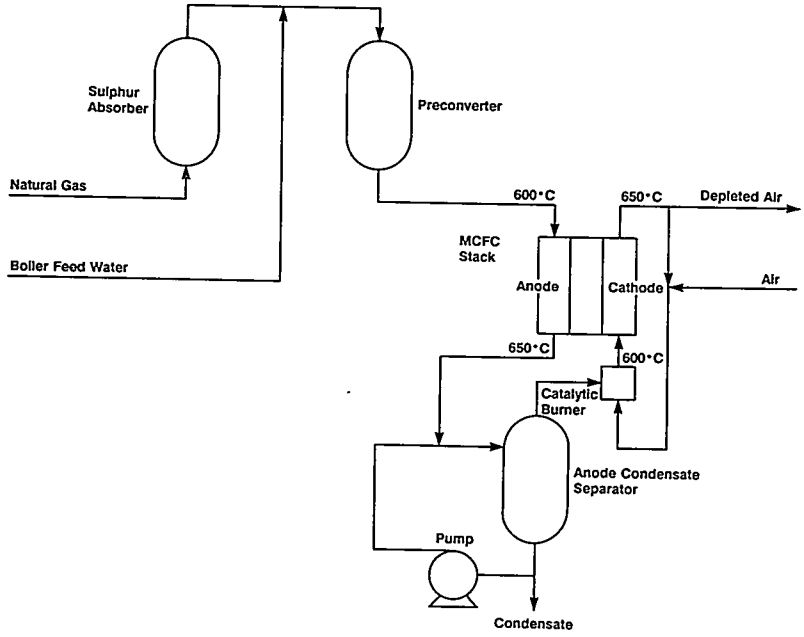

Figure 2
Lay-out of 7 kW MCFC Plant

References:

1. N.R. Udengaard, L.J. Christiansen, and D.M. Rastler: "Demonstration Results of a Heat Exchange Reformer for Fuel Cell Application". Abstracts from the 1988 Fuel Cell Seminar, Long Beach, California.

2. N.R. Udengaard, L.J. Christiansen, W.A. Summers, and D.M. Rastler: "Endurance Testing of a High-Efficiency Steam Reformer for Fuel Cell Power Plants", EPRI AP-6071, Project 2192-1, Final Report, October 1988.

SUBSCALE IMHEX™ MCFC STACK TESTING AT IGT

R. J. Petri, C. Sishtla, E. Ong,
R. Remick, R. Platon, D. Vasil, B. Evans
Institute of Gas Technology
3424 S. State Street
Chicago, IL 60616
FAX: (312) 567-5209

T.G. Benjamin, R.A. Jurish
M-C Power Corp.
8040 S. Madison Ave
Burr Ridge, IL 60521

INTRODUCTION

The objective of this project is to develop and demonstrate a novel molten carbonate fuel cell (MCFC) design concept. This concept is based on an internally manifolded heat exchanger (IMHEX™) cell/stack configuration. The program is structured into three main areas: System Design and Analysis; Stack Design and Technology Development; and Stack Testing and Scale-up. The Program Team is comprised of: The Institute of Gas Technology (IGT), M-C Power (MCP), and ABB-CE. As part of a commercialization strategy, IGT is responsible for technology research and development, MCP is responsible for the manufacture of the MCFC subsystem, and ABB-CE is responsible for the design, marketing and construction of MCFC power plants.

During the last two years, our team has: successfully fabricated, assembled, and operated five internally manifolded stacks with 1 ft^2 IMHEX, sheet metal separator plates; designed, installed and commissioned the largest and most advanced in the U.S., dedicated full-size, continuous fuel cell tape casting and sintering furnace production facilities; and designed and scaled up the IMHEX separator plate from 1-ft^2 to the 10-ft^2, full area size. This paper will focus on Technology and Stack Development.

TECHNOLOGY DEVELOPMENT ISSUES

The IMHEX stack is internally manifolded and is patterned after commercial plate and frame heat exchanger plates. No external gaskets are required, resulting in only unidirectional forces for all clamping and sealing, with no side clamping forces required. The path for electrolyte migration and segregation is therefore eliminated.

During the past two years, we have successfully designed, pressure and flow tested, *and* scaled up from 0.1 to 1-ft^2 sized, thin sheet metal, internally manifolded MCFC separator plates. Our 1-ft^2 separator plates are hydraulically capable of handling the flows for an 8-ft^2 separator plate; which at the time was the projected "full area" size.

The IMHEX plate sheet metal pressing step has undergone numerous iterations of Statistical Process Control (SPC) die-modifications; improving certain key, dimensions to within 0.002 inch of design and to tolerances of ±0.002 inch. The welding/joining step has undergone numerous modifications,

resulting in separator plates with 50% less welding and no need for flattening via heat treating prior to assembly.

The active area components have also been successfully scaled up from 0.1 to 1-ft^2 size. These parts are routinely fabricated by tape casting on an 18-inch bench-scale unit. Slurry processing scaleup, drying, and sintering studies have been completed; yielding final production components with thicknesses within 0.0025-inch of design and total anode-package tolerances of ±0.0018-inch and cathode-package tolerances of ±0.001-inch. Additionally, a new electrolyte formulation has been developed which has been verified at the bench-scale 100-cm^2 testing level to yield improved electrolyte integrity, performance, and endurance. This technology improvement is scheduled for testing at the 1-ft^2 scale at the end of 1990.

STACK DEVELOPMENT

Systems Analysis - ABB-CE has completed an initial Commercial Scale Systems Analysis of IMHEX-based, Coal-Fired MCFC Power Plants. The present results indicate an electrical efficiency of up to 50%. When heat recovery is included, the plant yields an overall thermal efficiency of 80% to 85%, depending on effluent gas temperatures. M-C Power economic analyses predict a total installed cost for a full size commerical unit of less than currently competitive technologies. The cost of electricity is projected to be less than 60 mils/kW-h.

Subscale Stack Testing - During the past two years, we have successfully completed the fabrication, assembly, and testing of five, 1 atm, 1-ft^2 MCFC IMHEX stacks. We have pursued an aggressive test matrix and each stack test was voluntarily terminated to accommodate the schedule. The number of cells per stack has varied from 3 to 24. Figure 1 is a plot of power versus current density for each stack at 75% fuel utilization, normalized to a ten-cell stack. The power output has improved 278% from Stack 1 to 5, yielding a stack power rating of 96 W/ft^2 per cell.

The latest, Stack 5, started up April, 1990. It operated for 1225 load hours. The maximum output was 2.54 kW. Two cells in this stack were mis-assembled with electrode exchanges which resulted in two anodes in the cell, and two cathodes in the other cell. Thus, the power plot of Figure 1 normalized Stack 5's average data on the basis of 22 cells rather than 24 cells, excluding these two "mis-built" cells.

Figure 2 depicts the lifeplot of Stack 5 at OCV and 160 mA/cm^2 load, as well as its IR losses, in volts. On a similar, 22-cell basis, the average performance per cell at 160 mA/cm^2 and 75% fuel utilization was 695 mV, exceeding the test goal of 650 mV per cell.

Bench-scale, 100 cm^2, tests are routinely conducted with current collectors, electrodes and electrolyte matrices from the same production batch of any given stack. These bench-scale cell

tests are used to establish benchmark stack performance characteristics and to provide trouble-shooting data. Stack 5 attained another milestone of matching the state-of-the-art (SOA), baseline performance defined by this benchmark, 100 cm^2 cell. At 75% fuel utilization and 160 mA/cm^2, both the reference cell and Stack 5 Cell No. 20 attained 740 mV.

One of the main advantages of the IMHEX stack configuration is the elimination of the primary communication paths for axial electrolyte migration and segregation. In externally manifolded stack configurations, electrolyte typically migrates from the cathode to the anode end of the stack, with a compositional skewing of Li_2CO_3 at the cathode and K_2CO_3 at the anode (1).

This characteristic has been evaluated through post-test analyses of IGT Stacks 1, 2, 3, and 5. (Stack 4 is in dry storage, awaiting possible re-start.) Figure 3 provides a plot of carbonate content as a percent of original, versus cell number. This data confirms that up to 1200 hours of operation at 650°C and for 24 1-ft^2 cells, zero carbonate pumping has been observed. Figure 4 is a graph of mole percent Li_2CO_3 in the electrolyte versus cell number. This data also indicates that the Li_2CO_3 distribution is uniform and not preferentially skewed to the cathode end.

An additional advantage of internally manifolded designs is the higher pressure differences which can be maintained between the cell interior compartment and the exterior furnace environment. In "manifold pressure" runs made on Stack 3, constant, greater than 85% anode and 98% cathode wet sealing efficiencies were demonstrated at internal stack pressures of up to about 2 psig.

Modeling - To date, all modeling efforts at IGT have been based upon the modification and expansion of the Physical Sciences Incorporated (PSI) MCFC Performance Model. One modification involves the estimation of the temperature profile of a single cell in the center of an IMHEX stack. Figure 5 portrays the temperature profile calculated by a modified version of the PSI model using as input parameters the actual specifications and operating conditions of IGT Stack 5. The solid circles represent the relatively closely matching actual temperature measurements made in Cell No. 12 of the 24-cell stack under steady-state conditions. Additional work is necessary, however, to be able to model the end cells of a multi-cell stack.

Scale up - During this program, IMHEX and MCFC technology was scaled up from 3 to 1028 cm^2 ($\approx$1 ft^2) and subscale stack concept verification testing was accomplished at the same time. The IGT/MCP/ABB-CE Program Team has completed a first generation IMHEX design scale-up to about 10,000 cm^2, or 10 ft^2, "full area", sheet metal separator plates. The full area plate pressing die has been fabricated and preliminary full area protoypes are being pressed at the time of this writing. The full area plates will be cell-tested in 1991.

Another milestone has been the design, procurement, installation and commissioning of continuous tape casting and sintering

equipment for the fabrication of full-size active area cell components. Both of these facilities are the largest in the U.S.A. - specifically designed and operated exclusively for production of fuel cell components.

MCP has recently installed the sintering furnace and preliminary sintering runs are underway. Through close collaboration, MCP and IGT have also begun operation of the full area tape caster to scale up IGT's 1-ft^2 component technology to the full area production facility (Figure 6). Anode, bubble barrier, cathode and matrix taping runs have been completed. A full-width, 50-ft anode tape has been made and this run was used to evaluate and improve the slip delivery section. The program plan includes the use of these two production units for upcoming stack tests at the end of 1990 and 1991.

CONCLUSIONS

- The viability of the IMHEX MCFC stack design concept has been verified.
- SOA bench-scale performance has been demonstrated in IMHEX subscale stack tests.
- The IMHEX internally manifolded MCFC stack concept eliminates the problems of carbonate pumping in external manifolds.
- Cell sealing has been demonstrated at internal stack pressures up to about 2 psi.
- The 1-ft^2 IMHEX stack design has been scaled up to the 10-ft^2, full area size with prototype, sheet metal pressings underway.
- The IGT 1-ft^2 component production technology base has been scaled up in the design, installation, and commissioning of tape casting and sintering furnace facilities capable of manufacturing full area, 10-ft^2 parts.

REFERENCES

1. H. R. Kunz, I.F.C., "Transport of Electrolyte in Molten Carbonate Fuel Cells," Journal of the Electrochemical Society, Vol. 134, No. 1, pp. 105-113, January. 1987.

ACKNOWLEDGMENTS

The work reported in this paper was funded by the U.S. Department of Energy, Morgantown Energy Technology Center; Electric Power Research Institute; M-C Power Corporation; and IGT.

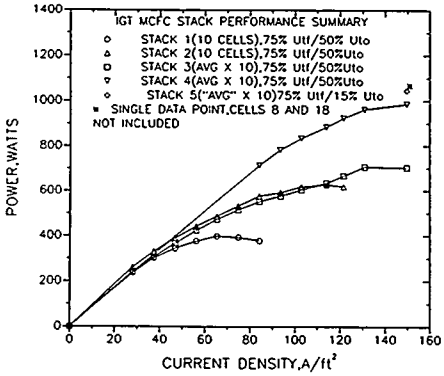

Figure 1. IGT MCFC Stack Performance Summary

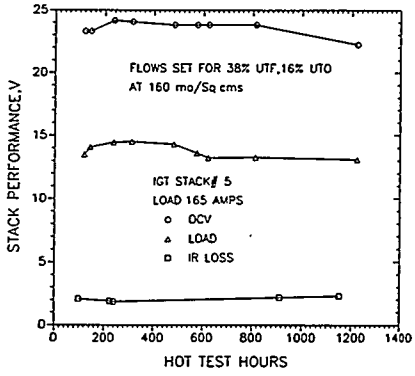

Figure 2. IGT Stack No. 5 Lifeplot

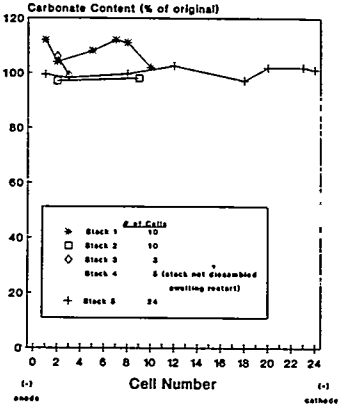

Figure 3. Carbonate Inventory of Stacks

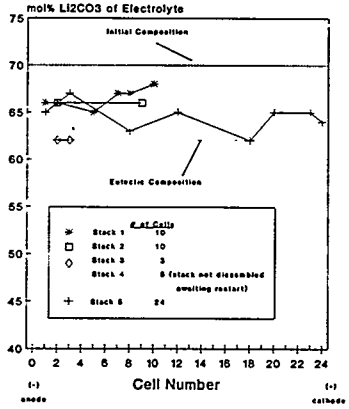

Figure 4. Li_2CO_3 mole percent in Electrolyte Versus Cell Number

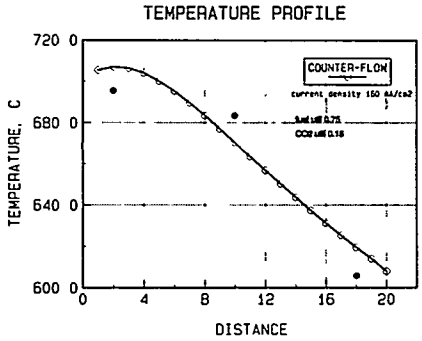

Figure 5. Model Predicted and Actual Temperature Cell Profile for Stack No. 5, Cell 12 of 24

Figure 6. Full Area Tape Caster Installed at M-C Power

MCFC DEVELOPMENTAL ISSUES

Tom J. George and Mark C. Williams
Department of Energy
Morgantown Energy Technology Center
P.O. Box 880
Morgantown, WV 26505

INTRODUCTION

This paper deals with the efforts of the U.S. Department of Energy/Morgantown Energy Technology Center to assist the private sector in the commercialization of the molten carbonate fuel cell technology. A description of the current state of developmental readiness of the technology is presented. The development issues which must be overcome to commercialize the technology are discussed.

READINESS OF THE MCFC TECHNOLOGY

Stack Designs -- Two DOE-funded stack designs are sufficiently advanced to allow commitment to commercial production of full-area components. Cost reduction studies are under way for all three stack designs funded by DOE. One design has resolved carbonate migration issues; however, confirmation by endurance testing is needed. No design has been operated sufficiently long (i.e., 5,000+ hours) to resolve all life issues.

Power Plant Systems Designs -- Power plant systems designs indicate technical feasibility of standard engineering subsystems and economic competitiveness with alternative technologies. Coal gas systems indicate 45% to 49% systems efficiencies and capital costs at 45 to 60 mils per kilowatt-hour. Coal gas systems employing advanced gasification processes indicate the potential of 55% to 60% efficiencies. The Gas Research Institute has sponsored systems studies of small, on-site natural gas fired systems. On a higher heating value basis, the on-site efficiencies have reached 48% with an indication that overall systems efficiencies could exceed 80% in a cogeneration mode.

Performance and Utilization -- State-of-the-art stack performance is 0.60 to 0.75 volts at 180 to 250 amperes/ft2. Eighty five percent fuel utilization continues to be a realistic design target. Oxidant utilization ranges from 10% to 50% dependent on current density, temperature difference across the plate (inlet to outlet), gas flow configuration (counterflow, co-flow, cross-flow, or combination), desired fuel utilization, and system costs.

Designs and Operating Pressure -- Dual-fuel (natural gas and coal gas) fired designs have emerged. Natural gas on-site market entry units are expected to operate at atmospheric pressure. In the longer term, coal gas units are expected to operate at elevated pressure (4 to 6 atmospheres). Improved stack

electrical efficiency is an incentive for high pressure operation. Higher pressure operation could also result in reduced costs or improved gas distribution.

Stack Height and Area -- Larger area and taller stacks imply reduced site construction costs (i.e., piping and electrical interconnects), and to a lesser degree, reduced stack manufacturing costs. Stacks with active areas of 10 ft2 containing 250 cells per building block and two building blocks per stack, have been proposed. Building block height in external manifolded stacks may be limited by changes in vertical height during stack life; whereas, the height might be limited in internal manifolded stacks by gas distribution problems. Since the highest carbonate stack, to date, has only been 60 cells, the issue on stack height is still speculative. The limitation on stack area is availability of manufacturing equipment to cast active area components and to form separator plates and current collectors.

Scale Up and Manufacturing -- Development has progressed to the point where 10- to 30-cells have operated for several thousand hours. The goal now is to integrate several hundred cells into a module capable of generating 100- to 300-kilowatt modules. The first commercial power plants are expected to link 10 to 20 stacks to create power plants of 2-megawatt size. Scale up and manufacturing of full-area components is now under way.

MCFC DEVELOPMENTAL ISSUES

Cathode Dissolution -- Due to cathode dissolution, at 10 atmosphere pressure, cell life is projected to be 4,000 hours as compared with the 25,000- to 40,000-hour target. System designs that require stacks to operate at pressure will require development of cathodes less susceptible to nickel oxide dissolution. Some bench scale work indicates solutions, but no sub-scale stack testing has been conducted.

Electrolyte Management -- Several engineering approaches to minimize electrolyte migration are being developed, but none have been demonstrated in sub-scale endurance stack tests (10,000 plus hours). Initial indications in tests up to 3,000 hours indicate that the internally manifolded stacks may experience no electrolyte migration.

Gas Crossover Management and Seal Efficiency -- Crossover can occur through seals, corroded separator sheets, or an imperfect electrolyte structure. However, the term "gas crossover" is commonly restricted to crossover through the electrolyte structure. Recently, there has been movement away from the use of separate bubble barriers to building fine pore structures into the electrodes. Matrices fabricated with more uniform porosity and slightly lower porosity provide good resistance to gas

crossover. As a result of improvements in matrix fabrication, gas crossover is not as serious a problem as it once was, but endurance testing is necessary to measure the effect of thermal cycling, corrosion, carbonate migration, etc. on gas crossover.

Internally manifolded stack seals have maintained a pressure differential of 55 inches of water. Externally manifolded stack seals have been demonstrated at least to 15 inches of water. Gas crossover from cell to cell in the interior area of the cells has been reported to be as low as 0.3% in internal stacks.

Thermal Management -- Optimization, considering cooling oxidant flow, oxidant utilization, stack temperature, MCFC stack design, and pressure drop restrictions remains an important consideration in all MCFC designs.

Corrosion of Materials -- In MCFC's, the reducing and oxidizing environments to which various components are exposed are highly corrosive. In some cases, a particular material is exposed to a range of conditions. For example, in the fuel chamber during operation, the inlet gas is considerably more reducing than the spent gas at the outlet. Another problem is the separator plate in that one side is exposed to a reducing environment while the other is exposed to an oxidizing environment. These environmental variations impose a number of constraints in selecting construction materials. Contractors are considering plated metals and alternative approaches that allow the use of different material in the two fundamentally different environments because no single material has yet been identified as satisfactory.

Stack Mechanical Design -- Mechanical design problems include the maintenance of electrical contact between adjacent cell components, the accommodation of dimensional changes that occurs during thermal cycling, the establishment and maintenance of tight seals to prevent gas leaks, the selection of materials that will have the required high-temperature properties, the accommodation of changes in overall stack height that occurs during cell operation, and the simplification of design in order to reduce cost and assembly time. The lack of resiliency of the individual cell components leads to many of these problems which are exacerbated by dimensional changes occurring during thermal cycles.

Improper design can lead to gap formation, leaks, and crushed components. Some of these design problems can be addressed during the design and operation of single cells, but many are apparent only at a larger scale when stacks of cells are in operation.

Contaminants -- The amount of raw coal gas cleanup needed is system and process specific. Today's major concerns are hydrogen sulfide and hydrogen chloride. Experimental results indicate that a sulfur level below 1 part per million (ppm) in the fuel is satisfactory. Also, performance recovery is likely if short-term upsets do not result in more than 5 ppm sulfur in the fuel gas. If sulfur dioxide is present in the cathode gas stream, it will tend to sulfate the carbonate electrolyte. Recent experiments indicate that corrosion of cell metal hardware in the cathode gas stream is accelerated in the presence of sulfur. Hydrogen chloride will also react to increase the electrolyte evaporation rate. Recommended tolerances for hydrogen chloride are 1 ppm or less.

Stack Cost and Endurance -- Costs to manufacture and assemble stack components into full-area, full-height stacks must be determined in order to direct cost reduction, design, and research efforts such that maximum cost benefit is achieved. The material in a cell package may be as much as 50 to 70% sheet metal by weight with the electrochemical components (electrodes and electrolyte matrix) weighing less but representing the components with greatest cost reduction potential. Cost reduction of electrodes might be accomplished by the use of alternative materials. Cell designs that minimize sheet metal requirements have the potential to contribute to substantial cost reductions. Endurance testing in the MCFC program has been insufficient.

SEE REVISED PAPER

RESEARCH AND DEVELOPMENT OF A PROTON EXCHANGE-MEMBRANE (PEM) FUEL CELL SYSTEM FOR TRANSPORTATION APPLICATIONS

H. F. Creveling and R. D. Sutton
Allison Gas Turbine Division, General Motors Corp.
Indianapolis, Indiana

Increasing environmental and strategic fuel concerns, and a potentially changing fuel base continue to dictate the need for advanced vehicular power plants that exhibit improved fuel efficiency, reduced emissions, and alternate fuel capability. The electric vehicle has been suggested as one means of decoupling petroleum from the transportation sector and dramatically reducing vehicular environmental emissions. [redacted] Among the candidate power plants for the engine/charging component within the hybrid system, the indirect methanol proton-exchange-membrane (PEM) fuel cell is potentially the most efficient, as the device is unrestricted by heat engine (Carnot cycle) limitations. Further, the fuel cell system directly produces electric power that drives propulsion motors mounted on the vehicle wheels, thus eliminating the need for a generating system.

The PEM fuel cell electrochemical engine converts processed fuel (hydrogen and carbon dioxide extracted from methanol using an on-board fuel processor) and air directly into DC electricity and may be thought of as a battery to which the reactants are being continuously supplied. This type of fuel cell power plant appears to be an excellent candidate for vehicular application; power densities are similar to spark-ignition engines. Further, since the part-load efficiency of the PEM fuel cell power plant is relatively high, substantial fuel economy improvement and total emission reduction over a typical driving cycle could occur through replacement of a conventional engine with a fuel cell power plant. Preliminary simulations of a methanol fuel cell/battery hybrid vehicle indicate installed fuel economy improvements exceeding 60% (accompanied by a ~ 40% reduction in CO_2) with a concurrent 90% reduction in regulated emissions.

While there has been considerable interest within General Motors (GM) during the past thirty years regarding various fuel cell technologies, most prior programs were terminated. Recent developments, however, gave rise to the potential of achieving break-throughs in PEM technology. Consequently, GM's Delco Remy Division, with GM Research Laboratories support, conducted a limited PEM fuel cell power plant research and development effort. The general conclusion of this effort indicated that, although system technology was immature and material/component costs (in the absence of sustained and intensive effort) were high, the technology to build and successfully operate a fuel cell system on the component level could be demonstrated. Continuing work

at Los Alamos National Laboratories, the Dow Chemical Co., Ballard Power Systems, and within General Motors now indicates that material and component costs have the potential to become competitive with those of future internal combustion engines that may well be required to meet extremely stringent emission and fuel economy standards.

The potential advantages of a fuel cell/battery hybrid vehicle and the demonstrated interest of the Department of Energy (DOE) [redacted] led to GM's designation of Allison Gas Turbine as the lead GM division to coordinate a joint government/cost-shared funded effort between DOE, the South Coast Air Quality Management District, Allison, the General Motors Technical Staffs, Los Alamos National Laboratory, Dow Chemical Co., and the Ballard Power Systems Co. to develop an advanced PEM fuel cell propulsion system for vehicular applications. The first two-year phase of this program was initiated September 1, 1990. General Motors views this initial two-year effort as the first phase of a six and one-half year program that develops an advanced reformate/air PEM fuel cell power plant, and culminates in an actual fuel cell/hybrid vehicle demonstration. The preliminary milestone schedule for the multiyear program is presented in Figure 1.

General Motors envisions a four phase program leading to the final test and evaluation of a fuel cell/hybrid vehicle demonstrator. The first phase was initiated with the award of the present contract and extends over a 24-month (two year) period. The objectives of this first phase, as presented in the milestone schedule, are the development of a 10-kW power source system evaluator and delivery of a Conceptual Design Study for automotive application (denoted RPD on Figure 1).

The second phase of the program initiates in the third year following program go-ahead and also extends over a two year period. The objectives of this phase are the development of a 40-kW brassboard power plant, its integration with vehicle drivetrain components, and the initiation of brassboard power plant dynamometer testing. Other activities occurring during this second phase include system optimization of the 10-kW unit and continuing design/fab/procurement of the components/drive train of the vehicle propulsion system. The 10-kW system optimization will produce the control capability required for a 40-kW power source system. As this second phase concludes, effort will also focus on preparing a "mule", or laboratory vehicle, ready to accept the components/drive train and 40-kW fuel cell power source.

The third phase, initiating in the fifth year of the program, extends for 18 months, and emphasizes development of an 80-kW fuel cell power source prototype, its dynamometer testing, and initial installation in the mule vehicle. As presently envisioned, the 80-kW fuel cell stack is [redacted] composed of two 40-kW stacks. Optimization of the test program will be achieved by evaluating a 40-kW power source thoroughly, first on a dynamometer and then in the mule vehicle.

Following development of an 80-kW reformer, the 80-kW power source can be integrated, dynamometer tested, and then installed in the same mule vehicle.

The final phase of the program extends from the middle of the sixth year to the middle of the seventh year. This final one year phase involves further prototype mule testing, installation in the actual demonstration vehicle, and proof-of-concept evaluation of the fuel cell/hybrid vehicle.

The twenty-four month initial phase currently under contract emphasizes the development of technologies that GM believes are critical to the success of this propulsion system concept. The initial program is designed to produce a methanol fueled 10-kW power source that demonstrates system feasibility and can also be used to develop an initial evaluation of fuel cell use in transportation applications. Key elements of this effort, as presented in the first phase preliminary milestone schedule depicted in Figure 2, are tasks addressing the fuel cell, a fuel processor, electronic controls, a gas pressurizing system, versatile water and heat management systems, low thermal inertia, a proper battery (to help with transients and start up), and other ancillaries. Technology feasibility is demonstrated at the end of this initial phase by delivery [redacted] of a complete 10-kW PEM reformate/air fuel cell power plant ready for further laboratory evaluation, Figure 3. In addition to significant R&D efforts on critical components, a propulsion system conceptual design study will be conducted during the first year of the program to define the actual reference power train design (RPD) specifications for a full-scale fuel cell/hybrid vehicle. The study will include appropriate tradeoff determinations and a prioritization of future research and development requirements. Finally, a detailed multiyear program plan for the effort summarized above will be developed during this initial 24-month period.

The current program to develop the 10-kW power source system and demonstrate the initial feasibility of the system for use in transportation applications, combined with the fuel cell/hybrid vehicle system conceptual design study, is a major step in evolving new families of alternative transportation applied power sources.

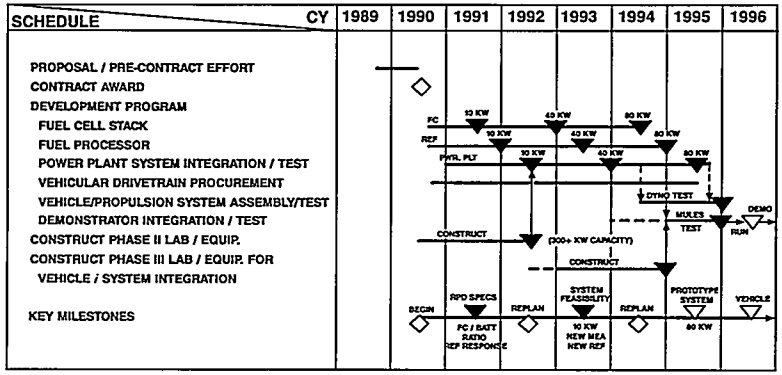

FIGURE 1. MULTIYEAR PROGRAM PRELIMINARY MILESTONE SCHEDULE.

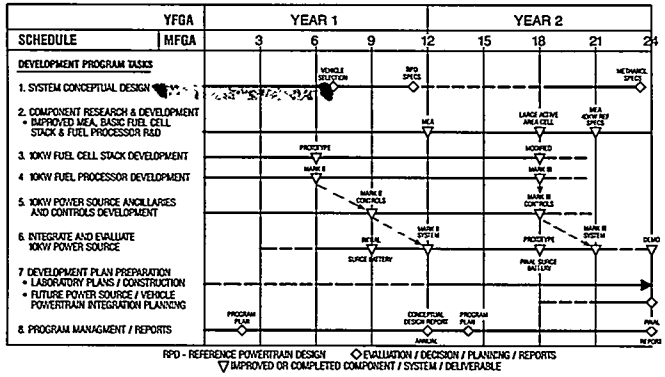

FIGURE 2. FIRST PHASE PRELIMINARY MILESTONE SCHEDULE.

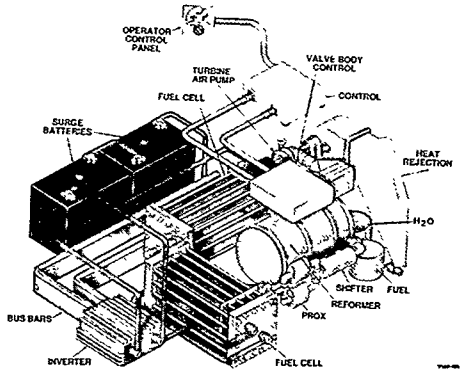

FIGURE 3. 10KW CONCEPTUAL POWER SOURCE.

ADVANCED SYSTEM ANALYSIS FOR INDIRECT METHANOL FUEL CELL POWER PLANTS FOR TRANSPORTATION APPLICATIONS

N. E. Vanderborgh, R. D. McFarland and J.R. Huff
Advanced Engineering Technology
Los Alamos National Laboratory
Los Alamos NM 87545

The indirect methanol cell fuel concept being actively pursued by the United States Department of Energy and General Motors Corporation is based on an "electrochemical engine" (e.c.e.), an electrical generator capable for usually efficient and clean power production from methanol fuel for the transportation sector. This on-board generator works in consort with batteries to provide electric power to drive propulsion motors for a range of electric vehicles. Success in this technology could do much to improve impacted environmental areas and to convert part of the transportation fleet to natural gas- and coal-derived methanol as the fuel source. These developments parallel work in Europe and Japan where various fuel cell powered vehicles, often fueled with tanked or hydride hydrogen, are under active development.

Transportation applications present design challenges that are distinctly different from utility requirements, the thrust of most previous fuel cell programs. In both cases, high conversion efficiency (fuel to electricity) is essential. However, transportation requirements dictate as well designs for high power density, rapid transients including short times for system start up, and consumer safety. Moreover most studies conclude that cost targets are more stringent for transportation applications.

The e.c.e. *system* is shown in Figure 1. This hardware is formed from four interacting components: 1.) the *fuel processor* that includes vaporization sections to form gaseous water and methanol and post processing devices to clean the output stream, 2.) the *fuel cell stack* that reacts the product hydrogen with air to generate electrical power, 3.) the *air compression and decompression device* that supplies the cathode air supply at appropriate flow rates and pressures and then recovers some fraction of the pressure-volume work, and 4.) the *condensing cross flow heat exchange device* that results in significant water recovery so that the water product can be recycled to meet essentially all of the water input requirements to component 1. (In this way, no water is required as a separate input stream.) This paper will describe status of each of these components, and describe a model that predicts the steady state performance of the e.c.e.

1. FUEL PROCESSING COMPONENTS

The fuel processing components generate hydrogen from liquid methanol. This process involves reaction of gaseous methanol and steam on surfaces of heterogeneous catalysts. The energetics for input energy to drive this reaction are demanding. The total fuel energy is based on heat of oxidation of methanol ($\Delta H = -715.4$ kJ/mol). On a mole basis, about 25% of the total energy is required for hydrogen production following the steam reforming route:

$$CH_3OH + H_2O = CO_2 + 3\,H_2$$

The reaction is usually done with excess steam, using a steam to methanol ratio between 1.1 and 1.3. Although earlier studies suggest that steam generation is the primary heat input for this process, analyses show that each of the three required processes, 1.) heating methanol to reaction temperatures, 2.) heating steam to reaction temperatures, and 3.) providing the heat of reaction, require significant and approximately equal inputs of thermal energy.

The sum for heat of combustion of the three moles of hydrogen produced by this process is slightly higher than the heat of combustion of the one mole of methanol required as the fuel input— steam reforming increases the fuel enthalpy. This means on a joule basis that the methanol to hydrogen conversion is approximately 75% efficient, assuming a processing

step with a steam to methanol ratio of 1.3/1.0. (Lowering the steam to methanol ratio improves this situation.) The required thermal input, equal to 25% of the total fuel energy content, can come largely from heat generated in other parts of the e.c.e system. In fact, most of the design challenges in the e.c.e.engineering development involve thermal management to increase system efficiency by moving "waste heat" generated in other parts of the system into the fuel processing components.

In general, the overall e.c.e. system efficiency is the product of the fuel cell stack efficiency and the net reformer efficiency, modified by various thermal inputs from nominal values. A stack operating at 0.800 volt/cell has a maximum efficiency of 65%, assuming complete hydrogen utilization in the anode compartment. If this stack is coupled with a fuel processing section that operates with a maximum efficiency of 75%, the overall maximum system efficiency falls just below 50%. The e.c.e. system efficiency can be improved by transferring heat from the fuel cell stack and other ancillary system components in the fuel processing section, thereby decreasing the thermal inputs that come from direct fuel oxidation. The most efficient e.c.e.system is the one that uses the smallest fraction of fuel for direct heat production to drive the fuel processing reactions.

Figure 2 shows a schematic diagram of current fuel processing concepts. The fuel processing is accomplished in three stages, 1.) *steam reforming convertor* using forced convection to provide thermal input, 2.) *shift convertor* with the introduction of additional water to cool and lower the CO content, and 3.) *preferential oxidation convertor* to lower the carbon monoxide content to acceptable levels. The first two steps produce reactants in thermodynamic equilibrium, while the third depends upon kinetics for a sharp decrease in carbon monoxide concentration, a severe poison in PEM fuel cell stacks.

2. FUEL CELL STACK COMPONENTS

Thermal management and water management are two key system aspects of fuel cell stack engineering. Because PEM fuel cells operate below the boiling point of water, two phase water management is essential. These heat and water management issues are strongly influenced by the temperature, pressure and the flow stoichiometry of the anode and cathode compartments, in addition to the current density, the fuel cell voltage, and the internal stack resistance. To date, most PEM fuel cell stacks rely on internal water flow for thermal management. Heat, removed at the stack temperature is produced as sensible heat in a water flow system. Although it is not required, most contemporary stack designs integrate this water flow with internal humidification systems, especially for anode feed humidification. Because of the required high humidification levels in the anode feed (R.H. > 80%), stack cooling occurs during this humidification step.

Water management is complicated by the electroosmotic processes that couple water transport with the anode-to-cathode flow of the proton flux in PEM fuel cells. Although this flow is less than that found during electrolysis processing (the H_2O/H^+ ratio is between 1 and 2), at higher current densities this water transport process can cause anode dehydration. Anode moisture levels are replenished in part by a water transport process within the membrane, flowing from cathode to anode. This process is driven by the water gradient between the cathode and anode. Water removal from the cathode is simplified in air breathing systems by the high nitrogen flow rate. Even with relatively low flow stoichiometries (< 2.0), the mass transport rates through the cathode compartment are necessarily high. For instance, an oxygen-based flow stoichiometry of 1.5 results in a flow rate of approximately seven and one half times that necessary for pure oxygen. This extra flow operates to accelerate water removal from the cathode compartment.

Waste heat from the stack or cathode exhaust is sufficient to vaporize most of the methanol flow. The anode vent stream, assuming a hydrogen utilization rate of 85%, is then available for contributing to the thermal input for water vaporization. Unused waste heat is discharged, probably through a water-air heat exchanger (not shown).

3. AIR MANAGEMENT COMPONENTS

Pressurized air most likely is required in the cathode so that stack operating temperatures can be increased. At higher stack temperatures, the membrane conductivity increases, a condition required for high power density At higher total pressure the steam pressure can also be increased to sufficient levels. Most likely, a pressure near 2 bar will be the required operating condition. This permits high stack performance, but does not dictate complex pressure-volume machinery. A simple turbine component, similar to an automotive turbocharger, can generate the required gas flows and pressures.

The pressure-volume work in the cathode gas exhaust provides in part the required input energy for pressured operation. In the schematic shown in Figure 1, the enthalpy of the air exhaust is increased by introducing the hot gas from the fuel processing burner vent. This "pressurized burner" scheme boosts the enthalpic flow through the expander, and, in some simulation examples, provides full work for the air compression step. If that is not the case then a motor must be used to supplement the power for moving the air compressor.

4. WATER RECOVERY COMPONENTS

Water recovery is required for an efficient system. The alternative is to fuel the system with a "premix" fuel, or to add water during the fueling process along with methanol. The system described here combines the fuel cell cathode exhaust with the combustor exhaust. This concept merges the product water coming from both the electrochemical oxidation processes (fuel cell stack) and the chemical oxidation processes (heat inputs for fuel processing) into one stream. This stream is cooled by cross-flow using incoming air, or through incorporation of the methanol vaporization processing in that section (not shown). The overall input water requirements are one third of the total product water volume. Water recovered in excess of the input requirements will be discharged once the relatively small storage volume is full.

5. E.C.E. SYSTEM MODEL

The analytical model describes energy and mass flows in this indirect methanol fuel cell. Currently steady state simulations are available. These show these results:

a. *Thermal Management:* A variety of simulations show balanced thermal situations in which the waste heat is sufficient to provide essentially all of the required input energies. Other system heat sources including cooling of power electronics, cooling of drive motors, *etc.* will improve this situation. The fact that the waste streams can be cooled to the boiling point of methanol is an advantage.

b. *System Efficiency:* The system efficiency is a function of fuel cell voltage, assuming a constant hydrogen utilization (85%). Increases in stack voltage efficiency will result in improved system efficiencies at least until high fuel cell voltages are established (> 1.0 V). Depending upon operating conditions, First Law system efficiencies exceed 55%. Under certain conditions, the power output from the expander exceeds compression work. c. *Transients:* Start up transients are controlled by the thermal mass of the system. With current designs that mass is large, so start up is a slow process. Water vaporization rates are difficult to change rapidly. It is expected that varying the steam generation rate is the current rate limiting step in meeting transients. The compressor-expander system may well not operate well over a wide range of flow, as is required for a load following system. This suggests that some level of battery power, operating as a fuel cell-hybrid system, may be required to permit the e.c.e. system to move swiftly between load points.

ACKNOWLEDGMENT: These studies were supported by the Office of Transportation Technology of the U.S. Department of Energy.

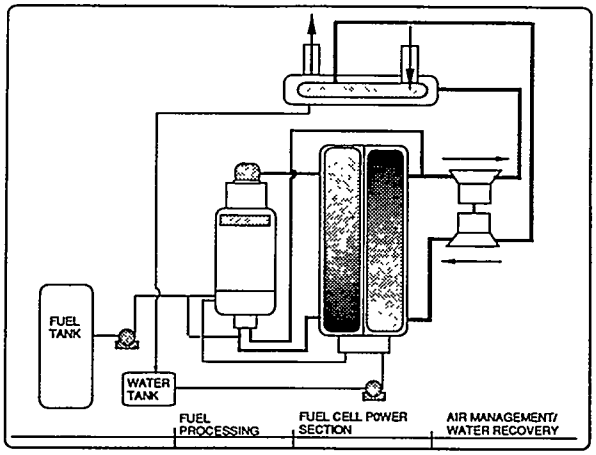

Fig. 1: Electrochemical Engine: This system combines a fuel processing component that generates hydrogen from liquid methanol with a fuel cell power component to generate electrical power. Air management is achieved using a compressor-expander to deliver pressured air. Water recovery involves a cross-flow heat exchanger to preheat the incoming air with the combined exhaust of the system.

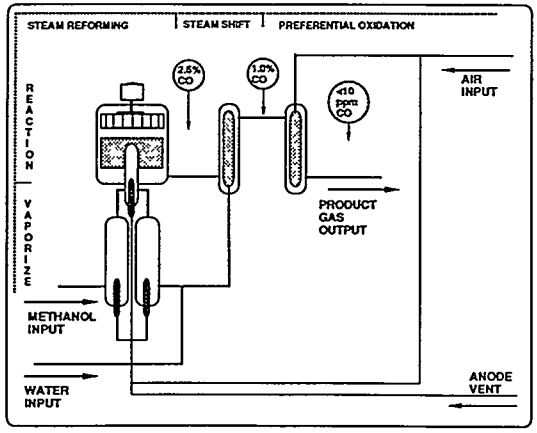

Fig. 2: Methanol Fuel Processing: Fuel processing requires three sequential processes designed to extract heat from waste streams from the fuel cell stack. Heat is extracted by combustion of the anode vent to drive the water vaporization and system preheat. Vaporized reactants are fed to the steam reforming section. Subsequent processes then 1.) react "breakthrough" methanol and 2.) lower the CO content. The preferential oxidation step also removes other higher molecular weight compounds prior to fuel cell stack feed.

STATUS OF SOLID POLYMER FUEL CELL DEVELOPMENT AT BALLARD

D.S. Watkins et al.
Ballard Power Systems
North Vancouver, Canada

Ballard Power Systems (BPS) is a Canadian company focused upon the development and sales of portable energy products. Batteries, fuel cell power generators and solid polymer fuel cell (SPFC) membranes are included.

With respect to fuel cells, Ballard has been working towards the commercialization of Solid Polymer Fuel Cell (SPFC) systems for military and civilian applications since early 1984. The work has been done in conjunction with the Canadian Department of National Defence.

Corporate Structure & Facilities

Figure 1 shows BPS Inc. and its two subsidiaries; Ballard Battery Systems Corporation (BBS) and Ballard Advanced Materials Corporation (BAM). The private investors in the parent company are also shown.

BBS manufactures non-rechargeable lithium/sulfur dioxide batteries which are being sold to the Canadian and US military. The company has a current backlog of $30 million with options to $82 million.

BAM is developing advanced polymeric/composite materials including a new membrane for the SPFC.

BPS including BAM employs 60 people and occupies approximately 25,000 ft^2 of space. This area consists of office, manufacturing, training, testing and product development space. In a separate location, BBS maintains a 22,000 ft^2 battery production facility with an additional 6,000 ft^2 of office space and employs 45 people.

Product Development & Manufacturing

SPFC product development at Ballard consists of Electrical & Control, Stack, System and Membrane/Electrode Assembly (MEA) development groups. Currently, H_2/O_2, H_2/air and methanol-/air systems are being developed. In addition, funding from Ballard, Canadian Department of National Defence, Province of British Columbia and the Federal Ministry of Energy Mines and Resources is supporting a $3.1 million methanol reformer program.

Figure 2 shows a 2.5 kW demonstration prototype fueled with H_2 and air. This packaged unit consists of a Nafion membrane stack and, electrical & control, heat rejection, water recovery and gas management subsystems. Inputs are process H_2 and air at 30 psig and cooling air. Outputs are spent process air, cooling air, product water and unregulated DC power. Weight is about 280 lbs with a volume of

6.5 ft^3. A 5 kW unit, with approximately the same volume and weight but using a Dow membrane is being built. A 10 kW unit using the Dow membrane and about twice the size of the 5 kW version was built previously for a customer.

Manufacturing consists of document control, quality control, manufacturing engineering, materials management and operations. Currently, a pilot line for stack manufacturing is being developed. A production rate of 3, 5 kW stacks per month has been achieved. During the pilot effort, quality control problems have been experienced. These problems are being addressed using Statistical Process Control (SPC) methodology. Alternative materials and processes are being evaluated to further increase plant capacity. Figure 3 shows the manufacturing group with stack serial numbers 015, 017 and 018.

Target Applications

Target applications are military, utility and motive. For the military, methanol and H_2 fuels are anticipated. The applications include a variety of maned and unmanned submersibles, tactical field generators and tanks.

Mine Counter Measures (MCM) underwater unmanned vehicles, small manned vehicles such as the Canadian Navy's SDL-1 to full size Atmosphere Independent Propulsion (AIP) submarines are being pursued. Figure 4 shows the Perry PC-1401 which is powered by a Ballard SPFC. The 2 man observation submersible uses H_2 and O_2 bottles which together with the fuel cell system supply 3 times the energy of the original battery pod but is one half the size. Recharging the system is as quick and simple as changing the gas bottles. For the batteries, this was an eight hour operation.

For utilities, natural gas and H_2 fuels are anticipated. Chemical plants and distributed power units of greater than 100 kW are included. A 10 kW demonstration program at Dow Chemical in Sarnia, Ontario, Canada is underway. The unit uses by-product H_2 from the Dow Sarnia chlor-alkali as the fuel and plant air as the oxidant.

For motive, H_2 and methanol fuels are anticipated. Applications include a 100 kW unit for a Canadian bus program and a variety of automobiles from a number of manufacturers. The automobile applications run from the replacement of the alternator, from battery/fuel cell hybrids to full propulsion using the fuel cell alone.

Conclusions

Ballard is developing fuel cell power generator and fuel cell manufacturing technology. In parallel Ballard is demonstrating and has plans for demonstrating fuel cell

systems in a variety of applications in the military, utility and motive areas.

Acknowledgements

Ballard acknowledges the continuing support of the Canadian Department of National Defence for Ballard SPFC technology.

Also acknowledged is support from the Federal Ministry of Energy Mines and Resources, The Province of British Columbia, The Ontario Ministry of Energy, Dow Chemical Canada Inc. and Dow Chemical USA.

References

1) Chemical Week, p 13, March 18, 1987

2) G.A. Eisman, The Application of a New Perfluorosulfonic Acid Ionomer in Proton-Exchange Membrane Fuel Cells: New Ultra-High Current Density Capabilities, Fuel Cell Technology and Applications, International Seminar, The Netherlands, 26-29 October, 1987, p 287.

3) D.S. Watkins, K. Dircks and D. Epp, Canadian Solid Polymer Fuel Cell Development, 33rd International Power Sources Symposium, June 1988, The Electrochemical Society, Pennington, New Jersey, p 782.

4) Perry Oceanographics Press Release, 7/28/89.

5) Chemical Week, p 20 November 9, 1988

6) D. Watkins, K. Dircks, D. Epp and A. Harkness, Development of a Small Polymer Fuel Cell, 32nd International Power Sources Symposium, 9-12 June 1986, The Electrochemical Society, Pennington, New Jersey, p 590.

7) D. Watkins, K. Dircks, D. Epp and C. De La Franier, Canadian Solid Polymer Fuel Cell Development, FCN Supplement, Fuel Cell News, Vol. VI No. 2, June 1989.

8) D. Watkins, K. Dircks, D. Epp and C. De La Franier, Canadian Solid Polymer Fuel Cell Development, Proceedings of the 4th Annual Battery Conference on Applications and Advances, January 17-19, 1989, California State University, Long Beach.

9) D. Watkins, K. Dircks, D. Epp and J. Blair, Canadian Solid Polymer Fuel Cell Development, Proceedings of the 5th Annual Battery Conference on Applications and Advances, January 1990, California State University, Long Beach.

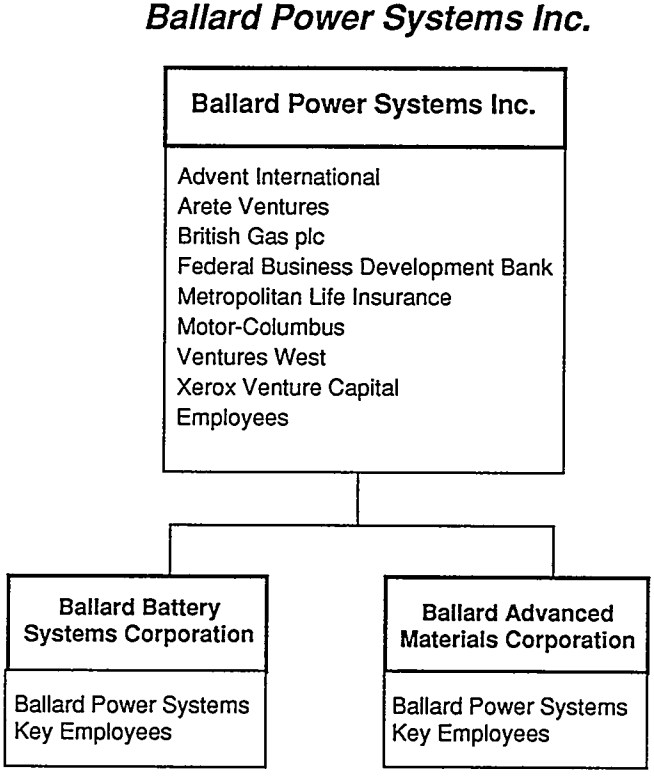

FIGURE 1

BALLARD CORPORATE STRUCTURE

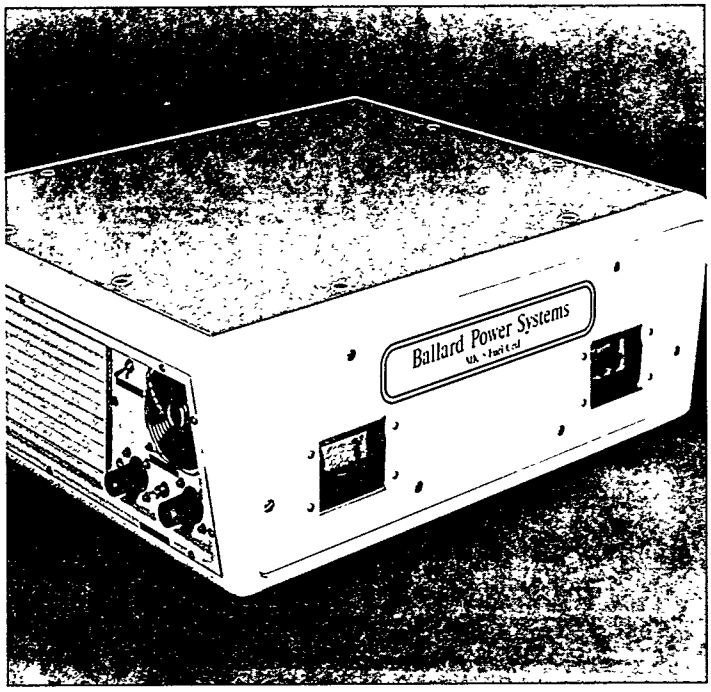

FIGURE 2

2.5 kW NAFION MEMBRANE DEMONSTRATION PROTOTYPE

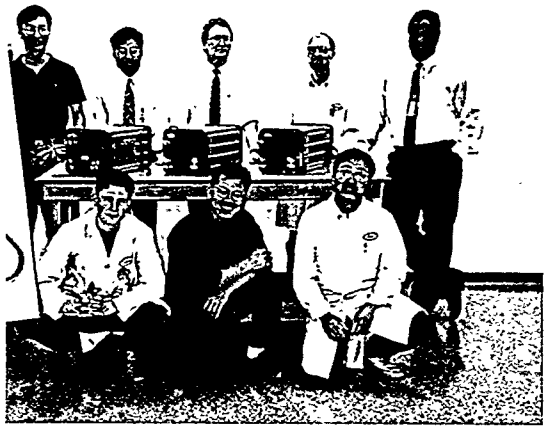

FIGURE 3

5 KW STACKS

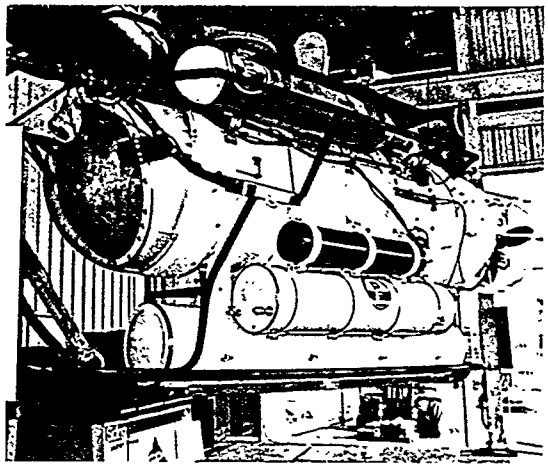

FIGURE 4

FUEL CELL POWERED PC-1401

STATUS OF SOLID OXIDE FUEL CELLS FOR TRANSPORTATION

Dennis W. Dees and Romesh Kumar
Electrochemical Technology Program
Argonne National Laboratory
9700 South Cass Avenue
Argonne, Illinois 60439-4837

As energy conversion devices for transportation applications, fuel cells are attractive alternatives to internal combustion engines because they are less harmful to the environment and have a high theoretical efficiency. Lower noise levels and improved acceleration are also among the prime motivating factors for the use of fuel cells for transportation applications. A phosphoric acid fuel cell based system is presently being developed for testing in a bus, and a polymer exchange membrane fuel cell system is also being considered for transportation applications (1). But the potentially high power density of solid oxide fuel cells (SOFC's), along with their ability to internally reform hydrocarbon fuels, electrochemically oxidize carbon monoxide, and generate water on the fuel side of the solid electrolyte (which can be used for the internal reform reactions), makes the SOFC a potentially even better candidate for transportation applications. One example of a SOFC system, shown in Figure 1, is a 60 kW power block measuring 5x3.5x2 ft. Such a package could fit easily into a van and provide enough power for acceleration.

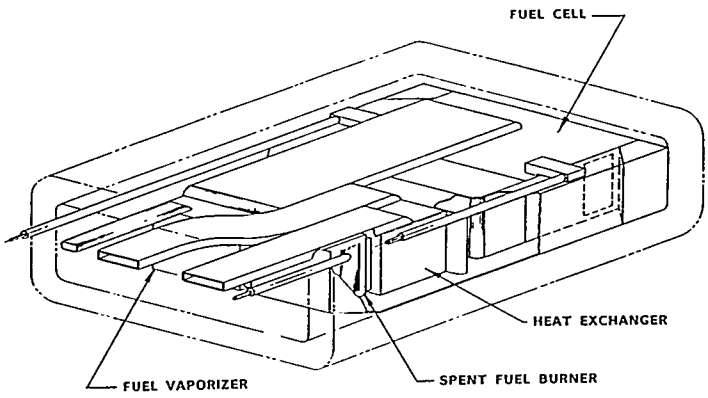

Figure 1. Schematic arranangement of the SOFC system package

The system is based on the flow schematic shown in Figure 2. The methanol fuel is vaporized using the hot fuel-side exhaust gas from the SOFC as a heat source, and then fed directly into the fuel cell. Spent fuel is burned to preheat the incoming air. A fraction of the SOFC air and fuel streams is recirculated to limit thermal stresses in the ceramic fuel cell. Such a system has only four major components, making it inexpensive to manufacture and easy to package into a compact enclosure.

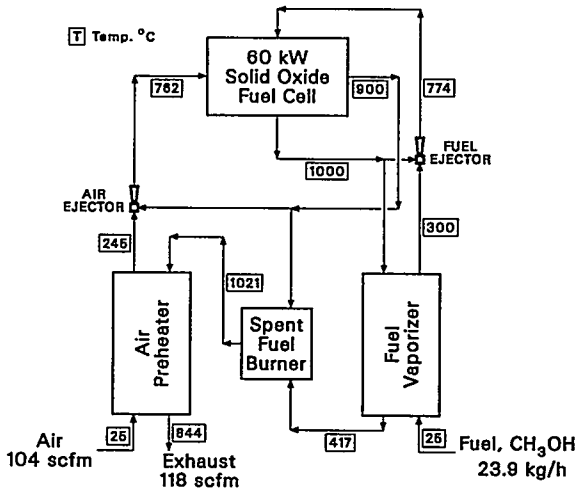

Figure 2. SOFC system for transportation application

SOFC's are generally all ceramic and have a doped (usually with yttria) zirconia electrolyte that is an oxygen ion conductor. Since the electrolyte has significant conductivity at high temperatures only, the operating temperature of SOFC's is nominally 1000°C. Requirements of thermal expansion matching, electrical conductivity, and chemical stability put severe limitations on what other materials can be used in the fuel cell. The anode is a nickel-zirconia cermet, and the cathode is a perovskite, usually a doped lanthanum manganite. The interconnect material is either ceramic (a doped lanthanum chromite) or a metal. Generally, non-precious metals or alloys are not stable in air at the SOFC's operating temperature, but they can be used if the oxide coating formed on the metal is conductive, stable, and non-porous.

Of the many SOFC designs under current development, the main three are tubular, flat plate, and monolithic. Although the tubular design is at a later stage of development than the other two, it was designed for stationary applications and does not have a high enough power density for transportation. Both the flat plate and monolithic designs should have high enough power densities, and currently, small laboratory-scale stacks (less that 100 W output) of both designs are being built and tested.

The flat plate design, also referred to as the planar design, is being developed in the United States, Europe, and Japan. Although the power density of this design would probably not be as high as that of the monolith, it has received more attention world wide because it is generally perceived to be easier to fabricate. The fuel cell in the flat plate design consists of a three-layer (anode/electrolyte/cathode) composite and an interconnection unit. The interconnection unit in the flat plate design contains the flow passages in a cross-flow pattern. The electrolyte composite and the interconnection unit are fabricated separately and then laid up into the fuel cell stack. The size of the gas passages

and the thickness of the three-layer electrolyte composite are similar in the monolithic design. In the United States, Cerametec is pursuing the flat plate design using a ceramic interconnection unit (2). Several foreign companies are developing their own versions of the flat plate design using either ceramic or metallic interconnection units.

The monolithic SOFC, named a monolith because of its stack of cells sintered into a single unit, can be fabricated into either cross-flow or co-flow configurations, both invented at Argonne National Laboratory. The two basic building blocks in the cross-flow design are thin (approximately 100 μm total thickness), planar three-layer composites of electrolyte and interconnect (doped $LaCrO_3$) materials with the appropriate electrode material layers on each. Corrugated anode and cathode material layers are used to create the gas passages (approximately 1 mm in height) and connect, both electrically and physically, the alternating electrolyte and interconnect composites together. The cross-flow design is being developed by Allied Signal Airesearch (3).

To estimate the power capability of the system shown in Figure 1, it was assumed that 16 monolithic SOFC stacks are arranged into a single, insulated unit. While this modular concept complicates the manifolding and electrical connections somewhat, it allows for a system with smaller fuel cell stacks that can be fabricated much more easily, thus decreasing the wait for the technology needed to build the system. At 85% fuel utilization and an operating point of 0.6 V at 0.735 A/cm^2, each module produces 3.75 kW. Other calculated operating and design parameters are shown in Table 1.

Stack Power, kW	3 75
Current Density, A/cm^2	0.735
Gas Passage Height, mm	0.7
Area Specific Resistance, Ω-cm^2	
Materials	0 122
Interfacial	0 150
Air Flow (x Theoretical)	4 00
Fuel Utilization, %	85
Pressure Drop, psi	
Air	0 43
Fuel	0.31
Stack Dimensions, cm	
Length	13.2
Width	8.9
Height	13.3
Stack Power Density, kW/L	2.32

Table 1. Operating and design parameters for monolithic SOFC stack

The fuel cell performance calculations in Table 1 are based on averaged fuel cell current density and other properties. A comparison of these results with more accurate nodal calculations that include heat transfer, flow, and current distribution indicate that the monolithic SOFC should actually perform better than the results in Table 1 indicate. Because the results of the SOFC calculations are conservative, the overall system calculations may also be applicable for the flat-plate design as well.

In transportation applications, the system load will vary dramatically during acceleration, braking, hill climbing, and cruising. Ideally, the fuel cell power

system should have the dynamic response capability to meet all conditions. More rigorous engineering will be required to determine whether a stand-alone SOFC system would have that capability or whether batteries will be needed to provide peak power capability. However, as a first step we have estimated the system parameters for the system shown in Figure 1 is operated at a reduced power level of 25 kW. A comparison of the SOFC system performance at 60 and 25 kW, given in Table 2, indicates that the corresponding efficiency increases from approximately 40% to nearly 50%.

	Power Level	
	60 kW	25 kW
CH_3OH Feed, kg/h	23.9	8.2
Energy Input (HHV), kW	150.8	51.6
Cell Energy Losses, kW		
$T\Delta S$	47.0	16.15
I^2R	20.0	2.35
Heat Duties, kW		
Fuel Vaporizer	15.3	5.2
Air Preheater	15.5	9.7
Spent Fuel Burner	22.6	7.7
Air Supply Blower Power, kW	1.17	0.42
Net Power, kW	60.0	25.0
Efficiency, %	39.9	48.6

Table 2. Thermal balance of SOFC system

The specific power of the entire assembly shown in Figure 1 is 0.5 kW/kg, while that of the SOFC alone is 1.4 kW/kg. Even with this relatively simple system, the SOFC only accounts for approximately one-third of the total weight, and increasing the performance of the SOFC even by a factor of two increases the system performance only by approximately 20%. Therefore, as the performance of the SOFC improves, it has a diminishing effect on the overall system performance. This is generally true for all fuel cell systems where the peripheral equipment typically accounts for a majority of the system weight.

Although the high operating temperature of the SOFC enables the fuel cell to operate directly on methanol, thus simplifying the system, it also has drawbacks. A vacuum-insulated casing is needed to reduce heat losses so that the system can be kept in standby mode, with approximately 0.5 kg of fuel per day from which power is immediately available.

Clearly, cold start-up of the system is a significant concern, and placing the system in standby mode would be advised, even if the vehicle would not be used for days at a time. While it is difficult to determine the dynamics of the complete SOFC system in cold start-up, the dynamics of the fuel cell stack itself have been examined. If one assumes that the stack can withstand a 200°C temperature difference between the inlet and outlet air flows, then the stack can be brought up to 900°C in less than two minutes.

The potentially high power density of the monolithic and flat plate SOFC's, along with their ability to internally reform hydrocarbon fuels and electrochemically oxidize carbon monoxide, makes them attractive for transportation applications. Also, SOFC's generate water on the fuel side of the solid electrolyte, which can be

used for the internal reform reactions. Our analysis of a 60 kW monolithic SOFC system indicated efficiencies of 40% at 85% fuel utilization.

ACKNOWLEDGMENT

This work has been supported by the Electric and Hybrid Propulsion Division, Office of Propulsion Systems, U. S. Department of Energy, under contract number W-31-109-Eng-38. We are especially grateful to Dr. Pandit G. Patil for his guidance and encouragement throughout this study.

REFERENCES

1. R. A. Lemons, "Fuel Cells for Transportation," J. Power Sources, Vol. 29, pp. 251-264, 1990.

2. A. Khandkar et al., "Proceedings of the First International Symposium on Solid Oxide Fuel Cells," S. C. Singhal, ed., The Electrochemical Society, Pennington, NJ, Vol. 89-11, pp. 377-383, 1989.

3. N. Q. Minh, et al., ibid., pp. 307-316.

The submitted manuscript has been authored by a contractor of the U S Government under contract No W-31-109-ENG-38 Accordingly, the U S Government retains a nonexclusive, royalty-free license to publish or reproduce the published form of this contribution, or allow others to do so, for U S Government purposes

METHANOL REFORMERS FOR FUEL CELL POWERED VEHICLES: SOME DESIGN CONSIDERATIONS

R. Kumar, S. Ahmed, M. Krumpelt, and K. M. Myles
Argonne National Laboratory
Argonne, Illinois 60439

Fuel cells are being developed for use in automotive propulsion systems as alternatives for the internal combustion engine in buses, vans, and passenger cars (1,2). The major motivations for developing fuel cell powered vehicles are as follows: low emissions of pollutants, high fuel energy conversion efficiencies, superior acceleration, low noise and vibration, and the possibility of using coal- or biomass-derived alcohols rather than petroleum-based fuels.

The two most important operational requirements for a stand-alone fuel cell power system for a vehicle are the ability to start up quickly and the ability to supply the necessary power on demand for the dynamically fluctuating load. The rapid start-up requirement is obvious. An example of the dynamic performance requirement is given in Fig. 1, which shows the simulated velocity and power profiles for a small car, the IETV-1, operated on the Simplified Federal Urban Driving Schedule (SFUDS). On this schedule the power varies 15 times over 6 min; in actual driving the power fluctuations are typically more numerous and more complex.

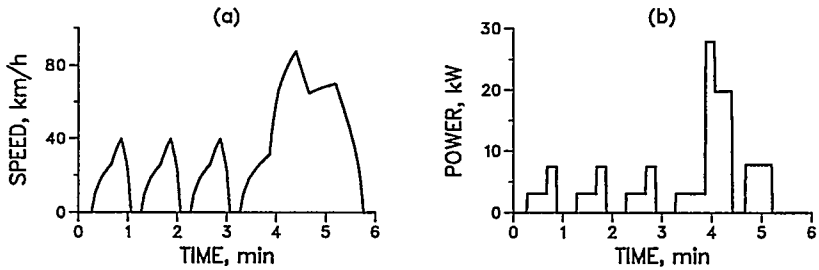

Fig. 1 Velocity and power profiles for the IETV-1 simulated on the SFUDS driving schedule: (a) Velocity vs. time; (b) Power vs. time.

Methanol is a likely fuel for use in fuel cells for transportation applications. It is a commodity chemical that is manufactured from coal, natural gas, and other feedstocks. For use in a fuel cell, however, the methanol must first be converted (reformed) to a hydrogen-rich gas mixture. The desired features for a methanol reformer include rapid start-up, good dynamic response, high fuel conversion, small size and weight, simple construction and operation, and low cost. In this paper we present the design considerations that are important for developing such a reformer.

Reforming of Methanol

Hydrogen may be produced from methanol by either partial oxidation or steam reforming, for which the overall reactions are:

$$CH_3OH(\ell) + \tfrac{1}{2}O_2(g) \rightarrow 2H_2(g) + CO_2(g) \qquad \Delta H^\circ_{298} = -154.86\,kJ \qquad (1)$$

$$CH_3OH(\ell) + H_2O(\ell) \rightarrow 3H_2(g) + CO_2(g) \qquad \Delta H^\circ_{298} = +130.99\,kJ \qquad (2)$$

$$CH_3OH(g) + H_2O(g) \rightarrow 3H_2(g) + CO_2(g) \qquad \Delta H^\circ_{298} = +49.48\,kJ. \qquad (3)$$

Thus, partial oxidation reforming is exothermic, while steam reforming is endothermic.

Mechanism of Methanol Reforming

There are two schools of thought regarding the mechanism by which methanol is reformed to hydrogen. Amphlett et al. (3) believe that the methanol first dissociates into carbon monoxide and hydrogen, and the CO is subsequently oxidized, by oxygen in partial oxidation reforming and by steam in steam reforming. On the other hand, Springer et al. (4) and Vanderborgh et al. (5) feel that the reaction occurs through an alternate oxidation and reduction of active sites on the catalyst, where the methanol first reduces a site by taking away the lattice oxygen and producing CO_2 and H_2. The reduced site is then oxidized by water to produce H_2.

Catalysts for Methanol Reforming

Variously supported oxides of copper and zinc have been used most often for the steam reforming of methanol, although additions of alumina (6), iron and chromium (7), and alkaline earth metals have also been employed successfully (8). A combination of oxidation catalysts, e.g., NiO-ZrO_2, NiO-Al_2O_3-CaO, and Cu-Pd-SiO_2, and reforming catalysts, such as NiO-Al_2O_3-MgO and Cu-SiO_2, is used for the partial oxidation reforming of methanol (9,10).

Partial Oxidation vs. Steam Reforming

Product Gas Composition

Both in partial oxidation and in steam reforming the product gas contains residual carbon monoxide. For use in a phosphoric acid fuel cell (PAFC), this CO must be reduced to less than 1%; for use in a proton exchange membrane (PEM) fuel cell, the residual CO must be reduced to trace amounts. The concentration of residual CO in the product gas can be reduced by injection of H_2O along with the CH_3OH in partial oxidation, and the use of excess H_2O in steam reforming. Even so, reducing the CO concentration to acceptable levels may require a follow-on selective oxidation step, using an appropriate catalyst (1).

In partial oxidation reforming, the product should nominally consist of 41% H_2, 21% CO_2, and 38% N_2, if all the CO is oxidized to CO_2. In practice, however, the addition of H_2O is required to reduce CO to low levels. Using a 1:1 molar mixture of CH_3OH and H_2O and selective oxidation of the residual CO, the product gas mixture contains 48% H_2, 20% CO_2, 11% H_2O, and 21% N_2. In steam reforming with 50% excess H_2O and after residual CO removal, the product gas composition is 63% H_2, 22% CO_2, 11% H_2O, and 4% N_2. The lower hydrogen concentration from the partial oxidation reformer compared to that from the steam reformer (48% vs. 63%) leads to a Nernst voltage decrease of ~6 mV.

Energy Conversion

Partial oxidation reforming of CH_3OH produces excess thermal energy which can be used to vaporize the methanol and water and to heat the reformed product gas. The net energy effect is that, from the 726.5 kJ of the higher heating value (HHV) of one mole of the input CH_3OH, the partial oxidation reformer yields H_2 with a theoretical maximum electrochemically available energy of 474.4 kJ.

Steam reforming of CH_3OH requires the input of external energy. If the vaporizing and reforming energy is obtained from the fuel cell stack waste heat and the combustion of the spent fuel leaving the stack, the net effect is to convert the 726.5 kJ of the HHV of an input mole of CH_3OH to a theoretical maximum electrochemically available energy

of 711.6 kJ as H_2. If the stack waste heat and spent gas combustion are not used to provide the vaporizing and reforming energy, then the maximum electrochemically available energy is 512.6 kJ.

Dynamic Response and Start-Up

The dynamic response and start-up performance of the partial oxidation reformer can be much superior to that of the steam reformer. This is because the partial oxidation reformer uses *direct* heat transfer, which provides very high heat fluxes, and therefore, the required heat transfer loads can increase or decrease rapidly. In contrast, a steam reformer must use *indirect* heat transfer, which limits heat fluxes. The high heat fluxes in *direct* heat transfer can make a partial oxidation reformer/fuel vaporizer start-up quickly; the lower heat fluxes in *indirect* heat transfer do not permit as rapid a start-up for a steam reformer/vaporizer, even if process gas recirculation is used to enhance the convective heat transfer.

Miscellaneous Features

The partial oxidation reformer is an intrinsically simple device due to the absence of burners, baffles, heat transfer surfaces, and combustion manifolding and ducting. In comparison, a steam reformer is relatively complex; it contains one or more burners, extended heat transfer surfaces, combustion air and exhaust ductwork, and perhaps even a process gas recirculator. Because of the high heat fluxes available, the partial oxidation reformer can be more compact than a steam reformer of equal methanol processing capacity. Also, since the combustion products form part of the reformed gas itself, there is no separate reformer combustion exhaust stream from the partial oxidation reformer.

Discussion

In a fuel cell power system it is possible to thermally integrate the fuel vaporizer, reformer, and the cell stack. Waste heat is available at ~80°C from the PEM stack and at ~190°C from the PAFC stack. In either fuel cell, the spent gas from the anode contains 10–30% of the H_2 in the anode feed, and its heat of combustion can also be used.

There are two major considerations in implementing such an integration. One is the quantity and quality of waste energy available, and the other is the dynamic relationship between the need for this energy and its availability. In a low temperature fuel cell system, such as the PEM, the stack waste heat is available at too low a temperature to vaporize water or pressurized methanol. In a higher temperature system, such as the PAFC, the stack waste heat can be used for this purpose. In either system, energy in the spent anode gas can be used.

In a dynamically varying automotive power system, the availability of the energy from the fuel cell stack and spent anode gas *lags behind* the demand for that energy. For instance, for a step increase in the power output required from the fuel cell stack, vaporizing and reforming of the additional fuel needs energy *before* the excess stack waste heat and the excess spent fuel become available; this only happens *after* the stack begins delivering power at the higher demand level. This temporal difference in the requirement and availability of thermal energy in the fuel cell power system suggests that the thermal subsystems of the stack should be independent of the vaporizer/reformer. In addition to being more responsive, the independent systems should be easier to operate and control.

Conclusion

A reformer developed for stand-alone fuel cell automotive power systems must be capable of rapid start-up and good dynamic response. To meet these requirements, it should incorporate: (1) a small catalyst bed for quick starting, small size, and low weight; (2) multiple catalysts for optimum operation of the dissociation and reforming reactions; (3) reforming by direct heat transfer partial oxidation for rapid response to fluctuating loads; and (4) thermal independence from the rest of the fuel cell system.

Acknowledgment

This work has been supported by the Electric and Hybrid Propulsion Division, Office of Propulsion Systems, U. S. Department of Energy, under contract number W-31-109-Eng-38. We are especially grateful to Dr. Pandit G. Patil for his guidance and encouragement throughout this study.

References

1. R. A. Lemons, "Fuel cells for transportation," *J. Power Sources*, **29**, 251–264 (1990).
2. R. Kumar, M. Krumpelt, and B. Misra, "Fuel cells for vehicle propulsion applications: A thermodynamic systems analysis," *Proc. 24th Intersoc. Ener. Conv. Eng. Conf.*, pp. 1601–1606, August 1989.
3. J. C. Amphlett, R. F. Mann, and R. D. Weir, "Hydrogen production by catalytic steam reforming of methanol. Part 2: Kinetics of methanol decomposition using C18HC catalyst," *The Canadian J. Chem. Eng.*, **66**, 950–956 (1988).
4. T. E. Springer, H. S. Murray, and N. E. Vanderborgh, "Methanol reformer system and design for electric vehicles," *Proc. 20th Intersoc. Ener. Conv. Eng. Conf.*, Vol. 1, p. 723, August 1985.
5. N. E. Vanderborgh, B. E. Goodby, and T. E. Springer, "Oxygen exchange reactions during methanol reforming," *Proc. 32nd Inter. Power Sources Symp.*, p. 623, 1986.
6. M. Matsukata, S. Uemiya, and E. Kikuchi, "Copper-alumina spinel catalysts for steam reforming of methanol," *Chem. Lett.*, **5**, 761 (1988).
7. Q. D. Vu, M. Davidson, D. Durand, and P. Courty, "Process for producing hydrogen by catalytic steam reforming of methanol," Euro. Pat. Appl. EP 272182, June 1988.
8. Y. S. Lee, C. S. Han, M. S. Cho, and K. S. Rhee, "Decomposition of methanol-water on Mg/Cu/ZnO system," *Taehan Hwahakhoe Chi*, **32** (1), 22 (1988).
9. M. Flytzani-Stephanopoulos and G. E. Voecks, "Conversions of hydrocarbons for fuel cell applications," JPL Report 82-37, DOE/ET-11326-1, October 1981.
10. J. W. Jenkins and E. Shutt, "The Hot Spot™ reactor. Hydrogen generation using a novel concept," *Plat. Met. Rev.*, **33** (3), 118–127 (1989).

The submitted manuscript has been authored by a contractor of the U S Government under contract No W-31-109-ENG-38. Accordingly, the U. S Government retains a nonexclusive, royalty-free license to publish or reproduce the published form of this contribution, or allow others to do so, for U S Government purposes

STATUS OF ONTARIO MINISTRY OF ENERGY PROJECTS RELATED TO FUEL CELLS AND TRANSPORTATION

ROBERT G. GREVEN, P.ENG.
MANAGER
ENERGY, RESEARCH AND
DEVELOPMENT
ONTARIO MINISTRY OF ENERGY
56 WELLESLEY STREET WEST
TORONTO, ONTARIO M7A 2B7

Several years ago, staff at the Ontario Ministry of Energy identified fuel cells as an emerging technology that offered good potential for vehicle power as well as stationary electrical generation.

Over the past three years, our EnerSearch program has funded four research and development projects designed to promote the PEM fuel cell and electric vehicle technologies. One other project offers the potential to significantly improve the economics of the PEM fuel cell.

The primary purpose of this paper is to describe the status of these projects as of November 1st, 1990.

The initial project involves the installation of a 10 kW PEM fuel cell, supplied by Ballard Technologies Corporation, at the Sarnia Ontario plant of Dow Chemical Canada. This fuel cell has been in operation since May, 1990. Test results to date are described.

A second project, directly related to vehicles, involves the installation of an aluminum-air fuel cell or battery supplied by Alupower Canada in a Chrysler mini van. In this case, the fuel cell will act as a range extender to a conventional electric vehicle.

The electric and/or fuel cell vehicle is now being promoted for environmental reasons. Although the actual vehicle emissions are either nil or significantly reduced compared to conventional vehicles, the production of the required electricity or hydrogen does create environmental problems. One pollution free source of vehicle power could be photovoltaic hydrogen. EnerSearch is funding the Electrolyzer Corporation's program to develop lower cost photovoltaic hydrogen by modifying the electrolyzer so that it can directly accept the output of a photovoltaic array. Progress to date and plans for a field demonstration that will be co-funded by the California South Coast Air Quality Management District are described.

It is becoming apparent that cost pressures and the desire to utilize regenerative braking are leading to the development of hybrid vehicles rather than those powered solely by fuel cells. Ontario Bus Industries and Unique Mobility are developing a hybrid electric drive bus actually powered by a natural gas fueled internal combustion generator. The initial vehicle is expected to be on the road by September, 1991. Since the storage batteries could easily be recharged by fuel cells and hydrogen could be stored in place of natural gas, additional units could be the basis of a relatively low cost fuel cell bus.

Finally, one major deficiency of the PEM fuel cell is that operating temperatures are too low to permit recovery of useable waste heat. The Ministry has been funding the program of Ravendahl Energy Research Corporation of Toronto which is developing a device that can recover electrical energy from low temperature ($160^{o}F$ to $190^{o}F$) waste heat. While this concept, when fully demonstrated, will be applicable in many industries and applications, it does offer the potential to raise the electrical efficiency of the PEM fuel cell considerably above the usually quoted 50%. The current status of this activity is described.

This paper also briefly describes a future fuel cell powered bus program that we would recommend based upon information coming from these individual projects. It highlights a number of R & D activities and studies that seem to be required.

ECONOMIC FEASIBILITY STUDY OF 5-MW FUEL CELL POWER GENERATION SYSTEM AND RESEARCH FOR THE 1000-KW CLASS MCFC PILOT PLANT IN JAPAN

K. Doi, T. Yoshida, T. Segawa, N. Horiuchi
MCFC Research Association
3-3-10 Minami-Ohtsuka, Toshima-ku,
Tokyo 170 Japan

1. INTRODUCTION

The introduction of the fuel cell, a new energy technology, is widely anticipated to consume less energy and to lighten the burden on the environment, vital factors in dealing with global environmental problems caused by CO_2 emission and the increasing international demand for energy.

The 5.7-million-W fuel cell is expected to be introduced into the Japanese market by 2010. The Research Association thus considered it timely to compare and analyze plant efficiency and economic efficiency of fuel cell power generation systems which use natural gas fueled PAFC, MCFC, and SOFC. The latter are considered to be the main representatives of diversifying power sources.

In this report, we would like to explain the basic concept of the 1000 W class MCFC pilot plant which is targeted to go into operation by the late 1990's. The developments to date of the plant's system and component technology as well as the results of system analyses are also described.

2. ECONOMIC FEASIBILITY OF FUEL CELL POWER GENERATION SYSTEMS

In order to clarify the areas for the development of the PAFC, MCFC and SOFC power generation systems, the economic feasibility of each natural gas-fueled 5-MW class fuel cell power generation system was analyzed. The results are shown in Table 1.

These results allowed us to clarify the following about the economic efficiency of the fuel cell power generation system:

(1) The MCFC power generation system has the possibility of being the most efficient economically.

(2) The cost of materials for the fuel cell body in the SOFC power generation system is high. It would be necessary to reduce the production cost by putting the current density at a level several times higher than that of other fuel cells.

(3) It is essential to further advance the performance of the fuel cell body in order to compete with existing technology in thermal power generation.

(4) At present, the production cost of the fuel cell body, represents most of the cost of plant construction and since the production cost ratio of peripheral equipment

will rise about the time of entry into the market, reducing the cost of this equipment is an important factor.

3. ANALYSIS OF THE 1000-KW CLASS MCFC POWER GENERATION PLANT

The development objectives set by the Japanese Government are shown in Table 2. The basic policy and the systems construction to achieve the targets are shown in Table 3 and Fig. 1 respectively.

This is the first pilot plant in Japan to aim for both dispersedand centralized facilities. In order to achieve the target plant efficiency, it is necessary to achieve the optimal plant and operating conditions as well as improving the characteristics of the cell and reducing the auxiliary electric power. Net plant efficiency can be expected to achieve 45% (3 ata., HHV), if the average cell voltage reaches 0.8 V (atmospheric pressure, fuel utilization rate: 80%, current density: 150 mA/cm^2) and the system has a turbine compressor and a cathode output gas recycle blower 5% more efficient than the existing ones (Fig. 2).

The operating pressure of the cell is determined to be 3 ata., viewed from cathode electrode dissolsion control, but if the cell is improved and can be operated at 7 to 8 ata., over 50% plant efficiency can achieved.

The plant requires a site area of about 1 m^2/kW. However, if the plant gets larger, the required area /kW could become equivalent to or smaller than that of existing thermal power plants.

Based on research results thus far, facilities used for testing the MCFC power generation system component technology will be installed at Akagi General Research Laboratory (Akagi Stack & System Square) in the Akagi Testing Center of the Central Research Institute of the Electric Power Industry to be established by the Research Association.

The basic data required for the design and production of the 1000-kW class pilot plant will be obtained there. Fig. 3 is a drawing of the planned demonstration test facilities.

Table 2. Target Value of 100 kW Class MCFC Pilot Plant (Moon-light project)

Item	Target Value
A.C Output	100 kW class
Net Plant Efficiency	≥ 45% (HHV)
Fuel Gas	LNG
Environmental Impact	≤ Regulation

Table 1. Investigation Results of Fuel Cell Generation System

[Appraisal condition] Fuel gas : Natural gas
Plant size : 5 MW (Transmission base)
Cell operation press.: 8 kg/cm²A

Fuel Cell Type	PAFC	MCFC	SOFC
Cell Voltage (Rated conditions)	0.759 V/cell at 200 mA/cm²	0.781 V/cell at 200 mA/cm²	0.689 V/cell at 200 mA/cm²
Net Plant Efficiency (HHV base)	∿ 43%	∿ 51%	∿ 45%
Unit Post of Construction per kW (Contain transmission credit)	∿ ¥240,000	∿ ¥230,000	∿ ¥320,000
Cell Stack	∿ 33%	∿ 27%	∿ 38%
B.O.P	∿ 67%	∿ 73%	∿ 62%
Unit Cost of Generation (Fuel cost ¥2/Mcal)	∿ ¥13/kWh	∿ ¥12/kWh	∿ ¥16/kWh

Table 3. Basic Principle of 1000 kW MCFC Pilot Plant Concept

Item	Contents
Equipment	The equipment used in normal operation should be minimized. Start-up or shut-down operation should be coped with the equipments for normal operation
Mass.Heat Balance	Mass.Heat Balance should be provided inside of the system
Control Point	Control Point should be minimized in the control-grade without any difficulty

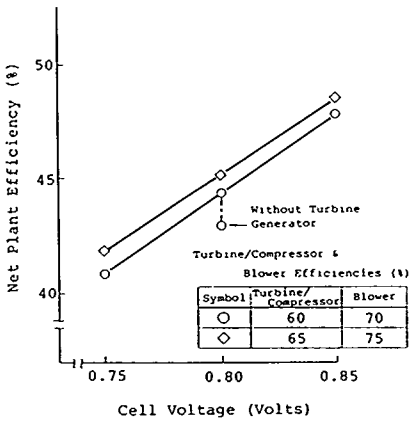

Fig. 2. Net Plant Efficiency vs. Cell Voltage

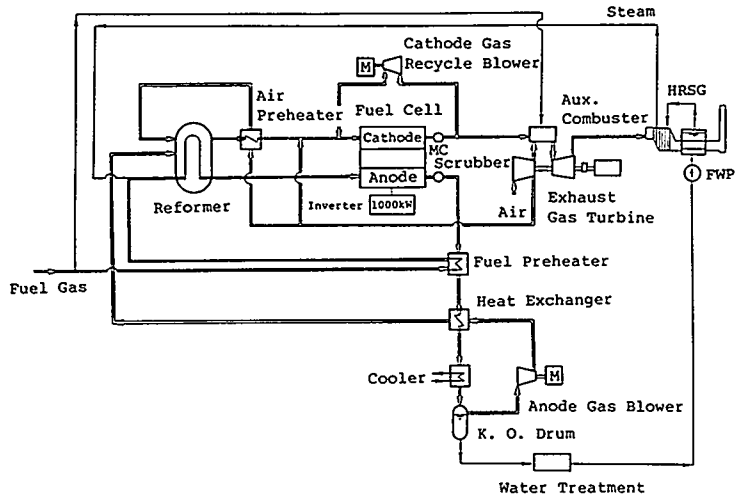

Fig. 1. Schematic Flow Diagram of the 1,000 kW MCFC Pilot Plant

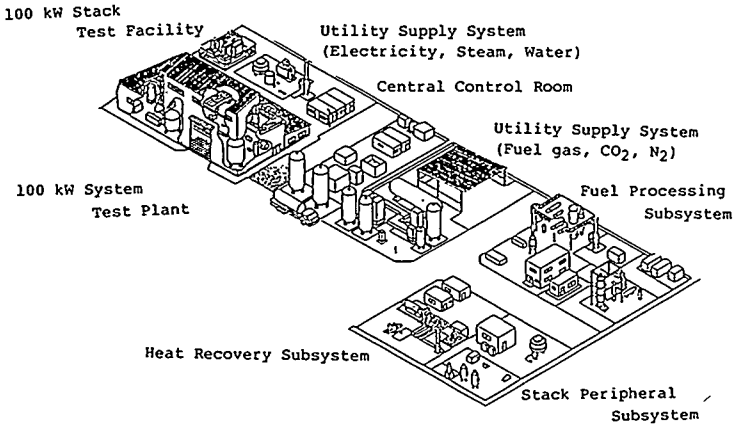

Fig. 3. Bird's View of Component Facilities at Akagi Stack and System Square

OPERATING TEST OF 2 KW MCFC PLANT

K. Kobayashi, N. Kinoshita and M. Koga
Ishikawajima-Harima Heavy Industries Co., Ltd.
3-1-15 Toyosu, Koto-ku, Tokyo 135, Japan

1. INTRODUCTION

Development of the molten carbonate fuel cell (MCFC) started in 1983 in the author's firm, where work has since progressed in parallel also on the MCFC generation system. The 2 kW MCFC installation described here has been test operated with the aims held in view of examining:-

- System performance characteristics, e.g. those under both rated and partial load, response to load variations, effect of cathode gas recycling, condensate/exhaust gas properties
- Consistency of process configuration and methods of control constituting the system, e.g. for catalytic combustion of dilute fuel (anode exhaust) with rarefied air (cathode exhaust), air-fuel ratio control, absence of control of the pressure difference between electrodes.

2. EXPERIMENTAL INSTALLATION

The experimental installation (Fig. 1) comprises the key components of fuel cell, reformer, recycling blower. Notable features of the system are:-

- Anode and cathode gases both channeled directly to reformer combustion chamber, to dispense with control of the pressure difference between electrodes --which used to be one of the most crucial control items in MCFC systems
- Cathode exhaust cooled down to the temperature of release to atmosphere, and recycled in part back to the cathode, to raise CO_2 partial pressure in cell, and thus improve the

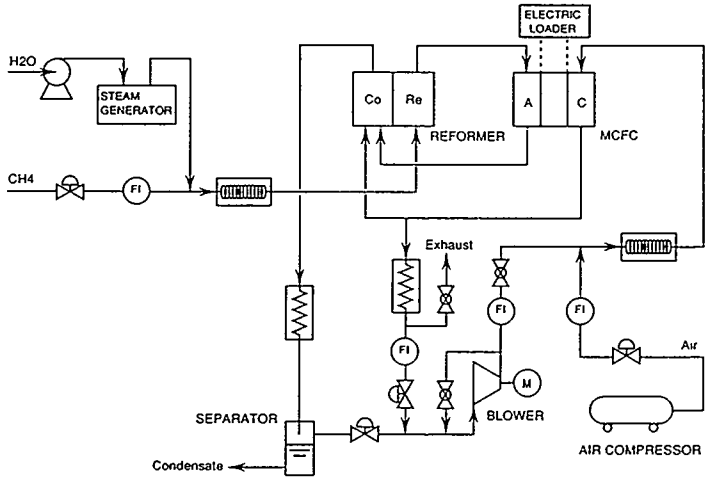

FIG. 1 Schematic Diagram of 2 kW MCFC Plant

generating efficiency without requiring a high-temperature blower.

Particulars of the principal components are:-
- Fuel gas : Methane gas
- Fuel cell : Parallel flow, internal manifold MCFC
  : = Output: 2 kW
  : = Electrode surface area: 1,000 cm^2/cell
  : = Number of cells: 20
  : = Operating temperature/pressure: 650°c/atmospheric
- Reformer : Plate type, catalytic combustion
- Blower : Roots type
- Control : By computer.

3. RESULTS OF TEST OPERATION

After operating stably for over 3,000 hours, the installation was subjected twice over to cell heating cycle tests, retracing the cycles of heating up/cooling down and fusion/solidification of electrolytes, followed by scheduled shutdown.

During operation, the power attained was 2.1 kW, and the average cell voltage was 0.7 V at 150 mA/cm2 with 66 % utilization of fuel gas (Fig. 2).

Performance under Partial Load

With the fuel utilization rate held constant, reducing the load lowered the current density and raised the cell voltage, resulting in improved fuel cell efficiency. The relation between current density and cell voltage was as shown in Fig. 3.

Cathode Gas Recycling Characteristics

With the fuel flow and the load held constant, runs were performed with the air flow regulated so as to maintain at approximately constant level the total gas volume flowing

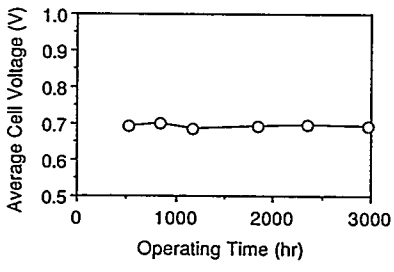

FIG. 2 Variation in Time of Average Cell Voltage

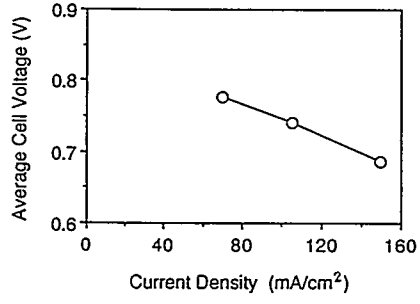

FIG. 3 Average Cell Voltage vs. Current Density

through the cathode under varying cathode gas recycling rate. As indicated in Fig. 4, increasing the cathode gas recycling rate lowered the O_2 concentration and conversely raised the CO_2 concentration, to raise the cell voltage.

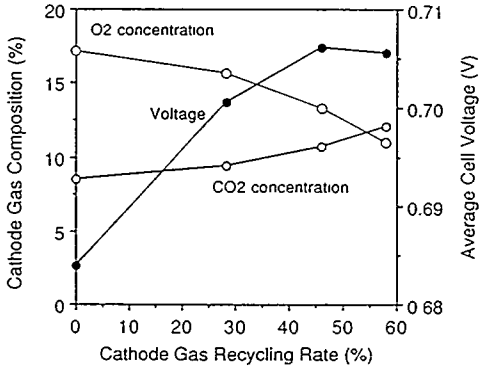

FIG. 4 Cathode Gas Recycling Characteristics

Response to Load Variations

A record of operating performance upon rapid rise of load is reproduced in Fig. 5-(a): cell voltage dropped sharply upon rapid rise of load, and several minutes elapsed before restoration. This proved to be due to lag in the resumption of gas supply --particularly CO_2 recycling to the cathode.

In order to minimize this lag, a run was made with the rise of air flow rate accompanying load increase restricted to the extent of not depriving the cell and reformer of requisite

(a) Without regulation of operating conditions

(b) With rise of air flow rate restricted

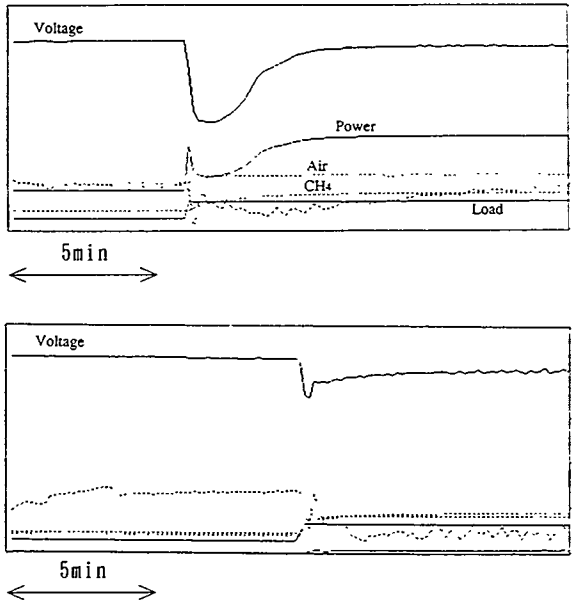

FIG. 5 Load Following Characteristics With and Without Regulation of Operating Conditions

O_2. The result, shown in Fig. 5(b), was a markedly smaller drop of cell voltage, followed by rapid restoration. Thus, response to load variations could well be improved through appropriate regulation of operating conditions, such as momentary restriction of air flow increase on occasions of load increase. Such means of minimizing the lag in CO_2 gas recycling should be tied into the system design and into operating instructions.

Pressure Difference between Electrodes

Adequacy of the present system dispensing with control of the pressure difference between electrodes (by principle not necessary) was demonstrated in actual test operation: the pressure difference never exceeded 200 mmAq whether under constant or varying load. Records of cell output voltage and anode gas analysis indicated that a pressure difference of this amount did not increase cross leaking nor impair cell performance.

Condensate and Exhaust Gas Properties

The condensate sampled from separator proved to possess:-
- pH: 4 - 4.5
- K, Li, Fe and other metal ions:
  Detected but only in amounts not exceeding 0.5 ppm.

Much the same properties were shown by anode exhaust sampled directly at anode exit, disproving the suspected possibility of these ions being contained in the cell exhaust gas depositing in the piping upstream of the separator.

Analysis of the cathode exhaust gas resulted in:-
- No detectable NO_2
- Unburned fuel detected to the extent of
  10 - 45 ppm CO and approx. 150 ppm CH_4.

The above gases in the exhaust are considered to derive from fuel incompletely burned in the reformer combustion chamber.

4. CONCLUDING REMARKS

The scale of the present installation (2 kW), while permitting self-contained operation in terms of material balance, called for auxiliary electrical heating of individual components to compensate local heat dissipation in order to maintain their requisite operating temperatures. The present test operation noneless clearly demonstrated the validity of the basic process adopted in the installation, and valuable data were obtained that should serve in further improving the power generating efficiency and response to load variations.

It is hoped to utilize the knowledge acquired so far to the design of generating systems for a wide range of applications --from on-site power supply to utility plants-- and thus to realize an attractive new system of electric power generation. For this, further examination of the operating characteristics, of the reliability aspects and of the economics is called for.

MCFC TECHNOLOGY DEVELOPMENT IN TOSHIBA

T. Terayama (Fuel Cell Systems Division)
K. Murata, M. Yamamoto, M. Hori (R&D Center)
M. Sasaki (Keihin Product Operations)
Toshiba Corporation
1-1-6,Uchisaiwai-cho, Chiyoda-ku, Tokyo, 100, Japan

Toshiba Corporation initiated MCFC technology development in 1980. Toshiba participated in the MOON-LIGHT project, and that effort culminated in demonstration of 10-kilowatt MCFC stack in FY 1986. Since that time Toshiba has established its own independent MCFC development program aimed at resolving the issues impeding commerciallization of this promising power generation technology.

To be commercially feasible, the cost of electricity produced by an MCFC power plant must be competitive with the cost of electricity produced by conventional plants. Toshiba is focusing on electricity cost reduction by improving cell endurance and by developing low-cost repeat-component manufacturing processes. Reasonable levels of cell performance have already been achieved. Recent Toshiba activities include:

1. Cell endurance improvement by development of countermeasures to cell degradation

2. Manufacturing process development for large-size repeat components, with emphasis on durability, unformity, and reproducibility

3. Design, analysis, and verification of a cell stack assembly of practical size

CELL ENDURANCE IMPROVEMENTS

In order to predict cell life, Toshiba has studied the relation between change in porous structure with time and electrolyte loss. To clarify the mechanism of electrolyte loss, the structures of the porous components of cells run for various lengths of time were analyzed. For the anode, strengthening the porous plate against thickness reduction by using an alumina dispersion was found to be effective.

Figure 1 shows Toshiba's progress in improving cell performance and endurance as measured in 15 x 15 cm single cell tests. Electrolyte loss countermeasures greately contributed to such improvements.

The effects of nickel oxide dissolution from the cathode on cell performance and endurance have been analyzed. Blocking of the ionic conduction path in the electrolyte layer by nickel and nickel oxide precipitates was found to be important. Based on the analysis, nickel oxide dissolution was estimated to limit cell life to about 15,000 hours. However, it was found that some alkaline earth carbonate additives could effectively suppress nickel cation diffusion and increase cell life.

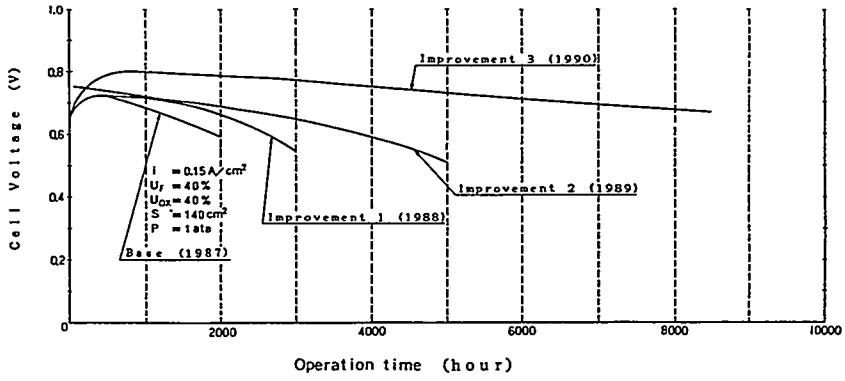

Figure 1 -- Toshiba's progress in improvement of cell performance and endurance, as measured by results of 15 x 15 cm cell tests without electrolyte replenishment.

MANUFACTURING OF LARGE SIZE REPEAT COMPONENTS

Manufacturing Process development was carried out on large-size repeat components. The objective was to reduce manufactured cost (both raw materials and value added) while meeting performance and endurance goals. The effort concentrated on uniformity, reproducibility, and projected productivity.

A 1.2-meter-wide tape-casting machine and drying oven were installed, and full-width matrix tapes were manufactured reproducibly. Finished matrices were made from the tapes and were evaluated in single cells and stack.

Equipment for a proprietary dry-casting process was installed and developed to produce 1-meter-square electrodes. The dry-casting process has the advantage of avoiding the binder and binder burn-out process required for wet tape-casting process. Nondestructive ultrasonic density distribution measurement methods were developed for in-process quality control.

STACK STRUCTURE DEVELOPMENT

In order to reduce the possibility of damage to porous parts during stack assembly, a process was developed for unifying the matrix and electrodes before stacking. The process incorporates matrix binder burn-out and electrolyte fill as well.

A new cell stack configuration using a mechanically sealed manifold was developed. An advantage of this type of manifold is that there is no path for electorolyte migration from cell to cell. The configuration also permits co-flow of fuel and oxidant. Performance calculations verified that more uniform temperature and current density distributions are obtainable with this cell configuration.

Figure 2 shows an assembled stack of five 50-cm-square cells of the new configuration. Post-test analysis will be carried out after completion of 1000 hours of operation.

COOPERATION BETWEEN TOSHIBA AND IFC

Toshiba has recently entered into cooperative arrangement with International Fuel Cells Corporation for joint development of MCFC stacks and systems. This relationship will be strengthened and will move into a utility demonstration stage as further progress is made toward commercialization.

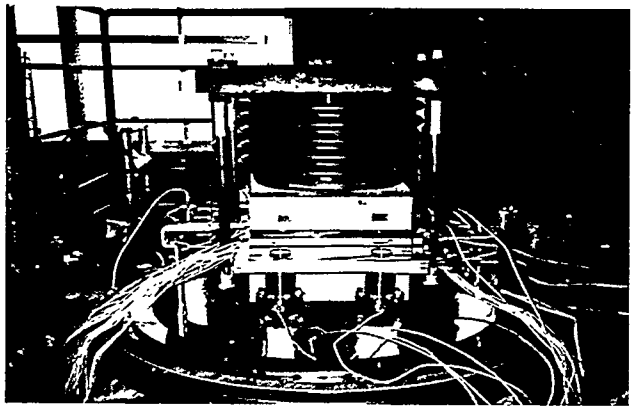

Figure 2--Assembled MCFC stack containing pre-unified cells and mechanically sealed manifolds.

REFERENCES

1. K. Murata, T. Shirogami, K. Ogimoto and Y. Sakamoto, STATUS OF MCFC DEVELOPMENT AT TOSHIBA", Fuel Cell Seminar Abstracts, pp147-150, Oct, 1986.

STATUS OF LARGE SIZED MCFC CELL & STACK TECHNOLOGY DEVELOPMENT AT HITACHI

Toshiki Kahara, Keizou Ohtsuka, Sei Takashima
Hitachi Works, Hitachi, Ltd.
1-1, Saiwaicho 3-chome, Hitachi-shi, Ibaraki-ken, 317 Japan

Masato Takeuchi, Yutaka Fukui
Hitachi Research Laboratory, Hitachi, Ltd.
4026, Kuji-cho, Hitachi-shi, Ibaraki-ken, 319-12 Japan

Shozou Nakamura
Hitachi Mechanical Engineering Research Laboratory, Hitachi, Ltd.
1-1, Saiwaicho 3-chome, Hitachi-shi, Ibaraki-ken, 317 Japan

SUMMARY

Hitachi, Ltd. has devised Multiple Large Capacity Type MCFC to achieve large size MCFC and developed a 25 kW class stack in FY1989. This stack was constituted of 22 cells with 1.21 m^2 electrode area. 28.3 kW generation which was the largest output by MCFC was successfully accomplished under the conditions of atmospheric pressure and 60 % fuel utilization at current density of 150 mA/cm^2.

INTRODUCTION

Research and development program of MCFC in Japan started in 1981, as a part of the Moon Light Project by the Agency of Industrial Science and Technology, Ministry of International Trade and Industry (AIST/MITI). This program is being promoted by MITI and New Energy and Industrial Technology Development Organization (NEDO). Hitachi, Ltd. has participated in this project from the first and the second phase program is being conducted.

In the first stage of the second phase, the targets are the development of a 100 kW class stack with large size (1 m^2 class) electrode and the trial of endurance test to be operated over 5000 hours. The development of a 1000 kW class stack is planned in the second stage.

Hitachi, Ltd. devised the multiple cell structure which is called Multiple Large Capacity Type (MLC Type) for enlarging the electrode area over 1 m^2 and has been engaged in researches of the cell components and the stacking technology. This paper described the development of a 25 kW MLC Type stack.

CELL STRUCTURE

The structure of MLC Type cell is shown in Fig. 1. The MLC Type cell has four pieces of unit electrode (unit small cell) in a cell plane. The unit electrode area was 3025 cm^2 at the 25 kW class stack; therefore, the total electrode area of MLC Type cell was 1.21 m^2. The merits of the MLC Type MCFC are as follows; (1) small gas pressure drop from inlet to outlet of a cell, (2) uniform gas distribution in a cell, (3) uniform temperature distribution of a cell, (4) handling feasibility of cell components, and so on.

CELL COMPONENT TECHNOLOGY

3600 cm^2 class cell components have already been made satisfactorily, and these technologies have been used for the MLC Type cells. Minor changes of the cell components, especialy electrodes and separator plates, are going on for higher performance and longer life. To maintain good cell performance during long term operation, a stabilized porous anode whose morphological condition and thickness do not change substantially needs to be developed. For this purpose, the addition of secondary elements in the porous nickel plate has been studied.
The addition of Al and Mg in nickel anode is very effective for the resistance to the shrinkage of an anode.

The separater plate is assembled in a process of soldering thin sheet metal plates with amorphous nickel under vacuum and at temperature of about 1000 ℃. The addition of Al and Y in 25Cr steel is very effective for improvement of anti-corrosion characteristics of the separator plates.

STACK TECHNOLOGY

A type of modules using an intermediate gas header has been developed as the basic configuration of the large capacity stacks, and a 10 kW stack with the module was operated over 3000 hours. A 25 kW class MLC Type stack was developed on the basis of this technology.

Fig. 2 shows a photograph of the 25 kW class MLC Type stack. The electrode area of a cell was 1.21 m^2 and the stack was constituted of 22 MLC Type cells. This stack adopted internal gas manifolds and cathode gas cooling system.

The result of long term performance of the 25 kW class MLC Type stack is shown in Fig. 3 under the operating conditions of atmospheric pressure and 60 % fuel utilization at current density of 150 mA/cm^2. This stack was operated successfully for 1612 hours.

ACKNOWLEDGMENTS

Most of the work described in this paper was performed under the support of the Agency of Industrial Science and Technology, Ministory of International Trade and Industry (AIST/MITI), and New Energy and Industrial Technology Development Organization (NEDO) in Japan.

REFERENCES

1. M.Takeuchi, K.Tamura, Y.Hishinuma and K.Ohtsuka; " Development of Electrode and Electrolyte Plate for Molten Carbonate Fuel Cell. ", 1986 Fuel Cell Seminar Abstracts, pp.215-218, Oct.,1986.
2. K.Ohtsuka, T.Kahara, R.Oshima and S.Akimaru; "Status of Molten Carbonate Fuel Cell Technology Development at Hitachi.", 1987 Fuel Cell Technology and Applications, Extended Abstracts, pp.51-60, Oct.,1987.
3. K.Ohtsuka, T.Kahara, S.Takashima, R.Oshima, M.Takeuchi, Y.Fukui and N. Kobayashi; " Status of MCFC Cell & Stack Technology Development at Hitachi." 1988 Fuel Cell Seminar Abstracts, pp.394-397, Oct.,1988.
4. M.Takeuchi, H.Okada, T.Mori, I.Sone, Y.Hishinuma, K.Ohtsuka and T.Kahara ; " The Stabilization of Electrodes for Molten Carbonate Fuel Cell." 1988 Fuel Cell Seminar Abstracts, pp.331-334, Oct., 1988.

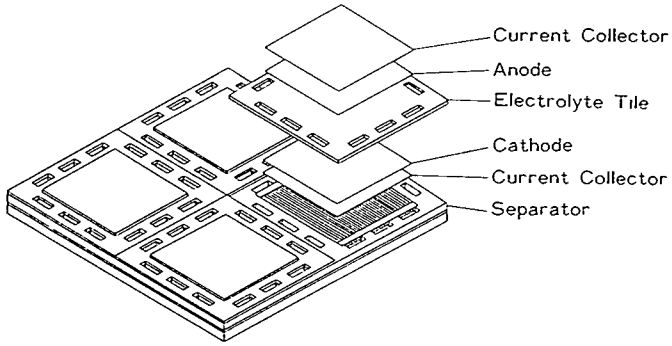

Fig.1 Cell Struture of Multiple Large Capacity Type (MLC Type) MCFC

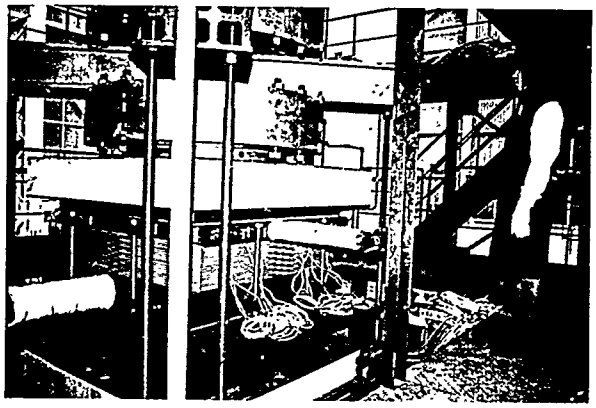

Fig.2 25 kW Class Multiple Large Capacity Type Stack

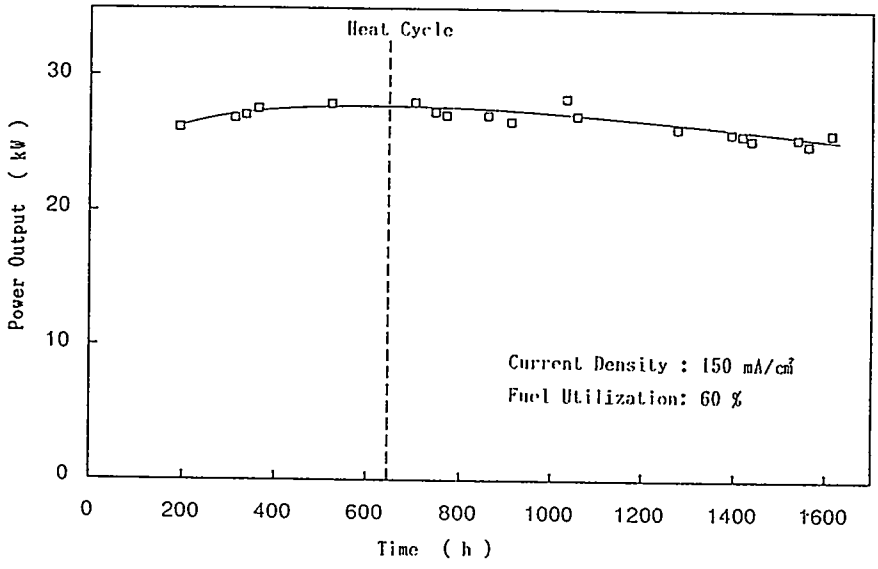

Fig.3 Long Term Performance of 25 kW Class Stack

IHI LARGE SIZE MOLTEN CARBONATE FUEL CELL ADVANCEMENTS

M.Hosaka, Y.Yamamasu, Y.Kato
A.Suzuki and S.Sato
Ishikawajima-Harima Heavy Industries Co., Ltd
Tokyo, Japan

1. INTRODUCTION

The molten carbonate fuel cell (MCFC) is a promising option for highly efficient and enlargeable power generation. IHI has been studying large size parallel flow MCFC stacks with internal manifolds. In 1987FY, the single cell test which had $1m^2$ electrode area was conducted. Since then we made several $1m^2$ stacks and a $1.4m^2$ stack.

2. POST TEST ANALYSIS OF $1m^2$x9 CELL STACK

We presented the test results of $1m^2$x9 cell stack before.[1] Cells showed stable performance except one cell. The evaluation test of the stack was terminated after 2250 hours atmospheric operation. Fig.1 shows the distribution of carbonate loss in a cell. There is some relation between the temperature distribution and potassium carbonate loss. The loss of potassium carbonate is higher at the outlet than at the inlet. The loss of lithium carbonate is almost uniform but larger than that of potassium all over the cell. This is caused by lithiation of chromium in the anode and the corrosion of hardware. These tendency was almost the same as the results of other tests conducted before.

For the external manifolding system, it is known that the migration of electrolyte from the positive end to the negative end of the stack takes place by the reason of carbonate transport through the manifold's gasket. The mobility of lithium ion is different from that of potassium ion, thereby the cationic composition changes locally. Fig.2 shows the result of the stack. The change of the Li/K ratio was small. For internal manifolding system, the migration seems to be small.

3. PRESSURIZED TEST OF $1m^2$x10 CELL STACK

The $1m^2$x10 cell stack was assembled at IHI and was equipped into the facility of CRIEPI. Fig.3 shows each cell voltage in the case of 80% fuel utilization. The deviation of voltage were small and the stack generated 11kw. The average voltage 0.66v was lower than the past small stacks. The high electric resistance of $0.06m\Omega$ was the reason for the lower cell voltage. Fig.4 shows the effect of pressure on the cell voltage. There is approximately semi-logarithmic relationship between the voltage and operated pressure.

4. SHORT STACK TEST WITH 1,4m^2 ELECTRODE AREA

Enlargement of electrode area has advantages to manufacture a large-sized internally manifolded stack in respects of improving the flow distribution and decreasing the ratio of ineffective area of separator. A 1.4m^{2}x2cell stack was tested to decide the cell size for the 100kw stack which will be fabricated under the NEDO program. The test made clear the following requirements.

(1)The accuracy of separator height should be higher. This was caused by the process of plastic deformation.

(2)The manufacturing technologies should be studied to get larger and uniform electrodes.

This test was terminated after 2100 hours operation. The stack generated 3.4kw at 175mA/cm^2 and 70% fuel utilization. The electric resistance was from 0.05 to 0.06 mΩ which was larger than that predicted from 1m^2 cell as well as small cells. This might be caused by the accuracy at separator fabrication. Fig.5 shows the performance of the stack. If the electric resistance of the large cell can make same as that of bench scale cell, both potentials will be almost the same. This means that the difference of the potential is mainly caused by the contact resistance of each components of cell. The contact of large cell is worse than that of small cell. Fig.6 shows the relation between electric resistance and electrode area. Fig.7 shows the distribution of gas utilization in the stack. The deviation was ± 5%. The distribution of gas flow was better than that of ordinary 1m^2 cells.

5. CONCLUSION

(1)By operating the large size MCFC including the largest 1.4m^2 cell, we get a perspective to construct large cell and we find that it is important to improve the contact resistance for large cell in order to get higher cell performance.

(2)For internal manifolding system, the migration problem seems to be negligible.

ACKNOLEDGEMENT

This work are performed under the sponsorship of MITI and NEDO. The evaluation of pressurized test was supported by CRIEPI.

REFFERENCE

(1)M.Hosaka;"The Development of Parallel Flow MCFC Stack at IHI",Sep.1989 Japan, Proceedings of the first International Fuel Cell Work-Shop.

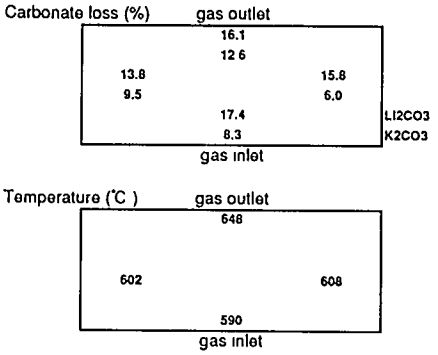

Fig. 1

DISTRIBUTION OF CARBONATE LOSS IN A CELL
(1m²x 9 cell stack)

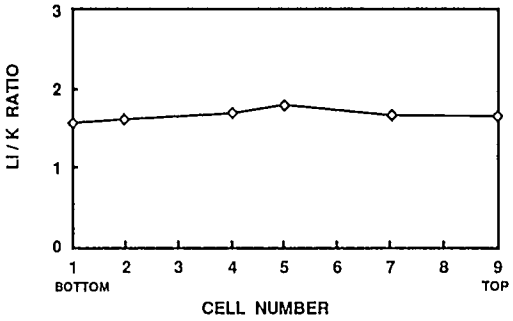

Fig. 2

DISTRIBUTION OF Li / K RATIO OF CARBONATE
IN THE TILE (1m²x 9 cell stack)

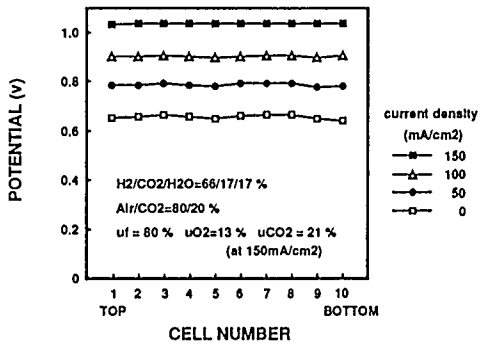

Fig. 3

DISTRIBUTION OF CELL POTENTIALS
FOR 1m²x 10 CELL STACK

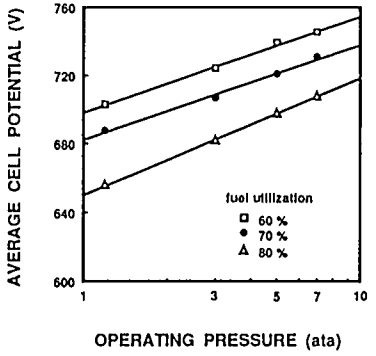

Fig. 4

EFFECT OF PRESSURE ON CELL POTENTIAL
FOR 1m²x 10 CELL STACK

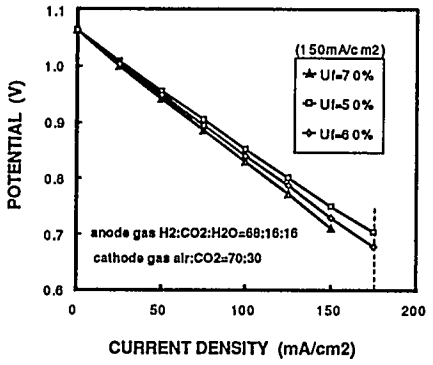

Fig. 5
PERFORMANCE OF 1.4m^2 x 2 CELL STACK

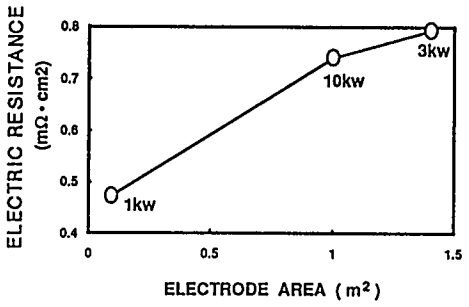

Fig. 6
RELATIONS BETWEEN ELECTRIC RESISTANCE AND ELECTRODE AREA

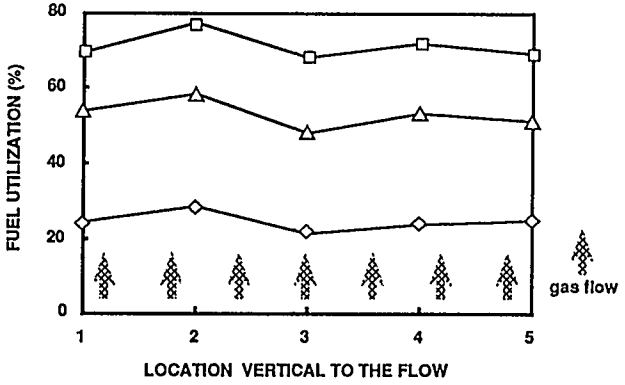

Fig. 7
UTILIZATION DISTRIBUTION OF 1.4m^2 x 2 CELL STACK

6kW CLASS MCFC TEST WITH GAS RECYCLING

Y.Mugikura, T.Watanabe ,Y.Izaki, H.Saitoh, K.Shimazu
and T.Abe
Central Research Institute of Electric Power Industry
(CRIEPI)
6-1, Nagasaka 2-chome, Yokosuka-shi, 240-01, Japan

T.Matsuyama, T.Shimizu, S.Sato and M.Ogoshi
Ishikawajima-Harima Heavy Industries Co., Ltd. (IHI)
1-15, Toyosu 3-chome, Koto-ku, Tokyo, 135, Japan

1. Introduction

For early realization of a molten carbonate fuel cells (MCFC) power plant, it is necessary to establish the operation technology of MCFC with gas recycling (cathode gas recycling, anode gas recycling, and carbon dioxide recycling) which are indispensable for a MCFC power plant. However, hardly anyone has studied this technology. In November 1988, CRIEPI has established a test facility which can be used for the tests of 10 kW class MCFC stacks with three gas recycling under pressurized condition.

Recently, CRIEPI and IHI jointly conducted the tests of 6 kW class MCFC with the gas recycling under pressurized conditions. The basic characteristics of the stack with three gas recycling were obtained by these test results.

2. Stack specification and its basic characteristics

The stack used in the tests consisted of 18 cells with an electrode area of 3,120 cm^2 each. The stack was designed as co-flow configuration with the internal manifolding.

At the initial stage of the tests (heated for about 250 hours), the average cell voltage was 751 mV at 150 mA/cm^2 and the power output was 6.33 kW under the atmospheric pressure with 80% fuel utilization. The stack was tested for about 2,000 hours.

3. Gas recycling characteristics

The purpose of the cathode gas recycling is to cool the stack through a heat exchange process, which is achieved by returning the part of the cathode outlet gas to the inlet of the cathode. The cathode gas recycling ratio β is defined by Equation (1). These gas flow rates in the Equation (1) were estimated from the pressure drop between the inlet and the outlet of the cathode.

$$\beta\ (\%) = \frac{\text{Recycled gas flow rate}}{\text{flow rate at the cathode outlet}} \times 100 \quad (1)$$

The tests were conducted on the cathode gas recycling only. Fig.1 summarizes the relationship between the overall oxygen utilization and the amount of cathode inlet gas flow. The cathode gas recycling ratio was adjusted to keep the

stack temperature constant when the overall oxygen utilization was changed. As a result, it was possible to control the stack temperature by the cathode gas recycling to remove the heat generated in the stack.

The purpose of the anode gas recycling is to increase the overall power generation efficiency by recycling the unreacted fuel included in the anode outlet gas. The anode gas recycling ratio α is defined by Equation(2). These gas flow rates in the Equation(2) were estimated from the pressure drop between the inlet and the outlet of the anode.

$$\alpha\ (\%) = \frac{\text{Recycled gas flow rate}}{\text{gas flow rate at the anode outlet}} \times 100 \quad (2)$$

The tests were conducted on the anode gas recycling only. In the tests, the anode gas recycling ratio was changed keeping the supplying fuel flow rate constant. As a result, it was possible to use the fuel more effectively by recycling and raising the overall fuel utilization up to 90 %. The relationship between the anode gas recycling ratio and the energy conversion efficiency of the stack is shown in Fig.2. When the anode gas recycling ratio rose to 71 % with the overall fuel utilization of 90 %, the energy conversion efficiency reached to about 53 % (LHV).

The Carbon dioxide recycling is a method to supply carbon dioxide generated at the anode to the cathode. The anode outlet gas contains the combustible gases that have not yet reacted. Hence, These are supplied to cathode only after they are mixed with air and burned by the catalytic combustor.

In the case of the tests with the carbon dioxide recycling, we used a catalytic combustor located in the cathode gas recycling line. The reason for using the cathode gas recycling with the combustor was not only to keep the stack temperature constant, but also to keep the temperature at the outlet of the combustor from rising. The condition when the carbon dioxide recycling was accomplished is presented in Fig. 3. As the figure shows, the carbon dioxide flow rate at the cathode which had to be supplied in the usual MCFC operation tests, became zero. As a result, it was possible to oprerate a MCFC power plant merely by supplying fuel and air to the plant as the conventional thermal power plants.

The fuel utilization characteristics of the stack with the gas recycling are summarized in Fig. 4. When the fuel utilization changed, the tendency of the change of the average cell voltage did not vary significantly in any case. These results suggest that the anode has significant influence on the performance of the stack with gas recycling.

4. Conclusion

The test results presented here demonstrate that it is possible to generate power by supplying only fuel and air to

a MCFC power plant. Moreover, the test results clearly show that the anode gas recycling is an effective way of increasing the efficiency of a MCFC power plant at this stage. We believe that these test results will accelerate further the realization of a MCFC power plant.

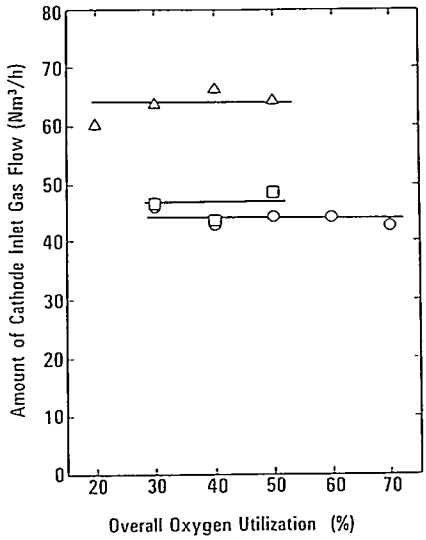

Fig.1 Effect of Cathode Gas Recycling

Temperature of Stack	: About 630°C
Fuel Composition	: $H_2/CO_2/H_2O=66/17/17$
Fuel Utilization	: 50%
Oxidant Composition	: $Air/CO_2=70/30$
Current Density	: 150mA/cm²
Operation Pressure	Hot Time
○ 6 kg/cm²G	: About 1250 hours
□ 2 kg/cm²G	: About 870 hours
△ 0 kg/cm²G	: About 310 hours

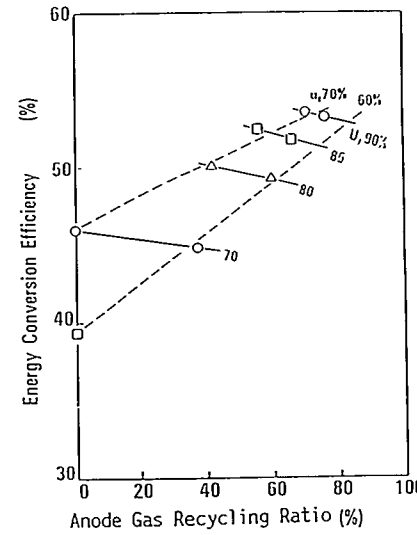

Fig.2 Effect of Anode Gas Recycling

U_f : One Pass Fuel Utilization
U_F : Ovreall Fuel Utilization (Including Anode Gas Recycling)

Fuel Compositions	$H_2/CO_2/H_2O=66/17/17$
Oxidant Compositions	$Air/CO_2=70/30$
Oxidant Utilization	23~45%
Current Density	150 mA/cm²
Operation Pressure	6 kg/cm²G
Hot time	1250 hours

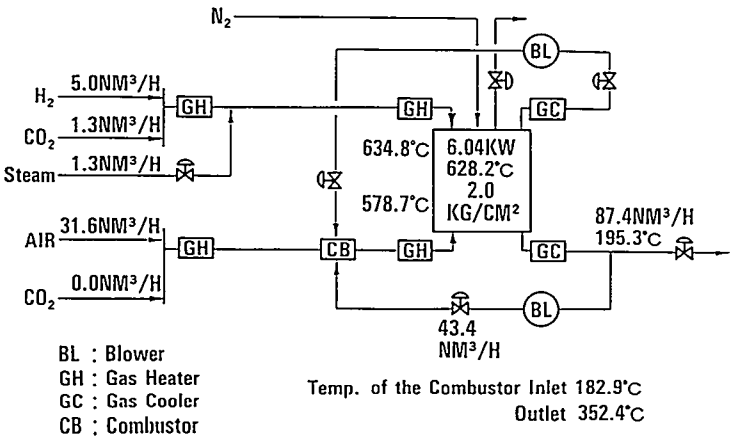

Fig.3 Result of Carbon Dioxide Recycling

Fig.4 The Fuel Utilization Characteristics of Gas Recycling

Fuel Composition : $H_2/CO_2/H_2O=66/17/17$
Oxidant Composition : $Air/CO_2=70/30$
(Air=100 For Carbon dioxide Recycling)
Overall Oxygen Utilization : 30%
(Except Case With No Gas Recycling and Case With Anode Gas Recycling)
Curreat Density : 150mA/cm²
Operation Pressure : 6 kg/cm²G
Hot Time : About 1200~1300 hours

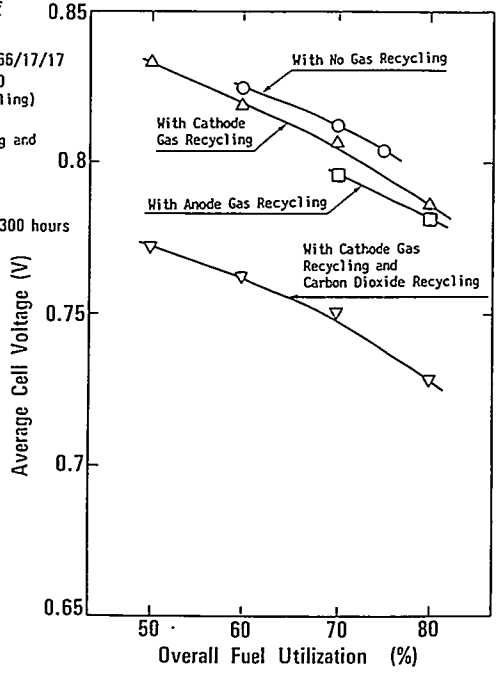

SOLID OXIDE FUEL CELL DEVELOPMENT AT FUJI ELECTRIC

K. Koseki, N. Kusunose, K. Shimizu, H. Shundo
T. Iwata, S. Maruyama and T. Nakanishi
Fuji Electric Corporate Research and Development Ltd.
2-2-1, Nagasaka, Yokosuka City, 240-01, Japan

1 Introduction

We have been developing planar solid oxide fuel cells because planar type fuel cells appear to have a high power density and to be economical. Two planar fuel cells, with the designs shown in Figure 1, are being developed. One is a conventional thin tri-layer (anode/electrolyte/cathode) design which we call a self-supported structure. The other is a new design which we call a substrate structure. In this design, thin electrolytes and cathodes are applied to thick porous anode substrates. An alternate design using thick porous cathodes as substrates is feasible if the porous cathodes are mechanically strong.
The self-supported structure has a higher power density than the substrate structure because the thick substrate of the substrate structure hinders gas diffusion, which restricts current density. The thin electrode of the self-supported structure does not hinder gas diffusion. The self-supported structure is also relatively easy to fabricate. However, its thin structure is mechanically too weak to permit large cell areas. The maximum electrolyte plate size is limited to about 10 $\times$10cm with a thickness of 0.2$\sim$0.3mm. Therefore, the applications are restricted to military or space applications, where small, compact, high power density power sources are required.
On the other hand, the substrate structure permits the fabrication of large electrolyte plates because the thick anodes can support the thin electrolyte plates. Electrolyte plates as large as 40$\times$ 40cm can be obtained with 2$\sim$3 mm thick anodes, although the power density will be lower than that of similar self-supported structures for the reasons given above. The fabrication of substrate structures is more difficult than that of self-supported structures. However, large electrolyte plates make it possible to construct large capacity fuel cells, which allows applications to be extended to power plants for dispersed or central power stations.
The following is the present status of development of these two structures at Fuji Electric.

2 Self-supported structure planar SOFC

2-1 Fabrication

The materials used for electrolyte plates, anodes and cathodes are 8 mol% Y_2O_3 stabilized ZrO_2 (YSZ), NiO-YSZ and

$La(Sr)MnO_3$ respectively. Electrolyte plates of 300 μm thickness were obtained commercially. NiO-YSZ and $La(Sr)MnO_3$ were applied in a slurry coating to the surface of the electrolyte plate, and were sintered at elevated temperatures.
The tri-layer plate thus obtained was assembled in a cell housing made of a heat resistant alloy, and was subjected to single cell tests. A stack was assembled by alternating tri-layer plates and alloy interconnections with ribs in sequence and by attaching fuel and air manifolds to the sides of the stack.

2-2 Cell performance
Single cells with active electrode areas of 10 cm^2 and 60 cm^2 were tested. The solid lines in Figure 2 show the typical I-V characteristics obtained. The maximum power obtained with the 10 cm^2 and 60 cm^2 cells was 0.48 W/cm^2 at 1 A/cm^2 and 0.3 W/ cm^2 at 0.6 A/cm^2 respectively.
A three-cell stack with an electrode area of 40 cm^2 was also built and tested. The stack was successfully operated, although its performance was a little worse than that of single cells.

3 Substrate structure planar SOFC

3-1 Fabrication
A 3 mm thick porous NiO-YSZ cermet disc was made by cold pressing, followed by sintering. Integral ribs were machined on one side of the disc. The ribbed disc was used as a substrate and anode. A thin YSZ electrolyte layer was plasma sprayed on the flat side of the disc. Then, a $La(Sr)MnO_3$ cathode was applied in a slurry coating to the YSZ layer. Fuel and air inlet holes were made near the center of the disc.
The single cell thus obtained was assembled with a ribbed interconnection made from $La(Sr)MnO_3$ and metal end plates, and was subjected to single cell tests.
A stack was fabricated by alternating single cells and interconnections in sequence. Although the interconnections should be made from a $La(Sr)MnO_3$/ $La(Ca)CrO_3$ composite in practical cells, $La(Sr)MnO_3$ covered with a metal sheet on the cathode side was used instead.

3-2 Cell performance
Single cells with electrode areas of 10 cm^2 and 50 cm^2 were tested. The dotted lines in Figure 2 show the typical I-V characteristics obtained. The open circuit voltage of these cells is about 0.1 V lower than that of cells with self-supported structures. This is probably caused by cross leakage of gas through the plasma-sprayed electrolyte because of its low density. In spite of this defect, the 10 cm^2 cell produced 0.25 W/cm^2 at 0.5 A/cm^2, and the 50 cm^2 cell produced 0.13 W/cm^2 at 0.25 A/ cm^2.
A stack with an electrode area of 50 cm^2 is under

construction, and will be tested in the very near future.

4 Future tasks

Some technical issues must be resolved before a reliable large stack can be developed:
(1) Matching the thermal expansion coefficient of components,
(2) Producing denser plasma-sprayed electrolyte layers,
(3) Producing denser plasma-sprayed $LaCrO_3$ interconnection layers,
(4) Reinforcing substrates,
(5) Sealing gases,
(6) Reducing contact resistance.
At present, the prospects are good for the resolution of the first two items. The last two problems are more difficult. The technologies that will allow us to solve them are the key to the success of planar SOFC.

5 Conclusion

We have been developing two types of planar SOFC structures, a self-supported one and a substrate one. Both types have shown good I-V characteristics in single cell tests. Stack performance is still not as satisfactory as that of single cells. Some issues remain yet to be solved.
Although building a stack of substrate structures is difficult, the substrate structure is very attractive because large fuel cells can be constructed using it. At present, we are focusing our efforts on this type.

6 Acknowledgement

This work has been supported by NEDO. We would like to express our thanks to NEDO for their help with it.

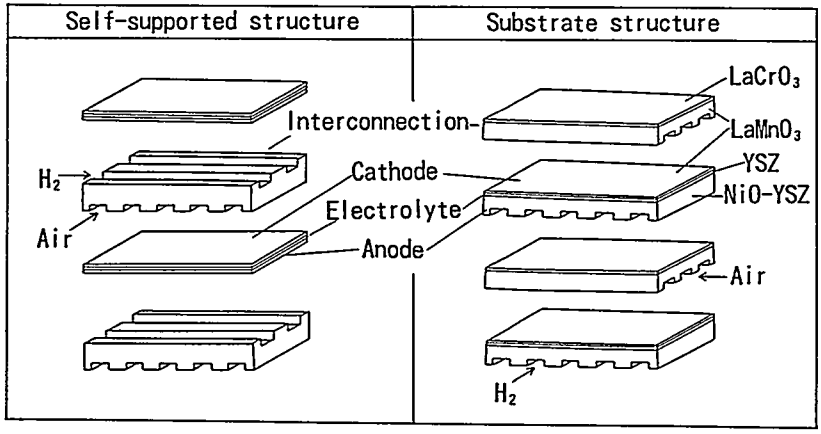

Fig. 1. Configuration of planar SOFC

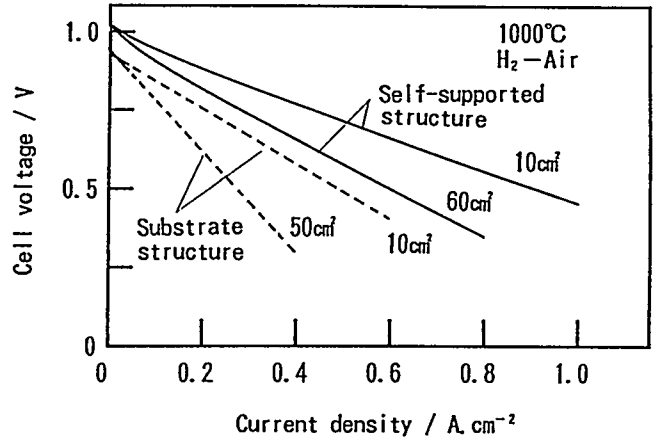

Fig. 2. I-V characteristics of planar single cells

SOLID OXIDE FUEL CELLS: CFP DESIGN AND CELL PERFORMANCE

R. F. Singer, F. J. Rohr and A. Belzner

ABB Corporate Research
Eppelheimer Str. 82
D - 6900 Heidelberg, Germany

The pioneering work on Solid Oxide Fuel Cells (SOFCs) was done in the 1960s and 1970s at Westinghouse Research and Development Center in Pittsburgh and ABB Corporate Research Center in Heidelberg (then Brown Boveri). ABB stopped its work in 1978 because it seemed unlikely that the cost goal could be reached. The concept pursued at the time was a tubular one [1]. Work has been resumed recently with the emphasis on design concepts which promise to lower the costs significantly as compared with the tubular concept.

Fig. 1 shows our Ceramic Flat Plate (CFP) design. The individual cells are mounted on a porous ceramic support plate. The exact geometry of the cells and the interconnect will depend on the fabrication processes to be used. So far we have produced the support plate by extrusion and the active layers by tape casting, screen printing or plasma spraying.

The CFP design promises important reductions in fabrication costs as compared to tubular designs:

- The single element size is much larger. There is a smaller number of parts to be inspected, installed and connected to build up a SOFC system. A larger piece can be fabricated in one production step.

- The flat geometry makes it easier to use modern low cost ceramic fabrication technologies like tape casting, screen printing etc.

In the following some experimental results on single cells will be reported. We have prepared single cells by tape casting of the electrolyte and air plasma spraying of the electrodes. The cell size was 44 mm x 44 mm, layer thicknesses were 220 µm, 80 µm, and 50 µm for the electrolyte, air electrode, and fuel electrode resp. As materials $(ZrO_2)_{0.92}(Y_2O_3)_{0.08}$, $(La_{0.84}Sr_{0.16})$ Mn O_3, and Ni/ZrO_2 30/70 were used for the electrolyte and the electrodes resp.

For power density measurements single planar cells were spring loaded between two alumina tubes as shown in Fig. 2. Rings of platinum sheet were used as current collectors and as gas seals. This measurement method yields power densities which decrease with increasing cell diameter. Ohmic losses in the electrode layers are more significant for large cells, where the conduction paths in the electrode planes are longer.

We performed a series of measurements where we varied the active cell diameter using identical samples of trilayer composite. Hydrogen was used as fuel with an utilization of up to 8 %. The oxidant side was supplied in turns with pure oxygen and air with an excess ratio of about four compared to the total fuel flow. In Fig. 3 maximum power densities measured at 1000°C are shown as a function of the cell diameter. Information of this kind will be crucial for the final optimization of the geometry of the CFP design.

By extrapolation of the measured power densities to cell diameter zero we obtain an "upper bound power density" which is not affected by size or shape of the active cell area. Our data as plotted in Fig. 3 indicates "upper bounds" of about 3.5 kW/m^2 for hydrogen versus air, and 9 kW/m^2 for hydrogen versus oxygen at 1000°C. These are satisfactory results.

The extrapolation to cell diameter zero can be performed in an analytical way, if cell resistances rather than power densities are used. Cell resistances are determined from experimental IV curves as the slope of the linear part of each curve. The resistance as a function of the cell diameter was derived earlier for our geometry (2). In Fig. 4 data points for the cell resistances are shown together with interpolation lines obtained by a least square fit using the analytical formula from Ref. (2).

It should be noted that the cell resistance depends not only on the ohmic resistivities of the cell components, but also contains terms describing diffusion polarization, as far as they are proportional to the current density, i. e. as far as the diffusion polarization behaves "pseudo ohmic". Measurements with oxygen yield lower cell resistances than measurements with air. This is due to a reduction of the diffusion polarization in the cathode layer in the former case.

In Fig. 3 the interpolated cell resistances are converted to power densities. For this purpose, an open circuit voltage of 1 V was assumed and power losses by non ohmic diffusion polarization were neglected. The "pseudo ohmic power densities" shown in Fig. 3 exceed the measured values, especially at lower cell diameters. Both the comparison of air and oxygen resistances in Fig. 4 and the comparison of measured and calculated values in Fig. 3 illustrate a potential for further improvement which will result from the optimization of structure and thickness of the electrode layers.

REFERENCES

1. F. J. Rohr, in:
T. Takahashi (Ed.), Application of Solid Electrolytes, JEP Press, Cleveland, 1980, p. 196.

2. H. J. Böhme, Raumfahrtforschung **4**, 154-156 (1970)

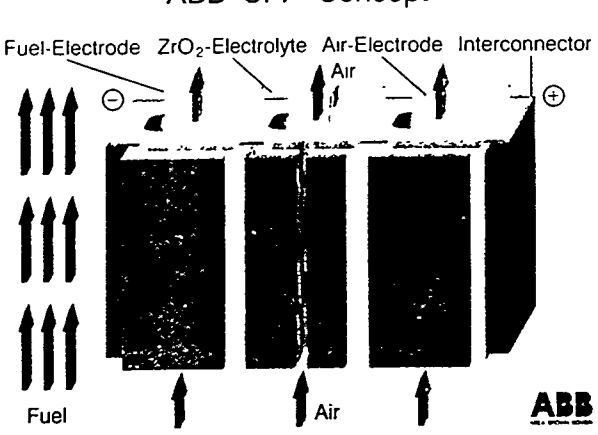

Fig.1 The new CFP design promises a reduction in fabrication costs through the larger element size and the flat surface.

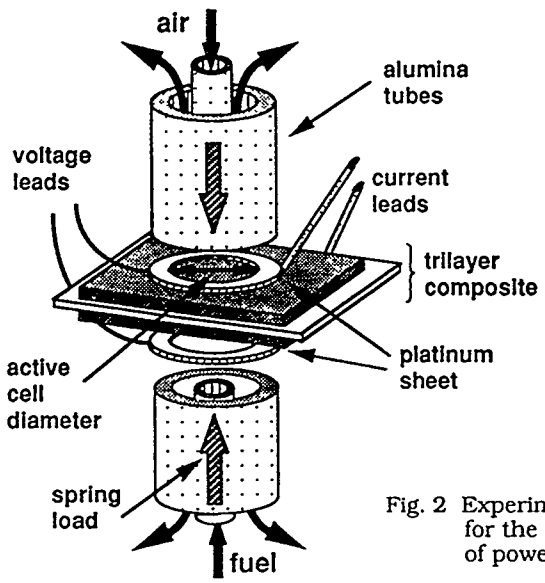

Fig. 2 Experimental set-up for the measurement of power densities

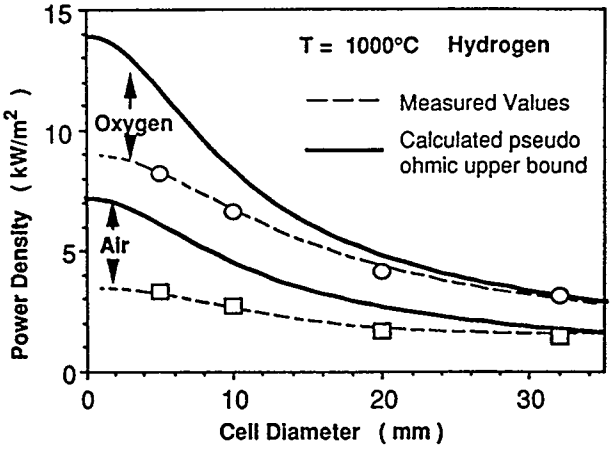

Fig. 3 Measured power densities for CFP single cells as a function of the cell diameter. The calculated curves serve to illustrate the improvement potential.

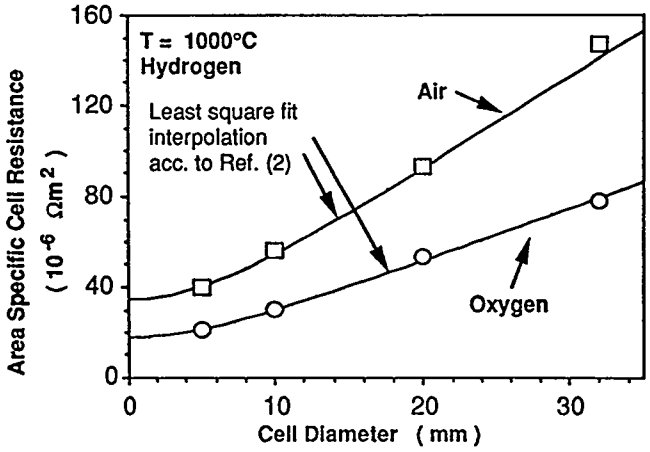

Fig. 4 Area specific cell resistances as a function of the cell diameter. The least square fit interpolation of cell resistances is used to calculate the pseudo ohmic upper bound power densities in Fig. 3.

PLANAR SOLID OXIDE FUEL CELL TECHNOLOGY DEVELOPMENT

Michael Hsu and Harold Tai

Ztek Corporation
Lincoln, MA 01773

INTRODUCTION

In recent years the application of fuel cells for commercial power generation and cogeneration has gained worldwide recognition. Most obvious benefits of the fuel cell systems include high efficiency; quiet, pollution-free operation; and multi-fuel capability including natural gas, petroleum based fuels and coal derived fuels.

Among the various choices of fuel cells, solid oxide fuel cells have the following distinct advantages:

1. Reforming of hydrocarbons occurs directly in the fuel cell assembly at an elevated operating temperature, eliminating the need for a separate reformer.
2. Accepting CO, CO_2, and a range of variations in impurities in fuel composition with minimum impact to cell performance, alleviating the need for fuel treatment.
3. The zirconia electrolyte, a solid material, serves as its own structural support, resulting in compact and lightweight assembly.
4. The zirconia electrolyte is physically and chemically stable. The requirement of electrolyte management in operation, a demanding task with other types of fuel cells, is eliminated. The system can have an indefinite shelf life.

Since 1974, the principals of the company have been engaged in the research and development effort of the solid oxide fuel cells of planar configuration using zirconia electrolyte. The work has resulted in low-cost components fabrication techniques, a compact packaging approach, and a simple integration approach for zirconia cell stacks. The work includes commercial applications and space applications.

ZIRCONIA CELL

Zirconia, a refractory ceramic material, can be used as the electrolyte in electrochemical cells due to its unique property to conduct oxygen ions but not electrons at an elevated temperature of 1000°C. Ztek's baseline technology comprises:

- Fabrication of free-standing electrolyte/electrodes plates
- Fabrication of free-standing interconnector plates
- Assembly of the plates by compression and flux seal
- Internal manifolding for reactants distribution

The Zirconverter®, the zirconia power package as assembled, is constructed of thin plates of zirconia electrolyte alternately arranged with interconnector plates. A cell stack is shown in Table I. The electrolyte plates are made of thin zirconia

plates with electrode coatings. The interconnector plates are fabricated from corrosion-resistant conducting materials.

Internal gas passages through the plates provide the reactants, and permit the resultants to exit. The distribution of gases to the surface of the electrode occurs along grooved networks formed in interconnectors. Gas seals and electrical contact between plates are obtained in the assembly by spring loading the interconnector plates against the surface of the electrolyte/electrodes plates. The interconnectors have a multi-function role as gas separator, gas manifold, thermal path, electric collector, cell interconnector and sealing gasket. The material selections for the interconnector plates are based on the following requirements:

1. The material is able to maintain its strength, and electrical and thermal conductivities at 1000°C, which is the operating temperature of the device.
2. The material has good oxidation resistance up to the working temperature.
3. The material is chemically stable with fuel species.
4. The material can be economically formed in a corrugated plate configuration.

To facilitate heat rejection radially in the cell stacks, plates of 10-15 cm diameter are considered to be the proper choice for either near-term demonstration devices (kilowatts) or future larger power systems.

The zirconia cell of modular design can be conveniently packaged as a small kW-level generator and also serve as the building block in scaled-up MW-level applications. Table I summarizes the performance specifications and power capability of the Zirconverter® assembly. A schematic in Table II shows the megawatt packaging where the columnar shaped modules of 10-20 kW size are constructed from the planar cell stacks. Additional information is available. The distinctive features that make this cell stack suitable for practical power applications are:

- High power density
- Structural ruggedness
- Ease of heat removal
- Low stress assembly

One technical challenge in dealing with the zirconia electrolyte is its brittleness in tension, which can be caused by the thermal differential expansion among materials used in the assembly, as well as by temperature gradient in a system. The Ztek design utilizes a unique composite structural technique to take advantage of the high compression strength of zirconia. The approach applies the complementary properties of the components to alleviate tensile stress in the ceramic component while enabling high-power density packaging. Efforts that others have pursued, such as the tubular configuration zirconia fuel cell by Westinghouse, and the monolithic stack by Argonne/Allied Signal, use compounds which have matching thermal expansion. These approaches have led to

materials of inferior mechanical and electrical properties. Furthermore, they do not eliminate the stress condition due to thermal gradient. A comparison of the three assembly techniques is given in Table II.

TECHNOLOGY STATUS Commercial/Industrial/Utility Applications

Ztek has successfully fabricated full-size electrolyte and interconnector plates. A ten-cell stack was tested for 1000-hours continuous operation. The major accomplishments are as follows:

1. A prototype fuel cell system with automatic control for unattended operations has been demonstrated.
2. Low-cost, high-yield fabrication processes have been established.
3. The engineering techniques for scaling to 20kW modules have been established.
4. Projected life of the cells will exceed 5 years.
5. The stack can withstand thermal cycling without damage. A quick thermal transient capability of 100°C/min was demonstrated.
6. A surface power density of 250mW/cm^2 has been demonstrated in a single-cell experiment. The ten-cell stack test achieved 25W of power output.

The fuel cell stack integrated with a gas/electric dual-mode furnace was tested, demonstrating operational safety, and start-up and shut-down procedures. Self-reforming of light-weight hydrocarbon fuel has been demonstrated. Continuous operation without carbon deposition was maintained.

ECONOMIC POTENTIAL

Preliminary study of the production costs has been conducted. The direct material cost for the Zirconverter® has been estimated to be less than $150/kW(e). The peripherals in the system, including an enclosure, reactants conditioning equipment, and piping, is about $150/kW(e). The fabrication and assembly cost is estimated to be about $50/kW(e). The low peripherals cost resulting from the elimination of the reformer, more than compensates for the relatively high cost of the stack. The total estimated direct cost (material and labor) of the assembled fuel cell system is about $350/kW(e). Ztek will produce and market the Zirconverter® under a fully patented technology in design, fabrication and integration.

COMPLEMENTARY ACTIVITIES

Ztek is proceeding simultaneously in various efforts on technology or system development of the zirconia cells:

1. Continuous development of high yield, mass production methods for electrolyte/electrodes plates.
2. Development of compatible heat-exchanger/reformers for direct thermal integration with the zirconia cell stacks.

3. Engineering and construction of a kW-level on-site cogeneration system for industrial applications.
4. Evaluation of zirconia fuel cells for electric utility applications.
5. Development of lightweight systems for space applications.

The above activities have been carried out via cost sharing with corporate funds and external contracts with agencies including the Electric Power Research Institute, the Department of Energy and the Department of Defense.

TABLE I ENGINEERING SPECIFICATIONS OF ZIRCONVERTER®

ZTEK

100 WATT STACK

	English Units		Metric Units	
Current Density	300	Amp/ft^2	3000	Amp/m^2
Voltage Per Cell	0.7	Volts	0.7	Volts
Cell Diameter	4	Inches	10	cm
Cell Height	1/16	Inch	1.6	mm
Cell Planar Area (80%)	0.07	ft^2	0.007	m^2
Cell Number/Unit Length	192	/ft	600	/m
Total Current	21	Amp	21	Amp
Voltage Per Unit Length	135	V/ft	420	V/m
Power Per Unit Length	2.8	kW/ft	8.8	kW/m
Volumetric Power Density (70% Pack)	28	kW/ft^3	880	kW/m^3
Stack Weight/Power Near Term	2	lb/kW	1	kg/kW

TABLE II COMPARISON OF ZIRCONIA PACKAGING TECHNIQUES

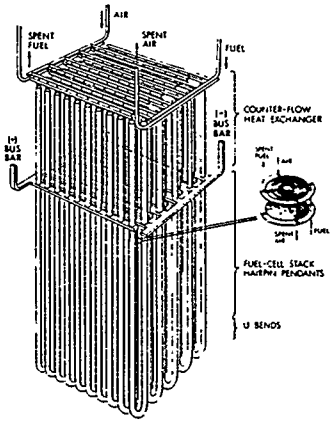

	Monolithic	Tubular	Zirconverter®
Compactness	Yes		Yes
Ease of Fabrication			Yes
Integration Simplicity			Yes
Good Thermal Characteristics			Yes
Mechanical Ruggedness		Yes	Yes
MW Scaling Feasibility		Yes	Yes

PEROVSKITE SOLID ELECTROLYTES FOR INTERMEDIATE TEMPERATURE SOLID OXIDE FUEL CELLS

Anthony F. Sammells, Ronald L. Cook, Daniel J. Kuchynka
Eltron Research, Inc.
4260 Westbrook Dr.
Aurora, IL 60504

and

Kevin Krist
Gas Research Institute
Chicago, IL 60631

Discussed here will be investigations directed towards the identification of perovskite solid electrolytes (ABO_3) possessing sufficiently high ionic conductivities, such that they may be attractive candidates for consideration in intermediate temperature ($\cong 600°C$) solid oxide fuel cells (SOFC's) operating at practical current densities. Our strategy has involved identifying empirical crystallographic related parameters which could be correlated to experimentally measured activation energies for ionic conduction and ionic conductivity in perovskite solid electrolytes. Considerations we are currently using for predicting new perovskite solid electrolytes include:

a) That cations introduced into perovskite A and B lattice sites are absent of multiple oxidation states, thereby avoiding electronic transport via this mechanism.

b) Ensuring that the perovskite crystallographic lattice possesses a relatively open structure or 'free volume' compatible with facilitating ionic mobility.

c) That weak association is present between mobile anions and the lattice bulk.

d) Ensuring that the aliovalent dopant cation introduced into the B lattice site for creation of oxygen vacancies necessary for promoting anionic conduction will possess a similar ionic radii to the B-cation it replaces.

e) That the saddle point critical radius (r_c) formed by two A and one B lattice site, through which mobile anions must pass between vacancies, are large enough so that minimal disturbance of the lattice occurs.

f) That the perovskites selected possess high thermodynamic stability.

g) That the inherent band gap between valence and conduction bands within the perovskite solid electrolyte is large enough to suppress parasitic electronic conductivity.

Empirical experimental observations found between perovskite crystallographic parameters and ΔE for anion conduction will now be addressed.

EMPIRICAL CRYSTALLOGRAPHIC PARAMETERS INFLUENCING ANIONIC CONDUCTION IN PEROVSKITES.

The ionic conduction pathway for oxygen anions through cubic perovskite lattice proceeds via octahedral oxygen edge sites.(1) The most important prerequisite for a stable perovskite structure is the existence of a stable BO_3 skeletal sublattice. Here, from geometric considerations, the B cation radii must exceed 0.51Å to achieve stable octahedral coordination in oxide based perovskites. The BO_3 skeletal sublattice can be further stabilized by large A site cations in cuboctahedral coordination at the center of six BO_6 octahedra. The presence of the A site cation generally distorts the BO_3 skeletal sublattice in order to attain optimal A-O bond lengths. When this distortion is too large, other crystal geometries such as orthorhombic or rhombahedral become favorable. The tolerance limits for cation radii in the A and B lattice site have been defined by the so-called Goldschmidt Tolerance Factor S given by:(2)

$$S=\frac{(r_A+r_o)}{\sqrt{2}(r_B+r_o)}$$

where r_A, r_B and r_o correspond to the respective ionic radii of lattice constituents. From geometric analysis, the ideal cubic structure should possess a tolerance factor of 1. However, cubic crystal structures for perovskites have been observed for tolerance factors between S = 1.04 to S = 0.95. Nominally, the perovskite structure should only be stable for $1.0 < S < .75$. To also achieve stability, the perovskite A lattice site must be stable in twelvefold coordination.(2) This places a lower limit on the A site cation size of $r_A >$ 0.90Å. For tolerance factors smaller than 0.90 but larger than 0.75, a cooperative buckling of the corner shared octahedra occurs (3), optimizing the A-O bond lengths, giving for most perovskites an O-orthorhombic crystal structure.

We have recently identified three empirical parameters which have been shown to exhibit strong correlations with activation energy for anion transport. These parameters are: 1) the average metal-oxygen bond energy in the perovskite, 2) the lattice free volumes, obtained by subtracting the ionic volumes of cations and O^{2-} in the unit cell from the overall crystallographic unit cell volume, and 3) the parameter $r_{critical}$ (r_c) which corresponds to the radius of the opening between the two A site cations and one B site cation through which the mobile anion must pass. These empirical parameters will now be briefly discussed.

i) Average metal-oxygen bond energy.

To estimate oxygen binding energies within perovskite solid electrolytes, we selected a relationship from which the average metal-oxygen bond energy (ABE) could be calculated from the starting oxide heat of formation, the metal heat of sublimation and the oxygen dissociation energy.(3) For perovskites where the A site cations are 12 coordinate and those for B sites 6 coordinate, the average perovskite bond energy can be given by:

$$ABE = \frac{1}{12 \cdot m}\left(\Delta H_{A_mO_n} - m\Delta H_A - \frac{1}{n} D_{(O_2)}\right) + \frac{1}{6 \cdot m}\left(\Delta H_{B_mO_n} - m\Delta H_B - \frac{1}{n} D_{(O_2)}\right)$$

where $\Delta H_{A_mO_n}$ and $\Delta H_{B_mO_n}$ are the heats of formation of the A_mO_n and B_mO oxides, respectively; ΔH_A and ΔH_B are the heats of sublimation of the metals A and B, respectively; and $D_{(O_2)}$ is the oxygen dissociation energy. These calculated average metal-oxygen bond energies were found to be linearly related to the activation energy for anion transport in perovskite solid electrolytes where activation energy for O^{2-} migration decreased with oxygen lattice bonding energy.

ii) Lattice free volumes.

We define the crystallographic 'free volume' (FV) as the difference between the perovskite unit cell volume and the summed volume occupied by all ions present within the perovskite unit cell of interest. Here, tabulated empirical ionic radii values were used (4) and corresponding perovskite unit cell volumes calculated from:(5)

$$a_o^3 \text{ (unit cell lattice edge)} = 2.37r_B + 2.47 - 2.00\ (S^{-1}-1)$$

which relates the ionic radii of the ions A^{n+} (r_A), B^{m+} (r_B) and O^{2-} (r_o) with the corresponding perovskite unit cell volume, where S is the Goldschmidt Tolerance Factor.(2) For perovskite solid electrolytes ΔE was found to increase as FV decreased.

iii) A-A-B perovskite crystallographic saddle point r_c.

The saddle point for ionic migration between two anion sites occurs via a triangle formed by two A site cations and a B site cation (Figure 7). The radius of a circle just touching the radii of these three cations is defined as r_c. We have calculated r_c values for over 400 ($A^{3+}B^{3+}O_3$ and $A^{2+}B^{4+}O_3$) perovskites found that the value of this parameter does not exceed 1.1Å while that for O^{2-} is 1.4Å. Thus, the crystallographic dimensions of the A-A-B saddle point through which O^{2-} migration proceeds would reasonably be expected to contribute

to ΔE. A relationship has been found between ΔE and the saddle point associated with r_c in the perovskite lattice.

With this thought in mind we plotted ΔE for O^{2-} migration through the perovskite lattice versus r_c for known O^{2-} conducting perovskite electrolytes. Here, as suggested by others (6), the value $(r_c/r_O 2-)^2$ was used as the correlation parameter. A smooth decline in ΔE for O^{2-} transport with increasing r_c was observed.

These three empirical trends relating perovskite crystallographic parameters to ΔE were incorporated with the Goldschmidt Tolerance Factor S in a multivariable analysis which assisted in the selection of perovskite solid electrolytes for intermediate temperature solid oxide fuel cells, several of which are summarized in Table 1.

TABLE 1

Perovskite Solid Electrolytes	σ_i ($\Omega^{-1}cm^{-1}$) at 600°C	t_i	ΔE(eV)
$SrZr_{0.9}Sc_{0.1}O_{3-\alpha}$	2.02×10^{-4}	.89	.89
$SrCe_{0.9}Gd_{0.1}O_{3-\alpha}$	5.3×10^{-3}	.84	.62
$LaGd_{0.9}Cd_{0.1}O_{3-\alpha}$	2.2×10^{-5}	.78	.80
$EuTh_{0.9}Gd_{0.1}O_{3-\alpha}$	6.1×10^{-5}(700°C)	.65	.64
$BaCe_{0.9}Gd_{0.1}O_{3-\alpha}$	2.3×10^{-3}	.86	.52
$BaTb_{0.9}In_{0.1}O_{3-\alpha}$	5.4×10^{-2}	.87	.45
$LaSm_{0.9}Ca_{0.1}O_{3-\alpha}$	2.8×10^{-4}	.80	.71
$LaEr_{0.9}Ca_{0.1}O_{3-\alpha}$	2.6×10^{-4}	.75	.50
$CaCe_{0.9}Gd_{0.1}O_{3-\alpha}$	1.8×10^{-3}	.86	-

Several of the above solid electrolytes have been incorporated into SOFC's possessing the general configuration:

$$H_2, Ni/ABO_3/La_{0.9}Sr_{0.1}MnO_3, air$$

and were operated at 600°C.

REFERENCES

1. J.A. Kilner, P. Barrow and R.J. Brook, J. Power Sources, 3, 67 (1978).
2. V.M. Goldschmidt, Akad. Oslo I. Mat. Natur. 2, 7 (1926).
3. R.J.H. Voorhoeve, J.P. Remeika and L.E. Trimble, Ann. N.Y. Acad. Sci., 272, 3 (1976).
4. R.D. Shannon, Acta. Crystallogr., A32, 751 (1976).
5. O. Fukunaga and T. Fujita, J. Solid State Chem., 8, 331 (1973).
6. J.A. Kilner and R.J. Brook, Solid State Ionics, 6, 237 (1982).

OPTIMISATION OF PLANAR CONFIGURATION SOFC STRUCTURAL COMPONENTS.

B.C.H.Steele, C.A.Leach, R.A.Rudkin, N.Khan and M.H.Huang.
Centre for Technical Ceramics,
Imperial College, London, SW7 2BP U.K.

The ceramic components of a SOFC are exposed to external and internal thermal and mechanical stresses during fabrication and operation. Most of the design methodologies of mechanical and chemical engineers today are based on the experience of designing with metals. However metals can deform plastically whereas ceramics usually fail by brittle failure. An important point in the evaluation of failure criteria based on stress and strain analysis of the ceramic components is that the fracture strength is a matter of statistical probability. In contrast to metals, which break at a very narrow well defined fracture stress, some components fabricated from ZrO_2, for example, will break at very low stress levels, while some survive up to very high stresses. In general, the Weibull modules of ceramics is low due to processing difficulties. Slow crack growth and cyclic fatigue are other factors which also need to be taken into account in designing the precise configuration of SOFC systems. Unfortunately most of the high temperature data required for the ceramic components are not available at present. Projects have been started at Imperial College to provide some of these data and some of the initial results are provided for the electrolyte and bi-polar plate materials which are the principal structural components in the planar SOFC configuration. These data emphasise the importance of optimising both electrical and mechanical properties and also illustrate how techniques developed to measure electrical properties can also be used to provide information about mechanical behaviour.

At present cubic fully stabilized zirconia-yttria compositions are favoured for use as the solid electrolyte component. This material is selected primarily because its ionic conductivity values at 900°C are higher than the tetragonal and partially stabilized zirconia compositions. This is illustrated in Table 1 and, provided clean powders are used, specific resistivity values below 10 ohm.cm can be attained at 900°C for the cubic phase. Values for the other zirconia phases are only slightly higher but as the zirconia electrolyte plates are typically only 200μm thick, the electrolyte resistance only contributes around 0.2 Ω/cm^2 and the dominant resistance is then usually associated with the electrode structure and bonding (1-2 Ω/cm^2). The electrode resistance is dependant upon the degree of yttria segregation at the interface and on details of the fabrication process which influence surface finish. The

large difference in electrode resistance for materials with nominally the same composition is illustrated in Table 2.

The fabrication route can also influence the quality of solid electrolyte plates as shown in Fig. 1 which reports Weibull statistics for cubic zirconia electrolyte plates made by tape-casting and extrusion. The superior mechanical strength and Weibull modulus of the extruded material is evident, although it must be noted that neither process is fully optimised. It is however the high temperature properties that are important and in this respect the behaviour of a selected ZrO_2-CeO_2-Y_2O_3 composition is illustrated in Fig. 2. These data illustrate the importance of optimising both the mechanical and electrical behaviour. A composition, of 2% CeO_2, 3% Y_2O_3 for example has a conductivity value at 800°C of 0.28 Scm^{-1}, and exhibits high temperature (900°C) fracture strengths of 180 MPa and fracture toughness values of 4.5 MPaml/2 respectively, this should be compared with the room temperature data illustrated in Table 3.

Similar work is in progess on doped $LaCrO_3$ ($LaCr_{0.9}Mg_{0.1}O_{3-\delta}$) bi-polar plate material. Powders have been developed at Imperial College which allow dense (~97% theoretical density) components to be fabricated by sintering at 1500°C in air. At present the fracture strengths of this material are 210 $\pm$ 16 MPa and 60 $\pm$ 10 MPa at room temperature and 900°C respectively. It is considered that these values need to be improved by at least 50% as the $LaCrO_3$ bi-polar plate will probably function as the main structural component in the SOFC planar configuration.

Slow crack growth and cyclic fatigue also need to be addressed for the ceramic components used in SOFC system. Room temperature data (1) suggests that certain zirconia ceramic compositions can rapidly fail when subjected to relatively low cyclic tensile stresses. These observations need to be repeated at high temperatures and for the zirconia compositions used in fuel cells. Experiments at Imperial College involve the use of impedance spectroscopy to monitor crack growth and stress variations initiated by the passage of a current past a crack tip.

Finally the I-V characteristics of single cells incorporating optimised electrolyte sheets are shown in Fig. 3.

Ref. 1 R.H. Dauskardt et al. Cyclic fatigue - crack propagation in magnesia partially stabilised zirconia ceramics. J. Am. Ceram. Soc. 73 [4] 893-903 (1990).

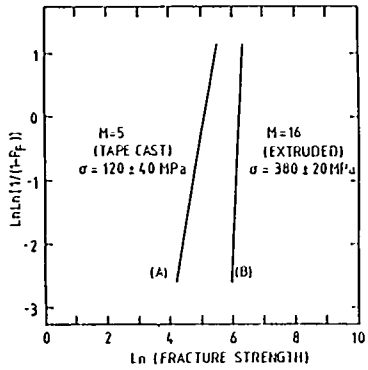

Fig. 1. Weibull plots for ZrO_2-Y_2O_3 (8 mole %) electrolyte sheets prepared by: (a) tape casting (b) extrusion.

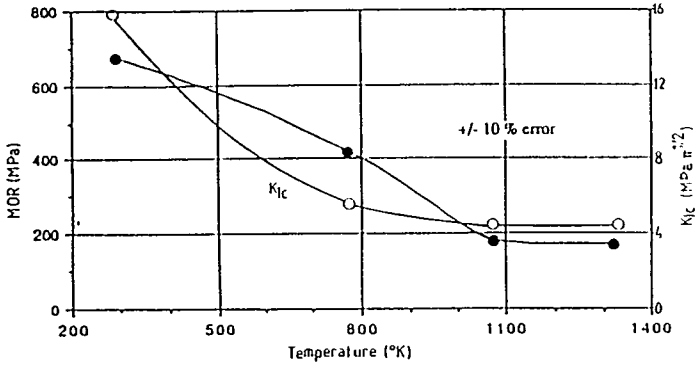

Fig. 2.Temperature dependence of fracture strength and fracture toughness of 2% CeO_2, 3% Y_2O_3 zirconia.

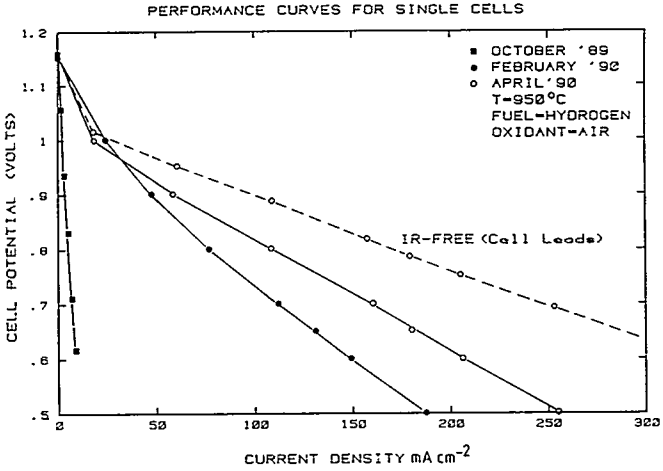

Fig. 3. I-V characteristics of Optimised Planar SOFC Electrodes.

		Conductivity				Resistivity (900°C)		
		Bulk (B)		Grain boundary (GB)		ρ_B	ρ_{GB}	ρ_T
Powder source.	Compn. m% Y_2O_3	log σ_o (S/cm)	Ea(eV)	log σ_o (S/cm)	Ea(eV)	ohm.cm	ohm.cm	ohm.cm
Mandoval (UK)	3	5.41	0.83	5.74	0.98	16	44	60(E)
Toya Soda	3	5.63	0.86	5.94	1.05	16	4	20(E)
Daiichi Kigenso	3	5.55	0.87	6.44	1.01	20	11	31(E)
Toya Soda	8	6.37	0.96	7.23	1.11	6	4	10(E)
Toya Soda	8	6.90	1.01	7.14	1.02	4	3	7(T)
Toya Soda	6	5.73	0.89	6.47	1.06	17	12	29(T)
Z.Tech	4-5	6.17	0.91	7.03	1.02	10	1	11(T)

E - Extruded T - Tape-cast

TABLE 1. Summary of conductivity and resistivity data for ZrO_2-Y_2O_3 electrolyte sheets.

Electrodes	R_E ohms /cm^2	R_E (after etching in HF)	Sample Description
Platinum painted	4.5-7	-	Pressed and sintered at ICST Toya Soda 8m/0 Y_2O_3
Platinum painted	13 - 21	< 10	ICI HSY8 sintered between 96% Al_2O_3
Platinum painted	35 - 45	6 - 16	ICI HSY8 sintered between 99% Al_2O_3
Platinum painted	10 - 17	8	ICI HSY8 sintered between ZrO_2 board
Platinum painted	3 - 4	-	ICI Toya Soda 3YS
Platinum painted	20 - 25	7	ICI Toya Soda 3Y
Platinum/LaSrMn	3 - 5	-	ICST pellet + tape cast LaSrMn
Platinum/LaSrMn	21	-	ICI HSY8 + tape cast LaSrMn
Platinum/LaSrMn	3 - 4	-	GEC tape cast TS8Y + screen printed LaSrMn
Platinum painted	12	-	HSY8 powder pressed and sintered ICST
Platinum painted	10	-	ICI Toya Soda 8Y
Platinum painted	3 - 5	-	GEC tape cast Toya Soda 8Y

TABLE 2. Summary of Electrode Resistance Measurements for ZrO_2-Y_2O_3 Electrolyte (900 ± 2°C).

Composition mol % CeO_2	Composition mol % Y_2O_3	Strength MOR MPa	Toughness K_{IC} MPa m$^{\frac{1}{2}}$	Phase(s) Present	Conductivity σ Scm^{-1} (800°C)
2	3	850 ± 50	13 ± 1	T	0.28
4	2	660 ± 80	15 ± 3	T	0.26
2	6	225 ± 20	3 ± 0.3	T+C	0.82
6	4	140 ± 10	3 ± 0.5	T+C	0.95
2	8	147 ± 20	-	C	1.40

TABLE 3. Room temperature mechanical and electrical properties of selected compositions in the system ZrO_2-Y_2O_3-CeO_2.

RESEARCH AND DEVELOPMENT OF SOFC

F. Umemura, H. Ohta, K. Amano
Tokyo Electric Power Co., Inc.
Engineering Research Center
2-4-1 Nishi-Tsutsujigaoka Chofushi
Tokyo, Japan

T. Saishoji
Electric Power Development Co., Ltd.
6-15-1, Ginza, Chuoku
Tokyo, Japan

S. Kaneko, N. Murakami, T. Gengo, S. Uchida
Mitsubishi Heavy Industries, Ltd.
2-5-1, Marunouchi, Chiyodaku
Tokyo, Japan

INTRODUCTION

Mitsubishi Heavy Industries, Ltd. (MHI) and The Tokyo Electric Power Co., Inc. (TEPCO) have been making a joint research on SOFC, and succeeded in developing a tubular cell which could achieve initial goals of both its out put and durability, in the year of 1988.

Based on these results, three firms including Electric Power Development Co., Ltd. (EPDC) commenced to tackle the development of moduling techniques and succeeded in a power generation test using a 1 kW module.

Parallel to the developing of tubular cell and module, MHI and TEPCO have been making a development of planar typed cells and various fundamental researches not only on SOFC but also on solid ionics.

TUBULAR CELL

A stack of tubular cell consists of multiple cells in series on one support tube. (Fig. 1)

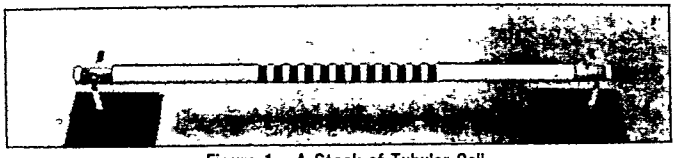

Figure 1 A Stack of Tubular Cell

The specification is determined by optimizing performance of the selected component materials, the thickness of each layer, and the configuration, etc.

All layers are made by plasma or flame spraying method, especially for electrolyte layer a low pressure plasma spraying technique is employed to make the layer as gas tight as possible.

Initial characteristics are as follows.

(1) Maximum output : 35 W/stack
(2) Cell voltage : 0.78 V (200 mA/cm²)
(3) Fuel utilization : 70% (200 mA/cm²)

A long-term endurance test of 5000 hours (Fig. 2) and test of 46 thermal cycles were also conducted.

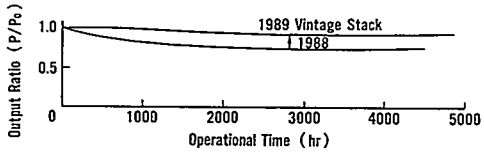

Figure 2 Endurance Test Result of Stack

1 kW MODULE

In March, 1990, 1 kW module put into operation at MHI.

1 kW module consists of 48 tubular stacks (one stack consists of 15 cells), built-in type air heater, automatic control system, high temperature seal and high temperature current collector, etc. External view of module is shown in Fig. 3. The specifications are as follows:

Rated output : 1 kW (D.C.)
Open circuit voltage : 180 V
Operating voltage : 120 V
Operating current : 10 A
Number of stacks : 48
Dimension : $\phi 700 \times {}^{H}1625$

One of major features of this module is to be able to exhaust fuel exhaust gas separately from air exhaust gas due to applying high temperature seal.

I-V characteristics and an assembly of stacks are shown in Fig. 4 and Fig. 5. The maximum output was about 1.3 kW and the fuel utilization was about 57%.

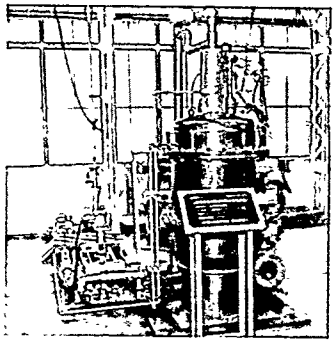

Figure 3 External View of 1kW Module

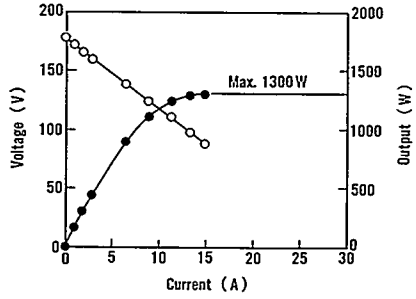

Figure 4 I-V Characteristic of Module

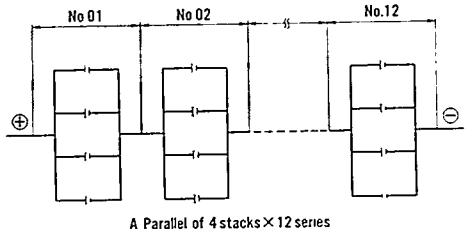

Figure 5 Assembly of Stacks

As successor to this 1 kW module, next step will start in this December at a power station of EPDC and 10 kW class module will be put into operation in 1992.

PLANAR CELL

Based on the various test results obtained by tubular cells, planar cells ideal for mass production have been also developed.

Each component layer is formed by tape casting and the fuel electrode, the electrolyte and the air electrode are integrally sintered at approx. 1300°C.

The shrinkage profile of each layer is matched by controlling grain sized distribution and sintering aids.

Fig. 6 shows the sectional view of planar cell of 100 cm^2 area.

Fig. 7 shows one example of I-V characteristics of planar cell. It suggests higher performance due to have good connections between the respective layer interface.

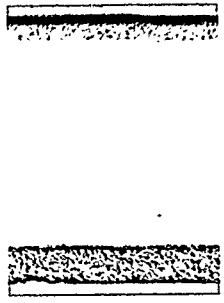

Figure 6 Crosssection of Planar Cell

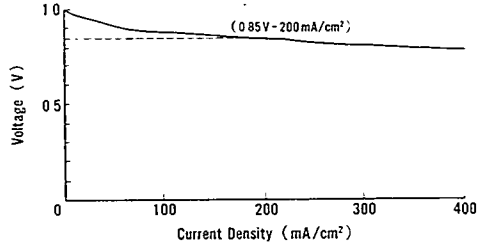

Figure 7 I-V Characteristic of Planar Cell

FUNDAMENTAL TEST

Various fundamental test are also conducted to improve I-V performance and endurance characteristics.

They are Laser-Raman measurements, acoustic emission method, current interrupt method, impedance method etc.

For example, using the impedance method, we examine the change over time of activation polarization between air electrode and electrolyte.

Time dependence of impedance plots of activation polarization of $LaCoO_3$/YSZ at 900°C, 1 atm is conducted in Fig. 8.

This figure says that activation polarization increases as time passes.

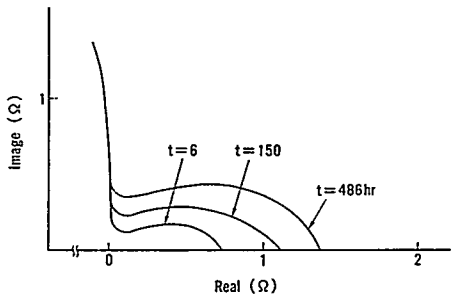

Figure 8 Time Dependence of Impedance Plot for YSZ/$LaCoO_3$ Activation Polarization at 900°C, 1 atm

CONCLUSION

The development stage of tubular cells already reaches a level capable of producing several kW-class modules.

Furthermore, we develop the most attractive SOFC with studying planar cells parallel to tubular cells.

REFERENCES

1. Fumio Umemura et al. 'Development of Solid Oxide Fuel Cell' - SOFC NAGOYA, pp. 15-20, Nov. 1989.

THIN ELECTROLYTE LAYERS FOR SOLID OXIDE FUEL CELLS BY ELECTROCHEMICAL VAPOR DEPOSITION (EVD)

L.G.J. de Haart, R.A. Kuipers, K.J. de Vries and A.J. Burggraaf
Laboratory of Inorganic Chemistry, Materials Science and Catalysis
Faculty of Chemical Technology, University of Twente
P.O. Box 217, 7500 AE Enschede, The Netherlands

INTRODUCTION

In the state-of-the-art SOFC design the thick yttria stabilized zirconia (YSZ) electrolyte layer (thickness 50 - 150 μm) requires a high operating temperature of 1000 °C in order to reduce the ohmic polarization losses in the electrolyte layer. This high operating temperature lowers the obtainable open cell voltage (OCV) considerably. Lowering of the operating temperature (to 700 - 800 °C) in order to increase this OCV and thereby the efficiency of the SOFC can only be done when very thin (about 1 μm) YSZ electrolyte layers are employed. These very thin electrolyte layers require to be supported when produced. A suitable production technique for thin supported YSZ layers is Electrochemical Vapor Deposition (EVD). The EVD technique has been introduced by the Westinghouse Co. [1] for the production of layers of about 40 μm and is also applied in other groups [2,3]. Our group has demonstrated the unique ability of the EVD technique to form very thin (2 - 5 μm) gas tight YSZ films on porous substrates [4].

The present investigations demonstrate the production by EVD of very thin YSZ electrolyte films for SOFC applications. Aimed at are layers of about 1 μm or smaller. The program is carried out in cooperation with the Netherlands Energy Research Foundation ECN (Petten, The Netherlands). Reported is on the EVD of YSZ on supported porous fuel cell electrodes and the performance properties of the thin electrolyte SOFC.

Previous EVD experiments [4] showed deep penetration of the deposited metal oxide in the pores of the substrate during the initial CVD phase of the process. In order to prevent the deep penetration of the YSZ in the pores of the fuel cell electrode, experiments were performed on the filmcoating of a ceramic membrane intermediate layer on the fuel cell electrode prior to the EVD of YSZ. The incorporation of the ceramic membrane intermediate layer offers also the possibility to produce submicron (< 1 μm) layers.

EVD OF YSZ

The experimental procedures for the EVD of YSZ on porous substrates has been given in detail elsewhere [5]. To study the CVD and EVD phases of the process depositions were made on a α-alumina substrate with a mean pore size of 0.2 μm. The results obtained for this model substrate could be very well explained within the mathematical models derived for the CVD [6] and the EVD [7] phase.

For the production of the electrolyte layer for SOFC applications, investigations were carried out here by the deposition of YSZ on a 2-layer substrate manufactured by ECN [8]. This consisted of a 35 μm thick layer of the perovskite cathode material $Sr_{0.15}La_{0.85}MnO_3$ (15SLM) with a mean pore size of 0.4 μm and a porosity of 70% on a wide porous (10 μm mean pore

size and 50% porosity) 1 mm thick α-alumina support. During EVD the perovskite layer was exposed to the metal chloride vapor, resulting in a gas tight YSZ layer on top of the 15SLM layer. Figure 1 shows a SEM photograph of the cross-section of a sample after EVD at 1000 °C. In a total deposition time of 1 hour an YSZ layer of around 8 μm was formed. The three layers α-alumina/15SLM/YSZ can be clearly distinguished in the SEM picture (see Fig. 1). In-situ Ar gas permeation measurements showed the pore closure time to be around 30 minutes. The actual time of the EVD phase to grow the 8 μm thick layer was thus also 30 minutes. The EVD film growth rate, which is a function of the substrate properties (e.g. mean pore size) and experimental conditions (e.g. total pressure, temperature, vapor phase concentration) [7], was for YSZ deposition on these type of substrates reproducibly around 16 - 20 μm/h. Gas permeation measurements performed after the deposition showed the YSZ layer to be gas tight. Several of these samples are being tested for their thermal stability.

Figure 2 shows the results of 4-point DC conductivity measurements performed on EVD YSZ films. The specific conductivity at 1000 °C of all samples is within the range 0.03 - 0.11 $S.cm^{-1}$, which means that these layers are quite suitable for use in a SOFC. The activation energy for the conductivity in the temperature range 700 - 1000 °C is for all samples around 102 kJ/mol. According to Ioffe et al. [9] this activation energy corresponds to an yttria content of the layer of 12 mol% Y_2O_3. This is in line with previous XRD results where we found an yttria content of 13 mol% Y_2O_3 [5].

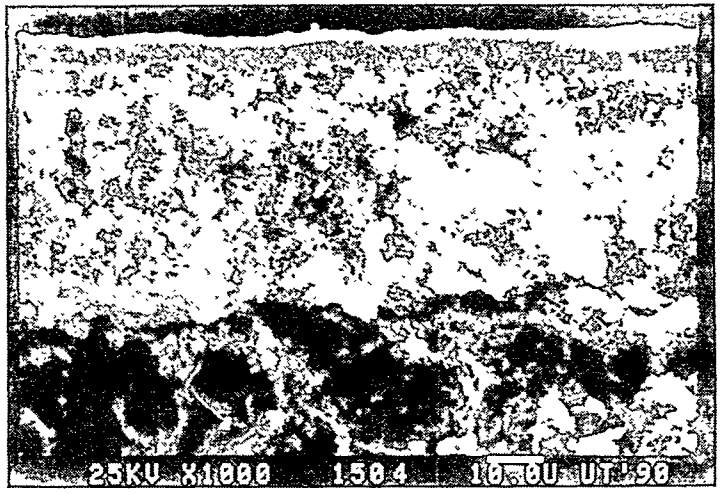

FIGURE 1
SEM photograph of a gas tight EVD YSZ layer (top; 8 μm thick) on top of a two-layer substrate 15SLM (middle; 35 μm thick) / α-alumina (bottom).

At the 3-layer half cell system α-alumina/15SLM/ EVD YSZ three-point I-V measurements and impedance measurements are being performed, which will be reported. Cell test results on the with an EVD thin YSZ electrolyte layer provided SOFC are not yet available.

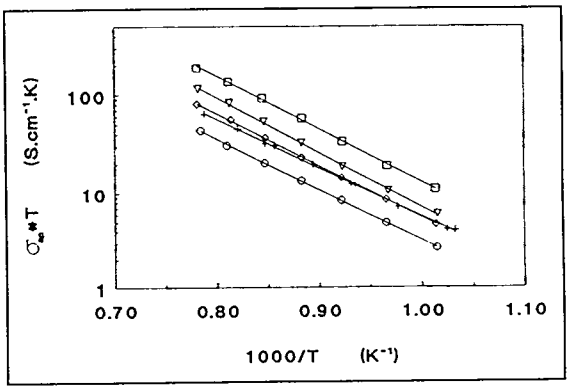

FIGURE 2
Arrhenius plot of the conductivity of EVD YSZ layers

MEMBRANE MODIFICATION

Ceramic membrane intermediate layers of YSZ are filmcoated on porous substrates from a suspension of the YSZ powder. Commercial available YSZ powders were used (Tosoh TZ8Y). Figure 3 shows a filmcoated porous YSZ layer on top of the ECN supplied 2-layer system α-alumina/15SLM. The top layer is around 2.5 μm thick.

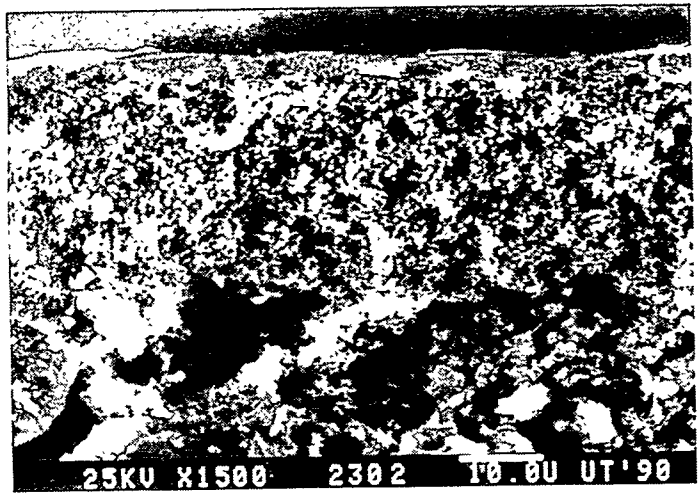

FIGURE 3
SEM photograph of a porous filmcoated YSZ layer (top; 2.5 μm thick) on top of a two-layer substrate 15SLM (middle; 35 μm thick) / α-alumina (bottom).

Hg-porosimetry measurements on unsupported layers show the filmcoated layers to have a porosity of around 55% and a mean pore size of around 90 nm. This mean pore size of the filmcoated layer is thus 4 times smaller than the mean pore size of the 15SLM electrode layer and will very likely prevent deep penetration of the YSZ deposit in the pores of the 15SLM layer in the initial CVD phase of the EVD process. Momentarily the EVD of YSZ is being performed on these YSZ membrane provided ECN substrates, which will be reported.

Acknowledgment

The investigations are performed under contract partly with the Commission of the European Communities (CEC) within the Non-Nuclear Energy R and D Programme (Research Contract 'Membrane Based Thin Layer SOFC Technology', No. EN3E-0175-NL) and partly with the Netherlands Agency for Energy and the Environment (NOVEM) within the program Fuel Cells, which is financed by the Ministry of Economical Affairs (Research Contract 'Thin electrolyte layer solid oxide fuel cells, No. 19.103-001.1).

References

1. A.O. Isenberg, "Growth of refractory oxide layers by electrochemical vapor deposition (EVD) at elevated temperatures", ECS Symp. Electrode Materials, Processes for Energy Conversion and Storage, vol. 77-6 (1977) pp. 572-83.
2. G. Dietrich and W. Schäfer, "Advances in the development of thin-film cells for high temperature electrolysis", Int. J. Hydrogen Energy, vol. 9 (1984) pp. 747-52.
3. M.F. Carolan and J.N. Michaels, "Growth rates and mechanism of electrochemical vapour deposited yttria-stabilized zirconia films", Solid State Ionics, vol. 37 (1990) pp. 189-95.
4. Y.S. Lin, L.G.J. de Haart, K.J. de Vries and A.J. Burggraaf, "Modification of ceramic membranes by CVD and EVD for gas separation, catalysis and SOFC application", in: 'Euro-Ceramics (G. de With, R.A. Terpstra and R. Metselaar, eds.), vol. 3, pp. 590-5, Elsevier Science Publishers Ltd, London, 1989.
5. L.G.J. de Haart, Y.S. Lin, K.J. de Vries and A.J. Burggraaf, "Modified-CVD of nanoscale structures in and EVD of thin layers on porous ceramic membranes", J. Europ. Ceram. Soc., submitted for publication.
6. Y.S. Lin, K.J. de Vries and A.J. Burggraaf, "CVD modification of ceramic membranes: simulation and preliminary results", J. de Phys., Colloque C5, vol. 50 (1989) pp. 861-72; Y.S. Lin, P. Fransen, K.J. de Vries and A.J. Burggraaf, "Experimental study on CVD modification of ceramic membranes", to be presented at the 11th Intern. Conf. on CVD, Seattle, Oct 14-19, 1990.
7. Y.S. Lin, L.G.J. de Haart, K.J. de Vries and A.J. Burggraaf, "A kinetic study on the electrochemical vapour deposition of solid oxide electrolyte films on porous substrates", J. Electrochem. Soc., (1990) in press.
8. J.P.P. Huijsmans, S.B. van der Molen and E.J. Siewers, "Membrane based thin layer SOFC components", in: "Euro-ceramics' (G. de With, R.A. Terpstra and R. Metselaar, eds.), vol. 3, pp. 626-30, Elsevier Science Publishers Ltd, London, 1989.
9. A.I. Ioffe, D.S. Rutman and S.V. Karpachov, "On the nature of the conductivity maximum in zirconia-based solid electrolytes", Electrochimica Acta, vol. 23 (1978) pp. 141-2

Characterization of High Temperature Fuel Cells based on Electrochemical Impedance Measurements

H. Landes, K. Mund

Siemens AG, Corporate Research and Technology, Erlangen, Germany

High temperature fuel cells are designed for a highly effective energy conversion in decentralized power generation. The development will be successful if a current density of more then 0.2 A/cm^2 at a voltage of more than 0.85 V can be maintained over several years.

Impedance measurements are our preferred tool to analyze the behaviour of the electrodes and to improve the characteristic of the cells.

We have performed experiments with laboratory cells of both types of high temperature fuel cells: Molten carbonate (MCFC) and solid oxide (SOFC) fuel cells. For both systems we have found that the voltage loss in the cells is not only caused by the electrolyte layer but also by the polarization of the electrodes. Electrochemical impedance measurement were carried out to differentiate between the voltage loss influenced by the electrode structure, the electronic and the electrolytic conductivity and the catalytic activity of the electrode material.

Compared to tests with low temperature fuel cells both electrodes reveal a reversible behaviour in MCFC and in SOFC. Therefore, we use a symmetrical arrangement of one type of electrode and analyze the result of the impedance measurement.

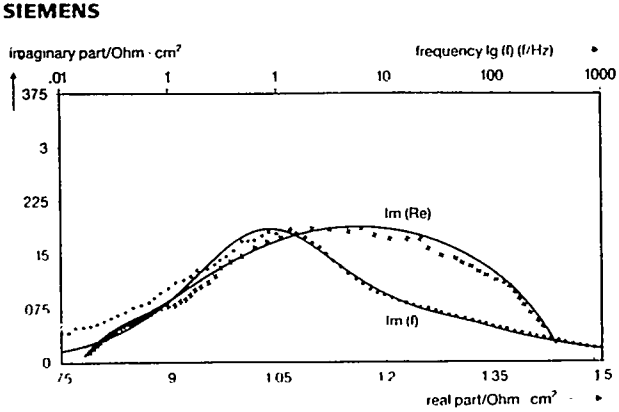

Ni-electrodes, symmetrical arrangement: $[H_2] : [CO_2] = 2 : 1$

fig.1

MCFC anodes consist of Nickel powder. An impedance diagram of these electrodes is shown in fig. 1. The analysis showed that the electrolytic resistivity of the electrolyte in the working layer and the charge transfer reaction at the catalyst powder have comparable influence on the polarization resistance. The experimental results with MCFC cathodes could be explained by assuming the diffusion of O_2 and CO_2 through an electrolyte film around the catalyst particle as a rate determining step (fig. 2). The polarization of the cathode is larger than for the anode. In small MCFC cells we measured a current density of 0.15 A/cm^2 at a voltage of 0.78 V.

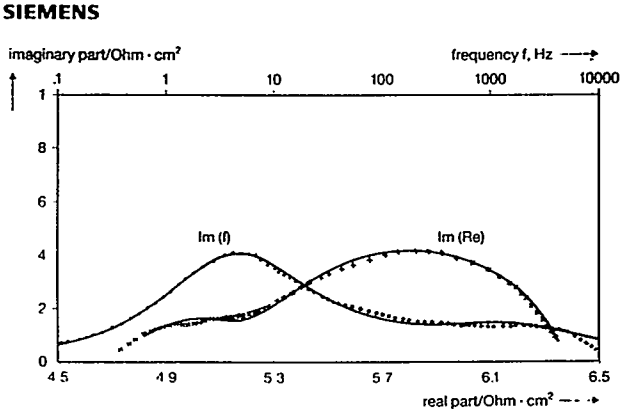

Nickel electrodes, oxidized, symmetrical arrangement:
$[O_2] : [CO_2] = 1 : 1$

fig. 2

Our development of the solid oxide fuel cell is based on the concept of a planar configuration. The ZrO_2-electrolyte sheet has a thickness of 170 um and surface related resistance of 0.15 ohm*cm^2. The polarization resistance of the electrodes should be in the same order of magnitude or even smaller. Impedance measurements with our electrodes showed that they can be improved. The cathodes made of a porous La-manganate layer have a higher resistance than the anodes prepared as a porous Ni-cermet structure. By interpretation of the results of impedance measurements we assume that the electrolytic conductivity of the working layer is poor and therefore only a thin layer takes part in the reaction.

MULTILAYER ELECTRODES FOR PLANAR SOFC

E. Ivers-Tiffée, W. Wersing and B. Reichelt
Siemens AG, Corporate Research and Development,
Otto-Hahn-Ring 6,8000 Munich 83, FRG.

Abstract

This work presents a planar design for the SOFC using a metallic bipolar plate. The different expansion coefficients of solid electrolyte and metal are adapted by intermediate layers in the form of multilayer electrodes (functional gradient materials). For the anode, cermets with a Ni-content between 31% and 100% can be used. The stack design can be realized by various coating techniques (screen printing, tape casting, plasma spraying).

1. Planar SOFC Design

Three different construction concepts exist for high temperature fuel cells of the SOFC-type (tubular, monolithic, planar). The planar design employs ceramic as well as metal as interconnector materials (ICM). As part of the current CEC fuel cell R&D programs (1990-1993), Siemens (FRG) develops in cooperation with ECN (NE) a 1 kW SOFC-stack with a bipolar plate (figure 1) [1].

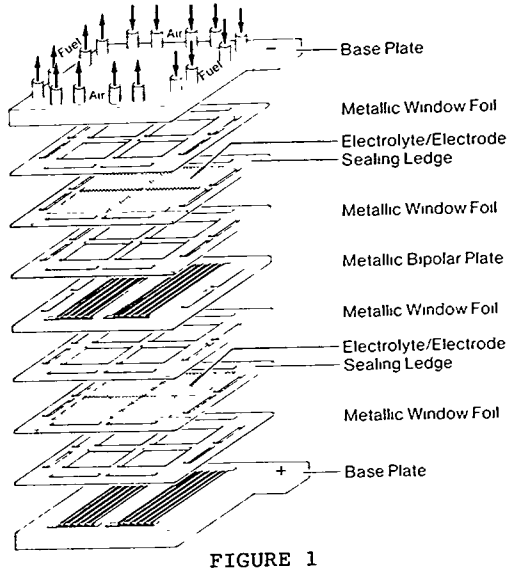

FIGURE 1
PLANAR SOFC WITH METALLIC BIPOLAR PLATE

For the solid electrolyte cubic YSZ is used, for the anode Ni/YSZ cermets, and for the cathode $La_{1-u}Sr_uMn_{1-x}Co_xO_3$ [2]. After preliminary experiments with respect to corrosion behavior, metallic alloys based on FeNiCr, NiCrW, NiCrAl and FeCrAl qualified for use as bipolar plates [3]. In the two last alloys the electrically isolating Al_2O_3-surface layers have, however, to be modified.

2. Multilayer Electrodes

If one takes into account the difference in thermal expansion between solid electrolyte ($\approx 11 \cdot 10^{-6}$ K^{-1}) and metallic bipolar plate ($\approx 15\text{-}18 \cdot 10^{-6}$ K^{-1}), one will not only need material-oriented cell design but also multilayer electrodes (functional gradient material). The cathode comprises a series of layers with increasing expansion coefficient while electrical conductivity remains constant. This can be accomplished by varying the Mn:Co ratio [3]. For the anode the same is in principle possible by varying the Ni(O):YSZ ratio. Different electrode textures and thicknesses are realized by a combination of different coating techniques (e.g. screen printing, tape casting, plasma spraying).

3. Production and Preparation of Ni/YSZ Cermets

3.1 Bulk Material

The interactions between cermet properties and raw material properties were first investigated for bulk material [4]. The results presented in this work were measured on samples produced from NiO-powder with a specific surface of 4.5 m^2/g (average particle size 3 µm), and from YSZ-powder with 14 m^2/g (average particle size 1.2 µm). The raw materials were homogenized in ball mills, pressed to disks together with a binder (PVA), and sintered at 1300°C. For the electrical 4-point resistance measurements (d.c.) small sample bars ($10 \cdot 1 \cdot 1$ mm^3) were contacted with Pt-wire (0,1 mm). The following reduction in 5% H_2/95% N_2 at 1000°C created cermets with a porosity between 10% and 40%. The change in electrical conductivity during reduction, and the conductivities that can be gained with porous samples are shown in figure 2.

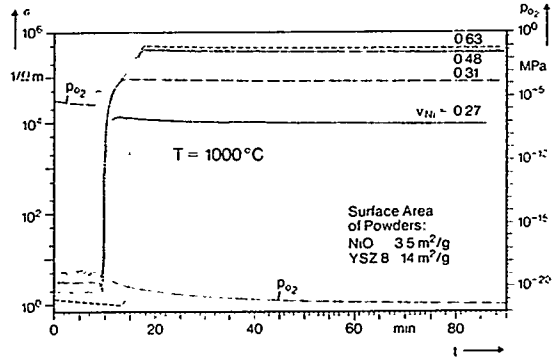

FIGURE 2
ELECTRICAL CONDUCTIVITY OF Ni/YSZ CERMETS VS. O_2-PARTIAL PRESSURE AT 1000°C

Figures 3 and 4 show the conductivities (calculated for 0% porosity after Bruggeman [6]) and expansion coefficients of reduced cermets as a function of Ni-content. Starting at the value for YSZ (≈ 10 $\Omega^{-1}m^{-1}$), conductivity increases drastically as soon as the percolation limit is reached ($\approx$ 31 vol% Ni), and connectivity between the Ni-particles is ensured. The expansion coefficient of a cermet with 31% Ni is approxi-

mately $12 \cdot 10^{-6}$ K^{-1}. In a multilayer anode one can therefore gain expansion coefficients of up to $16 \cdot 10^{-6}$ K^{-1} [5] and conductivities up to $4 \cdot 10^{6}$ $\Omega^{-1}m^{-1}$ [5], depending on composition and porosity.

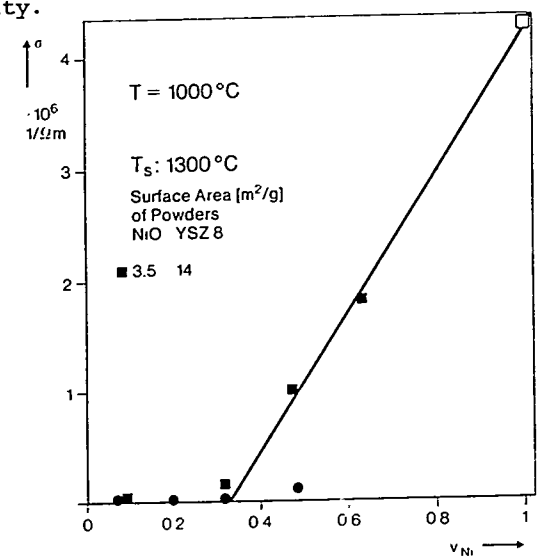

FIGURE 3
ELECTRICAL CONDUCTIVITY OF Ni/YSZ CERMETS
(0% POROSITY CALCULATED) AT 1000°C (5% H_2/95% N_2)

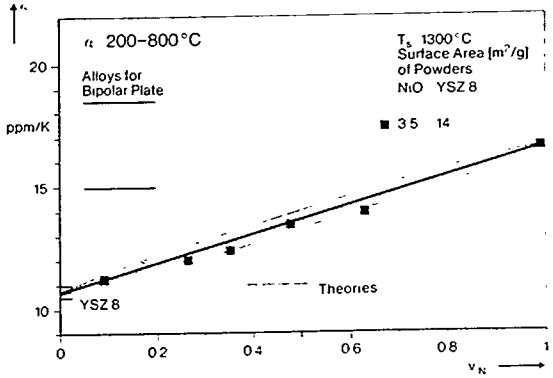

FIGURE 4
MEAN THERMAL EXPANSION COEFFICIENTS OF Ni/YSZ CERMETS BETWEEN 200°C AND 800°C (5% H_2/95% N_2)

3.2 Electrode Layers

For the production of anode layers on solid electrolyte, cermets with Ni-contents ≥ 31 vol% were measured. Anodes (40•40 mm^2) with varying composition and thickness were applied to the solid electrolyte (50•50•0.15 mm^3) by screen printing, and fired at 1300°C. The paste used for screen printing was

mixed from the above mentioned raw materials and an organic binder system (solid content of the paste between 50 and 60 weight %). The layer thickness was modified by differently coated screen printing nets (325 mesh), the layer design was controlled by multiple printing. Figure 5 shows a scanning electron micrograph of a single layer screen printed anode.

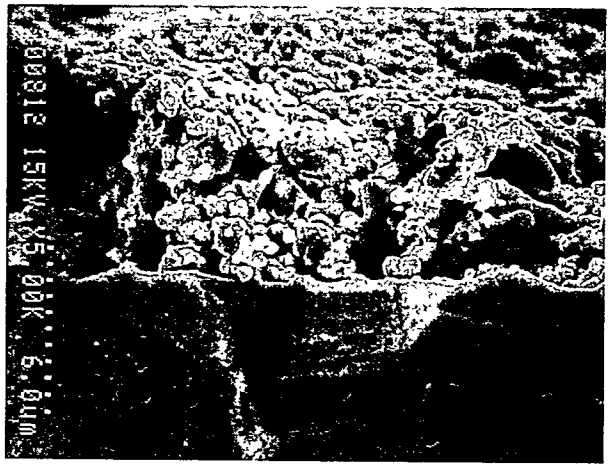

FIGURE 5
SCANNING ELECTRON MICROGRAPH OF A FRACTURED SURFACE OF A CERMET/ELECTROLYTE WITH 47.5 VOL% Ni (SCREEN PRINTED)

In the presentation further microtextures of electrode layers will be shown. The connections between layer design and current-voltage curves will be discussed.

Patents

[1] H. Greiner, W. Wersing, E. Ivers-Tiffée, German Patent Application P 3935722.8, 1989.

Journal Articles

[2] M. Schießl, E. Ivers-Tiffée, W. Wersing, Proc. 7th CIMTEC World Cer. Congr., June 24-30, 1990, Montecatini, Italy.

[3] E. Ivers-Tiffée, W. Wersing, M. Schießl, and H. Greiner, Ber. Dt. Bunsen Gesellschaft, to be published 1990.

[4] B. Reichelt et al., to be published.

[6] D.A.G. Bruggeman, Ann. Phys. Lpz., 24, 636 (1935)

Books

[5] K. E. Volk, Nickel und Nickellegierungen, Springer Verlag, Berlin Heidelberg, New York, 1970.

AIR SINTERABLE SOLID OXIDE FUEL CELL INTERCONNECTS

H. U. Anderson, D. Carter, R. Koc and M. Nasrallah
University of Missouri-Rolla
Rolla, MO 65401

Considerable attention has focussed on perovskite-type oxides for their potential applications both as electrodes and interconnects in high temperature solid oxide fuel cells (SOFC). The $LaCrO_3$ system appears to be the prime candidate for interconnects. The latter is subjected to severe conditions that require material stability in both air and fuel environment ($1-10^{-16}$ atmos) at the operating temperature (1000°C), compatibility with other cell components, low resistivity, negligible volatility as well as gas tightness to prevent fuel leakage to the cathode and air leakage to the anode.

Undoped $LaCrO_3$ and $YCrO_3$ do not satisfy any of the mentioned requirements for interconnect application, however, upon doping a significant improvement in properties is observed. For example, the substitution of Sr for La in $LaCrO_3$ is known to lower the transformation temperature, stabilizing the rhombohedral symmetry at room temperature[1]. Sr doping also improves electrical conductivity[2,3] and sinterability under oxidizing conditions[4]. Furthermore, Sr additions has been found to increase the thermal expansion coefficient (TEC) to match that of YSZ electrolyte[1]. Mg doping also improves the electrical conductivity and stability over a wide range of oxygen activity[5,6]. $YCrO_3$ is very stable at high temperature and Ca doping appears to improve its electrical conductivity[3]. Although the properties of both Y and La chromites can be made to match the requirements for SOFC applications, however, they are extremely difficult to fabricate under conditions compatible with other SOFC components, due to the vapor phase transport of higher valent oxides of Cr. Typically, the sintering involves temperatures as high as 1775°C and at oxygen activities as low as 10^{-12}-10^{-9} atmos. These conditions are not suitable for other cell components that might have to be cosintered with the interconnect material for monolithic structures of planar or tubular SOFC designs. It is therefore very desirable to process La and Y chromites under conditions favorable for other cell components, this requires lower sintering temperature (not exceeding 1400°C) and in air without deterioration of the electrical conductivity or structural stability.

In this work Ca and Co dopings were used to enhance air sinterability and improve properties of La and Y chromites. Compounds of the general formula $A_{1-x}Ca_xCr_{1-y}Co_yO_3$ (where A = La or Y) were synthesized using our well established liquid mix polymer precursor techniques[7]. The Ca content varied between 10-30% and the Co content up to 30%. The amount of dopants

did not exceed the solubility limit of the perovskite structure as detected by x-ray diffraction studies. The synthesized powders were consolidated in the form of bars or discs and sintered in air at 1000-1500°C for 2-10 hours. Bulk densities were determined by the liquid displacement technique and the microstructure identified by the use of scanning electron microscopy on both the La and Y series. DC electrical conductivity as a function of temperature and oxygen activity as well as dilatometric measurements were conducted on the $LaCrO_3$ series.

Our results show that Co substitution for Cr improves air sinterability. Addition of up to 20% Co in $LaCrO_3$ ($LaCr_{.8}Co_{.2}O_{.3}$) improved its sinterability in air (about 85% of theoretical density was achieved at 1500°C). In $YCrO_3$, 30% Co addition resulted in a 93% TD at 1500°C. It is not recommended to add Co in excess of 30%, although the solubility limit is not exceeded yet it is not favorable in fuel cell environment. The undoped and Ca containing chromites did not show any significant sintering up to 1500°C. However, we have observed that Ca additions have a remarkable effect on the sintering of $LaCoO_3$ (90% TD obtained at 1100°C in $La_{.7}Ca_{.3}CoO_3$). It was accordingly concluded that the incorporation of Ca in the Co containing compounds will have a positive effect on sintering and properties. Indeed a significant increase in sinterability of both the $A_{1-x}Ca_xCr_{.9}Co_{.1}O_3$ and $A_{1-x}Ca_xCr_{.8}Co_{.2}O_3$ series was observed for x = 0.2 and 0.3 at temperatures between 1200 and 1400°C. Similar results were also observed for the 20% Co containing series. The results clearly show that 95% TD or better can be achieved at 1400-1500°C in air, when 20-30% Ca and 10-20% Co is incorporated in the chromite structure.

The enhanced sintering process that occurs above 1200°C suggests a reactive sintering mechanism which takes place in the presence of both Ca and Co and is believed to be due to a transient liquid phase. The latter was studied using SEM and EDS techniques on rapidly quenched samples after heating at 1100-1400°C in air for 15 minutes. The microstructure reveals the presence of a viscous liquid that only appears during the early stages of sintering, it spreads and penetrates along the solid-solid contacts and completely wets the grains. The rapid spreading of the liquid caused the generation of the observed minimal porosity which is expected in transient liquid formation mechanisms. EDS analysis of the liquid phase indicates that it contains a higher Ca content and a lower La content as compared to the matrix. SEM analysis of the completely sintered samples did not show any evidence of the liquid phase, this clearly indicates that the liquid forms during the early stages of sintering and goes into solution as the sintering process continues, thus inducing an enhanced solution-reprecipitation type of densification.

Ca and Co additions did not only improve the sinterability at lower temperatures in air, but also allowed a better control of properties to match SOFC requirements. For example the thermal expansion coefficient of $La_{.7}Ca_{.3}Cr_{.9}Co_{.1}O_3$ was found to match that of YSZ electrolyte. Table I shows the effect of dopants on the TEC of $LaCrO_3$, the measurements were conducted using an Orton automatic dilatometer coupled with a data acquisition system, at a heating rate of 5°/min. and temperatures between 25-1100°C in air.

TABLE I

Dopant	TEC ($X10^{-6}$/°C)
$LaCrO_3$	9.5
$LaCr_{.9}Mg_{.1}O_3$	9.5
$La_{.98}Sr_{.02}CrO_3$	10.24
$LaCr_{.9}Co_{.1}O_3$	13.1
$LaCr_{.8}Co_{.2}O_3$	13.6
$LaCr_{.7}Co_{.3}O_3$	15.9
$La_{.9}Ca_{.1}Cr_{.9}Co_{.1}O_3$	12.3
$La_{.8}Ca_{.2}Cr_{.9}Co_{.1}O_3$	11.1
$La_{.7}Ca_{.3}Cr_{.9}Co_{.1}O_3$	10.4
YSZ	10.3

Furthermore, Ca and Co doping increased the electrical conductivity. Since Ca^{2+} enters the structure substitutional on the A^{3+} site, charge compensation will occur either electronically via $Cr^{3+} \rightarrow Cr^{4+}$ transitions resulting in a P_{O2} independent electronic conductivity, or by ionic compensation causing the formation of oxygen vacancies (V_o) as postulated in our model[5]. The P_{O2} independent region extended to lower oxygen activities upon doping and a 1/4th power dependence was observed at lower P_{O2} for the ionic compensation. The experimental data was found to be in good agreement with the postulated model.

In conclusion, La and Y chromites are sintered to above 95% TD at temperatures below 1500°C in air. A reactive sintering process is induced due to the presence of dopants, this process involves the presence of a lower temperature transient liquid phase. The dopants allowed alteration of properties to match those of other SOFC components.

Acknowledgement

The authors express their gratitude to the Department of Energy - Morgantown Energy Technology Center (DOE-METC) and Basic Energy Science (BES) for their financial support.

References

1. C. P. Khattak and D. E. Cox, "Structural Studies of the (La,Cr)CrO_3 system", Mater. Res. Bull., 12, 463-72 (1977).

2. D. P. Karim and A. T. Aldred, "Localized Level Hopping Transport in La(Sr)CrO_3", Phys. Rev. B, 20[6] 2255-63 (1979).

3. W. J. Weber, C. W. Griffin and J. L. Bates, "Effects of Cation Substitution on Electrical and Thermal Transport Properties of $YCrO_3$ and $LaCrO_3$", J. Am. Ceram. Soc., 70[4] 265-70 (1987).

4. D. B. Meadowcraft, "Some Properties of Sr-doped $LaCrO_3$", Br. J. Appl. Phys., 2, 1225-33 (1969).

5. B. K. Flandermeyer, M. M. Nasrallah, A. K. Agarwal and H. U. Anderson, "Defect structure of Mg-doped $LaCrO_3$, Model and Thermogravimetric Measurements", J. Am. Ceram. Soc., 67[3] 195-98 (1984).

6. H. U. Anderson, M. M. Nasrallah, B. K. Flandermeyer and A. K. Agarwal, "High Temperature Redox Behavior of Doped $SrTiO_3$ and $LaCrO_3$", J. Solid State Chem., 56, 325-34 (1985).

7. N. G. Eror and H. U. Anderson, Mat. Res. Soc. Symp. Proc., Vol. 73, "Better Ceramics Through Chemistry II", Eds. C. Brinker, D. Clark and D. Ulrich, MRS, 1989.

IMPROVED CERAMICS - THE KEY TO ECONOMIC FUEL CELLS

K Kendall
ICI, PO Box 11, Runcorn
Cheshire, WA7 4QE, UK

Ceramic materials are used in many fuel cell designs:- as inert porous matrix materials to contain the electrolyte in alkaline and molten carbonate fuel cells (MCFC); as porous supports for solid oxide fuel cells (SOFC) components; as oxygen ion conducting electrolyte in the zirconia fuel cell; as conductive electrode or catalyst layers in MCFC and SOFC; and as interconnect material in any high temperature cell where metals cannot be used because of corrosion.

It is evident that ceramics will be used even more extensively in future fuel cell designs as these devices are used at higher and higher temperatures to improve reaction kinetics. For this reason, SOFC are the main target for ceramics at the present time [1].

When devising ceramic components for fuel cells, two major economic problems stand out. The first is in the processing of the intractable ceramic powder to obtain the required geometry at the correct density. Many ceramics cannot readily be formed and joined by traditional powder methods to form the dense ~100 μm layers required for fuel cells. The second problem is obtaining the mechanical strength, thermal shock resistance, and long term reliability, out of ceramic components which are theoretically very strong, but in practice are limited by defects some 20 to 100 μm long, introduced through the forming process [2].

This paper demonstrates that these two problems of poor processing and properties arise from the van der Waals forces which bind ceramic powder grains together during mixing and moulding [3]. Such van der Waals forces are so strong that the powder agglomerates are not broken down during mixing and forming unless very high shear forces are applied [4]. The agglomerates have several deleterious effects. They interfere with the moulding of the ceramic; they inhibit sintering to full density; and they act as flaws in the final product, reducing strength and reliability [5].

By overcoming these van der Waals forces, using a plastic mixing process, the agglomerates can be broken down into individual grains and prevented from subsequent flocculation. This means that the plastic mix is much easier to form into thin membranes. The product also

sinters at lower temperatures to give impermeable material. Moreover, the strength and Weibull modulus values are much improved over the ordinary products [6].

For example, cubic zirconia sheets have been made with oxygen conductivities of 0.13 S/cm at 800 C, with a 3-point bend strength of 472 ± 128 MPa. Impermeable interconnect sheets of lanthanum chromite have been made with conductivity in air of 35 S/cm at 800 C plus a bending strength of 290 MPa.

Figure 1 shows the improvement in strength and Weibull modulus for a three mol% yttria stabilised zirconia when made by this new process. The conductivity in this case ranged from .05 to 0.1 S/cm.

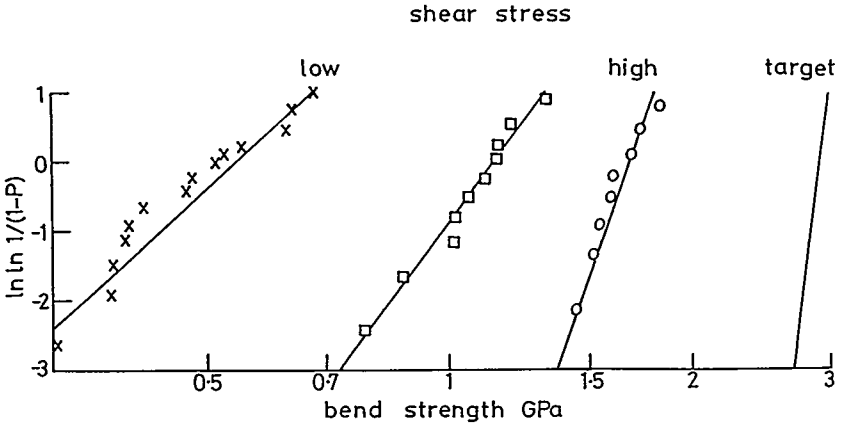

FIGURE 1: BEND STRENGTH STATISTICS FOR 3Y-ZrO2 MADE BY PLASTIC MIXING, SHOWING IMPROVEMENT IN CURVES FROM LEFT TO RIGHT BY INCREASING THE SHEAR STRESS DURING PROCESSING IN ORDER TO BREAK DOWN AGGLOMERATES.

Figure 2 shows the comparable improvement obtained by better processing of lanthanum chromite powder. The left-hand curve gives the bend strength results for a commercial agglomerated powder, illustrating the low strength and Weibull modulus. K1c for this material was 3.2 MPa$\sqrt{m}$, only half that of 3Y zirconia. The right hand curves demonstrate the gain in both strength and reliability after breaking down the agglomerates during processing. The mean strength increased from 75 to 290 MPa and the Weibull modulus rose from 4 to 5. These results represent a substantial improvement in the processing and properties of fuel cell ceramics [7]. Further enhancement is possible to the target values shown in the figures, if agglomerates could be broken down to the 1 μm size range.

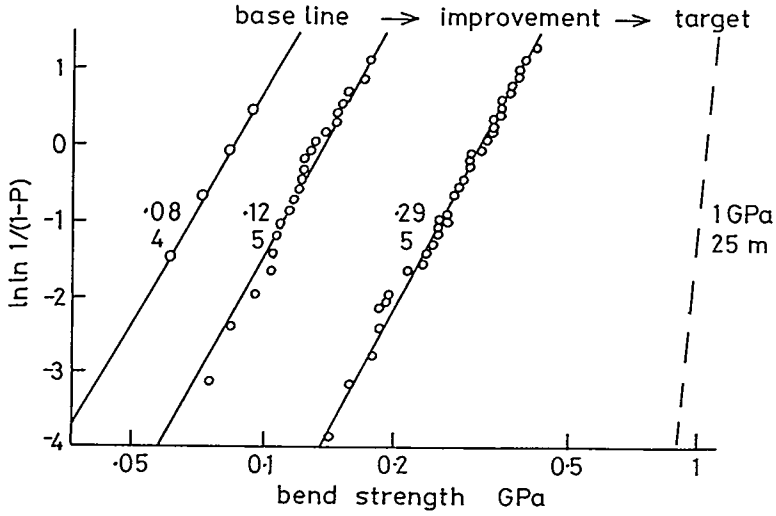

FIGURE 2: BEND STRENGTH PLOTS FOR LANTHANUM CHROMITE, SHOWING IMPROVEMENT FROM LEFT TO RIGHT AFTER AGGLOMERATE BREAKDOWN.

References

1 B Riley, "Solid Oxide Fuel Cells - The Next Stage". J Power Sources, Vol 29, pp223-237, 1990.

2 N McN Alford, J D Birchall and K Kendall, "High Strength Ceramics through Colloidal Control to Remove Defects". Nature, Vol 330, pp51-53, 1987.

3 K Kendall, "Influence of Powder Structure on Processing and Properties of Advanced Ceramics". Powder Technol, Vol 58, pp151-161, 1989.

4 K Kendall, "Agglomerate Strength". Powder Met, Vol 31, pp28-31, 1988.

5 K Kendall, "Microstructure of Sub-Micron Powders and Green Compacts". Birt Ceram proc, Vol 42, pp81-90, 1989.

6 K Kendall, N McN Alford, W J Clegg and J D Birchall, "High Strength and Weibull Modulus from Colloidal Processing of Ceramics". Brit Ceram Proc, Vol 45, pp79-89, 1990.

7 K Kendall, "Revolution in Ceramic Processing". Third European Symposium on Engineering Ceramics, London, November 1989.

THE USE OF MOLTEN CARBONATE FUEL CELLS IN AN INTEGRATED COAL TO TRANSPORTATION LIQUIDS FACILITY

H.T. Chen, J.H. Hirschenhofer, M.G. Klett, M.D. Rutkowski
Gilbert/Commonwealth, Inc.
Reading, PA 19603

In early 1989, the Department of Energy, Office of Coal Conversion Systems directed Gilbert/Commonwealth (G/C) to investigate the integration of various processes to produce transportation liquids via indirect liquefaction of coal, i.e., synthesis. The purpose was to figure out if a pattern could be established to direct Fischer-Tropsch (F-T) liquids production toward economic viability.

The general scope of the study consisted of siting a plant at a mine mouth with a throughput of 30,000 tons per day of dry coal. The coal would be gasified to produce synthesis gas (syngas) for a F-T reactor that, in turn, produced predominantly diesel fuel and gasoline. The scope departs from conventional F-T synthesis in that the product gases are not recycled to extinction. This required G/C to explore alternative approaches for using the off-gases which led to a once-through F-T concept. The scope also required that the plant produce all liquid products and useful byproducts, e.g., electricity. By combining the MCFC with the once-through slurry F-T reactor, G/C developed a synergism that used the available product gas effectively and increased the level of power production significantly. Figure 1 depicts the major plant concept.

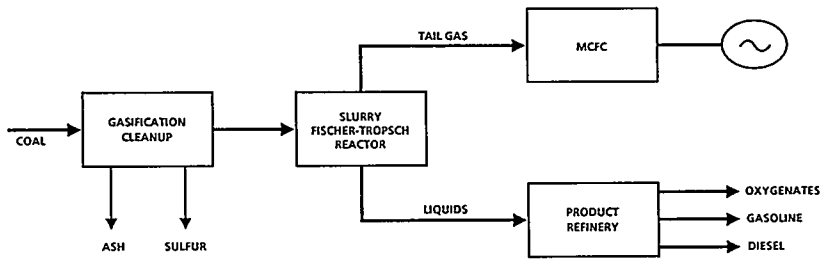

FIGURE 1
BASIC PLANT CONCEPT

The production of diesel fuel and gasoline by indirect liquefaction of coal requires the integration of gasification, cleanup, liquefaction, and refining processes. In this concept, the F-T reactor operates in a once-through mode that has a tail gas consisting of unreacted H_2 and CO with CO_2, C_1, C_2 and other non-condensed vapors. The CO_2 is in a separate stream than the H_2 and CO. The availability of these particular gases suggested that it might be economical to use them in a molten carbonate fuel cell than burn them in a waste heat recovery boiler for use in a combustion turbine/combined cycle. Figure 2 is a schematic of the plant's molten carbonate subsystem of the plant showing the two gas stream feeds from the F-T tail gas subsystem. The operating conditions selected for the fuel cell were determined using the Fuel Cells A Handbook, Kinoshita et al., DOE/METC - 88/6090, May, 1988. The cell operating point is: V = 0.799 volt, J = 220 mA/cm^2, U_f = 85% (CO + H_2), P = 180 psia, and T = 1,200^{o}F.

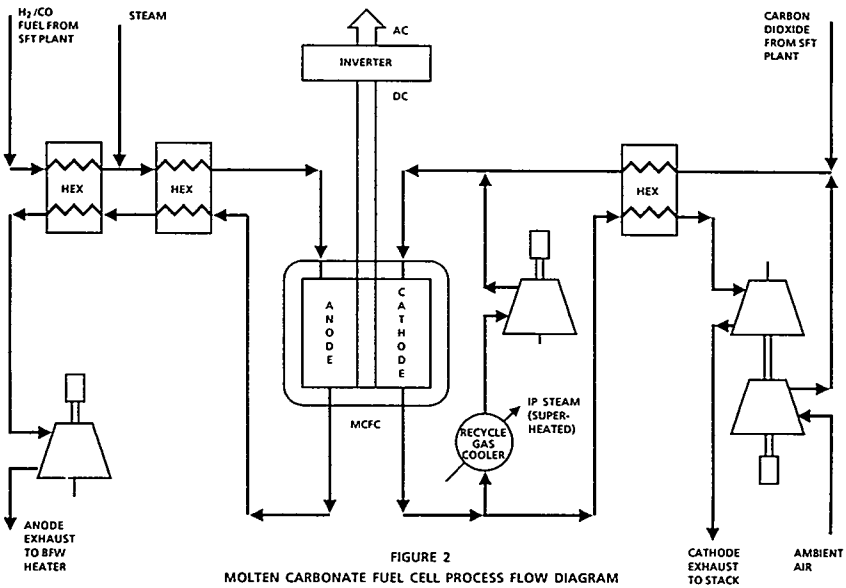

FIGURE 2
MOLTEN CARBONATE FUEL CELL PROCESS FLOW DIAGRAM

Thus, the syngas produced in the gasification plant is used in a form of grand cascade: first as the feedstock in the F-T plant for gasoline diesel production, the MCFC plant then processes the unreacted fraction to provide electro-chemical power generation followed by expansion of the anode/cathode exhaust gases in turbo-machinery for mechanical work recovery and, finally, combustion of the remaining poor quality exhaust fuel gas (with other waste fuel gases generated in the entire complex) in a furnace in support of a central Rankine cycle steam power plant for additional electric power generation. In this way, the energy in the coal is best utilized and hence make the technologies involved more economically feasible. Tables 1 and 2 summarize the plant thermal efficiencies, consumables, and products.

Table 1

PERFORMANCE SUMMARY

MATERIAL		
Coal Feed Rate (Dry)	2,500,000	lb/hr
Oxidant Feed (99.8% Oxygen)	2,000,305	lb/hr
Clean Gas to F-T	4,222,820	lb/hr
Sulfur Recovery	71,683	lb/hr
Slag/Char Production (Dry)	400,254	lb/hr
POWER PRODUCTION		
Gross Steam Turbine Power	1,101,802	kW
Net Steam Turbine Power	1,055,526	kW
Gross Fuel Cell Power	611,871	kW
Net Fuel Cell Power	492,448	kW
Process Plant Power Needs	458,464	kW
Net Power Production	1,089,510	kW
LIQUID PRODUCTS		
LPG Production	0	lb/hr
Oxygenates Production	40,311	lb/hr
Gasoline Production	239,564	lb/hr
Diesel Production	380,613	lb/hr
OVERALL PLANT EFFICIENCY (HHV)	56.43	percent

Table 2

**SHELL COAL GASIFICATION/F-T/REFINERY/MCFC PLANT
OVERALL THERMAL EFFICIENCY**

	pph	MWe	$10x^9$ Btu/h HHV	Btu%
INPUT				
Coal (Dry)	2,500,000		30.950	100.00
USEFUL OUTPUT				
Transportation Liquids				
Diesel	380,613		7.726	24.95
Gasoline	239,564		4.943	15.96
Oxygenates	40,311		0.581	1 88
LPG (C_1 C_2)	0		0.000	0 00
Total Liquids	660,488		13.250	42 79
Sulfur (By-product)	71,683		0.509	1.64
Electricity				
Steam Plant/Gross		1,102		
Net		1,056		
MCFC Plant/Gross		612		
Net		492		
Process Plant Needs		458		
Overall Power Systems		1,090	3.718	12.00
TOTAL USEFUL OUTPUT	732,171	1,090	17.477	56 43

The two major findings of the study were:

- By designing the plant to operate in a once through F-T mode, substantial amounts of high value electricity are produced. By using the molten carbonate fuel cell, conversion to electricity is more efficient resulting in about 12 percent of the HHV value of the coal feed ending up as electricity. Since electricity has the highest value of the products produced, this results in over a third of the revenue coming from electricity. Hence, economics of the plant depend upon both the product mix and selling price.

- Prospects for this concept improve in view of the leverage that electric power can provide for pricing liquids. The revenue required from the sale of liquids decreases with the rising price of electricity. For this study, the effect of pricing electricity from 2 to 8 cents per kWh is to reduce the required selling price of the liquids from $55 to $28 per barrel. Although the cost of products from the plant continues to be higher than the cost of an equivalent barrel of product produced from crude oil, recent events in the mid-east swing the balance close to plant economic feasibility.

Thermodynamic Analysis on Reactions between Molten Carbonates and Alloys

Harumi Yokokawa, Natsuko Sakai, Tatsuya Kawada
and Masayuki Dokiya
National Chemical Laboratory for Industry
Tsukuba Research Center, Ibaraki 305, Japan

Reactions between alloy and molten carbonate are of quite technological importance in view of a long term stability and compatibility required for materials in MCFC. Experimental investigations(1,2) reveal that reaction products form multi-layered scales. Hsu et al.(3) made chemical equilibria calculations and summarized results into a log $P(O_2)$ vs. log $P(CO_2)$ diagram. Such a diagram is convenient to see how reaction products change as functions of oxygen partial pressure and carbon dioxide partial pressure. Even so, this diagram does not provide anything about possible phase arrangement under gradients of thermodynamic variables. Such information should be given in chemical potential diagrams.

Yokokawa et al.(4,5) have written a program, CHD, of constructing a chemical potential diagram in a generalized manner; any linear combination of chemical potentials can be adopted as coordinates, and extension to multicomponent systems can easily be made by fixing some chemical potentials at selected values throughout a series of calculations. In particular, the Li-Fe-C-O system has been investigated to see whether or not this approach can be applied for molten carbonate-metal systems(6). This confirmed that phase equilibria among three differently categorized substances, namely, alloys, carbonates and oxides, can actually be represented as two-dimensional diagrams by selecting proper coordinates and chemical potentials to be fixed. Here, we extend further to the more complicated, Fe-Cr-Li-K-C-O, system. Calculational results are compared with experimental results(1,2) of corrosion test on SUS316L and SUS310S in molten carbonates.

Double Oxides Stable in Molten Carbonates

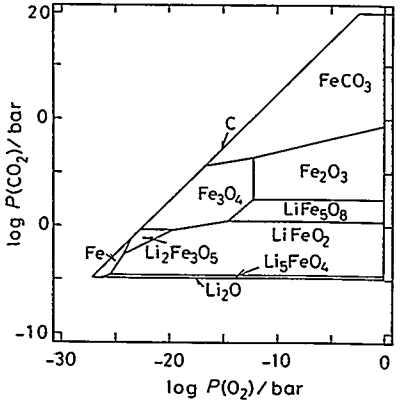

Fig. 1 Chemical potential diagram for Li-K-Fe-C-O system at $a(K_2CO_3)$ = 0.38 and $a(Li_2CO_3)$=0.62.

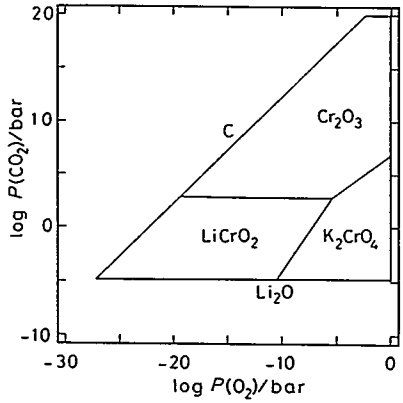

Fig. 2 Chemical potential diagram for Li-K-Cr-C-O system at $a(K_2CO_3)$ = 0.38 and $a(Li_2CO_3)$=0.62.

When the chemical potentials of carbonates are fixed, a diagram shows phases in equilibrium with carbonates. Fig. 1 was constructed for the Fe-Li-K-C-O system under conditions of $a(K_2CO_3)=0.38$ and $a(Li_2CO_3)=0.62$; this fixation was adopted to simulate molten carbonates at the eutectic composition. Although this diagram shows stable iron oxides in the molten carbonates, this is essentially the same as that for the Fe-Li-C-O system under a condition of $a(Li_2CO_3)=1$(6). This means that potassium carbonate is stable against reaction with iron, while lithium carbonate easily reacts with iron to form double oxides. The analogous diagram for the Cr-Li-K-C-O system (Fig. 2) shows that in a high oxygen partial pressure region, chromium reacts with the potassium carbonate component to form potassium chromate, while in a reducing atmosphere, it in turn reacts with the lithium component to form $LiCrO_2$.

Reaction product arrangement

In order to account thermodynamically for multilayered scales, it will be convenient to construct such a diagram that can provide relations among binary oxides, double oxides, and carbonates. Figs. 3 and 4 show phase relations when partial pressures of oxygen and carbon dioxide are simultaneously fixed at selected values; in both cases, chromium exists as Cr_2O_3. Since a log [a(Cr)/a(K)] vs. log [a(Cr)/a(Li)] plot is adopted, the upper region shows phase relations in the Cr_2O_3-Li_2CO_3 subsystem, while those in the Cr_2O_3-K_2CO_3 subsystem are given in the right hand side. Since the molten state of carbonate is not treated as mixture, it should appear at the border between Li_2CO_3 and K_2CO_3. Note that Li_2CO_3 and K_2CO_3 form three phase points with K_2CrO_4 and $LiCrO_2$ in oxidizing and reducing atmospheres, respectively. This suggests the formation of the following layered oxide scales: (molten carbonates)/ K_2CrO_4/Cr_2O_3/(Cr) and (molten carbonates) /$LiCrO_2/Cr_2O_3$/(Cr) for oxidizing and reducing atmospheres, respectively.

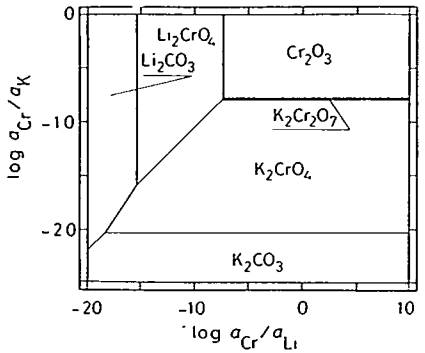

Fig. 3 Chemical potential diagram for Li-K-Cr-C-O system at $P(O_2)$ = 1 bar and $P(CO_2)$ = 0.1 bar.

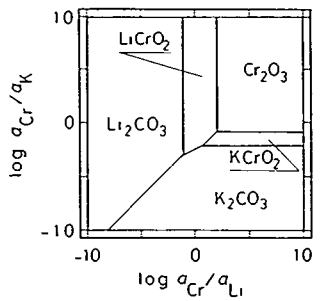

Fig. 4 Chemical potential diagram for Li-K-Cr-C-O system at $P(O_2)$= 10^{-20} bar and $P(CO_2)$=1 bar.

Comparison with experimental results

Some corrosion tests in molten carbonates have been made on SUS316L and SUS310S(1,2). The following layered scales are reported as reaction products in air(2):

$K_2CrO_4/LiFe_5O_8/Cr_2O_3$,Fe,Ni for SUS310S
$LiFe_5O_8/FeCr_2O_4$,Ni for SUS316L

The diagram for the Cr-Fe-Li-K-C-O system was first constructed to see what double oxides of iron or chromium are dominant in molten carbonates. As shown in Fig. 5, $LiFeO_2$ or K_2CrO_4 should be formed according to chromium activity. It is most likely that oxide scale on high chromium content alloys should appear in a high chromium activity region. In this sense, Fig. 5 is consistent with the above experimental results, because SUS310S contains higher chromium content than SUS316L. Even so, Fig. 5 alone cannot provide the thermodynamic basis for the observed layered scales, since phase relations concerning Cr_2O_3, $FeCr_2O_4$ and other oxides are not shown. It is worthy of note that similar phase relations are shown in Figs. 1 and 2 as a function of carbon dioxide partial pressure; that is, with increasing partial pressure of carbon dioxide, the predominant compound of iron or chromium changes from their double oxides to binary oxides. This strongly suggests that extension of Fig. 5 can be obtained by changing partial pressure of carbon dioxide. For this purpose, graphite and iron carbonate appearing in Fig. 1 are not necessary and were excluded in Fig. 6.

To account for the layered arrangement of SUS316L and SUS310S simultaneously, dissections were setup. A dissection ABCD (b), shows that oxide scales can be well accounted for by simple parallel paths (solid and dashed lines for SUS316L and SUS310S, respectively). Fig. 6(c) was constructed to compare with results of Nakagawa et al.(1) who maintained SUS316L potentiostatically at -0.95 V and obtained a porous double layered scale (outside Fe;inside Cr), which was equilibrated with carbonates. In such a case, SUS316L may form a $LiFeO_2/LiCrO_2$ scale instead of a $LiFeO_2/FeCr_2O_4$ scale obtained without applying voltage.

The present diagrams can explain that the multilayered arrangement is resulted from monotonical changes in chemical potentials along diffusion paths. This implies that the local equilibrium approximation can hold in the corrosion processes.

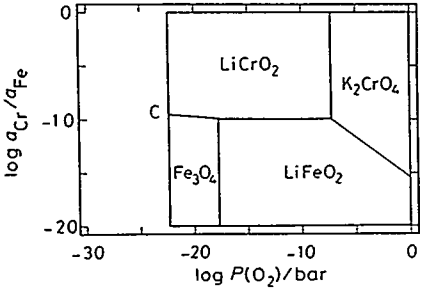

Fig. 5 Cr-Fe-Li-K-C-O system at $a(K_2CO_3)$=0.38, $a(Li_2CO_3)$ =0.62 and $P(CO_2)$= 1 bar.

References

1. K. Nakagawa et al., Boshoku Gijutsu,36,438(1987);37,473(1988)
2. Y. Fujita et al. Proc. Fall M. Electrochem. Soc. Japan, 2E04, 115 (1989).
3. H. S. Hsu et al. J. Electro-

chem. Soc. 133, 2077 (1986); 134 2146, 3038 (1987).
4. H. Yokokawa, T. Kawada and M. Dokiya, Denki Kagaku 56, 751 (1988); J. Am. Ceram. Soc. 72, 2104 (1989).
5. H. Yokokawa et al. J. Electrochem. Soc. 137, 388 (1990).
6. H. Yokokawa et al. Denki Kagaku, 58, 57 (1990).
7. T. B. Lindemer et al. J. Nucl. Mater., 100, 178 (1981).

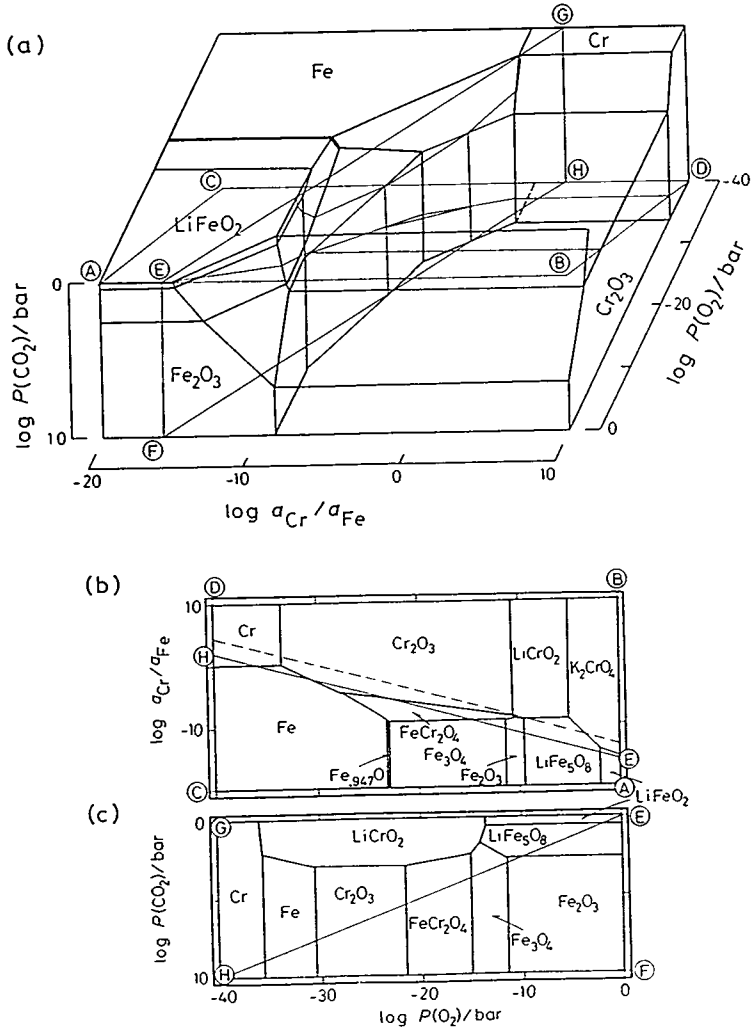

Fig. 6 Chemical potential diagram for the Cr-Fe-Li-K-C-O system under conditions of $a(K_2CO_3)$ =0.38 and $a(Li_2CO_3)$=0.62. (a) three dimensional diagram, (b) dissection ABCD, (c) dissection EFGH.

Chemical Stability of Interface between Air Electrode and Electrolyte in Solid Oxide Fuel Cell

Harumi Yokokawa, Natsuko Sakai, Tatsuya Kawada
and Masayuki Dokiya
National Chemical Laboratory for Industry
Tsukuba Research Center, Ibaraki 305, Japan

Tedmon et al.(1) first reported in 1969 on potential use of transition metal perovskites as air electrode for a solid oxide fuel cell. Since then, some experimental investigations have been made to clarify electrode-electrolyte reactions(2-4): Hayami and Yabuki(2) clarified that $LaCoO_3$ reacts with ZrO_2 to form $La_2Zr_2O_7$ and CoO at high temperatures and as a result, give rise to a non-uniform concentration profile, which has been confirmed recently by Echigoya et al.(3) more clearly. On the other hand, Lau and Singhal(4) found that reaction between $La_{0.9}Sr_{0.1}MnO_3$ and YSZ gave rise to the formation of $La_2Zr_2O_7$; however, no manganese binary oxide was detected.

We have made a series of thermodynamic analyses to clarify the thermodynamic nature of reactions between perovskites and zirconia(5). Thermodynamic explanation can be thus given for whether or not reactions take place between perovskites and zirconia; in other words, results of powder reactions can be well taken into account. On the other hand, diffusion couple experiments reveal interesting distribution of reaction products. In the present study, an attempt has been made to account for such a concentration profile in terms of diffusion paths in chemical potential diagrams.

Thermodynamic Data

Echigoya et al.(3) have recently found $La_2Zr(Ni,Co)O_6$ as reaction products. Similar compounds, $La_{2n}M_nZrO_{4n+2}$ (M=Ni, Co), might therefore exist and be formed as reaction products. Since the thermodynamic properties of such ternary oxides were not available, they were estimated as follows: For La_2MZrO_6, use was made of an empirical correlation between enthalpy of formation and tolerance factor(t):

$$\delta/\text{kJ mol}^{-1} = 2\ [\ -90 + 720\ (1 - t)], \qquad [1]$$

in which t was calculated from the averaged radii of B-site cations (Zr^{4+} and M^{2+}). The entropy of formation is assumed to be zero. The thermodynamic properties of $La_4M_2ZrO_{10}$ were obtained from the estimated enthalpy change, -10 kJ/mol, for the following reaction:

$$La_2MO_4 + La_2MZrO_6 = La_4M_2ZrO_{10}. \qquad [2]$$

This is about the same as that for $Sr_4Ti_3O_{10}$.

$LaCoO_3$/YSZ

When the oxygen potential is fixed at $P(O_2) = 1$ bar in the La-M-Zr-O system, three phase coexistence leads to the invariant point, which can be characterized in terms of chemical potentials of the three metallic elements, μ(La), μ(M) and μ(Zr). This implies that phase equilibria in the La-M-Zr-O system at a constant oxygen potential can be well represented

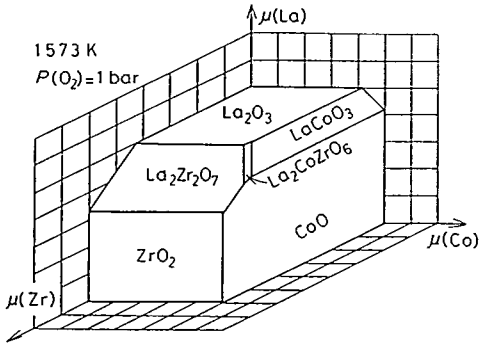

Fig. 1. Three dimensional chemical potential diagram for La-Zr-Co-O system at $P(O_2)$ = 1 bar.

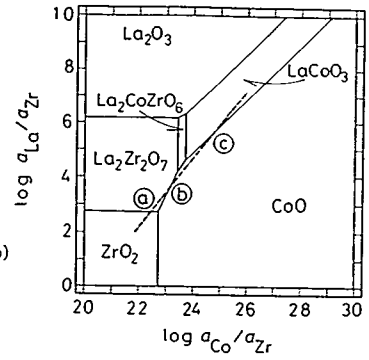

Fig. 2. Chemical potential diagram for La-Zr-Co-O system at 1573 K and $P(O_2)$ = 1 bar: a dashed line is a possible diffusion path.

in a three-dimensional chemical potential diagram. An example is shown in Fig. 1 for the La-Co-Zr-O system. In this diagram, binary oxides are represented by flat planes which are perpendicular to the respective axis and form a cubic polyhedron. Similarly, $LaCoO_3$ is represented by a plane cutting off the edge between CoO_2 and La_2O_3. In this way, all stable phases form a polyhedron in the three dimensional chemical potential space. Although this is quite appropriate for providing the whole phase equilibria, two dimensional diagrams may become convenient in some cases; Fig. 2 shows a log [a(Co)/a(Zr)] vs. log [a(La)/a(Zr)] plot, in which phase equilibria among La_2O_3, $La_2Zr_2O_7$ and ZrO_2 are given in the left-hand side, whereas those among La_2O_3, $LaCoO_3$ and CoO are given in the right-upper part. The important point in Fig. 2 is that the stability area of $LaCoO_3$ is separated from that of ZrO_2; in other words, $La_2Zr_2O_7$ and CoO intervene between $LaCoO_3$ and ZrO_2. This polygon configuration corresponds to the following reaction;

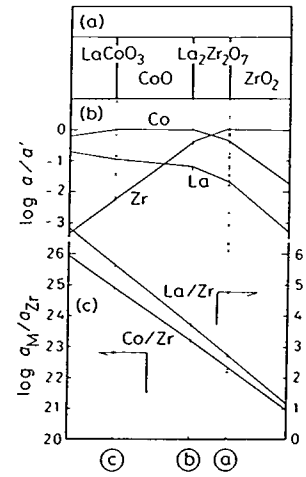

Fig. 3. Chemical potentials along diffusion path: a) dominant products;b) elemental chemical potentials relative to CoO, ZrO_2, La_2O_3 at $P(O_2)$ = 1 bar; c) driving force.

$$LaCoO_3 + ZrO_2 = 1/2\ La_2Zr_2O_7 + CoO + 1/4\ O_2(g). \quad [3]$$

This is accompanied with reduction of cobalt ions; its Gibbs energy change at 1573 K is negative.

The most interesting point in diffusion couple results is that the reaction products, $La_2Zr_2O_7$ ($Pr_2Zr_2O_7$) and CoO, tend to be formed separately; that is, CoO appears immediately adjacent to $LaCoO_3$ ($PrCoO_3$), while $La_2Zr_2O_7$ ($Pr_2Zr_2O_7$) is formed between CoO and ZrO_2. Fig. 2 shows that there is some possibility of accounting for this layered arrangement in terms of the chemical potentials. Since reactant are $LaCoO_3$ and ZrO_2, chemical potential differences of Zr and of La(Co), μ(La) - μ(Zr) or μ(Co) - μ(Zr), should change monotonically from the ZrO_2 side to the $LaCoO_3$ side; this can be represented as a line having a positive slope in Fig. 2. In order to account for the formation of CoO next to $LaCoO_3$, we can draw a diffusion path as a dashed line in Fig. 2. Along this line, chemical potentials change as given in Fig. 3; the present driving force, gradient of log [a(Co)/a(Zr)] or log [a(La)/a(Zr)], is presented in Fig. 3(c). Note that in Fig. 3(b), the chemical potential of cobalt has the maximum in the cobalt oxide phase. In addition, lanthanum ions diffuse beyond the La_2O_3-depleted CoO phase to form $La_2Zr_2O_7$ with ZrO_2; the chemical potential of lanthanum, however, decreases monotonically.

$LaNiO_3$/YSZ

The chemical potential diagram for the La-Ni-Zr-O system is shown in Fig. 4. At 1573 K, $La_4Ni_3O_{10}$ as well as La_2NiO_4 are stable at $P(O_2)$= 1 bar. La_2NiZrO_6 and $La_4Ni_2ZrO_{10}$ appear among $La_2Zr_2O_7$, NiO, $La_4Ni_3O_{10}$, La_2NiO_4 and La_2O_3. Among reactions associated with these compounds, only the following reaction evolves oxygen:

$$La_4Ni_3O_{10} + ZrO_2 = La_4Ni_2ZrO_{10} + NiO + 1/2\ O_2(g). \qquad [4]$$

In diffusion couple between $La(Ni,Co)O_3$ and YSZ, Echigoya et al.(3) found that nickel and cobalt ions diffuse and form monotonically decreasing concentration profiles. Fig. 4 indicates that this feature may be due to the formation of ternary Ruddlesden-Popper phases. Actually, the polygon arrangement in Fig. 4 is quite similar to the experimental phase arrangement(3) between perovskite and YSZ. Note, however, that the layered structure of NiO and $La_2Zr_2O_7$ was not developed in this case. This is probably because of no evolution of oxygen at NiO precipitation or of different diffusion rates in NiO phase.

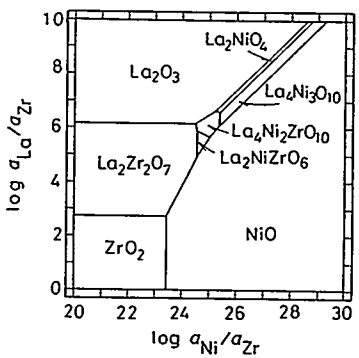

Fig. 4. Chemical potential diagram for La-Zr-Ni-O system at 1573 K and $P(O_2)$ = 1 bar including estimated $La_4Ni_2ZrO_{10}$ phase.

La_yMnO_3/YSZ

The chemical potential diagram is shown in Fig. 5. Since the lanthanum nonstoichiometry in the manganite perovskite affects its reaction with ZrO_2, a chemical potential diagram was first constructed by CHD without taking into account the lanthanum nonstoichiometry; this is presented by dotted lines in Fig. 5. Solid lines show phase relations among the nonstoichiometric lanthanum manganite, $La_yMnO_{3-\delta}$, and cubic solid solutions, $(ZrO_2)_{1-x}(YO_{1.5})_x$, calculated using the CTC/SOLGASMIX program.

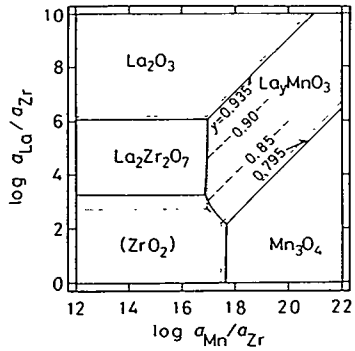

Fig. 5. Chemical potential diagram for La-Zr-Mn-O system at 1573 K and $P(O_2)$= 1 bar. Dotted lines were for stoichiometric compounds for $LaMnO_3$, solid lines being for La_yMnO_3 and $(ZrO_2)_{1-x}(YO_{1.5})_x$.

No diffusion couple has been done between $LaMnO_3$ and YSZ. Instead, it has been done between $(La_{0.9}Sr_{0.1})MnO_3$ and YSZ by Lau and Singhal(4); their results show some interdiffusions of La, Mn and Zr. However, it is not clear that whether $La_2Zr_2O_7$ phase was formed at the interface.

Recently, Yamamoto et al.(6) have investigated effects of La nonstoichiometry of La_yMnO_3 on reaction with YSZ and found that when La nonstoichiometry is large, after about 100 h or longer period of time, $La_2Zr_2O_7$ eventually formed together with enlargement of YSZ cubic lattice. This indicates that some La component in La_yMnO_3 dissolved into YSZ. Figure 5 implies that the $La_2Zr_2O_7$ precipitation should be accompanied with significant Mn depletion from perovskite phase. Although the manganese dissolution is not included in Fig. 5, the stability area of Mn dissolved ZrO_2 can be regarded to be essentially the same as that of nondissolved ZrO_2; the Mn-rich side of its stability area therefore corresponds to Mn-dissolved ZrO_2. This implies that when y is small, the manganese component significantly dissolves into YSZ, and the precipitated $La_2Zr_2O_7$ phase would be in equilibrium with La_yMnO_3 and Mn-dissolved YSZ.

References

1. C.S.Tedmon,Jr. et al. J. Electrochem. Soc. 116,1170(1969).
2. R. Hayami and T. Yabuki, Bull. Government Industrial Research Institute, Osaka, 28, 98 (1977).
3. J.Echigoya, et al. Mater.Trans.JIM,30, 789(1989).
4. S. K. Lau, S. C. Singhal, National Fuel Cell Seminar May 1985 Tuscon, Arizona, Courtesy Associate, 1985, p. 107.
5. H. Yokokawa, et al., Denkikagaku 56, 751(1988);57, 821 (1989);57,829(1989);58,161(1990);58,489(1990): J. Am. Ceram. Soc. 72, 2104(1989): J. Electrochem. Soc. 137, 388 (1990).
6. O. Yamamoto et al. Proc. 1st International Symp. Solid Oxide Fuel Cell, ed. by S.C.Singhal, ECS, 1989, pp242-253.

DEFINITION OF PROCESS STEPS FOR MCFC COMPONENTS AND CELLS OF LABORATORY SCALE

Hartmut Wendt, Olaf Böhme, Frank Udo Leidich
Institut für Chemische Technologie, TH Darmstadt
Petersenstraße 20, 6100 Darmstadt, Ger. Fed. Rep.

1. Introduction

Preparation of precursors of MCFC-anodes, cathodes and electrolyte matrices in polymer-bonded tapes and the in-situ formation of molten carbonate fuel cells by thermal curing of such stacked tapes are the key steps in MCFC-production. /1/. Tape casting, tape composition and the appropriate heat treatment decide the eventual cell performance. This paper reports on investigations which are intended to obtain fundamental knowledge and engineering data concerning tape casting and heat treatment.

2. Self supporting cells

The mechanical conditions within a compressed fuel cell stack do not allow for exerting pressure separately on the wet seal and on the fuel cell surface and current transducting structures of the cell separately.

It is therefore necessary to perform the formation of the stack in a way which would allow for good and permanent electronic contacts between both electrodes and the bipolar plate and assures simultaneously a good electrolytic contact between either electrodes and the electrolyte. The formation procedure and the formation of the anode and cathode - precursor foils must therefore provide for the possibility to solder in a way the metallic nickel-anode and nickel oxide cathode to the metal-structure of the bipolar plate or cell frame respectively. It is the aim of the procedure, described in this paper to arrive at a process which starts from foils avoiding any preceding high temperature sintering step and which allows to form the cell in situ from tapes.

3. Formation and Casting of precursor foils

3.1 The anode foil

To assure sinterability at formation temperatures of approx. 650°C of the metallic anode structure (the normal sintering temperature of nickel amounts to 900°C) the nickel incorporated into the precursor tape has to be highly dispers. Therefore Mond-nickel with a mean particle diameter of approximately 3 µm is chosen, which forms on sintering porous structures which are mechanically too soft, so that shrinking and loos of inner surface with deterioration and seizable performance losses in very short time can be obsorved. It is state of the art to use Cr-additives in presintered electrodes which affect a type of dispersion hardening of the nickel structure. By use of appropriate (still propriatory) oxidic additives to the anode-precursor tape the same effect can be achieved-avoiding the relative expensive sintering of Ni(Cr)-structures in very dry reducing atmosphere.

Fig. 1a and 1b show sintered nickel anodes with and without this additive.

3.2 The cathode tape

It is state of the art to form lithiiated, porous MCFC-cathodes by in situ oxidation of presintered porous nickel structures being in contact and soaked with the Li/K-carbonate electrolyte.

Presintering can be avoided by preparing cathode precursor tapes which are similarly composed as the anode foils but which contain an active additive (proprictory) which initiates a dissolution-redeposition process of oxidatively formed nickel oxide which renders good electronic contact to the surface of the oxidized bipolar plate and improves the lateral electronic conductivity within the porous nickel cathode. Fig. 2a and 2b compare the appearance of nickel oxide cathodes without and with this additive.

3.3 The matrix tape

The matrix tape is prepared from prefabricated $LiAlO_2$ which - due to the reaction mode, by which it is formed from alumina and lithium carbonate - comes immediately in correct granulometry, e.g. with a particle size of 0.5 to 1 µm.

Although $LiAlO_2$ is seizably hydrolysed in aqueous solution a proprietary procedure allows to work it into tapes by dispersing it in aqueous solutions of polyvinyl alcohol which is the polymeric organic binder for all three precursor foils.

4. Evaporation and removal of the organic binder

4.1 DTG-experiments

Fig. 3a depicts a DT-gram of an anode-precursor tape. The curve allows to distinguish the removal of residual water and glycerol in the temperature range of 140 to 220°C followed by depolymerization and evaporation of polyvinylalcohol.

Fig. 3b. depicts the behaviour of the matrix-precursor and shows that $LiAlO_2$ binds water and polyvinylalcohol much stronger than metallic nickel. It is very important for a success of the in-situ formation of the cell that accordingly the release of vapours and combustibles is retarded and therefore the precursor-assembled cell has the chance to be cured without destruction by avoiding violent gas evolution from its initially shielded central matrix.

4.2 Electrolyte supply

From the DTG there follows the temperature-strategy for cell-curing in inert atmosphere. Finally the matrix is provided at 650°C with electrolyte, which is soaked from the rim of the cell into the matrix. Only after this procedure the working gas are given access to their respective electrodes.

5. Cell performance

Fig. 4 depicts the evolution of current densities at a cell voltage of 750 mV (upper trace) and 900 mV (lower trace; anode gas: 0.85% H_2, 0.15% H_2O; cathode gas: 67% air, 33% CO_2) with time. During the first 50 hrs the cell current keeps nearly constant (100 and 200 mA/cm^2) increases sizeably from 60 to 100 hrs and stays unchanged (300 mA/cm^2 and 200 mA/cm^2 resp.) for the next 400 hrs. Deterioration cannot be observed during the first 3000 hrs.

6. Conclusion

An in-situ formation of molten carbonate fuel cells from component precursors which are all made from film-casted foils with polyvinyl alcohol as organic binder can be performed with good reproducibility and rehability on bench scale size.

Performance of fuel cells prepared by in situ formation match published data so that the method can be expected of practical use - provided it can be extended to larger cell surfaces.

7. References

/1/ J.R. Selman, L.G. Marianowski, "Fuel Cells" in D.G. Lovering ed., Molten Salt Technology, Plenum Press, 1982

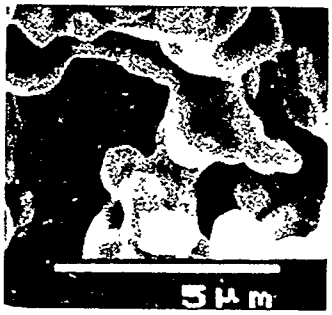

Fig. 1a: standard anode

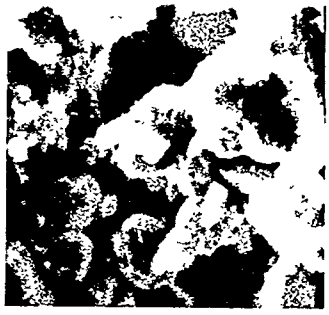

Fig. 1b: modified anode

Fig. 2a: standard cathode

Fig. 2b: modified cathode

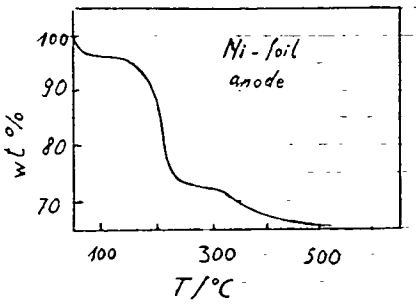

Fig. 3a: DTG of anode foil

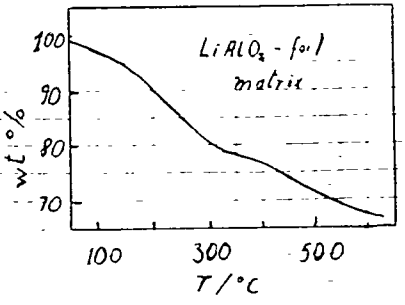

Fig. 3b: DTG of matrix foil

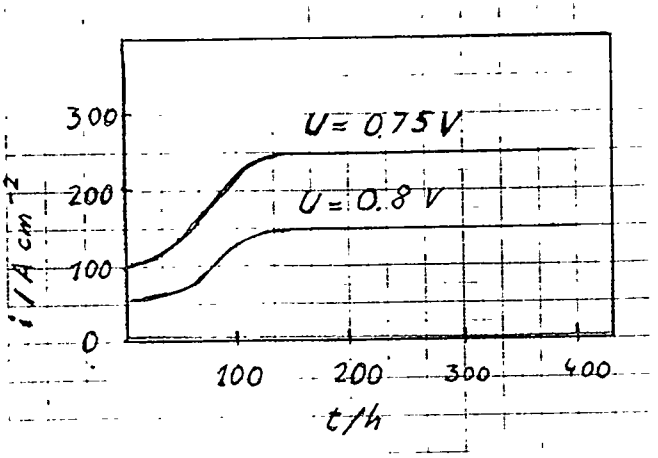

Fig. 4: low term behaviour of in-situ formed MCFC

- VOLATILITY OF ALKALI CARBONATE MELTS - BASIC ENGINEERING DATA FOR THE MOLTEN CARBONATE FUEL CELLS

Holger MOHN and Hartmut WENDT

Institut für Chemische Technologie der TH Darmstadt,
Petersenstr. 20, D-6100 Darmstadt, F.R.G.

Introduction

Molten salt fuel cells (MCFC) are expected to become important devices for medium to large scale highly efficient energy conversion during the coming decennium. But still a number of unsolved problems hampers the rapid development of MCFCs. Among these problems there is the important question of electrolyte management because the used mixed akali carbonate melts exhibit finite vapor pressures which give rise to electrolyte evaporation into the working gases with corresponding long term electrolyte losses. This type of dynamic electrolyte loss is caused by the enhanced vapor pressure of the alkali hydroxides due to the sensitivity of the alkali carbonates to hydrolysis.
Equilibria between alkali carbonate melts and water vapor, oxygen and carbon dioxide are known from the literature but need a confirmation as well as experimental proof if applied to mixed molten alkali carbonate melts.

Experimental

The volatility of purified and molten alkali carbonates and their binary mixtures was investigatd applying the perspiration procedure using as carrier gases mixtures containing water vapor together with carbon dioxide under a total pressure of 1 bar. The amount of carbon dioxide in the carrier gas determines the mole fraction of alkali oxide in the melt defined by the equilibrium (equ. 1)

(1) Me_2CO_3 ----------> $Me_2O + CO_2$

Whereas the amount of water vapor together with the amount of carbon dioxide in the carrier gas determines the degree of melt hydrolysis (equ. 2),

(2) $Me_2CO_3 + H_2O$ --------> $2MeOH + CO_2$

the ratio of metal oxide to metal hydroxide in the melt depends only on the water vapor pressure and not on the carbon dioxide pressure.
Perspiration measurements were performed at seizeably enhanced temperatures of 750°C to 940°C for lithium-, sodium- and potassium carbonate melts as well as for the mixed lithium/potassium and lithium/sodium carbonate melts because in the temperature range, which is typical for MCFC process (650°C) the vapor pressures were inconveniently low.

Extrapolating the obtained data over a temperature range of at most 200°C was supposed to be a safe procedure.
Measurements were performed under two different gas atmospheres. At first a CO_2/H_2O gas mixture (4/1 for the pure alkali carbonates, 1/1 for the mixed carbonates) was used as carrier gas in order to simulate cathodic.
A reducing gas mixture $H_2/CO_3/H_2O$ (1/1/1) was applied to simulate anodic conditions.

Results

Vapor pressures under "cathode gas"

For Li_2CO_3 the measured effective vapor pressures under CO_2/H_2O(1/1)-atmosphere were compared with lithium hydroxide vapor pressures calculated from data of the JANAF tables. At a temperatur of 800°C one calculates a LiOH- vapor pressure of approximately $4 \cdot 10^{-6}$ bars for lithium carbonate melts in contact with the gas atmosphere mentioned above.
Experimentally much higher vapor pressures are obtained: at 750°C for instance one measures $1,2 \cdot 10^{-5}$ bars (a monomeric lithium species being assumed) and the vapor pressure increases to $1 \cdot 10^{-4}$ bars at 885°C. The effective vaporization enthalpie for the unknown volatile lithium species amounts to 172 kJ/mole.

Potassium carbonate is much less volatile than the lithium salt melt. At 900°C $8 \cdot 10^{-5}$ bars are determined.
This agrees quiet well with to the data calculated from the JANAF tables for potassium hydroxide. The effective vaporization enthalpie was determined to be 219 KJ/mole, from data of the JANAF tables one calculates 225 KJ/mole. This good agreement is an indication for KOH to be the volatile gas species.

The eutectic mixture of lithium and potassium carbonate, which contains 68 (Li) and 32 (K) mole % had been investigated in the temperature range from 850 to 932°C .

Interestingly the observed vapor pressures of volatile lithium species of the melt is much lower than anticipated from the vapor pressures of pure lithium carbonate melts. Across the temperature range the effective lithium vapor pressure does not exceed 10^{-6} bars whereas the effective vapor pressure of volatile potassium species changes from $4,8 \cdot 10^{-6}$ bars to $2,8 \cdot 10^{-5}$ bars.
This is obviously an indication that in the eutectic mixture of Li_2CO_3 and K_2CO_3 the vapor pressures of lithium and potassium are decreased by a factor of almost hundred due to the formation of the compound $LiKCO_3$.

The eutectic mixture of lithium and sodium carbonate 52 (Li) and 48 (Na) mole% that is also beeing discussed for the use as electrolyte in MCFC, had been investigated in the temperature range from 825 to 910°C with the same CO_2/H_2O (1/1)-carrier gas mixture.
The effective vapor pressure of sodium changes from $1.4 \cdot 10^{-6}$ bars at 906°C to $7.5 \cdot 10^{-7}$ bars at 825°C.
It has to be noted that the effective sodium pressure at 900°C is one order of magnitude lower than the effective potassium vapor pressure.

Vapor pressure under "anode gas"

Applying the reductive carrier gas ($H_2/CO_3/H_2O$ = 1/1/1), measurements on the Li/K- mixture (62/38 mole%) were performed between 765 and 900°C, on the Li/Na- mixture (52/48 mole%) between 690 and 797°C.
For the Li/K- mixture the effective vapor pressures of lithium and potassium are almost the same in this temperature range; for 780°C the effective Li- and K- pressures are determined to be $4.5 \cdot 10^{-6}$ bars and for 900°C to $1.3 \cdot 10^{-4}$ bars.

For the Li/Na- mixture at 800°C $3 \cdot 10^{-6}$bars and at 700°C $4 \cdot 10^{-7}$ bars are determined for the Na-vapor pressure. The Li- vapor pressure does not exceed 10^{-6} bars.

The result of the transpiration measurements indicates that vapor loss from the standard Li_2CO_3/K_2CO_3 electrolyte is **significantely higher**, namely a factor of approximately 10, than from the Li_2CO_3/Na_2CO_3 melt under oxidizing as well as under reducing conditions.
It must also be recognized that under reducing atmosphere the alkali vapor pressures are lower than under oxidizing conditions. Both is clearly to be seen in figure 1.

Extrapolating the observed vapor pressure data to 650°C - which is actually the working temperature of molten carbonate fuel cells, shows that vaporization of the electrolyte in the oxidizing cathode atmosphere does not pose a real problem for maintaining the fuel cell process.
Although the effective alkali pressures are about one order of magnitude higher in reducing atmosphere, evaporation losses are still tolerably small.

Figure I: Overview of the effective Na- and K- vapor pressures over Li_2CO_3/Na_2CO_3 (52/48 mole%) and Li_2CO_3/K_2CO_3 (62/38 mole%) melts under the more oxidizing CO_2/H_2O (1/1) - and the reductive $H_2/CO_2/H_2O$ (1/1/1) atmosphere as a function of the temperature.

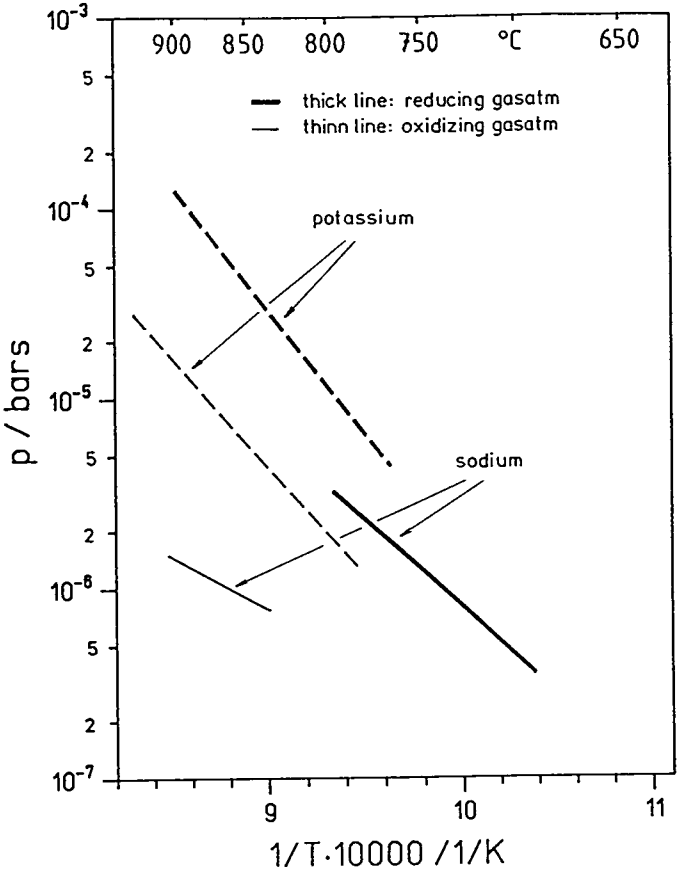

New Process Design for a Solid Oxide Fuel Cell Power Plant

Masamichi Ippommatsu, Hirokazu Sasaki, Akira Hirano, and Kimio Ishimaru

Fundamental Research Laboratories, Osaka Gas Co.,LTD.
6-19-9 Torishima Konohana-ku Osaka, 554 Japan

1. Introduction

Solid oxide electrolyte fuel cell (SOFC) is high efficiency co-generation system, and this development is one of the most important theme for gas industry. There is a strong relationship between cell structure design and system design to improve SOFC system, and good cell structure design must be supported by good system design. It is because SOFC is composed by all ceramics and controling the stress caused by thermal expansion is more difficult than other type fuel cell. In this paper, the authors report their studies of a new process design for SOFC power plant using chemical process simulation and cell simulation including current density , chemical spcies and temperature distribution.

2. Simulation method

We have developed three main simulation modules . One simulates tubular cells incorporating inner reforming process ,temperature distribution, heat transfer and gas diffusion in electrode. Second is isothermal SOFC simulation module incorporating inner reforming to both tubular and cross flow planar cells. Third is system simulation module. Our computer is SONY NEWS NWP-3860 (Max 20MIPS) that is the fastest desk top workstation and this computer is enough to calculate. Basic equations are shown in the reference [1] that contents Isothermal cell simulation , and non-isothermal cell simulation will be published in near future.

3. Design and results of simulation

Our new process design of the SOFC power plant is shown in Fig.1. The innovative points of this new design are a fuel recycling and supplying oxygen rich air to reduce diffusion resistance. All reaction vessels except CO_2 removal are adiavatic vessel, and it is possible to construct the plant with low cost and easy to control. Our simple feasibility study suggest a high probability that the cost of the new design is less than that of the conventional design when we adapt to more than MW plant. Four examples of simulation that include thermal distribution are shown in Fig.2. (1) Conventional system including pre-reformer. [Fuel utilization factor UF = 85 % , Air utilization factor UA = 25 % , Output voltage 689 mV ,Output current 20A , Cell length 300 mm tubular type] (2) Fuel recycle system [UF = 15 % for one cycle , Pure oxygen , Output Voltage 984 mV] (3) Fuel recycle system [Output voltage 689 mV] (4) Fuel recycle system [Output voltage 585 mV]

Case(1) and case(2) were calculated to compare the output voltages and so the output current is same . Efficiency of power generation of case(2) is about 1.8 times in comparison with case(1) . Case(3) and (4) are prepared to show the probability to increase output current. Output current of case (4) is 5.7 times of case (1) at same efficiency. Case(3) and Case (4) show the new system enables to cool the cell when the cell is operated at high loading.

4. Conclusion

The results of simulation show that the new system design has a good probability to improve efficiency of power generation , output current, and cell cooling . This design has a little difficulty to let enter into market such as development of low cost CO_2 removal system. However high potential of this new design is illustrated.

[1] A.Hirano et al. Denki Kagaku P842 vol.9 1990

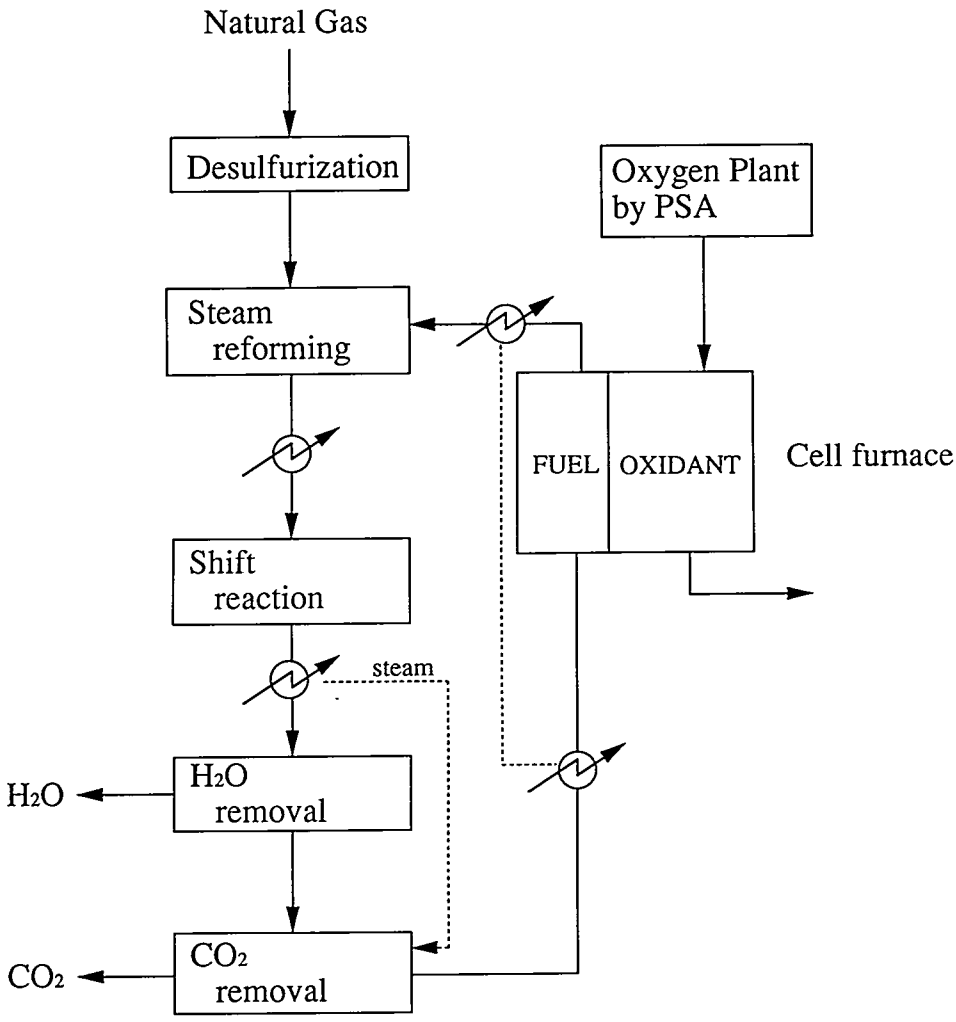

Fig.1 New System Design

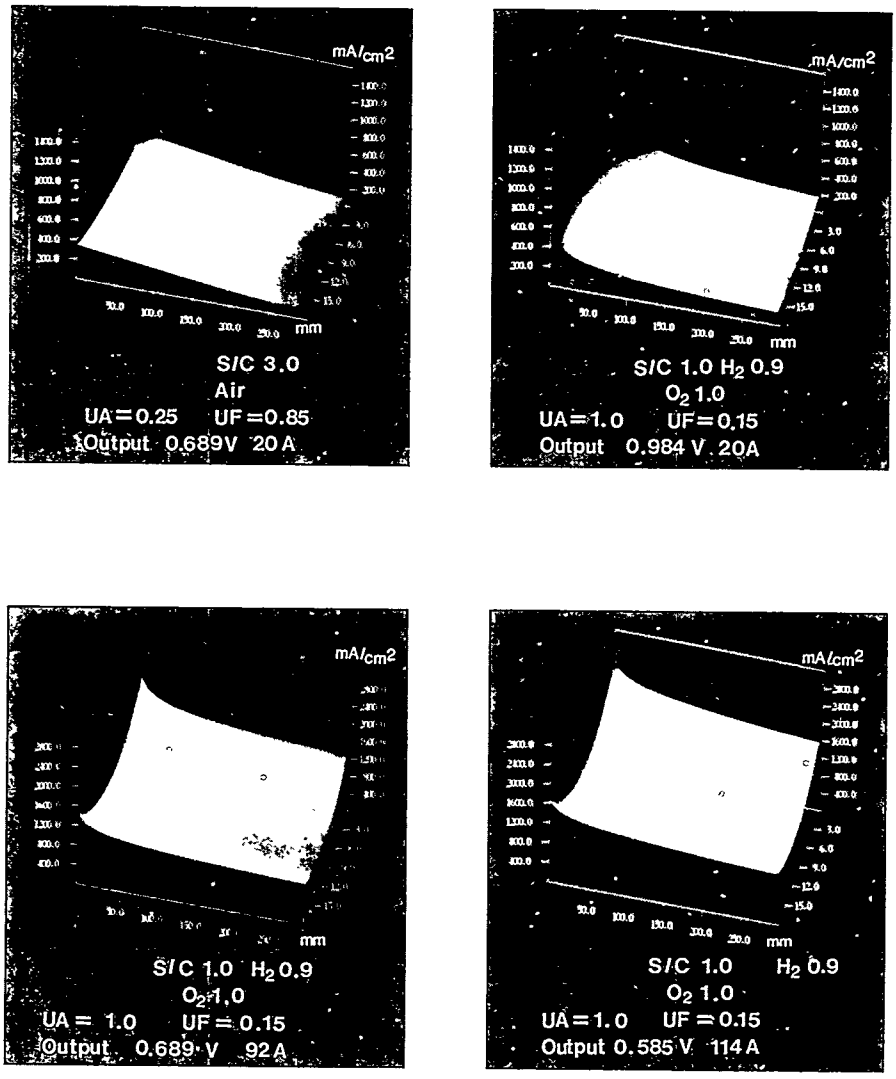

Fig.2 Calculated current density distribution using non-isothermal model

DEVELOPMENT OF NEW MATERIAL FOR MCFC SEPARATOR

T. Shimada, Y. Kuriki, N. Yamanouchi and M. Tamura
Steel Research Center, NKK Corporation
1-1 Minamiwatarida-cho, Kawasaki-ku, Kawasaki, 210 Japan

INTRODUCTION

Development of new materials for the major components of molten carbonate fuel cell (MCFC) is under way at MCFC Research Association as a part of MCFC Power Generation System Research Development in the Moonlight Project in Japan. Development of alternative material to AISI 316L and 310S steels for metallic components such as the separator, current collector and gas channel has been being conducted at NKK and a highly corrosion resistant 30%Cr-40%Ni-1%Al-0.05%Y-Fe alloy has been obtained so far. This paper is focused on the results of an electrochemical corrosion test simulating highly peculiar corrosion environment of MCFC.

EXPERIMENTAL

The 30%Cr-40%Ni-1%Al-0.05%Y-Fe alloy, along with AISI 316L and 310S steels, was tested for its performance in terms of the corrosion resistance by the electrochemical method, that is, the measurement of the change in the anodic current during the immersion in the molten carbonate. The chemical compositions of the tested materials and the test conditions are shown in Table 1 and Table 2, respectively. In this test, test specimens were polarized to the fixed potential equivalent to that of the cathode or anode potential of MCFC. For the evaluation of the corrosion resistance of the separator materials of MCFC, this method is more suitable than the widely used dip type or coating type corrosion tests because the metallic components are electrochemically in contact with and polarized to the potential of either electrode during the operation of MCFC and the corrosion behavior of the materials is significantly affected by the electrochemical polarization. Testing setup was composed of the image furnace, high purity alumina crucible, test specimen (working electrode), reference electrode ($33\%O_2/67\%CO_2/Au$), counter electrode (Au), potentiostat and recorder. Immediately after the test specimen was immersed in the molten carbonate into which the environmental gas had been kept bubbling for 1 hour, the specimen was polarized to the cathode or anode potential of MCFC and the measurement of the anodic current was started. Tests were conducted for 20 hours.

RESULTS AND DISCUSSION

Measured change of the anodic current with time at anode potential of MCFC for tested materials are shown in Fig.1. It is clear that the anodic current for the 30%Cr-40%Ni-1%Al-0.05%Y-Fe alloy was smaller by about an order than that of AISI 316L steel and several times smaller than that of 310S steel. Considering that the anode potential of

MCFC is in the region of active dissolution for all tested materials, this result can be explained by the effect of Cr to restrict the anodic current in the active dissolution region and also by the effect of Al to shift the rest potential to noble potential. AISI 316L and 310S steels are usually used with Ni cladded on the side exposed to anode environment because they suffer especially severe corrosion at anode side. From the data shown in Fig.1, it can be said that the 30%Cr-40%Ni-1%Al-0.05%Y-Fe alloy is much more corrosion resistant in the anode environment of MCFC and can possibly be used without Ni cladding.

Measured change of the anodic current with time at cathode potential of MCFC for tested materials are shown in Fig.2. At the early stage of the measurement, the anodic current of the 30%Cr-40%Ni-1%Al-0.05%Y-Fe alloy was larger than those of AISI 316L and 310S steels. The smallest anodic current was observed for 316L steel. However, with time the difference in the anodic current for these materials became smaller. The decrease in the anodic current was more significant for 30%Cr-40%Ni-1%Al-0.05%Y-Fe alloy than for other steels and it was thought that in a relatively short time the anodic current for these materials would be reversed. To confirm this, the data were rearranged according to the equation (1) which can be derived from the Wager's oxidation law assuming that the controlling process of the corrosion in MCFC cathode environment is mainly a diffusion of atoms through the surface scale.

$$\log i = \log k + \{(1-n)/n\} \cdot \log t \quad \cdots \quad (1)$$

where i is the current density, k is a constant, n is the exponent used in the Wagner's law and t is the time. The rearranged data is shown in Fig.3. The straight lines were obtained for all materials, implying that the assumption mentioned above is reasonable. It should be noted that the slope of the straight line is larger (corresponding to larger value of n) for 30%Cr-40%Ni-1%Al-0.05%Y-Fe alloy than for other steels. It is clear that after about 100 hours the anodic current will become smallest for 30%Cr-40%Ni-1%Al-0.05%Y-Fe alloy and largest for 316L steel. These results can be understood as follows. For high Cr materials the cathode potential of MCFC is in the transpassive region of the polarization curve and the selective dissolution of Cr occurs predominantly. This Cr dissolution corresponds to the large anodic current observed for 30%Cr-40%Ni-1%Al-0.05%Y-Fe alloy at the early stage of the measurement. With time, however, the Cr depletion in the vicinity of the surface becomes significant and the relative concentration of Al increases, resulting in a formation of compact alumina rich surface scale. Because of this highly protective surface scale, 30%Cr-40%Ni-1%Al-0.05%Y-Fe alloy begins to show smaller anodic current in a relatively short time than other steels whose surface scale is composed of less protective Fe and Cr oxides. Thus, it can be said that 30%Cr-40%Ni-1%Al-0.05%Y-Fe is more corrosion resistant and

reliable than the currently used AISI 316L and 310S steels in MCFC cathode environment considering the practical long-term operation.

In summary, the corrosion resistance of the 30%Cr-40%Ni-1%Al-0.05%Y-Fe is much higher than the currently used materials in both anode and cathode environments of MCFC. This alloy can possibly be used as a separator and other metallic components without Ni cladding to anode side. Final adjustment of the alloying elements for further corrosion resistance is still being conducted at NKK.

CONCLUSIONS

(1) Result of an electrochemical corrosion test showed the superior corrosion resistance of a 30%Cr-40%Ni-1%Al-0.05%Y-Fe alloy over AISI 316L and 310S steels in both anode and cathode environments of MCFC.
(2) This alloy can possibly be used as the material for the separator and other metallic components without Ni cladding to anode side.
(3) Modification on this alloy for further improvement of corrosion resistance is being continued in the Moonlight Project.

Table 1 Chemical compositions of the used materials (wt%).

	C	Si	Mn	Cr	Ni	Others
AISI 316L	0.02	0.51	1.49	17.0	13.9	2.13Mo
AISI 310S	0.06	0.72	1.62	25.0	20.6	
30Cr-40Ni-Al-Y-Fe	0.05	0.24	tr.	30.0	40.4	1.07Al,0.06Y

balance:Fe, tr.:trace, P,S < 0.003 for all materials

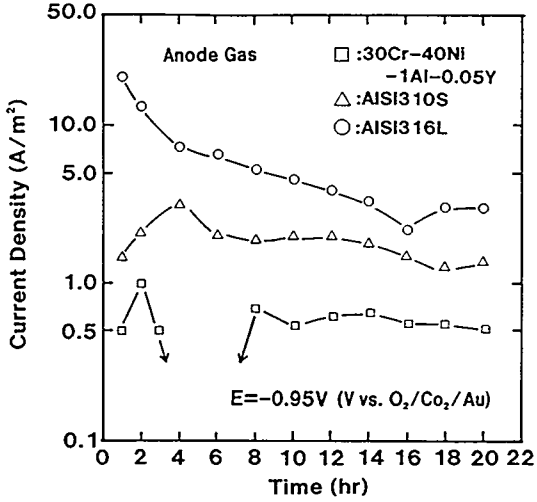

Fig.1 Results of the measurement of anodic current in anode environment of MCFC.

Table 2 Test conditions for measurement of anodic current.

	Measurement at Cathode Potential	Measurement at Anode Potential
Salt Composition	62%Li_2CO_3/38%K_2CO_3	
Gas Composition	70%Air/30%CO_2	80%H_2/20%CO_2
Test Temperature	650℃	
Test Potential (vs. 33%O_2/67%CO_2/Au)	-0.1V	-0.95V
Test Duration	20 hours	

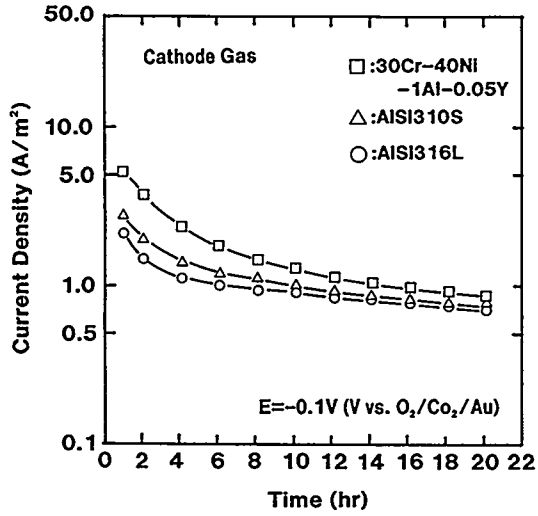

Fig.2 Results of the measurement of anodic current in cathode environment of MCFC.

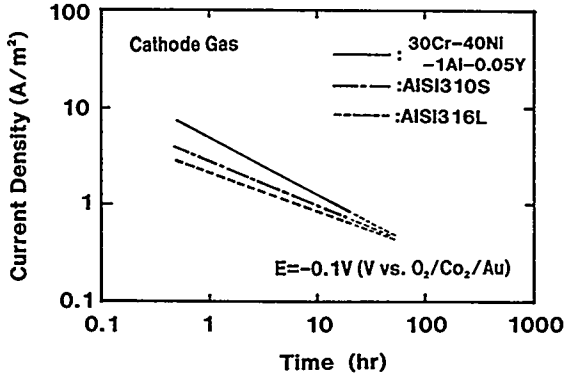

Fig.3 Log i vs. log t plot of anodic current in cathode environment of MCFC.

INTERNAL REFORMING - MCFC SYSTEM PERFORMANCE STUDY UNDER FULL- AND PARTIAL-LOAD CONDITIONS

Peter C. van der Laag
Netherlands Energy Research Foundation ECN
Box 1, 1755 ZG Petten, The Netherlands

SUMMARY

An investigation into the steady state full- and partial-load behaviour of an internal-reforming molten carbonate fuel cell system is performed, with natural gas as fuel. The study shows an increase in conversion efficiency when the gas feed level is reduced, whereby the fuel utilization remains constant. This is opposed to a previous study on external-reforming BOF-fueled MCFCs, by Lugten [1]. The increase holds for both ambient pressure operation and for raised pressure operation. The system design is highly synergetic, since it is capable to produce the required hydrogen, carbondioxyde and steam from the natural gas feed.

I. THE INTERNAL REFORMING MCFC

Since the active fuel for the MCFC is hydrogen, methane must be converted into hydrogen, by the endothermic reform reaction:

$$CH_4+H_2O \longleftrightarrow CO+3H_2 \quad (1)$$

The carbonmonoxide forms a secondary source for hydrogen, due to the exothermic water-gas shift equilibrium reaction:

$$CO+H_2O \longleftrightarrow CO_2+H_2 \quad (2)$$

In the internal reforming scheme, these processes take place inside the anode chamber of the MCFC. Thus, a separate reform reactor unit can be omitted from the MCFC system, which leads to a simpler flow sheet (fig. 1). In order to reduce the activation energy for reforming, the

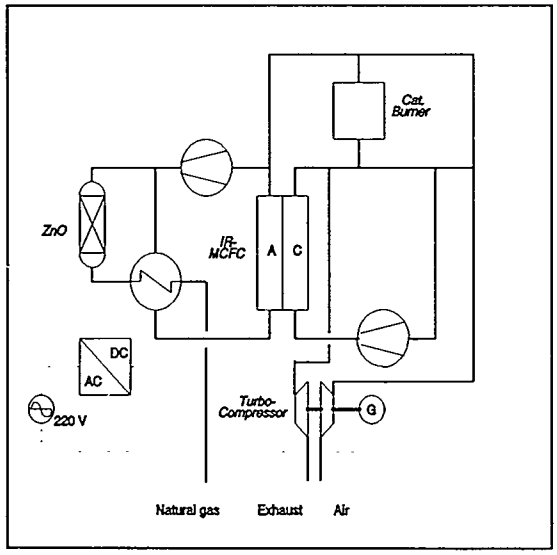

F.1 The internal-reforming MCFC system flow sheet and a bottoming cycle for pressurized operation.

anode chamber must be equipped with an effective catalyst, whose surface has to be maintained large- and effectiveenough, throughout the fuel cell's expected life time.
In our calculations, we assume full thermodynamic equilibrium across the cell's active surface, which is an idealization, giving an upper limit for the cell's performance. This results in full methane reforming, due to the continuous consumption of hydrogen. This provides us with a criterion for the catalyst's activity requirements.
The cell behaviour is predicted by the PSI model, which solves the local mass and energy balances. The system behaviour is computed with the DesignII process simulator from ChemShare. The process flow diagram works as follows: The system is fed with natural gas, consisting for 90 % of methane. H_2S is effectively extracted in a ZnO guard bed. The fuel is mixed with the anode outlet recycle flow to provide steam for the reform reaction and to prohibit carbon formation. The cell's inlet temperature is 600 °C. The cathode outlet, at 700 °C, is recycled to raise the CO_2 partial pressure. The anode outlet flow is burned to produce more CO_2 and to prohibit H_2 from entering the cathode, where it might reduce the NiO electrode.

II. FULL LOAD PERFORMANCE

Full load performance of a 1 MWe-class fuel cell system is examined at different operating-pressure levels: ambient, 3 bara and 5 bara. Table 1 gives an overview of these cases, with key data. All cases assume 85 % fuel utilization by the fuel cell, 100 C° temperature rise across the cell and a current density of 150 mA/cm².
The exergy of the fuel feed equals 810 kJ/mol CH_4 (ΔG at 1 bara, 25 °C); LHV equals 801 kJ/mol CH_4. The exergy is the amount of energy available for conversion into (electric) work. Therefore, the exergy efficiency is the most natural measure for any system's ability to convert chemical binding energy into work. Alas, it is seldomly used.

Case id.	1_150	3_150	5_150
Exergy of fuel [kW]	1823	1823	1823
Topping AC power [kW]	1036	1013	890
,, exergy eff. [pct]	56.8	55.6	48.8
Net AC power [kW]	1116	1245	1251
,, exergy eff. [pct]	61.2	68.3	68.6
Pressure [bara]	1.0	3.0	5.0
Curr.density [mA/cm2]	150	150	150
Cell voltage [mV]	695	749	768
Cell DC power [kW]	1070	1149	1174
Exhaust temp. [°C]	103	575	543

Table 1. System performance data, at different operating pressures (case id. = pressure_current density).

Compressor isentropic efficiencies of 72 % are used, while a full-load isentropic expander efficiency of 84% is used. DC/AC conversion efficiency of 97 % is used. Pressure drops across the anode and cathode chambers are 20 and 25 mbar respectively. In the ambient pressure case (1_150), a bottoming steam cycle is used to generate steam of 180 bar, 540 °C. The ambient pressure exhaust is first compressed to 1.4 bar, to overcome pressure losses inside boiler feedwater heatexchanger and the steam boiler. The steam turbine's exhaust is 1 bara, 102 °C.

III. PARTIAL LOAD PERFORMANCE

The steady-state partial load behaviour of the system is examined, when the natural gas feed is reduced. A constant fuel utilization of 85 % is assumed. The resulting key data for the ambient pressure system are given in table 2.

Case id.	1_135	1_120	1_105	1_90	1_75
Exergy of fuel [kW]	1640	1458	1276	1094	911
Topping AC power[kW]	952	861	763	660	553
,, exergy eff. [%]	58.0	59.1	59.8	60.3	60.7
Net AC power [kW]	1024	925	817	705	591
,, exergy eff. [%]	62.4	63.4	64.0	64.4	64.9
Curr. dens. [mA/cm2]	135	120	105	90	75
Cell voltage [mV]	708	719	727	733	737
Cell DC power [kW]	1012	913	808	698	585

Table 2. Partial load behaviour (ambient system).

Increasing the operating pressure results in a partial load behaviour, that is given in table 3. The expander, has a poor partial load behaviour. The cases at 120 mA/cm2 and 90 mA/cm2 are computed with 80 % and 84 % isentropic expander efficiency respectively. In the latter case one of two expanders is switched off.

Case id.	3_120	3_90	5_120	5_90
Exergy of fuel [kW]	1458	1094	1458	1094
Topping AC power [kW]	807	619	731	557
,, exergy eff. [pct]	55.3	56.6	50.1	50.9
Net AC power [kW]	978	749	998	763
,, exergy eff. [pct]	67.1	68.5	68.4	69.7
Pressure [bara]	3.0	3.0	5.0	5.0
Curr.density [mA/cm2]	120	90	120	90
Cell voltage [mV]	762	779	778	795
Cell DC power [kW]	964	739	981	751
Exhaust temp. [°C]	519	510	447	434

Table 3. Partial load behaviour of the pressurized system.

IV. DISCUSSION AND CONCLUSIONS

The IR-MCFC system design, as depicted in figure 1, is highly synergetic in a sense that it is capable of producing the required hydrogen, steam and carbondioxide from the natural gas feed. The system shows a high exergetic conversion efficiency, both at ambient and at raised operating pressures. All full load cases (150 mA/cm^2) show an efficiency that is higher than conventional STEG (steam and gas turbine) methods, currently in use for electricity generation.
A bottoming steam cycle for the ambient pressure system adds 4.6 %-points to the topping efficiency. Hereby steam is generated of 540 °C, 180 bar, as is possible by current methods. This system makes a good candidate for demonstration purposes.
The system's conversion efficiency raises even further at partial loading conditions, when the natural gas feed is reduced. This holds both for ambient and pressurized operation.
The bottoming expander efficiency drops sharply, when operated at less than 80 % of its design capacity. Therefore the use of two or more expanders, used in parallel, is recommended to enhance the bottoming conversion efficiency. One or more expanders can be switched off at partial load conditions.

Assumptions that underly these results are:
- Full methane conversion by the fuel cell, which gives an indication of the required catalyst activity (estimated at more than $2.5 \cdot 10^{-4}$ m^3/g-kat/s, including diffusion limitation inside the porous catalyst).
- 85 % Fuel utilization, which is realistic according to Tanaka's experimental results [2].
- A temperature rise of 100 C° across the fuel cell, also at partial load conditions. If this can be realised in practise the heat contents of the fuel cell hardware remains near stationary, enhancing dynamic behaviour of the cell. Furthermore, a large temperature difference enhances the cooling effect of the cathode flow, which thereby remains limited. A higher flowrate causes a higher associated auxiliary power consumption by the air- and cathode-recycle fans.

REFERENCES

1. P. E. Lugten; System efficiencies for a BOF (basic oxygen furnace) fueled MCFC power plant at full load and partial load conditions, ESTS/Hoogovens (Dutch iron and steel industry), IJmuiden, 1988 FCS, pp. 149 - 152.

2. T. Tanaka, M. Matsusura, Y. Gonjo, C. Hirai, T. Okada, M. Miyazaki; Development of internal reforming molten carbonate fuel cell technology, Mitsubishi Electric Corporation, Japan, Energy Conversion Conference, U.S., august 1990.

MATERIAL STUDIES ON MOLTEN CARBONATE FUEL CELL

Y.Miyazaki, M.Yanagida, S.Tanase, K.Tanimoto, T.Kojima
H.Okuyama, T.Kodama, H.Itoh*, C.Nagai* and S.Terada*
Government Industrial Research Institute, Osaka
1-8-31, Midorigaoka, Ikeda, Osaka 563 Japan
*Akashi Technical Institute, Kawasaki Heavy Industries, Ltd.
1-1 Kawasakicho, Akashi 673 Japan

INTRODUCTION

Government Industrial Research Institute, Osaka (GIRIO) started studies on cell materials of molten carbonate fuel cell (MCFC) since 1981 in the Moonlight Project.

At present, our surveying efforts of electrode, electrolyte matrix and bipolar plate materials are continued, and the physical properties data such as melting point, electric conductivity, vapor pressure etc. are being accumulated for binary or ternary systems of carbonate electrolytes.

Our activities mentioned above are introduced and some recent results are shown in this paper.

SURVEY CELL MATERIALS

We are surveying cell materials mainly by means of immersion method into molten carbonate. Fe-based or Ni-based alloys and electronic conductive ceramics for electrodes and bipolar plates and non or ionic conductive ceramics for electrolyte matrix were investigated. Over a hundred kinds of materials have been surveyed so far.

We chose $LiInO_2$, $LiGaO_2$ and Li_2SnO_3 as alternative electrolyte matrix materials[1] and have been studying the characteristics of these materials. At this time, we considered that, if these materials with some additive have considerably high electrical conductivity and the amount of the dissolution of the materials in carbonates is little, they could be used as the alternative cathode materials. From this consideration, we examined the electrical conductivity of $LiInO_2$, $LiGaO_2$ and Li_2SnO_3 with one of NiO, ZnO and CuO as the additive. FIGURE 1 shows the relationship between electrical conductivity and NiO content in $LiInO_2$-NiO system.

PHYSICAL PROPERTIES OF ELECTROLYTE

The physical properties data of binary and ternary systems of molten carbonate were being accumulated.

In order to obtain less corrosive molten carbonate, we are trying the addition of alkaline earth metal carbonate such as $CaCO_3$, $SrCO_3$, and $BaCO_3$ to conventional binary alkaline metal carbonate systems.

In addition to that, in order to optimize the electrolyte composition from the viewpoint of cell performance and endurance, we extend the surveying range of carbonate electrolytes for MCFC and accumulate the physical properties data of these carbonates. The phase diagram of melting points of binary system, Li_2CO_3-Cs_2CO_3 is shown in FIGURE 2. Conductivity measurement was also carried out for the binary system. FIGURE 3 shows the conductivity of Li_2CO_3-Cs_2CO_3 at 900°C.

CELL TESTING

Cell testings are being carried out to investigate the effects of pressure, electrolyte composition etc. on cell performance and to evaluate suitability of candidate materials.

We construct the "standard" cell for the evaluation of suitability of candidate materials. It needs the "standard" cell components such as anode, cathode and electrolyte plate. This paper presents the development of the "standard" electrolyte matrix. In order to develop the "standard" electrolyte matrix, studies have been made to determine the effect of aluminum oxide fibers on the performance of a matrix. Electrolyte matrices were fabricated by adding aluminum oxide fibers ranging 5 to 70 wt% to the $LiAlO_2$ fine particles using the tape casting method. FIGURE 4 shows the fabricating process of the electrolyte matrix by tape casting method. A performance of a candidate matrix has been evaluated by a 10 cm^2 single cell test. It was found that the optimum addition of 20 wt% aluminum oxide fibers improved the life of the cell.

REFERENCE

1. Y.Miyazaki, M.Yanagida, K.Tanimoto, S.Tanase, T.Kodama, H.Itoh, C.Nagai and K.Morimoto, 1988 Fuel Cell Seminar Abstracts, pp304-307 (1988).

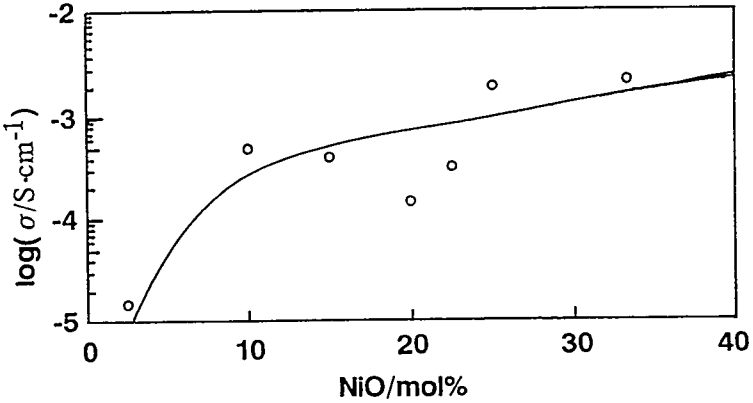

FIGURE 1 Relationship between Electrical Conductivity of $LiInO_2$-NiO and NiO Content at 650 ℃ in Air

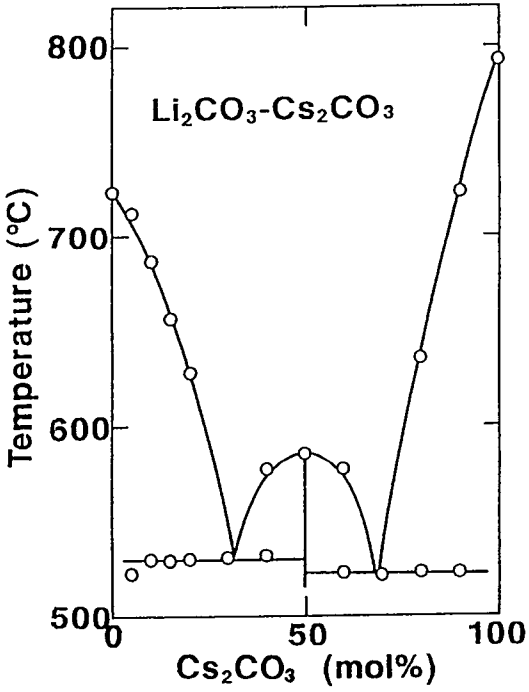

FIGURE 2 Phase Diagram of Melting Points of Binary System, Li_2CO_3-Cs_2CO_3

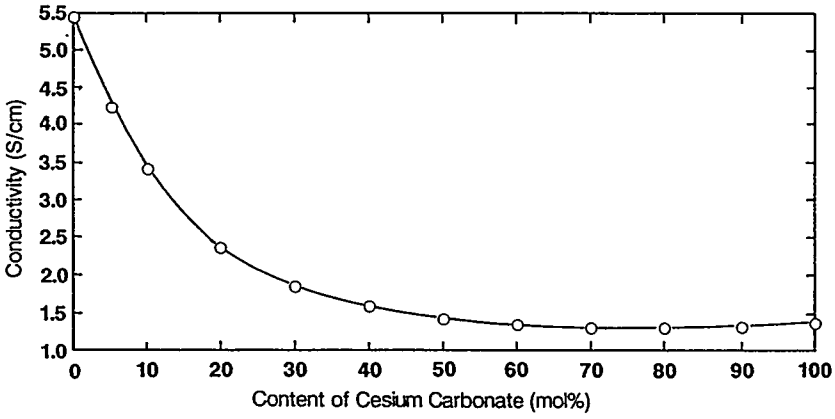

FIGURE 3 Electrical Conductivity of Li_2CO_3-Cs_2CO_3 at 900 ℃

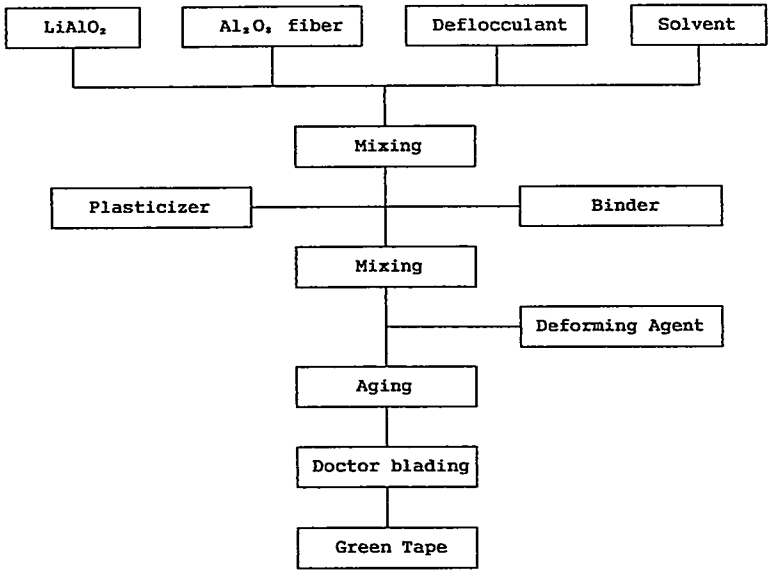

FIGURE 4 Fabrication Process of Electrolyte Matrix

DEVELOPMENT OF PETROLEUM NAPHTHA FUELED MCFC SYSTEM

Y. AOYAGI, A. SAIAI, S. SAKURADA
Tonen Corporation
1-3-1, Nishitsurugaoka Ohi-machi Iruma-gun,
Saitama 354, JAPAN

M. NISHIOKA, T. SAITO, N. FURUKAWA
Sanyo Electric Co., Ltd

T. SAKAMOTO
Toyo Engineering Corp.

INTRODUCTION

Our goal is to develop an MCFC system using petroleum naphtha($C_{6.4}H_{14}$ as an average molecular formula) which is more economical than natural gas. Naphtha-reformed gas usually has higher humidity than reformed natural gas and so hydrogen partial pressure is relatively low. The high humidity may not only reduce cell performance but also affect cell material durability.

Our approach was to develop a new naphtha reforming catalyst which enabled reforming under lower S/C(steam to carbon ratio) and stable cell materials under high humidity. A new reforming catalyst and improved cell components have achieved stable and efficient performance in both 100W and 300W stacks' operation using naphtha as a source of fuel.

1. DEVELOPMENT OF HIGH PERFORMANCE CATALYST

According to the definition of steam reforming of hydrocarbons, naphtha-reformed gas is composed of H_2, CO, CO_2, H_2O and CH_4 and the composition is theoretically calculated by the shift and the methanation equilibrium. The relation between the composition and S/C is shown in fig 1, which implies the higher S/C causes lower hydrogen partial pressure resulting in the lower cell performance. So it was necessary to find a new catalyst which enabled reforming under lower S/C.

We have developed new catalysts with noble metal as active metal on partially stabilized zirconia (3YSZ) support. From the view point of reforming reactivity, Ru/3YSZ catalyst was compared with D11, a commercial Ni catalyst, which showed the least carbon formation. When S/C was reduced to 1.5, carbon formation was observed on D11, but not on Ru/3YSZ catalyst. In the condition of high GHSV(Gas Hourly Space Velocity[1/hr]) D11 produced more CH_4 than Ru/3YSZ catalyst(Table 1). Though neither produced unconverted hydrocarbons over C_2^+ at 800℃, D11 produced them at lower temperature(600℃) (Table 2). As a result it was found that Ru/3YSZ catalyst was very active and enabled lower S/C operation than any other commercial catalysts.

2. DEVELOPMENT OF CELL COMPONENT MATERIALS TOLERABLE TO HIGH HUMIDITY

(1)Optimization for carbonates supporting material

In out-of-cell test, we have already found the grain of $LiAlO_2$ grows larger and the matrix holds less carbonates as the humidity gets higher. From

both of in- and out-of-cell tests using several matrices made from $LiAlO_2$ with different surface area from 1 to 19m^2/g, it was found that there must be optimum surface area between 6 and 14m^2/g.

(2)Anti-corrosive treatment of wet seal area

In the cell tests, higher humidity of anode gas caused more serious degradation of cell performance not only at 150mA/cm^2 but also at OCV in spite of little cross leakage. A systematic experiment revealed that this was due to a semi-shortage by some conductive oxides from stainless steel at the wet seal area. In order to solve this problem, the wet seal area was protected with Al or Al_2O_3, hence the cell durability has been improved. The cell performance with or without Al or Al_2O_3 is shown Fig 2.

3. STACKS OPERATION COMBINED WITH A NAPHTHA REFORMER

(1)A long term performance test of stacks and Ru/3YSZ catalyst

The naphtha reformer with Ru/3YSZ catalyst was connected with 100W (250cm^2*4) or 300W(777cm^2*4) scale stacks with the improved matrix material and the wet seal protection. These stacks were fed with standard gas (H_2:CO2=4:1, 10% humidity) as well as reformed gas (mainly S/C=3). The 100W stack was operated for about 1800 hours, during which it experienced one thermal cycle. The 300W stack was operated for 500 hours. Depending on kinds of feed gases, the cell performance varied, but no degradation of performance was recognized at all. The reformer itself was operated totally for about 3000 hours. The new reforming catalyst showed good performance throughout the operation, since high naphtha conversion, high H_2 yield and low methane leakage were not changed. In addition the mechanical strength of the catalyst was maintained satisfactorily.

(2)Stack performance efficiency

Fig 3 shows the efficiency of the 300W and 100W stacks fed with naphtha-reformed gas(S/C=3). The 300W stack is more efficient than the 100W stack, it seems to be due to good gas sealing effect at manifolds. Both satcks achieved more than 45% efficiency at Uf=75%, which was intended to be practical fuel utilization. Moreover when the fuel utilization was raised, the efficiency over 50% was attained. (The efficiency(η) is defined by a formula ① , and is the efficiency of a stack itself.)

$$\eta = \frac{\Delta G^0(H_2)}{\frac{X_{H2}}{X_{H2}+X_{CO}} \cdot \Delta H^0(H_2) + \frac{X_{CO}}{X_{H2}+X_{CO}} \cdot \Delta H^0(CO)} \cdot \frac{V \cdot Uf}{E^0} \qquad ①$$

x_i : molar fraction of inlet gas
E^0 : standard potential
V : average cell voltage
ΔG^0 : standard Gibb's energy(650℃)
ΔH^0 : standard enthalpy(650℃)

4. CONCLUSION

The reformer using a newly developed catalyst and the stacks with treatment against high humidity were combined and they achieved stable and efficient performance. Now a 10kW stack is being operated with simulated gas of naphtha-reformed gas. By the end of this year, another 10kW stack with CO_2 recycling loops is to be operated with a naphtha reformer using Ru/3YSZ catalyst.

5. ACKNOWLEDGEMENT

This work was supported by the Petroleum Energy Center which is a subsidiary of MITI.

Table 1 The effect of GHSV on methane leakage(S/C=3, dry base) [%]

GHSV	CAT.	H_2	CO	CO_2	CH_4
2500	D11	71.46	13.70	13.46	1.38
	Ru	72.27	14.83	12.07	0.83
7500	D11	70.84	11.59	15.28	2.28
	Ru	70.93	14.13	13.52	1.42

Table 2 The effect of temperature on C_2^+ production(S/C=3, GHSV=5000)

CAT.	600℃	800℃
D11	++++	ND
Ru	ND	ND

ND:not detected

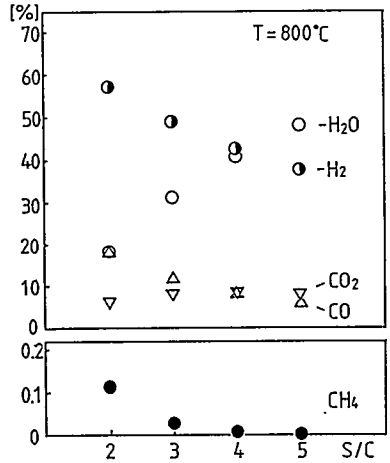

Fig 1 The equilibrium gas composition of naphtha-reformed gas (reformer outlet temperature is 800℃)

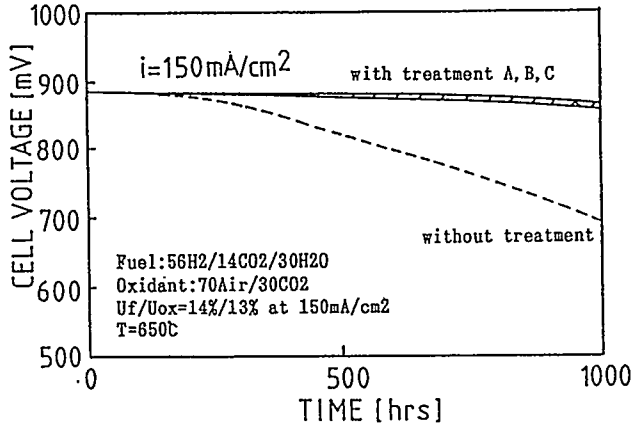

Fig 2 Performance stability of a single cell with or without wet seal treatment (Treatment A:Al(5 μm thick), Treatment B: Al2O3(100 μm thick), Treatment C:Al(50 μm thick)

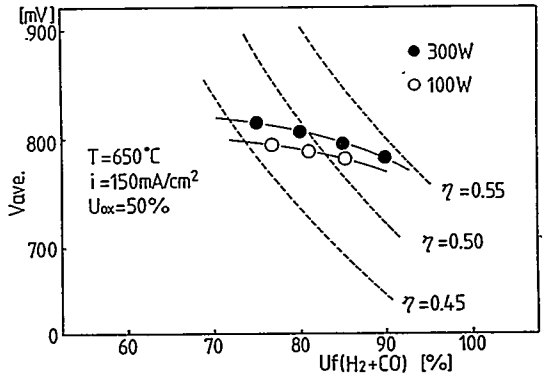

Fig 3 The efficiency of the stacks fed with naphtha-reformed gas (S/C=3)

STUDY OF THE HYDROGEN OXIDATION AT GOLD IN MOLTEN LI+K (68/32) CARBONATE USING IMPEDANCE MEASUREMENTS AND CHRONOAMPEROMETRY

R.Weewer, K.Hemmes and J.H.W. de Wit
Delft University of Technology, Laboratory for Materials Science
Division of Corrosion Technology and Electrochemistry
Rotterdamseweg 137 2628 AL Delft The Netherlands

INTRODUCTION

The mechanism of the hydrogen oxidation reaction has been studied by several authors (1- 5). Ang and Sammells (1) proposed the most probable mechanism for the hydrogen oxidation at nickel and cobalt electrodes to be:

$$H_2 \rightleftharpoons 2\,H_{ads} \qquad [1]$$

$$H_{ads} + CO_3^{2-} \rightleftharpoons OH^- + CO_2 + e \quad (rds) \qquad [2]$$

$$H_{ads} + OH^- \rightleftharpoons H_2O + e \qquad [3]$$

The applicability of this mechanism was confirmed independantly for copper electrodes by Lu and Selman (2). Suski et al (3) discussed mechanism [1-3] and proposed a second mechanism, yielding the same reaction orders:

$$H_2 \rightleftharpoons 2\,H_{ads} \qquad [4]$$

$$2\,(H_{ads} + CO_3^{2-} \rightleftharpoons OH^- + CO_2 + e\,) \qquad [5]$$

$$2\,OH^- + CO_2 \rightleftharpoons H_2O + CO_3^{2-} \qquad [6]$$

A modification of mechanism [4-6] has been proposed by Bienasz (4), assuming steps [4] and [5] to have equal rates. Nishina et al (5) confirmed the applicability of mechanism [4-6] on account of their chronocoulometry experiments at various electrode materials (Au, Ag,Pt, Ir, Ni, Pd).
Most mechanistic studies are carried out using chronoamperometry. Due to the effect of the double layer charging current and the finite rise time of the potentiostat the interpretation of potential step data is tricky, especially for fast electrode processes (6). There are several methods to extract kinetic data from the current transient. Ang and Sammells (1) determined the current at zero time by linear extrapolation between 300µs-500µs. This method was discussed later (2,7), and it was shown that $\sqrt{t}$ extrapolation resulted in more accurate, and higher values for i_0.
Using impedance measurements Nishina et al (5) showed the exchange current density of Ni and Pd electrodes to be much higher (≈130 $mAcm^{-2}$) than i_0 for the other materials (Au:22 $mAcm^{-2}$). They proposed an equivalent circuit consisting of a charge transfer resistance in series with a parallel circuit reflecting the adsorption process to describe their impedance plots satisfactorily. They determined the charge transfer resistance and the adsorption resistance to be of the same order of magnitude. The impedance plot for nickel electrodes essentially showed a Warburg impedance, indicating mass transport to be ruling the overall electrode process. (5,8). This phenomenon complicates the determination of the charge transfer resistance using computer fit techniques.
The purpose of this study is to determine reaction orders for the hydrogen oxidation reaction using impedance measurements, and to compare the results with those obtained from chronoamperometry experiments.

EXPERIMENTAL

The experiments were carried out in a half cell configuration consisting of an alumina crucible containing the molten 62 mole% Li_2CO_3 / 38 mole% K_2CO_3 eutectic carbonate mixture loaded in a quartz reactor which was held at 923K. Flag type gold electrodes of 0.5 cm^2 area were used. The gold lead wire was 0.1mm in diameter to minimize meniscus effects. Cyclic voltammograms were taken to ensure the absence of the meniscus effect. Equilibrium potentials were measured vs the Au / 33% O_2 / 67% CO_2 reference electrode. All measurements were carried out at a quiescent melt. Inlet gases consisted of H_2/CO_2 mixtures humidified at appropriate temperatures. The gas flow was kept at approximately 10 ml/min. Complete establishement of the shift equilibrium in the gas phase was assumed.This was checked by measuring the equilibrium potential. Over 32 gas compositions were measured covering a range of water, carbon dioxide and hydrogen partial pressures as wide as possible. Table I lists an outline of the gas compositions measured.

Impedance measurements were carried out using the EG&G model 378 Electrochemical Impedance System within a frequency range between 95kHz and 10 mHz. The impedance data were analyzed using the analysis and fit program Equivcrt.
Chronoamperometry experiments were carried out using the EG&G 273 potentiostat. Step potentials were 10,20,30,40,60,80 and 100 mV anodic of the equilibrium potential. During the measurement the potentiostat was kept in the 1 A current range to obtain the shortest RC-time for the double layer charging. No IR compensation was applied since due to the low uncompensated resistance of the setup (0.6 Ω) this had no noticeable effect on the current response curve. The current was measured with a Philips PM9355 current probe, and recorded with a Philips PM 3350 digital storage oscilloscope.

RESULTS AND DISCUSSION

The impedance plots obtained at gold electrodes showed only one well defined high frequency semi circle followed by a Warburg impedance at lower frequencies (see figure 1), as for a simple Randless equivalent circuit. An equivalent circuit including an adsorption process as proposed by Nishina et al (5) did not give satisfactory fit results (i.e. $\chi^2 > .01$ and undetermined values for R_{ct}). This indicated the adsorption step to be absent on gold. At frequencies below 50 mHz the signal became disturbed by fluctuations in open circuit potential. Also the imaginairy part of the impedance tended to bend back to the real axis, probably due to the finite diffusion layer thickness caused by thermal convection in the melt. The frequency where deviation from the 45° angle occurred was not well reproducable, but was always in the range 10 to100 mHz. The diffusion layer thickness estimated from this frequency range assuming $D = 10^{-5}$ cm^2s^{-1} was $\delta = \sqrt{2D/\omega}$ or about 0.1 to 0.4 mm. To obtain Warburg coefficients and charge transfer resistances the Randless circuit was fitted to the data at frequencies >100mHz. In fact, we used CPEs instead of C_{dl} and W in the fitting procedure. A value for $Q = ((j\omega)^n Y)^{-1}$ was obtained. Theoretically, for a double layer capacitance n=1 and thus $Y = C_{dl}$, and for the Warburg impedance n=0.5 and $Y=(\sqrt{2}\,\sigma)^{-1}$, with σ the Warburg coefficient. For the double layer capacitance we found n=0.95- 1 and for the Warburg impedance n=0.45-0.5. These values were very close to the theoretical values, so we treated the values for Y as real double layer capacitances and warburg coefficients. The double layer capacitance was fitted to be 80-100 μFcm^{-2} dependant on gas composition. For comparison figure 2 shows an impedance plot of nickel. This plot features a pure Warburg impedance, and no semi circle, indicating a much higher charge transfer rate for Ni.

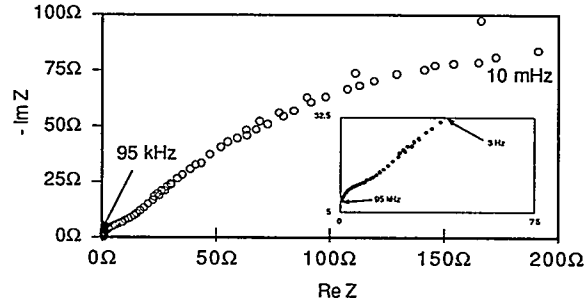

Figure 1: Impedance plot of a gold flag electrode in Li/K carbonate under 80%H_2/20% CO_2 inlet gas atmosphere. Inlay: high frequency impedance plot.

The results of the fitting are listed in Table I. The standard exchange current densities were calculated from the charge transfer resistances using $i_0 = RT/\,nFR_{ct}$, assuming n=2. Our data are of the same order of magnitude as data obtained by Nishina et al (5) taking into account that they assumed n=1.
Exchange current densities obtained from chronoamperometry experiments are within 10% of the exchange current densities obtained from impedance measurements.
In Table II the obtained reaction orders and standard exchange current densities are listed.

Figure 3 shows a typical current response curve for gold in a 80% H_2 + 20 % CO_2 inlet gas atmosphere. The current at zero time was obtained by linear extrapolation of the current vs $\sqrt{t}$ plots in the range between 200 µs and 500 µs. The exchange current density was determined from the intercept at η=0 of the so called Allen-Hickling plots (2), and α_A from its slope assuming n=2. Using n=1 the value for α_A would be 0.23, which is unlikely to be the correct value.

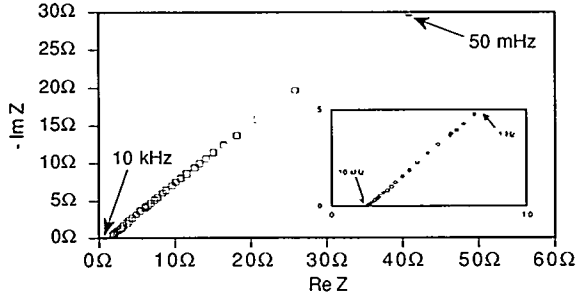

Figure 2: Typical impedance plot for a nickel cylindre electrode in Li/K carbonate under 80%H_2/20% CO_2 inlet gas atmosphere. Inlay: high frequency impedance plot.

Table I: Outline of gas compositions measured (Inlet gas compositions after humidification in %). Warburg coefficients (σ) ($\Omega cm^2 s^{-1/2}$) and exchange current densities (i_0) ($mAcm^{-2}$) determined using impedance measurements and chronoamperometry

H_2 inlet	CO_2 inlet	H_2O inlet	E shift	E observed	i_0 impedance measurements	i_0 chrono amperometry	σ $\Omega cm^2 s^{-1/2}$
80	20	0	-1157	-1160	13.8	11.0	60
64	16	20	-1111	-1110	11.3		33
55	14	31	-1095	-1088	10.0		34
42	11	47	-1076	-1073	7.4		47
60	40	0	-1074	-1075	15.7	13.5	40
56	37	7	-1065	-1070	13.8	13.9	26
32	21	47	-1029	-1033	7.2		42
40	10	0	-1184	-1180	8.4		70
32	8	20	-1112	-1110	6.0		57
28	7	31	-1093	-1086	5.2		66
40	40	0	-1054	-1070	11.6		64
32	32	20	-1032	-1045	10.0		39
28	28	31	-1022	-1023	9.1		43
20	20	0	-1081	-1077	5.6		95
16	16	20	-1040	-1048	3.9		77
20	80	0	-964	-1020	9.4	7.3	59
19	74	7	-961	-1001	9.2	9.5	47
14	55	31	-951	-968	5.5		72
11	42	47	-944	-948	3.7		133
10	20	0	-1049	--1020	2.8		133

According to White and Twardoch (9) presence of the meniscus effect would give rise to an extra current peak in the cyclic voltammograms. Typical voltammograms are shown in figure 4. Since no extra current peaks were observed we concluded that the meniscus effect did not influence our results.

The difference between the reaction orders determined from chronoamperometry and impedance measurements is probably caused by the fact that less gas compositions were measured using the former technique. This is also demonstrated by the larger standard deviation of the multilinear fit.The experimental reaction orders clearly suggest that the hydrogen oxidation reaction at gold follows a completely different mechanism than at nickel. The high reaction order of 0.71 for hydrogen from impedance measurements may be explained by an Heyrovski- type mechanism , e.g.:

$$H_2 + CO_3^{2-} \rightleftharpoons H_{ads} + OH^- + CO_2 + e \quad \text{(rds)} \qquad [7]$$

$$H_{ads} + CO_3^{2-} \rightleftharpoons OH^- + CO_2 + e \qquad [8]$$

$$2OH^- + CO_2 \rightleftharpoons H_2O + CO_3^{2-} \qquad [9]$$

For scheme [7-9] the theoretical reaction order for hydrogen is 0.75, and for water and carbon dioxide 0.25. The experimental reaction order for water however, does not agree with mechanism [7-9]. In fact, to our knowledge, a negative reaction order for water cannot be explained by any mechanism.This is probably caused by the particular role water and hydroxyl ions play within the melt. The existence of water molecules in the melt has never been proved experimentally and it may be expected that water is present in the melt only as hydroxyl ions through the hydrolysis reaction. Since this reaction probably takes place at the melt/gas interface, and the kinetics of the hydrolysis reaction are unknown, the OH^- concentration at the electrode may differ from equilibrium and thus influence the reaction order for water and carbon dioxide. This issue will be further elaborated in our future research.

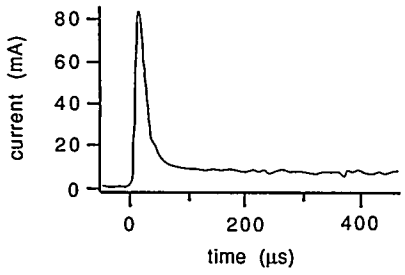

Figure 3: Typical step response curve for a potential step of 100mV vs open circuit potential at gold in 80% H_2+20%CO_2gas atmosphere.

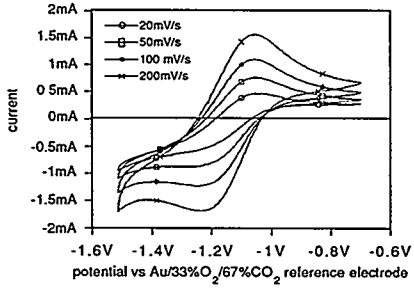

Figure 4: Cyclic voltammograms at a gold electrode scan rate 20-200 mVs^{-1}, inlet gas 80%H_2+20% CO_2

Table II: Reaction orders, standard exchange current densities and anodic transfer coefficient for gold determined using impedance measurements and potential step measurements.

	H_2	CO_2	H_2O	$i^0_0(mAcm^{-2})$	α_A
impedance measurements	0.71±0.09	0.45±0.07	-0.23±0.07	40±2	
potential step measurements	0.50±0.13	0.34±0.13	-0.12±0.10	30±2	0.59±0.04

CONCLUSIONS

Impedance data and potential step data of the hydrogen oxidation at gold electrodes give comparable results. The exchange current density at gold is smaller by a factor of ten than the exchange current density at nickel. The reaction orders suggest the mechanism of hydrogen oxidation at gold to proceed through an Heyrovski-type mechanism. The rather surprising reaction orders obtained for water suggest water and hydroxyl ions in the melt to play an important role. Further research is needed to elucidate the role of the hydrolysis reaction.

Acknowledgement: This work was supported by the Dutch Energy Research Centre under contract SC02 and SC03.

REFERENCES

1. P.G.P. Ang and A.F. Sammells, J.Electrochem. Soc. Vol.127 No. 6 p 1279, 1980
2. S.H. Lu and J.R. Selman, J.Electrochem. Soc. Vol. 131, No 12, p 2827, 1984
3. L.Suski, J.Jewulski and J.Wyrwa, Proc. Electrochem. Soc. 84-13, p 113, 1984
4. L.K. Bienasz, J.Electroanal. Chem., Vol 197, p 387, 1986
5. T. Nishina, M.Takahashi and I.Uchida, J.Electrochem. Soc. Vol 137., No. 4, p 1112, 1990
6. L.H. L. Miaw and S.P. Perone, Anal. Chem. Vol 5., No. 11, p 1645, 1980
7. S.H. Lu and J.R.Selman, J.Electrochem.Soc. Vol 136, No.4, p1068, 1989
8. R.Weewer, R.C. Makkus, K. Hemmes and J.H.W. De Wit, J.Electrochem. Soc., 137, No. 10, p 3156, 1990
9. S.H.White and U.M. Twardoch, J.Electrochem.Soc.Vol135, No.4, p892, 1988

TEMPERATURE INFLUENCE ON THE MCFC LIFE TIME

S. Freni [a], S. Cavallaro [b] and N. Giordano [a]

(a) Istituto C.N.R.-T.A.E., Salita S. Lucia sopra Contesse, 39 - 98126 S. LUCIA - MESSINA (ITALY).

(b) Dipartimento di Chimica Industriale - Università di Messina P.O. Box 29 - 98010 SANT'AGATA DI MESSINA (ITALY).

Introduction

The effect of the temperature (T) is paramount in determining the rates of the various mechanisms which contribute to the performance and the endurance of a MCFC (1). Several tests have been carried out on MCFC operating at different T (873, 893 and 923 K) for length of time (t) corresponding to a 90% of the initial activity. Considerations on the amount of the released energy, voltage and the averaged power suggest the most useful temperature for a practical purpose.

Experimental

Experimental tests on MCFC isothermal monocell were carried out on a completely automated test-facility. Work conditions are detailed in Table 1.

TABLE 1

Temperature (K)	873	893	923
Power at full load (W)	9.5	10.7	11.0
Initial IR losses (mV)	120	109	120
Final IR losses (mV)	180	134	150
Life time/T (h/K)	7.33	4.93	2.38
cathode weight (NiO) (g)	9.93	10.05	9.72
anode weight (g)	28.40	29.30	28.10
filled tile weight (g)	56.50	55.80	56.00

Active area = 94 cm2; H2 utilization = 75%; CO2 utilization = 44%; Current at full load = 15 A; fuel [H2(.480), CO2(.322), H2O (.195)] flow rate = 0.236 mmole/s; oxidant [O2(.139), N2(.593), CO2(.244), H2O(.024)] flow rate = 0.698 mmole/s.

In our tests fresh anodes (Ni with 10 wt% of Cr) and prelithiated (Li 1 wt%) Ni cathodes manufactured by tape-casting, were used. The cathodes were oxidized "in-situ", by the same oxidant stream, after the cell assembling. The LiAlO2 tiles, made by the hot-pressing technique, were charged with 55 wt% of the eutectic Li, K carbonates mixture. The electrodes were located in two AISI 316 housings and aluminum foils were interposed between the tile and the edges of the housings. Chemical analysis for Li, K, Ni, Cr, Fe and Al, on the fresh and spent cell components, were carried out by using an atomic adsorption (AA) PERKIN ELMER model 4000 spectrophotometer. Scanning

electron micrographies (SEM) were made by an AUTOSCAN "E TEC" 45A instrument coupled with a PV-9100 EDAX microprobe.

Results

The electrochemical parameters, the morphological characteristics and the chemical analysis on samples of spent electrodes and tiles, were collectively evaluated. As evidentiated by SEM, the cathodes structures, after the initial "in situ" oxidation, look as agglomerates of 0.9 μm NiO crystallites and it appears to be weakly sensitive to the inverse effect of the life-time and the temperature (t/T). Contrarywise, structural and chemical modifications were very evident on the used tiles. Long-term operations evidenciated some modifications in the pores distribution and in the electrolyte partition among the used components.The total porosity and the micropore volume fraction have been found increasing with the temperature (and decreasing with the cell life time) as reported in fig.1. Moreover, the SEM micrographs show the presence of different $LiAlO_2$ forms depending upon the tested conditions. The phase distribution evaluation, starting from the structural observations reported by Selman and Maru (2), demonstrates that, although the $LiAlO_2$ phases were present together in each tested sample, only negligible traces of γ-phase were always detected. The low-T sample (873 K) showed high percentage of the α-phase, whilst at the intermediate temperature, the β-phase was slightly predominant. No noticeable differences were detected within spent anodes.

Due to the effect of the t/T, the energy released showed a maximum for the 873 K run-test. The initial IR values were found to be 7-8 mOhm, while the final values ranged between 9 and 12 mOhm. The output power appears to depend upon the working temperature: at the reference current density of 160 mA/cm2, the initial power varied from 118.1 (923 K) to 102.0 (873 K) mW/cm2, while the final one from 103.7 to 91.0 mW/cm2 respectively. As expected from Nernst equation, the open circuit voltage (OCV) was found to vary from 1000 to 1020 mV, inversely with the temperature trend. The measured electrolyte total losses rate seems to be correlated directly with the time and inversely with the temperature. Instead, the existing relationship between the electrolyte distribution and the time/temperature (t/T) variations is not immediately evident. A better overview of these aspects could be taken from the fig. 2.

Discussion

Performance and endurance tests on MCFC evidenced that the electrolyte management is one of the most critical factor affecting the life of the cells (3). Within a temperature range of only 50 K, a remarkable difference on the life-times was found: 2200 h for the highest-T test and 6400 h for the lowest-T one. Another meaningful aspect is related to the relative low difference in the residual electrolyte

content. In fact, independently from testing conditions, the output power drops off until the 90% of its starting value is reached with a corresponding electrolyte losses in the order of 20÷25 wt% of the original charge (33.0 g). Post-mortem analysis revealed that electrolyte partitions among the cell elements (tile-electrodes) are very similar at any tested temperature (Fig.1): anode = 5.2 ÷ 6.9 wt%; tile = 15.8 ÷ 19.4 wt%; cathode = 1.2 ÷ 2.3 wt%. A correlation between the OCV drops and the tiles filling degrees (TFD) was found (Fig. 3). Porosimetry and SEM micrographies on the spent cells demonstrated a good maintenance of the fresh anode framework, while some $LiAlO_2$ phases transition has been recorded for the tiles employed at different temperatures. The cathodic NiO-agglomerate structure, produced by the action of oxidant stream on the fresh cathode, appears to be slowly dissolved by the CO_2 action. The released energy linearly decreases vs. the MCFC temperature, while the output power shows an inverse behaviour (Fig. 4). This allows us to conclude that if the MCFC system is finalized to the cheapest energy production, it seems more convenient to work at lower temperature, while if an high power is required, the system benefits from the highest temperature (923 K).

Conclusion

Tiles structure modifications produced a decrease in the electrolyte capability and a bad electrolyte redistribution among the components. In the highest temperature test, the original electrolyte amount on the tile was retained to its highest extent, demonstrating a good tile capability. Instead, in the lowest-T range, the residual electrolyte content, low in the tile, was high in the cathode and only the anode appeared to be well filled. Besides, the total released energy increases by lowering temperature, while Vm and Pm show an opposite trend. This suggests that if the MCFC system is finalized to the cheapest energy production, it seems more convenient to work at lower T, while if an higher power density is required, the system benefits from the highest temperature (923 K).

References

1. N. Giordano, S. Freni, R. Quagliata, S.Cavallaro and P. Carbonaro, J. Electrochem. Soc., 135, 910 (1988).

2. J.R.Selman and H.C.Maru, Advances in Molten Salt Chemistry,4, G.Mamantov and J.Bramstein eds., Plenum Press, NY (1981).

3. J.R. Selman, S.S. Penner, DOE/ER/30060-T1 report (1985).

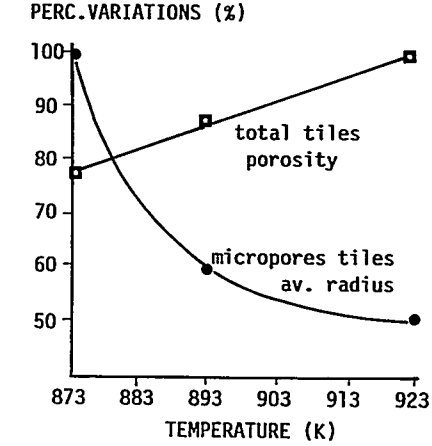

FIG.1-Variations of total pores volume and total micropore volume in the tiles vs. temperature.

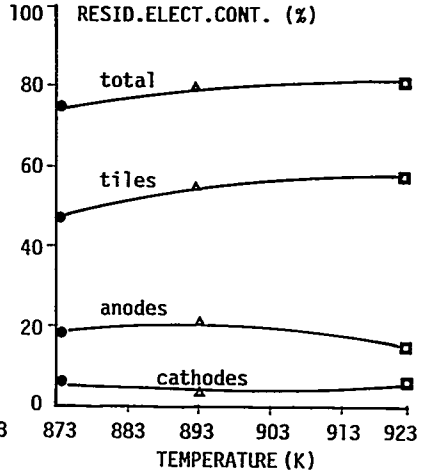

FIG.2-Distribution of resid electrolyte content among the spent components vs. temperature.

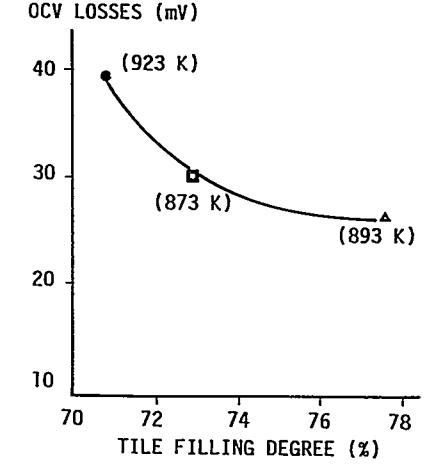

FIG.3-OCV's losses vs. tile filling degree (TFD).

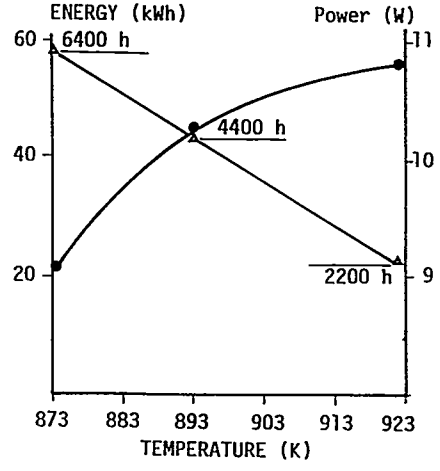

FIG.4-Total energy and averaged power released vs. temperature.

ON THE PROSPECTS OF OPERATING AN SOFC ON DRY NATURAL GAS

Mogens Mogensen, Bruno Kindl and Bjørn Malmgren-Hansen
Materials Department, Risø National Laboratory
DK-4000 Roskilde, Denmark

INTRODUCTION

Most fuel cell types have been developed to be fuelled with hydrogen. Usually, it is necessary to produce H_2 from primary fossile fuels containing carbon. Thus, a step of reforming carbon or hydrocarbons has to be added to the fuel cell systems making them more complex and decreasing the efficiency (1). In the cases of the molten carbonate fuel cell (MCFC) and the solid oxide fuel cell (SOFC) the high temperature makes it possible to avoid these problems, at least in principle, by means of internal reforming. However, the endothermicity of the steam reforming reaction gives rise to high temperature gradients by cooling the fuel electrode at the inlet, and the reforming catalyst may deactivate (2,3). On this background research on the simple, electrochemical oxidation of dry CH_4 in SOFC has been started (4,5).

THE CH_4/Ni-YSZ-CERMET ELECTRODE

The Ni-YSZ-cermet electrode (YSZ = yttria stabilized zirconia) has been demonstrated to be an excellent H_2-electrode at 1000°C (6,7). So it was natural to test if it also could be used as a CH_4-electrode. Fig. 1 shows the results of a Ni-YSZ- cermet electrode tested at 1000°C in H_2 with 3% H_2O and in CH_4 with 3% H_2O. This is here called "dry CH_4" in contrast to the steam-CH_4 mixture used for internal reforming which typically consists of 75% H_2O and 25% CH_4.

The experiments were done with a tree-electrode setup, the counter and reference electrodes being air/Pt.

Fig. 1 reveals that the CH_4 oxidation rate (current density) is more than a factor of 10 lower than the oxidation rate of H_2 at a given potential. It should be noted that the open circuit potential of the CH_4-electrode was some 50 mV more negative than that of the H_2-electrode so this much slower CH_4 oxidation is at considerably higher polarizations.

THE CH_4/CeO_2 ELECTRODE

Recently, it was reported that it was possible to oxidize CH_4 on a CeO_2-Gd_2O_3 type of electrode at 1000°C (5). The continuation of this work has resulted in improved CH_4 electrodes. Fig. 2 shows the oxidation rates of H_2 and CH_4 both with 3% H_2O on a CeO_2 electrode with an additive as developed at Risø. By comparison with Fig. 1 a similar H_2 oxidation rate is observed whereas the CH_4 oxidation rate is about 100 times higher than for Ni-YSZ at -1000 mV.

The explanation why the CeO_2 electrode is much more efficient in CH_4 oxidation may be that the CeO_2 becomes non-stoichiometric when it is exposed to a reducing atmosphere. CeO_{2-x} is a conductor for O^{--} as well as for electrons (8). In the Ni-YSZ-cermet the Ni conducts electrons only and the YSZ conducts O^{--} only. If the first step of the CH_4 oxidation is that a CH_4 molecule adsorbs on the Ni-metal surface and dissociates (9) the difference in the reaction steps might be (in simplified terms) for the two electrodes:

$$\text{On Ni: } CH_{4,\,ads} \rightarrow C_{ads}^{4+} + 4\,H_{ads}^{+} + 8e^{-} \qquad (1)$$

Surface diffusion to YSZ (2)

On YSZ: $4\,H^+ + 2O^{--} \rightarrow 2H_2O$ and (3)

$C^{4+} + 2O^{--} \rightarrow CO_2$ (4)

Otherwise for a mixed e^- and O^{--} conductor:

On CeO_{2-x}: $CH_{4,ads} + O^{--} \rightarrow CH_3OH_{ads} + 2e^-$ (5)

$CH_3OH_{ads} + O^{--} \rightarrow CH_2O + H_2O + 2e^-$ etc. (6)

On the CeO_{2-x} the reaction can go on at the same site (without surface diffusion). For the simpler reaction of H_2 oxidation this feature is less important probably because the surface diffusion of H^+ (or OH^- in the other direction) is fast but this is not the case for C-atoms.

THE CARBON DEPOSITION PROBLEM

In the temperature range of SOFC operation (800-1000°C) CH_4 is not thermodynamical stable, and deposition of solid carbon may happen (10). This can block the hot tubings through which gas is fed. Furthermore, it poses a special problem for utilizing the Ni-YSZ-cermet for CH_4 oxidation, because the carbon deposition will make the Ni-YSZ-electrode spall off the YSZ electrolyte. This is illustrated by the experimental results shown in Fig. 3, where the area specific series resistance (as measured by impedance spectroscopy) is plotted versus time. At time 0, the anode gas is switched from H_2 to CH_4 (both with 3% H_2O). The correlation between anode/electrolyte contact area and area specific resistance, is so that the contact area decrease even faster than the area specific resistance increases. The detachment of Ni-particles from their support has also been observed in the field of catalysis (9).

No carbon precipitation has been observed on the CeO_2-based electrodes.

For CH_4 the non-catalysed pyrolysis reaction kinetics may be slow enough to avoid carbon formation even at 1000°C due to the strong C-H bonds in CH_4 ($CH_4 \rightarrow CH_3 + H$: $\Delta H = +435$ kJ/mol) (11). The homogeneous pyrolysis reaction proceeds via CH_3 radicals which couple to higher hydrocarbons. These in turn make other radicals which further catalyse the CH_4 pyrolysis. Thus factors like flow rate, and content and type of higher hydrocarbons are of importance for the carbon deposition behaviour (11). The probability of carbon deposition increases with the concentration of higher hydrocarbons especially if these are aromatics.

Of greatest importance for the carbon deposition reaction rate is the type of surface in contact with the gas. Transition metals like Ni and Fe are very good catalysts (9,11) for the CH_4 pyrolysis whereas metal oxides like α-Al_2O_3 are rather inert (11). Also the surface finish may be decisive for the nucleation of solid carbon (11), and according to Holmen (12) SiC tubing with mirror quality surface is an excellent material for heating natural gas without cracking it. For heat exchange, metal tubes are to be preferred, and here deactivation of the metal surface by a sulfur treatment can suppress carbon formation in steam reforming at low H_2O/CH_4 ratios (9,13).

It is considered that for natural gas of Danish type (91.1 vol% CH_4, 5% C_2H_6, 1.8% C_3H_8, 0.9% C_4H_{10}, 0.2% C_5H_{12}, 0.1% C_{6+} and 0.9% $CO_2 + N_2$ (14)), there is a fair chance to avoid carbon deposition in a SOFC system by proper design and material selection.

CONCLUSION

The prospects of using dry natural gas as the feed for the SOFC system seem promising. Therefore, more experimental work as well as system analysis are being carried out by Risø in cooperation with other Danish partners.

ACKNOWLEDGEMENTS

This work was supported by the Danish Ministry of Energy under contract no. 1443/89-6. The help from K. Larsen in preparing the cells and performing the experiments is gratefully acknowledged.

REFERENCES

1. J. Appleby, "Phosporic Acid Fuel Cells", Energy, Vol. 11, No. 1/2, pp. 13-94, 1986.
2. K.A. Trimble and E.R. Ray, "A Solide Oxide Fuel Cell/Module for Utilization of Pipeline Natural Gas", in: 1988 Fuel Cell Seminar Abstracts, pp. 22-24, Long Beach, CA, Oct. 1988.
3. K. Kishida et al., "Evaluation of IR Molten Carbonate Fuel Cell for On-Site Application", in: Fuel Cell Technology and Applications, pp. 40-49, Abstracts of International Seminar, The Netherlands, Oct. 1987.
4. B.C.H. Steele et al., "Direct Electrochemical Oxidation of Methane in Ceramic Electrochemical Reactors", in: 1988 Fuel Cell Seminar Abstracts, pp. 179-182, Long Beach, CA, Oct. 1988.
5. M. Mogensen and J.J. Bentzen, "Oxidation of Methane on Oxide Electrodes at 800-1000°C", in: Solid Oxide Fuel Cells, pp. 99-110, Proceedings Volume 89-11, The Electrochemical Society, Inc., 1989.
6. J.T. Brown, "Solid Oxide Fuel Cells" in (T. Takahashi, ed.), High Conductivity Solid Conductors, Recent Trends and Applications, pp. 630-663, World Scientific Publishing Co., 1989.
7. A. Kandkar and S. Elangovan, "Development of Planar SOFC Technology: Progress and Problems", Denki Kagaku, Vol. 58, No. 6, pp. 551-556, June 1990.
8. H.L. Tuller, "Mixed Conduction in Nonstoichiometric Oxides", in (O. Toft Sørensen, ed.), Nonstoichiometric Oxides, pp. 271- 335 (1981).
9. J.R. Rostrup-Nielsen, "Catalytic Steam Reforming", Springer- Verlag, Berlin 1984.
10. G.H.J. Broers and B.W. Trijtel, "Carbon Deposition Boundaries and other Constant Parameter Curves in the Triangular Representation of CHO equilibria with Applications to Fuel Cells, pp. 365-382, "Advanced Energy Conversion, Vol. 5, Pergamon Press, 1965.
11. L.F. Albright et al., "Pyrolysis: Theory and Industrial Practice", Academic Press, 1983.
12. A. Holmen, University of Trondheim, Private Communication.
13. E. Riensche and H. Fedders, "Conversion of Natural Gas into CO- rich Syngases", Paper presented at the Natural Gas Conversion Symposium, Aug. 12-17, 1990, Oslo, Norway.
14. J. de Wit, The Danish Center of Gas Technology, Private Communication.

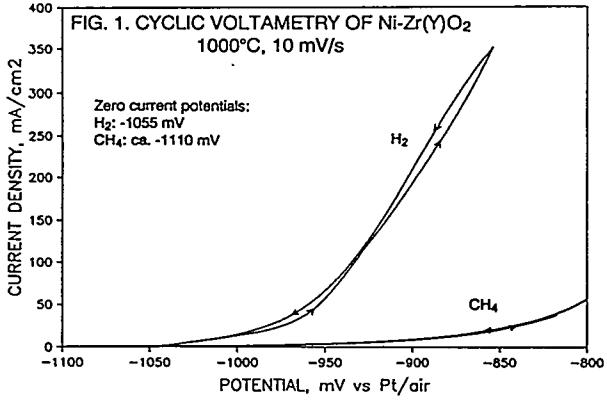
FIG. 1. CYCLIC VOLTAMETRY OF Ni-Zr(Y)O2
1000°C, 10 mV/s
Zero current potentials:
H2: -1055 mV
CH4: ca. -1110 mV
H2
CH4
CURRENT DENSITY, mA/cm2
POTENTIAL, mV vs Pt/air

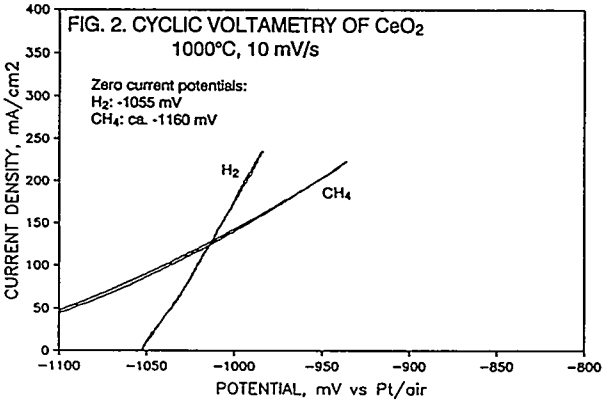
FIG. 2. CYCLIC VOLTAMETRY OF CeO2
1000°C, 10 mV/s
Zero current potentials:
H2: -1055 mV
CH4: ca. -1160 mV
H2
CH4
CURRENT DENSITY, mA/cm2
POTENTIAL, mV vs Pt/air

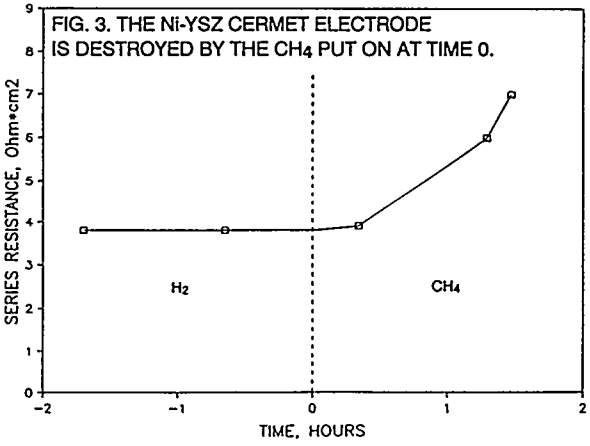
FIG. 3. THE Ni-YSZ CERMET ELECTRODE
IS DESTROYED BY THE CH4 PUT ON AT TIME 0.
H2
CH4
SERIES RESISTANCE, Ohm*cm2
TIME, HOURS

HYBRID COMBUSTION OF MCFC ANODE EXHAUST GAS FOR HEAT EXCHANGE STEAM REFORMER

Osamu Togari

Chiyoda Corporation R & D Center
13, Moriyacho 3-chome, Kanagawa-ku,
Yokohama 221, Japan

Introduction

A process in which MCFC anode exhaust gas combustion system has been employed as a heat supply method for the heat exchange steam reformer, is quite rational because the off gas treatment and the production of fuel hydrogen can be practiced concurrently. The exhaust gas, however, is so rarefied a fuel that it is difficult to burn by ordinary burners and so the catalytic combustion method must be applied. But the combustion catalyst working stably in high temperature circumstances over 1000°C has not been developed so far. Consequently in such a case necessitating 1200°C combustion gas as heat resources, Hybrid Combustion System, namely a combination of catalytic combustion and following gaseous combustion will have been adopted. In this system regenerating materials put in gaseous combustion zone hold the key to the solution of the problem. In this report details in selection of the regenerating materials are stated.

Hybrid Combustion

Under high temperature such as 1200°C, a combustion catalyst accepts so heavy thermal loads that the degradation of ability or breakage often occurs in a short time. Then it is proposed a specific process in which the burning temperature of a catalyst bed are maintained below 1000°C (really below 800°C) and the heat shortage is made up by gaseous combustion in the later section. In this process a part of fuel and all quantity of air are premixed enough and sent to the catalytic combustion chamber in the previous section. After the combustion gas containing unconsumed oxygen are mixed with the remaining fuel, this mixture is burned in the vacant room. However in this system there are two weak points as follows.

(1) Extinguished easily when it happens condition changes accompanied with reduction of the fuel concentration.

(2) Formation of NOx more than catalytic combustion

About item (1), it is the unavoidable phenomenon in a perfectly premixed combustion because of the low flame temperature. Concerning item (2), such a phenomenon is caused by insufficient mixing of fuel and the gas containing air. Insufficient mixing gives rise to the local heating and NOx is generated in large quantities at high fuel concentration portions.

Necessity of the Regenerating Materials

To improve Hybrid Combustion System having faults described above, it is desired that regenerating materials having a large surface area will be set in the later gaseous combustion section. This regenerating material not only prevents the extinguishing of fire but can re-ignite automatically whenever the gas compositions return as before in a short time, even if the fire extinguished temporarily.

Consequently, the regenerating materials are considered to be a requisite for Hybrid Combustion System.

If these regenerating materials present in the later chamber, even perfectly premixed gas can be flamed stably, so that NOx formation is suppressed to minimum value. Therefore in order to reduce NOx formation the combustion gas from the primary chamber and SAE gas must be mixed as perfectly as possible.

Properties required to the regenerating materials

The regenerating materials should have the following four characteristics.

(1) structural materials such as honeycomb or foaming boards
(2) s high melting port (higher than theoretical combustion temperature of anode exhaust gas)
(3) high resistance to thermal shocks
(4) high resistance to oxidation

It is very difficult to find out the materials which satisfy the above mentioned 4 necessitating characteristics. Besides there is little information concerning to the durabilities of ceramics in high temperature gas containing high concentration of CO2, H2O such as MCFC anode exhaust one.

About item (1) the regenerating materials must be supported by themselves on surrounding refractories, therefore, their form should be plain board. Besides in order to have high contact area with gas, it is desired that they consist of honeycomb or foaming structure. Typical samples of regenerating materials used in this experiment are shown in Fig. 1. Requirements described in items (1), (2), (3) will not need to be explained.

Durability Test of Various Regenerating Materials with Simulated MCFC Anode Exhaust Gas (SAE Gas)

Many kinds of ceramics were selected as samples for regenerating materials, and were repeatedly entered and removed from an electric furnace maintained at 1000°C. Only nine kinds of these samples could bear 50 times thermal shocks. The properties of these nine samples are given in table-1 and all of then were supplied to durability tests using SAE gas. A profile of two combustion chambers of experimental Hybrid Combustor is shown in Fig.-2. Combustion catalysts set in the primary chamber were selected from commercial ones. In an experiment a mixture of a quarter a SAE gas and all of the air flew through the primary chamber. The resultant combustion gas was mixed enough with the remaining three quarters

SAE gas at a central orifice and the mixed gas was burned in the secondary chamber set up with several regenerating materials. The compositions of SAE gas are given as follows.

The Compositions of Simulated MCFC Anode Exhaust Gas

H2	24.7 vol%
CH4	3.7 vol%
CO2	53.7 vol%
H2O	17.9 vol%

A maximum of 6 regenerating materials can be set at one time. The temperatures of various parts in chambers are described in Fig. 2. The experiments were conducted continuously but a shut-down and a restart took place once a week to give thermal shocks to the samples. Sometimes by taking out the samples set in the secondary chamber, their external appearance, weight and bending strength were examined. The results of durability tests of these regenerating samples are given in table-2. HC, HE, S3 were cracked in a short time. These samples appear to be active for high temperature steam. Other samples showed no external changes until 500 hr'th. However, at 900 hr'th HT changed to white and began to collapse. The other remaining five samples were tested for 2000 operation hours. At 2000 hr'th HI showed a color change to white and swelled to be collapsed considerably. Although at almost the same time the other four samples were not observed any large external changes, S2, S4 are broken by the hand bending test.

Finally SA are broken by the hand bending test at 2150 hr'th and only HA showed more than 3000 hrs durability.

About the Durability of HA (Si impregnated SiC honeycomb)

The results shown in table-2 suggest the following two conclusions.

(1) SiC is strong to thermal shock but weak to oxidation.
(2) Oxide ceramics are strong to oxidation but weak to thermal shocks.

HA is superior in oxidation resistance to any other SiC and it is the reason why HA exhibited the most durability. Only HA is prepared by the reaction bonding method and other SiC by the pressureless sintering method. It is noted that the pore volume of HA is Zero as shown in table-1. The reaction bonded SiC such as HA, was made by impregnating metal silicon into the honeycomb consisting of SiC and pitch at 1450°C or higher. Therefor, after reaction bonding, the excess of metal silicon remains between SiC crystals and thus non-porous Si-SiC material is formed. In comparison oxidation of porous SiC progresses from everywhere of the honeycomb, but oxidation of non-porous Si-SiC progresses only from the surface of the honeycomb. Fig. 3 shows the EPMA line Analyses of O Kα on cross sections of cell walls for HA and HI which were taken out at the halfway point of the experiment. It shows clearly that HA is oxidized in a mere ten microns depth from the surface at 1100 hr'th while HI have been oxidized everywhere in a short time less than 200 hours.

Subsequently the cell walls of HI was cut sharply by a diamond cutter in order to examine the oxidation rate of SiC crystals. SEM

photograph and EPMA line analyses of O Kα on the cross section of HI's cell wall are shown in Fig. 4. About 1μ width periphery of SiC crystal differs in darkness from the bulk and the results of EPMA line analysis suggests that the brighter periphery portion is an oxidized phase. The oxidation rates of the HA surface and monocrystal of HI are tabulated as follows.

	oxidation time	thickness of oxidized phase	rate of oxidation
HA	1100 hrs	10μ	9 nm/hr
HI	150 hrs	1u	7 nm/hr

Both rates of oxidation appear nearly same and then the oxidation rate of non-porous SiC (or Si-SiC) is considered a little less than 10 nm/hr in these experimental conditions. Consequently, a regenerating material made of non-porous SiC (or Si-SiC) is considered to have more than one year of life as far as it could bear 70 ~ 80μ reduction of thickness.

Conclusions

For usage of MCFC anode exhaust gas as heat resources of steam reformer it is necessary to employ a Hybrid Combustion System -combination of catalytic combustion and following gaseous combustion. However, it requires regenerating materials to maintain gaseous combustion stably. These regenerating materials must have a high melting point, strong resistance to thermal shocks and high resistance for oxidation. Si impregnated SiC is a quite hopeful material which satisfies these severe requirements.

Acknowledgement

This study was done as one of the key components of MCFC power generation system development project sponsored by NEDO.

The author would like to appreciate NEDO for giving an opportunity of this presentation.

Table-1 Properties of the Ceramics Used in the Durability Test

Sample Name	Material	Shape	Size	Cell Number (/in²)	Porosity	
					Pore Volume (cc/g)	Surface Area (m^2/g)
HI	SiC*1	honeycomb	56φ x 25L	324	0.291	0.0
HE	SiC*1	honeycomb	40φ x 25L	200	0.067	0.45
HT	SiC*1	honeycomb	50φ x 25L	200	0.128	0.0
HA	SiC*2	honeycomb	40 x40 x25L	6	0.000	0.0
HC	Al_2O_3-TiO_2	honeycomb	50φ x 25L	200	0.068	-
S1	Al_2O_3-ZrO_2	foam	50φ x 20L	30 - 40	0.034	2.5
S2	ZrO_2-Mullite	foam	50φ x 20L	30 - 40	0.091	-
S3	ZrO_2	foam	50φ x 20L	30 - 40	0.012	-
S4	Al_2O_3	foam	50φ x 20L	30 - 40	0.085	-

*1. Pressureless sintered
*2. Reaction bonded

Table-2 Durability Test Results of Regenerating Materials

Sample Name	Operation Time (hr)	Extenral Appearance Observation		Weight Change (%)	Hand Bending Test	Evaluation
		color change	damage			
HI	190	no	no change	+ 6.8	-	
	900	whitening	small crack	-	-	x
	2,000	do.	collapsed	-	-	
HE	59	no	cracked	+ 2.5	-	xx
HT	159	no	no change	+ 1.1	-	x
	900	whitening	cracked	+ 12.8	-	
HA	1,150	whitening	no change	+ 3.1	OK	
	2,200	do.	no change	+ 4.1	OK	o
	3,200	do.	exfoliation	+ 2.6*	OK	
HC	111	no	cracked	- 3.1	-	xx
		no				
S1	160	no	no change	- 2.0	-	
	900	no	do.	- 0.8	-	Δ
	2,000	no	do.	- 1.2	OK	
	2,150	no	do.	-	cracked	
S2	160	no	no change	- 0.9	-	
	900	no	do.	- 1.9	OK	x
	2,000	no	do.	- 1.8	cracked	
S3	160	no	cracked	- 0.2	-	xx
S4	160	no	no change	- 0.5	-	
	900	no	do.	- 1.1	OK	x
	2,000	no	do.	- 0.5	cracked	

* Weight loss by exfoliation

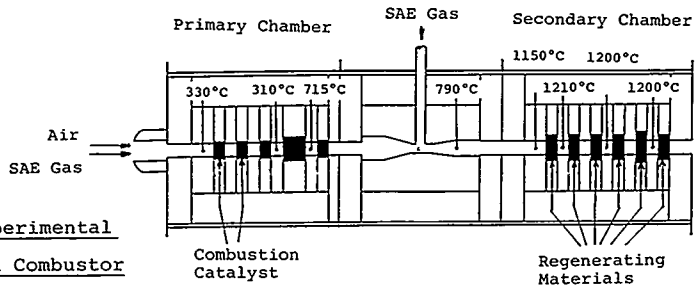

Fig.-2 Experimental Hybrid Combustor

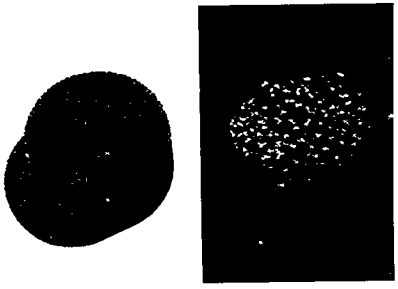

Fig. 1 Typical Samples of Regenerating Material

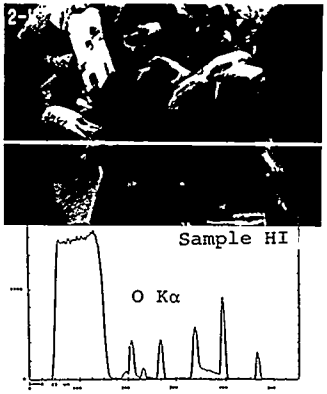

Fig. 4 EPMA Line Analysis of SiC Crystals

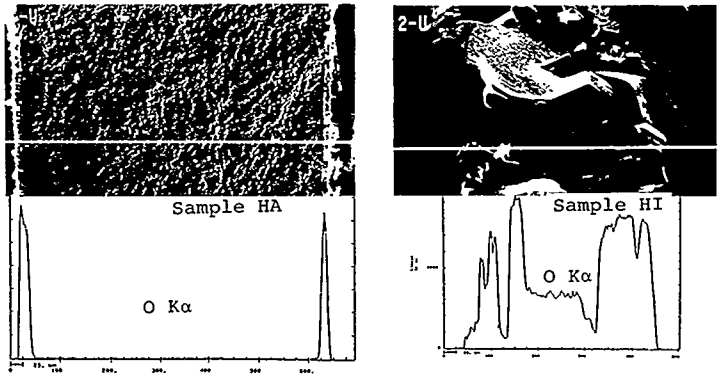

Fig. 3 SEM Images and EPMA Line Analyses on the Cross Sections of Cell Walls

DEVELOPMENT OF A 25kW CLASS SOFC COGENERATION SYSTEM UNIT

Kenichi Shinozaki
Fuel Cell Development Department
Osaka Gas Co., Ltd.
Chiyozaki, Nishi-ku, Osaka 550, Japan

Shoichi Kaneko
Research & Development Institute
Tokyo Gas Co., Ltd.
Shibaura, Mita-ku, Tokyo 105, Japan

Introduction

Osaka Gas and Tokyo Gas have high expectation for the potential of natural gas fueled SOFC cogeneration system. The SOFC cogeneration system has advantages over systems employing the PAFC or the MCFC as Follows:

1. High electrical efficiency of over 50 %
2. High pressure steam (over 10 kg/cm3)as heat recovery
3. High system simplicity

We are carrying forward a project with the Westinghouse Electric Corporation for the design, manufacture and test verification of a 25kW class SOFC cogeneration system. The system design is responsive to requirements provided by Osaka Gas and Tokyo Gas. We expected to initiate operation of the unit in either Osaka or Tokyo at the end of 1991. The results of design studies conducted as part of the system design effort are reported in this paper.

SOFC COGENERATION SYSTEM

The SOFC cogeneration system shall be capable of providing nominally 30 kW of AC electrical power using natural gas as fuel. In addition, the system shall be capable of providing steam at 10 kg/cm sq pressure.

The system configuration consists of two SOFC generator modules, a DC to AC power conditioner, and ancillary systems for the distribution and thermal management of air, fuel, exhaust and steam. The system flow circuit is shown schematically in Figure 1. Note that a heat recovery steam boiler is located in the exhaust line.

Each generator module is mated with an exhaust gas heated prereformer which is designed to reform approximately 75% of the incoming natural gas fuel before it is introduced to the cells. The water vapor needed to support reformation and to suppress carbon deposition is provided solely by spent fuel which is recirculated and mixed with incoming natural gas within the SOFC generator module/prereformer assembly. No externally sourced steam is required.

The physical arrangement of components can be seen in Figure 2.

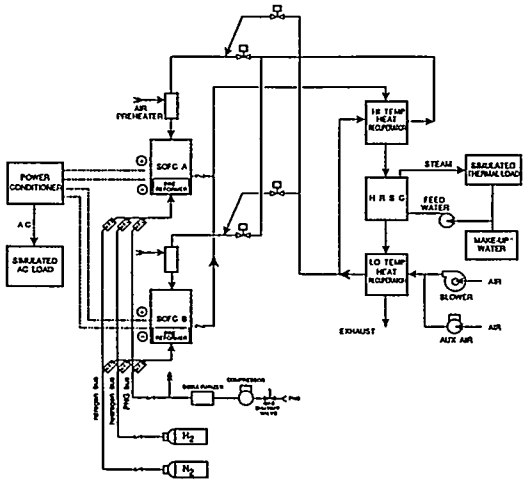

Figure 1 System Flow Diagram

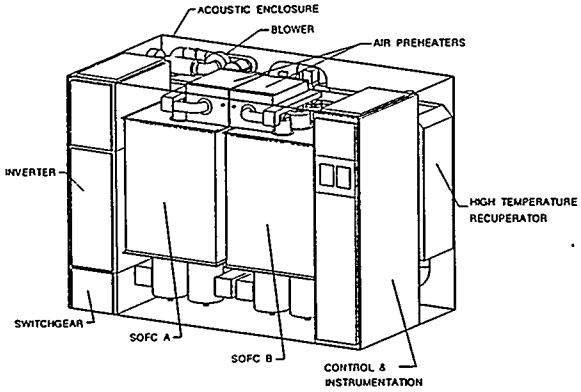

Figure 2 System Front View

ESTIMATED PERFORMANCE

Estimated performance for a 25kW class system is shown in Figure 3. The maximum electrical generating efficiency is

40% at electrical output of 30kW. At that point, 19% of the fuel's LHV can be recovered as steam at 10kg/cm sq.

The maximum electrical efficiency occurs at that operating point where the system is in thermal balance - no fuel is consumed beyond the electrochemical requirements for power generation.

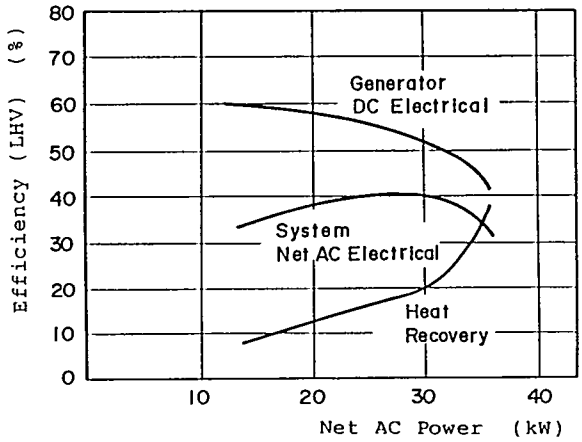

Figure 3 25kW SOFC Cogeneration System Efficiency

SOFC SYSTEM RATING EFFECTS

The estimated performance of the 25 kW SOFC cogeneration system reflects the limitations imposed by small scale. The relative importance of envelope heat losses is proportional to the surface to volume ratio of the SOFC generator module and ancillary high temperature equipment. Hence,as the module capacity level becomes larger, the envelope heat losses become less important. The result of a capacity sensitivity analysis for single module systems are shown in Figure 4.

Results summarized in Figure 4 show that for the same cell technology proposed for the 25 kW SOFC (except for cell length) peak

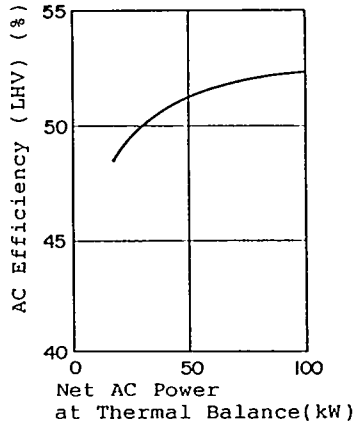

Figure 4
System Efficiency
as a Function of Capacity

efficiency values greater than 50% (AC/LHV) are achievable with systems that balance thermally with net AC electrical outputs greater than 30 kW, corresponding to systems with a peak power greater than 70kW.

PROJECTED COMMERCIAL- CLASS SOFC COGENERATION SYSTEM PERFORMANCE

Performance estimates have been developed for commercial-class SOFC cogeneration systems using the system model applied in the performance studies for the 25 kW SOFC cogeneration system. The performance estimates of Figure 5 indicate the feasibility of achieving 50% AC/LHV efficiency in the over 50kW commercial-class system employing advanced cell and generator technology.

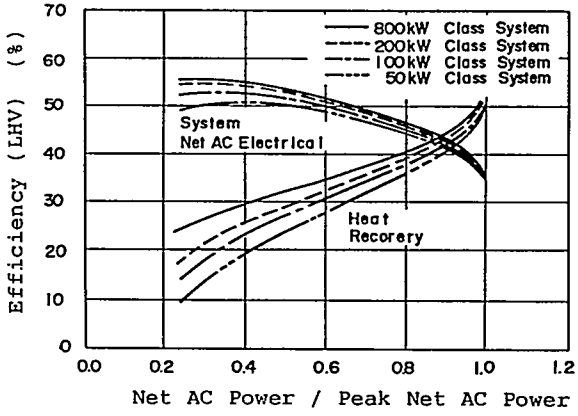

Figure 5 Commercial-Class SOFC System Efficiency with Advanced Cell and Generator Technology

CONCLUSION

1. The SOFC cogeneration system is simple compared with that of the PAFC and the MCFC.
2. An electrical efficiency greater than 50% (AC/LHV) that is coincident with the recovery of high quality heat (190 degC) can be expected for power systems with the relatively small power ratings associated with on-site applications.
3. Improvements in generator design and thermal insulation technology directed toward reducing heat loss are important in achieving higher efficiency at lower capacity levels.

RECENT PROGRESS ON A FUEL CELL R&D PROJECT OF NEDO

Hiroshi Ayada, Hideo Totuka and Yoshihiro Yamazaki
New Energy and Industrial Technology Development Organization (NEDO)
Sunshine 60 3-1-1,Higashi-Ikebukuro,Toshima-ku,Tokyo,170,Japan
Yoshiki Kurihara and Masahiro Yanagida
Agency of Industrial Science and Technology (AIST), MITI

NEDO, an implementing agency of the Japanese government acting, has been promoting a fuel cell R&D project as a part of the Moonlight Project founded and sponsored by MITI. The 15-year project started in fiscal 1981 covers phosphoric acid, molten carbonate and solid oxide types of fuel cells. The recent status of its activities is as follows.

Phosphoric Acid Fuel Cell

NEDO has started field tests of two on-site types of 200 kW power generating systems in late 1989, one for detached islands and another a cogeneration type for commercial use.(Table 1)

Table 1 200kW Power Generating Systems

Item	Detached Island	Commercial Use
AC Output(HHV)	200 kW	200 kW
Fuel	methanol	city gas(LNG)
Operation Temp.	190 ℃	205 ℃
Operation Press.	atmosphere	atmosphere
Dimension(meter)	11 ×3.0 ×3.9h	10 ×3.1 ×3.2h
Test Site	a power station in Okinawa	a hotel in Osaka

The detached island type uses methanol fuel and is located at a test site, an utility power station,on a small island in Okinawa prefecture. Field tests were started in October 1989 by Okinawa Electric Power Co. Up to July 31, 1990, the unit experienced 40 start-ups, which covered 3,287 hours with an accumulated 452,759 kWh of electricity generated. The performance of this system is summarized in Table 2.

Table 2 Peformance of a 200 kW Power Generating System for Detached Islands

Item	Design	Measured
Overall Efficiency	> 37 %	39.7 %
Cold Start-up	< 3 hr	2 hr 59 min
Load Response (20-100 %)	< 30 sec	25 sec
Harmonic Voltage Distortion	< 3 %	—
Noise at 5 meters	55 dB	—

The second 200 kW system is for cogeneration use in such facilities as office-buildings, hotels, hospitals, etc. This system, using liquid natural gas, is located at a prestigious hotel in Osaka. Field tests to supply both electricity and heat to the hotel have been conducted jointly by Osaka Gas Co. and Kansai Electric Power Co. The electricity generated by this system amounts 10% of total hotel use. The higher-grade heat energy of 170 ℃ steam recovered from this system is used as the heat energy for one of the air-conditioners for guest room services, and the lower-grade heat energy of 70 ℃ hot water is supplied to guest rooms. Up to July 31,1990,the unit had 40 start-ups, which covered 4,344 hours with an accumulated 682,700 kWh of electricity generated. The performance of this system is summarized in Table 3.

Table 3 200 kW Co-generation System Performance

Item	Design	Measured
Overall Efficiency	> 36 %	36.0 %
(co-generation)	(> 80 %)	(80.2 %)
Cold Start-up	< 3 hr	3.5 hr *
Load Response (0-100 %)	< 60 sec	75 sec *
Harmonic Voltage Distortion	< 2 %	0.2 %
Steam	170℃	170℃
Hot water	70℃	70℃
Noise at 5 meters	55 dB	—

*: adjustment is ongoing

Molten Carbonate Fuel Cell

Research on basic the molten carbonate fuel cell (MCFC) technology was started under the Moonlight Project in FY 1981. NEDO promoted a first phase program from FY 1984 with the target of developing a 10kW class cell stack by FY 1986. The successful first phase program offered some bright prospects for enlargement and performance improvement of MCFC by improving on matearials and manufacturing technologies.

The second phase program was started in FY 1987 with the target of developing a 1,000kW class pilot plant with more than 45% efficiency and more than 5,000 hours of operating time by FY 1995. As interim targets, we have been developing 100kW class cell stacks, balance of plant (BOP) for the 1,000kW class pilot plant and system technology, etc. The outline of the second phase program is shown in Figure 1.

Figure 1 Second Phase Program R&D Schedule

Item FY	1987		1995
Cell stack	10kW class	100kW class	1MW Plant (LNG type)
BOP	Component study	Components for 1MW Plant	
Materials,etc.	Elements study		Large size plant
Overall system	System design, Market research		System economies

With regard to the development of cell stacks, three types of cell stack, such as a multiple large capacity type, a rectangular large capacity type, a internal reforming type are beeing developed.

The multiple large capacity type,consisting of an electrode which has four square pieces of unit electrode in a cell plane, is being developed by Hitachi, Ltd., the contractor for this project. Hitachi, Ltd. constructed 25kW class cell stack of the atmospheric pressure type by the end of March 1990 and carried out operation tests of this cell stack from April 5 through June 22, 1990. The specifications of the 25kW class cell stack are shown in Table 4.

Table 4 25kW Class Cell Stack Specifications

Item	Specification
Type of Cell Stack	Multiple Large Capacity Type
Effective Electrode Area	12,100 cm^2 (3,025cm^2 ×4)
Stacking Cells	22 Cells
Operating Gas Pressure	Atmospheric Pressure
Gas Supply	Internal Manifold type
Gas Flow	Cross Flow Type
Cooling	Cathode Gas Cooling Method

Up to June 22, this cell stack covered 1,612 hours with a maximum output of 27.8 kW, which is the largest output by a MCFC in the world.

The rectangular large capacity type, consisting of an electrode which is a rectangular large-scale type, is being developed by Ishikawajima-Harima Industries Co.,Ltd.(IHI), the contractor for this project. IHI constructed a 10 kW pressurized type cell stack by the end of January 1990 and carried out operation tests from February 19 through April 26. The specifications of this cell stack are shown in Table 5.

Table 5 10kW Class Cell Stack Specifications

Item	Specification
Type of Cell Stack	Rectangular Large Capacity Type
Effective Electrode Area	10,000 cm^2 (56 cm×180 cm)
Stacking Cells	10 Cells
Operating Gas Pressure	1 ~ 7 ata
Gas Supply	Internal Manifold type
Gas Flow	Co-Flow Type
Cooling	Cathode Gas Cooling Method

Up to April 26, this cell stack had accumulated 1,621 hours with a maximum output of 10.8 kW under the condition of 80% fuel utilization, 7 ata.

The internal reforming type is being developed by Mitsubishi Electric Corp., the contractor for this project. Mitsubishi Electric Corp. completed construction of a 3 kW class cell stack of the atmospheric pressure type on January 12, 1990 and started the operation tests of this cell stack on January 20.

The specifications of this stack are shown in Table 6.

Table 6 3 kW Class Cell Stack Specifications

Item	Specification
Type of Cell Stack	Internal Reforming
Effective Electrode Area	5,016 cm^2
Stacking Cells	5 Cells
Operating Gas Pressure	Atmospheric Pressure
Gas Supply	External Manifold type
Gas Flow	Cross Flow Type
Cooling	Internal Reforming, Cathode Gas Cooling Method

Up to August 19, the operation tests of this stack were still ongoing, and to date had covered 4,023 hours with an average voltage of more than 0.7 V at 150 mA $/cm^2$.

With regard to the development of BOP, the Technology Research Asociation for MCFC Power Generation System (MCFC Research Asociation), which is sponsored by NEDO, is developing 1,000 kW class plant components and the basic design of a 1,000 kW class system during the first half of the Second Phase Program. The MCFC Research Asociation started construction of the test site for 1,000 kW class plant components at Akagi in FY 1990.

Solid Oxide Fuel Cell

The development of solid oxide fuel cells(SOFC) was started under a project of the Agency of Industrial Science and Technology in 1981. NEDO began to study and develop SOFC in September 1989. The R&D schedule for SOFC is shown in Figure 2.

Figure 2 SOFC R&D Schedule

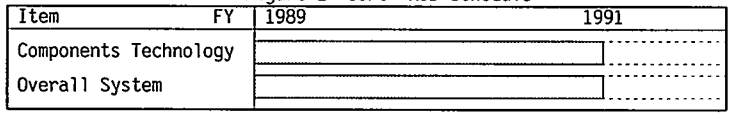

The purpose of this project is to examine the various fabrication technologies for large sized cells and to explore the prospect of future tasks in research and development with regard to elemental technology development and study on power generating systems. Performance tests for 100 W class cell stacks are scheduled in FY 1991.

Conclution

On the basis of NEDO's successes, activities to realize commercialization of PAFC has accelerated in Japan. With regard to the R&D of MCFC, the cell area was achieved to 1 m^2 class successfully and cell stack technology is being developed steadily aiming for interim targets of the second phase program. The R&D of SOFC is making steady progress.

MONOLITHIC SOLID OXIDE FUEL CELLS

FOR DIESEL BASED SYSTEMS

Solid oxide fuel cells (SOFC's) are currently under development for electric utility power generation and other applications utilizing fossil fuels. SOFC's present several significant advantages over other types of fuel cells (phosphoric acid and molten carbonate). For example, the solid electrolyte of the SOFC eliminates corrosion and electrolyte management problems facing the phosphoric acid and molten carbonate fuel cells. In the SOFC, carbon dioxide recycling is not required, as in the molten carbonate fuel cell. Higher system efficiency is possible with SOFC's. The higher operating temperature of the SOFC allows fast reaction kinetics and produces high-quality by-product heat for cogeneration and bottoming cycles.

AiResearch is currently conducting a system study for the U.S. Army Materials Technology Laboratory investigating the use of Monolithic Solid Oxide Fuel Cells (MSOFC's) for diesel based electric power generation systems. Recent improvements in the performance of single cells coupled with advances in the fabrication technique allow significant improvements over competing technologies.

ELECTROLYTE CHEMISTRY AND WETTING EFFECTS ON MCFC CATHODE KINETICS AND PERFORMANCE

J.R. Selman, T. Nishina and Y.P. Lin
Department of Chemcial Engineering
I.I.T., Chicago, IL, USA
and
D.B. Tryk and E.B. Yeager
Case Center for Electrochemical Studies
Case-Western Reverse University
Cleveland, OH, USA

Despite the concentrated efforts of a number of investigators, the rate determining factors in the cathodic reaction in molten carbonate fuel cells is still not well-understood. While there is a consensus that O_2 itself is not the primary species undergoing electroreduction, there remains a great deal of uncertainty as to whether peroxide or superoxide is the primary species. The extent to which acid-base reactions are rate determining also remains uncertain. The fact that these reactions are strongly affected by melt and gas compositions and the nature of the electrode surfaces makes the situation even more difficult. The present research, reported in more detail in Ref. [1], aims to address the above questions using several complementary electrochemical and spectroscopic techniques.

This research was carried out as a joint research effort at Illinois Institute of Technology (IIT) and Case Western Reserve University (CWRU). It was aimed at developing novel experimental approaches to the chemistry and electrode kinetics of oxygen reduction under MCFC conditions, and improving our fundamental understanding of the reaction mechanism as it applies to the MCFC.

At IIT, a rotating disk electrode (RDE) for electrode-kinetic measurements in molten carbonate has been constructed and tested. The method of constructing this RDE was finalized after methodical testing of several preliminary assemblies. Based on these experiences, a pre-treatment procedure was developed. Tests of the final RDE assembly showed very good mechanical stability (up to 4000 rpm) and stable open-circuit potentials close to the theoretically expected values. The method of simultaneously obtaining concentration and diffusivity of the reacting species by a single measurement at such a RDE has been demonstrated (Fig. 1) and numerous data have been obtained for peroxide species in pure Li_2CO_3.

Cyclic voltammetric measurements have also been made at a partially immersed gold flag electrode with simultaneous optical observation of the electrolyte film at such an electrode. Rapid wetting/dewetting was observed in the potential range from -0.4 to -0.6 V vs SOE.(Fig. 2) This is believed to be significant for electrolyte movement in the MCFC.

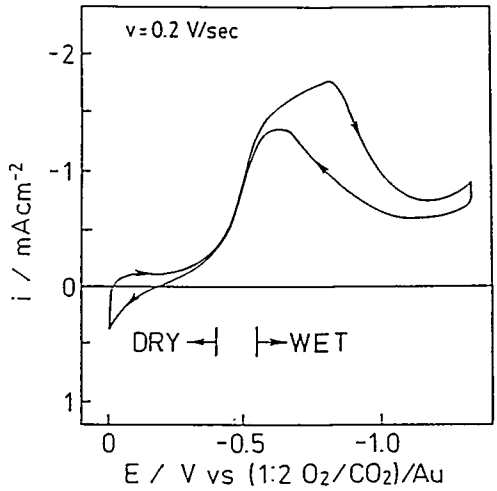

Fig. 1 Stationary Polarization Curve at a Rotating Disk Electrode in Li_2CO_3 at 800 °C, in 0.9 atm. O_2 and 0.1 atm. CO_2.

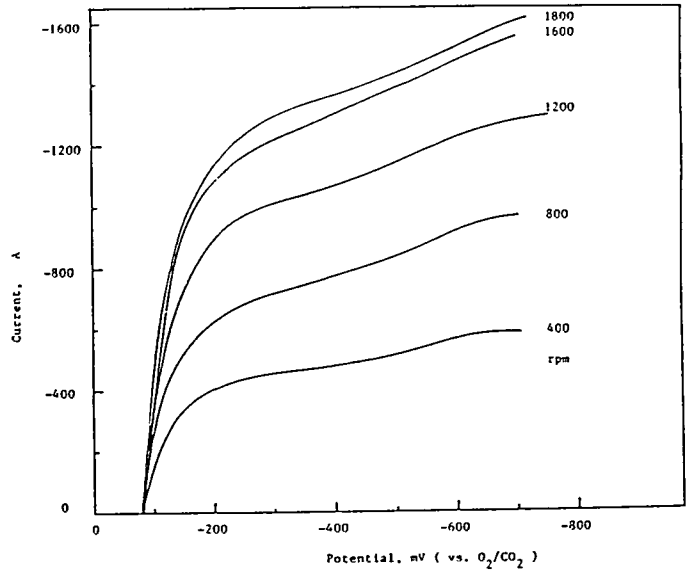

Fig. 2 Multi-cycle Cyclic Voltammograms of Oxygen Electrode at a Partial Immersed Gold Flag Electrode in 62 mol% Li_2CO_3 + 38 mol% K_2CO_3 Melt under 0.9 atm O_2 and 0.1 atm. CO_2 at 650 °C. scan rate =0.2v/s, A=0.83 cm^2.

At CWRU, several different types of microelectrodes were constructed, including a disk, a cylinder and a band type micro-electrode. All were based on gold as the electrode material and either polycrystalline alumina or sapphire as the insulator.
Raman spectroscopy was used to examine both quenched melt samples as well as melts at high temperature. The O-O stretching bands for both superoxide and peroxide were detected in quenched melt samples. The superoxide band at 1145 cm^{-1} was observed in a quenched K_2CO_3 melt to which KO_2 had been added at high temperature. The peroxide band at 685 cm^{-1} was observed in a quenched Li_2CO_3 melt to which Li_2O_2 had been added at high temperature.

Electron spin resonance (ESR) spectroscopy was found to be a good method for the quantitative analysis of quenched melt samples for superoxide. It was found necessary to quench the melt samples rapidly so that the equilibrium concentration of superoxide does not change. The spectra were obtained with the samples at liquid nitrogen temperature.

ESR measurements were carried out on a number of different melt and atmosphere compositions. The preliminary results were generally consistent with the thermodynamic data available in the literature. (Fig. 3)

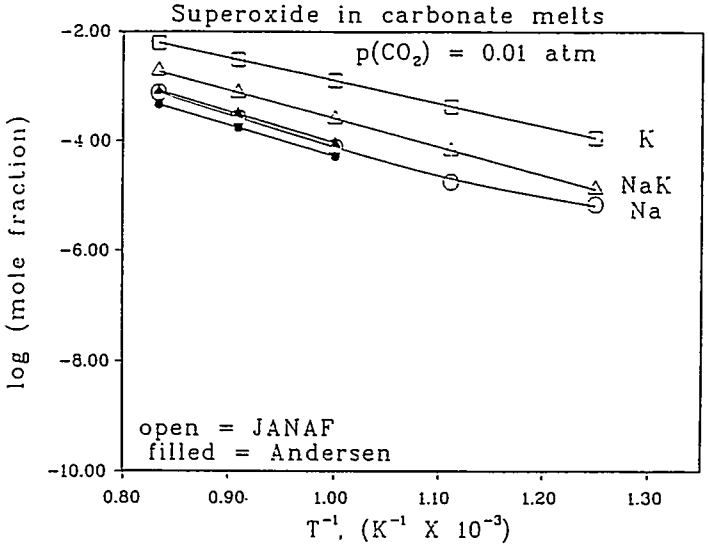

Fig. 3 Peroxide Mole Fractions for Various Carbonate Melts under 1.0 atm. O_2 and 0.01 atm. CO_2 (Note: Open symbols were calculated using JANAF data provided by Andersen, and closed symbols were calculated from Andersen's experimentally obtained data[2].)

These measurements were extended to include several melt and gas atmosphere compositions of interest from both MCFC technology and fundamental standpoints. The ESR measurements were found to provide a much higher level of precision than had been available before, with excellent sensitivity as evidenced by the fact that superoxide was detected in a quenched Li_2CO_3 melt. As expected, the superoxide concentration was very low (~10-5 mol %) (Table 1)

Table 1
ESR Measurement of Superoxide Concentration
in Carbonate Melts Cooled to 77 K

Melt	T(°C)	pO_2	pCO_2	Time (h)	$x(O_2^-)$
Na_2CO_3	900	1.0	-	8	$5x10^{-4}$
Na_2CO_3	900	1.0	-	8	$1x10^{-6}$*
Na_2CO_3	900	1.0	-	1	$4x10^{-6}$
Na_2CO_3	900	0.98	0.02	0.5	$1x10^{-5}$
$NaKCO_3$	900	1.0	-	1	$9x10^{-7}$
$NaKCO_3$	900	0.98	0.02	1	$6x10^{-7}$
Li_2CO_3	900	1.0	-	1	$2x10^{-7}$

* after 5 months

Acknowledgment : This work was supported by the U.S. Department of Eneregy, Morgantown Energy Technology Center (contract DE-AC21-86MC23266)

References

[1] J. R. Selman, T. Nishina, Y.P. Lin and D.A. Tryk, E.B. Yeager, "Electrode Reaction Mechanisms in Molten Carbonate Fuel Cells", Final Technical Report submitted to U.S. Department of Energy, Morgantown Energy Technology Center, under contract DE-AC21-86MC23266, July 1989.
[2] B.K. Andersen, Ph.D. Dissertation, The Technical Univer sity of Denmark, 1975.

THERMOCHEMICAL CONSIDERATIONS AND PERFORMANCE OF SOLID OXIDE FUEL CELLS

Christopher Milliken, David Tucker, S. Elangovan and Ashok Khandkar

Ceramatec, Inc.
2425 South 900 West
Salt Lake City, Ut 84119

Introduction:

In a Solid Oxide Fuel Cell (SOFC), intimate contact between various cell components such as electrolytes, electrodes, and bipolar interconnects is required to minimize polarization losses and achieve high performance characteristics. However, interactions at component interfaces during high temperature fabrication processes and/or under cell operating conditions may lead to performance degradation. Consequently, it becomes important to recognize the "materials limitations" of the cell components of choice.

The candidate materials, used along with a stabilized zirconia electrolyte, are $La_{1-x}Sr_xMnO_3$ as the cathode, NiO/ZrO_2 as the anode and $La_{1-y}Sr_yCrO_3$ as the interconnection. The cathode and the interconnection materials, being isostructural, lend themselves to interdiffusion of chromium and manganese. This interdiffusion has been shown to decrease the conductivity of both materials(1). Formation of lanthanum and strontium zirconates ($La_2Zr_2O_7$ and $SrZrO_3$, respectively) in powder mixtures of the electrolyte and cathode materials at high temperature has been reported(2). Cathodic overpotential losses have been found to increase with increased annealing temperature and are believed to be related zirconate formation(2). Reactions are not expected between the anode material and the electrolyte, however, limited solubility of of NiO in ZrO_2.has been reported(3).

Experimental:

Fully densified samples of $La_{1-y}Sr_yCrO_3$ (LSC) and $La_{1-x}Sr_xMnO_3$ (LSM) were prepared from liquid-mix synthesized powders. Pellets of commercially available coprecipitated (8 mole % Y_2O_3) ZrO_2 (YSZ) and NiO/ZrO_2 mixtures were also prepared. Archemedian measurements were made to ensure that all specimens had densities in excess of 95% and open porosities below 0.05%. X-ray diffraction analysis showed that no impurity phases were present. One face of each sample was polished and optically examined to ensure a clean, flat, contamination-free surface. Diffusion couples consisting of electrolyte/cathode, cathode/interconnect and electrolyte/anode pellets were made by placing polished surfaces of the samples in intimate contact and burying them in powders composed of a 50:50 mixture of the component materials. The diffusion couple and powder were contained in a high purity alumina crucible.

The diffusion couples were annealed at temperatures between 1200°C and 1650°C for various lengths of time. Furnace temperature was monitored and maintained at a constant temperature within ±5°C for the duration of the runs. The annealed samples were quenched in air to room temperature, mounted in an epoxy resin and ground and polished to expose the diffusion region. The samples were examined using an electron microprobe. Determination of the compositional profile, perpendicular to the original weld, was achieved by observing the X-ray intensities of Cr Kα, Mn Kα, Sr Lβ, La Lα, Zr Lα and Ni Kα. The bulk powders used to bury the samples were examined using X-ray analysis.

Results/Discussion:

The concentration profiles of Cr and Mn in the $La_{1-y}Sr_yCrO_3/La_{1-x}Sr_xMnO_3$ system after 24 hours of annealing at 1500 and 1650°C are shown in Figure 1. These profiles were analyzed using both the Matano method (4) and linearized error function analysis(5) to determine the interdiffusion coefficient, $D_{Mn,Cr}$. The interdiffusion coefficient was found to be independent of composition in the temperature range investigated. The experimentally determined values for $D_{Mn,Cr}$ are plotted as a function of

temperature in Figure 2, and are found to follow the Arrhenius relation, $D = 0.361\exp(-378.3\ kJ / RT)\ cm^2/s$. From the experimental data and assuming solid state diffusion, an interdiffusion region of approximately 1.5μm is expected after 50,000 hours at 1000°C. In an SOFC, the cathode will be porous,with an open porosity ranging from 20 to 30% and an average pore size of 1 to 3 μm. Since Cr is known to migrate by vapor transport, the actual interdiffusion distance will be greater than predicted.

In the $La_{1-x}Sr_xMnO_3$-YSZ system, formation of $La_2Zr_2O_7$ as an interfacial reaction product was observed. As shown in Figure 3, Lanthanum Zirconate forms along the interfacial weld with a typical thickness ranging from 1μm to 5 μm when held at 1450°C for 48 hours. X-ray analysis on cofired powder mixtures revealed $La_2Zr_2O_7$ formation after 24 hours at temperatures as low 1200°C. It is believed that zirconate formation leads to high overpotential losses at the cathode/electrolyte interface and reduced cell performance.

Microprobe analysis of the interdiffusion region also reveals pronounced Mn diffusion into ZrO_2 along grain boundaries, with measurable quantities of Manganese extending >40 μm into the electrolyte after 168 hours at 1350°C. This agrees with earlier work where Mn diffusion into polycrystaline YSZ to a distance of more than 1500μm when held at 1400°C for 328 hours was observed(6). Figure 4 shows Mn diffusion into ZrO_2 when held at 1350°C for 168 hours. As shown in Figure 5, Mn diffusion is discontinuous within the zirconate region indicating a very low solubility of MnO_x in $La_2Zr_2O_7$.

The investigation of NiO diffusion into YSZ has yielded little information. Microprobe analysis has shown that there is less than 0.2% bulk NiO solubility in this system which is in agreement with literature values(3). X-ray analysis indicates no additional phase formation at temperatures as high as 1500°C. Scanning Electron Microscopy of the interfacial region shows reagions of good bonding, however, microprobe analysis reveals that there is less than 2μm interpenetration in these areas when held at 1420°C for 168 hours. More sensitive analysis, such as TEM or STEM, might reveal additional information.

References:
(1) R. Koc, H.U. Anderson and S.A. Howard, Proceedings of the First International Symposium on Solid Oxide Fuel Cells, vol. 89-11, p. 220, The Electrochemical Society, New Jersey, 1989.
(2) O. Yamamoto, Y. Takeda, R. Kanno and T. Kojima, Proceedings of SOFC-Nagoya, Nagoya, Japan, Nov. 13 - 14, 1989.
(3) V.B.Tare, et.al., Extended Abstracts from the 177th Meeting of the Electrochemical Society, Montreal, 1990.
(4) C. Matano, Japan Journal of Physics 8, p. 109, 1894.
(5) Siv Killie, "Interferometric Technique for Determination of Diffusion at Elevated Temperatures and Pressures, ", Doctoral Thesis, University of Trondheim, Norway
(6) S.K. Lau and S.C.Singhal, "Potential Electrode/Electrolyte Interactions in Solid Oxide Fuel Cells," Corrosion, 1985

Acknowledgments:
This work was funded by the Gas Research Institute under contract #5086-294-1292

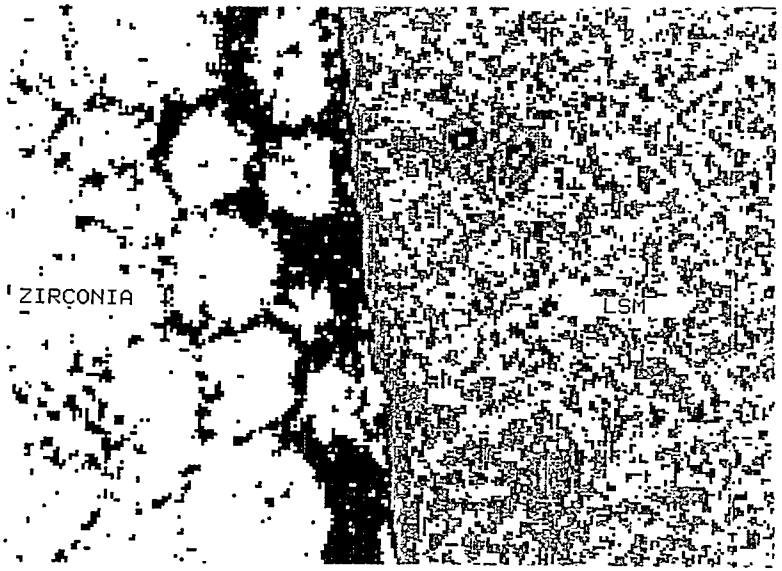

Figure 4 - Manganese Diffusion along Grain Boundaries in YSZ

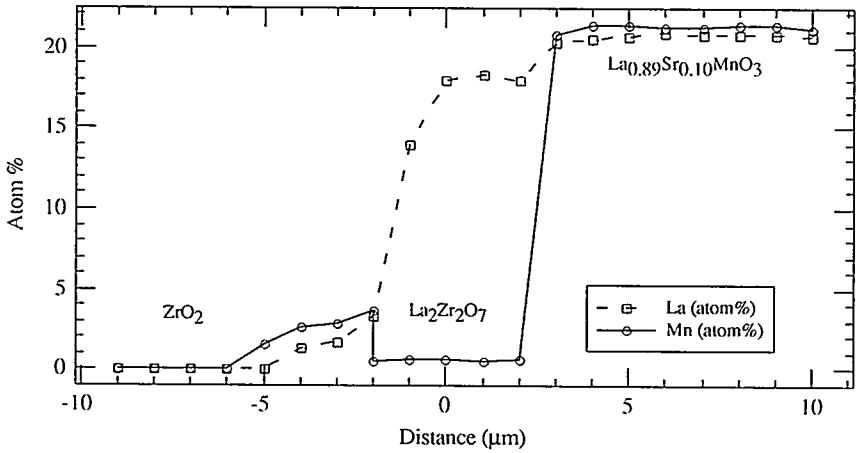

Figure 5 - Lanthanum and Manganese Diffusion in $LaMnO_3$-ZrO_2 System.

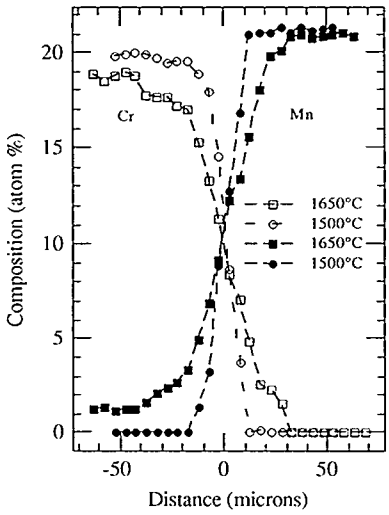

Figure 1- Interpenetration of Cr and Mn in $LaCrO_3$-$LaMnO_3$

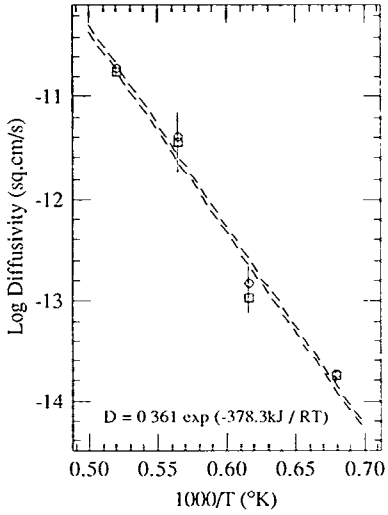

Figure 2 - Interdiffusion Coefficient as a Function of Temperature

Figure 3 - $La_2Zr_2O_7$ Formation along Interfacial Weld

DEVELOPMENT OF ALTERNATE CERAMIC CATHODE MATERIAL FOR MOLTEN CARBONATE FUEL CELLS

S. Elangovan, Ashok Khandkar,
Dave Tucker and Robert Mayhew
Ceramatec, Inc
2425 South 900 West
Salt Lake City, UT 84119

Introduction:

The state-of-the-art cathode material used in molten carbonate fuel cells is lithiated nickel oxide which is a p-type electronic conductor. The lithiated NiO cathode is known to have stability problems in molten carbonate and is not suited for long term operation of the cell (25,000 hrs), especially at high pressure. The NiO cathode forms nickel carbonate which dissolves in the molten carbonate electrolyte. Nickel ions in the electrolyte then reduce to nickel metal at the anode causing dendritic nickel growth, which leads to internal shorting of the cell (1). The current technological status of NiO cathode has been reviewed extensively in literature(2).

Various alternate cathode materials have been investigated over the years to replace NiO . Many of the alternate materials suffer from low conductivity and poor stability in the corrosive carbonate environment. All investigations are based on achieving the following criteria:

- High p-type electrical conductivity,
- phase stability under cathode environment at 650° to 700° C, and,
- corrosion resistance to molten (Li-K)CO_3 eutectic mixture.

After screening several possible alternate cathode materials, garnets were chosen as the candidate material for further evaluation. The selection was based on preliminary corrosion tests and conductivity measurements under simulated cathode gas conditions.

Synthesis and Characterization:

The Yttrium Iron Garnet, $Y_3Fe_5O_{12}$, compositions with various dopants were synthesized by the liquid mix process using cation nitrate precursors. Systematic evaluation of "A" site dopants was carried out. A candidate dopant with an optimum dopant level was chosen based on conductivity measurements. X-ray diffraction was employed as the primary technique for phase characterization. The conductivities, measured at 650° C, ranged from 0.1 to 0.2 $(\Omega\text{-cm})^{-1}$ compared to a value of 0.08 $(\Omega\text{-cm})^{1}$ for NiO. The conductivity of NiO, however, increases with Li+ doping(3) and it can be as high as 47 $(\Omega\text{-cm})^{-1}$. The doped garnets showed excellent high temperature phase stability when held at 700° C in air for more than 200 hours. The conductivity values decreased very little after the test. Immersion tests in molten carbonate at 650° C showed good corrosion resistance for this composition. These tests were performed using the doped YIG material in a ~50% dense pellet form as well as in the powder form. Atomic absorption analyses of the carbonate, after 200 hours at temperature, showed the presence of Y ions in the range of 200 ppm. The corrosion product, Y_2O_3, is highly stable in the anode environment and is not expected to reprecipitate causing internal shorting. There was no appreciable change in conductivity after immersion in molten carbonate for 200 hours.

In-cell Testing:

Based on the promising out-of-cell test results of A-site doped YIG, limited in-cell tests were conducted at the Institute of Gas Technology. The test cells consisted of electrolyte tiles made of $LiAlO_2$ impregnated with molten Li-K carbonate, porous Ni-Cr anode, doped YIG cathode and stainless steel current collectors. The cell arrangement was held together by external pressure. Molten carbonate was periodically added to the cell to make up for any loss during the test.

In the first test in a 3 sq. cm. fuel cell, the cathode showed a very high polarization, 457 mV, compared to 27 mV for the state-of-the-art cathode, at a load of 80 mA/cm^2. The high polarization loss could be attributed to unoptimized microstructure (porosity and pore size distribution). The cell resistivity was about 20 Ω-cm, an order of magnitude higher than that for a cell using the current NiO cathode. The results of the in-cell test are given in Figure 1.

In order to recheck the results of the first test and to determine if the poor performance was due to cathode flooding, a second in-cell test was performed using two YIG samples, thereby doubling the cathode thickness. The initial cell resistivity, measured after the cell temperature had stabilized at 650° C, was 91.4 Ω-cm. This is slightly more than twice the value from the previous test,with the additional interface between the two YIG samples contributing to the cell resistance.

In the cell arrangement used for these tests the cathode is the only component that was expected to contribute to cell resistivity. The cell resistivity during the second test varied from 36 to 112 Ω-cm whereas the out of cell resistivity of doped YIG measured at 650° C in air was of the order of 5 Ω-cm. The cell resistivity increased as a function of time; but, it dropped steeply when molten carbonate was added to the system. X-ray characterization of the cathode material after the test showed that it did not undergo any phase transformation.

Alternate Compositions:

Even though out-of-cell conductivity of doped YIG was higher than that of NiO, lithiation of NiO during cell operation increases its conductivity by an order of magnitude The conductivity of Li^+ doped NiO can be as low as 47 $(\Omega\text{-cm})^{-1}$ (3). The in-cell conductivity of NiO, however, is typically 0.5 $(\Omega\text{-cm})^{-1}$. Thus, it becomes necessary to improve the conductivity of YIG comparable to lithiated NiO. In order to improve the conductivity of the YIG composition, comparable to that of lithiated NiO, effects of various B site dopants were evaluated. After screening several dopants, based on coordination number, ionic radius, and valency, a dopant was successfully identified that increased the conductivity of 50% porous samples to >0.5 $(\Omega\text{-cm})^{-1}$. The conductivity as a function of temperature using the 4-point measuring technique is given in Figure 2. The 200 hour corrosion tests (1 atm. in air as well as 10 atm. under cathode gas) were conducted and the leach liquors were analyzed for the presence of various ions. Under both test conditions, the material exhibited excellent corrosion resistance.

Conclusions:

An alternate ceramic cathode material for molten carbonate fuel cells has been identified through out-of-cell and limited in-cell characterization. In-cell evaluation

identified that the primary loss in performance is due to high ohmic resistance and polarization losses. Through multiple dopants, the conductivity of YIG has been increased to a value comparable to the in-cell conductivity of NiO cathode. The corrosion resistance also appears to have improved for this composition. The polarization losses are expected to be minimized through optimization of cathode microstructure.

Acknowledgements:

This work was funded by Electric Power Research Insitute under contract number RP+1085-14. Mr. Len Marianowski of IGT is acknowledged for in-cell evaluation of the material.

References:

1. Vogel, W.M. et al., Proceedings of the Symposium on Molten Carbonate Fuel Cell Technology, The Electrochemical Society Proceedings Volume 84-13, p. 443 (1984)

2. N.Q. Minh, J. Power sources, vol. 24, p.1, 1988.

3. Z. M. Jarzebski, Oxide Semiconductors, Int. Ser. Monographs Sci. and Solid St., Vol. 4, Ed. by B. R. Pamplin, Pergamon Press, New York, 1973, pp. 150 - 189.

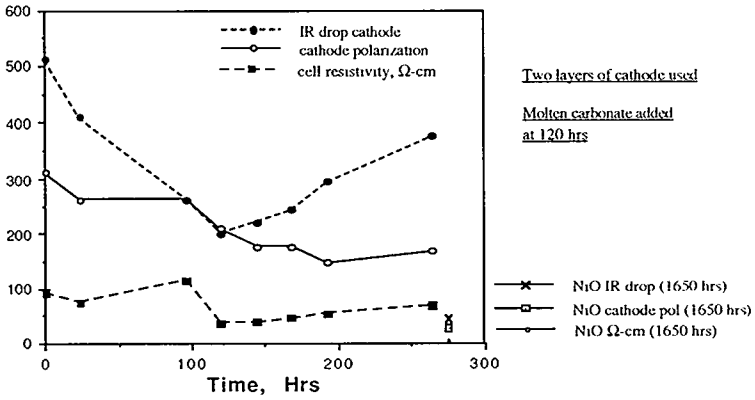

Figure 1
In-cell Testing of A-site doped YIG Cathode

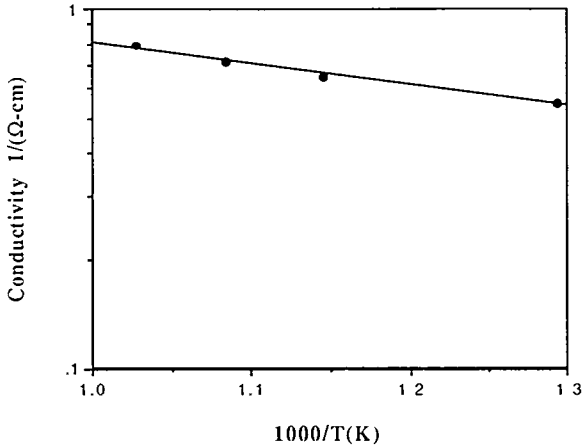

Figure 2
Conductivity of Alternate YIG Composition

HALF-CELL ELECTROCHEMICAL CHARACTERIZATION OF MATERIALS FOR MCFC CATHODES

L. Bigoni*, G. D'Antonio*, U. Ducati°
F. Parmigiani*, M. Scagliotti*
*CISE Tecnologie Innovative SpA, P.O.Box 12081
I-20134 Milano
°Dip. Chimica Fisica Applicata,Politecnico di Milano
P.za L. da Vinci 32, Milano

INTRODUCTION

The oxygen electrode is the main source of energy dissipation in most electrochemical systems - both cells and electrolyzers - where this gas is involved in electrodic reactions.

The situation is even more dramatic in the specific case of MCFC, where a mixed feed of oxygen and carbon dioxide must be converted into carbonate ions.

The requirements of the cathodic material are easily obtained from the reaction mechanism: good adsorption capacity of oxygen molecules (including low impedance with reference to mass flow), good oxygen exchange capabilities, good electron exchange properties to complete the reaction, good stability in a very reactive environment, as molten carbonates are, good mechanical properties to ensure adequate time stability.

A thorough examination of the behavior of some candidate materials for MCFC cathode has been carried out at CISE in the purpose of optimizing the cathode as to:

- electrocatalytic activity, with reference to the global reaction resistance (including mass flow impedance, ion and electron exchange ability, a.s.o.);
- stability towards the working environment;
- effects of surface area changes at constant porosity and surface doping on electrodic activity and stability.

EXPERIMENTAL

All data presented herein have been collected by a half cell, schematically shown in fig. 1, developed a few years ago at CISE Labs. The main feature of the work is the use of a Piontelli-type RE probe, machined from a sintered alumina rod, embedded within the electrolyte tile during the hot pressing procedure. The RE probe is electrochemically connected to the tile through a 10 μm dia hole laser drilled on the side surface at approximately 200 μm from the base.

In comparison with the conventional RE probes described in the literature, the Piontelli probe does not affect the equipotential surface distribution within the electrolyte. Moreover it is bound up with an equipotential surface whose geometrical characteristics are invariant over current density (c.d.).

The half cell (5 cm^2 apparent area) has been operated with different - but home made - cathodes; namely:

i) "in situ" oxidized and lithated sintered nichel electrodes of various texture (felt, foam, sintered powder);

ii) sintered prelithiated nichel oxide structures;
iii) physically modified (PVD coating of lithiated nichel oxide) prelithiated sintered nichel oxide structures;
iv) chemically modified cathode environments, through the addition of dopants to the electrolyte or to the cathode during the preparation procedure. Acidic or basic (as from Lewis) dopants have been selected among the lantanide, actinide and 2b or 4b elements;
v) some alternative cathode materials, such as Zn(Cr)O, have been considered for comparison.

As far as the above items are concerned, the aim of the research strategy is:

i) the effect of cathode texture and porosity in respect to the electrochemical performance of the NiO(Li) cathode material:
ii) the effect of thermal treatments, at temperatures higher than the MCFC working temperature, on the removing of surface inhomogeneities, which can promote the dissolution of Ni ions from the cathode;
iii) the effect of a further procedure to eliminate the surface inhomogeneities by PVD coatings to reduce the Ni ion solubility in the electrolyte;

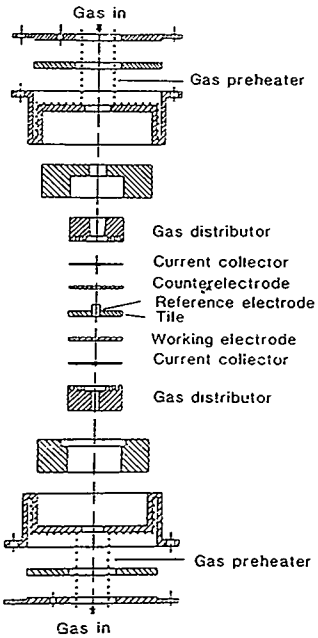

FIGUR E 1

SCHEMATIC OF THE HALF CELL

iv) the effect of acid base equilibria at the electrode surface;
v) the potential of materials which are considered alternative candidates over the lithiated nichel oxide.

The experimental procedure of the investigation is based on standard electrochemical techniques, such as intensiostatic runs, fast voltage recording during current transients and, in some cases, amperodynamic experiments. Gas side polarization effects have been evaluated by changing the composition of the gas fed to the working electrode.

RESULTS

Some typical polarization results obtained on individual but representative cathodes made of different materials are shown in fig. 2.

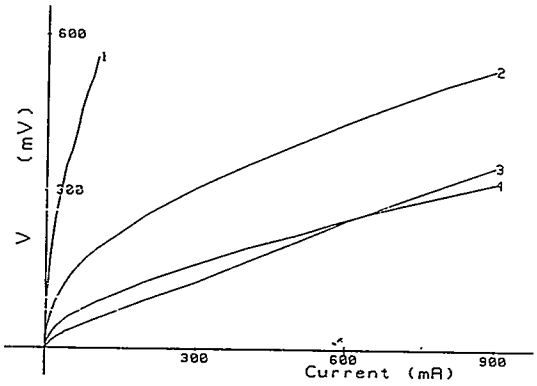

FIGURE 2

POLARIZATION RESULTS ON DIFFERENT CATHODES:1: Zn(Cr)O; 2: IN SITU OXIDIZED Ni FOAM;3: SINTERED PREOXIDIZED PRELITHIATED NiO;4: THE SAME MATERIAL PVD COATED

Here, the effects of the chemical nature (ZnO and NiO), of the structure and of the preparation procedure including physical treatments are summarized.

Of course, the global electrochemical behavior of an electrode is a combination of different properties: internal ohmic drops, which may be very high at increasing porosity, may be responsible for the comparatively high voltage drops on "in situ" oxidized Ni foam; crossing over of the characteristics of the prelithiated sintered NiO electrodes may be due to the change of porosity in the surface layer, brought about by PVD treatment.

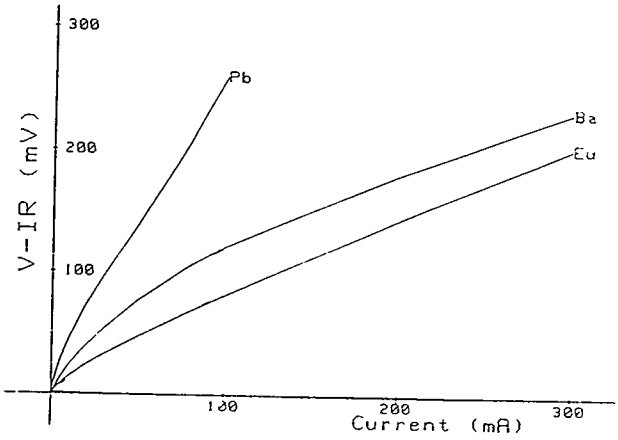

FIGURE 3

EFFECT OF DOPANTS (1°/₀₀ WT) ON POLARIZATION CHARACTERISTICS: 1 Pb; 2 Eu; STANDARD (Ba) CATHODE

In fig. 3, the effect of dopants on the cathode behavior is shown: the results appear to neatly stress the role of acid-base equilibria at the surface.

Even more impressive results have been obtained with actinide and 2b group elements from the work in progress at the time of the presentation of this paper.

One of the problems encountered with NiO-based cathodes is the dissolution of Ni compounds in the electrolyte; fig. 4 shows how this can be managed, at least to some extent, by carefully controlling the preparation procedure of the cathode.

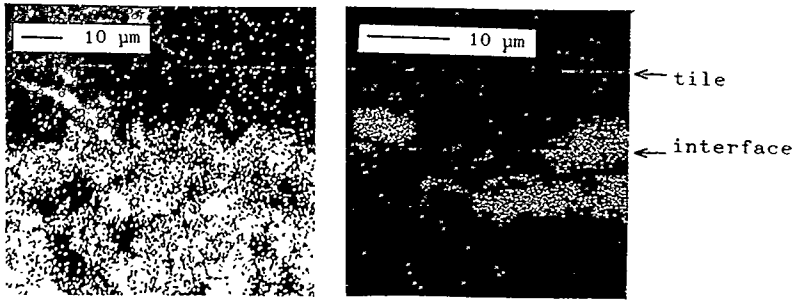

FIGURE 4

Ni DOT MAP ON A SECTION OF THE TILE
A: STANDARD CATHODE; B: PVD COATED

It is worth noting that all the observed doping effects have been proven volatile in nature in a one hundred-hour time range or so: a restoring capacity of the cell prevails, eventually.

Fast recording of voltage transients at current pulses may help in discriminating about the various power dissipation mechanisms at the electrode.

In fig. 5 gas side diffusion polarization and ion exchange overvoltages are easily evidenced. By this technique, parameters i_l and i_o and α_n of the Butler-Volmer (BV) equation have been evaluated.

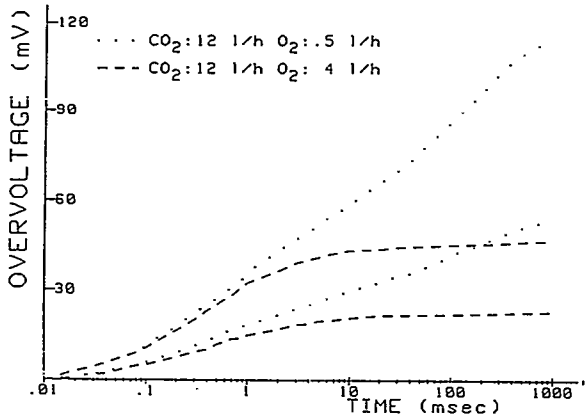

FIGURE 5

FAST RECORDING OF VOLTAGE TRANSIENTS
(LOGARITHMIC TIME AXIS)

CONCLUSIONS

A clear representation of the electrochemistry of Ni(Li)O cathodes for MCFC can be obtained from the work carried out at CISE: a reaction mechanism comprising a fast ionization stage of oxygen to superoxide followed by a rather slow reduction process in solution is confirmed by doping experiments and the value of α_n in the BV equation. The solubility of Ni in the electrolyte is probably largely dependent on the presence of surface inhomogeneities on the cathode, so that it may be limited by adsorption of strong basic species or removal of the inhomogeneities by PVD coatings of the same material.

Work supported by ENEA under grant no. 39100 serie 3.

DEVELOPMENT AND CHARACTERIZATION OF MOLTEN CARBONATE FUEL CELL ANODES

M. Takeuchi, H. Okada, K. Iwamoto, Y. Iwase, S. Kuroe and T. Yoshioka.
Hitachi Research Laboratory, Hitachi, Ltd.
4026, Kuji-cho, Hitachi-shi, Ibaraki-ken, 319-12, Japan

T. Kahara and K. Ohtsuka
Hitachi Works, Hitachi, Ltd.
3-1-1, Saiwai-cho, Hitachi-shi, Ibaraki-ken, 317, Japan

INTRODUCTION

A research and development program for molten carbonate fuel cell (MCFC) in Japan was started in 1981, as a part of the Moon-Light Project. Hitachi, Ltd. has been participating in the program from the beginning. This program is now being promoted by the Agency of Industrial Science and Technology, Ministry of International Trade and Industry (AIST/MITI) and New Energy and Industrial Technology Development Organization (NEDO). Since entering the program's second stage in 1987, Hitachi has been engaged in the development of a 100kW class large capacity stack(1), and basic research on the MCFC, focusing on the stabilization of cell components and improvement of cell performance and durability.

ALUMINUM DIFFUSION STRENGTHENED NICKEL ANODE

To maintain good cell performance during long term operation, a stabilized porous anode whose morphological conditions and thickness do not change substantially during use needs to be developed (2-6).

Aluminum diffusion strengthened nickel anodes were prepared by heating sintered porous nickel plates with the aluminum diffusing reagent (mixture of Al, Al_2O_3 and NH_4Cl powders) at different temperatures (450-750°C) under an inert gas (Ar) atmosphere.

Figure 1 shows the scanning electron microscope photograph and the results of electron probe micro analysis (EPMA) of the aluminum diffusion strengthened nickel anode. The existence of aluminum in bulk nickel was confirmed by EPMA of the anode cross-section and this aluminum was diffused throughout the bulk nickel.

Figure 2 shows the relationship between the aluminum diffusion temperature and the thickness loss after a creep test and the overpotential of the aluminum diffusion strengthened nickel anodes. The shrinkage of the anode due to the sintering and creep process was suppressed by rising the aluminum diffusion temperature. As shown in Figure 3, the morphological conditions of anodes treated at 550°C and 650°C did not change significantly compared to that of the anode treated at a lower temperature. On the other hand, the overpotential of the anode increased with the rise in temperature. The tendency correlated to the aluminum contents

in bulk nickel which increased with the temperature. The crystal structures of the anodes were checked by X-ray diffraction and intermetallic Ni-Al compounds, $AlNi_3$ at 550°C, AlNi and AlNi at 650°C and Al_3Ni_2 at 750°C were observed.

It seems that the formation of the intermetallic Ni-Al compounds was more effective in providing resistance to shrinkage and thickness loss of the anode and in reducing the progression of sintering and creep of the anode.

CELL PERFORMANCE

A lab-scale single cell (effective electrode area:100cm^2) was assembled with a NiO cathode containing Ag, the aluminum diffusion strengthened nickel anode, a $LiAlO_2$ electrolyte plate made by a tape casting method and stainless steel separators in which the wet seal zone was aluminized. Figure 4 shows the results of the durability test of the single cell when operated under atmospheric pressure. The cell voltage was kept at over 0.8V at a current density of 150 mA/cm^2 for 2000 hours.

ACKNOWLEDGEMENT

Most of the work described in this paper was performed under the support of the Agency of Industrial Science and Technology, Ministry of International Trade and Industry (AIST/MITI) and New Energy and Industrial Technology Development Organization (NEDO).

REFERENCES

1. T. Kahara, K. Ohtsuka, S. Takashima, M. Takeuchi, Y. Fukui and S. Nakanuma, "Status of Large Sized MCFC Cell and Stack Technology Development at Hitachi", 1990 Fuel Cell Seminar Abstracts, to be presented, Nov., 1990
2. L. Paetsch, J. Doyon, R. Chamberlin and C. Yuh, "Molten Carbonate Fuel Cell Materials Status", 172nd Electrochemical Society Meeting Abstracts, pp.277, Oct., 1987
3. D. S. Erickson, E. T. Ong and R. A. Donado, "Oxide Dispersion Strengthened (ODS) Anode", 1986 Fuel Cell Seminar Abstracts, pp.168, Oct., 1986
4. M. Takeuchi, H. Okada, T. Mori, I. Sone, Y. Hishinuma, K. Ohtsuka and T. Kahara, "The Stabilization of Electrodes for Molten Carbonate Fuel Cell", 1988 Fuel Cell Seminar Abstracts, pp.331, Oct., 1988
5. P. Petty, S. Elangovan and A. C. Khandkar, "Development and Characterization of Metal Coated Ceramic Anodes for Molten Carbonate Fuel Cells" 1988 Fuel Cell Seminar Abstracts, pp.356, Oct., 1988
6. E. T. Ong and R. A. Donado, "MCFC Component Technology", 1988 Fuel Cell Seminar Abstracts, pp.390, Oct., 1988

SEM Image of Bulk Ni
(Cross-Section)

Al Distribution in Bulk Ni
(Al Map by EPMA)

FIGURE 1

ALUMINUM DIFFUSION STRENGTHENED NICKEL ANODE

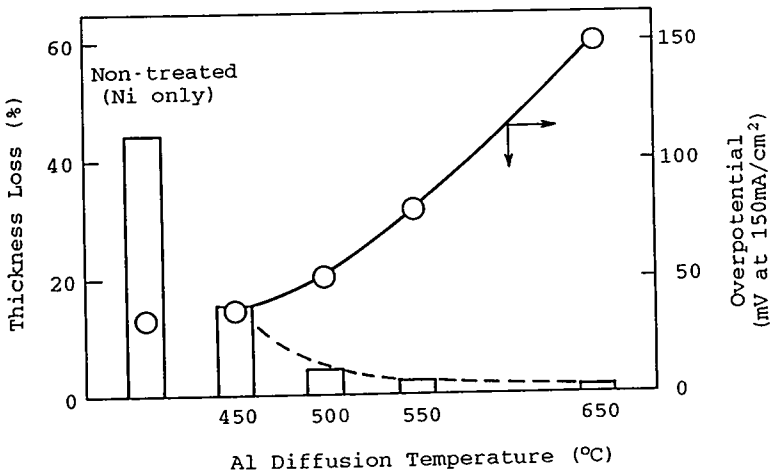

FIGURE 2

RELATIONSHIP BETWEEN THE ALUMINUM DIFFUSION TEMPERATURE AND THE THICKNESS LOSS AFTER A CREEP TEST AND THE OVERPOTENTIAL OF ALUMINUM DIFFUSION STRENGTHENED NICKEL ANODES

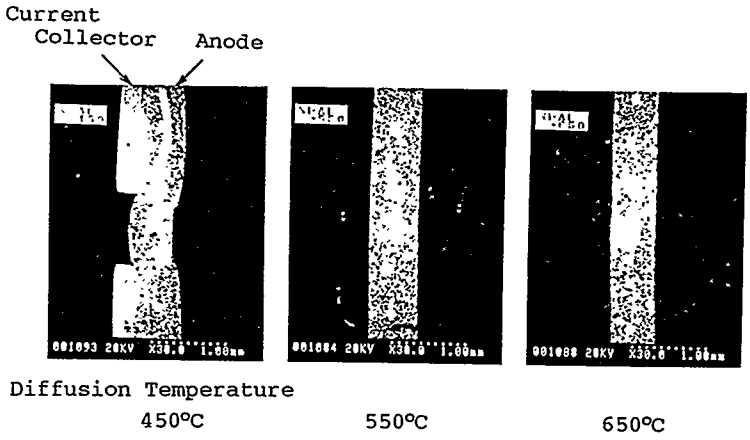

FIGURE 3

SEM PHOTOGRAPHS OF THE ANODE CROSS-SECTIONS AFTER A CREEP TEST

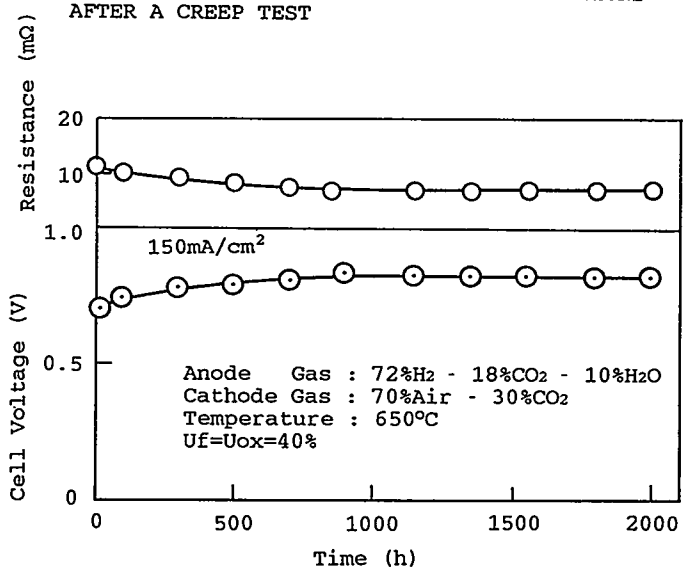

FIGURE 4

DURABILITY PERFORMANCE OF A SINGLE CELL ($100cm^2$) USING THE ALUMINUM DIFFUSION STRENGTHENED NICKEL ANODE UNDER ATMOSPHERIC PRESSURE

IMPEDANCE MEASUREMENTS OF THE OXYGEN REDUCTION IN MOLTEN CARBONATES AT 650 °C

R.C. Makkus, K. Hemmes, J.H.W. de Wit
Delft University of technology, Laboratory for materials Science
Division of Corrosion Technology and Electrochemistry
Rotterdamseweg 137, 2628 AL Delft, The Netherlands

Introduction.

A proposed reaction path for the oxygen reduction in the eutectic mixture of Li_2CO_3/K_2CO_3 (62/38 mol%)at 650 ° C consists of two chemical reactions, followed by three electron transfer reactions and a succeeding chemical reaction [1,2,3]:
a) Oxygen dissolves in the melt and reacts with carbon dioxide to form peroxide:

$$O_2 + 2\,CO_3^{2-} \underset{\leftarrow}{\overset{\rightarrow}{}} 2\,O_2^{2-} + 2\,CO_2 \qquad (1)$$

b) Dissolved oxygen reacts with peroxide to form super oxide:

$$O_2 + O_2^{2-} \underset{\leftarrow}{\overset{\rightarrow}{}} 2\,O_2^{-} \qquad (2)$$

c) Three electron transfer reactions:

$$O_2^{-} + e \underset{\leftarrow}{\overset{\rightarrow}{}} O_2^{2-} \qquad (3)$$

$$O_2^{2-} + e \underset{\leftarrow}{\overset{\rightarrow}{}} O^{2-} + (O^{-}) \qquad (4)$$

$$(O^{-}) + e \underset{\leftarrow}{\overset{\rightarrow}{}} O^{2-} \qquad (5)$$

d) The recombination of oxide and carbon dioxide forming carbonate:

$$O^{2-} + CO_2 \underset{\leftarrow}{\overset{\rightarrow}{}} CO_3^{2-} \qquad (6)$$

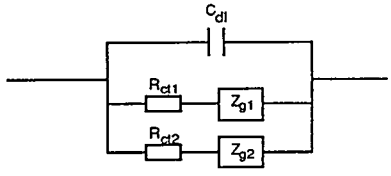

Figure 1. The equivalent circuit.
C_{dl} Double layer layer capacitance
R_{ct1} Charge transfer resistance 1
Z_{g1} Gerischer impedance 1
R_{ct2} Charge transfer resistance 2
Z_{g2} Gerischer impedance 2

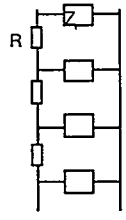

Figure 2. The transmission line approximation.

An impedance model has been derived based on this reaction path [4]. The equivalent circuit is shown in fig. 1. The Gerischer impedances are due to the chemical reactions 1 and 6 respectively. The Gerischer impedance (Z_g) has the form [5]:

$$Z_g = \frac{\gamma}{\sqrt{\omega}} \cdot (m - j \cdot n) \qquad (7)$$

with γ as the Gerischer coefficient, $m = \left(\frac{\sqrt{1 + A^2} + A}{1 + A^2}\right)^{1/2}$, $n = \left(\frac{\sqrt{1 + A^2} - A}{1 + A^2}\right)^{1/2}$ and $A = \frac{k}{\omega}$,

with k as the apparent reaction rate constant. The porous cathode in a molten carbonate fuel cell

can be described by the filmed agglomerate model [6]. A more simplified model is the thin film model. Using this simplification the impedance model for the flat electrode is extended to describe the impedance of a porous cathode.

Porous electrode model.

The impedance of the thin film model can be described by the transmission line approximation [7], see fig. 2 if the following condition is satisfied:

$$\sqrt{\frac{Z_i}{\rho \cdot \delta}} \gg 1 \tag{8}$$

with Z_i as the interfacial impedance, ρ as the specific electrolyte resistance and δ as the film thickness. The impedance of one pore is then:

$$Z_{pore} = \frac{1}{\pi \cdot b} \cdot \frac{\sqrt{Z_i \cdot \rho / \delta}}{\tanh(\sqrt{\delta \cdot \rho / Z_i} \cdot L/\delta)}, \text{with L as the pore length and b as the pore diameter.} \tag{9}$$

For long films, i.e. for $L/\delta \geq 3 \cdot \sqrt{Z_i / (\rho \cdot \delta)}$, the tanhyperbolic term in (9) equals 1, thus:

$$Z_{pore} = \frac{1}{\pi \cdot b} \cdot \sqrt{\frac{Z_i \cdot \rho}{\delta}} \tag{10}$$

For short films, i.e for $L/\delta \leq 1/3 \cdot \sqrt{Z_i / (\rho \cdot \delta)}$, $\tanh(\sqrt{\delta \cdot \rho / Z_i} \cdot L/\delta) = \sqrt{\delta \cdot \rho / Z_i} \cdot L/\delta$, thus:

$$Z_{pore} = \frac{Z_i}{\pi \cdot b \cdot L} \tag{11}$$

The interfacial impedance is similar to the equivalent circuit shown in fig. 1, except that the Gerischer impedance for semi-infinite diffusion has to be changed in a Gerischer impedance for limited diffusion.

In a gas pore with a thin film of electrolyte with thickness δ on the inner pore walls there are no transport limitations for the diffusing species at the electrolyte/gas interface. Following an analogous calculation as in [5] this yields a finite Gerischer impedance with unlimited transport at the diffusion boundary:

$$Z_{gu} = \frac{\gamma}{\sqrt{\omega}} \cdot (m - j \cdot n) \cdot \tanh\left(\delta \cdot \sqrt{\frac{2 \cdot \omega}{D}} \cdot \frac{1}{m - j \cdot n}\right) \tag{12}$$

For $\omega = 0$ this becomes: $Z_{gu}(\omega=0) = \frac{\gamma}{\sqrt{k}} \cdot \tanh\left(\delta \cdot \sqrt{\frac{2 \cdot k}{D}}\right)$. In case of a slow chemical reaction (1 and 6), i.e. as $\sqrt{k} \leq 1/3 \cdot \frac{\sqrt{D}}{\delta \cdot \sqrt{2}}$, the impedance at $\omega = 0$ becomes: $Z_{gu}(\omega=0) = \frac{\gamma \cdot \delta \cdot \sqrt{2}}{\sqrt{D}}$. At $\omega=0$ $R_{ct} \ll Z_{gu}$, thus the interfacial impedance is approximately equal to the finite Gerischer impedance or two in parallel as for fig. 1. For long films the pore impedance (Z_{poreg}) is thus proportional to: $\sqrt{\gamma}$ / b. For short films the pore impedance is proportional to: $\gamma \cdot \delta / (b \cdot L)$.

In a completely flooded pore the symmetry axis can be regarded as the diffusion boundary at which no transport is possible, the film thickness δ equals then the radius of the pore (1/2b). This results in a finite Gerischer impedance with no transport at the diffusion boundary:

$$Z_{gn} = \frac{\gamma}{\sqrt{\omega}} \cdot (m - j \cdot n) \cdot \operatorname{cotanh}\left(1/2b \cdot \sqrt{\frac{2 \cdot \omega}{D}} \cdot \frac{1}{m - j \cdot n}\right) \tag{13}$$

For $\omega = 0$ this becomes: $Z_{gn(\omega=0)} = \frac{\gamma}{\sqrt{k}} \cdot \text{cotanh}\left(1/2b \cdot \sqrt{\frac{2 \cdot k}{D}} \right)$. In case of a slow chemical reaction this can be simplified to: $Z_{gn(\omega=0)} = \frac{\gamma}{k} \cdot \frac{\sqrt{2 \cdot D}}{b}$. At $\omega = 0$ the pore impedance (Z_{poref}) is thus proportional to $\sqrt{\frac{\gamma}{k} \cdot \frac{1}{b^2}}$ for long films and proportional to $\gamma/(k \cdot b^2 \cdot L)$ for short films.

Regarding the porous electrode as a set of parallel gas pores and flooded pores, with N as the number of pores and α as the fraction of gas pores and assuming that all gas pores are equal and all flooded pores are equal, the electrode impedance (Z_{el}) is:

$$\frac{1}{Z_{el}} = \frac{\alpha \cdot N}{Z_{poreg}} + \frac{(1 - \alpha) \cdot N}{Z_{poref}} \qquad (14)$$

At high frequencies only the kinetics will contribute to the interfacial impedance, which will be small. The long film approximation can therefore be used, thus the pore impedance will be proportional to square root of the kinetic R-C impedance. The initial phase angle will be 45° and the maximum of the imaginary part is proportional to $\sqrt{R_{ct}}$, see also [6]. At low frequencies the Gerischer impedances dominate the interfacial impedance. The phase angle will be between 22.5° (long film) and 45° (short film).

Experimental

The porous electrode studies have been performed using a symmetrical laboratory scale cell (3 cm^2) with two $LiFeO_2$ cathodes. The cell was held at a temperature of 923 K in a DC furnace. The electrolyte was an eutectic mixture of Li_2CO_3/K_2CO_3 (62/38 mol%). The impedance of the cell was measured with the Zahner Im5d system in the frequency range of 50 mHz to 100 kHz, under several gas atmospheres.

Results and discussion

In figure 3 and 4 the measured impedances are shown. At high frequencies the inductive behaviour of the connecting wires can be observed. In figure 4 it can be seen that the uncompensated resistance decreases slightly with decreasing carbon dioxide partial pressure, indicating the resistance of the $LiFeO_2$ cathodes to be a function of the carbon dioxide partial pressure. The data obtained under several oxygen partial pressures (P_{CO_2} = 0.3 atm.) show only one arc, which increases with decreasing oxygen partial pressure. In figure 5a the logarithm of the maximum of imaginary part of the impedance is plotted versus the logarithm of the oxygen partial pressure. The slope is: -0.50 ± 0.01. The data obtained under several carbon dioxide partial pressures (P_{O_2} = 0.5 atm.) show for pressures below 0.1 atm. two arcs. Above 0.1 atm. only one arc is observed. The logarithm of the maximum of the imaginary part of the impedance for the first and second arc are plotted versus the logarithm of the carbon dioxide partial pressure in figure 5b and 5c. The slopes are respectively : 0.32 ± 0.02 and -0.79 ± 0.05. Using the long film approximation and assuming that the first arc is due to the kinetics, the maximum of $Z_{imaginary}$ is proportional to $\sqrt{R_{ct}}$, so the reaction order for oxygen and carbon dioxide will be twice the slope of fig. 5a and 5b, hence -1.00 ± 0.02 and 0.64 ± 0.04 respectively. These reaction orders do not agree with the theoretical reaction orders for the peroxide (-0.375 and 1.25) or the super oxide (-0.625 and 0.75) mechanism. If for the low oxygen partial pressures the long film approximation can not be applied, the reaction order for oxygen will become less negative and lie between - 0.5 and -1.0. This is in agreement with the reaction order for oxygen for the super oxide mechanism. The determined carbon dioxide reaction order is slightly too small.

Conclusion.

The two types of finite Gerischer impedances have been derived. Assuming the first arc in the impedance data to be due to the kinetics we may conlude that the super oxide mechanism dominates the electrode reaction.

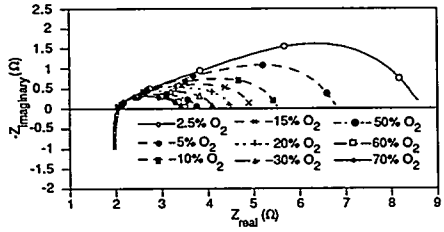

Figure 3.Measured impedance of a $LiFeO_2$ symmetrical laboratory cell obtained under several oxygen partial pressures,P_{CO_2}=0.3 atm.

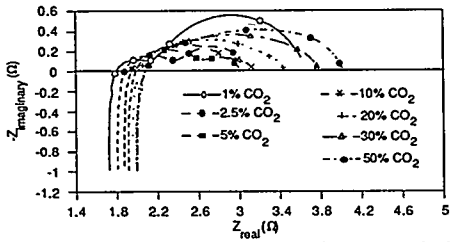

Figure 4. Measured impedance of a $LiFeO_2$ symmetrical laboratory cell obtained under several carbon dioxide partial pressures,P_{O_2}=0.5 atm.

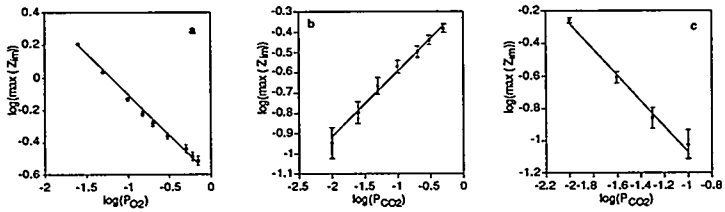

Figure 5. The oxygen and carbon dioxide dependency of the maximum of the imaginary part of the impedance for the first (a,b) and second semi circle (c).

Acknowledgement
This work was supported by the Commission of the European Communities under contract EN3E-0151-NL and by the Dutch Energy Research Centre (ECN) under contract SC03.

[1].A.J.Appleby and S.B.Nicholson, J. Electroanal. Chem., 53 (1974), 105-119
[2].A.J.Appleby and S.B.Nicholson, J. Electroanal. Chem., 83 (1977), 309 - 328
[3].A.J.Appleby and S.B.Nicholson , J. Electroanal. Chem., 112(1980), 71 - 76
[4]. R.C. Makkus , K. Hemmes and J.H.W. de Wit, proc. of the 178th meeting of the Electrochem. Soc., oct 1990, Seattle.
[5].M.Sluyters-Rehbach and J.H.Sluyters in Comprehensive Treatise of Electrochemistry vol. 9, E.Yeager, J.O'M.Bockris, B.E.Conway, S.Sarangapani eds.,Plenum Press,New York (1984)
[6].C.Y.Yuh, Ph.D.Thesis,Illinois Institute of technology,Chicago Illinois,1985
[7].G.H.J.Broers, M.Schenke, Abhandl. Sachs. Akad. 49 (5), Berlin 1968, 299 - 315

PERFORMANCE PREDICTIONS FOR MONOLITHIC SOLID OXIDE ELECTROLYZER ARRAYS

Thomas M. Maloney* and George A. Coulman
Fenn College of Engineering
Cleveland State University
Cleveland, Ohio 44115

Monolithic solid oxide fuel cells (MSOFC) were devised at the Argonne National Laboratory in the early 1980's (1) and are presently in the fabrication development stage at Allied Signal Aerospace (2) for various applications. The monolithic fuel cell is an all-ceramic structure which is assembled in a "honeycomb" shape similar to that of corrugated cardboard. While fuel cell operation has been demonstrated (3), it is also possible to operate the monolithic structure in the reverse, or electrolysis, mode. Performance characteristics of monolithic solid oxide electrolyzer (MSOEZ) arrays were estimated in order to determine the effects that inlet gas temperatures, i-V relationship, and the average current density, have upon the average cell temperature and upon the applied voltage requirements.

Performance predictions of MSOFC arrays have been previously reported (4,5) and the computational algorithm formulated by Lu and Maloney (4) was revised to predict performance characteristics of MSOEZ arrays for the Mod 0 design. The algorithm consisted of a finite difference scheme to solve the mass and energy balance equations which pertain to the electrolyte and to the anode and cathode gas channels. The inlet reactant gas stream is a hydrogen-steam mixture and the water in that stream is electrolyzed to produce hydrogen (in the H_2-H_2O channel) and oxygen (in the pure O_2 or air channel). The solid electrolyte mass and energy balance equations were derived elsewhere (6) and Table I lists the operating conditions which were maintained constant unless otherwise noted.

TABLE I

ELECTROLYZER ARRAY OPERATING CONDITIONS

Operating Pressure	= 1 atm
Average Current Density	: 500 mA/sq.cm.
Water Utilization Ratio (WUR)	: 86.6 %
Array Dimensions	: 10 cm x 10 cm
Inlet Gas Temperatures	: 1423 K

*Present Address : Sverdrup Technology, Inc.; NASA LeRC Group ; 2001 Aerospace Pkwy; Brook Park, Ohio 44142

i-V Relationship

Current-voltage characteristics for single solid oxide fuel cells were predicted by Maloney (6) and simplified for implementation to both fuel cell and electrolyzer array analyses. For MSOEZ arrays, two i-V relationships were used: A Best Case i-V relationship which included only material resistance; and an Estimated Case i-V relationship which encompassed all overpotential sources. Figure 1 represents typical Best Case and Estimated Case i-V curves for electrolysis operation while Figures 2 and 3 represent calculated Temperature Distributions and Current Density Distributions, respectively, for the solid electrolyte.

Effect of Inlet Reactant Gas Temperature

MSOEZ array performance is affected by the inlet gas temperatures. As the inlet gas temperatures increased, the average MSOEZ array temperature increased for both the Best Case and Estimated Case i-V relationship, as expected. Furthermore, average array temperatures for the Estimated Case were higher than those for the Best Case since more resistive heat is generated using the former case. The required applied voltages varied with the inlet gas temperatures in the manner shown in Figure 4.

Effect of Average Electrolyzer Array Current Density

The average current density of the MSOEZ array influenced both the average array temperature and the applied voltage requirements. Array voltage increased with average current density in the manner shown in Figure 5. The effect of current density on the average MSOEZ array temperature is shown in Figure 6.

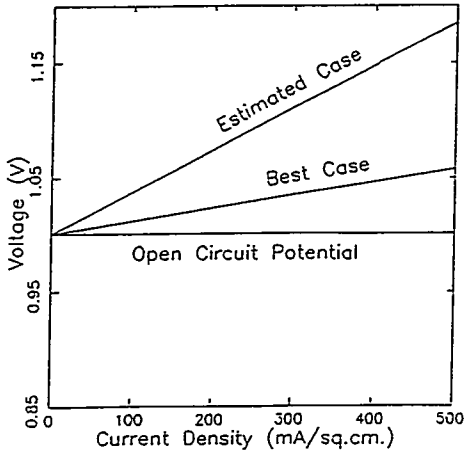

Figure 1. i-V Relationships used for Mod 0 Electrolyzer Array Analyses

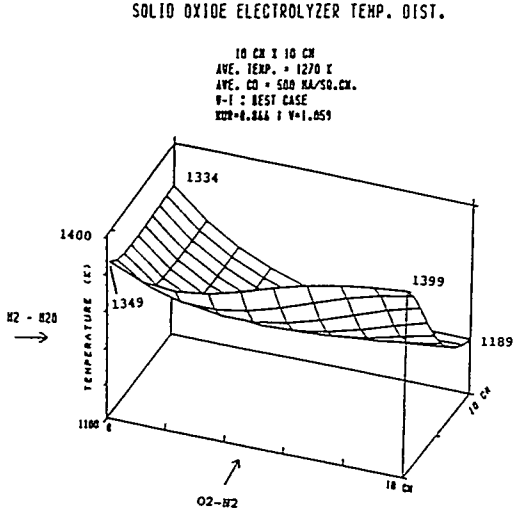

Figure 2. Temperature Distribution in 10 cm x 10 cm Mod 0 Electrolyzer Array Electrolyte With Best Case i-V Curve

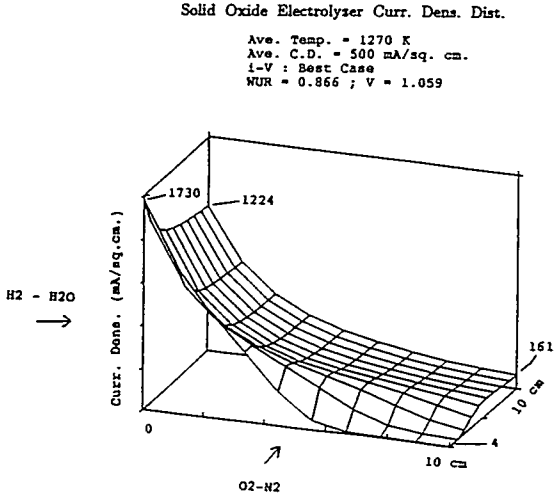

Figure 3. Current Density Distribution in 10 cm x 10 cm Mod 0 Electrolyzer Array Electrolyte With Best Case i-V Curve

Conclusion

Performance estimations for Mod 0 MSOEZ arrays were completed and some of the results were provided. Computer modeling results of this type may be used to aid the design of a monolithic solid oxide electrolysis sub-system and of a regenerative fuel cell system with various applications. An assessment of thermal stresses should also be undertaken as part of the design study.

REFERENCES

1. D.C. Fee, R.K. Steunenberg, T.D. Claar, R.B. Poeppel, and J.P. Ackerman, "Monolithic Fuel Cells", National Fuel Cell Seminar Abstracts, Courtesy Associates, Inc., Washington, DC., pp. 74-77, November 1983.

2. N.Q. Mingh, et al., "Fabrication and Characterization of Monolithic Solid Oxide Fuel Cells", Proceedings of the 1990 IECEC Vol. 3, Reno, Nevada, pp. 230-234, August 1990.

3. C.C. McPheeters, D.W. Dees, S.E. Dorris, and J.J. Picciolo, "Argonne Monolithic Solid Oxide Fuel Cell Fabrication", National Fuel Cell Seminar Abstracts, Courtesy Associates, Inc., Long Beach, CA, pp. 29-32, October 1988.

4. C.-Y. Lu and T.M. Maloney, "Mathematical Modeling of Solid Oxide Fuel Cells", National Fuel Cell Seminar Abstracts, Courtesy Associates, Inc., Long Beach, CA, pp. 78-83, October 1988.

5. T.M. Maloney, C.-Y. Lu, and G.A. Coulman, "Predicted Restrictions on Reactant Gas Utilizations in Monolithic Solid Oxide Fuel Cell Operation", Progress in Batteries & Solar Cells, Vol. 8, pp. 298-301, 1989.

6. T. M. Maloney, Doctoral Dissertation, Chemical Engineering Department, Fenn College of Engineering, Cleveland State University, March, 1990.

Acknowledgement

This study was supported by the U.S. Department of Energy, Morgantown Energy Technology Center, through the NASA Lewis Research Center Fuel Cell Project Office.

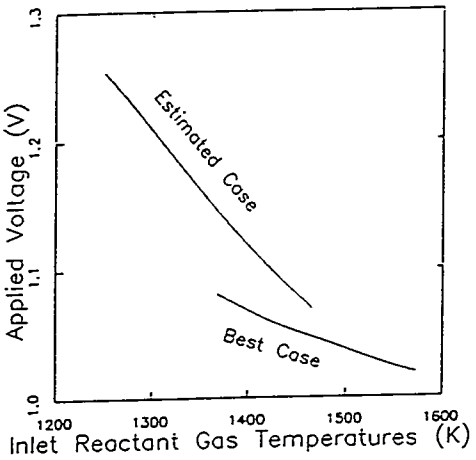

Figure 4. Effect of Inlet Electrolyzer Gas Temperature on Applied Electrolyzer Voltage

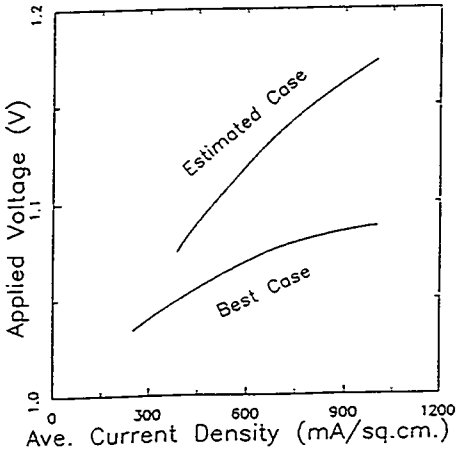

Figure 5. Relationship Between the Average Electrolyzer Array Current Density and the Applied Voltage

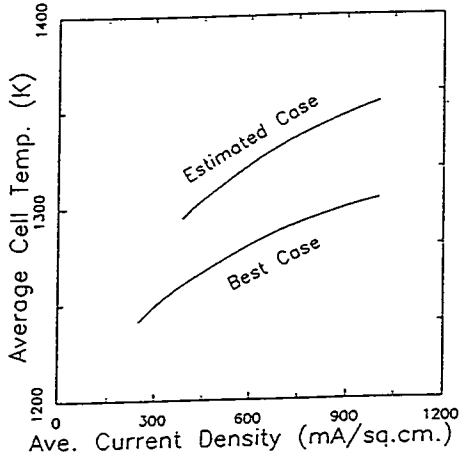

Figure 6. Effect of Electrolyzer Array Current Density on the Average Electrolyzer Array Operating Temperature

MATHEMATICAL ANALYSIS OF THE THERMAL CHARACTERISTICS OF A 25 KWe REGENERATIVE FUEL CELL ENERGY STORAGE SYSTEM

T.M. Maloney
Sverdrup Technology, Inc. ; NASA LeRC Group
Cleveland, Ohio 44142

H.F. Leibecki and P.R. Prokopius
NASA Lewis Research Center
Cleveland, Ohio 44135

Introduction

The Planetary Surface Power Program is a key element of the National Aeronautics and Space Administration's Space Exploration Initiative. The program objectives include development of regenerative fuel cell (RFC) energy storage systems with the capability to support Mars and Lunar operational activities. Design goals are a 25 kWe system (25 kWe electrolyzer stack ; 12.5 kWe fuel cell stack) operating for 20,000 hours in an autonomous mode. One element of the program is the development of techniques to predict the performance characteristics of the energy storage system and to provide design guidelines. Precursory heat transfer analyses have been completed and some of the impacts upon the overall system design are discussed.

Numerous RFC computer modeling efforts have been completed to date for small power levels and a short list of such work is given in reference (1). Transient RFC performance has also been predicted for Space Station applications (2). The present analysis pertains to higher power planetary surface missions. Fuel cell systems are generally predicted to have lower specific masses and specific volumes than battery systems for the 12 hour day/night cycle for Mars surface application and for the 2 week day/night cycle for Lunar surface applications. Much technological progress has been achieved in recent years regarding lifetime and performance of fuel cell and electrolyzer stacks, but various system issues must be addressed, including heat transfer requirements.

Fuel Cell Sub-section

A symbolic diagram of the fuel cell sub-system is shown in Figure 1. During the night portion of the cycle, hydrogen and oxygen gas will be consumed and electricity, steam, and heat will be produced. The major heat generation source is the fuel cell stack, which must be cooled. The condenser section must also be cooled to remove the latent heat of water condensation. An assortment of heat exchangers are employed to carry out sensible heating or cooling of the reactant and product gas streams. For steady state operation, all thermal requirements will remain constant, except for the oxygen gas heat exchanger duty (and a hydrogen gas heat exchanger duty if no condenser is used), which will vary with time since the thermodynamic states of the gases within the storage vessels change as the stored gases expand during fuel cell operation. For fuel cell designs which do not utilize a condenser, the latent heat of water

condensation must still be considered in the energy balance.

Estimation of Fuel Cell Sub-section Thermal Conditions

Net energy generated in the fuel cell stack is a function of the stack temperature, pressure, current density, and the fuel cell efficiency. Energy is generated from the heat of reaction and the electrical resistance incurred during fuel cell operation. The equations which describe the net energy generated in the fuel cell (and other pertinent equations) are recorded elsewhere (3) and are not duplicated here. The overall fuel cell energy balance includes generation and convective energy terms. Condenser cooling requirements are estimated from the latent heat of condensation as well as appropriate sensible cooling. Some calculated heat duties for the fuel cell stack and condenser are shown in Figure 2 as a function of fuel cell efficiency.

Transient Thermal Analysis of Stored Reactant Gases

The temperature and pressure of the stored hydrogen and oxygen gases will change as the storage vessels are depleted during fuel cell operation. If a constant inlet fuel cell temperature is desired, then it is necessary to heat the reactant gases. Temperature behavior versus operation time for ideal reactant gases are shown in Figure 3 where the transient behavior depends upon the molar residual and initial storage temperature and pressure. Isobaric storage would probably not be implemented since the required temperature rise would be too great and since pressure can be easily regulated. If a condenser is used, adiabatic storage would offer a slight advantage since the decrease in the hydrogen gas temperature would better cool the incoming condenser gas. The average heating rate required to maintain the isothermal condition in Figure 3 is 140.5 kcal/hr.

Electrolysis Sub-section

A symbolic diagram of the electrolysis sub-system is shown in Figure 4. During the sunlit portion of the cycle, electricity and water will be consumed while gaseous hydrogen and oxygen will be produced. Since the overall electrolysis reaction is endothermic and electrical energy must be added to the electrolyzer stack, the thermal requirements for this sub-section are less demanding than those for the fuel cell sub-section ; furthermore, the electrolyzer efficiency may dictate whether the electrolyzer heat duty is positive or negative. Stored water must be pre-heated before entering the electrolyzer stacks and this modest requirement is included in electrolyzer sub-section analysis. Some calculated heat duties for the electrolyzer sub-section are shown in Figure 5 as a function of electrolyzer efficiency.

Transient Thermal Analysis of Storing Product Gases

The temperature, pressure, and flow rates of the product hydrogen and oxygen gases exiting the electrolyzer are assumed to remain constant. As the gases are added to the respective

storage vessels, the temperature, pressure, and number of moles inside of the tanks will change. For gaseous storage systems, the electrolyzer products must be cooled sufficiently so that excess storage pressures do not develop. Temperature behavior versus operation time for an ideal product gas is shown in Figure 6 where the heat required to cool the gas from the electrolyzer exit temperature of 450 K (from Figure 5) to the inlet storage tank temperature of 370 K is 167 kcal/hr for hydrogen.

System Issues

When electrochemical conversion technologies have been sufficiently developed and qualified for space applications, various system issues must already have been addressed. Considerations regarding the energy available (ie. from fuel cell stack) for electrolysis sub-section heating during the dark segment of the cycle is one example. Since heat is available during the sunlit period and the electrolyzer efficiency increases with addition of heat, designs should address the increased efficiency of the electrolyzer as shown in Figure 5. Temperature and pressure of the various reactant and product streams must be controlled to permit or to avoid phase changes and to reduce corrosion. Water condensation within the fuel cell reactant gas streams may be intolerable whereas icing within the water storage tanks may be allowable. Special considerations must also be given to electrolyte freezing. In summary, thermal characteristic of the entire regenerative fuel cell system must be considered to optimize performance.

References

1. T.M. Maloney and H.F. Leibecki, "Modeling and Optimization of a Regenerative Fuel Cell System Using the ASPEN Process Simulator", 25th IECEC, Vol. 6, pp. 114-118, Reno NV, 1990.

2. R. Simon and M. Rothmeyer, "Simulation of Regenerative Fuel Cell Systems Including Thermal Control", Proceedings of the European Space Power Conference, Madrid, Spain, 2-6 October, 1989, Vol. 1, page 233.

3. C.-Y. Lu and K.A. Alkasab, "Manual of Phosphoric Acid Fuel Cell Stack Three-Dimensional Model and Computer Program", NASA CR-174722, May 1984.

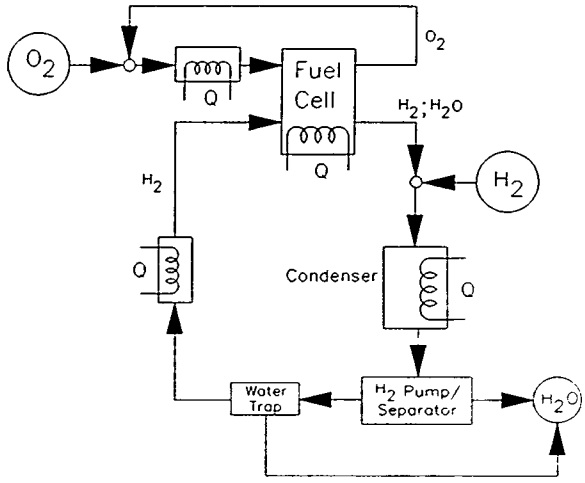

Figure 1. Fuel Cell Sub-section of Illustrative Regenerative Fuel Cell System

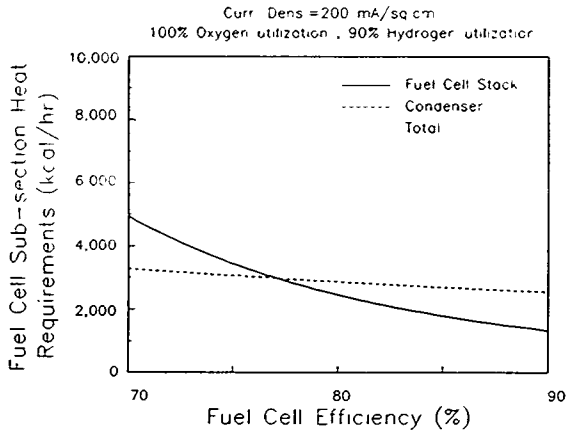

Figure 2 Effect of Fuel Cell Efficiency on the Fuel Cell Sub-section Heat Requirements

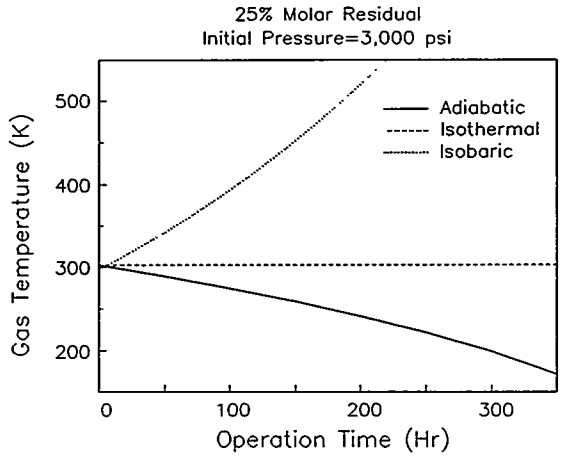

Figure 3. Transient Temperature Behavior of Stored Reactant Gases

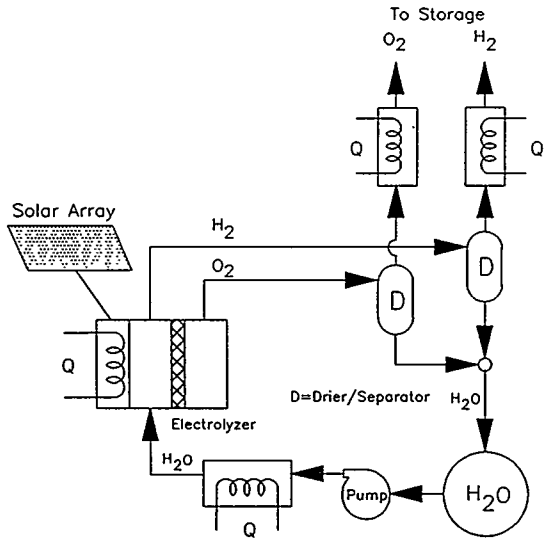

Figure 4. Electrolysis Sub-section of Illustrative Regenerative Fuel Cell System

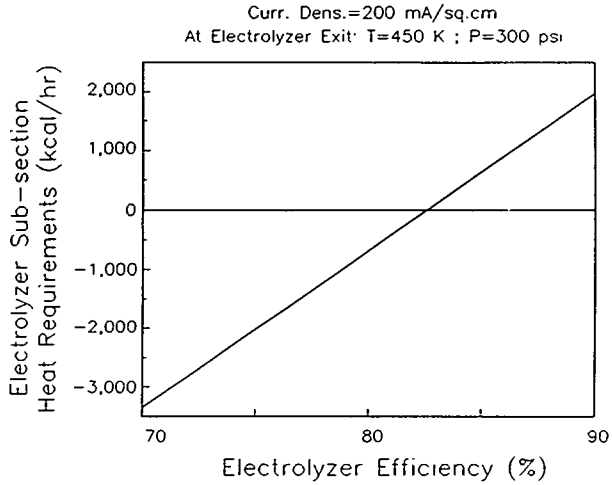

Figure 5 Effect of Electrolyzer Efficiency on the Electrolyzer Sub-section Heat Requirements

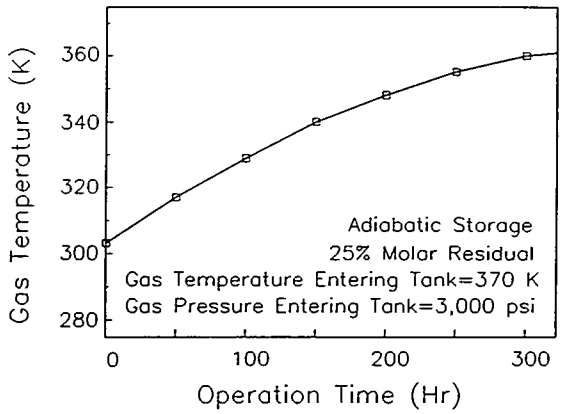

Figure 6. Transient Temperature Behavior of Stored Product Gases

A PRACTICAL REVIEW OF COMPOSITE UTILITY GENERATION OPTIONS

M R Fry MSc Epsom England
H Watson BSc Bramhall England

1. Introduction

This Abstract is based on studies carried out under contract for the United Kingdom Department of Energy by WS Atkins and Watson Engineering Consultants, supported by Professor B. Steele from Imperial College, London and Professor R. Singh from Cranfield Institute of Technology. However, the views expressed are those of the Contractors, and are based on their own work, reviews of the international literature and consultations with participating organisations in European Countries, including the United Kingdom, the Netherlands, Switzerland and Germany. It is, of course, accepted that other countries are playing a vitally important role in developing this technology.

The main thrust of the work has involved a review of high temperature (i.e. Solid Oxide, SOFC, and Molten Carbonate, MCFC) Fuel Cell R & D and system studies, with emphasis on large scale integrated Fuel Cell/Turbine or 'Composite' utilities. The objectives have been to identify the major issues, seek relevant views from selected fieldworkers and draw conclusions such as to place these possible long term developments into context with the underlying environmental issues. Parallel developments with more conventional technologies are considered important and have been reviewed also.

Inevitably, with this sort of overview, the role of associated technologies such as the Phosphoric Acid Cell (PAFC) has had to be recognised, as has the small scale cogeneration market, within which Fuel Cells must have a role. Additional work is now underway to investigate the latter in more detail.

2. Observations and Critical Issues

We have made no attempt to probe the basic Cell R & D, and have taken the 'black box' approach. However, we do conclude that it will be some time before there is a clear indication as to which of the SOFC or MCFC type will ultimately reach commercialisation. There is a possibility that both will and a risk that neither will, but the latter is considered small in view of the shear weight of international commitment and ever increasing environmental pressures.

The route to success with Fuel Cells must be a step by step one. There is much speculation, evidenced by the wide ranging, international activities on system studies, about ultimate configurations and performance of large scale Composite Fuel Cell/Turbine utility systems. Some of these studies conclude that, through the economies of scale, this is where the ultimate market lies, rather than with smaller, modular cogeneration units. However, in some cases, the gain in generation efficiency over the

basic stack may be only five to ten percentage points at the expense of turbine plant which itself may, in specific cost terms, be as much or more than the Fuel Cell stack. One therefore has to weigh a relatively small gain in performance against a much more complex plant, with all the associated system problems of optimisation, control, safety, availability, etc.

Whilst it must be accepted that large scale Fuel Cell based power stations may one day be built, it must not be forgotten that the route to them must be through the cogeneration market. The Fuel Cell is inherently small, modular and offers enormous potential in this rapidly growing market, provided costs and efficiencies can be got right. At the small end, the economies of scale are surely replaced by the economies of high volume production. We would caution that, if the cogeneration application cannot be addressed, then the chances of the technology leapfrogging to the 100 MW plus power station must be questionable. It has to be said that there is considerable support for this view among fieldworkers.

The PAFC tends to be seen in a fairly negative light by many, in view of its relatively high cost and low efficiency compared with the targets being set for the high temperature Cells. It also requires external fuel processing, which will probably be avoided by the latter variants. However, it exists today at the pre-commercial stage, unlike any other type. Whatever its long term future, in our view it has a key part to play today, as a technology demonstrator. It will be important, in the way that it is presented to the market, that its relative shortcomings are recognised and that it is seen as part of a long term programme and a precursor to a much more competitive second generation. Its Demonstration will also enable us to learn some important lessons, based upon operational experience, about overall system design, integration and reliability. Such activities do exist, and more are planned, and it is hoped that the results and operational experience will be made fully available to the international community.

The question of internal v external reforming remains to be resolved - the point being argued is that, if large scale plant is considered, it may be more economical to employ one central external system. However, if the thesis that small must come first is accepted, and small cogeneration will have to employ internal reforming, then will going to external for large systems be a retrograde step?

3. Likely Developments of Competing Technology

The timescales pertaining to high temperature Cell development are such that it will probably be ten to fifteen years before the fully commercial stage is reached. In this situation, there is always a danger in comparing tomorrow's new technology with today's alternatives.

Part of our work has therefore involved a review of the possible evolution of one type, as an example, and gas fired combined cycle generation was selected. Here, there are three aspects which are relevant: the development of the coregas turbine, the integration of the steam and gas plant and the emissions of NOx.

The core plant will be developed over this time period in terms of increased turbine entry temperature, (i.e. higher thermal efficiency) reduced bleed air flows (i.e. lower losses) and more efficient blading design (i.e. higher stage efficiencies). The integration of the two systems to provide a fully optimised dual fluid power plant is really just beginning, as evidenced by recent mergers/collaborations between Aero and Industrially based companies. Our assessment indicates that these advances are likely to lead to net thermal efficiencies in the low to mid sixties by perhaps 2010. This would compare with figures in the mid fifties today.

With regard to emissions of NOx, whose virtual absence from the Fuel Cell is a significant advantage, one again has to look to the future. At present the gas turbine emits about 150 ppm on natural gas, with no passive clean up. It is likely that active measures to eliminate NOx may reduce levels to 10 - 15 ppm over this timescale. It is not clear today what minimum levels may be dictated in the future, in other words how much better almost zero is than 10 ppm!

The above indicates that the combined cycle plant will be offering efficiencies of the same order as claimed for the Composite Fuel Cell Utility. It is also highly competitive on cost, as Figure 1 shows. However, it will have the unbeatable additional advantage that it is well developed now, and by the time that the Fuel Cell Utility is at the pilot stage, it will have benefited from another fifteen years' evolution. This, in our view, adds further weight to the argument that the Fuel Cell should be targeted at the cogeneration market where, particularly at the very small end, such competition as exists is perhaps less likely to make such significant advances. In addition, the Fuel Cell already has a significant edge in efficiency terms.

4. Costs

The target figure of $1000/kW is used, and Fig 1 suggests that it is probably a maximum. Ultimately, of course, a higher efficiency will help to reduce the lifetime costs. Fig 2 indicates, for a 40 MW Composite plant, a trade-off between efficiency and stack costs for two fuel prices. This approach may be a useful tool in bracketing costs and efficiencies as target bands, albeit here for what we consider to be the wrong market. Further work will enable us to develop this for small cogeneration plant.

5. Concluding Remarks

It is suggested that system study work to date indicates that large Fuel Cell utilities will not be able to compete with conventional alternatives in the ten to twenty year time-frame. We accept that our work in this respect has just scratched the surface, and that more detailed assessments are needed, to include pressurised fluid bed combustion, etc.

Small applications, perhaps even the integration of the Fuel Cell with the domestic gas water heater, must be where the future lies.

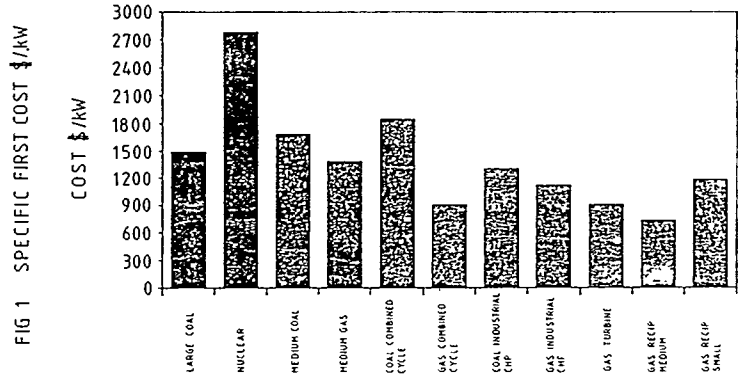

FIG 1

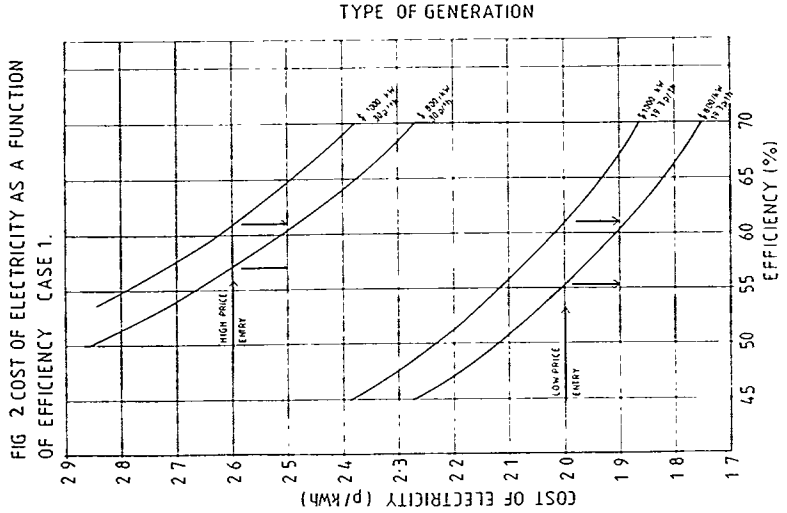

FIG 2 COST OF ELECTRICITY AS A FUNCTION OF EFFICIENCY CASE 1.

TECHNOLOGY ADVANCEMENTS IN THE WESTINGHOUSE AIR-COOLED PHOSPHORIC ACID FUEL CELL PROGRAM

Maynard K. Wright, Jerome M. Feret and Mai T. Le
Westinghouse Electric Corporation
Advanced Energy Systems, NATD
Pittsburgh, PA 15236-0864

Westinghouse is nearing completion of its highly reliable air-cooled phosphoric acid fuel cell (PAFC) technology that is directed towards the electric utility and industrial markets. The Westinghouse PAFC program has been jointly sponsored by the U.S. Department of Energy (DOE) and Westinghouse along with its team members. The Westinghouse industrial and utility team has funded the needed facilities and the power plant design.

The overall program success is highly dependent upon the DOE sponsored PAFC Development Program. This program's key objective is to provide the basic fuel cell and cell stack technology needed to demonstrate the air-cooled PAFC performance, performance stability and cost goals associated with successful energy service. This program has achieved significant technical progress over the past several years. At the rated operating conditions of 190°C, 70 psia, 267 mA/cm^2, SRG fuel at 83%, air at 50% the baseline cell technology selected was demonstrated to have met or exceeded the initial performance and endurance goals of an average cell voltage of 690 mV and voltage loss of $\leq$ 8 mV/1000 hours, respectively. These performance goals have been reproducibly achieved in numerous cell stacks rated between 2.5 and 100 kW.

Extensive development efforts have also established an improved baseline cell and stack technology of up to 200°C and 60% air utilization. Two 2.5 kW cell stacks and a 100 kW stack with this improved technology are being tested for up to 10,000 and 1,000 hours, respectively to demonstrate the early commercial performance goals of 705 mV initial performance and voltage loss of 4 mV/1000 hours. The costs when adjusted for learning curves and volume production will meet the commercial cost goals.

Completion of the cell and stack technology development efforts will culminate in the projects end product, the "375" kW module. Westinghouse is in the process of building an Engineering Model Module for testing in early 1991. An artist rendition of the module is shown in the figure.

A joint 400 kW demonstration power plant is actively being designed for an industrial application in a user environment. The second DOE sponsored module is committed to this demonstration for start-up in early 1992.

WESTINGHOUSE PAFC MODULE

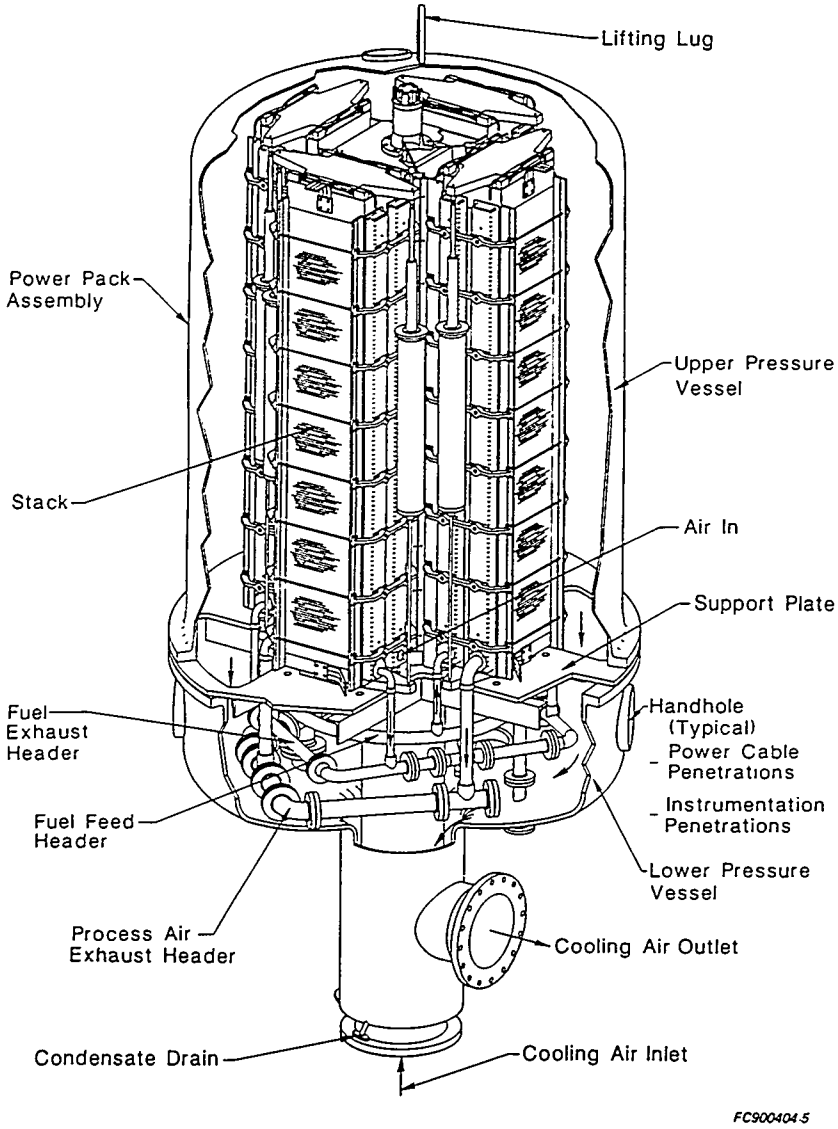

FIELD TEST RESULTS OF 50 KW PRESSURIZED PHOSPHORIC ACID FUEL CELL PILOT PLANT FOR ELECTRIC UTILITY

T.Saito, S.Yasuda and M.Kadowaki
Touhoku Electric Power Co.,Inc.
3-7-1 Ichiban-cho Aoba-ku Sendai-shi 980,Japan

K.Kubota
Fuji Electric Co.,Ltd.
K.Harashima
Fuji Electric Corporate Research and Development Ltd.
7 Yawatakaigan-dori Ichihara-shi 290,Japan

Introduction

Touhoku Electric Power Co., Inc. and Fuji Electric Co., Ltd. started a joint research on a phosphoric acid fuel cell pilot plant in September 1985. From May 1987 to October 1989, a field test was performed at the Niigata Thermal Power Station of Touhoku Electric Power Co., Inc. The objectives of this joint research and field test were to confirm the technical problems of fuel cell power generators and to establish the operating technologies for electric utilities. Therefore, in spite of the small 50 kW capacity of the pilot plant, we decided on a pressurized phosphoric acid fuel cell for this project. The pilot plant was designed to simulate a large scale power plant. The specifications of the pilot plant are shown in Table 1 and an outside view of the pilot plant is shown in Figure 1.

Results of field test

Accumulated operating time

From May 1987 to October 1989, the pilot plant recorded about 9500 hours of accumulated operation including 2205 hours of uninterrupted operation and about 306 MWh of power generated. The period of accumulated operation is the longest ever recorded in the world for a pressurized type PAFC plant.The period of uninterrupted operation is also the longest ever recorded. Figure 2 shows the history of operation of the pilot plant.

Load changing test

Load changing tests were performed with the four patterns as shown in Figure 3,to simulate the actual load changing pattern of a power station. The pilot plant achieved a maximum load changing rate of 64 %/minuite.

Operation with LPG fuel

The pilot plant was normally operated with natural gas. Liquefied petroleum gas was used as fuel in trials,to provide for a diversity of energy sources. When the fuel was changed from NG to LPG, it was confirmed that operation was possible with LPG if the steam carbon ratio was changed and flow meters adjusted. The accumulated operating time with LPG was 588 hours.

Grid connection to commercial distribution line

This pilot plant normally suppied the house line of the thermal power station. It was also temporarily connected to a 6.6 kV high voltage commercial distribution line for the first time in Japan. We confirmed the high quality of the electricity during this connection. The major results obtained are as follows.

(1) There was little voltage or power factor fluctuation when the pilot plant and commercial distribution line were connected and disconnected.

(2) The increase of voltage harmonic distortion was less than 0.1 %, which is a very good value.

Environmental acceptability

Pilot plant emissions were meassured to investigate thier effect on the environment. NO_x was only 6.5 ppm and SO_x could not be detected at all at rated power. These results show the high environmental acceptability of PAFC.

Conclusion

A pilot plant was constructed to simulate a large scale PAFC for electric utilities and various tests, such as connection to commercial distribution lines, were conducted. The results we obtained from these tests have allowed us to isolate several subjects for further study. In the near future, we will apply this knowledge to the development of a large scale commercial power plant.

Table 1 Specifications of the pilot plant

Rated Output	50 kW, AC
Voltage,Frequency	220 V/ 6600 V, 50 Hz
Fuel	Natural Gas/ LPG selectable
Stack Operating Conditions	2 kg/cm² A, 190 deg C
Grid Connection	House Line / Commercial Distribution Line selectable
Inverter	Self-Commutated PWM type
Operating Mode	Full-Automatic (Manned Monitor)
Heat Recovery	Control Room Air Conditioner & Hot Water

Figure 1 An outside view of the pilot plant

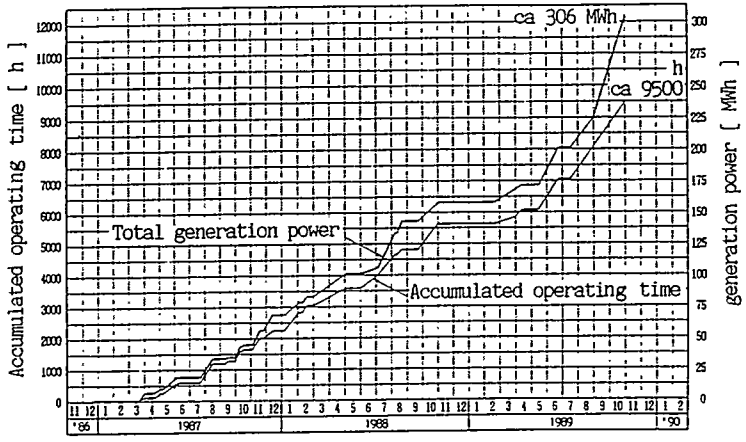

Figure 2 History of operation

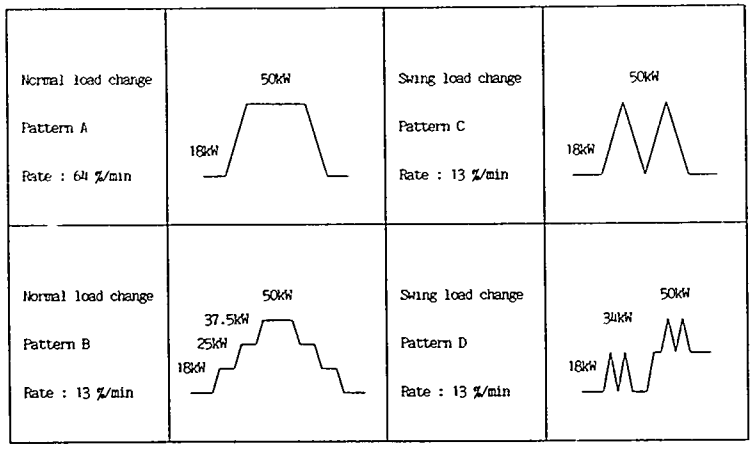

Figure 3 Load changing patterns

PRODE PROJECT - 1MW PAFC EUROPEAN DEMONSTRATOR DESIGN PROGRESS AND LICENSING ASPECTS

B. G. Marcenaro[†] M. Mazzieri[†] U. Haus[•] V. Cincotti[‡] F. Di Mario[‡]

(†) Ansaldo Ricerche - Genoa - Italy
(•) Azienda Energetica Municipale - Milan - Italy
(‡) ENEA - Rome - Italy

INTRODUCTION

The first design phase of the 1MW PAFC Power plant that ANSALDO is going to install in Milano has been concluded in march 1990. During this phase all of the technical choices has been made and detailed subsystem design has been exploited.

Meanwhile a one to one scale test rig has been designed and erected to verify the operation and the control logics for the turbomachinery to be adopted in the actual power plant.

As part of the first design phase a dynamic model of the plant is being established that will eventually be converted into an operator training system.

ACTIVITY STATUS

The feasibility study (1) for this plant ended in 1987 and reference was made, at that time, to four 260 kW fuel cell stacks (Fuji), operated at 5 bar and 190 C and a power conditioning subsystem with a line commuted inverter. Even if the general process flow sheet hasn't changed so much from then, orders have been placed for two 670 kW IFC stacks, operated at 8 bar and 205 C, and a self commuted GTO inverter, designed by ANSALDO, will be tested during this year.

A big effort has been spent in designing a system that can withstand any single failure with no consequences for people and major pieces of equipment. Particular attention has been devoted to introduce passive, intrinsic, features as a backup to the control system to make it possible to bring the plant to a "safe" condition even with the control system not functioning.

Based on the general criteria developed during the conceptual design phase the detailed design of major plant subsystems has been performed and is now being verified using dynamic analysis and a turbomachinery test rig that has been erected at ANSALDO site in Genova.

The rig was originally conceived to gain experience in running a turbocompressor but, on the way, it was given many other objectives like, for instance:

- Testing and fine tuning of the Air Pressurization System controls.
- Verification of the auxiliary burner design during pressurized operation.

The erection was completed July 1990 and tests will be performed from September to December of this year.

In order to obtain the maximum possible results from the dynamic analysis activity, a tool has been selected allowing real time dynamic simulation that can easily be used as the starting point of a simulator for training of operators. An other possible development in this field consists in using the real time simulator in connection with the actual control system (2) in order to validate the application software without having to run extensive test on the field.

Erection of the building for the power plant has been started in Milan during last June. The building has been designed following architectural criteria that allows installation in highly populated urban areas with minimum impact on the residents.

EXPECTED PERFORMANCE

The expected performances for the PRODE power plant are:

- REAL POWER:

  RATED: 1150 kW
  MINIMUM: 0 MW GROSS AC (STANDBY)
  OPERATING RANGE: 30% - 100% RATED POWER
  STEP CHANGES: 10% RATED (115 kW) PER MINUTE
  OUTPUT VOLTAGE: 23 kV / 50 Hz

- EFFICIENCY: 40% (AC net power over LHV)
- FUEL: NATURAL GAS
- HEAT AVAILABLE FOR COGENERATION: 1000 Mcal/h
- NO_x EMISSION: < 10 ppm

A big effort is being spent in finding a turbocompressor that fits the requirements of the project, in terms of flowrate and pressure ratio. At the moment an ABB machine has been selected for testing on the experimental rig that corresponds to a flow which is almost twice the flow required by the plant.

In the case that a suitable machine is not found, a reduction in the actual efficiency will happen. However it has been decided to take out the extra amount of energy, required to compress the excess air, form the efficency evaluation.

ADDITIONAL FEATURES AND POSSIBLE DEVELOPMENTS

In parallel with the design activity attention is devoted to additional features that can make plants of this kind more attractive to the potential clients.

In particular work is in progress on the fields of automatic operator training and expert systems for on line fault diagnosis. As mentioned the dynamic model of the power plant is being developed using a tool that allows real time operation, thus allowing the model to be used as a simulator for training of operators. Plans have been made to build emulation of the operator interface of the actual control system to be integrated in the simulator and to provide the model with handling for remote functions

and malfunctions in order to be able to test the operator's skill even in non standard situations.

Dynamic models will be also used as part of a fault diagnosis system based on artificial intelligence techniques. This system will use mixed qualitative (rules and logical relationships between components and subsystems) and quantitative (dynamic response of components and/or subsystems) knowledge to determine, basing on the actual value of key parameters coming from the field, if an undesired trend is in course and, in the affirmative case, what the possible causes could be.

On the electrical side a firts study on the status of the electrical grid has been performed in order to verify the harmonic content to be specified for the PCS design. The first results show that the PCS, as actually being designed, does not generate any indesired effect on the local grid.

LICENSING ASPECTS

In spite of its experimental nature and of the growing worries of the italian authoriries over environmental impact after the Seveso accident, the PRODE power plant has now got all of the permissions required by the italian law for industrial installations.

In submitting the design to the various authorities the following aspects were particularly stressed:

As far as safety is concerned it has been demonstrated with an Hazop analysis that, thanks to the design criteria adopted, no significant safety problems exist, either inside or outside the plant.

However, to make the plant absolutely safe even in case that an unbelievable accident occurs, the building has been designed in such a way that it acts as a completely safe barrier towards the extenal world. An architectural design of the building has been followed to better integrate the plant in the outstanding urban area.

For what concerns the environmental impact, the first results of the analyses carried out to evaluate the plant emissions seem to be far below the limits imposed by the existing codes and rules.

The italian mandatory code on pressure vessel design and construction, ISPESL code, required many additional test and manufacturing procedure reports to be carried out with respect to ASME code.

CONCLUSIONS

Even though a few other power plants has been developed in the past to demonstrate the viability of PAFC based power plants, the PRODE project has its own validity in that it will demonstrate how a power plant of this kind can be designed and erected without having the technology of either the fuel cells or the reformer.

During each stage of the power plant design, fabrication, installation and operation, experience will be accumulated as evidence to support the feasibility of future commecialization of PAFC power plants.

The efforts spent in licensing this plant in accordance with the restrictive rules existing in Italy make it reasonable to foresee the installation of Fuel Cell power plants into highly populated urban areas, with the additional advantage of better cogeneration opportunitites given by district heating technologies.

REFERENCES

1. G. Caserza et al., "A 1MW PAFC Demonstration Plant in Europe: Feasibility study technical results", proc. of F.C. Tech. and applications, pp 189-196, Oct. 1987.

2. O. Paladino et al., "Dynamic Simulation of a Fuel Cell Power Plant and Tuning of the Control System", proc. of ESM 89, Rome Jun 1989.

PAC TEST OPERATION OF 11 MW PAFC POWER PLANT AT TEPCO GOI THERMAL POWER STATION

Toshio Iino
Tokyo Electric Power Company
Chiyoda-ku Tokyo, 183 Japan

J.S. Caraceni
International Fuel Cells
South Windsor, CT 06074

Y. Shiba, N. Kato and K. Hayakawa
Toshiba Corporation
Chiyoda-ku Tokyo, 183 Japan

1. Introduction

This is a report on the progress of 11 MW PAFC Power Plant constructed at Tokyo Electric Power Company (TEPCO) Goi Thermal Power Station.

Construction of the plant and instruments/cable checkout were completed in spring of 1990. Preparation for the start of the Process and Control (PAC) test were begun in May 1990 and the PAC test was started in August 1990. As of the end of August, the PAC test has progressed to completion of the Fuel Processing System and Power Section System pressurization, and the Air Pressurization System start up.

At the time of the seminar, remaining PAC test operations such as Power Section Cooling System operation and Fuel Processing System heat-up and operation to fuel/steam transition will be completed. The detailed results of the PAC test will be presented at the seminar.

2. Construction

Power plant construction at the site was started in January 1989. Major components such as reformer, turbocompressors, heat exchangers and catalyst bed vessels were shipped to the site in "pallet structure" by July to September 1989. The microprocessor based control system and the Power Conditioning System (PCS) were shipped to the site on October 1989 and November 1989 respectively. Meanwhile, the piping work and inspection were continued. All of the construction work was completed by January 1990. Figure 1 shows the plant overview. The cable installation was completed in February 1990. Following the cabling work, the instruments which were installed at site were checked and point to point checkout was conducted to confirm that the cables between the control system and individual components (sensor, actuator, etc.) were correctly connected.

3. PAC Test Preparation

Before starting the PAC test, the following operations were conducted.

a. Cleanup coolant lines

In order to clean up the coolant line, fill and drain method was used, then recirculating water through the Heat Rejection System (HRS) was conducted to remove particles in water using the in-line filters.

b. Fill coolant lines

After completion of the cleaning operation, the coolant lines were filled with glycol water as heat rejection material (coolant). Because gas in the coolant is not desirable, gas vent operation was done during the HRS test operation.

c. HDS catalyst conditioning

The catalyst bed was conditioned (deoxidized) at site.

4. PAC Test

The plant control software was designed so that individual systems can be operated independently in order to conduct the PAC test efficiently. The PAC test is carried out in accordance with the startup procedure of the power plant. Up to this date (the end of August 1990), the following two steps have been completed.

a. FPS/PSS pressurization

FPS and PSS are pressurized to 115 psia simultaneously by nitrogen. Coordination of pressurizing speed between FPS and PSS was tested. Also, depressurization was tested for plant shut down.

b. APS startup

Major components of APS are an auxiliary burner, a low pressure turbocompressor (LPTC) and high pressure turbocompressor (HPTC). Fuel (natural gas) and air flow controls of auxiliary burner were tested and tuned. APS pressurization to 115 psia was successfully achieved and performance of the auxiliary burner and turbocompressors are verified.

5. Plant Operation

The PAC test is expected to be completed by the end of the year. The fuel cell stack assemblies (CSA) will be installed in the early part of 1991 and the plant will be operational by the spring of 1991.

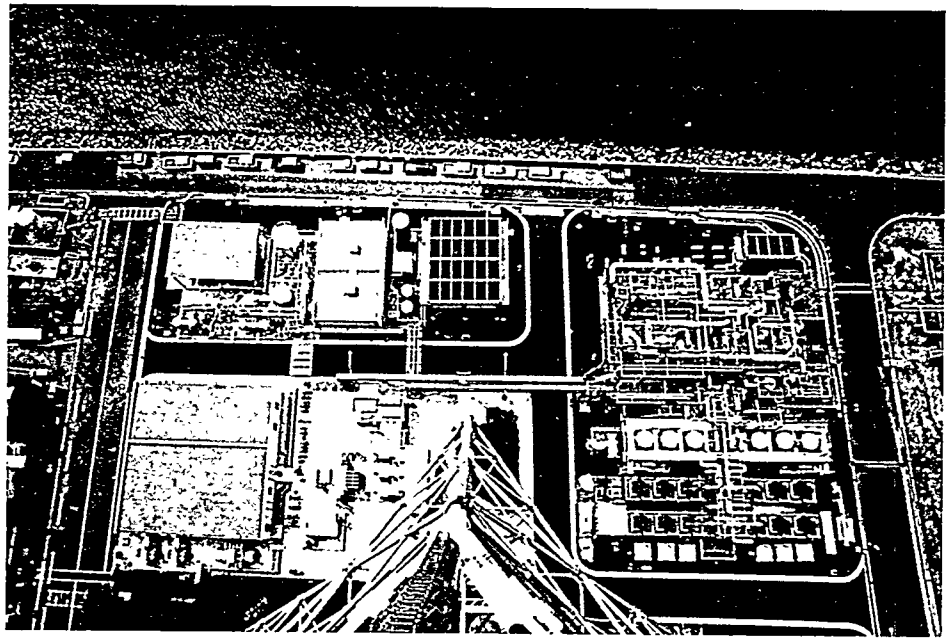

Figure 1. Plant Overview

NATURAL GAS/DIRECT FUEL CELL POWER PLANTS: DEVELOPMENT AND COMMERCIALIZATION ACTIVITIES

H.C. Maru, G. Steinfeld and B.S. Baker
Energy Research Corporation
3 Great Pasture Road
Danbury, CT 06813

P.H. Eichenberger, P.E.
The City of Santa Clara
Electric Department
1500 Warburton Avenue
Santa Clara, CA 95050

1. INTRODUCTION

A DIRECT FUEL CELL (DFC) is a unique type of fuel cell technology being developed by Energy Research Corporation. The DFC eliminates the need for a separate fuel processor and the associated heat transfer equipment. Natural gas fuel can be directly supplied to an internal reforming carbonate-type fuel cell, where it is converted to a hydrogen-rich stream and subsequently to electricity. The intimacy of the heat and mass transfer arrangement within the fuel cell results in a highly efficient, simple and reliable power plant. The DFC utilizes a mixture of alkali metal carbonates as an ionic conductor, nickel-based electrodes, and operates at 1200°F and atmospheric pressure.

Because of the direct conversion of fuel to electricity, DFCs promise very high electrical efficiencies even in MW-size power plants--surpassing any other practical power plant, including conventional phosphoric acid and solid oxide type fuel cells, combined cycles and other thermo-mechanical generators. DFCs can utilize a variety of fuels, including natural gas, methanol, ethanol, propane and coal-derived gases. The internal reforming capability of DFCs is also advantageous for providing multifuel capability and increasing the availability in case of an interruption of the primary fuel.

These unique characteristics, combined with other advantages, such as siteability, low pollution, low noise, modularity, improved power factor, low or no water requirements, and high-grade waste heat, make DFCs a highly attractive power plant option for utility applications.

ERC has been aggressively pursuing the technology and power plant development, as well as commercialization of DFCs. An account of these activities is presented below.

2. TECHNOLOGY DEVELOPMENT

The technology development programs at ERC have been supported by the Department of Energy, Electric Power Research Institute, Gas Research Institute, private utility companies and corporate funds.

Beginning with laboratory-size cells in the mid 1970s, the DFCs have been scaled to 4-ft^2 size cells. Basic materials are non-noble metal catalysts and stainless steels, which have been demonstrated in tests for up to 10,000 hours. Individual cells are stacked in a multicell configuration. A tall stack of 60 subscale cells has already been tested to examine the effect of height. A 54-cell stack has been assembled and will be tested in late 1990, followed by a 100-kW full-size stack to be tested at Pacific Gas & Electric Company's San Ramon, CA site. Additional 100-kW stacks have also been proposed to be tested.

The cell components can be made by well-established processes such as sheet metal bending and tape casting. These processes have been developed at ERC and detailed manufacturing studies have been conducted to ascertain that DFC stacks can be built economically.

3. POWER PLANT DESIGN AND DEVELOPMENT

Extensive system engineering and economic studies have been conducted for megawatt-size natural gas fueled DFCs in collaboration with Fluor Daniel. Two types of natural gas fueled DFC power plants have been designed:

1. an "Integrated" Design
2. a "Simplified" Design

Extensive design work to date has been carried out on the Integrated Design. The Simplified Design was recently proposed which requires minimal equipment but has slightly lower efficiency as compared with the Integrated Design. A description of the Simplified Design is presented below.

As shown in Figure 1, sulfur impurities (odorants) are first removed from natural gas and the fuel is fed to the anode side along with steam for suppressing soot formation, and for reforming reaction. The fuel is reformed internally and electrochemically oxidized by carbonate ions which are formed on the cathode side by reaction with oxygen and carbon dioxide. Spent fuel containing hydrogen, carbon monoxide, carbon dioxide and water is fed to a burner along with fresh air. The resulting hot gases containing oxygen, carbon dioxide, water and nitrogen are fed to the cathode side of the fuel cell to serve as the oxidant as well as a heat-removal medium. The spent oxidant gases are sent to a boiler to raise steam and then to an optional cogen unit before exhausting. DC power produced by the fuel cell is converted by using a high-efficiency inverter. The efficiency of this system is estimated to be 54% (LHV). Subsystem engineering for the Simplified System has already begun in collaboration with Pacific Gas & Electric Company--as discussed in a separate paper by Herman and Patel at this Seminar.

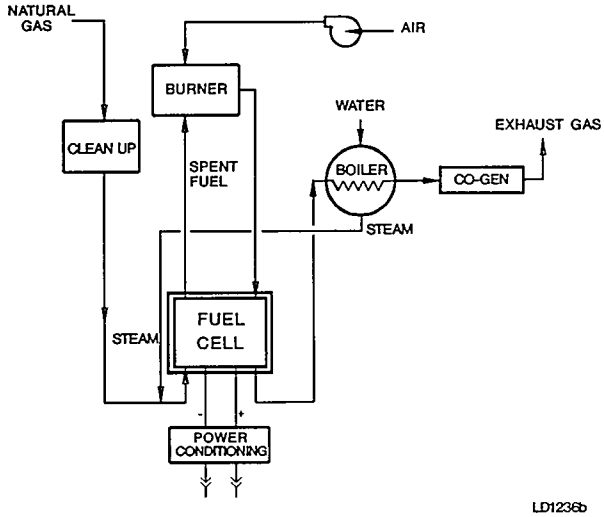

Figure 1. SCHEMATIC OF DIRECT FUEL CELL POWER PLANT (SIMPLIFIED DESIGN)

A recent in-depth DOE study at ERC investigated the feasibility of coal-gas fueled DFCs. This study concluded that such power plants can provide up to 47% efficiency at a competitive cost of electricity. Acid rain precursor (SO_x, NO_x) emissions from these power plants are at least an order of magnitude lower than the most stringent environmental standards existing today. Carbon dioxide emissions are also lower because of the high efficiency. Such power plants can initially utilize natural gas, and can be later converted to coal-gas fuel in a "Phased Construction" approach. Thus a broad application based, from MW to 100-MW sizes, from natural gas to coal-gas, exists for DFCs.

4. COMMERCIALIZATION ACTIVITIES

Significant activities have already been initiated towards stack manufacturing, collaborative effort with utilities, and demonstrations. These activities are briefly summarized below.

4.1. Manufacturing

Manufacturing is the keystone for commercialization of a technology. Conceptual design studies for a commercial fuel cell manufacturing facility (400- to 1600-MW/yr production) have been conducted to obtain a reliable estimate

of manufacturing cost. A 100% owned subsidiary, Fuel Cell Manufacturing Corporation (FCMC), has been organized to build a pilot manufacturing facility by 1991. Funding for this facility is already in place. This facility will supply fuel cells at affordable costs for field demonstrations. Another subsidiary, Fuel Cell Engineering Corporation (FCEC), is currently being organized to carry out power plant engineering and supply complete power plants to the utility industry. A commercial manufacturing facility will be established following the field demonstrations and initial set of firm orders from utilities.

4.2 Collaborative Effort with Utilities

An early involvement of utility customers is considered valuable in product development. A utility advisory group has been formed to provide utility input and to critique the direction of ERC's technology and power plant development.

A significant development of utility interest in the Direct Fuel Cell came from American Public Power Association's (APPA) initiative. In October 1988, APPA issued a "Notice of Market Opportunity for Fuel Cells" (NOMO). The NOMO Review Team received five bona fide responses. Energy Research Corporation was the only supplier to receive the Review Team's endorsement after 15 months of evaluation and in-depth discussions. APPA's Board of Directors and EPRI also endorsed ERC's Direct Fuel Cell Program. Following the endorsements, a "Briefing" was organized in February 1990, which was attended by 22 electric utility companies representing public power, private utilities and rural electric cooperative organizations. At the meeting, the City of Santa Clara announced a strong interest in hosting a demonstration unit. Following the positive reaction at the "Briefing," a buyer's group, Fuel Cell Commercialization Group (FCCG), was formed in April 1990.

The FCCG now has 17 members, consisting of municipal and investor-owned utility companies. An expanded Information Exchange meeting was organized by FCCG in September 1990, which was attended by 72 representatives from various utility companies.

4.3 Demonstration

Demonstration of prototype units is important to gain field experience, shake out design issues, train utility personnel and familiarize potential customers. Energy Research Corporation is planning to demonstrate several 2-MW size DFC power plants in cooperation with interested utility companies and government and other funding organizations. Stacks for these demonstrations will be fabricated cost-effectively in the pilot manufacturing facility being built by ERC.

Following the successful demonstrations, a commercial manufacturing facility will be built and early production units will be offered in 1996. A total order of 50 units of 2-megawatt size each is expected from private and public utilities. This would be a key step for committing to build a factory. After supplying the early production units at somewhat higher cost, mature units will be offered at competitive prices in the late 1990s. ERC plans to provide plant installation, checkout and personnel training services, as required. In addition, provision will also be made for maintenance and replacement parts.

Utilities participating in the demonstration and early production unit orders will receive preferred treatment in terms of price and delivery.

Preliminary power plant specifications for the DFC power plants are being defined under detailed studies in progress. General characteristics and design/performance data based on the system analyses carried out to date are shown in Table 1 for demonstration, early production and commercial units.

The first demonstration is expected to be carried out at the City of Santa Clara. An ad-hoc Steering Committee, consisting of the City of Santa Clara, Los Angeles Department of Water and Power, Pacific Gas and Electric Company, National Rural Electric Cooperative Assoc., Southern California Edison, and Electric Power Research Institute, has already been formed and a project schedule has been developed to begin the demonstration. Current activities include review of participant agreements, the agreement with ERC, and the hiring of a consultant to begin the balance of plant identification process. An update of the Demonstration Group will be presented at the Seminar.

Additional demonstrations are being envisioned for the United States as well as Europe.

Table 1. GENERAL DESIGN AND PERFORMANCE CHARACTERISTICS OF DFC POWER PLANTS (SIMPLIFIED DESIGN):

Three Categories of Progressive Units are Offered

	DEMO	EARLY	COMMERCIAL
PLANT			
Nominal Capacity (MW)	2	2	2
Nameplate Capacity (MW)	1.8	1.8	1.8
Maximum Capacity (MW)	2.25	2.25	2.25
Minimum Capacity (MW)	0.45	0.45	0.45
First Year for Orders (yr)	1991	1994	1994
First Year for Delivery (yr)	1993	1996	1998
Plant Life (yr)	-	20	30
Site Construction Time (yr)	1	1	1
Site Requirements			
Area (sqft)	5500	4500	4500
Footprint (sqft/kW)	3.1	2.25	2.25
Maximum Height (ft)	12	12	12
PLANT CAPITAL			
Total Plant Cost (Million $ (1990))	16	2.7	1.8
$/kW	9000	1500	1000
O&M EXPENSE			
Var O&M (No Fuel) ($/MWh)	-	-	12.7
Fixed O&M ($/kW-yr)	-	-	15.8
Stack Cost ($/kW)	5000	600	300
Stack Life (hr)	10,000	25,000	40,000
OPERATING			
Fuel Type	Natural Gas	Natural Gas	Natural Gas
Heat Rate (LHV)			
Full Load (Btu/kWh)	6850	6515	6350
75% Load (Btu/kWh)	6905	6570	6400
50% Load (Btu/kWh)	8095	7695	7500
25% Load (Btu/kWh)	11,870	11,290	11,000
Cold Start (Hr)	20	16	10
Standby to Full Load (min)	10	1	1
Cogeneration Option	yes	yes	yes
Waste Heat (MMBtu/hr)	2.3	2.2	2.1

MARINE APPLICATIONS OF FUEL CELLS

V W Adams
(Procurement Executive, Ministry of Defence,
Room 72, B Block, Foxhill, Bath, BA1 5AB, UK)

(Any views expressed are those of the author and do not necessarily represent those of the Department/HM Government)

INTRODUCTION

Fuel cells have already been used or demonstrated in land, space and military applications (1, 2). The purpose of this paper is to consider which types of fuel cell systems are best suited for marine use to provide extended operational capability within the restraints of limited space and weight for both the power conversion plant and the stored fuel (fuel/oxidant for submarines) required for their safe operation.

ADVANTAGES AND DISADVANTAGES

Advantages (3) of replacing diesel-generators with fuel cell systems are high efficiency, lower noise output, lower running and maintenance costs, savings in weight, direct generation of dc for some applications, dispersal of generators and no increase in through life costs. Disadvantages (3) are new development, higher procurement costs, the need for dc to ac conversion, reformation of fuel and in submarines, the need to dispose waste products discreetly.

FUEL CELL TYPES

In principle any fuel cell type could be used for marine applications but important parameters in selecting a choice are power density and power per unit weight. Other criteria are fuel and oxygen consumption, operating temperature (warm-up time), complexity, such as auxiliary systems required, and whether proven in demonstrators or applications. Data and comments for fuel cells, including an aluminium/oxygen or air fuel cell sometimes referred to as an aluminium/air battery (4), are given in the paper.

SUBMARINE SYSTEMS

It is assumed that system power levels of between 100 kW and 300 kW are required, built up of modules of at least 50 kW with, for reformed fuels, each module working with its own reformer. The major space requirement is for the oxidant and in practical terms, the choice is limited (3) to gaseous or liquid oxygen or a peroxide such as High Test Peroxide. The choice of fuel is wide but in practical terms is limited (3) to hydrogen stored in a metal hydride or, by reforming liquid fuels. Data and comments for both fuel and oxidant storage and comments on waste disposal are given in the paper.

Figure 1 presents overall volumes against stored energy for four groupings dominated by: (i) Gaseous oxygen, (ii) LOX or (iii) HTP, all with liquid fuels (methanol or diesel), and

(iv) by using solid hydride fuel with any of the three oxidants, where the estimated volumes of fuel and oxidant storage vessels and associated compartments have been taken into account. Storage of HTP or methanol is assumed to be in collapsible vessels outside the pressure hull in a free flooded compartment, and storage of gaseous oxygen could be in a toroidal design of pressure hull (5). Data for lead acid batteries (6) are included for comparison. Overall weights against stored energy are shown in Figure 2.

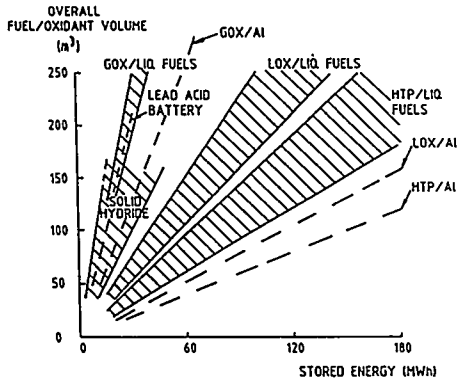

FIGURE 1 VOLUME AGAINST STORED ENERGY
GOX - Gaseous Oxygen
LOX - Liquid Oxygen
HTP - 85% High Test Peroxide
LIQ FUELS - Methanol or Diesel Fuel

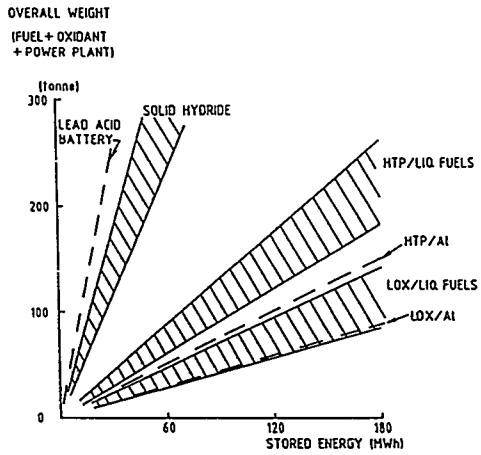

FIGURE 2 WEIGHT AGAINST STORED ENERGY
LOX - Liquid Oxygen
HTP - 85% High Test Peroxide
LIQ FUELS - Methanol or Diesel Fuel

SURFACE SHIP SYSTEMS

It is considered that it would be impracticable to use high power (tens of MW's) fuel cell stacks for the generation of power to drive large ships at their maximum speed using electric propulsion (3). Application is thus confined to replacing diesel-electric generators used for auxiliary power and low to medium speed electric ship drives. Thus, it is assumed that system power levels of between 500 and 1500 kW are required, built up of modules of between 50 kW to 500 kW, each module working with its own fuel reformer.

Since existing prime movers, such as gas turbines, would be retained for higher speeds, it is highly desirable that fuel cells should operate on diesel fuel reformate, assumed to be a mixture of hydrogen and carbon dioxide, provided from onboard reformers. Reforming of fuels such as methanol and diesel oil has been considered elsewhere (1, 3, 7) and development work is needed for compact systems suitable for the marine environment. The best solution is to use desulphurised fuel, which would also be advantageous for the prime mover life, but the availability of such fuel needs to be established.

It is assumed that fuel cell types for surface ship application are limited to those which can use either methanol reformate or desulphurised diesel oil reformate, as a fuel and air as an oxidant. This choice limits the options to PAFC's or PEMFC's for low temperature operation with external reformers and MCFC's or possibly SOFC's for high temperature operation with integrated fuel reforming. Estimated system sizes, based on new data for reformers (7), are shown against output power in Figure 3. In calculating system volumes a packing factor of 1.3 has been included.

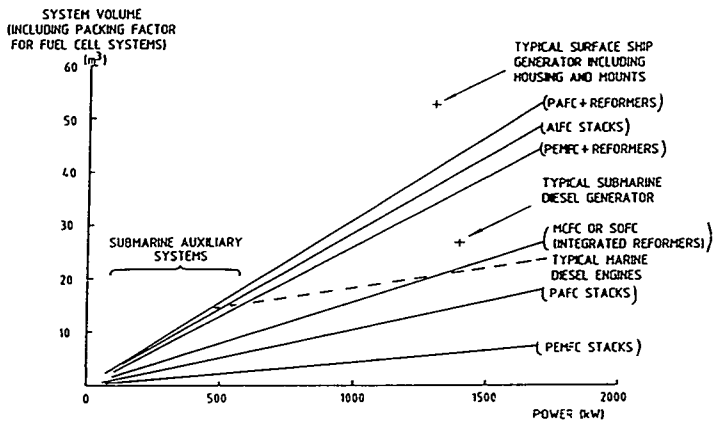

FIGURE 3 ESTIMATED SYSTEM VOLUMES

Estimated weights and fuel consumption are shown in Figures 4 and 5.

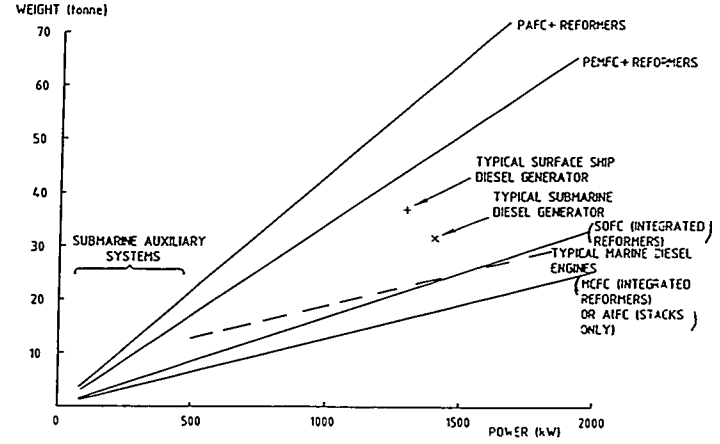

FIGURE 4 ESTIMATED SYSTEM WEIGHTS

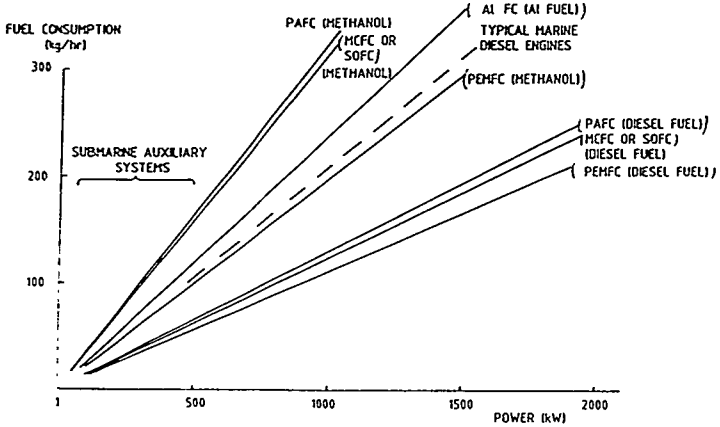

FIGURE 5 ESTIMATED FUEL CONSUMPTION

Areas of risk applicable to both surface ship and submarine systems are summarised in the paper.

CONCLUSIONS

The potential advantages offered by fuel cell systems, particularly low noise signature, reliable automatic operation and high efficiency are considered to outweigh the disadvantages. In terms of power density, fuel consumption, fastest start-up time, shortest development time and least complexity, proton exchange membrane fuel cells have the greatest potential for marine applications, although the reformation of fuels would be required to obtain the greatest benefits.

For longer term development molten carbonate and solid oxide cells, although operating at a significantly higher temperature, offer greater overall power density and savings in weight because of integrated reforming.

For submarine systems particular attention needs to be given to the safe storage of fuel and oxidant; hydrogen stored in a metal hydride and oxygen in a shock protected cryogenic tank are the safest, although there are advantages in storing liquids such as methanol as a fuel and high test peroxide as an oxidant. Gaseous oxygen could also be stored in high pressure vessels by using a radical change to a toroidal hull design. The more complex aluminium fuel cells with liquid oxygen storage offer higher stored energy density with a penalty in the fuel cell volume and weight, but compensated for by using internal aluminium electrodes as the fuel.

Copyright (C) Controller, Her Majesty's Stationery Office, London England 1990.

REFERENCES:

1. A J Appleby and F R Foulkes, "Fuel Cell Handbook", Van Nostrand Reinhold, 1989.

2. D Foxwell, "Staying Under Longer: The SSK Closes the Gap", Military Technology, No 11/88, Nov 1988, pp 61-71.

3. V W Adams, "Possible Fuel Cell Applications for Ships and Submarines", Grove Anniversary Fuel Cell Symposium, 18-21 Sep 1989, The Royal Institution, London, published in Journal of Power Sources, Vol 29, No 1/2, 1990, pp 181-192.

4. D Linden, "Handbook of Batteries and Fuel Cells", McGraw Hill Book Company, 1984.

5. R Compton-Hall, "Minisubs: a small revolution", Jane's Defence Weekly, 23 Sep 1989, pp 590-593.

6. N E Bagshaw, "Batteries on Ships", Research studies Press, John Wiley and Sons Ltd, 1982.

7. W Kumm, "Feasibility Study of Small Submersible Fuel Subsystem and Energy Converter System Integration Analysis", Phase 1 Final Report SBIR Topic N88-94, AEL/N88-94/SBIR 89, Sponsored by NAVSEA R&D Office US Navy Dept, Nov 1989.

FUEL CELLS IN NAVAL APPLICATIONS

David P. Bloomfield
ANALYTIC POWER CORPORATION
123 SOUTH STREET
BOSTON, MA 02111

Joseph A. Woerner
DAVID TAYLOR RESEARCH CENTER
ANNAPOLIS, MD 21402

The Navy has sponsored and continues to sponsor studies of fuel cells, in Naval missions. It has conducted studies within its own research laboratories, such as DTRC, as well as outside organizations. In the past, the fuel cell's low power density precluded its use aboard ship. The DSSV power system was a notable exception and this alkaline fuel cell, built by IFC, actually powered a submersible (Lockheed Deep Quest).

These early studies evaluated fuel cells for submarine and weapons power missions. The Navy has prepared exhaustive studies of potential fuels and oxidants which might be used in a variety of underwater missions. The latest being the Unmanned, Underwater Vehicle (UUV). The Navy's recent interest in fuel cells was partially triggered by Ballard's success in high power density IEMFC's, and the development of DOW membrane. These advances warranted a study of fuel cell power in surface vessel applications. The study was completed by Analytic Power under a SBIR Phase I program. The objective of the study was to determine whether fuel cells could compete with advanced heat engines in surface vessel applications.

This paper summarizes our findings on the role of fuel cells in Naval surface vessel applications. We have investigated ion exchange membrane (IEMFC), molten carbonate (MCFC) and phosphoric acid (PAFC) technologies. We have studied alternative fuels in conjunction with several surface vessel missions. The missions ranged from emergency power applications with 1 MW capability and 12 to 24 hr operating time; to a cruiser propulsion unit with a capacity of 62.5 MW for 300 to 500 hr. The quantitative basis for the comparison between heat engines and fuel cell power plants is given in Tables 1 and 2, and consists of system weight, volume, and cost - including fuel. In a qualitative sense, fuel cells can be built in relatively small (200 KW), efficient modules. These power packages can be distributed around a ship, eliminating the traditional engine room and enhancing the ship's damage control capability. The fuel cell power plant, with its high current capability, is also well suited for both advanced propulsion and weapons power.

We compare fuel cell power plants with diesels and gas turbines operating in Naval missions. The power plant flowsheet for the fuel cells is shown in Fig 1. In the case of the MCFC, it is assumed that reforming is internal to the stack and the external reformer and shift converter is eliminated. The fuel processor subsystem is comprised of a conventional, high pressure desulfurizer, a catalytic steam reformer and a shift converter. Condensation water recovery

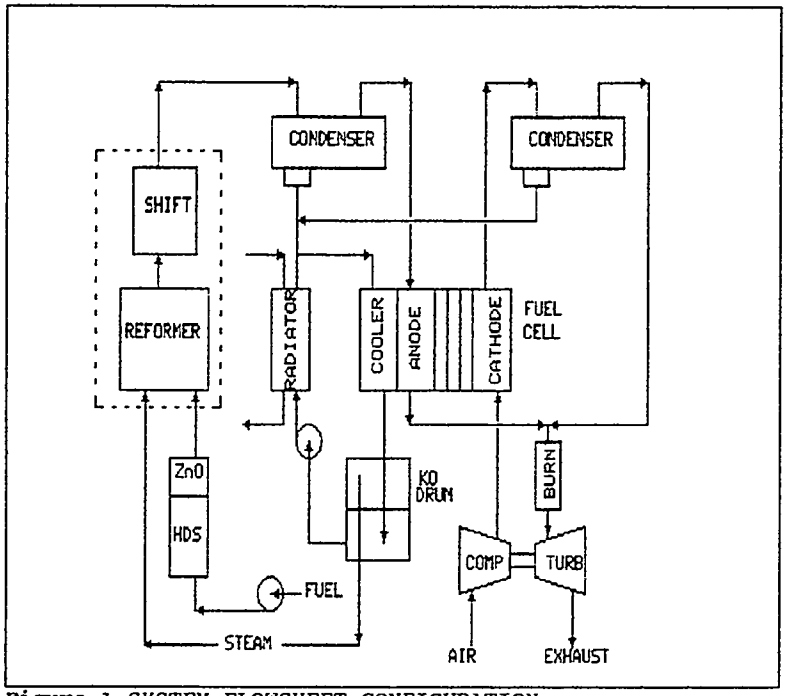

Figure 1 SYSTEM FLOWSHEET CONFIGURATION

is used and a turbocharger is used when the air supply system is pressurized. Low AC power levels do not require inverter magnetics, and high power applications assume DC power. Figure 1 does not show any heat exchangers. Regenerative heat exchange networks are resolved automatically by Analytic Power's systems codes. All fuel cell power plants were evaluated with a consistent set of economics, and weight & volume codes.

The results of the comparison for the Cruiser mission are given in Table 3 and the weight volume and cost results for the Enclave Mission are given in Table 4. These tables show the high and low values of weight volume and cost that are obtained in parametric studies. The independent variables in the studies were: power plant pressure, reactant utilizations, and cell voltage. We conclude that IEMFC based systems are competitive with diesel engines and gas turbines on a weight and volume basis but they are more costly. Molten carbonate fuel cell power plants were found to be competitive on a cost basis but were heavier and larger than the competition. Phosphoric acid fuel cells were found to be heavier, larger and more costly than conventional systems.

We concluded that the most significant problem with fuel cells is fuel. Easily reformable fuels, such as methanol are

attractive to fuel cell manufacturers, but from the Navy's perspective, diesel fuel is the fuel of choice for surface vessels. It is available on a world-wide basis and is already in the Navy fuels inventory. The principle problem with alternative fuels is their low energy content and low availability. The problem with desulfurization of diesel fuel is that it has, in the past, required very high equipment volume. Analytic Power is addressing this problem experimentally.

TABLE 1
HEAT ENGINE SOURCE CHARACTERISTICS

DIESEL		
FUEL CONSUMPTION	0.44 - 0.52	LB/KWH
WEIGHT	20	LB/KW
VOLUME	0.7 - 0.88	FT^3/KW
GAS TURBINE		
RATED POWER	1 MW 62	MW
FUEL CONSUMPTION	0.47 - 0.86	LB/KWH
WEIGHT	23 6	LB/KW
VOLUME	0.75 0.27	FT^3/KW

TABLE 2
FUEL CELL POWER PLANT CHARACTERISTICS

TECHNOLOGY	MCFC	PAFC	IEMFC
STACK WEIGHT lb/ft^2	4.1	1.4	0.9
PITCH cells/in	3.2	3.2	7.0
COST \$/ft^2	\$15	\$40	\$120
CURRENT DENSITY asf @ 0.7 VOLTS	430	270	880
PRESSURE 8 atm	8	8	8
HYDROGEN UTILIZATION	0.85	0.85	0.85
OXYGEN UTILIZATION	0.6	0.6	0.6
COST \$/KW	50	211	195

We found that pressurization improved the performance, weight and volume of all fuel cell technologies. However the gains in weight and volume one would normally expect with MCFC and PAFC cell stack performance improvements are offset by the large weight of encapsulation materials required. Encapsulation is required because both of these technologies employ liquid electrolytes and capillary seals. This fact coupled with their low cell pitch results in high encapsulation weight. Using conventional MCFC cathodes, the MCFC would not survive long at high pressure. IEMFC's do not require encapsulation.

The competitive position of all fuel cell technologies improves as mission duration increases. While MCFC's were up to 235% heavier and up to 271% larger than gas turbines in enclave missions, they were only 12% to 38% heavier and 10% to 35% larger than gas turbines in propulsion missions. In longer missions they might undercut the gas turbine weight and volume. IEMFC's can compete with heat engines on a weight and volume basis irrespective of mission length.

In the trade-off studies we performed, we did not include the effect of the power system on the ship. Our studies only compared power generator to power generator. There may be many other advantages to fuel cells than we accounted for in our study. For example the high air flow rates required by gas turbines may require a larger superstructure on a ship to accommodate ducting. The pulse power capability of fuel cells may also offer additional advantages to the Navy by allowing the integration of weapons power and propulsion or auxiliary power generators.

TABLE 3
CRUISER MISSION 62.5 MW/300 hr RESULTS

	MCFC		IEMFC	
	HIGH	LOW	HIGH	LOW
WEIGHT (TON/KW)				
FUEL CELL	108	87	74	66
GAS TURB.	78			
DIESEL	81			
VOLUME (FT^3/KW)				
FUEL CELL	4127	3378	3387	3101
GAS TURB.	3068			
DIESEL	3357			
COST ($/KW)				
FUEL CELL	720	639	1,438	1,170
GAS TURB.	464	400		
DIESEL	184	156		
STACK COST % OF SYSTEM	21.88%	12.84%	31.16%	48.43%

TABLE 4
ENCLAVE MISSION 1 MW/24 hr RESULTS

	IEMFC		MCFC		PAFC	
	HI	LO	HI	LO	HI	LO
WEIGHT (TON/KW)						
FUEL CELL	20	18	67	44	46	27
GAS TURB.	20	16				
DIESEL	18	15				
VOLUME (FT^3/KW)						
FUEL CELL	1025	946	4204	2153	2916	1693
GAS TURB.	1133	939				
DIESEL	1274	1007				
COST ($/KW)						
FUEL CELL	1278	1211	813	564	1944	1200
GAS TURB	680	616				
DIESEL	178	161				
STACK COST % OF SYSTEM	25.9%	28.1%	36.7%	18.1%	44.0%	30.0%

ACKNOWLEDGMENT

This work was sponsored by the U.S. Navy under an SBIR Phase I Program, Contract N61533-89-C-0008. Mr. Joseph Woerner was the Technical Contract Officer.

SPE® REGENERATIVE HYDROGEN/OXYGEN FUEL CELLS FOR SPACE AND MARINE APPLICATIONS

J. F. McElroy
Chief of Advanced Systems, Electro-Chem Products

United Technologies Corporation
Hamilton Standard Division
One Hamilton Road
Windsor Locks, Connecticut 06096-1010

INTRODUCTION:

High energy density storage is a critical element for future space and marine applications. SPE water electrolyzers and SPE hydrogen/oxygen fuel cells can be combined into a system providing this high energy density storage capability as shown in Figure 1. Demonstrated SPE cell lifetimes of over 100,000 hours and voltage stability of one microvolt per cell hour enable very long missions and/or repeated use. The storage of the hydrogen and oxygen reactant gases at pressures between 3000 psi and 6000 psi has a major impact on overall system volume. For space applications, the high pressure gas storage permits the use of high strength fiber wound tankage with its greatly reduced mass per cubic foot of gas stored.

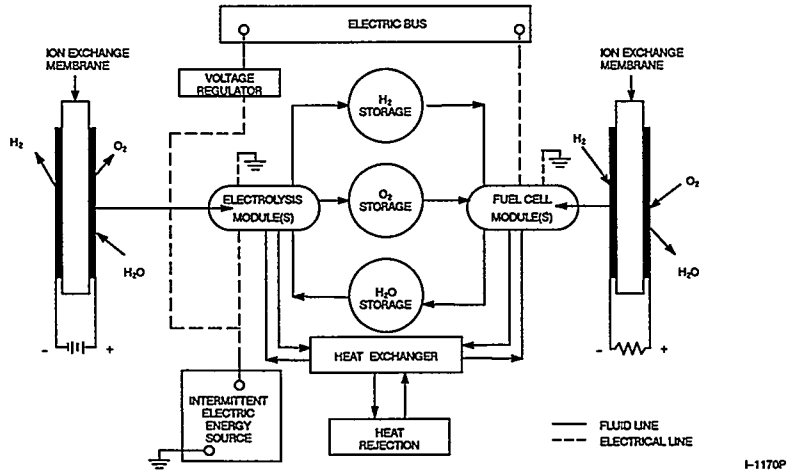

FIGURE 1. POWER PLANT FUEL SCHEMATIC INCLUDING HYDROGEN/OXYGEN REGENERATIVE FUEL CELL ENERGY STORAGE SYSTEM

HIGH PRESSURE SPE ELECTROLYZER CHARACTERISTICS:

A 3000 psi SPE water electrolyzer system has been fully developed for U.S. Navy nuclear submarine oxygen generation. This hardware is in the process of being modified, under NASA contracts, for space applications in the pressure range from 3000 to 6000 psi These low weight/low volume derivatives will be suitable in the gas changing portion of an energy storage system for either space or naval applications.

Converting the naval electrolyzer to a space flight configuration requires a lighter and smaller package. The high pressure naval SPE electrolyzer design features a cylindrical cell stack pressure vessel pressurized with nitrogen. The mass of the 100-cell naval stack is approximately 200 lbs. The mass of the pres-

SPE® is a registered trademark of United Technologies Corporation, Hamilton Standard Division

sure vessel surrounding it adds an additional 800 lbs. Recent design work conducted for NASA-JSC has produced a prototype cell stack for space propulsion that weighs <200 lbs. total, demonstrating several weight and volume enhancements.

Cell Stack Hardware Design Base

Typically, an SPE cell stack is supported and compressed between two terminating plates, one fixed, one free, tied together with high strength rods under tension. Compression loading of 34 tons is applied by springs located between the tie rods and the free end plate. The free end plate incorporates an insulated positive plate and post assembly for applying the electrolysis current to the cell stack. The fixed end plate serves as the negative current collector plate as well as a manifold passage of water and gas to/from the cell stack.

In the naval SPE electrolyzer, the fixed end plate also forms one end of the pressure vessel, so that it carries the pneumatic load of 3000 psi in addition to the cell stack compression load. To resist deflection and deformation under the resulting combined load of 197 tons, the fixed end plate of the naval SPE electrolyzer must be 4 in. thick stainless steel plate. The cylindrical pressure vessel that bolts into the fixed end plate requires 2 in. thick steel walls.

Enhancements for Space Flight

To reduce weight and decrease volume, configuration changes were made to the pressure vessel, fluid end plate and positive plate and post. The prototype SPE high pressure water electrolyzer that results in significantly smaller and lighter.

Domed Pressure Vessel – In the prototype high pressure SPE electrolyzer, the pressure vessel is two torispherical domes opposed on either side of a central fluid plate. This configuration is shown in Figure 2. The domed design allows for a wall thickness of as low as 1/4 of an inch when using Inconel or other high strength materials.

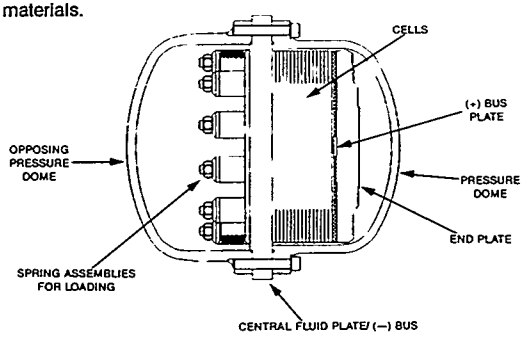

FIGURE 2. CROSS SECTION, SPE PROPULSION ELECTROLYZER PROTOTYPE

Central Fluid Plate – The fluid plate is pressure balanced between the two pneumatic domes, eliminating the need for a thick plate to resist the pneumatic load. The prototype fluid end plate is only 1 in. thick. In the prototype, the cell stack is located on one side of the fluid plate within the volume of one dome.

The compression springs are located in the volume of the opposing dome. Volume is available for incorporation of an in-stack gas/water separators and/or other system ancillaries, allowing for additional savings in system weight and volume as development progresses. Larger cell stacks may be packaged as half-stacks in each dome on either side of a central fluid plate.

Other Design Enhancements – A height and weight reduction to the cell stack was realized in the prototype by incorporating edge electrical connections with a low profile positive terminal plate instead of using a plate and post assembly.

The prototype SPE high pressure water electrolyzer is shown in Figure 3. The dimensions of the prototype are 13 in. across the domes and 13 in. in diameter at the dome flanges.. The total weight of the prototype cell stack for space station propulsion is 193 lbs which is 20% of the naval version. The volume is reduced 70% from the naval stack.

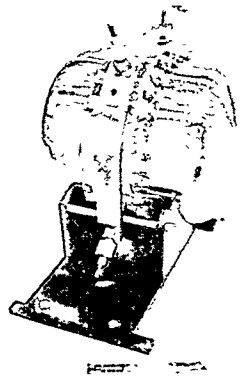

FIGURE 3. ASSEMBLED SPACE SPE ELECTROLYZER

Performance

The prototype SPE propulsion electrolyzer is designed to convert 2pph normal rate/4pph emergency rate of water into oxygen and hydrogen gas at 3000 psia, 120° F at an efficiency of greater that 70%. Performance of the prototype SPE high pressure water electrolyzer is shown in Figure 4 for conditions of 3100 psia, 120° F.

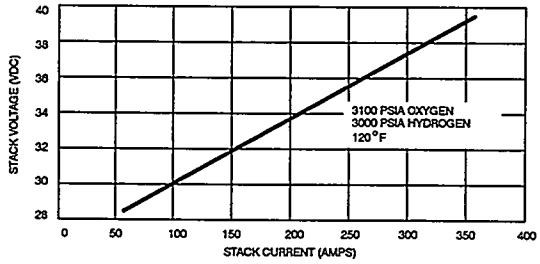

I-1171P

FIGURE 4. SPACE SPE ELECTROLYZER PERFORMANCE (STACK VOLTS VS. AMPS)

SPE FUEL CELL CHARACTERISTICS:

The U.S. Navy SPE water electrolyzer design has been scaled to an SPE hydrogen/oxygen fuel cell configuration. The resultant 0.78 square foot active area per cell design has been performance tested in single and multi-cell stacks.

Hamilton Standard's circular screen-type fuel cell hardware has proven versatility and reliability. The membrane electrode assembly represents the most vital component of the cell design. This component is similar in design to production water electrolyzer hardware in that materials and manufacturing procedures are nearly identical. The major differences are the oxygen electrocatalyst material and the fact that the oxygen electrode has a wetproofing film attached in order to prevent water buildup on the surface of the catalyst. A package of metal screens is placed in intimate contact with the membrane electrode assembly, thus forming a means for reactant and product transport as well as current distribution. A circular nonconducting frame surrounds this screen package, providing overboard sealing. A similar screen package and frame design placed on the alternate side of the membrane forms the hydrogen cavity of the cell. Cell units are assembled in bipolar fashion, with conductive separators placed in between.

The benefits obtained via the utilization of the round screen type cell hardware are numerous. High pressure sealing capability is enhanced due to the evenly compressed perimeter of the circular cell. Also, the round design has demonstrated excellent stackability characteristics, as demonstrated by the fact that stacks of up to 100 cells are commonly manufactured at Hamilton Standard. Round cells have shown greater sealing reliability than square cells. Importantly, more than 100,000 hours of life have been

demonstrated in circular single-cell hardware. These factors become important when reliable hardware must be produced.

Another important feature of the circular screen-type hardware is its inherent capability to withstand high shock loads. This has been demonstrated on Hamilton Standard hardware in the U.S. Navy oxygen generator plant program. As a part of this effort, an oxygen generator system was exposed to greater than 100G shock loads with no resultant module or system damage.

Stack Compression

The cells, fluid distribution assemblies, and separators are compressed between end plates connected by insulated tie rods. Belleville spring washers on the tie rods provide for thermal expansion and prevent component creep, therefore maintaining uniform compression over time. Figure 5 displays a stack of 0.78 ft^2 cells compressed between end plates with spring washers. This stack operates at 100 psia and 180°F. Cooling is performed by the circulation of water and the product water is passively discharged.

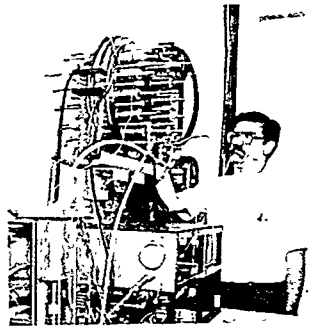

FIGURE 5. SPE FUEL CELL STACK (EACH CELL ACTIVE AREA - 0.78 FT^2)

Performance

To date both single-cell and multi-cell stacks have been performance evaluated. Membrane types evaluated include Nafion®120 and Nafion 117. Figure 6 provides the performance characteristics of the 0.78 ft^2 cells at 100 psia and 180°F.

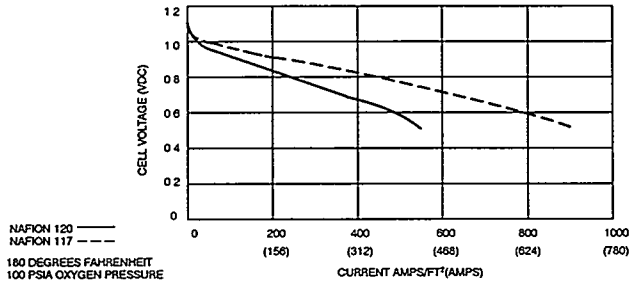

I-1172P

FIGURE 6. PERFORMANCE CURVES FOR 0.78 FT^2 FUEL CELLS

SUMMARY:

During the past year advances in both SPE electrolzers and SPE fuel cells have been directed toward the regenerative hydrogen/oxygen energy storage systems as well as other unique applications. These advances have placed the SPE eletrolyzers and SPE fuel cell in position to meet the need of both space and naval customers.

Nafion® is a trademark of Dupont

REGENERATIVE FUEL CELL SYSTEMS TRADE-OFF ANALYSIS

J.R. Huff, J.C. Hedstrom and N.E. Vanderborgh
Los Alamos National Laboratory
Los Alamos, New Mexico 87545

P. Prokopius
NASA Lewis Research Center
Cleveland, Ohio 44135

The Surface Power Program is one of five elements under the Exploration thrust of Project Pathfinder. Besides Surface Power, the other elements include Planetary Rovers, Sample Acquisition, Analyses and Construction, Autonomous Rover, and Photonics. The objective of the Surface Power Program, simply stated, is to develop power technology to a level of readiness sufficient to enable or enhance extraterrestrial surface missions to the Earth's moon or Mars. To meet this objective, technology development will be conducted in the areas of solar power generation, energy storage, and electrical power management. The highest potential for successfully achieving surface power capabilities that will satisfy currently understood mission and system requirements lies in regenerative fuel cell (RFC) energy storage subsystems and photovoltaic power generation subsystems. This paper describes an investigation of alkaline and proton exchange membrane (PEM) fuel cell and electrolyzer technologies as possible candidates for use in a regenerative energy storage system.

The technology assessment and system trade-off studies addressed the following RFC system characteristics: (1) 25-kWe continuous for approximately one-half of the 20,000-hour lifetime required for the lunar mission, (2) stand-alone operation, (3) compatibility with lunar and Martian surface environment, (4) 65% fuel cell system efficiency, (5) 500 Wh/kg Martian surface, and (6) 800 Wh/kg lunar surface. These characteristics place emphasis on life, reliability and, to a lesser extent, performance.

From an electrochemical performance point of view, the alkaline and PEM fuel cells and electrolyzers are now at a satisfactory state of development. Any further improvement would result in higher efficiencies, but the impact of higher efficiencies on the overall system is yet to be determined. Electrodes and stack structural components appear satisfactory. The PEM membrane has demonstrated adequate lifetime and stability. The major area of concern and risk is the unknown long-term stability of the alkaline matrix component and the susceptibility of this component to operational upset during the long mission requirement.

Permeability of the fuel cell and electrolyzer separators by the reactant gases is a parameter that must be understood and controlled. This permeation results in losses in faradaic efficiency in both devices. Within the electrolyzer, these losses mean that the size of the photovoltaic array, or any other primary power source, must be increases. A loss in faradaic efficiency within the fuel cell is more critical. This loss results in additional thermal energy being generated and also adds to the supply and tankage of hydrogen and oxygen. These changes increase the system mass and volume through the requirement for larger radiators, larger storage tanks, and additional reactants.

Existing fuel cell and electrolyzer systems are fabricated now with a number of rotating machinery components, especially water pumps, coolant pumps, and recirculating fan-water separators. None of these rotating components

have demonstrated 20,000-hour operation. Therefore, the inclusion of such components presents a high level of risk for successfully achieving mission requirements.

Another critical element in successful system design is the control of water and thermal flows. Water control includes maintaining appropriate water content in the fuel cell electrolytes, transferring water to storage and for use in the electrolyzer, separating water from gas streams, and preventing water from freezing (or boiling) in critical places within the system. Thermal control involves either using excess heat within the system or removing heat through suitable heat exchange under all lunar surface conditions.

The system components with significantly high mass are the reactant storage tanks and the reactants. The reactant mass must be minimized by high efficiency electrochemical designs. The tank mass must be minimized by suitable design. The storage tanks must be able to withstand the lunar environment, both the extremes of temperature and the intermittent bombardment with solid particles.

An important technical question is the storage pressure for reactant gases and the resulting electrolyzer reactant pressure. Storage of wet oxygen at 204 atm (3000 psi) raises concern about tank material corrosion. Moreover, higher pressure operation impacts electrolysis efficiency. Gas storage pressure has only a minor impact on tank mass. Further study is needed to consider the details of the effect of storage pressure on storage tank design.

Based on the above considerations and the technology assessment, a system design option is formulated. The regenerative fuel cell hardware is subdivided into a series of components, as follows:

1. 25-kW Fuel Cell Stack: The fuel cell stack needs to operate at a voltage efficiency over 65% for approximately 10,000 hours and be of a design that allows the repeated start-up and turn-down cycles necessary to follow the solar cycles on the lunar surface. A PEM, metal hardware fuel cell stack appears to be the only candidate that will meet these targets. A system that incorporates multiple stacks is probably a reasonable approach. Most likely, three 15-kW stacks should be included so that any two of these stacks can more than supply the required 25-kW.

2. 35-kW Electrolyzer Stack: The electrolyzer stack hardware must follow much the same design requirements necessary for the fuel cell stack. Good voltage performance, probably 1.55 mV/cell or less, and high faradaic efficiency are required. These characteristics are needed to achieve the necessary hydrogen and oxygen resupply rates with a 35-kW electrolyzer unit. Moreover, the device must operate successfully for approximately 10,000 hours following a cycle that includes a 14-day turn-on and a 14-day turn-down. Some element of freeze protection may be required during the lunar night. The conclusion was reached that PEM electrolysis stacks are superior in voltage performance, ruggedness, and reliability. Therefore, PEM electrolyzer stacks are the apparent choice. Most likely, the same degree of redundancy is required for PEM electrolysis hardware as for PEM fuel cell stacks. Three stacks, each operating at 18-kW can be configured so that any two stacks can deliver design yields of oxygen and hydrogen.

3. Gas Drying Hardware: Both electrolyzer stack types generate gas saturated with water at the stack operating temperature. Considerable attention was given to the need to remove water from the gases before storage. Because the regenerative fuel cell designs require full recovery of water, the extent of gas cooling possible and the heat exchange system required to facilitate that extent of cooling were considered. Alternatively, the storage tanks could be maintained at a temperature that precludes condensation and freezing. Neither of these alternatives were particularly attractive because of the energy requirements and because of the additional required mechanical components. A third solution would be to process the gases through a gas-liquid static separator following a modest cooling step, then gas saturated with water at 20 to 40°C would be stored. This smaller amount of water would be collected as it condensed in the tanks or allowed to freeze on the walls. It is recommended that this alternative be included in the initial design.

4. Reactant Storage Tanks: Although tank architecture was not a primary focus, without question reactant gas storage must be a design concern. Tank mass is one of the predominating components of total system mass and is directly related to fuel cell efficiency. However, the mass of the tanks and reactants is not influenced by storage pressure. Thus, generation and storage pressures are parameters that are yet to be determined. The recommendation is that spherical tanks be considered that are designed to operate well through a wide temperature range. Tank linings must be used that minimize corrosion rates or mitigate the effects of corrosion, even through the very long design lifetime. A series of smaller tanks, in contrast to one large tank, is required to decrease the chance of system failure because of bombardment. Even with multiple tanks, some elementary cladding may be necessary.

5. Thermal Management: The thermal management subsystem is considered as a separate component even though the actual design is still not firm. In general, thermal management for previous electrochemical systems has led to the inclusion of active heat transfer systems driven by centrifugal fans and blowers or using liquid coolants transported with pumps. These active heat transfer systems involve components with suspected short lifetimes. Indeed, the concensus of opinion is doubt that existing active heat transfer components could operate in excess of 2,000 hours. Therefore, it is essential that new designs be considered that minimize the number of these rotating components and that include redundant components at a level sufficient to influence system reliability.

ACKNOWLEDGEMENT

This work was supported by the NASA Lewis Research Center.

PHYSICAL PROPERTY OPTIMIZATION OF LITHIUM ALUMINATES FOR FABRICATION OF MOLTEN CARBONATE FUEL CELL MATRICES

Patrick M. Brown
Cyprus Foote Mineral Company
Malvern, PA 19355

Stable molten carbonate fuel cells are dependent upon the stability of individual components exposed to a high temperature molten salt environment; i.e., anodes, cathodes and electrolyte matrix.

While numerous molten salt electrolytes have been tested,(1,2,3) the majority have fixed upon a 62 mole percent lithium carbonate and 38 mole percent potassium carbonate composition. Researchers have also investigated various dopants from zirconium oxide(4) to alkaline earth oxides(5) to aid in matrix stabilization and limit nickel oxide dissolution.

Many studies have been done on various matrix materials including magnesium oxide up to the early 1960's. But most have now fixed upon lithium aluminate as the material of choice. This selection was based upon its stability at 650°C in the presence of molten lithium carbonate/potassium carbonate electrolyte(6). Various crystal modifications of lithium aluminate have been investigated including the alpha (α), beta (β) and gamma (γ)forms. Gamma lithium aluminate which is developed at high temperatures in excess of 650°C has been found to be the most stable form.(7)

Lithium aluminate physical properties are very important for optimization of an effective and stable matrix for molten carbonate fuel cell production. High surface area, fine particle size lithium aluminate was developed for electrolyte retention. The capillary pressure acting to retain the electrolyte is directly proportional to pore size by virtue of the equation relating surface tension to the column height of liquid in a capillary.

Hence

$$h = \frac{2T\cos\theta}{rdg}$$

Where T = surface tension
r = pore radius
h = height of liquid rise in a pore
d = liquid density
θ = contact angle

The pore radius in turn is directly related to particle size, smaller particles generating finer pores.

Coarse particles of lithium aluminate limit crack propagation and provide matrix compressive strength(8). Fibers of lithium aluminate strengthen the matrix to prevent cracking during forming and thermal cycling.

Proper fabrication of a tape cast matrix requires adequate information on the chemical and physical properties of the matrix particulates themselves. Also, a thorough understanding of what part each type of particulate plays in the final matrix structure. Therefore, the major forms of lithium aluminate are characterized here along with examination of typical tape cast matrix.

Table I shows the chemical properties of lithium aluminate indicating a relatively low impurity level. Loss on ignition is a particularly important parameter. It is composed of two components, surface adsorbed water which can be removed by heating to 110°C and normally represents 0.1-0.3 percent by weight. The second component is in the form of hydroxylated, chemically bound moisture which is not removed until substantially higher temperatures. It is formed by the hydration reactions:

$$LiAlO_2 + nH_2O \xrightarrow{\text{limited water}} LiAlO_2 \cdot nH_2O$$

$$2LiAlO_2 + 6H_2O \xrightarrow{\text{x's } H_2O} LiOH \cdot 2Al(OH)_3 \cdot 2H_2O + LiOH$$

The lithium alumina hydrate thus formed in the presence of limited or excess water has been characterized by x-ray diffraction file No.'s 20-618 and 31-704, respectively.

The presence of varying amounts of moisture can have a negative influence upon tape casting if not properly controlled. Moisture can hamper dispersion of the lithium aluminate particulates due to surface adhesion between particles and their hydrophilic nature. In addition upon hydration with excess water and recalcination, gamma lithium aluminate can be converted to the less stable alpha crystal modification. While exposure to moisture should be limited, predrying at 300°C prior to dispersion in the tape casting solvents can give more reproducible and consistent results.

Table II illustrates the physical characterization of lithium aluminate particles. The high surface area particulates are required for electrolyte retention.

The lithium aluminate fibers shown in Figures 1 closely resemble the leg of a fly. This form which allows a fly to climb walls is a fortuitous result of the fiber forming process and results in providing added tensile strength to the tape cast matrix. This interlocking nature

can reduce the potential for crack generation during thermal cycling and prevent gas cross over.

TABLE I
LITHIUM ALUMINATE TYPICALS - CHEMICAL

Typical Analysis	High Surface Area HSA-10	HSA-19	Low Surface Area LSA-15	LSA-50
Chemical				
% Li_2O	22.2	22.2	22.5	23.5
% Al_2O_3	75.1	75.1	76.2	75.9
% LOI (550°C)	0.5-1.0	0.5-1.0	1.0	0.3
% Fe_2O_3	0.016	0.016	0.03	0.03
% Cl	0.02	0.02	0.05	0.05
% Na	0.21	0.21	0.18	0.18
% K	0.009	0.009	0.007	0.007
% Mg	0.003	0.003	0.007	0.007
% Ca	0.015	0.015	0.02	0.02
% SO_4	0.028	0.028	0.044	0.044
% Alpha-$LiAlO_2$	0.3	0.4	0.3	0.3

TABLE II
LITHIUM ALUMINATE TYPICALS - PHYSICAL

	High Surface Area HSA-10	HSA-19	Low Surface Area LSA-15	LSA-50
Phase Composition				
% gamma	>99.5	>99.5	>99.5	>99.5
% alpha	<.5	<.5	<0.5	<0.5
Surface Area (B.E.T.)	9-11m^2/gm	18-20m^2/gm	<1.0m^2/gm	<0.1m^2/gm
Particle Size				
% minus 325 mesh by wet screening	>97	>97	<92	<50
Wet Screen Analysis:				
+60 mesh	<0.1	<0.1	0.1	trace
+100	0.1	0.1	0.9	0.7
+140	0.1	0.1	1.7	4.6
+200	0.1	<0.1	2.0	10.0
+325	0.1	0.1	4.0	43.0
-325	>99.5	>99.6	90.5	41.7
Average particle size(μ)	2	2	15	50
Bulk Density (p.c.f.)				
Free Fall	23	14	35	60
Packed	43	36	82	85

Tape cast matrix were produced with 10%, 20% and 30% fiber levels. The matrix containing 30% fiber had qualitatively greater strength. Comparative SEM photographs of the 10%, 20% and 30% (Figure 2) fiber samples show some vertical cracks in the 10 and 20% fiber matrix which could explain the strength differences. Furthermore, mercury porosimetry shows secondary pores developed in the 30% fiber sample. These 1-2 μ pores would result when fibers begin to overlap. Again one would anticipate this would lead to increased matrix strength.

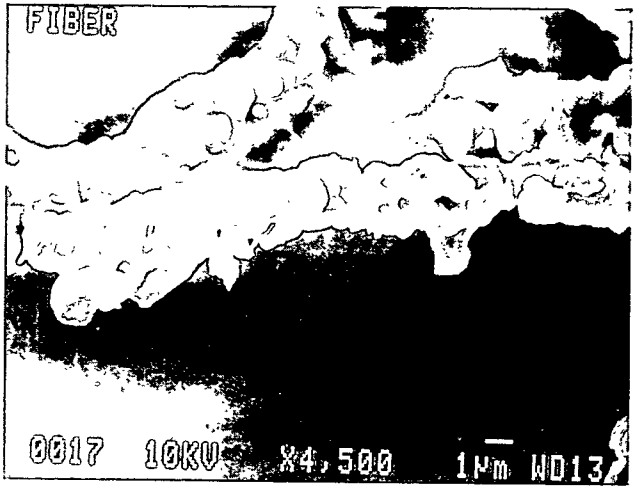

FIGURE 1

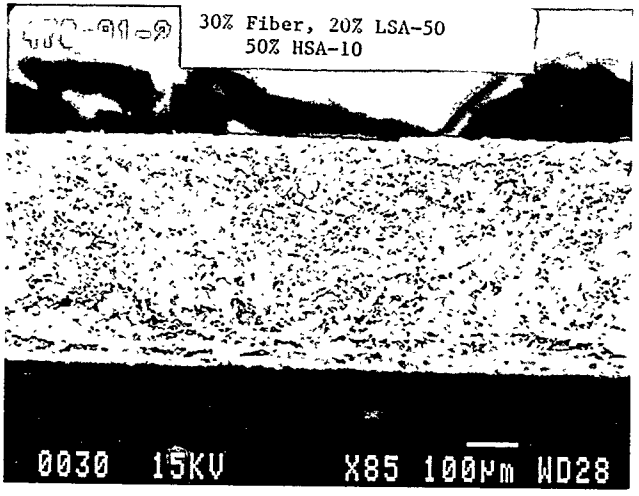

FIGURE 2

REFERENCES

(1) Braers, G.H.J. and Ketallaar, "Fuel Cells", Reinhold N.Y. p. 78 (1960)

(2) Kronenberg, M.L., J Electrochem Society, 109, p. 753 (1962)

(3) Sandler, Y.L., J Electrochem Society, 109, p. 1115 (1962)

(4) Hatoh, K., Nakura, J., Taniguchi, N. and Gamo, T., "Study on Electrolyte Tile of Molten Carbonate Fuel Cell Particle Growth Behavior of Electrolyte Supporting Material", Denki Kagaku 57, No. 7 p. 728 (1989)

(5) Ohzu, H., Agawa, T., Akasaka, Y., Yamamoto, M. and Murata, K., "Effect of Alkali-Earth Carbonate Addition in Electrolyte on NiO Cathode Dissolution" presented October 23-26, Fuel Cell Seminar (1988).

(6) Kucera, G., "DTA Study of $LiAlO_2$ Polymorphic Transformations" Extended Abstracts, Electrochemical Society Meeting, Hollywood, Florida, Oct. 5-19, Vol. 80-2, p. 365-7 (1980)

(7) Kucera, G., "Thermal Characterization of Lithium Aluminate/Alkali Carbonate Electrolyte Structures", proceedings of the 11th North American Thermal Analysis Society Conference, New Orleans, October 18-22, p. 89-94 (1981).

(8) Appleby, A. J. and Foulkes, F.R., "Fuel Cell Handbook" Van Nostrand Reinhold, N.Y. p. 301 (1989).

(9) Pigeaud, A. and Yuh, C.Y., "Determination of Optimum Electrolyte Composition for Molten Carbonate Fuel Cells" work performed under Department of Energy Contract No. DE-AC21-86MC23264, June (1989).

(10) Tapes produced by Argonne National Laboratories Molten Carbonate groups under DOE Contract No. DE-AC21-90MC-21187 (August 1990).

DEGRADATION OF NiO CATHODES: MODELING AND EXPERIMENTAL STUDIES*

David A. Shores
University of Minnesota
Corrosion Research Center
Minneapolis, MN 55455

J. Robert Selman
Illinois Institute of Technology
Chicago, IL 60616

Estela T. Ong
Institute of Gas Technology
Chicago, IL 60616

The dissolution of the NiO cathode into the electrolyte and the subsequent precipitation of Ni in the tile is an important limitation of the operating lifetime of current design MCFCs. Experience with laboratory cells and pilot plant sized cell stacks has shown that the Ni precipitates can grow sufficiently to electronically short cathode to anode in less than the design lifetime. In this abstract we describe a mathematical model of cathode degradation together with some laboratory cell tests that were designed to help quantify and verify the modeling results.

The mechanism of cathode degradation involves several fundamental processes:

a) dissolution of (lithiated) NiO into the adjacent carbonate film throughout the wetted portion of the cathode,
b) transport of the dissolved Ni species through the carbonate film on the cathode structure to the cathode/tile interface,
c) transport of the dissolved Ni species through the electrolyte tile,
d) reduction of the dissolved Ni species and precipitation of metallic Ni within the electrolyte tile.

These processes constitute an example of "fluxing" in that there is a source and a sink for the soluble component (Ni ions) and a driving force for transport; therefore the degradation process proceeds continuously.[1,2] If only dissolution were involved, the loss of cathode to saturate the electrolyte at (≈ 30 - 50 ppm Ni) would be insignificant. The fluxing processes are coupled to each other and are

* This work was supported by the U.S. Department of Energy, Morgantown Energy Technology Center, under contract DE-AC21-86MC 23263.

coupled to other electrochemical reactions and transport processes involved in the MCFC operation. We have constructed a computer model that describes the above steps in terms of (a) chemical reactions and (b) transport equations, which are coupled together by the requirements of conservation of mass and charge. The relatively simple chemical reaction model contains only a single unknown kinetic parameter (i.e., the rate constant of NiO dissolution) and this was combined with a model for convective diffusion in the tile which, likewise, contained only a single unknown parameter (i.e., the convection velocity due to ion migration). Using the available experimental cell data, the values of these parameters have been determined, and they fall within a fairly narrow band. The kinetic rate constant is weakly dependent on current density and much less so on gas composition. This suggests that NiO does dissolve, after all, as the result of an electrochemical reaction; however, the chemical-reaction model is adequate as a first approximate. The convective velocity is, as expected, primarily dependent on current density. All other input values for the equations are fundamental physico-chemical parameters, such as diffusivities, solubilities, etc. The aim of the model is to be able to predict NiO dissolution rates and the location of the Ni deposit in the tile for any set of operating conditions.

The model calculates the "ideal" steady state activities of the gas components across the thickness of a cell for given cell operating conditions, including anode and cathode gas compositions and utilizations, current density, temperature, etc. This calculation fixes δ, the location of the Ni precipitates in the tile. Then the model calculates the activity profile and the flux of soluble Ni within the cathode and through the tile to the precipitation site. The cathode structure is assumed to follow an "open agglomerate" model.[3] A schematic representation of the results of a set of such calculations is shown in Fig. 1 for open circuit. For a cell under load, the concentration profiles differ in detail, but the general picture is the same, with the Ni precipitates located slightly further from the cathode.

A series of laboratory-scale (IGT) 3 cm^2 fuel cells were operated under specially selected and controlled conditions to provide data for the development of the cathode dissolution model. These conditions included constant NiO solubility with varying current density, constant oxidant with varying current density, various fuels and operating for times up to 4000 hrs. Nickel deposition rates and Ni distributions in electrolyte tiles were

measured for each run. Data from several experimental cells are included in Fig. 2 along with model predictions.

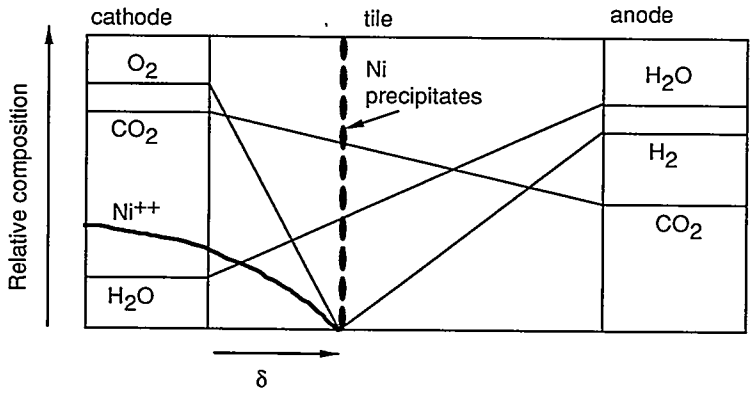

Fig 1 Model calculations of component activities across a cell thickness at steady state for a given set of cell operating conditions and open circuit.

The cell test efforts have led to the identification of current density as an important parameter. Under a given cathode solubility, the amount of nickel transported to the tile increases with increasing current density. For a given current density, the amount of nickel transported to the tile increases with increasing solubility. These are consistent with our proposed mechanism for nickel transport. However, at very low solubility, there appears to be a threshold current density below which the correlation changes. We infer that the rate controlling step shifts from transport to the dissolution reaction under these low solubility conditions.

Except for some uncertainty in the case of low CO_2/air ratios at low current densities, the model predicts with fair accuracy the location of the Ni deposit within the tile and the nickel dissolution rate. An electrochemical description of NiO dissolution is also feasible, but the electrochemical kinetic parameters are not sufficiently well characterized to permit a critical test of the model from cell data. Thus, a relatively simple two-parameter model encompasses satisfactorily the rather complicated composition-dependent behavior of the experimental cell data shown in Fig. 2. Further details about this study are available.[3,4]

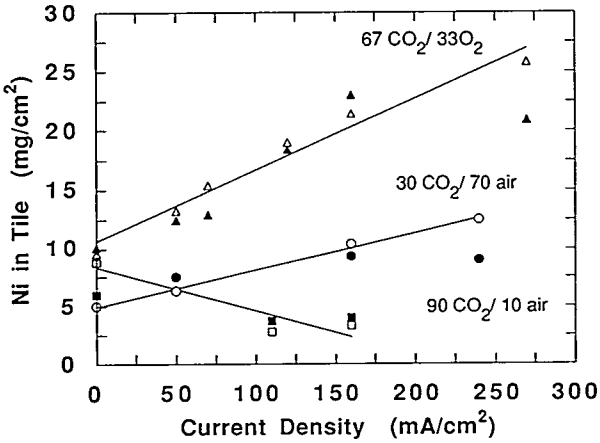

Fig. 2 Model predictions (solid lines) *vs* experimental values of Ni deposited in the tile as a function of operating current density for 2000 hrs for three oxidant compositions. The open symbols are model predictions; the filled symbols are measurements from cells.

REFERENCES

1. D. A. Shores, C. D. Iacovangleo and R. H. Wilson , "Solubility and Transport of Ni in MCFC Electrolyte Structures", presented at Fall Electrochemical Soc. meeting, (Detroit) Abst 344, 1982.

2. D. A. Shores, J. R. Selman and E. T. Ong,"Degradation of NiO Cathodes: Modeling and Experimental Studies", in Symp. on Molten Carbonate Fuel Cells, The Electrochemical Soc., Fall meeting, Seattle, 1990.

3. Yuh, C. Y. and J. R. Selman, J. Electrochemical Soc. *131*, p. 2062-2069, 1984.

4. D. A. Shores, J. R. Selman and E. T. Ong, "Cathode Dissolution", final Report to U. S. Dept. of Energy, Morgantown Energy Technology Center for contract DE-AC21-86MC23263, July, 1990.

TECHNOLOGY BASE RESEARCH FOR THE MCFC: STATUS AND NEEDS

J.R. Selman
Department of Chemical Engineering
Chicago, IL, USA

and

I. Uchida
Department of Molecular Chemistry and Engineering
Tohoku University, Sendai, Japan

1. Introduction

As the development of the MCFC rapidly approaches the 100-kW stage of pre-commercial demonstration, it is relevant to review the role of basic research in MCFC development from a new perspective. This perspective is two-fold: that of the drive to commercialization, and that of successful commercialization, in an international setting.

In this paper, we review first the present status of "basic" research related to the MCFC: the incentives for research, and the contributions it has made to development. Research has played an important role in bringing the MCFC to the pre-commercial stage. Now, however, the question is: How basic is "basic" research for the commercialization effort itself? And next: Which kinds of research would be required once the MCFC finds market acceptance?

2. Basic Research 1975-1990: Incentives

Technology base research specifically for the MCFC came into its own since 1975, when major development programs started in the USA, sponsored by DOE. A large part of this technology base research in the U.S. and in Japan (since 1980), has been aimed at improving our understanding of the operation of electrode processes.

Initially, the search for better electrode materials and improved structures, to minimize voltage losses under a typical load of 160 mA/cm^2, was one of the major research activities of developers in the U.S. This search was combined with the goal of formulating an optimized electrolyte composition. It was guided by the existing, far from complete, insight in the sources of electrode polarization, and it led to new questions about the reaction mechanism and transport processes in the porous electrodes.

Key questions concerned:
(1) the performance characteristics of various anode materials (replacement of nickel by less expensive and sulfur-resistant materials);
(2) the strong temperature dependence of the cathode polarization;
(3) the quite different sensitivity of the porous anode and cathode to overfilling by electrolyte.

By 1982 many of the critical factors responsible for electrode and cell performance had been clearly identified. Although important questions remained and work on the electrode

reactions continued, a certain consensus emerged about the level of performance made possible by improved structures and materials.

The operation of stacks under pressure then brought up several questions that had not been thoroughly analyzed yet. These are
(1) cathode (nickel oxide) dissolution;
(2) electrolyte migration and possible loss by evaporation;
(3) corrosion of hardware and consequent loss of electrolyte.
With these issues, the main incentive of basic research shifted to improving stack lifetime, i.e., understanding and preventing long-term performance decay. A fourth important issue concerned both lifetime and fabrication cost:
(4) the technology of preparing creep-resistant component materials, in particular for the anode.

In 1985 the Penner advisory working group of the U.S. DOE formulated a number of key priorities for basic research. These largely sprang from the endurance concerns of the MCFC developers, and they included Priority I items (conductive ceramics, electrode kinetics and mass transport; corrosion mechanisms and control) as well as Priority II items (direct hydrocarbon electrode; sulfur and HCl tolerant electrodes; fundamental physicochemical and engineering studies).

These recommendations were subsequently implemented in several multi-year basic research programs, carried out by companies, government laboratories and universities. They were mostly funded and managed by DOE, via METC. Some of these have yielded significant contributions to practical development.

In Japan, basic research in support of MCFC development has been carried out since 1981 in part by a few government laboratories and in part by five universities, among which several major universities. The government (national) laboratory programs are managed by the Agency of Industrial Science and Technology of MITI, while the university programs are under the direction of the Ministry of Education, Science and Culture (MESC), as Special Project Research. Coordination and practical relevance of these two separate research programs is ensured by overlapping advisory committees, in which companies strongly participate.

3. Basic Research 1975-1990: Practical Contributions

At this point, it is relevant to distinguish between **fundamental engineering** and **exploratory** approaches. The first stresses the need to understand the mechanisms and limitations of known materials or processes. The second approach explores alternative materials or processes to broaden the spectrum of potential applications, and often follows an intuitive or heuristic approach.

An example of the **fundamental engineering approach** is that of analyzing the capillary behavior of porous MCFC electrodes, starting from physical principles, and explain the effect of electrolyte filling on polarization. This analytical approach, supported by mathematical modeling, goes beyond simply

explaining empirically observed behavior. If a model can reproduce a carefully chosen set of experimental data, it may be possible to predict performance over a wide range of conditions, using estimated design and operating parameters.

This approach has been quite successful in several of the critical issues discussed above. Specifically, we mention:

(1) Predicting the rate of nickel oxide cathode dissolution, based on a few parameters derived from small-cell data;
(2) Explaining the difference in polarization behavior of the anode and the cathode, from the generic differences in electrode kinetics of anode and cathode materials and from differences in mass transfer of dissolved gas;
(3) Explaining and predicting the effect of electrolyte composition (Li-Na-K balance) on nickel oxide dissolution and on cathode kinetics, from the acid-base chemistry of the electrolyte and the complex chemistry of dissolved oxygen;
(4) Explaining, and in part predicting, the effect of migration on electrolyte movement in manifold gaskets and wet seals;
(5) Predicting the performance of scaled-up cells at high utilization by models making use of polarization data of small cells at low utilization.

Nevertheless, there remain significant gaps in our ability to understand quantitatively and predict, for example:
(a) a completely satisfactory prediction of the scaled-up cell performance polarization is not possible yet, in particular for pressurized operation;
(b) the wetting and capillary behavior of porous electrodes under load as a function of gas composition, and its effect on polarization, is poorly known. This is especially critical for predicting polarization, cathode dissolution, and corrosion tendencies at low CO^2 partial pressures.
These gaps are related, and in turn are related to gaps in our understanding of the reaction mechanism of the cathode. Another significant gap is:
(c) the lack of understanding and control over deactivation (by electrolyte wetting) of internal reforming catalyst.

Important contributions to development have also been made by the exploratory approach. In particular,
(1) the exploration of alternative cathode materials has yielded a few candidates, of which $LiFeO_2$ in particular looks very promising and is undergoing further scrutiny;
(2) the exploration of electrolyte additives to decrease the rate of NiO dissolution has yielded incremental improvements. In a combination of these approaches, Ni-ferrite has shown some potential for improvement over NiO as cathode material.

Nevertheless, we tentatively conclude that these efforts in exploratory research have not greatly increased the options available to MCFC developers, or introduced new designs and materials (with the possible future exceptions of $LiFeO_2$ and of Ni-ferrite). The reason may be simply that Edisonian exploration has its limitations under the complicated conditions of the MCFC. In any case, the planned pre-

commercial demonstrations rely on proven (i.e. established) materials and on incremental improvements in lifetime. However, clearly the search for better materials should be continued and refined, if the MCFC becomes commercial reality.

The science of metal/molten salt and ceramic/molten salt interactions is not developed enough to chart an informed and promising choice of exploration. A promising material has to have acceptable conduction, solid-state diffusion, and electrocapillary characteristics; it helps considerably if we control operating conditions to make this possible.

4. Research to Assist Demonstration and Commercialization

During the last three years the challenge and resolve to demonstrate and commercialize the MCFC, in the face of competition from other high-temperature fuel cells and from other advanced power generation systems, has opened a new era. To some extent the need for further exploratory research appears diminished. Based on a preliminary database of materials properties and cell performances, cell/stack components and materials have been selected and overall design features have been decided. These choices and decisions will largely be adhered to during further scale-up and stacking. How correct they are, will become evident ultimately in the final tests of stack and system performance.

The most critical need during this stage will be for:
(1) simple but reliable models useful in scale-up, and verification of these models, especially with respect to performance under pressure;
(2) experiments and models to assess the effect of low CO_2 partial pressure on polarization, corrosion, and electrolyte movement/loss.

However, in a longer-term perspective successful commercialization requires basic research aimed at three goals: (1) cost reduction in manufacturing; (2) longer life-time (contributing to cost reduction); and (3) incremental or quantum improvements of performance.

Cost reduction will require research into new techniques of manufacturing, especially that of nickel- or nickel-alloy coated metals and of separator-plate alloys or composites.

Above we have argued that (2) and (3) require a much deeper base of technology research than what has thus far been carried out, especially with respect to metal/electrolyte and ceramic/electrolyte interactions. This field needs much greater attention than it has received thus far. We believe that commercial success of the MCFC will make this kind of effort possible, and that it will greatly contribute to improved performance.

Acknowledgment: The authors acknowledge support from several funding agencies in the U.S. and Japan, respectively, and useful discussions with many colleagues in MCFC R&D.

DURABILITY STUDY OF A MOLTEN CARBONATE FUEL CELL AT ELEVATED PRESSURE

Isamu Sone, Masato Takeuchi, Takehiko Yoshida
Hitachi Research Laboratory, Hitachi, Ltd.
4026 Kuji-cho, Hitachi-shi, Ibaraki-ken, 319-12 Japan

Toshiki Kahara, Keizou Ohtsuka
Hitachi Works, Hitachi, Ltd.
3-1-1 Saiwai-cho, Hitachi-shi, Ibaraki-ken, 317 Japan

Summary

The Molten Carbonate Fuel Cell(MCFC) is expected to operate at elevated pressure when it is commercialized. We have been conducting a series of operation tests and subsequent post-test analyses in both lab-scale cells and cell stacks. One of the lab-scale single cells (effective electrode area: 64 cm^2), which was life-tested for the purpose of evaluating the MCFC durability, demonstrated a stable cell performance for 5600 operation hours under 3 ata. Study of the performance and components of the cell, which proceeded the scheduled 100kW-stack operation at elevated pressure, clarified the status quo and identified remaining problem areas for the MCFC.

Cell Components

We used Mg-impregnated Ni anode, Ag-impregnated NiO cathode, and tape-casted electrolyte tile for the active components of the cell.(1) For the cell housing materials SUS310S was used in the current collectors and separators.

Operation Conditions

Three independent reactions were proposed for the carbon monoxide in the fuel mix: water-gas shift reaction, methanation reaction, and Boudouard reaction.(2) In order to avoid carbon fouling at the anode, steam concentration of the fuel mix had to be increased as the operation pressure was increased. A partial equilibrium carbon deposition boundary, which neglected the methanation reaction from the above three reactions, was experimentally selected for a criterion of carbon free operation.

Cell Performance

Fig.1 shows a lifegraph of the cell. It was life-tested for a total of 5600 operation hours, which excluded the standby period and cold-hold period. During the course of the life test, various diagnostic check-ups were periodically and occasionally conducted to identify the cause of performance decay. Different degradation modes were apparent in each period (A-D). The voltage drop in period A synchronized with the resistivity increases of the cell.

There were three weeks of cold-hold and several shutdowns accompanying thermal cycle in period B; however those interruptions had no adverse effect on the subsequent performance of the cell. Cell performance was very stable in period B. Complete clogging of the inlet fuel flow by carbon-fouling at the end of period B caused a shutdown, and then a step-wise drop and subsequent decay of performance started in period C. Repair of gas sealing, which was undertaken at the end of period C, restored the cell performance to 0.7V. The cell demonstrated stable performance at elevated pressure. There were no signs of electrolyte depletion or electrical shorting during the course of the life test.

Cell Components

Corrosion: The non-conductive area of the separators was aluminized to evaluate the long-term corrosion resistance. Current collectors and other conductive area were not aluminized. Fig.2 is a photograph of a typical cross-section of the aluminized area of the separators. The aluminized SUS310S separator showed effective anti-corrosion performance.

Nickel Dissolution: Elements in the tile were analyzed by atomic absorption spectrometry and the inductively coupled plasma spectrometry. Assuming that aluminum content in the post-tested tile remained the same as before the test, total amount of nickel in the tile was calculated as about 53 mg/cm^2 per unit electrode area. Compared with previous reports about nickel dissolution and electrical shorting, (3)(4) the present data indicated that operation at elevated pressure accelerated the nickel dissolution from the NiO cathode. Distribution of nickel in the tile was investigated with electron probe micro analysis. As a result of it, nickel particles were detected which were locally deposited at the cathode-side of the electrolyte tile. Estimated lifetimes to electrical shorting have been discussed as a function of CO_2 partial pressure.(5) The present data confirmed that the NiO cathode dissolution was one of the remaining problems, especially for MCFC operation at elevated pressure.

Acknowledgement

This work is being supported by the Agency of Industrial Science and Technology, Ministry of International Trade and Industry (AIST/MITI), and the New Energy and Industrial Technology Development Organization (NEDO).

References

1. M. Takeuchi, et al.: "The Stabilization of Electrodes for Molten Carbonate Fuel Cell": 1988 Fuel Cell Seminar Abstracts, pp332-334, Oct. 1988.
2. D.O. Ham and G.W. Lord: "Carbon Deposition in Molten Carbonate Fuel Cells": 1987 Fuel Cell Seminar Abstracts, pp228-229, Oct. 1987.
3. E.T. Ong and R.A. Donado: "MCFC Component Technology": 1988 Fuel Cell Seminar Abstracts, pp390-393, Oct. 1988.
4. T. Murahashi: "Molten Carbonate Fuel Cell -On the life limiting factors": Proceedings of the 1st International Fuel Cell Workshop on Fuel Cell Technology Research & Development, pp61-70, Sept. 1989.
5. A.J. Appleby and F.R. Foulkes: Fuel Cell Handbook, Van Nostrand Reinhold, New York, 1988.

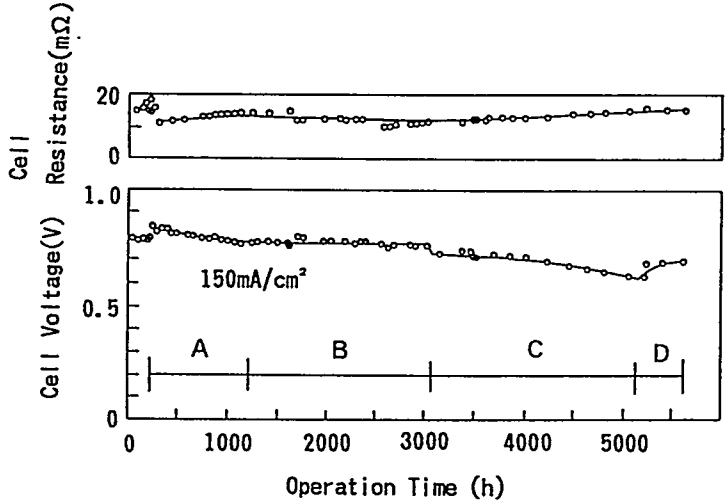

Fig.1 Lifegraph of Cell Operated at 3 ata

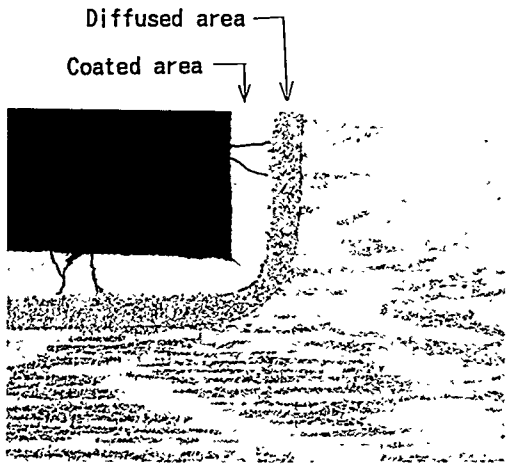

Fig. 2 Cross-Section of Aluminized SUS310S after the life test

OVERVIEW OF THE DOE-FUNDED FUEL CELL CONTAMINANTS R&D PROGRAM

Mark C. Williams and David A. Berry

U.S. Department Of Energy
Morgantown Energy Technology Center
Morgantown, WV 26506

INTRODUCTION

Integrated coal gasification fuel cell systems (CGFC) offer promise for high-efficiency, environmentally sound, and cost-competitive electric power generation. However, coal gas contains contaminants which may adversely affect fuel cell performance. The cleanup requirements of this gas need to be defined to order to permit interfacing of the gasifier and fuel cell.

OBJECTIVE

The near-term objective of the Department of Energy's (DOE) Contaminant Research and Development (R&D) Program is to assess the impact coal-derived contaminant species on the molten carbonate (MCFC) and solid oxide (SOFC) fuel cells. The long-term goal is to establish tolerance levels, characterize performance effects, and develop reaction mechanisms of various species. The tolerance levels will be used in coal gasification fuel cell (CGFC) system studies and in program planning that defines needs for gas stream cleanup technology for CGFC systems.

BACKGROUND

Coal-gas contaminants may affect MCFCs and SOFCs in many ways, such as:

a. Increased MCFC and SOFC anode polarization when contaminants adsorb on active anode surfaces lowering current/voltage output.

c. Plugging of MCFC and SOFC anode gas passages due to deposition of oxides, which increase diffusion losses and decrease fuel cell performance.

d. Increased MCFC electrolyte loss through enhanced melt vaporization, causing gas crossover and short circuiting.

PROJECT DESCRIPTIONS

The contaminant work is being performed by Energy Research Center (ERC) for the MCFC and Westinghouse Science and Technology Center for the SOFC.

In August 1988, a program was established with ERC to evaluate coal-gas contaminant effects on the MCFC. This ongoing program is studying the effects of major (hydrogen chloride (HCl), hydrogen sulfide (H_2S) and ammonia (NH_3)) and minor trace contaminant species (selenium (Se), lead (Pb), cadmium (Cd), mercury (Hg), tin (Sn), arsenic (As), and zinc (Zn)) are being investigated by various analytical methods.

An initial task was to perform a literature survey and thorough data analysis by a complete thermochemical study of all multiphase/multicomponent equilibria that can exist at 650°C for all possible products of contaminant/fuel cell component interaction. Individual trace species testing provided the experimental data for contaminant species. Both thermogravimetric (TGA) and electrochemical (½-cell) experiments were done to examine the different mechanisms of contaminant interaction and volatilization, before actual 300 cm^2 fuel cell testing was begun.

In September 1989, an effort was initiated with Westinghouse to evaluate the effect of H_2S, HCl, and NH_3 on SOFC performance. The effort also includes an analytical study to evaluate SOFC operation on various trace contaminant species. A test matrix involving contaminant level, current density, and temperature is being conducted to characterize a range of operation.

Table 1. Current Understanding of Coal-Derived Contaminant Effects on MCFC

Contaminant (Max. ppm Occurrence)	Short-Term 300 cm^2 Bench-Scale Performance Tolerance	Reaction Mechanism @ 650°C/1 atm Pressure	Conclusions
NH_3 10,000	No effect w. 1 v/o NH_3 injected in fuel ahead of cell. Greater than 95% passes through.	$2NH_3 \rightarrow N_2+3H_2$ With SS-oxide catalysis, equilibrium NH_3 concentration @ 650°C in coal-gas is 55 ppm.	10,000 ppm NH_3 from high temp/pressure gasifier dissociates down to 100 ppm at FC temp/pressure.
Cd 5	No effect w. 30 ppm Cd, such additions, however, clog exit manifold pipes with Cd/CdO.	$Cd(v)+H_2O \rightarrow CdO(s)+H_2$ No serious oxide formation inside cell even w. high fuel utilization.	Cd effects appear to be much less serious than those due to Zn contamination.
Hg 0.5	No effect w. 35 ppm Hg, as done by thermogravimetric (TGA) experiments.	No reactivity.	Mercury is least reactive of all suspect species.
HCl 500	No effect w. 0.1 ppm HCl injected in fuel ahead of the cell with much of it recovered as KCl in exit gas.	$HCl(g)+K^++e^- \rightarrow KCl(g)+\frac{1}{2}H_2$ Removal of K_+ from electrolyte by HCl is a long slow process. No direct Ni-interaction was noted.	No direct in-cell polarization effects. Carbonate loss from transfer outside cell is a concern.
H_2S 15,000	Minor effect w. 1 ppm H_2S injected in fuel ahead of cell. Performance is recovered upon OCV and removal of contaminant.	$xH_2S+Ni \rightarrow NiS_x+H_2$ Ni-surface adsorbs sulfur causing anode polarization which is reversible using high H_2 activity.	Minor surface adsorbe H_2S recovered under OC conditions. Shortterm tolerance up to 5 ppm H_2S.
H_2Se 5	No effect w. 0.5 ppm H_2Se injected in fuel ahead of cell. Performance is recovered upon OCV and removal of contaminant.	$xH_2Se+Ni \rightarrow NiSe_x+H_2$ Same type of reversible adsorption noted as with H_2S.	Minor surface adsorbe H_2Se poisoning also recoverable. Se of little concern after coal-gas cleanup.
Zn 60	No effect w. 15 ppm zinc vaporized in fuel ahead of the cell. Performance drop with 35 ppm not recoverable employing OCV.	$Zn(v)+H_2O \rightarrow ZnO(s)+H_2$ Increasing steam and decreasing H_2 activity in fuel, drives the reaction to the right.	ZnO deposits can clog anode pores depending on fuel utilization. Tolerance is for average fuel conversion.

Table 1. Current Understanding of Coal-Derived Contaminant Effects on MCFC
(Continued)

ontaminant (Max. ppm ccurrence)	Short-Term 300 cm^2 Bench-Scale Performance Tolerance	Reaction Mechanism @ 650°C/1 atm Pressure	Conclusions
b 15	Not yet MCFC tested.	TGA showed some wt. gain. There is a possibility of alloy formation with dry, porous Ni-plaque.	Metal vapors, if no oxides form, do not react with carbonate wetted components.
sH_3 10	No immediate effect w. 1 ppm AsH_3 eventual polarization effects result from stable NiAs formation.	$As^{3-}+Ni(s) \rightarrow NiAs+3e^-$ As^{3-} ion derives from $AsH_3(g)$ dissolving in the carbonate melt.	Stable NiAs reaction product accumulating on anode surface is not as easily purged as sulfur or selenium.
n 3	No effect of Sn itself SnS injected @ 40 ppm in fuel, showed only the typical sulfur effects.	$SnS(g)+H_2O \rightarrow SnO(s)+H_2S$	Fuel humidification precludes any Sn from reaching the cell.

ESULTS

ignificant progress has been made in defining the "safe" MCFC tolerance levels for lmost all species, as shown in ERC's Table 1.

s of the time of writing of this paper, ammonia testing at 1,000 degrees centigrade ad been completed for the SOFC. Results indicate that NH_3 level up to 5,000 parts er million dissociated into H_2 and N_2 and had no deleterious performance effect on OFC operation.

UTURE WORK

n the MCFC program, individual contaminant testing will be followed by a combined ontaminant testing effort consisting of three, fairly long-term (4,500 hours), bench-cale cells for which 7 out of 10 contaminants have been selected for consecutive ddition. This will be at their nominally tolerant concentrations in fuel gas, until ll these species are simultaneously present. The last task in this program will ntail a complete modeling effort to achieve a synthesis of all the data. Projections ay then be made to assist in future, integrated systems analyses.

n the SOFC program, testing will be continued for H_2S and HCl. An analytical study ill be completed to identify any additional characterization testing concerning coal-as trace contaminants.

MCFC MATERIALS RESEARCH AT THE NETHERLANDS ENERGY RESEARCH FOUNDATION ECN.

L.Plomp, F.P.F. van Berkel, J.B.J. Veldhuis, and S.B. van der Molen.
Netherlands Energy Research Foundation ECN
P.O. Box 1, 1755 ZG Petten,
The Netherlands.

Introduction.

The MCFC materials research and development programme at ECN aims at the improvement of long term performance through reduction of anode and cathode degradation.
The paper describes the anode microstructure change caused by the lithiation process and shows the effects on the electrical performance of the anode. The NiO dissolution appears to be the main life limiting process for the MCFC. Experimental results are compaired with modelling of the dissolution process. Furthermore, results on alternative cathode materials will be presented.

Anode materials.

Due to lithiation during cell operation part of the Cr in the Ni-11at%Cr alloy was transformed into LiCrO2. After the test the largest part of the Cr content is found at the grain boundaries, whereas the Cr was distributed rather well over the grains before the test. The process of lithiation occurs mainly in the first 1000 hours of operation (Figure 1). The remaining equilibrium Cr-content (3at%) is found in the Ni-grain as determined by XRD and SEM/EDX, which indicates the presence of Cr-oxide in the grains of Ni-Cr alloy. It can be concluded that the formed $LiCrO_2$ drastically changes the anode microstructure.
Besides Ni-Cr, the use of Ni-Al alloys as anode material is under investigation, because of their higher electrical performance. The lithiation process here gives $LiAlO_2$ and a similar diffusion of the Al to the grain boundaries. In spite of rather large changes in microstructure, cell tests (Table 1) for Ni-Cr and Ni-Al anode materials showed low contributions to the cell degradation.

Table 1. Degradation of cell performance in mV/1000h

Anode material	Ni-Cr	Ni-Cr	Ni-Cr	Ni-Cr	Ni-Al	Ni-Al
Operation time in hrs	2980	3032	3025	5459	3857	8746
Anode polarization	1.0	1.4	0.0	1.0	0.0	1.0
IR anode-reference	0.0	0.6	0.0	1.0	0.0	0.0
Cathode polarization	2.4	2.7	4.0	5.8	1.8	5.0
IR cathode-reference	2.4	1.8	3.5	1.4	2.1	0.6

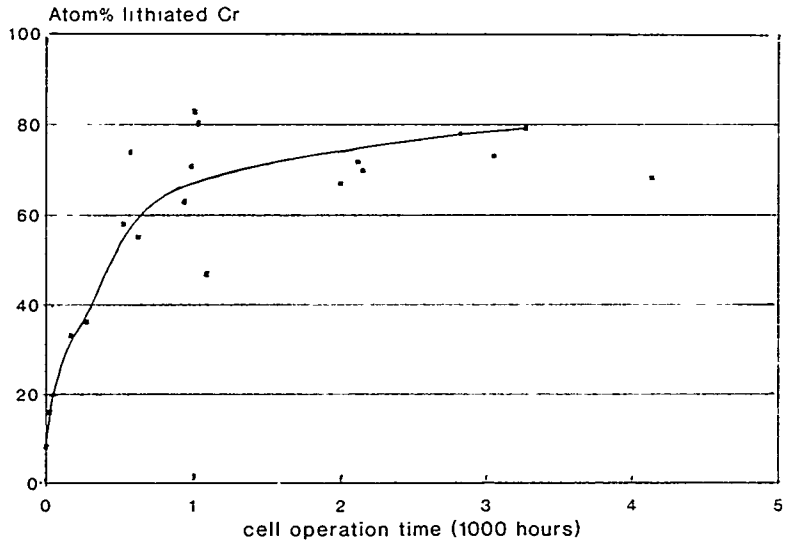

Figure 1. The atomic percentage of chromium converted to $LiCrO_2$ during cell operation.

Dissolution of NiO cathodes.
The dissolution of NiO cathodes was studied by observation of the location and amount of nickel found in the matrix-tile after cell testing in lab-scale (3 cm^2) cells at the usual conditions.
The dissolution rate for nickel was found to range from 7μg/cm^2h for operation times less than 1500 h to 2μg/cm^2h for a 20 000 h test.

The precipitation zone of nickel in the matrix tile showed a diffuse boundary at the cathode side and a sharp boundary at the anode side of the matrix-tile. These boundaries shifted to the anode during cell-operation, the latter more rapidly than the first. This resulted in an increase of the precipitation zone thickness. Note that, due to the increasing distance to the cathode, short-circuiting of the cell is not likely to occur. The diffuse boundary at the cathode side is thought to originate from the non-homogeneous transport of oxidizing and reducing species through the porous matrix-tile. The observed linearity of the anodic precipitation distance to the cathode interface, versus the square root of time suggests a diffusion mechanism. This phenomenon is not observed at the cathode side of the precipitation zone.

A simple model (1), based on the Nernst-Planck equation, was developed for the transport of nickel ions and oxygen entities from a flat nonporous cathode through a porous matrix to the precipitation zone, and hydrogen molecules from the anode to the precipitation side. Apart from the difussion and migration fluxes, it was necessary to introduce a (convectional) flux associated with the transport of nickel ions due to an interaction of these ions with the motion of the carbonate ions which carry the cell's current. This would enhance the transport of oxidizing species and diminish the transport of reducing species. From this model the precipitation distance and dissolution rate could be calculated. The model was fitted to the experimental results. The obtained figures accounted for the observed changing precipitation distance and dissolution rate for the nickel ions.

Alternative cathode materials.
The ECN research on new MCFC cathode materials was initially concentrated on $LiFeO_2$, properly doped to obtain sufficient electrical conductivity. Recently, also $LiCoO_2$ was taken into consideration (2). Both materials showed lower corrosion-rates than NiO. Porous cathode structures of these materials were made by means of tape-casting and sintering. These structures, as well as state-of-the-art (*in situ* formed) lithiated NiO cathodes, have been tested in lab-scale MCFC's. It turns out that there are significant differences in the polarization behaviour of NiO, $LiCoO_2$,and $LiFeO_2$ cathodes, as may be seen from the *iV*-characteristics presented in Figure 2.

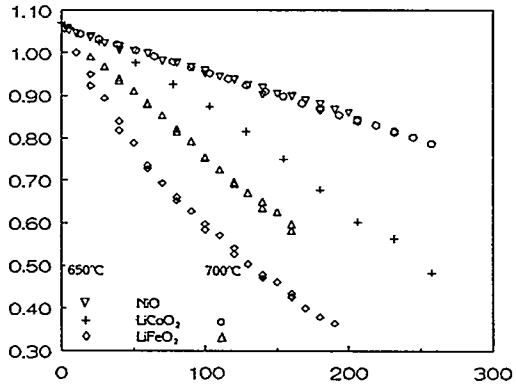

Figure 2. Cell potential (V) as a function of current density *i'* (mA/cm^2) for the three cathode materials.

The *iV*-characteristics were obtained through varying the cell current-load. These experiments were accompanied by current-interrupt measurements, utilizing oxygen reference electrodes, to extract *iR*-free cathode overpotentials. To elucidate the observed differences in polarization behaviour of the three cathode materials mentioned, a simple electrode-model was fitted to the experimental overpotentials. From these fits it could be concluded that at 650 °C NiO cathodes have a mass transfer controlled behaviour, while $LiFeO_2$ cathodes have almost complete kinetic control. For $LiCoO_2$ mass transfer and kinetics turn out to be about equally important.

Assuming current densities are related to the surface area as determined with mercury intrusion, absolute values could be obtained for the apparent exchange current densities i_0 and the limiting current densities i_l of the cathodes tested. Where i_0-values for $LiCoO_2$ differ less than one order of magnitude from those of NiO, $LiFeO_2$ has an i_0-value which is about *two orders* of magnitude lower. Values for i_l appear to be all on the same level. Therefore, the relative bad performance of $LiFeO_2$ cathodes is probably due to slow kinetics. $LiCoO_2$ on the other hand, seems to be much more promissing for application as an MCFC cathode material.

Acknowledgement
Financial support from the *Nederlandse maatschappij voor energie en milieu bv* (NOVEM) is greatfully acknowledged.

References

(1) J.B.J. Veldhuis, R.C. Makkus, S.B. van der Molen, G.H.J. Broers, Ber.Bunsenges.Phys.Chem. in press.
(2) L. Plomp, E.F. Sitters, C. Vessies, and F.C. Eckes, submitted.

COPPER-BASED ANODE

E. T. Ong, R. A. Donado, K. E. Hrdina
Institute of Gas Technology
3424 South State Street
Chicago, IL 60616
(312) 567-3650

Among the non-noble metals, Co, Ni and Cu are the only ones that may be considered for use as a molten carbonate fuel cell anode. Copper is most desirable because of its cost and availability. However, its exchange current density, a measure of electrochemical reaction rate, is just about half that of nickel.[1] Most notably, the toughest challenge facing the development of a copper anode is combating its creep property. The comparative creep behavior of unstabilized porous copper and porous nickel at 650°C and 50 psi load, as shown in Figure 1, clearly demonstrates this property.

Different approaches to stabilizing copper against creep have been tested at IGT. A composite copper anode structure has been produced which matches the creep stability of the baseline Ni + 10% Cr anode. It has been successfully operated in a 3-cm^2 laboratory-scale cell for 2000 hours with a good, stable performance. Its creep behavior at 650°C and 100 psi load is compared to that of the standard Ni + 10% Cr anode in Figure 2, and its cell performance lifegraph is presented in Figure 3. Its steady-state cell potential of 845 mV at 160 mA/cm^2 was about 40 to 50 mV lower than normally obtained for standard Ni + Cr anode. This lower cell potential was mainly due to higher polarization at the copper anode.

The higher polarization losses observed at the copper anode was a combination of a slower anode reaction rate and an unoptimized pore structure. For the cell presented in Figure 3, the anode polarization was 70 mV at 160 mA/cm^2. On the other hand, anode polarization of only 25 mV is obtained for Ni + Cr anode. The latter may be broken down to 9 mV Nernst loss and 16 mV activation and concentration polarization.

The activation polarization, for practical purposes, may be considered inversely proportional to the exchange current density. The exchange current density for Ni and Cu at 650°C with a high-Btu fuel was determined to be 50 and 28 mA/cm^2, respectively. Therefore, one would expect the activation polarization of the copper anode to be about twice as high as that for the Ni-based anode. This would be 32 mV at most, based on the 16 mV polarization observed with the Ni + Cr anode. Hence, the high anode polarization observed for the cell shown in Figure 3 was mostly concentration polarization which can be minimized through anode pore structure optimization.

Reference

1. Lu, S. H. and Selman, J. R., "Electrode Kinetics of Fuel Oxidation on Copper in Molten Carbon," J. Electrochem. Soc., 131, 2827 (1984).

Acknowledgment

The Electric Power Research Institute (EPRI) has been supporting this work under EPRI Contract RP-3059-2.

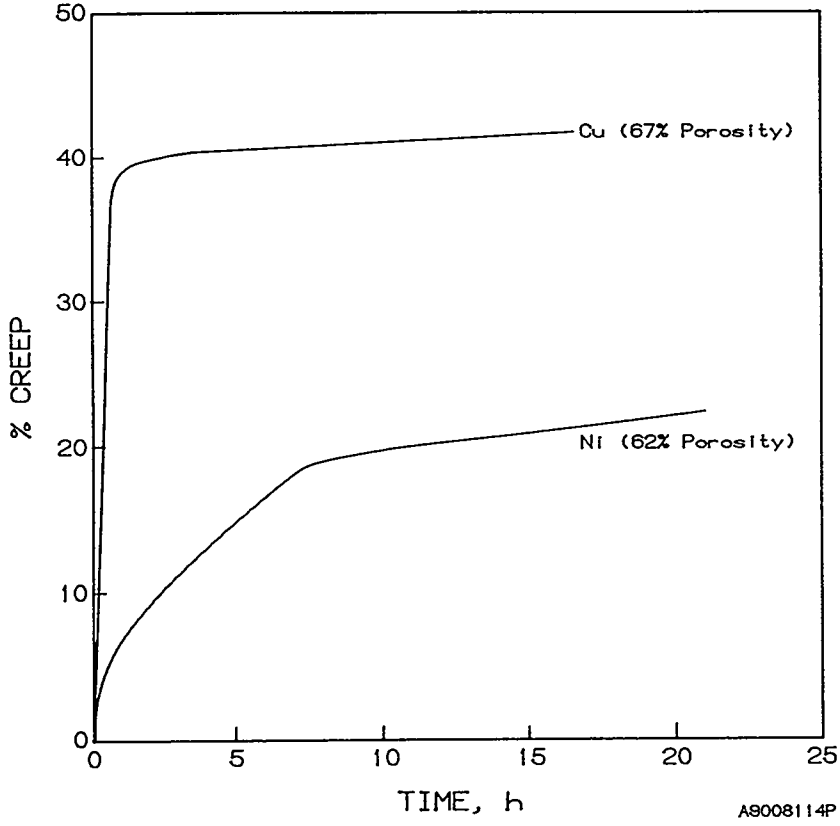

Figure 1. Comparative Creep of Porous Copper and Nickel at 650°C and 50 psi Load

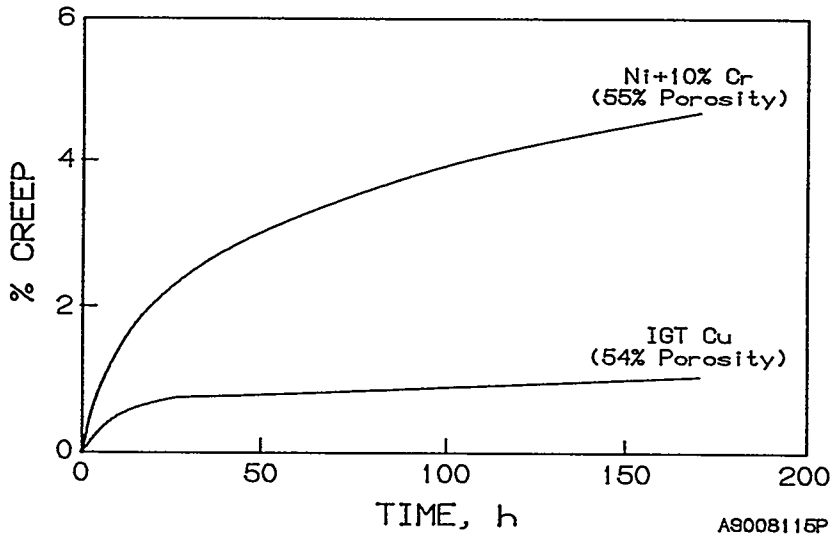

Figure 2. Comparative Creep at 650°C and 100 psi Load of IGT Stabilized Copper Anode and of Standard Ni + 10% Cr Anode

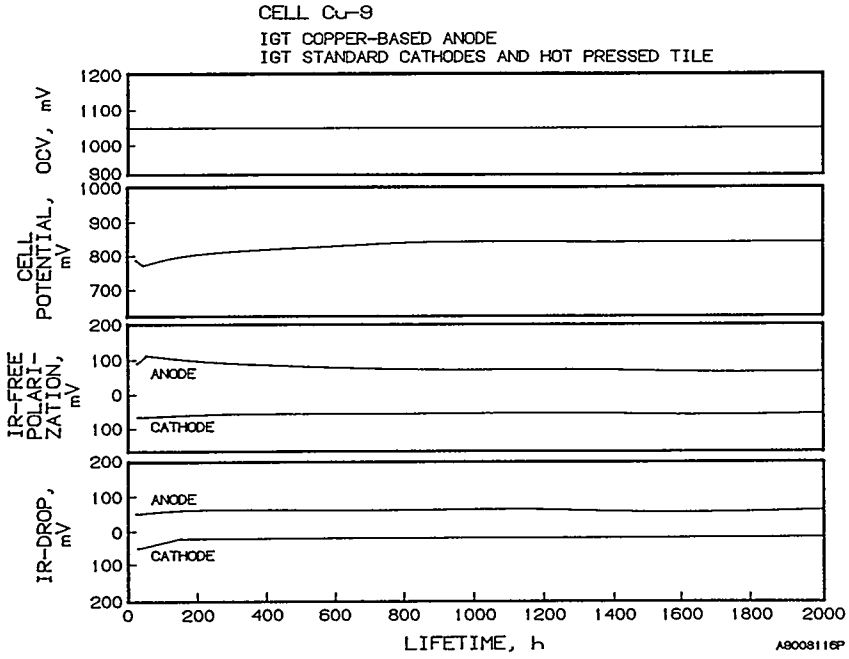

Figure 3. Cell Performance Lifegraph of IGT Stabilized Copper Anode

RESULTS OF 100KW METHANOL FUELED PAFC PILOT PLANT AND RECENT CELL TECHNOLOGY DEVELOPMENT

Hidekazu Ishioka, Tetsuo Koshimizu
The Hokkaido Electric Power Co.,Inc.
1-2,Odori-Higashi, Chuo-ku, Sapporo 060, Japan

Hideaki Miyoshi, Yoichi Mizumoto
Masaaki Matsumoto, Hideaki Tomei, Kazuo Usami
Mitsubishi Electric Corporation, Kobe Works
1-1-2, Wadasaki-Cho, Hyogo-Ku, Kobe 652, Japan

1.INTRODUCTION

The Hokkaido Electric Power Co.,Inc. (HEPCO) and Mitsubishi Electric Corp. (MELCO) have developed the PAFC (phosphoric acid fuel cell) power plant for electric utility use under the joint program. The 100kW PAFC pilot plant was constructed at Date Thermal Power Station. The operation study and evaluation were succesfully carried out from November 1987 to May 1989.

MELCO has been performing R&D of PAFC technologies since 1981 aiming at an early commercial use. We have developed several stacks for demonstration power plants and carried out basic research to improve performance and reliability of stacks.

This paper presents some results of 100kW methanol fueled PAFC pilot plant and recent cell technology development activities at MELCO.

2. RESULTS OF 100KW METHANOL FUELED PAFC PILOT PLANT

The objectives of operation study are as follows: (1) verification of plant operation performance, (2) verification of maintenance, safety and reliability, (3) examination of grid connected or grid independent operation, (4) confirmation of enviromental acceptability, (5) investigation of heat recovery characteristics.

Table 1 shows specifications of the pilot plant. This plant consists of a fuel processor, a fuel cell stack, a inverter, a heat recovery subsystem and a control unit. Figure1 shows process flow diagram of this plant and Figure 2 shows out view of this plant.

TABLE 1 SPECIFICATION OF 100 KW PILOT PLANT

ITEM	SPECIFICATION
Fuel Cell Type	Water Cooled PAFC
Output Power	100 kW AC
Efficiency	36% (HHV Base)
Overall Efficiency	79% (HHV Base)
Fuel	Methanol
Load Following	25 → 100% in 5 min

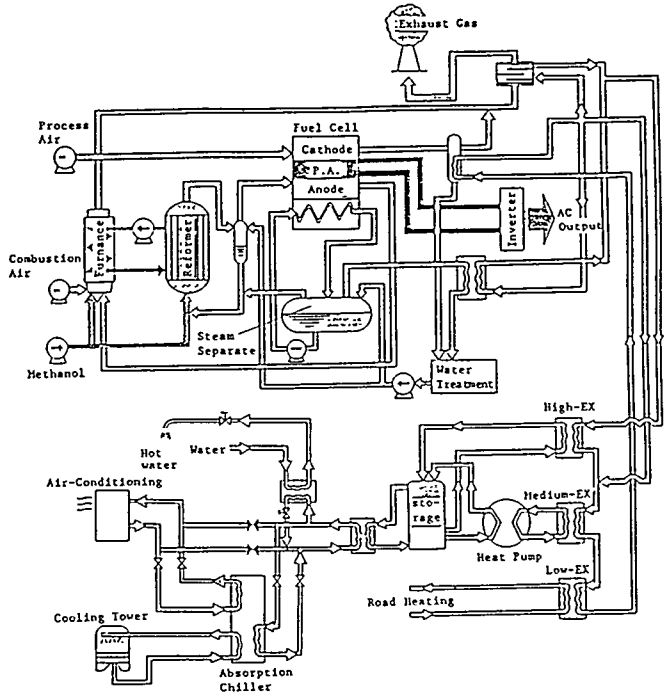

FIGURE 1 PROCESS FLOW DIAGRAM OF 100KW PILOT PLANT

FIGURE 2 100KW METHANOL FUELED PAFC PILOT PLANT

After the inspection by MITI, operation tests began in the begining of November 1987. Operation modes of this plant are DSS (dayly start and stop), WSS (weekly start and stop) and continuous operation. Table 2 summarizes field test results of this plant. The design targets were succesfully achieved.

Figure 3 shows the cell performance of the 100 kW pilot plant. The voltage decay after 4575 hours operation was 5.2% of the initial voltage. The voltage decay after 40000 hours operation was estimated to be 7.7%.

TABLE 2 FIELD TEST RESULTS OF 100KW PILOT PLANT

ITEM	RESULTS	TARGET VALUE
Generated Power	330,323 kWH	
Operation Time	4,575 Hrs	
Start-stop Cycle	245 Times	
Start-up Time (Cold)	2.0 Hrs	2.0 Hrs
(Hot)	1.5 Hrs	
Load Following	30%/min	15%/min
Efficiency	37.1%(Initial)	36% (HHV Base)
NOx Emission	< 1 ppm	< 20 ppm

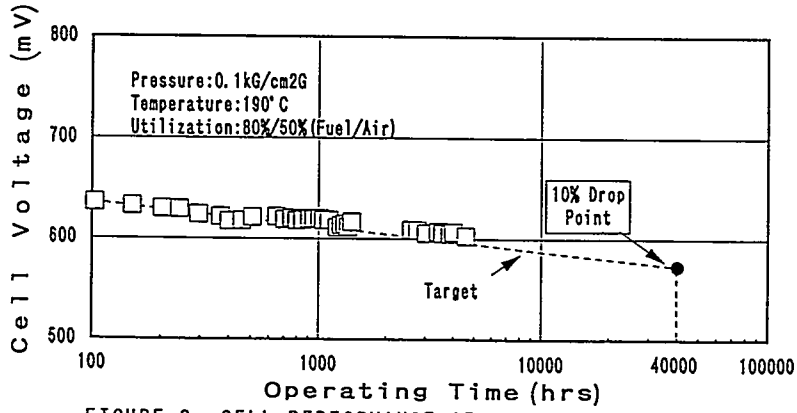

FIGURE 3 CELL PERFORMANCE OF 100 KW PILOT PLANT

3. RECENT CELL TECHNOLOGY DEVELOPMENT ACTIVITIES AT MELCO

Figure 4 shows the recent progress in the cell performance. Improvements of these cell perfomance were achieved by following cell technology developments: (1) improvements of catalyst activity and stability, (2) reduction of cell resistance by using thinner matrix, (3) development of alternative cell and stack configurations, (4) improvement of gas flow distribution.

Figure 5 represents typical features of improved performance and stability of short stacks with 3600cm² class electrode area. Stack A (21-cell) was tested for about 16000 hours (1987 -1989) and Stack B (18-cell) has been tested for over 4000 hours to date since December 1989. The voltage decay rate for the stack A and the stack B are 3-4 mV/1000 h and less than 2 mV/1000 h respectively.

The technical problems on PAFC have almost been solved and our program is focussed on subjects aiming at cost reduction and compactness.

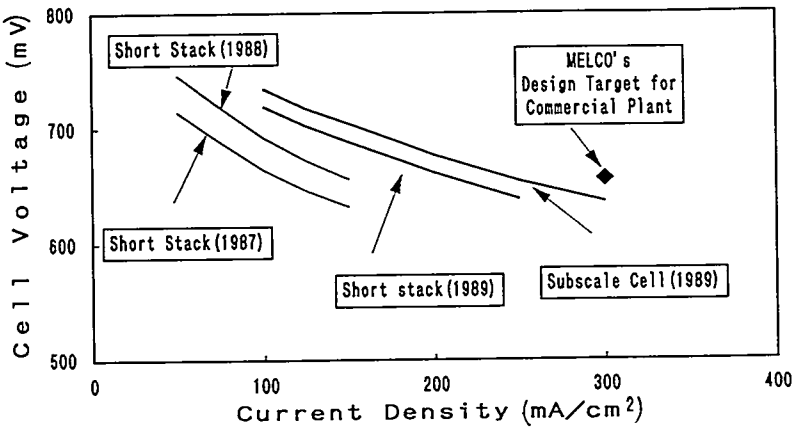

FIGURE 4 RECENT PROGRESS IN CELL PERFORMANCE

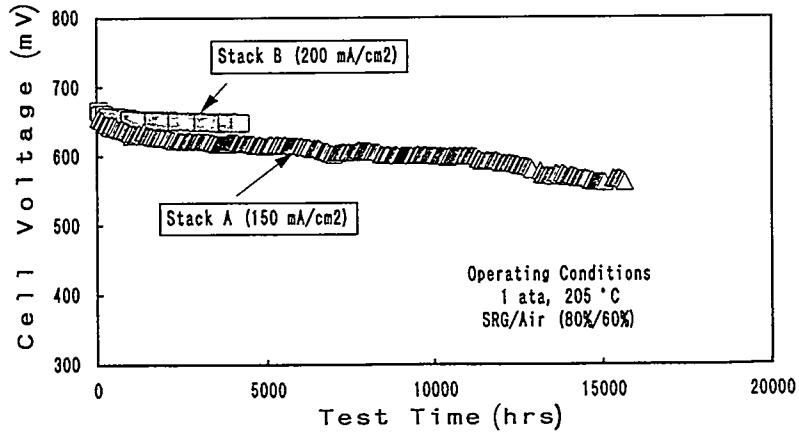

FIGURE 5 CELL PERFORMANCE OF SHORT STACKS

DEVELOPMENT OF 200kW PHOSPHORIC ACID FUEL CELL SYSTEM FOR DETACHED ISLANDS

T. Nogi
Fuji Electric Co., Ltd.
7 Yawata-Kaigandori, Ichihara, Chiba 290, Japan

T. Toma
The Okinawa Electric Power Co., Inc.
2-1, 5-chome, Makiminato, Urasoe Okinawa, 901-21, Japan

H. Yamazaki
New Energy and Industrial Technology Development Organization
Sunshine 60, 1-1, 3-chome,
Higashi-Ikebukuro Toshima-Ku, Tokyo, Japan

1. Introduction

This research and development, a part of the Moonlight Project by the Agency of Industrial Science and Technology, the Ministry of International Trade and Industry, has been promoted by New Energy and Industrial Technology Development Organization (NEDO).
The development of this system was started in 1986 and is planned to be finished with operational research scheduled till March 1991. This five year project was jointly undertaken by The Okinawa Electric Power Co., Inc. (conducting the system research and operational study) and Fuji Electric Co., Ltd.(carrying out the system development, design and manufacture of the plant) The schedule is shown in Table 1.

Table 1 Schedule of Research and Development

Fiscal Year	1986	1987	1988	1989	1990
R & D of Fundamental Technologies	▬	▬			
System development & Design	▬	▬			
Manufacturing Adjusting & Testing		▬	▬	▬	
Operational Study				▬	▬

There are more than 300 inhabited, detached islands around Japan. In almost all of them, power is supplied by diesel generators. In a detached island, electrical load fluctuates greatly not only during the day and annually. Fuel cells will be effective for such power demand since the generating efficiency is fairly constant at partial load.
Diesel generating plants totaling 1,900 kW have been installed in Tokashiki Island in Okinawa Prefecture, and the power system configuration includes the four neighboring islands.

The main purpose of this development is to investigate the parallel operation of a fuel cell system interconnected with the power system of the diesel generators.

2. Test Results
In October 1989, the fuel cell plant was interconnected to the power system in Tokashiki Island and successfully placed into operation.
Main test results so far obtained are shown in Table 2.

Table 2 Main Test Results

Items		Design	Results
Gross output		—	215 kW
Net output		200 kW	202 kW
Efficiency	Overall	> 37 %	39.7 %(H.H.V.)
	75% load	—	40.6
	50%	—	36.7
	20%	—	22.9
Cold start-up time		< 3 hr	3 hr
Load response (20-100%)		< 30 sec	25 sec tested before shipment
Harmonic voltage distortion increase		< 3 %	no change
NOx emission (O_2 7%)		regulated level	2 ppm
SOx emission			less than 1 ppm
Total generating time, as of August 31, 1990			3,600 hours
Total generated power, as of August 31, 1990			493,000 kWh

3. Features of the System
The system for detached islands is a pre-commercial prototype phosphoric acid fuel cells unit.
In this system, methanol is used as raw fuel which is comparatively easy to obtain, store, and handle in detached islands. The methanol reforming unit consists of a reformer heated indirectly by hot-oil and a hot-oil heater with catalytic combustor with a high load response.
The methanol-processing equipment is contained in a divided zone of the package. The power conditioning system is installed in the control house.
The generating unit has a packaged construction for outdoor use to shorten time for transportation and installation. First generating operation at site was carried out effectively for 3 weeks after the installation of the package inspite of the influence by typhoon.

The view of 200kW PAFC system is shown in Figure 1, the main system configuration, in Figure 2, and the electrical system diagram, in Figure 3. And Figure 4 shows a daily load sharing curve of Tokashiki power system.

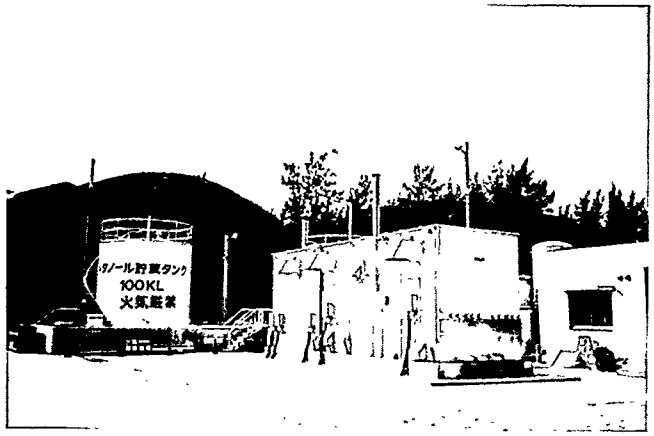

Figure 1 The view of 200kW PAFC system

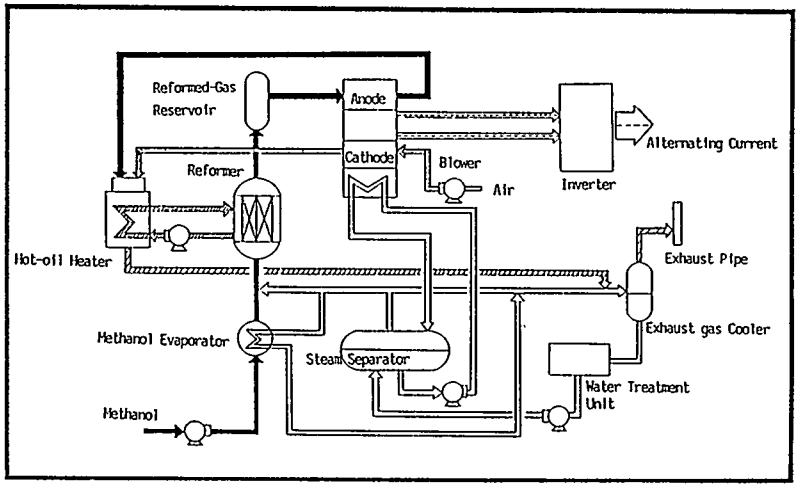

Figure 2 Main System Configuration

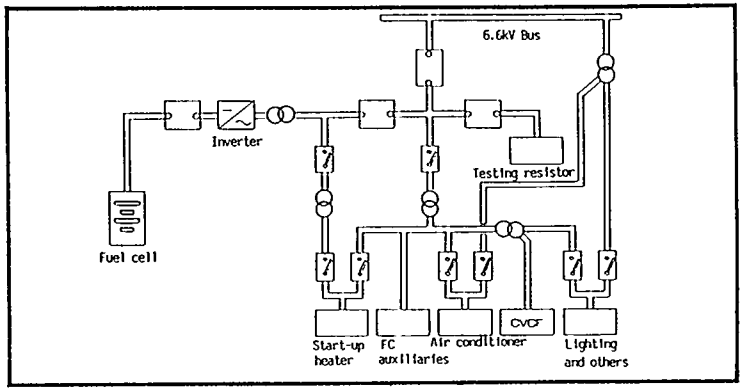

Figure 3 Electrical System Diagram

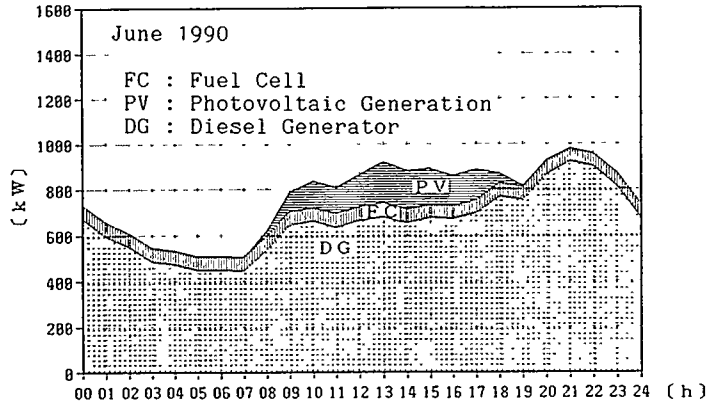

Figure 4 Daily Load Curve of Tokashiki Power System

4. Conclusion

A fuel cell power plant for detached islands was developed and was interconnected to the power system used by the islanders. Transmission operation was successful. Practical use was demonstrated.

The packaged unit verified availability in short term transportation and installation, which is a valuable step toward commercialization.

5. Acknowledgement

In preparing this presentation, we would like to acknowledge the continuing guidance and suggestions of the members of Agency of Industrial Science and Technology.

DEVELOPMENT OF ON-SITE PAFC BASED ON NAPHTHA AND KEROSENE

Shigeru Yanagida
R&D Section Yokohama Refinery
Nippon Petroleum Refining Co.,Ltd.
390 Koyasu-dori 3 Chome, Kanagawa-ku
Yokohama 221, Japan

Tomonori Sioiri, Shinichi Satake
R&D Group R&D Dept.
Nippon Oil Co.,Ltd.
3-12, Nishi Shimbashi 1-Chome, Minato-ku
Tokyo 105, Japan

INTRODUCTION

As part of the research activities sponsored by the Petroleum Energy Center(PEC), Nippon Oil Company(NOC) has been developing a commercial size PAFC plant utilizing Naphtha and Kerosene as feedstocks.
PEC is a foundation to carry out research on the various sectors relating to the usage of the petroleum energy.

The main hydrogen source to PAFC system has been LNG or town gas. However, it is now technically/economically feasible to produce hydrogen from petroleum products, because

1) unit fuel cost is lower than LNG or town gas with same heating value.
2) existing infrastructures for petroleum product transport /storage/delivery can be used for fuel cell feedstock delivery.

As shown in table 1, clean(low sulfur) petroleum products such as light naphtha for petrochemical use or home heating kerosene are considered as major commodity products. Since no major investment would be required for handling light naphtha/kerosene for fuel cell use, NOC has been innovating technology to produce hydrogen from these petroleum products.

TABLE 1
CHARACTERISTICS OF NAPHTHA AND KEROSENE

	LIGHT NAPHTHA	KEROSENE
Specific Gravity (15/4°C)	0.64	0.82
Sulfur Content (wt.ppm)	0.3	0.5
Boiling range (°C)		
IBP	28	198
50%	39	220
90%	53	241
EP	72	258
Hydrocarbon Type (%)		
Paraffinic	95	90
Naphthenic	0	
Olefinic	4	1
Aromatic	1	9

NOC PAFC RESEARCH ACTIVITIES

Since sulfur/carbon contents in petroleum products are higher than those in LNG or town gas, special technology needs to be developed to desulfurize and reform petroleum products. NOC has developed desulfurizing and reforming process for naphtha and kerosene by using experimental bench scale reactor. Based on this experimental work, naphtha base PAFC power plant(200kW) and kerosene fuel processing unit for 200kW class PAFC system have been installed for demonstration purposes.

NAPHTHA BASE PAFC PERFORMANCE TEST

Naphtha base PAFC performance test has been carried out by use of the custom-made equipment package including desulfurizer,reformer,cell stack and inverter(see Fig.1). With NOC desulfurization technology, the package is designed and manufactured by International Fuel Cells Corp.(Conneticut U.S.A.) as the world first model for naphtha as a fuel, although there are several experiences in LNG.

The naphtha base PAFC power plant was completed in Jan.1990 and has been in operation since March 1990.

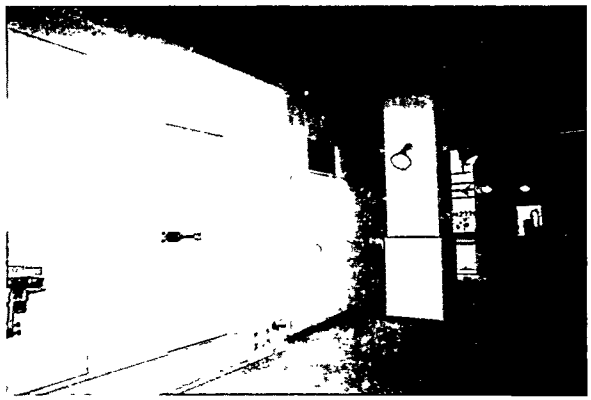

FIGURE 1

NAPHTHA PAFC POWER PLANT

The specification of the plant is shown in Table 2. As a result of performance test the plant has been generating 220 MW over the cumulative operation of 2,200 Hrs.

TABLE 2
SPECIFICATION OF NAPHTHA PAFC POWER PLANT

Name	PC25YX-2N
Power Section	PAFC(Water Cooled)
Feed Stock	Light Naphtha
Desulfurizer	Adsorption Type
Nominal Output Power	130 kWac (NET)
Power Conditioner	Two-stage transistorized Inverter
Voltage	210 Vac, 3 Pase (50 Hz)
Electrical Efficiency	32-35 % (at Nominal Power)
Operation Mode	Fully Automatic

KEROSENE FUEL PROCESSING UNIT

Kerosene fuel processing unit consists of desulfurizer, reformer,shift converter and water treatment section (see Fig.2).

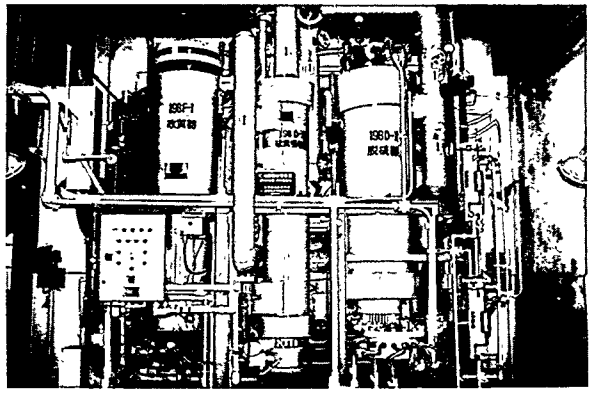

FIGURE 2

KEROSENE FUEL PROCESSING UNIT

NOC have installed the fuel processing unit in Nov.1988 after the detailed basic research jointly with Mitsubishi Kakoki Kaisha Ltd. on reduction of sulfur level of Japanese spec. kerosene from 10-100 wt ppm to 0.1 wt ppm to prevent the deterioration of the reformer catalyst.

The reformer is the world first product manufactured by Haldor Topsoe A/S, Denmark. This Heat Exchange Reformer is very compact in size requiring very small installation area.

The performance test of the kerosene fuel processing unit has been carried out since Jan.1989. The test result shows that:

(a) Load can be followed between 25% and 100% of design capacity within one minute.
(b) Cold start up takes 4.5 Hrs. while restart of the plant requires 30 minutes.
(c) Product gas component is as follows:
H2 : 73-74% , CH4 : 1%
CO : 0.5% , CO2 : balance
(d) Cumulative operation time is 4,850 Hrs.

FUTURE NOC PAFC RESEARCH ACTIVITIES

The naphtha base PAFC power plant and the kerosene fuel processing unit continue to be in operation to verify good performance, followed by detaile studies on kerosene base PAFC system especially on kerosene FPS and power generation system.

PEC wish to have demonstration operation of several 50-200 kW naphtha/kerosene base PAFC power plants in 1992-1994. We beleive that NOC technologies will contribute to this project.

We trust that these research activities will lead to successful development of the naphtha/kerosene base PAFC power plant, and they would be used for co-generation system or transportation system in the future.

DEVELOPMENT OF ON-SITE PAFC FOR COGENERATION IN TOKYO GAS

MASANORI KAIZAKI, SHOUICHI KANEKO, MOTOICHI IKEDA
R&D INSTITUTE OF TOKYO GAS
SHIBAURA, MINATO-KU, TOKYO 103, JAPAN

INTRODUCTION AND SCHEDULE

Tokyo Gas Co., has developed 50kW Phospholic Acid Fuel Cell unit (FP-50) as a joint development project with Fuji Electric Co. This paper describes targets of the project and test results of FP-50 as a cogeneration system.

The project had started in 1987. Some developments of components and system design had been carried out during 1988 and 1989. The complete system had been manufactured and installed at R&D Institute of Tokyo Gas in the beginning of 1990. (see Figure 1) After obtaining the Japanese government approval as a 50kW power station in April 1990, we have been carrying out various performance tests of FP-50. The acumulating generating time had become 2500 hrs by the end of August 1990.

OBJECTIVES AND TARGETS

The objectives of the project is to gather the state-of-the-art technologies of Japanese PAFC manufacturers so as to get the commercial prospect of on-site PAFC cogeneration system in Japan.

The main target of the project is size reduction (0.11m2/kW), which is the essential step to cost reduction and commercialization. The compactness of cogeneration system is indispensable condition in Japan where the system are required to be installed in a narrow space such as in a basement floor or on a roof floor.
The target performances were decided to be 40% of electrical efficiency with 40% of total heat recovery efficiency (LHV).

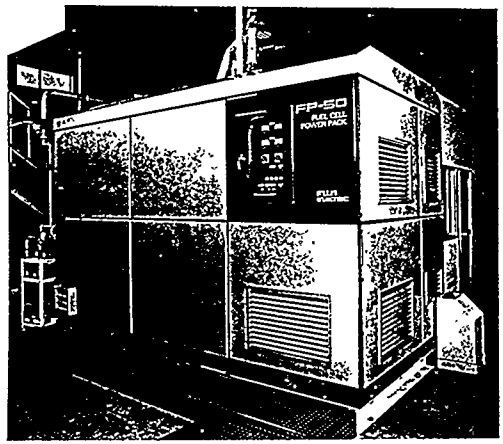

Figure 1 50kW PAFC UNIT (FP-50)

DEVELOPMENT OF THE SYSTEM

In order to accomplish the target performances, we have carried out following developments of components.
(1)Development of compact reformer (see Figure 2)
(2)Development of compact shift converter (see Figure 3)
(3)Development of ambient temperature desulfurizer (see Figure 4)

Figure 5 shows a process flow diagram of the system. The feature of the system design is simplification by applying following technologies.
(1)Application of plate-fin heat exchange system integrated 5 heat exchangers into 2 heat exchange systems.(H.E.1 & 2)
(2)The system has only 4 control valves operated by a simple preset control system instead of complex feedback control system. The application of the simple control system allowed us to eliminate many measuring equipments from the system.

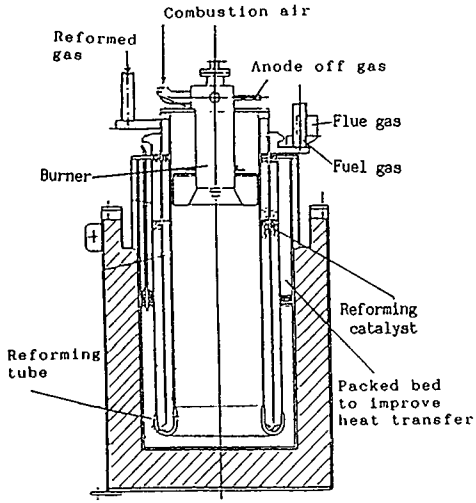

Figure 2

50kW COMPACT REFORMER

single burner and single tube system with packed bed to improve heat transfer

Figure 3

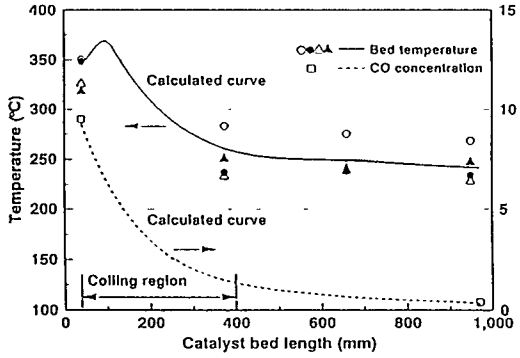

PERFORMANCE OF INNER COOLING TYPE SHIFT CONVERTER

Inner cooling system accelerats reaction by keeping the catalyst bed in rather high temperature range.

Figure 4

PERFORMANCE OF AMBIENT TEMPERATURE DESULFURIZER

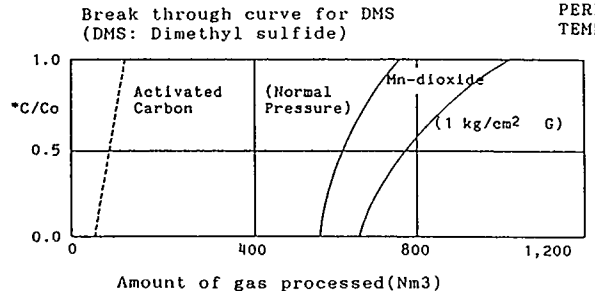

* $C/Co = \frac{\text{DMS outlet concentration}}{\text{DMS inlet concentration}}$

The advanced desulurization material (Mn-dioxide) shows a capacity approx. 10 times larger than that of usual activated carbon.

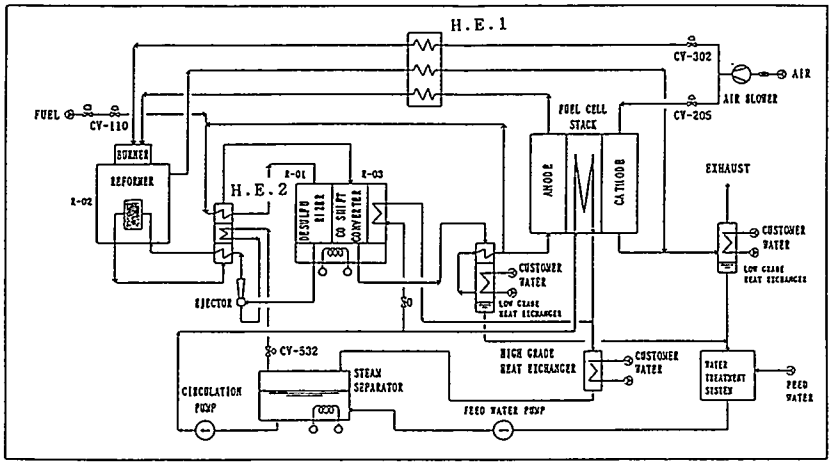

Figure 5 MAIN PROCESS FLOW DIAGRAM OF FP-50
(with hydro-desulfurizing system)

PERFORMANCE TEST RESULTS

Figure 6 shows the electrical efficiency measured over the AC output range from 0kW to 50kW. The target performance of electrical efficiency 40% are accomplished for AC output range from 35kW to 45kW. In the region of AC output less than 30kW, the electrical efficiencies are far below 40%, because some portion of the generated electricity are utilized to generate steam for natural gas reforming. Therefore reducing steam demand for reforming (i.e. low steam carbon ratio in steam reforming) is significant to improve the efficiency even in small AC output region.

Figure 6 also shows the heat recovery efficiencies measured over the same AC output range. The total heat recovery efficiency is approaching to the target value of 40% at the AC output 50kW, when the high grade (170C) heat recovered is around 15% and the low grade (60C) heat recovered is around 25%. The low grade heat is recovered fairly constant over the range of AC output 0kW to 50kW, while the system can not produce high grade excess heat in the range of AC output less than 20kW.

Figure 7 shows the transient response of process parameters when the electric demand instantaniously changes from 20kW to 40kW. All the parameters response instantaniously and are stabilized rapidly at the new value of them. The fractuation of the parameters are within fairly acceptable range to the system.

The wave form of AC output voltage shows fairly good shape of sine curve, having the THD of 3.5%. Since the quality of electricity is becoming important issue for the utilities, developing compact inverter with less THD output is needed.

The NOx emission measured was 2ppm at nominal power generation which is far below the target value 20ppm. The low NOx emission of Fuel Cells is significant and strong advantage in commercializing the system.

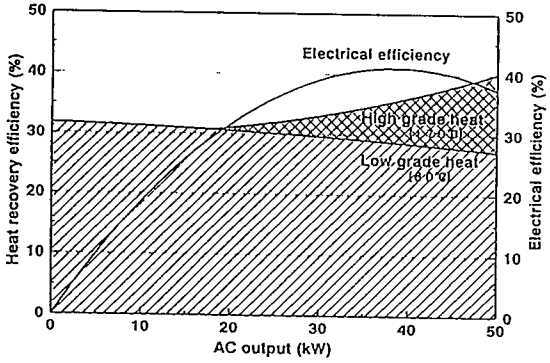

Figure 6

ELECTRICAL EFFICIENCY &
HEAT RECOVERY EFFICIENCIES

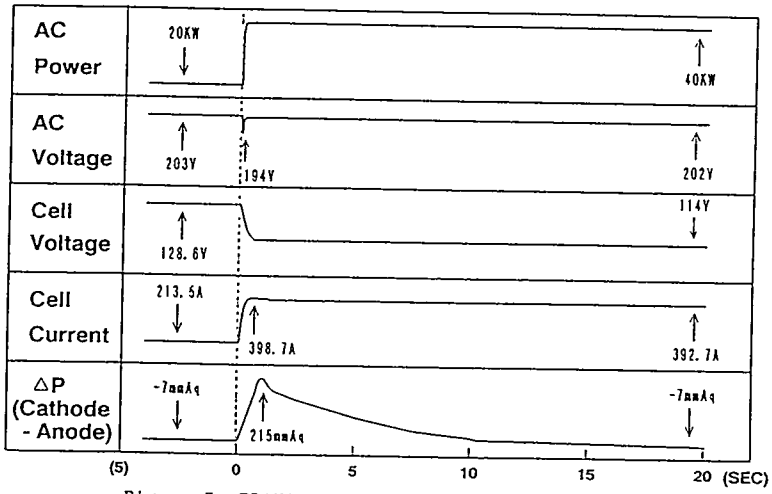

Figure 7 TRANSIENT RESPONSE OF SYSTEM PARAMETERS

CONCLUSIONS AND FURTHER PROSPECT FOR COMMERCIALIZATION

Through the development of FP-50 and the evaluation of the test results, we have obtained encouraging prospect to accomplish cost reduction for commercializing on-site PAFC. Succeeding this project, we had started new project in 1989 to commercialize on-site PAFC with major Japanese gas companies, Osaka Gas Co., and Toho Gas Co., and Fuji Electric Co., as the manufacturer. We are expecting to commercialize on-site PAFC cogeneration unit (Both 50kW and 100kW) by the middle of 1990s.

DEVELOPMENT OF FUEL CELLS FOR COMMERCIAL USE UNDER THE MOONLIGHT PROJECT

T. Omoto
Osaka Gas Co., Ltd.
2-95, 3-Chome, Chiyozaki,
Nishi-Ku, Osaka 550, Japan

H. Tomei
Mitsubishi Electric Corporation
1-2, 1-Chome, Wadasaki-Cho
Hyogo-Ku, Kobe, Hyogo 652, Japan

Y. Yuasa
Kansai Electric Power Company, Inc.
11-20, Nakoji, 3-Chome
Amagasaki 661, Japan

H. Yamazaki
New Energy and Industrial Technology Development Organization(NEDO)
Higashi-Ikebukuro, Toshima-Ku
Tokyo 170, Japan

INTRODUCTION

Osaka Gas and Kansai Electric Power have been involved in Japanese fuel cell development program for commercial use under the Moonlight Project sponsored by MITI(Ministry of International Trade and Industry). This program has been promoted for the purpose of verification of various characteristics of PAFC co-generation system through the field operation of a 200 kW unit. The NEDO is the promotional organ, while Mitsubishi Electric is responsible for development of component technology and manufacturing of the unit, and Osaka Gas and Kansai Electric Power are responsible for co-generation system design and field testing of the unit. The program is promoted as a 5-year plan from 1986 to 1990 as shown in Figure 2.

In July, 1989, the 200 kW PAFC unit was installed at Hotel Plaza, Osaka, Japan. The field operation for more than 5,000 hours has been carried out by the end of August, 1990, and successful results have been obtained in meeting the design goals of the program. Figure 1 shows 200 kW PAFC in operation at Hotel Plaza.

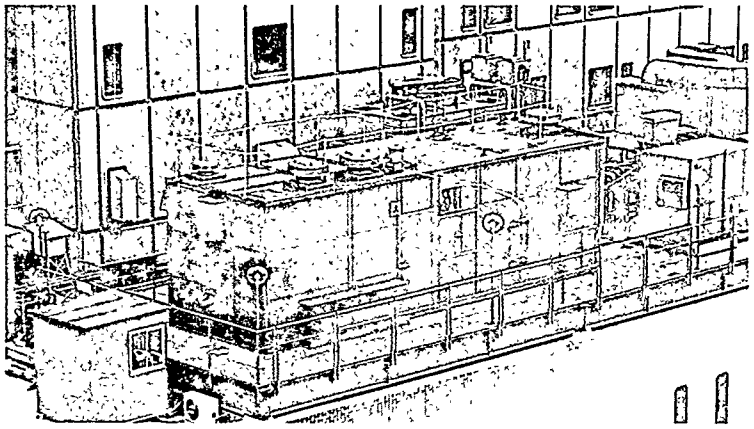

Figure 1 200 kW PAFC at Hotel Plaza

FIELD TEST SYSTEM

The field test system at Hotel Plaza is shown in Figure 3. The fuel cell is connected to the power system (400 V system) on the middle level floors, usually in the grid-connected mode, but by selecting a suitable load branch, grid-independent operation is also possible.

The heat from fuel cell is recovered at 2 levels: high grade heat (170℃ steam) and low grade heat (70℃ hot water). High grade heat (approx. 87 Mcal/h during rated operation)is used as heat source for steam driven double effect absorption chiller & heater (40 RT), which is utilized for the air-conditioning at a part of the hotel rooms. Low grade heat(approx. 124 Mcal/h during rated operation) is supplied to the storage tank for hotel hot water supply through the heat exchanger, which is utilized in kitchens and hotel rooms on the low and middle level floors.

The fuel cell provides approx. 10% of the entire hotel power and approx. 5% of the entire hotel thermal load.

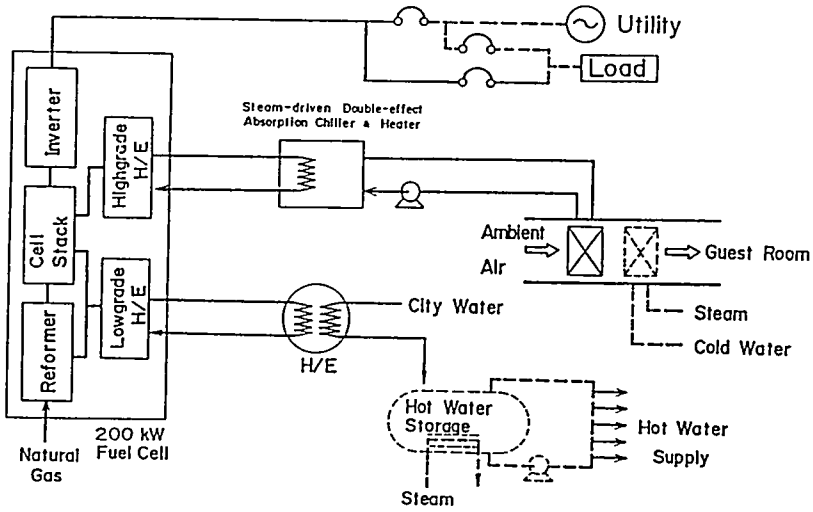

Figure 3 200 kW PAFC Field Test System

OPERATING EXPERIENCE

In July, 1989 the unit was delivered to the test site where, after the adjustment and trial operation, the field operation has been carried out successfully. The accumulated operation time after installation is approx. 5,000 hours including 1,555 hours continuous run as of August 31, 1990.

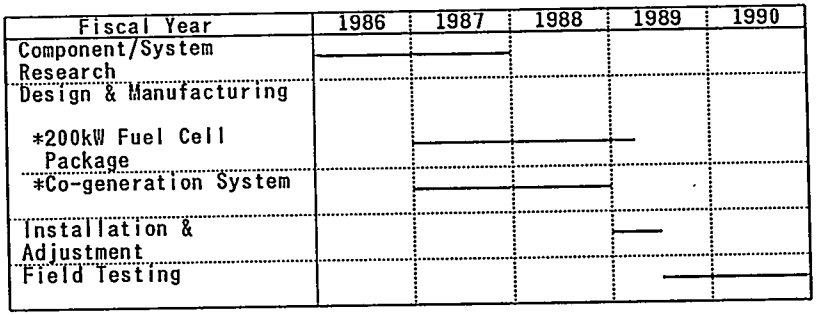

Figure 2 Development Schedule for 200 kW PAFC

FIELD TEST SITE

Hotel Plaza is a standard scale city hotel with 550 guest rooms, and 23 stories above and 3 stories under the ground. The hotel was built in 1969 and has contract power 2,200 kW and is equipped with air-conditioners of 1,250 RT, and boilers of 18 t/h.

200 KW PAFC

The fuel cell system is contained in single package, which has been developed and made first in Japan as such a complete package type on-site fuel cell. The specifications are shown in Table 1. The net power generation efficiency and overall thermal efficiency are as high as 36% (HHV) and 80% (HHV) respectively.

This system is characterized in that:
(1) unattended, fully automatic operation can be performed;
(2) the system can drive steam at 170℃ to utilize it for the heat source of double effect absorption chiller & heater;
(3) the system adopts a gas fired boiler as a means for heating up the cell stack, reducing auxiliary power at startup; and
(4) the plate fin type and plate type heat exchangers are adopted in place of the conventional shell & tube type in order to make it smaller.

Table 1 200 kW PAFC Specifications

Rated Power (Net)	200 kW
Electrical Efficiency	36% (HHV)
Overall Efficiency	80% (HHV)
Fuel	Natural Gas (City Gas)
Operation Mode	Grid-connected/Grid-independent
Start-up Time	Cold Start 3 Hrs, Hot Start 1 Hr
Thermal Output	70℃ Hot Water (124 Mcal/H) 170℃ Steam (87 Mcal/H)
NOx Emission	4 ppm (0, 7%, Measured)
Dimensios	3.1(W)X10.0(L)X3.2 m(H)

1. Performance
At the point of approx. 1,600 hours operation, the net power generation efficiency and overall thermal efficiency were 36.0% (HHV) and 80.2% (HHV) respectively at the rated load. Figure 4 and Figure 5 show the results of net power generation efficiency and heat recovery versus the load factor.

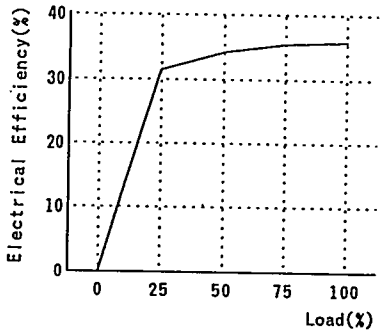

Figure 4 Electrical Efficiency

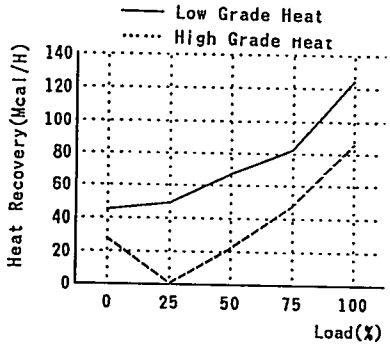

Figure 5 Heat Recovery

2. Start-up time
The start-up time from the cold state of reformer is 3 hours. The unit adopts the hot-hold mode, thus making it possible to generate power within one hour from the hot-hold mode.

3. NOx emission
Nitrogen oxide level in exhaust gas was 4 ppm (7% O_2 converted value) at the rated load.

4. Harmonic distortion
For overall voltage distortion, the measurement result of 0.6% was obtained on grid-connected operation.

CONCLUSIONS

1. The 200 kW PAFC was verified to show satisfactory performance through field testing.
2. No difficulties were found during the field operation and maintenance.
3. The issues to be solved for commercialization are reduction of the footprint size, simplification of the system, improvement of current density of cell stack and reduction of the cost.

ACKNOWLEDGEMENTS

We would express our sincere appreciation to all the Agency of Industrial Science and Technology of MITI officers for their great cooperation and guidance in promoting this research and development.

DEMONSTRATION TEST OF 200kW WATER-COOLED TYPE PHOSPHORIC ACID FUEL CELL PLANT

T.Makabe K.Ohkawara H.Maebayashi M.Abe Y.Usami
The Tokyo Electric Power Co.,Inc.
1-1-3,Uchisaiwai-cho,Chiyoda-ku,Tokyo,100 Japan

1. Introduction

TEPCO has been engaged in development of PAFC plant since 1978. Through the demonstration tests of a 4.5MW plant and an air-cooled type 220kW plant, valuable results were obtained. Currently, TEPCO has introduced two different types of PAFC plants: an 11MW plant of the distributed power generation type and two 200kW plants (so-called PCX) of the on-site type. This paper describes interim results of the PCX-1 and PCX-2 demonstration tests.

FIGURE 1. 200kW PAFC PLANT (PCX-2)

2. System Configuration

Table 1 shows the specifications. PCX is a package type PAFC plant manufactured by the International Fuel Cells Corp., featuring compactness and cost-reductions. Compactness was achieved by significant improvements in cell stack performance and simplification of system configuration. These improvements are based upon IFC technology and the valuable experience gained through previous demonstration tests. Fig.2 shows the system flow diagram of PCX. PCX employs a heat exchanger for heat-recovery. The overall thermal efficiency of the plant was greatly improved by utilizing waste heat.

TABLE 1. SPECIFICATIONS

Rated Power	200kW
Output Voltage	210V, 3 phase, 50 Hz
Fuel	City Gas (Natural Gas)
Cell Stack	Water-cooled , atmospheric pressure

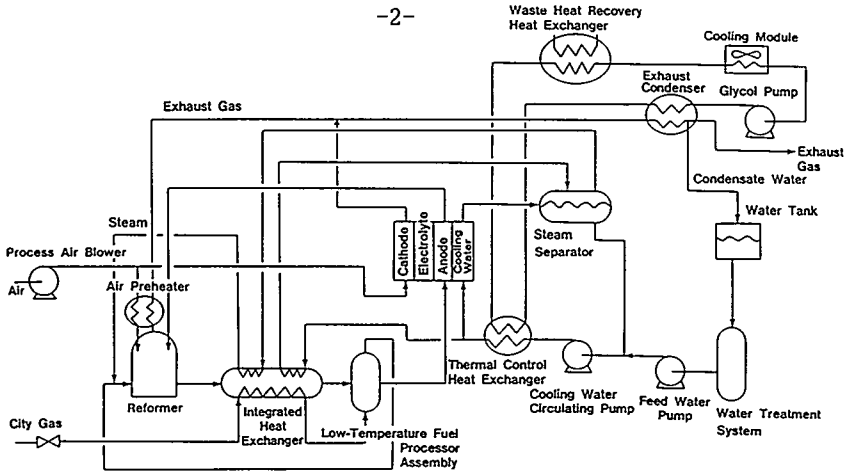

FIGURE 2. SYSTEM FLOW OF PCX

3.Installation and Operation

PCX-1 was installed outdoors at the Shin Tokyo Thermal Power Plant. Power generation tests started in Oct.'88, to verify basic plant performance and reliability.

PCX-2 was installed with a heat-recovery system comprising an adsorption refrigerator, heat exchangers, etc., in the basement of an office building in Shibaura, Tokyo. Power generation tests started in Mar.'89. With this sysytem, the cogeneration capability of the plant was demonstrated. Also, load-patterned operation was carried out to meet the electric power demand for the building. Site demonstration tests were completed in Mar.'90, with PCX-2 transferred to Shibaura DHC Plant. Cogeneration tests were performed in combination with commercial heat supply operation. These tests started in Sep.'90. Table 2 shows the operation record.

TABLE 2. OPERATION RECORD (Aug.'90)

	PCX-1	PCX-2
Cumulative Generating Hours	5210 hrs	3780 hrs
Max. Continuous Generating Hours	1393 hrs	417 hrs
Cumulative Gross Electric Power	876 MWh	409 MWh

4.Results of Demonstration Tests

1) Performance of Operation

All PCX operation was performed through the keyboard of the plant controller terminals. For plant start up, a "Start" command activates the heat-up sequence for automatic procedure. About 4 hours is required to generate power at a minimum load of 50kW. Load level can be changed by inputting the desired load level, ranging from 50 to 200kW, into the

controller. The load changing rate is 10kW/sec.

PCX has an operational mode, "Interrupt",to protect the inverter. When a utility line disturbance occurs, the inverter is stopped instantly. After disappearance of the line disturbance within 10 seconds, the inverter returns to previous power. The interrupt function was confirmed during PCX-1 operation.

2) Efficiency

Measured net electrical efficiencies for PCX-1 and 2 nearly matched the design value of 35%(HHV). Figure 3 shows the efficiency curves for PCX-1. The reduction in efficiency at low load is due to the use of the electrical heater for cell heating (max.65kW).

In the PCX-2 cogeneration tests, an overall thermal efficiency of 80% could be obtained at rated power.

3) Durability of cell stack

After more than one thousand hours of operation, cell voltage deterioration was observed in both plants. In particular, the cell stack for PCX-1 was replaced by a spare stack. Figure 4 shows V-I curves for PCX-1.

4) Environmental characteristics

NOx in the exhaust was less than 3ppm at 7% O_2 , and noise level was less than 50dB at site boundary, indicating good PCX environmentel characteristics.

5) Power quality

Harmonic distortion level and voltage fluctuation level were measured. The total voltage distortion level satisfies the design value of <3%. The current distortion level for PCX-1 satisfies the Government Guideline (total<5%), established in Jun.'90. However, utility line interferrence must be isolated to enable more accurate measurment.

6) Maintainance

Gas/steam line leakage and failures in sensors and the controll system were main trouble-shooting items. To maintain the water quality for WTS, about 1.6kl resin is required to be exchanged per year.

5. Conclusions

Test results obtained through the demonstration tests of both plants having different site conditions revealed that the design performance could be almost achieved. However, it is considered that the following improvements may be required for commercialization.

1) Improvement of cell stack life
2) Improvement of reliability of sensors and the control system

3) Increase of net electrical efficiency at low load
4) Reduction in quantity of exchanged WTS resin
5) Reduction in the quantity of nitrogen for plant start/stop

Prior to these water-cooled fuel cell systems, an air-cooled 220kW plant (developed in cooperation with SANYO Electric Co.,) began demonstration tests at the Shin Tokyo Thermal Power Plant in Sep.'87. These tests were completed in Oct.'89, with a power generating time of 5032hrs and a cumulative generation power of 581MWh. Valuable results were obtained for future plant design.

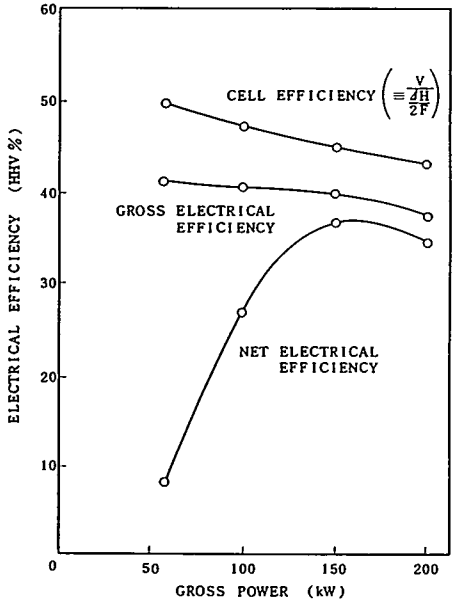

FIGURE 3.
EFFICIENCY OF PCX-1

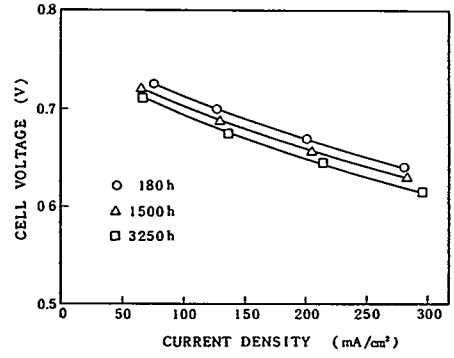

FIGURE 4.
CELL PERFORMANCE OF PCX-1

STABILITY OF PHOSPHORIC ACID FUEL CELL ELECTROCATALYSTS

K. Tsurumi, S. Kawaguchi, N. Nakamura, N. Yamamoto, N. Hara
Tanaka Kikinzoku Kogyo Technical Center
2-73 Shinmachi, Hiratsuka City, Kanagawa, 254 JAPAN

With Dr. P. Stonehart, and Professor M. Watanabe
Stonehart Associates Inc. Yamanashi University
Madison CT 06443. USA Kofu, 400 Japan

Phosphoric Acid Fuel Cell (PAFC) Power Generation Systems are now entering the final step of commercialization. As electrocatalyst vendors, we are continually developing new electrocatalyst structures to provide more advanced catalysts to the fuel cell manufacturers. The emphases are placed on increasing the electrocatalyst activity, lowering the catalyst degradation rate (increasing life time), and lowering the catalyst cost.

For the oxygen cathode electrocatalysts, Pt has been replaced with binary alloys, and then ternary alloys. It would appear from the patent literature that the development trends with time for the PAFC cathode electrocatalysts are from Pt, to Pt/refractory metal; to Pt/Cr;to Pt/Cr/Co, through to Pt/Fe/Co, and then the various Gallium additions to these combinations.

It has been a topic of some curiosity as to why these alloys should show increased activity for oxygen reduction.

Mass Activity of Electrocatalysts

In an examination of the mass activity for these Pt alloys in operating fuel cells, the alloy combinations shown in the patent literature were prepared in a highly dispersed form using our catalyst preparation technology, and performance comparisons were made in hot phosphoric acid. Those results are shown in Figure 1.

[Fig.1] INVERSE OF PARTICLE SIZE vs MASS ACTIVITY

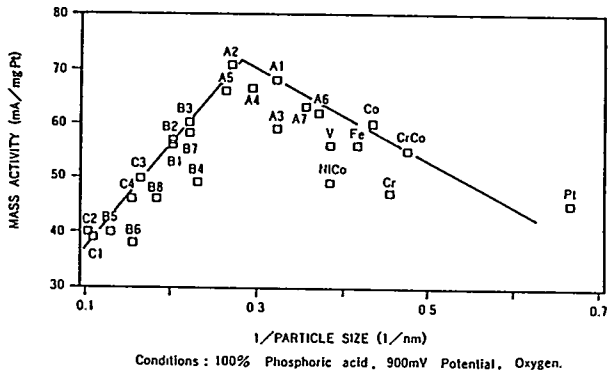

Conditions : 100% Phosphoric acid, 900mV Potential, Oxygen.

It can be seen from the figure that the mass activity (mA/mg Pt at 200 ℃ ;900mV vs RHE/O_2) for oxygen reduction increases with all of the alloys above that mass activity for Pt alone. In addition we have determined that new alloy combinations show significantly higher activities than demonstrated by the early alloy combinations. From Figure 1 it can be seen that a maximum in the mass activity occurs around 3.6 nm diameter crystallites. It is believed that the very high mass activities demonstrated by these new alloys are a combination of the enhanced surface reactivity of these alloys and the special crystallite distributions on the carbon support surface.

We have also observed that the apparent specific activity of the smallest alloy particles which are spaced closely together on the carbon supports have a lower activity than alloy crystallites that are more separated on the support. It has been shown previously [1] that when the intercrystallite distance for supported platinum crystallites is less than 17-20nm (about 10 times the crystallite diameter), an apparent diffusive interference occurs so that each individual crystallite becomes more like an individual microelectrode.

[Fig 2] INTER-CRYSTALLITE DISTANCE vs SPECIFIC ACTIVITY
[TEC80 SERIES]

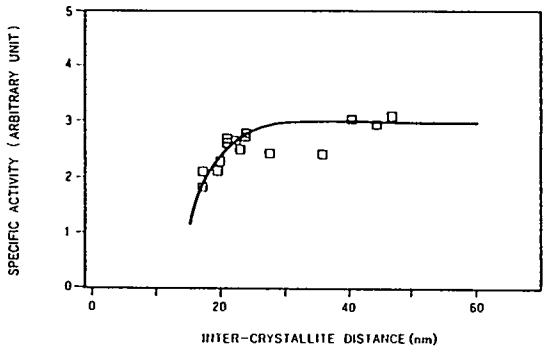

Figure 2 shows the apparent specific activity (Mass Activity × Crystallite Size instead of mA/Surface Area) for TKK advanced alloy electrocatalysts shown from Figure 1 as a function of the intercrystallite distance on the carbon support. It can be seen that the same phenomenon observed previously for Pt crystallites is observed for these alloys, in that when the intercrystallite distance decreases below 20nm the apparent specific activity decreases rapidly. The critical intercrystallite dimension in the alloys may be greater than in the supported platinum case since the alloy crystallites are larger due to the concentration of the alloying components. The design rules of 10x crystallite diameter still hold true.

In order to evaluate the performance advantages of alloying Pt with 3d transition metals, Buchanan, Keck and co-workers [2] examined Pt with first row transition elements to see whether or not there were significant improvements in the performance of the alloys in hot phos-

phoric acid as oxygen reduction catalysts. They concluded that alloying Pt with the first row transition elements significantly increases the performances above that for Pt alone. In their work they did not distinguish between the alloying elements, since they expressed the view that generally, the specific activities of all these Pt alloys were similar. The superiority of the alloys that they prepared, produced an improvement about 1.5 times the activity of Pt alone. Of greater importance was their finding that the alloys showed greater stability against sintering and degradation than did Pt alone. This translated into an increased lifetime with higher performance for the alloys. Although they tested their alloy combinations for the critical intercrystallite distance described by Watanabe et al.,[1] they were not able to determined that this effect was controllable under the conditions used to prepare their catalysts.

Dissolution of non-noble elements from alloys

Of greater importance is the question of the lifetime of these catalysts in the hot phosphoric acid reaction enveronment. Early statements in the patent literature indicated that for the Pt/V alloy then over 67% by weight of the V dissolved in the first 36 hours. In the case of Pt/Cr, only 37% had dissolved under the same conditions. It is not clear from the description in these patents whether or not there is any unreacted V or Cr active in the catalyst.

As a first approximation, we may assume:

a) spherical particles, with the alloy evenly distributed throughout the particle,

b) dissolution of the non-platinum component is potential dependent

c) the dissolution rate is linearly dependent on the surface concentration of the non-platinum component.

Then: the rate of concentration decrease is $-dC/dt = k_x C$

So: $\ln C = -k_x t + \text{const.}(V)$

and $C = C_0 \exp(-k_x t)$ where C_0 is the starting concentration.

It follows that $\ln C_{0.5} = -k_x t_{0.5}$ and $t_{0.5} = (2.303 \log 2)/k_x = 0.6932/k_x$

where k_x is a function of the alloy structure. Buried within k_x are the metallurgical diffusion driving forces, so that $k_x = fkD$, and D is a self diffusion coefficent, treating the alloy as a solid solution. This is not a constant, since the alloy composition is complicated by the formation of intermetallics.

The alloy composition is changing with time and although it is the self diffusion coefficient of the non-platinum component within a Pt matrix, surface segregation also may be operating. The rate constant will be related to the hardness of the alloys as a first approximation.

This means that to all intents and purposes we can plot logC vs t and obtain a relative figure of merit for the alloy stabilities, and project the lifetime where accelerated performance can be maintained. The real situation is more complicated, since the alloy particle grows with time, and that is a linear growth in the particle size with log time.

Analyses of Pt alloys from operating fuel cells have shown that at long operating times very little non-noble metal alloy component remains. Indeed, for long operating times and at high electrode potentials, Pt itself dissolves. The dissolution of bulk Pt/ Cr have been the most studied [3-7], but very little work has been done on real catalysts in operating environments. Most recently, Kroen and coworkers [7] have revealed extensive Cr loss as a result of electrode operation and have postulated that phosphorus from the phosphoric acid may have incorporated into both Pt and Pt/Cr catalysts during operation. Ross and coworkers [8] have concentrated on Pt/Co and have shown that Pt_3Co intermetallic is a more stable component of the Pt/Co system.

From these results, and from the results of other workers, it is suggested that the catalytic enhancement of the alloys for oxygen reduction is due to a roughening of the crystallite surface due to leaching of the non-platinum component. For Pt/Cr alloys with Cr dissolutions (or Co dissolution in the Pt/Co case) then a dissolution-deposition surface enhancement may be responsible for the observed catalyst activity increases.

It is difficult to accept that the catalytic enhancement of the alloy only is due to surface roughening of such small crystallites. Given the specific activity increases that are shown in Figure 1, it would be supposed that Pt atoms with a high degree of disorder and a high surface roughness would exhibit rapid surface diffusion and sintering to eliminate the surface roughness for the Pt/Cr, Pt/Cr/Co, Pt/Co, Pt/V, and Pt/Fe.

[Fig.3] THE RATE OF DISSOLUTION FOR VARIOUS ALLOY CATALYSTS

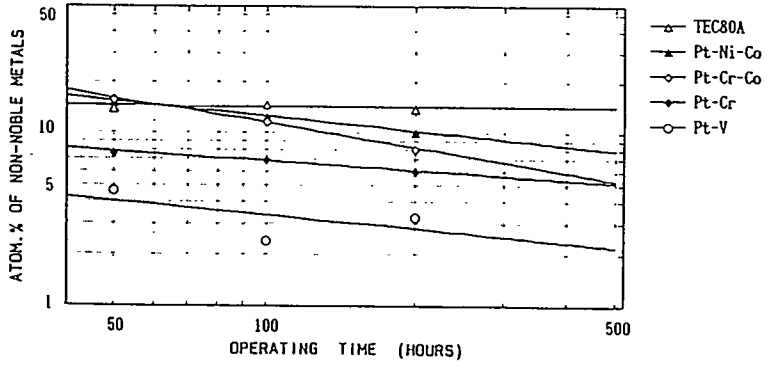

The rates of dissolution for various alloy catalysts described in the patent literature have been studied as a function of time in the hot PAFC environment. Preliminary results are shown in Figure 3.

In all instances for these alloys there is a rapid decrease in the non-platinum element concentration as a function of time. Performance testing of alloys does not reflect this demetallization of the catalyst for thousands of hours.

Further work is ongoing to develop more active catalysts with extended lifetimes.

References

1. M. Watanabe, H. Sei and P. Stonehart
"The Influence of Platinum Crystallite Size on the Electroreduction of Oxygen"
J. Electroanal. Chem. 261 375 (1989)

2. J. S. Buchanan, L. Keck, J. Lee, G. A. Hards, N. Scholey
"The Impact of Surface Area on Oxygen Reduction Activity of Supported Platinum Alloy Fuel Cell Catalysts"
First International Fuel Cell Workshop. eds. M. Watanabe and P. Stonehart Tokyo Sept. 16th 1989. pp. 29-39

3. K. Daube, M. Paffett, S. Gottesfeld, and C. Campbell
"Combined Electrochemical/Surface Science investigations of Pt/Cr Alloy Electrodes"
J. Vac. Sci. Tech. A4, 1617 (1986)

4. S. Gottesfeld, M. T. Paffett, and A. Redondo
"The Ellipsometric Characterisation of Pt+ Cr Alloy Surfaces in Acid Solutions"
J. Electroanal. Chem. 205 163 (1986)

5. M. T. Paffett, K. A. Daube, S. Gottesfeld, and C. T. Campbell
"Electrochemical and Surface Science Investigations of PtCr Alloy Electrodes"
J. Electroanal. Chem. 220 269 (1989)

6. M. T. Paffett, J. G. Beery, and S. Gottesfeld
"Oxygen Reduction at $Pt_{0.65}Cr_{0.35}$, $Pt_{0.2}Cr_{0.8}$ and Roughened Platinum"
J. Electrochem. Soc. 135 1431 (1988)

7. C. F. Kroen, G. E. Stoner, S. R. Taylor, and G. L. Cahen, Jr.
"Microstructural Properties and Electrocatalytic Behavior of Platinum and Platinum-Chromium Dispersed Catalysts"
Extended Abstract # 121, 90-2, ECS Meeting, Seattle, Washington, P.182 (1990)

8. B. C. Beard and P. N. Ross Jr.
"The Structure, and Activity of Pt-Co Alloys as Oxygen Reduction Electrocatalysts"
J. Electrochem. Soc. (submitted) (private communication)

OPERATIONAL EXPERIENCE OF A 100 W PHOSPHORIC ACID FUEL CELL STACK

V. Recupero, V. Alderucci, G. Zappalà, M. Laganà and N. Giordano
Institute CNR-TAE, Salita S.Lucia sopra Contesse, 39
98126 S.LUCIA - MESSINA (ITALY)

Abstract

A 100 W phosphoric acid fuel cell unit has been designed and developed at CNR (National Research Council) Institute for Transformation and Storage of Energy (Messina, Italy) in the framework of national programs (Progetto Volta, Enea contract). This prototype, an intermediate step toward the 1 kW stack, has been succesfully run in endurance tests for a total of 5000 hours. The results showed a good performance of the unit either in terms of scaling-up, time and procedure for the stack assembly and, finally, for the mechanical and chemical resistance of the bipolar plates. The capability for operating on a methanol reformer product gas has been demonstrated too.

Introduction

The Institute for Transformation and Storage of Energy, Messina,Italy, is involved in a program to develop a small phosphoric acid fuel cell stack (1 kW), integrated with a methanol reforming unit of the same size.
On the basis of the principal key features carried out /1-5/ (proprietary know-how related to the preparation of active Pt electrocatalyst supported on active carbon; proprietary design of the basic stack module; 40000 hrs of operation in monocell with a useful surface area of 72 cm2),a 100 W prototype has been built and tested as an intermediate step towards the 1 kW stack /6-7/.
This paper describes activities to verify the effectiveness of the unit, and particularly, the correct running of the bipolar plates based on an internal gas collector system; the acid replenishment system; the gas sealing system; the simplified stack hardware design with an integrated methanol reformer.
The information so obtained, besides confirming the working hypoteses, has added useful grounds for an improved design and optimization and scaling-up.

Experimental

The fuel cell stack (fig.1) is provided with bipolar plates of proprietary design and construction, and internal gas collectors for the working gases in order to have a more compact system and to simplify the gas sealing. The upper and lower stainless steel plates are the only external gas collectors (upper to outlet, lower to inlet) and the current collectors; fuel is supplied to the fuel cell stack via two separate systems: by a methanol reformer unit furnished by

Tecnars Srl, Bari, Italy, (gas composition 74.5 % H2, 24.5 % CO2, 1.0 % CO) or by H2 and CO2 tanks mixed under proper proportions.
Besides the voltage collector, each plate has seats for thermocouples; in the anode plate side there are moreover two reservoirs, which are filled with a suitable material for transferring, by capillarity, the phosphoric acid to the system. The inlet of the electrolyte in the stack occurs via a vertical path.
Various tests up to a total of 5000 hrs, on a 100 W stack (working conditions in table 1), have been carried out.
The goal of these tests have been to verify :
- the correct functionality of the internal gas collectors;
- the scale-up problems;
- the phosphoric acid replenishment;
- the capability for operating on a methanol reformer product gas;
- the engineering of the system.

Results and discussion

Fig. 2 shows a tipycal performance of the 100 W prototype versus the life time, the loss of performance in 1,500 hrs was 5 mV, the ohmic losses of the individual cells were 35 mV at 200 mA/cm2. Table 2 shows the performance of the monocell (useful surface 72 cm2) and of the 100 W stack (useful surface of the single cell 200 cm2): the identical values of the voltage, at low and high current density, shows both the good scaling-up, and the high efficiency of the internal gas collector system.
No particular problems were encountered during the life time of the test (the check system has worked well: the predetermined automatic sequence of events assured the correct behaviour of the run, in case of external failure).
The weight losses of the bipolar plates was negligible with no signs of plate corrosion observed.
The behaviour of the methanol reforming unit connected to the phosphoric acid stack has been analyzed: the performance decay for each cell, passing from pure H2 to the reformed gas, are 20-30 mV for a constant (< 1 %) CO content in the reformed gas.
Some problems have been identified regarding the phosphoric acid management, as the efficiency of the acid-replenishment system was found to decrease with the time. On the contrary, the time and the procedure for stack assembly was sufficiently low and simple, respectively.

Conclusions

A phosphoric acid prototype of 100 W, integrated with a methanol reforming unit has been designed and built, as an intermediate step to develop a 1 kW prototype.
Various tests have been carried out to verify the effectiveness of the unit. The results have shown:

- good stability of the performance during the life time (1500 hrs for each run);
- no problems in terms of scale-up: the performance of the monocell scale and the performance of the single cell of the 100 W stack were identical;
- stack performance is not affected by gas distribution pattern design;
- good mechanical/chemical resistance of the bipolar plates;
- time and procedure for stack assembly were sufficiently low and simple, respectively.

The capability for operating on a methanol reformer product gas has been demonstrated too.

Acknowledgements

We gratefully acknowledge the technical support of Tecnars Srl and the financial assistance of ENEA, Dept. FARE. This work was carried out under contract from ENEA as a part of Progetto Volta.

References

1. N. Giordano, E. Passalacqua, V. Recupero, M. Vivaldi, E.J. Taylor and G. Wilemski, " Influence of acid occupation on performance of PAFC gas-diffusion cathodes ", The 40th Meeting of the International Society of Electrochemistry, Kioto, Japan, September 17-22, 1989.
2. N. Giordano, E. Passalacqua, V.Recupero, P. Staiti, V. Alderucci, R. Di Leonardo, H. Mirzaian, Z. Poltarzewski, L. Pino, " Morphological and electrochemical characteristics of PAFC's electrodes: comparison and modelling ", Proceedings 1988 Fuel Cell Seminar, 69-73, Long Beach, 23- 26th October 1988.
3. N. Giordano, E. Passalacqua, V. Recupero, M. Vivaldi, E.J. Taylor and G. Wilemski, Electrochimica Acta, in press.
4. V. Alderucci, V. Recupero, G. Maggio, R. Di Leonardo and N. Giordano, " Evolution of the structural properties of PTFE bound gas diffusion electrodes ", 1990 Fuel Cell Seminar, Phoenix, Arizona.
5. V. Recupero, V. Alderucci, R. Di Leonardo, M. Lagana, N. Giordano, " Performance of a portable 100 W phosphoric acid fuel cell under different operating conditions ",Proceedings of the 25th IECEC, vol. 3, pp 269-274. Reno, Nevada, August 12-17, 1990.
6. V. Recupero, E. Passalacqua, " Progetto celle a combustibile, realizzazione di uno stack di celle a combustibile ad acido fosforico da 1 kW ", Estratto attività 1987, contract Enea, Aprile 1988.
7. V. Recupero, V. Alderucci, R. Di Leonardo, M. Lagana, G. Zappala, N. Giordano, " 1 kW PAFC stack: a case history", Proceedings of the 8th World Hydrogen Energy Conference, vol. 3, pp 1509-1518. Honolulu and Waikoloa, Hawaii, July 22-27, 1990.

TABLE 1

WORKING CONDITIONS OF THE 100 W STACK

Pressure	1 Atm
Cell Temperature	180 °C
Fuel utilization	70 %
Oxidant utilization	50 %
Fuel composition	METHANOL REFORMED GAS
Oxidant composition	AIR
Useful electrode surface	200 cm2
Working voltage	0.512 V
Current density	200 mA/cm2
Internal resistance (single cell)	2 mΩ
Cell number	6
Thermal power of the single cell	30 W
Electrical power of the single cell	20.5 W
Total output electrical power	123 W

TABLE 2

COMPARISON BETWEEN MONOCELL AND 100 W STACK PERFORMANCES
(Average value at t: 1000 hrs)

CURRENT DENSITY	MONOCELL VOLTAGE.	MONOCELL POWER	MONOCELL .VOLTAGE iR FREE	SINGLE CELL 100 W VOLTAGE.	SINGLE CELL 100 W POWER	SINGLE CELL 100 W .VOLTAGE iR FREE
mA/cm2	V	mW/cm2	V	V	mW/cm2	V
150	0.570	85.5	0.635	0.570	85.5	0.630
200	0.510	102.0	0.596	0.512	102.4	0.592

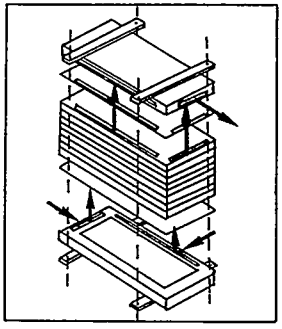

FIGURE 1

VIEW OF 100 W STACK

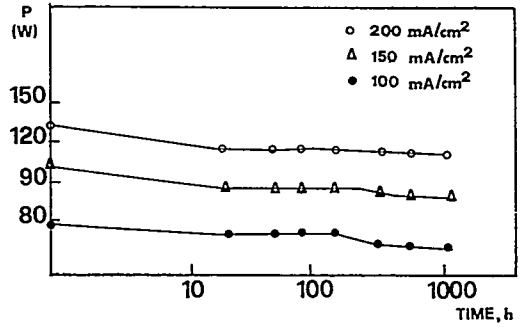

FIGURE 2

PERFORMANCE OF 100 W VS TIME

EVOLUTION OF THE STRUCTURAL PROPERTIES OF PTFE BOUND GAS DIFFUSION ELECTRODES

V.Alderucci, V.Recupero, G.Maggio,
R.Di Leonardo, N.Giordano

CNR Institute for Transformation and Storage of Energy,
S. Lucia 39, 98126 S. Lucia MESSINA - ITALY

Abstract

In the present study, an approach based on the examination of morphological changes of gas diffusion electrodes subjected to very severe working conditions has been made. Result of physical characterization have shown that long term operations induce profound modifications of the electrode surface which involve mostly carbon corrosion, platinum sintering and dissolution and changes in wettability. Deadhesion of PTFE-carbon interface monitored by XPS analyses has also been observed.

Introduction

In the last decade, progress in the phosphoric acid fuel cell technology led to it commercial status of development. Main current researches are aimed to enhance the efficiency as well as extending the lifetime of the electrode by a control of the catalyst deactivation and of the electrode degradation mechanisms which are, as well known (1-4), the main causes of performance decay.

Altough many studies have been reported on these subjects (5-8), information is lacking concerning weight loss, variations of catalyst pore size distribution and changes in wettability in their correlation with changes at the interface carbon-PTFE.

Accelerated tests at open circuit voltage (OCV) conditions are known to be useful to investigate such phenomena in a resonable time. In the light of these we have performed a set of tests at OCV, in concentrated phosphoric acid at 180°C, to obtain information regarding the evolution of the morphological properties of the electrode structure. By so doing it is possible to extrapolate with a good approximation the behaviour expected for electrodes in long term operations under standard conditions.

To make a complete model of the deterioration of the electrode structure, XPS analyses are also presented. Results of the spectral characteristics clarify the role of separation effects of the adhesive (PTFE) - substrate (carbon) couple in the observed structure disintegration phenomena and provide valuable information concerning the best thermal treatments at which the electrode should be subjected.

Experimental

The real electrodes used in accelerated tests have been

manufactured according to a procedure described elsewere /9/. Corrosion tests were carried out at atmospheric conditions by keeping the electrodes in 98% w/w H_3PO_4 in a teflon holder at 180°C. The potential of the cell, periodically checked, was 1.015 V. The weigth loss (W) was measured gravimetrically,after periods of 1, 5, 24, 120 and 300 hrs. The structural properties of such electrodes were analyzed by mercury intrusion technique and optical microscopy.

As the electrode sintering temperature (Ts) influences the morphological /10/ and the electronic properties of the teflon - carbon interface, model electrodes, prepared by deposition of a thin film of PTFE dispersion (61% w/w), have been sintered at 250, 300, 320, 340, 360 and 400°C for 30' intervals and the spectral characteristics monitored by an ESCA spectrometer.

Physical characterization

The structural changes occuring on electrodes subjected to OCV conditions are clearly manifested in Figs.1, a) and b), which show respectively the pore volume and the weigth loss evolution as a function of time.

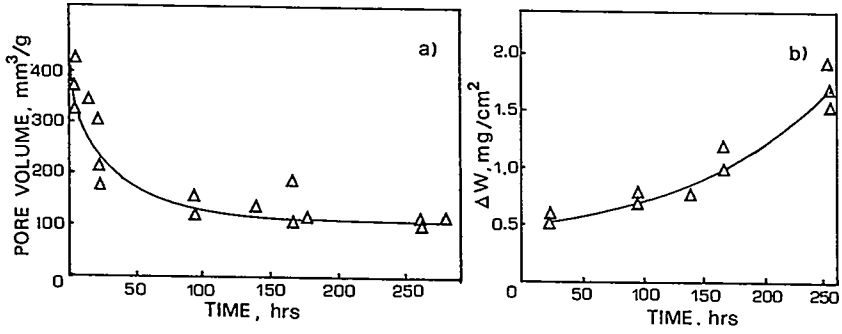

FIGURE 1

PORE VOLUME (a) AND WEIGTH LOSS (b) EVOLUTION VS. TIME

Optical micrographs, clearly reveal the progressive and drastic disruption process of the electrode surface as a consequence of the structural change induced by the cperating conditions. Such a phenomenon appears to be correlated with a failure of the adhesive contact between PTFE and active carbon driven by the changes in the free energy of the corrosion process, according to a mechanism which involves the working electric potential /11/ and/or a pre-existing non-equilibrium interaction between PTFE and carbon, due to an inadeguate thermal treatment of the electrode.

Surface characterization

XPS measurements were made on the model electrodes to investigate how the thermal treatments can modify (or stabilize) the joint PTFE - carbon. The surface effects by heating are clearly seen in the C 1s spectra (Figs. 2 a-d).

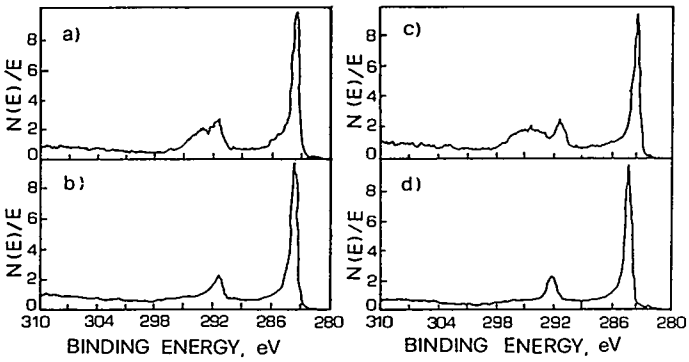

FIGURE 2

XPS C1s SPECTRA OF THE a) 250°C, b) 300°C, c) 320°C, d) 340-400°C TREATED SAMPLES

The broad peak at the highest binding energies (295 eV) is the charge shifted carbon bound to F in the PTFE, whose intensity changes during the thermal treatment.Corresponding changes are also noted in the F 1s spectra (Figs. 3 a-d) expecially in the component at the high binding energy (692 eV).

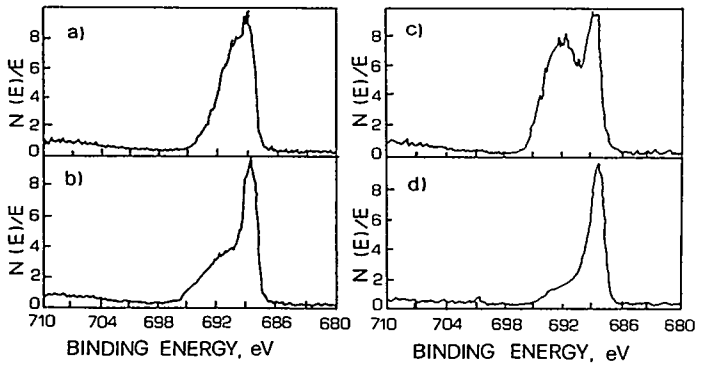

FIGURE 3

XPS F1s SPECTRA OF THE a) 250°C, b) 300°C, c) 320°C, d) 340-400°C TRATED SAMPLES

The evolution of the C1s and F1s spectra are an index of the modifications of the carbon - PTFE interface with the thermal treatment. From these results it can be stated that the adhesion of PTFE to the carbon increases until a Ts of 320°C where it changes dramatically to a poorer state. From 340°C and up the contact is reestablished and the quality of the PTFE - carbon interaction increases with increasing the temperature. However the range between 340 - 360 °C appears to be the best as the PTFE is in a good contact with the carbon and an optimization of hydrophobic - hydrophilic properties of the electrode surface is also achieved /12/.

Conclusion

Results from extensive physical characterizations point to the fact that morphological changes induced by long term operations involve concomitantly carbon corrosion, platinum sintering and dissolution, and changes in the wettability, the latter caused by a deadhesion and selective charging of the PTFE. This phenomenon is responsible for a drastic disruption process of the electrode structure due to modifications of the surface texture of the materials. Valuable information on the adhesion of the carbon-PTFE interface can be gleaned from XPS spectra which clearly monitor the charging characteristics of the electrode surface.

References

1. D.N. Patel, H.C. Maru, M. Farooque and C.H. Ware, J. Electrochem. Soc. 131 (1984) 2750.
2. J. Aragane, T. Murahashi and T. Odaka, ibid. 135 (1988) 844.
3. A. Honji, T. Mai, K.Tamura and Y. Hishimuma, ibid 135 (1988) 355.
4. V. Alderucci, V. Recupero, L. Pino, R. Di Leonardo, D.L. Cocke, N. Giordano and F. Parmigiani, J. Applied Electrochem. (accepted).
5. A.K.Kush, L.G.Christner and P.P.Yeh, Proceedings USA Fuel Cell Seminar, Tucson (1985) p.56.
6. P. Bindra, S.J. Clauser and F.Yeager, J.Electrochem. Soc. 126 (1979) 1631.
7. A.Pebler,ibid.133 (1986) 9.
8. K. Kinoshita, K. Routsis, J.A.S. Bett and C. S. Brooks, Electrochem. Acta 18 (1973) 953.
9. V. Alderucci, E. Passalacqua, N. Giordano, P. L. Antonucci, F. Parmigiani and N. Ricci, J. Applied Electrochem. 20 (1990) 235.
10. N. Giordano, E. Passalaqua, V. Alderucci, P. Staiti, L. Pino, H.Mirzaian, J.Taylor and G. Wilemski, Electrochim. Acta (accepted).
11. K. A. Klinedinst and W. M. Vogel, J. Adhesion 9 (1978) 123.
12. T. Mori, J. Imahashi, T. Kamo, K. Tamura and Y. Hishimuna, J. Electrochem. Soc. 133 (1986) 896.

INFLUENCE OF PARTICLE SIZE OF PLATINUM CATALYSTS SUPPORTED ON CARBON UPON ELECTROCHEMICAL O_2-REDUCTION IN PAFC

E. Passalacqua*, L. Pino*, M. Vivaldi*, N. Giordano*, M. Scagliotti** and N. Ricci**

*Institute CNR-TAE (Transformation and Storage of Energy) - S.Lucia - Messina (ITALY).

**Materials Department CISE S.p.A. - Segrate - Milano (ITALY).

ABSTRACT

Pt particle size effect on the activity (98% H_3PO_4, T=170°C) of oxygen reduction on a series of Teflon-bonded cathodes (40% Teflon, sintering temperature = 340 C) was investigated.

Electrodes were made from catalysts differing by the metal surface area (MSA from TEM=20 ÷ 200 m^2/g of Pt) and the intercrystallite separation (IS, from 12 to 310 nm). The activity was determined in terms of specific (SA, $\mu A/cm^2$) and mass (MA, mA/mg of Pt) activity at 0.9V vs. RHE in O_2. In the range of practical value of MSA, SA decreases with decreasing Pt particle size while MA increases showing no maximum but an ever increasing "lost activity" at the highest MSA.

Moreover, the effective Pt working area (EPWA) was determined by cyclic voltammetry. The correlation between MA and EPWA is more linear and scattering in the values is justified by a different degree of utilization of Pt in the electrocatalyst, depending on morphological-absorptive properties (PAO) of the cathodes.

INTRODUCTION

Several pubblications [1-4] have been made to understand the influence of Pt particle size upon catalytic activity resulting into widely differing and often contradictory results, mainly due to differences in the experimental conditions, and they are therefore difficult to compare.

The most important advancement was made by Bregoli [1] who studied the influence of platinum crystallites size on specific and mass activity for surface areas ranging from 20 to 80 m^2/g. He found that the specific activity increases with an increase in the Pt particle size; on the contrary, the mass activity increases decreasing particle sizes. Ross [2] extended this work to higher surface areas, i.e. 120 m^2/g and observed the same decay in the specific activity but more pronounced at surface areas greater than 80 m^2/g, while the mass activity linearly increases reaching a maximum at 3.5 nm and then decreases. Recently, Watanabe et al. [3] identified the crystallite separation (IS) as a significant factor for marking the activity of the electrocatalyst. They found that depending on carbon surface area, Pt loading, etc., at IS values in the order of 18-25 nm, a full utilization of the Pt crystallites is achieved.

The purpose of this paper is to extend the earlier study [1-4], by analyzing data of oxygen reduction performance of a series of cathodes made from catalysts differing by the Pt

surface areas (from 20 to 200 m^2/g), supported on a same high surface area carbon. Moreover, the extent of utilization of Pt has been studied, also in terms of morphological-absorptive characteristics of the electrodes,by relating the values derived from electrochemical measurements and morphological parameters to PAO, showing that for a given Pt surface area full utilization of Pt further depends upon good and reproducible preparations of the electrodes.

EXPERIMENTAL

The electrocatalysts consisted of Pt supported on a high surface area carbon black (950 m^2/g) which were prepared by liquid-phase reduction of H_2PtCl_6 , using two different preparative procedures [5] to broaden the range of Pt particle size. The platinum loading was 20% constant for all catalysts.

The Pt surface area (MSA, m^2/g) and the Pt crystallite sizes (nm) of the electrocatalysts were determined by Trasmission Electron Microscopy (TEM), from which the intercrystallite separation (IS, nm) was calculated by a simple equation previously proposed by Watanabe [6].

After preparation and characterization, the electrocatalysts were formed into gas diffusion electrodes (40% PTFE and sintering temperature=340°C). The Pt loading on the electrodes was about 0.5 mg/cm^2. Several cathodes were prepared with each catalyst.

The % phosphoric acid occupation (PAO) was determined from the ratio between the amount of absorbed acid and the electrocatalyst pore volume as described elsewhere [5,6].The electrocatalyst activity for oxygen reduction was determined at 900 mV (vs RHE) in 98% H_3PO_4 at 170°C in pure oxygen in a half-cell apparatus [7]. The electrode platinum working area, EPWA, on the gas diffusion electrodes was obtained from cyclic voltammetry [5].

RESULTS AND DISCUSSION

A series of Pt on carbon samples has been prepared which provide for a range of platinum particle size from 1.4 to 12.5 nm, corresponding to about 200-20 m^2/g of MSA. Choice of a very high surface area carbon and variations in the preparative procedure made it possible to broaden the range of MSA to upper and lower values not yet comprehensively explored in a single set of experiments. Experimental data in fig. 1 show the specific activity to decrease with an increase in MSA. A similar behaviour was previously reported by Bregoli [1] for a Pt surface area ranging from 20 to 80 m^2/g and by Ross [2] who extended the range of interest up to surface area of 120 m^2/g.

Fig. 2 shows the relationship binding SA to intercrystallite separation, IS. Again, variations in the preparative conditions and a choice of a high carbon surface area allowed us to extent the IS range to extremes not yet

covered in previous literature. The data in fig. 2 show no clear trend to indicate that a critical IS value exists, below which the SA dramatically decreases, instead they suggest that the specific activity of Pt decreases with a decrease in IS. Recently, a similar trend have been reported by Buchanan et al. [4] for IS. The AA found coincident values up to 100 nm on electrocatalysts prepared on acetylene black supports. Since in our experiments also a single carbon black has been used with a constant Pt loading (20%), it is evident that the influence of the IS upon SA should be attributed exclusively to Pt particle size and improvement in the SA can be obtained by increasing IS.

In fig. 3 the influence of the MSA on MA is shown. The mass activity increases with increasing Pt surface area but the data do not show a clear evidence for a maximum in mass activity at small Pt particle size, such as that reported by Ross [2]. Our results are essentially similar to those reported by Bregoli [1], still showing an ever increasing "lost activity" at the highest MSA, even if shifted at Pt surface areas higher than that reported by Bregoli.

As evident from our plots scattering in data is everywhere observed at any given Pt surface area. This appears to be in common with previous literature [1-4], although the interpretation should be quite different. Scattering in the data is probably unrelated to the nature of the catalysts, but it has to be attributed to different morphological-absorptive characteristics arising from reproducibility in the electrodes preparation. Because of this, effective Pt working areas (EPWA) were determined by CV and used to calculate the degree of Pt utilization. These values were correlated with %phosphoric acid occupation (PAO), an index of the relative hydrophobicity-hydrophilicity characteristics of the electrodes [5] and shown to be well interrelated. Use of EPWA gives a better correlation with MA (fig. 4), because it takes into account effects bound to the preparative procedure of the electrodes and therefore it furtherly determines the degree of platinum utilization in the electrodes for any given electrocatalyst. Altogether, it seems that whenever Pt particle size are too close each other, i.e. small, not only a "lost activity" is observed but this poses a limit to a full utilization of Pt, as evident from the broader differences recorded in the range of 100-200 m^2/g.

REFERENCES

1. L. J. Bregoli, Electrochim. Acta, 23, 489 (1978).
2. P. N. Ross, Precious Metals 1986, InternationalPrecious Metals Institute, Allentown, PA, 1986.
3. (a) M. Watanabe, H. Sei and P. Stonehart, 173rd Meeting of the Electrochem. Soc., vol 88-1, No. 510. p. 732, Atlanta, May 1988; (b) M. Watanabe, H. Sei and P. Stonehart, J. Electroanal.Chem., 261, 375 (1989).
4. J. S. Buchanan, L. Keck and J. Lee, Proceedings of the

1st International Fuel Cell Workshop, Tokyo, Japan, September 1989.
5. N. Giordano, E. Passalacqua, L. Pino, M. Vivaldi, M. Scagliotti and N. Ricci, 25th IECEC Reno, Nevada, August 1990.
6. N. Giordano, E. Passalacqua, V. Alderucci, P. Staiti, L. Pino, H. Mirzaian, E. J. Taylor and G. Wilemski, Electrochim. Acta, submitted for pubblication.
7. N. Giordano, E. Passalacqua, V. Recupero, M. Vivaldi, E. J. Taylor and G. Wileski, Electrochim. Acta, in press.

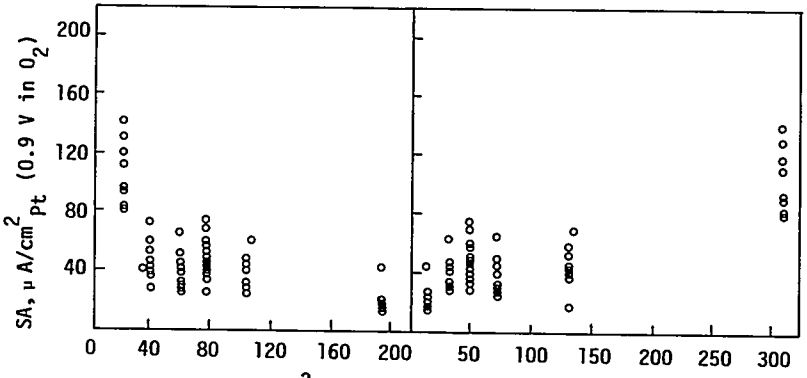

FIG.1-RELATION BETWEEN THE SPECIFIC ACTIVITY AND Pt SURFACE AREA FROM TEM.

FIG.2-SPECIFIC ACTIVITY AS FUNCTION OF INTERCRYSTALLITE SEPARATION.

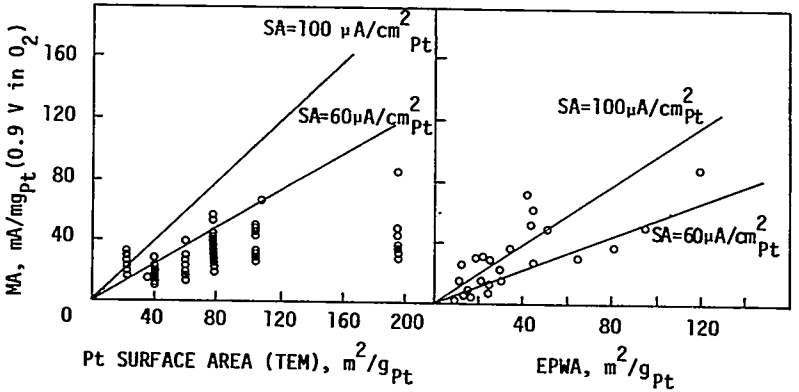

FIG.3-VARIATION OF MASS ACTIVITY WITH Pt SURFACE AREA FROM TEM.

FIG.4-VARIATION OF MASS ACTIVITY WITH ELECTRODE Pt WORKING AREA FROM CV.

DEVELOPMENTAL STATUS OF A 34 KW FUEL CELL MODULE IN PEM TECHNOLOGY AS AN AIR-INDEPENDENT POWER SOURCE

W. Bette, K. Strasser
Siemens AG, KWU, Erlangen

At the end of the sixties the fuel cell was already regarded as an important component for an air-independent power source in submarine propulsion systems.

A compact 100 kW alkaline H_2/O_2 fuel cell power plant consisting of 16 single 6.5 kW modules showed excellent operating performance on board a German naval submarine (1, 2). Analysis of different FC systems, however, favored the PEM principle for this submarine application, and at the end of 1984 Siemens initiated a developmental program for solid polymer fuel cells (3).

The basic know-how was transfered from GE to Siemens. The FC powerplant is scheduled to be developed in three stages:

- development and evaluation of a 5 kW stack
- development of a 34 kW laboratory-type module
- development and qualification of a 34 kW prototype unit.

The first phase was successfully completed by demonstrating, in September 1988, a 5 kW stack having the following features:

- outside dimensions 400 mm x 400 mm
- active area 1180 cm²
- number of cells 11
- rated cell voltage 685 mV

The typical current/voltage characteristic measured on a smaller test cell with 50 cm² active area, at 80 °C and 2 bar reactant pressure, is shown in Fig. 1.

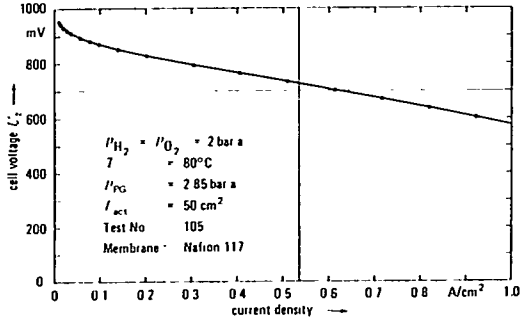

FIGURE 1

CURRENT/VOLTAGE CHARACTERISTIC OF A STANDARD TEST CELL

The advantage of the PEM fuel cell is its high output availability. Only a small voltage drop was observed during 20,000 hours of operation at rated current (see Fig. 2).

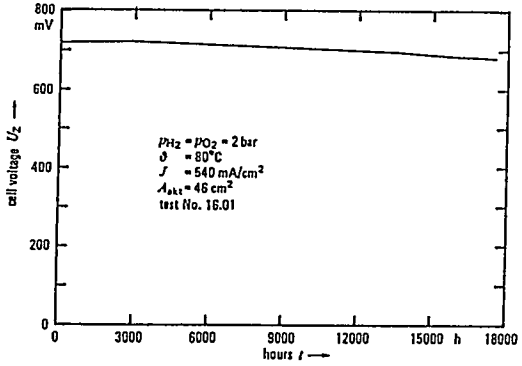

FIGURE 2

VOLTAGE OF TEST CELL AS A FUNCTION OF OPERATING TIME

The aim of the second developmental phase, which is scheduled for completion in 1991, is to integrate all subcomponents in a module assembly and increase module power up to 34 kW.

Fig. 3 shows a schematic functional diagram with the subcomponents: humidifier, product water separator, auxiliaries for gas supply and purging, and waste heat removal system.

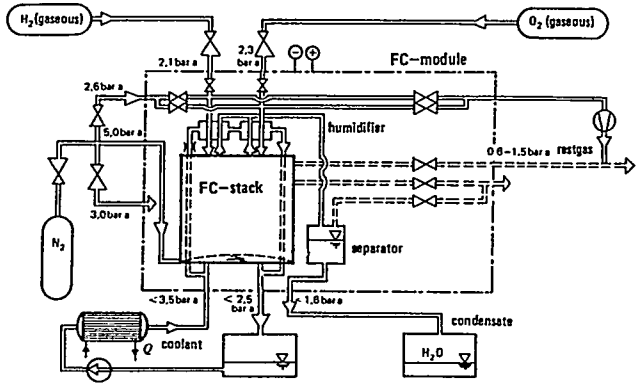

FIGURE 3

FUEL CELL MODULE: SCHEMATIC

The module will be assembled in a compact rectangular container. Fig. 4 shows a schematic outline drawing.

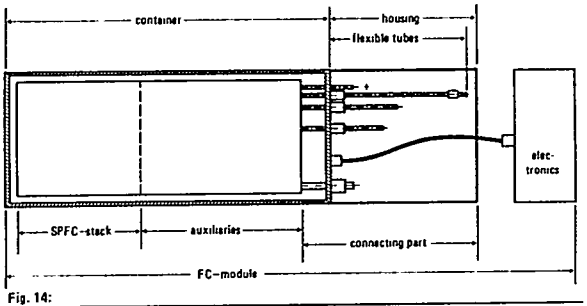

Fig. 14:
Outline drawing of the FC-module

FIGURE 4

OUTLINE DRAWING OF THE FC MODULE

The technical data are as follows

rated power	34 kW
rated voltage	53 V
rated current density	0,54 A/cm²
efficiency at rated power	55 %
efficiency at 10 % of rated power	75 %
temperature	80 °C
H_2 pressure	2.0 bar a
O_2 pressure	2.3 bar a
dimensions	0.5 x 0.5 x 1.6 m³

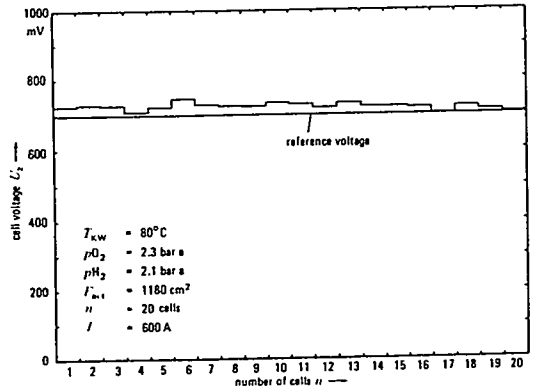

FIGURE 5

VOLTAGE VALUES OF 20 STACKED FUEL CELLS AT 600 A COMPARED WITH THE PROJECTED CELL VOLTAGE

In the meantime a further important step was taken in realizing the developmental aim by running a 20 cell FC stack. The voltages of the 20 individual cells at a load current of 600 A are compared with the projected voltage in Fig. 5.

The test bed of the 20 cell FC stack is shown in Fig. 6.

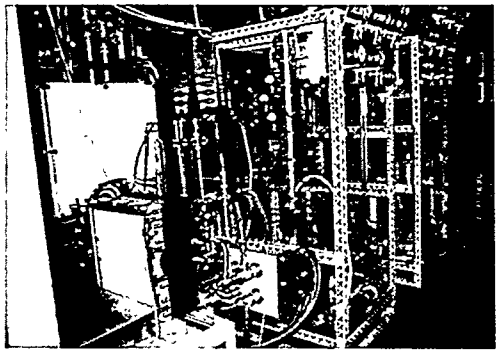

FIGURE 6

LABORATORY TEST SETUP OF THE 20 CELL FC STACK

Recently, the power of a single cell was increased by optimizing cell construction and improving product water management. The current/voltage characteristic achieved with a variety of single cells is shown in Fig. 7.

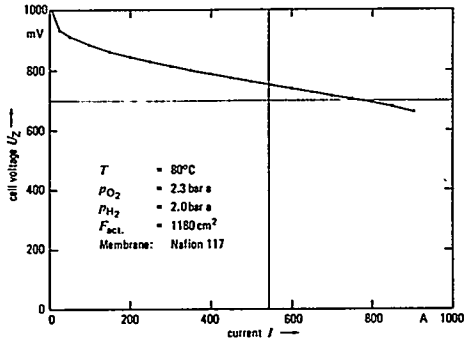

FIGURE 7

IMPROVED CURRENT/VOLTAGE CHARACTERISTIC OF THE CELL

The efficiency at nominal load was increased by 2.9 %. An FC stack has already been assembled. With a single cell characteristic as shown in Fig. 7 the 40 cell unit will deliver 18 kW of electrical power at a stack voltage of 30 V.

CONCLUSIONS

Up to now the aims in developing a high power PEM FC module have been exceeded. Only a small step has yet to be taken to allow the demonstration of a 34 kW module in the coming year. The developmental work done in the past has confirmed the high power availability of PEM fuel cells, i.e. their high overload capacity, low power degradation and high power at low temperature. These advantages, together with the possibility of using air instead of oxygen, may open up new applications for the fuel cell because of its environmentally friendly character.

REFERENCES

1 K. Strasser, L. Blum, W. Stühler
An advanced alkaline H_2/O_2 fuel cell assembly as a compact mcdule of a 50 kW power source
Proceedings of FC-Seminar, 1988, Long Beach, Cal. USA

2 K. Strasser
The design of alkaline fuel cells
Journal of Power Sources, 29 (1990) 149-166

3 K. Strasser
PEM-Fuel Cells: State of the Art and Development Possibilities
to be published Berichte der Bunsengesellschaft für Physikalische Chemie, 9/1990

METHODS TO ATTAIN HIGH ENERGY EFFICIENCIES AND HIGH POWER DENSITIES IN SOLID POLYMER ELECTROLYTE FUEL CELLS WITH LOW OR HIGH PLATINUM LOADING ELECTRODES

S. Srinivasan[1], E.A. Ticianelli[1], M.A. Enayetullah[1], A. Parthasarathy[1,2], D.J. Manko[1], O. Velev[1], H.P. Dhar[1], C.R. Martin[2] and A. J. Appleby[1]
[1]Center for Electrochemical Systems and Hydrogen Research, Texas Engineering Experiment Station, Texas A&M University System, College Station, Texas 77843-3577
[2]Department of Chemistry, Texas A&M University, College Station, Texas 77845-3255

1. Introduction

Fuel cells with high energy efficiencies and high power densities are vitally needed for extraterrestrial (space, underwater) and terrestrial (electric vehicles, stand-by or remote power) applications from the points of view of minimizing weight, volume, capital cost and fuel consumption. Our Center is actively engaged in research and development of solid polymer electrolyte fuel cell systems for these applications. This paper deals with two of the areas of our research activities: (i) investigations of electrode kinetic parameters for oxygen reduction at the platinum/solid polymer electrolyte interface, and of the mass transport parameters of oxygen in this electrolyte; and (ii) optimization of the structure of the electrode and of the membrane and electrode assembly to attain high energy efficiencies and high power densities. The other areas of on-going activities in our laboratory are scale-up of single cells, methods for thermal and water management and multicell stack development.

2. Electrode Kinetics of Oxygen Reduction Kinetics at a Platinum/Solid Polymer Electrolyte Interface and Mass Transport/Parameters of Oxygen - A Microelectrode Study (1)

A novel solid state electrochemical cell, which allows for investigations of electrochemical processes occurring at the Pt/Nafion interface, was designed and constructed (Fig. 1). The solid state cell consisted of a conventional three - electrode arrangement where the solid polymer electrolyte is sandwiched between the three electrodes under high mechanical pressure. The working electrode was a 100-μm diameter Pt fiber sealed in a flared capillary; the reference electrode was a solid state version of the dynamic hydrogen electrode; the counter electrode was a perforated foil Pt electrode. Equilibration of the electrolyte membrane with O_2 is provided by enclosing the entire apparatus in a gas-tight enclosure. The experiments were carried out at atmospheric pressure, 25°C and 99.9% relative humidity.

Cyclic voltammetry was used to assess the cleanliness of the Nafion film and of the electrode. Cyclic voltammetry was also used to determine the electrochemically active surface area of the working electrode. Low scan rate CVs (2 mV/s)

were recorded at the Pt/Nafion interface (O_2-equilibrated Nafion) to determine the kinetic parameters for O_2 reduction. The exchange current density and Tafel slope, were obtained via Tafel analysis of the pseudo-steady state CV data. A typical mass transfer-corrected Tafel plot [E vs $\log\{i_l i/(i_l - i)\}$] is shown in Fig. 2. The Tafel plot shows two well-defined linear regions extending over 2 orders of magnitude in current density. The exchange current density (Table 1) that was obtained at the Pt/Nafion interface was higher than that obtained at any other Pt-acid interface. Mass transport data were obtained from an analysis of chronoamperometric experiments. In these experiments, the potential was stepped from a value where no O_2 reduction occurred, to a potential where the O_2-reduction current was diffusion controlled. The diffusion coefficient, D and the solubility C are simultaneously determined from a current vs. $t^{-1/2}$ plot. The mass transport parameters for oxygen in Nafion determined from this study are shown in Table 2. The differences in mass transport data obtained by other workers is ascribed to the dependence of these parameters on the water content of the membrane.

3. Optimization of Electrode Structure of Solid Polymer Electrolyte/Electrocatalyst Interface (2)

(i) Alternate Methods for Localization of Platinum on the Front Surface

Electrodes with the platinum layer localized on the front surface using chemical or electrochemical methods exhibited similar performances to that of Pt sputtered electrodes. These electrodes, which were custom-made by Prototech, Inc., contained only 0.40 mg/cm^2 (20% Pt/C) prior to Pt localization. Platinum localization increased the Pt loading only by 0.05 mg/cm^2. Only a one-section Tafel line for oxygen reduction on these electrodes, with a slope of 60 mV/decade, was observed over the current density range of 1 mA/cm^2 to 2 A/cm^2. The reason for this behavior is that on the high surface area electrocatalyst, the potential of the oxygen electrode was in the oxide covered region over the entire current density range.

(ii) Reduction of Membrane Thickness and Use of Alternate Membranes to Enhance Power Density

In order to achieve high power densities, it is necessary to minimize the slope of the linear region in the cell potential versus current density plot. Two methods were used to reduce the slope of this line. In the first, thinner Nafion membranes (50 and 100 μm rather than 175 μm) and in the second, Dow membranes (125 μm thick) with better conductivities and water retention characteristics were used. Reactant gas cross-over and the consequent creation of hot-spots and pin-holes must be taken into consideration in the optimization of thickness of membranes. The best performance was obtained with the Dow membrane - a linear cell potential

vs. current density plot over the current density range 200 mA/cm^2 to 2 A/cm^2 with a slope of 0.11 ohm cm^2(Fig. 3). The current density at 2 A/cm^2 with H_2/O_2 as reactants, at 95°C and 5 atm pressure was 0.6 V. Mass transport limitations were negligible with the Dow membrane (125 μm thick) up to 2 A/cm^2; however, mass transport effects were noticed with the Nafion membrane at 1.6 A/cm^2 (Fig. 3). This result indicates that proton and/or water transport occurs more effectively through the Dow membrane. At relatively low current densities (< 200 mA/cm^2), the difference in cell potential when using H_2/O_2 and H_2/air as reactants was about 40 mV, the expected value based on electrode kinetics, but this value increased linearly with current density due to some mass transport limitations. At 1A/cm^2, this difference was about 100 mV and at 2A/cm^2, was about 200 mV.

(iii) Increase of Pt Loading to Attain Projected Power Density

The ultimate limit of lowering the slope of the linear region was approached with the 125 μm thick Dow membrane (if the resistance of the single cell test fixtures, 0.05 ohm-cm^2, were taken into account the slope reduces to 0.06 ohm-cm^2 for the single cell). The only possible methods for further increase of power density are by using higher platinum loading electrodes, or Pt alloy electrocatalysts. Until the present time, it was possible to only investigate electrodes with a higher platinum loading. These electrodes (10 mg/cm^2 unsupported Pt black/carbon), with a carbon cloth, Torray paper or Stackpole paper substrate, were tested in single cells with the Dow membrane as the solid polymer electrolyte. Activation overpotential was lower by about 50 to 70 mV, on these electrodes, as compared to that on the electrodes with the low platinum loading. The best performance was a cell potential of 0.7 V at a current density of 2 A/cm^2(Fig. 4). From these results, it was extrapolated that to attain still higher power densities, for example, current density of 8 A/cm^2 at a cell potential of 0.5 V, it will be necessary to use Dow membranes with a thickness of 75 μm.

4. Acknowledgements

This work was supported by the Defense Advanced Research Projects Agency - Office of Naval Research, (Contract #N00014-88-K-0389), Energy Research in Applications Program, Texas Higher Education Coordinating Board (Contract #249) and Electrochem, Inc., (Contract #L800079), and Center for Space Power - Texas A&M University (Contract #NAGW-1194).

5. References

1. A. Parthasarathy, C. R. Martin, S. Srinivasan, J. Electrochem. Soc., Submitted for publication, 1990.
2. S. Srinivasan, S. Somasundaram, D.H. Swan, D. J. Manko, M. A. Enayetullah, H. Koch and A. J. Appleby, Annual Meeting of the AIChE, Nov. 6-7. San Francisco, CA, 89-14, The Electrochemical Soc., Pennington, NJ, 1989.

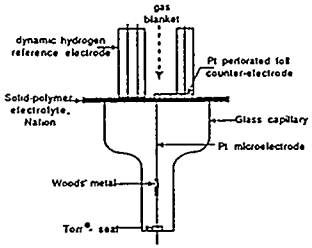

Fig 1. A schematic of the electrochemical cell

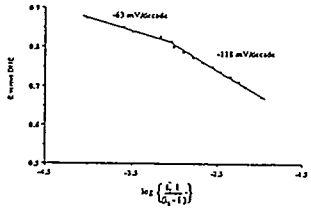

Fig 2.Tafel plot obtained for O_2-reduction at Pt/Nafion interface.

Table 1

Transport Parameters for Oxygen in Nafion	
Diffusion coefficient,D (cm^2/s)	7.4×10^{-7}
Solubility, C(mM)	26

Table 2

Electrode Kinetic Parameters for Oxygen Reduction at the Pt/Nafion interface.	
Tafel slope (mV/decade)	Exchange current density, i_o (A/cm^2)
-63 (E>0.8V vs DHE)	2.05×10^{-9}
-118 (0.650 V-0.8V vs DHE)	7.8×10^{-7}

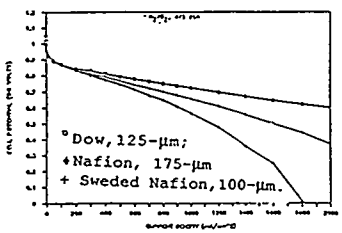

Fig 3. H_2/O_2 fuel cell performance with low Pt loading electrodes.@ 4/5 atm, 95 °C.

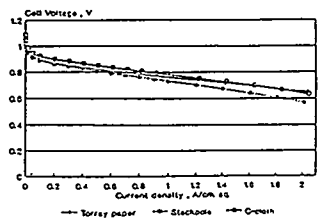

Fig 4.H_2/O_2 fuel cell performance for unsupported Pt (ElectroChem, Inc).

ONSITE FUEL CELLS AND A PACKAGED COGENERATOR AT THE SAME SITE.

Thomas Naples
Brooklyn Union Gas Co.
Brooklyn, NY 11201

ABSTRACT

The on site phosphoric acid fuel cell power plant can continuously transform the chemical energy of natural gas into usable electricity and heat. Conventional cogenerators utilize a prime mover such as an internal combustion engine driving an electric generator to produce similar outputs, recovering engine heat through heat exchangers.

In 1986, Brooklyn Union Gas completed a field evaluation of two 40-kW on site fuel cell power plants developed by the United Technologies Corporation.

Successful completion of this field test resulted in design of a commercial power plant which is in the pre-commercial stage.

In order to complete a baseline study of the results of the project, and to provide a comparison with existing cogeneration technologies, Brooklyn Union reused the fuel cell site. The 40 kW fuel cell power plants were removed, and a 75-kW packaged cogenerator designed by Tecogen,Inc. was installed. An upgraded data acquisition system was designed to provide a data base for comparison of the two technologies.

This paper will detail the results of both field tests, and provide a comparison of the data obtained.

Onsite Field Test - 40-kW Fuel Cell

In November, 1984, Brooklyn Union began operating two 40-kW power plants in a grid independent mode at JFK International Airport. The field tests were completed in September, 1986.

Performance and operating goals were set for each unit to achieve an operational availability range of 55-65% and a cumulative operating time of 8000 hours for successful fuel cell test operations. Both power plants at JFK exceeded these goals. The Staten Island Hospital unit exceeded the availability goal, but logged 6234 hours of operation. Overall electrical efficiencies for the grid independent power plants at JFK, based on the lower heating value for gas, met performance goals as specified by the manufacturer.

The three main power plant components: fuel processor, power section, and power conditioner, operated satisfactorily. Most unscheduled maintenance activities focused on ancillary components of the power plants related to the cooling system and inverter logic.

Maintenance activities, one of the unknowns at the start of the field test, were performed by Brooklyn Union personnel. With technical assistance from the manufacturer's field engineers, the in-house servicemen were competent enough to keep the units on line.

By operating and maintaining both grid independent and grid connected power plants over the course of the field test, Brooklyn Union personnel became familiar with the on site fuel cell service concept and were able to further their understanding of the fuel cell power plants operating capabilities.

75-kW Tecogen Cogenerator - JFK Airport

The 75-kW packaged cogenerator manufactured by Tecogen, Inc continues to run at the former Fuel Cell test site at JFK Airport, connected to the grid. The cogenerator is operating in a thermal following mode. It is one of two similar units being tested under a co-sponsored GRI program.

The cogenerator is a modified 60-kW Tecogen module. The manufacturer has redesigned the camshaft, and added high compression pistons. The oil circulation system has been enhanced to provide extended maintenance intervals , possibly to 4000 hours.

Operating Performance

The unit was started on February 25, 1988 for site testing purposes. After minor site modifications, the cogenerator was officially put on line on March 23, 1988.

As of August, 1990 the unit has operated approximately 12,500 hours.

Operating efficiencies have been:

Electrical	29.7%
Thermal	46.2%
PURPA	58.7%

The unit runs 21 to 22 hours a days; shutting down only in the early morning hours due to low requirement for thermal energy. There is no provision to dump the heat to keep the generator running.

Maintenance

Oil changes have been made at an average running time of 900 hours. After approximately 1500 hours, Mobil Delvac 1 oil was installed under the assumption that the interval could be increased to 1500 hours. However, Tecogen engineers monitoring the project suggested using Exxon XD oil.

The unit has been running with A C and Champion spark plugs. After an average of 500 hours, several experienced cracked insulators. Stitt spark plugs were installed and we report good experience with these plugs.

Summary

Preliminary comparison of the two systems is indicated below. Final analysis will be presented when the 75-kW field test is completed.

	Fuel Cell Power Plants		75-kW Tecogen
	Unit 8231	Unit 8236	
Duration of Test	18 mos.	19 mos.	28 mos.
Total Hours of Operation	8,502	10,064	12,500
Longest Continuous Run (hours)	1,502	1,654	750 (note 1)
Unadjusted Availability	67%	72%	72%
Estimated Electricity Generated	318.5 MW	354 MW	930 MW
Avg. Electrical Efficiency	43%	42%	29%
Estimated Recovered Heat	508.5 mmBTU	595 mmBTU	3,500 mmBTU

Note 1. Scheduled shut down for 750 hour maintenance.

References

Londos, T. "40-kW Fuel Cell Field Test Summary Report" June, 1987

Naples, J.F. "Packaged Cogenerator's Time Has Come - Fact or Fiction?" CSI Report, 27 , 9 Mar. 1990

CORROSION-RESISTANT CATALYST SUPPORTS FOR PHOSPHORIC ACID FUEL CELLS

J.A. Kosek, C.C. Cropley and A.B. LaConti
Giner, Inc.
14 Spring St.
Waltham, MA 02254-9147

INTRODUCTION

High-surface-area carbon blacks such as Vulcan XC-72 (Cabot Corp.) and graphitized carbon blacks such as 2700°C heat-treated Black Pearls 2000 (HTBP) (Cabot Corp.) have found widespread applications as catalyst supports in phosphoric acid fuel cells (PAFCs). However, due to the operating temperatures and pressures being utilized in PAFCs currently under development, the carbon-based cathode catalyst supports suffer from corrosion, which decreases the performance and life span of a PAFC stack.

The feasibility of using alternative, low-cost, corrosion-resistant catalyst support (CRCS) materials as replacements for the cathode carbon support materials was investigated. The objectives of the program were to prepare high-surface-area alternative supports and to evaluate the physical characteristics and the electrochemical stability of these materials. The O_2 reduction activity of the platinized CRCS materials was also evaluated.

The CRCS materials were prepared using a low-cost, energy-efficient, self-propagating high-temperature synthesis (SHS) method. Originally developed to produce dense, hard ceramics (1), the SHS technique can also be used to prepare loose powders (2). The general method of manufacture is to ignite a pressed pellet of the mixed reactant powders with a resistance heated coil inserted at one end of the reaction vessel; a drawing of the apparatus is shown in **Figure 1**. The reaction proceeds through the pellet from one end to the other spontaneously, due to the heat generated by the exothermic combustion. The process generally results in a nearly complete transformation with 0.2 wt% or less unreacted residue. An inert atmosphere is usually used to preserve product purity. Several variables, including the molar ratio, type, purity and particle size of the reactant powders affect the properties of the CRCS materials. In our work, the molar ratios of select corrosion-resistant reactant powders were varied. Subsequent to preparation, the CRCS materials were evaluated for surface area, electrical conductivity, particle size, corrosion resistance, and after catalyzation, oxygen reduction activity.

RESULTS

The surface areas (BET method), conductivities and particle sizes of the CRCS materials were measured and compared with similar properties of Vulcan XC-72 and HTBP, two state-of-the-art catalyst supports. As expected, surface areas of the CRCS materials were lower than those of Vulcan and HTBP, but respectable surface areas as high as

20 m^2/g were obtained. Particle sizes of the CRCS materials were comparable to those of Vulcan and HTBP, while electrical conductivities of the CRCS materials were higher by a factor of six.

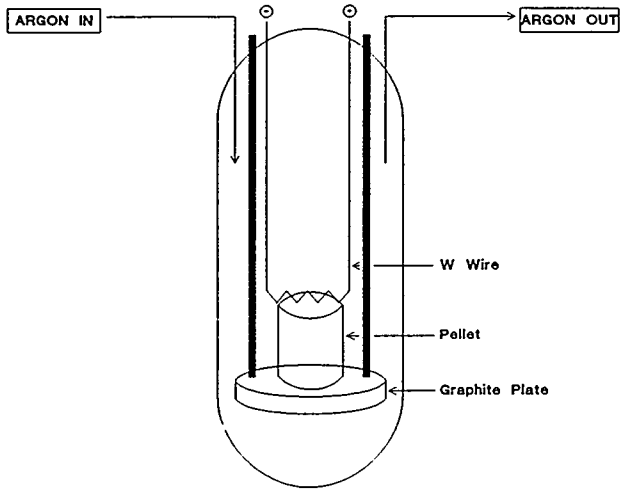

FIGURE 1. SHS REACTOR ASSEMBLY

Corrosion currents of the CRCS materials were measured at 1.0 V vs. a Dynamic Hydrogen Electrode (DHE) for 1,000 minutes in N_2 saturated, 190°C, 100% H_3PO_4. Typical results are shown in **Figure 2.** For several of the CRCS materials, duplicate samples were soaked overnight in air-saturated, hot, concentrated H_3PO_4 prior to the corrosion current measurements to leach out any unreacted starting materials; typical results are also shown in Figure 2. Corrosion currents for Vulcan and HTBP were also measured and plotted in Figure 2 as reference points.

The lowest corrosion current for the CRCS materials was observed for sample CRCS-8; a slightly lower current was observed for a duplicate sample which had been pre-soaked in H_3PO_4. However, this difference in corrosion currents was not considered to be significant. Corrosion currents of samples CRCS-8 and H_3PO_4 leached CRCS-8 were comparable to those observed for HTBP after 1,000 minutes and much lower than those observed for Vulcan.

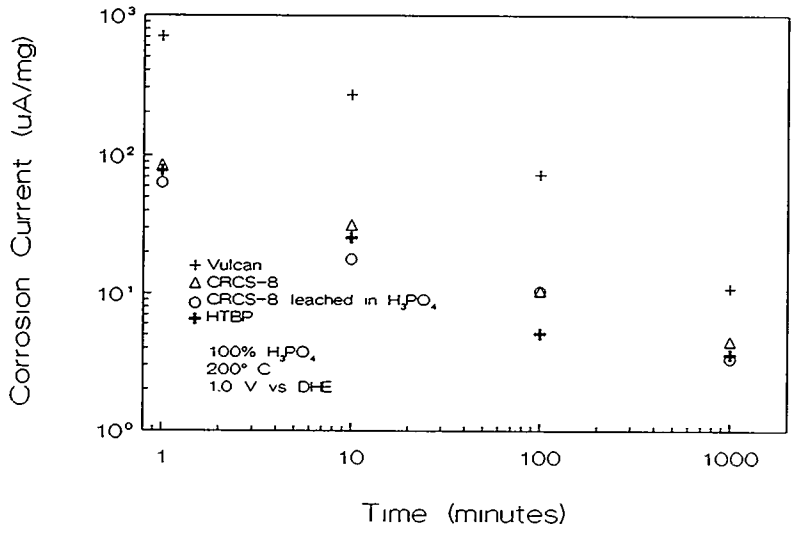

FIGURE 2. COMPARISON OF CORROSION CURRENTS OF CRCS-8, HTBP AND VULCAN

Samples of CRCS-8 and CRCS-16 were catalyzed with Pt and evaluated for O_2 reduction activity using a floating-electrode half-cell apparatus. Results are shown in Figure 3. At current densities below 100 mA/cm² the performance of Pt/CRCS-16 was superior to that of Pt/Carbon; below 20 mA/cm² the performance of the two CRCS materials was essentially identical. The drop-off in performance at the higher current densities was due to the use of unoptimized electrode structures which were partially flooded.

CONCLUSIONS

High-surface-area, conductive, corrosion-resistant catalyst supports can be prepared by the simple, efficient, SHS technique. The electrochemical stability of a CRCS material in hot, concentrated H_3PO_4 was greater than that of Vulcan and equivalent to that of HTBP. The O_2 reduction activity of platinized CRCS was superior to that of platinized carbon at low current densities.

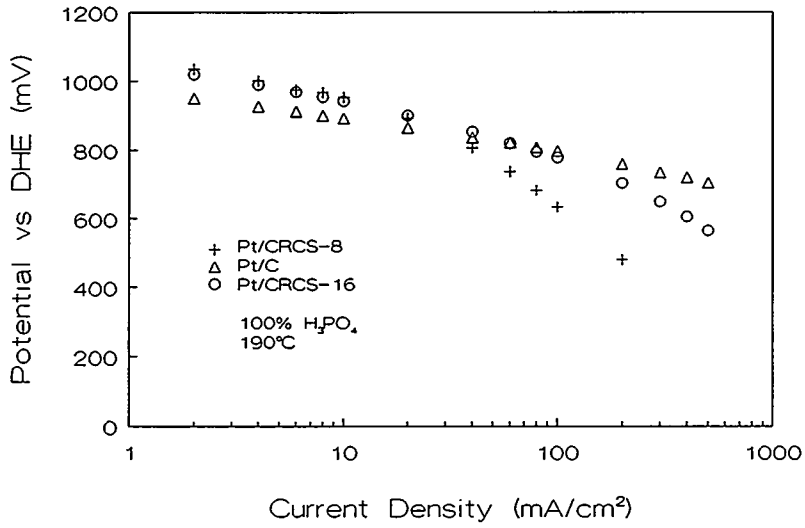

FIGURE 3. COMPARISON OF OXYGEN REDUCTION ACTIVITY OF PT/CRCS TO PT/CARBON

ACKNOWLEDGMENT

This work was supported by the U.S. Department of Energy under Contract DE-AC02-89ER80807. Continued funding is being provided under U.S. Department of Energy Grant No. DE-FG-90ER80861.

REFERENCES

1. A.G. Merzhanov and I.P. Borovinskaya, Dokl. Chem. [*Eng. Trans.*], **204**, 429 (1972).

2. E. Riley, R.J. Wright and M.A. Riley, "A Novel Method for Generation of Submicron Carbides and Borides," Paper presented at the 18th Annual Meeting of the Fine Particle Society, Aug. 3-7, 1987, Boston, MA.

WORK ON THE LARGE SCALE ADVANCED TYPE PAFC

M. YAMAGUCHI, N. UOZUMI, M. IZUMITANI
Hitachi Research Laboratory, Kokubu Works
1-1-1 Kokubu-cho Hitachi-shi Ibaraki-ken, 316 Japan
Y. TSUTSUMI
Ibaraki University
4-12-1 Nakanarusawa-cho Hitachi-shi Ibaraki-ken, 316 Japan

Introduction

Important problems for PAFC (phosphoric acid fuel cell) development are cost reduction and longer cell lifetime. We have been studying an advanced type PAFC as a means to solve these problems and a configuration was reported at the 1988 FC seminar[1]. Since then we have developd a large scale cell of this type. This paper reports on its test results.

Cell configuration

The cell configuration is shown in Fig.1. One stack is assembled from two types of components, namely, a unit cell and a porous ribbed bipolar plate. The unit cell is a flexible unified component composed of a matrix sheet, two catalyst sheets and surrounding solidified edge seal. This configuration needs less time for making the catalyst layers and for combining the edge seal with the catalyst layers and the matrix layer. Unit cell can be handled easily by hand since they are assembled in. The porous ribbed bipolar plate is a rigid unified component composed of a non-porous flat plate separator, porous ribs and four non-porous edge plates. The purposes of using this separator are to increase the mechanical strength of each structural element which allows

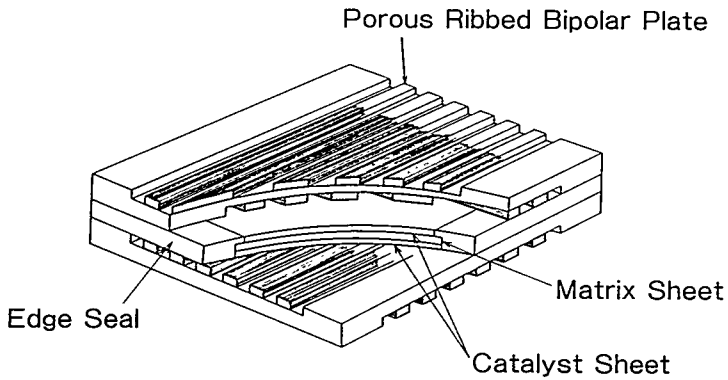

Fig.1 Cell Configuration

their thickness to be reduced and to reduce electrical and thermal contact resistance by conjugating porous ribs to the separator. With this configuration cell thickness is reduced to about half that of the conventional ribbed electrode type cell. Two cell sizes are used. One is a 3600 cm class large size cell and another is a 100 cm class small size cell. The latter is used to study the cell voltage-time characteristics of the PAFC.

Test Results

Fig.2 shows the voltage-current (V-I) characteristics of the advanced type large size cell compared with the conventional ribbed electrode type cell. The cell voltage of the advanced type cell is nearly the same as that of the conventional type cell. Taking cell thickness reduction into account, this means that the power generation density of the former is about twice as much as the latter. The cell resistance of the advanced cell which is calculated from the slope of the V-I characteristics also is less than that of the conventional type cell. Fig.3 shows the temperature rise-current density characteristics. The temperature rise of the advanced cell is about 20 % less than that of the conventional type cell. We think the lower cell resistance and temperature rise are due to the cell thickness reduction. Fig.4 shows the performance history of the advanced type cell. Cell voltage has been stable until 6000h and the cell is still undergoing testing. The drop in the voltage-time curve is under 5.0mV/1000h. We hope that these cell technologies will contribute to cost reduction in commercializing PAFCS.

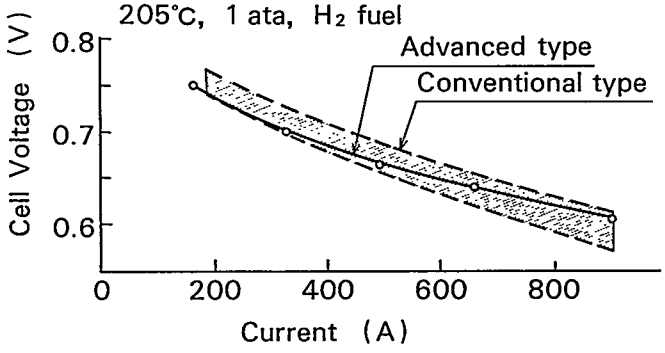

Fig. 2 V-I Characteristics of Cells

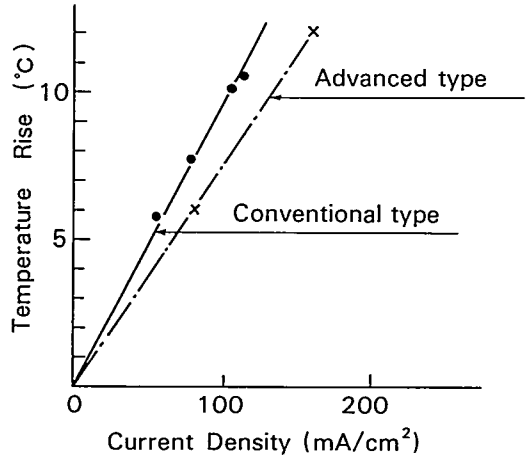

Fig. 3 Temperature Rise in Stack Direction

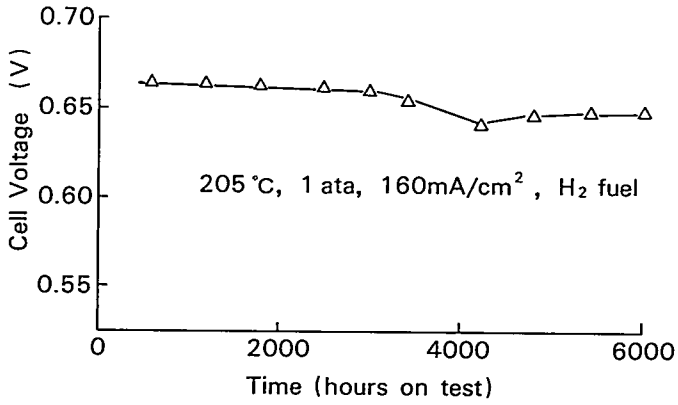

Fig. 4 Performance History of the Advanced Type Cell

Journal Articles
1.Y.Tsutsumi,"STUDY ON ADVANCED TYPE PHOSPHORIC ACID FUEL CELLS"
1988 Fuel Cell Seminar

A WORLDWIDE PERSPECTIVE ON FUEL CELL MARKETS

Diane Traub Hooie, P.E., Ph.D.
NORA Management, Inc.
Matawan, NJ 07747

Over the past three years, the author has developed a market model that encompasses five different types of fuel cells (alkaline, polymeric membrane, phosphoric acid, molten carbonate, and solid oxide systems) and fourteen applications, ranging in size from 1 kW to multi-MW. This model was developed to run on an IBM-compatible computer with at least 512 kB RAM.

In this model, fuel cells were compared, on a competitive life cycle cost basis, to gas engines, gas turbines, uninterruptible power supplies, other generator types of power supplies, combined cycle equipment, and the electric grid, to develop estimated market potentials worldwide. Data contained in this model was obtained from numerous literature sources, as well as personal contacts with each of the manufacturers. In addition, both objective information (such as energy consumption trends) and subjective information (such as technical viability) were included in the model. Assumptions utilized in the model as well and limitations of the model projections will be discussed. In addition, market opportunities for European, Asian, and North American market areas will be presented.

THE DEVELOPMENT OF AN SPFC POWER GENERATION SYSTEM DEMONSTRATOR

C.M. Seymour,
Vickers Shipbuilding & Engineering Limited,
Barrow-in-Furness, LA14 1AF, U.K.

R.A.J. Dams,
C.J.B. Developments Limited,
Portsmouth, PO3 5PG, U.K.

During late 1989, VSEL and CJBD embarked upon a project ultimately aimed at producing power generation systems based upon solid polymer fuel cell technology. The two companies already had certain specific markets in mind but believed that there was greater potential if the right approach to design and marketing could be taken.

The key factors for these markets were believed to be:-

i) The ability to use a readily available fuel which could be handled easily and safely.

ii) The emphasis on total system design so that the end user need have no involvement in further design or development.

ii) The system must show cost and/or performance benefits over existing power generation devices or the technology must allow power to be generated under conditions not otherwise possible using existing systems.

In order to produce a power generation package to meet these market requirements it is necessary to address the total system design. If attention is focused solely on fuel cell stack development to the detriment of supporting systems for instance the result will inevitably be an unbalanced design which fails to satisfy the needs of the application. VSEL and CJBD decided to base systems upon the Ballard Solid Polymer Fuel Cell Stack and concentrate their efforts on the development of the supporting systems and overall package. By working with Ballard in this way and feeding back system performance requirements, the fuel cell can be further developed to more closely match the applications.

In order to ensure that the system specification meets the market demands, the approach shown in Figure 1 was adopted, where the starting point was the identification of major attributes. Typically, these would be cost and performance issues as shown in Figure 2.

Different markets require emphasis on different attributes so it is necessary that these attributes be weighted in terms of importance for each application. This allows a balance to be drawn between the many conflicting requirements, notably maximum performance at minimum cost. This requires a great deal of market information and the early phase of this project concentrated on gathering these data.

Once the relative importance of key attributes is known it is possible to produce a range of design options for further study. In order to investigate these design options further, a series of parametric studies is conducted, aided by a mathematical model which ideally addresses the complete system. The VSEL/CJBD model uses empirical equations based upon actual equipment performance data. For the fuel cell stack for instance voltage is modelled as a function of current, temperature, air and fuel pressures as well as air and fuel utilisation rates based upon current fuel cell performance data. From this equation fuel cell efficiency is derived and hence gas consumption rates, etc.

Once completed, the parametric studies are subjected to a selection analysis procedure to identify the option which best meets the balance of key attributes identified earlier. At this point a system specification can be written and it is only after this that the specification for sub systems and components can be addressed in detail.

The current phase of the project is aimed at producing a 20kW system demonstrator. The system will be generic at this time, not being designed for a specific application. It will however serve to demonstrate the potential attractions to a variety of markets, both military and industrial.

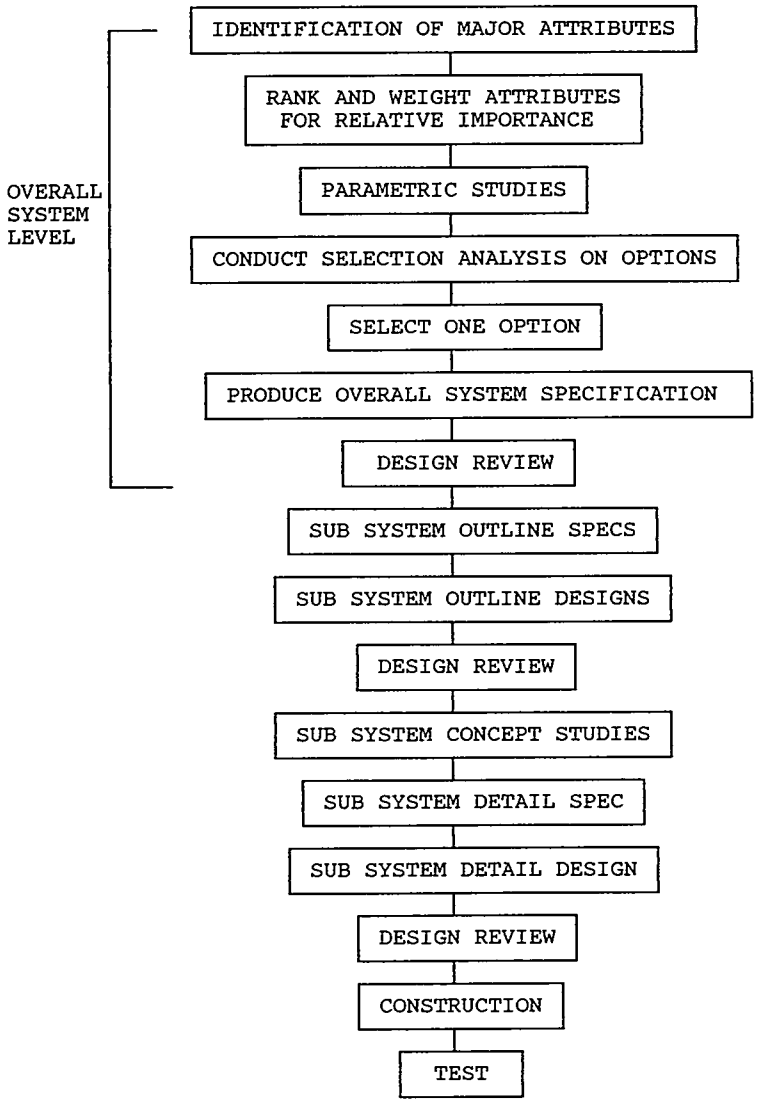

FIGURE 1

FUEL CELL SYSTEM DESIGN FLOW CHART

SYSTEM CONSTRAINTS

For a particular application:

Power required
Electrical output form
Fuel type

SYSTEM ATTRIBUTES

Volume
Weight
Unit Production Cost
Through Life Cost
Overall efficiency
Noise/vibration
Exhaust gas temperature
Exhaust gas composition
Life
Availability, Reliability & Maintainability
Development risk/timescale
Start up time
Transient response capability
Ability to accept alternative fuels with minimum further development
Environmental factors e.g. humidity, temperature, angles of inclination etc.

FIGURE 2

FUEL CELL SYSTEM CONSTRAINTS AND ATTRIBUTES

DEMONSTRATION TEST OF A 200 KW PAFC POWER PLANT AT AN OFFICE BUILDING

M. Harada and N. Hashimoto
Fuel Cell Development Dept.
Osaka Gas Co., Ltd.
2-95, 3-Chome, Chiyozaki,
Nishi-Ku, Osaka 550, Japan

Y. Tanohata and S. Sugiura
Building Design Dept.
Takenaka Corporation
1-13, 4-Chome, Hom-Machi,
Chuo-Ku, Osaka 541, Japan

INTRODUCTION

Osaka Gas, in cooperation with Takenaka Corporation, installed a natural-gas fueled 200 kW PAFC unit, developed and manufactured by International Fuel Cells Corporation (IFC), at the site of the Umeda Center Building in downtown Osaka in April, 1989, and has been conducting a demonstration test. The objectives of the demonstration test are as follows:

1. Technological evaluation
2. Accumulation of experiences in legal procedures and field operation
3. Demonstration of the advantages of a fuel cell unit as a co-generation system to potential customers.

Over 3,800 hours have been logged on the unit as of the end of July, 1990. Several system failures have been experienced.

TEST SITE

The Umeda Center Building is a 32-story office building with two basement levels and is well known for its "intelligent" design. The building was designed and built, and is owned by Takenaka, one of the biggest construction firms in Japan. The company is interested in introducing natural-gas fueled PAFC's for commercial building use to offer customers efficient energy services with less impact on the environment. The overall power demand of this building is 4,200 kW. Figure 1 shows a photograph of the building.

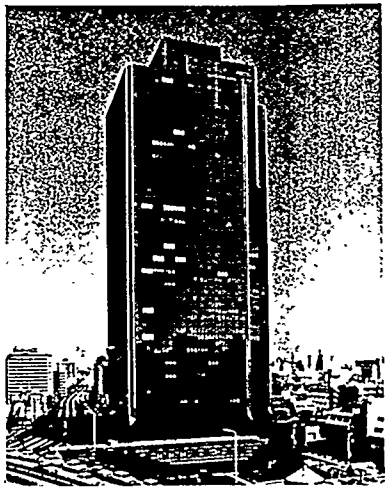

Fig. 1 The Umeda Center Building

200 KW PAFC UNIT

The PAFC unit being operated at the building is one of four PC25 pre-prototypes manufactured and sold to Japan by IFC, and is called the "PC25YX-1". These four units were designed and manufactured to demonstrate technical improvements which were made based on experience gained through GRI PC18 Manufacturing and Field Test Program. The improvements included higher power density, greater system simplicity, higher operational sophistication and better manufacturability.

The design features and specifications of the PC25YX-1 are shown in Table 1. Figure 2 shows a photograph of the PC25YX-1 installed at the site of the Umeda Center Building.

Table 1. PC25 Design Features and Specifications

	Pre-prototype (PC25YX-1)	Initial Lot (PC25)
Rated Power (Net)	180-190 kW	200 kW
Elec. Efficiency	37% (LHV)	40% (LHV)
Heat Recovery	Hot Water (Max. 75℃)	High-Grade Heat Option (90℃)
Fuel	Natural Gas(100-356mmH$_2$0)	Natural Gas(100-356mmH$_2$0)
Operating Mode	Grid Connected	Grid Connected/ Grid Independent
Dynamic Response	10 kW/S (Gross Power)	Grid Connected: 15 S (0 to 200 kW Net) Grid Independent: Load Following
Cooling System Heat-up Method	Electric Heater (75 kW)	Electric Heater (22 kW) and Gas Boiler
Start-up Time	3.5 Hrs	Less than 5 Hrs
Dimensions	3.0(W)×11.3(L)×3.5 m(H)	3.0(W)×7.3(L)×3.5 m(H)
Weight	36 Tons	30 Tons

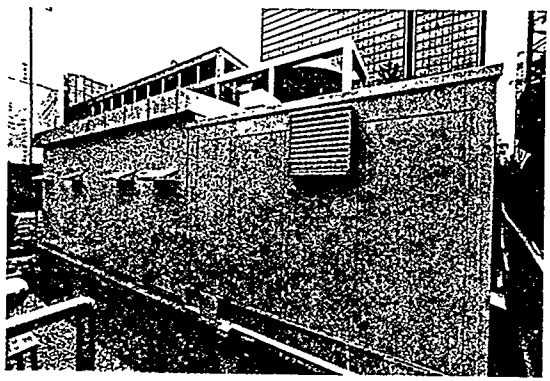

Fig. 2 PC25YX-1 at Umeda Center Building

SITE FACILITY

The PC25YX-1 is connected to the grid of the lower floors of the building. The power generated is supplied to the air conditioners and ancillary equipment. Unless interrupted by an

automatic shutdown, the power plant operates continuously at the set power level, 24-hours a day. The unit can provide, at maximum, approximately 10 % of the annual electric power demand of the entire building. The rejected heat from the cooling system and exhaust gas from the unit is recovered as hot water and supplied to the lower level of the building. Figure 3 shows the PC25YX-1 electrical and heat recovery system.

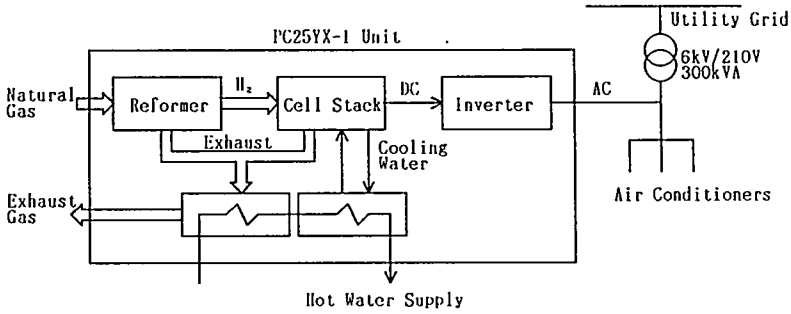

Fig. 3 Electrical and Heat Recovery System

OPERATING EXPERIENCE

After installation was finished, pre-start preparation was done at the site, including component checkout and simulation, operational simulation and stack dry out. Commencement of operation had to be delayed until September, 1989 due to various government procedures and was then interrupted for four months until the end of March, 1990 for the same reason. As of the end of July, 1990, the accumulated operation exceeded 3,800 hours. The longest continuous run was 833 hours and the unit was started a total of 20 times.

Various performance data were obtained during the operation. The electrical efficiency, component efficiency and cell performance at the beginning of operation are shown in Figures 4, 5 and 6 respectively.

So far, the operation has been suspended 12 times due to forced shutdowns. Table 2 classifies the reasons for the forced shutdowns. In all of these cases, the problemes were minor and operation was resumed after repair or replacement of parts. The durability of the power section is not so good as we expected.

Table 2 Forced Shutdown Causes

Cooling System Steam/Water Leak	4 Times
Diagnostic/Control System Failure	4
Solenoid Valve Failure	1
Causes Exterior to the Unit	3

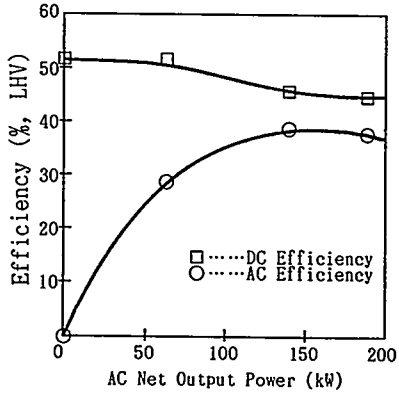

Fig. 4 Electrical Efficiency

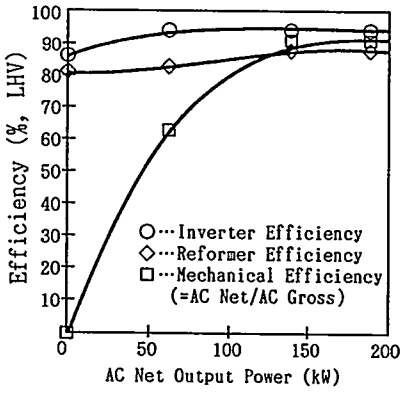

Fig. 5 Component Efficiency

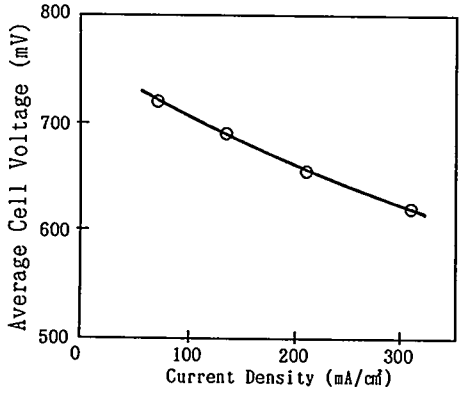

Fig. 6 Cell Performance

The level of emmissions from the power plant at the rated power were measured. NOx was less than 2 ppm. This ppm level represents the smallest amount detectable by the measuring equipment used.

CONCLUSIONS

PC25YX-1 unit met its specification requirements and showed good environmental characteristics. The system design has been simplified and its function made more sophisticated, leading to both easy operation and maintenance.

IFC has been developing the PC25, 200 kW commercial unit. The design features and specifications of the PC25 are shown in Table 1 as compared to those of the PC25YX-1.

A STUDY ON THE COSTS OF ELECTRICITY GENERATED BY FUEL CELLS AND CONVENTIONAL POWER PLANTS IN TAIWAN

Moses L. Ng, Cheng-Chih Chen and Yaw-Chung Cheng
Energy and Resources Laboratories
Industrial Technology Research Institute
Hsin Chu, Taiwan, Republic of China

INTRODUCTION

In recent years, Taiwan has experienced enormous economic growth. Per capita GNP increases from US$ 1,223 in 1969 to US$ 7,518 in 1989, representing an annual average growth rate of 7.2% [1]. However, the island is heavily dependent on imported energy. Last year, 48 million kiloliters of oil equivalent representing 93% of the total energy was imported [1]. On the other hand, like everywhere in the world, the general public concerns very much for clean living environments. This problem is particularly prominent here as the island is densely populated. For these reasons, both the Energy Commission of the Ministry of Economic Affairs of the Republic of China and the Taiwan Power Company have great interests in fuel cells as this technology is known to be more efficient and relatively benign to the environment.

In 1982, the U.S. Department of Energy conducted a study on assessing the potential value of U.S. fuel cell technology in foreign countries. The report [2] concludes that having examined the technical and fiscal facets of the problem in light of Taiwan's resources, abilities, trade experiences, needs, goals, and attitudes, there does exist an opportunity for commercial United States suppliers to furnish Taiwan with fuel cell systems. Consequently in 1987, the Energy and Resources Laboratories of the Industrial Technology Research Institute performed "A Feasibility Study on Development of Fuel Cell Power Plants in Taiwan" sponsored by the Taiwan Power Company. It is concluded [3] that now is the best time to introduce this new technology to Taiwan as fuel cell power plants are anticipated to be fully commercialized in the near future.

METHODS

In this study, the basic power generating costs comprising of installation, operation and maintenance as well as fuel costs were calculated for fuel cells and other conventional power plants including nuclear, coal-fired, oil-fired as well as gas-fired power plants. A set of common criteria such as inflation and interest rates, different load capacity factors as base, intermediate as well as peak loadings, etc., was used to determine the present value net revenue of each power plants including fuel cells. Similar conditions of reserve margin, plant lifetime and construction time of each individual power

plants were considered. This method was consistent with the one used in the study performed by the Lawrence Livermore Laboratories mentioned above [2]. Sensitivity tests on different inflation and interest rates were also included.

Both large and small fuel cell power plants representing the supply- and the demand-side-of-the-meter were considered because of the low environmentally intrusive characteristics of fuel cells making possible for both centralized and on-site applications. For centralized applications, the cost of electricity for both present (based on IFC's 11 MW PC23) and future (based on EPRI's prediction [4] of both market entry 16 MW uprated PC23 and 100 MW advanced) fuel cell power plants were calculated. For on-site applications, the costs of electricity (based on IFC's 200 kW PC25) were calculated with and without savings on fuels by cogeneration since it can easily be applied to fuel cell systems.

Table 1 is a summary of cost data and assumptions used in this study. Note that these data were provided by the Taiwan Power Company representing figures being used in the course of evaluating power plants of different technology to be constructed in Taiwan. The inflation and interest rates were chosen as 3% and 10% respectively as they were reported by the government.

RESULTS AND DISCUSSIONS

The results of the calculations using assumptions mentioned above are presented in Table 2. Understandably, the cost of electricity generated by IFC's PC23, being a demonstrator, is the highest among present power generating technologies. However, it is predicted that the market-entry 16 MW uprated PC23 will be competitive to thermal such as gas-fired power plants. Furthermore, the advanced fuel cells, being more efficient and less expensive as predicted by EPRI, can be seen may even be comparable to nuclear power plants. Note that these calculations do not include the costs on environmental pollution controls which will definitely raise the generation costs for conventional power plants, especially the coal-fired thermal power plants.

The results of sensitivity tests on different interest rates at 3% inflation rate on different power plants used for intermediate loading are plotted in figure 1. Figure 2 presents the results of sensitivity tests on different interest and inflation rates on intermediate loading of 200 kW PC25 for on-site applications with savings on fuels with cogeneration. As a reference, the national average electricity rate of Taiwan in 1989 was NT$ 2.15/kWh with slightly higher average charge in the commercial sector at NT$ 2.97/kWh.

CONCLUSIONS

(1) The installation costs of the present fuel cell power plant are high as PC23 is not a commercialized product. Costs of electricity generated by fuel cells will be lowered as fuel cells markets mature.

(2) Fuel cell power plants may be more competitive with the conventional power plants in Taiwan as the costs for environmental pollution controls are considered.

ACKNOWLEDGEMENTS

This work was initiated by the Taiwan Power Company and is now sponsored by the Energy Commissions of the Ministry of Economic affairs of the Republic of China under contract 798Q1.

REFERENCES

1. "The Energy Situation in Taiwan, Republic of China", Energy Commission, Ministry of Economic Affairs, 1990.

2. V. R. Latorre and L. R. Spogen, Jr, "Fuel Cell Technology Assessment: vol IV - Evaluation of Taiwan", Lawrence Livermore Laboratory, UCID 19412, 15 Aug. 1982.

3. M. L. Ng, Y. C. Cheng, C. H. Liao and C. C. Chen, "A Feasibility Study on Development of Fuel Cell Power Plants in Taiwan", (in Chinese), Energy and Resources Laboratories, ITRI, Taiwan, R.O.C., 1988.

4. E. W. Hall, L. M. Handley and G. W. May, " Capital Cost Assessment of Phosphoric Acid Fuel Cell Power Plants for Electric Utility Applications", EPRI report AP-5608, March 1988.

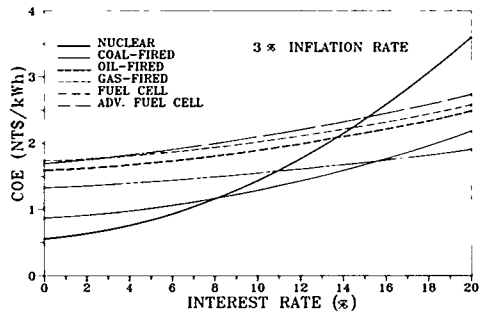

Figure 1. Effects of interest rates on the costs of electricity generated by power plants of intermediate loading at 3% inflation rate in Taiwan.

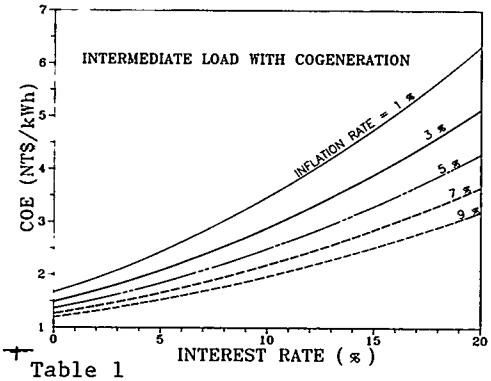

Figure 2.
Effects of interest and inflation rates on the costs of electricity of intermediate loading of on-site PC25 fuel cells with savings o fuels by cogeneration.

Table 1
Cost Data and Assumptions Used for Calculating Costs of Electricity Generated by Power Plants in Taiwan

	POWER PLANTS*							
	A	B	C	D	E	F	G	H
Inst'n Cost (10^3NT$/kW)	50.8	26.7	20.0	18.9	103.5	30.9	17.2	74.8
Inst'd Cap. (MW)	2000	2200	2200	2200	11	16	100	0.2
O & M Cost (NT$/kWh)	0.088	0.106	0.035	0.037	0.163	0.163	0.082	0.163
Const'n Time (years)	8	6	5	5	2	2	2	2

* A: Nuclear; B: Coal-fired; C: Oil-fired; D: Gas-fired;
E: Fuel Cell (PC23); F: Fuel Cell (uprated PC23);
G: Advanced Fuel Cell; H: Fuel Cell (PC25).
@ All costs in 1989 dollars.
# Exchange rate: 1 US$ to 26 NT$.

Table 2
The Cost of Electricity Generated by Fuel Cells and Conventional Power Plants of the Republic of China at 10% Interest Rate and 3% Inflation Rate

	POWER PLANTS*							
	A	B	C	D	E	F	G	H+
Base Load (NT$/kWh)	1.439	1.280	1.891	2.010	3.455	2.091	1.542	2.970 [2.298]
Int. Load (NT$/kWh)	1.904	1.510	2.057	2.167	4.234	2.323	1.672	3.554 [2.882]
Peak Load (NT$/kWh)	3.001	2.048	2.447	2.535	6.050	2.865	1.975	4.917 [4.245]

+ [] denotes COE with savings on fuels by cogeneration.

ELECTROCHEMICAL EVALUATION OF THE EFFECT OF PTFE CONTENT ON THE PERFORMANCE OF FUEL CELL ELECTRODES

D. Rocco de Sena, E.A. Ticianelli and E.R. Gonzalez
Instituto de Física e Química de São Carlos/USP
C.P. 369 - 13560 - São Carlos (SP) Brazil

In this work, the effect of PTFE content on the electrochemically active area and on the capacity and resistance of the interface of gas diffusion electrodes for phosphoric acid fuel cells is evaluated. It is believed that a knowledge of these parameters will contribute to establish better models for this type of electrode.

Gas diffusion electrodes were made with a filtration method . The Pt content for all electrodes was 0.6 mg cm^{-2}.The cell contained a PTFE support for the gas diffusion electrode, a Pt-gauze counterelectrode and a hydrogen reference electrode. Solutions were 0.5 M in H_2SO_4. Impedance measurements were carried out with a Solartron 1250 Frequency Response Analyser. All other measurements were done using a PAR 273 Potentiostat.

Figure 1 shows the Tafel plots for the oxygen reduction reaction (ORR) for some of the electrodes containing different amounts of PTFE. The corresponding Tafel parameters are shown in Table 1.

According to Fig. 1 the electrode with the best performance is that with 35% PTFE. Also, this is the only one presenting only two Tafel slopes. b_1 and b_2 have values that are very similar to those observed on flat Pt electrodes [1] while the third slope, when present, has values that are twice as much as those of b_2. This type of behaviour has been predicted by theoretical models already presented [2,3]. For the electrodes containing 0, 11.5 and 20.8% PTFE the flooded agglomerate model [2] is probably the one that suits best because of a low degree of hydrofobicity. Thus the presence of a third Tafel slope can be attributed to diffusional limitations. On the other hand, the electrode with 49.6% PTFE is highly hydrophobous and in this case the thin film model [3] may be more adequate. Thus, the third Tafel slope may be attributed to a larger potential drop within the pores responsible for an uneven current distribution. It may then

Table 1. Tafel parameters for the RRO on electrodes with different PTFE contents. b_1, b_2 and b_3 are the slops at low, medium and high current density, respectively.

% PTFE	b_1(mV)	b_2(mV)	b_3(mV)	$i_{(0,7V)}$ ($mAcm^{-2}$)
0	56	100	228	51.8
11.5	54	100	240	38.2
20.8	58	95	180	68.8
35.0	61	120	-	115.4
46.9	54	100	195	52.4

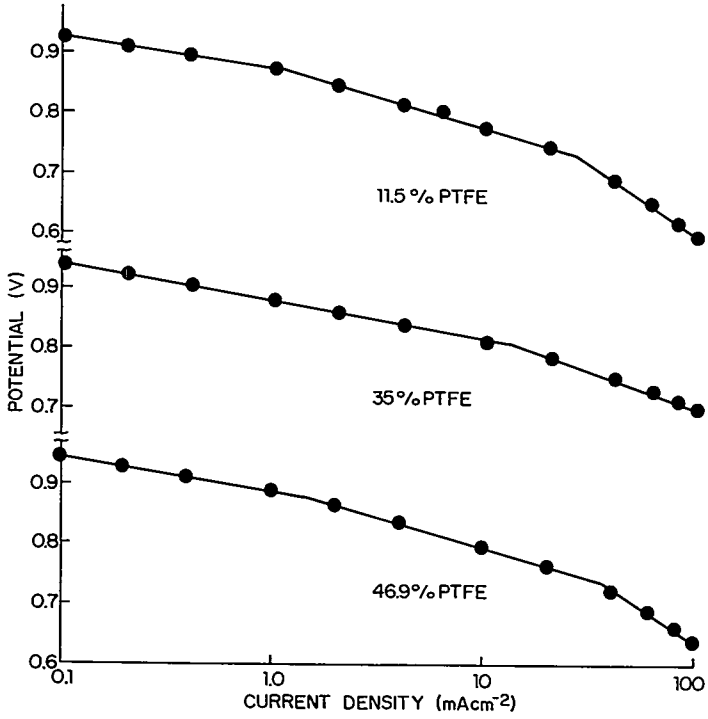

Figure 1. Tafel plots for different PTFE contents.

be concluded that for the electrode containing 35% PTFE the effects of either limiting diffusion or a high potential drop may appear at higher current densities when compared with the other compositions, thus showing a better performance, which is kinetic terms is very similar to that of a flat electrode.

Figure 2 shows cyclic voltammograms for two of the electrodes in the absence of oxygen. The active area of the electrodes can be evaluated through the characteristic hydrogen oxidation peak and the results are shsown in Figure 3. The active area decreases with the increase in PTFE content showing a reducced accessibility to the Pt particles. This result gives support to the proposed change from the flooded agglomerate to the thin film model as the PTFE content increases.

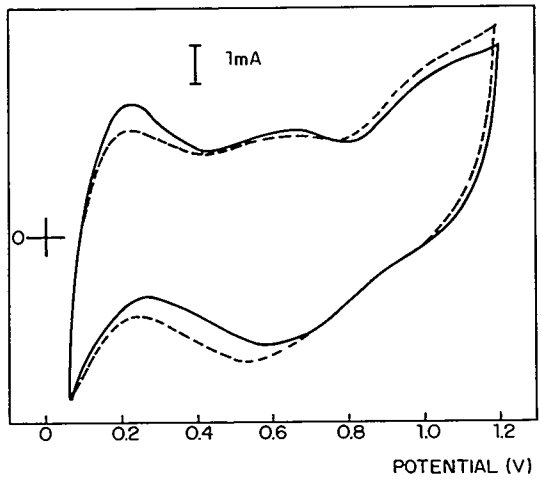

Figure 2. Cyclic Voltammograms for electrodes without (solid line) and 46.9% PTFE (broken line). v = 5 mV s^{-1}

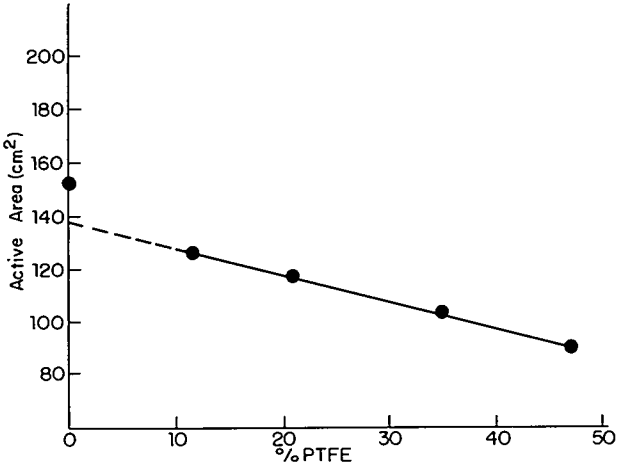

Figure 3. Active area as a function of PTFE content.

Figure 4 presents a Bode plot for the ORR on the electrode with 35% PTFE at 0.7 V. The response was essentially similar for the other electrodes. The Bode plot suggest a simple equivalent circuit of the type 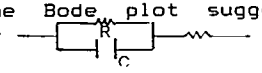

and the values of the parameters are presented in Table 2.

Table 2. Parameters of the equivalent circuit for electrodes with different PTFE contents.

% PTFE	R(Ω)	C(F)
0	6.04	0.220
11.5	5.44	0.072
20.8	3.59	0.088
35	3.28	0.085
46.9	4.19	0.077

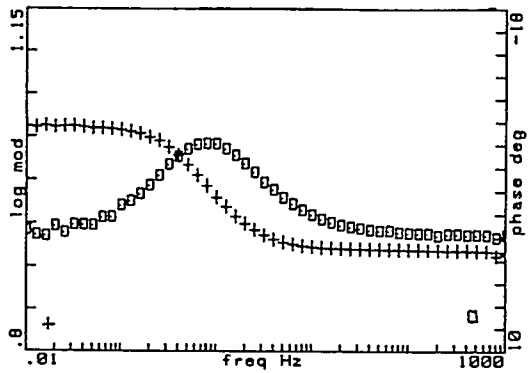

Figure 4. Bode plot for an electrode with 35% PTFE.

The dependence of R on the PTFE content shows that structural characteristics of the electrode influence the rate of the reaction. The electrode with the highest active area has also the highest value of R. From these results it may be proposed that resistances due to diffusion or potential drop within the pores are in series with the electron transfer resistance and do not appear sepparately in the Bode plot. The values of the capacity are essentially similar for all electrodes except the one without PTFE which presents a significantly higher value. This is probably due to the lack of hydrofobicity which allows a larger real area to be in contact with the electrolyte.

Acknowledgements. The authors thank FAPESP and FINEP, Brazil, for financial support.

REFERENCES

[1] D.B. Sepa, M.V. Vojnovec and A. Damjonovic, Electrochim. Acta., Vol. 26, pp. 1781, 1981.
[2] J. Gener and C. Hunter, J. Electrochem. Soc. Vol. 116, pp. 1124, 1969.
[3] J. O'M. Bockris and S. Srinivasan, "Fuel Cells: Their Electrochemistry". Mc Grow-Hill - N.Y., pp. 230-288, 1969.

OPTIMIZATION OF PLATINUM LOADING AMOUNT OF CARBON-SUPPORTED ALLOY CATHODE CATALYST FOR ADVANCED PHOSPHORIC ACID FUEL CELL

Takashi Ito, Katsuaki Kato, Shinji Kamitomai
and Masahisa Kamiya
N. E. CHEMCAT CORPORATION
Nakakokubun 3-19-3, Ichikawa, Chiba 272, Japan

INTRODUCTION

In the development of the improved electrocatalyst for the advanced phosphoric acid fuel cell (PAFC), one of the most important issues is the optimization of platinum loading amount on the catalyst with balancing between the catalyst cost and the cell output performance. Conventionally, 10 wt% platinum has been believed to be an optimum loading amount on the conductive carbon black carriers of BET surface area 70 - 240m^2/g. In order to improve the catalytic activity and performance stability, various types of platinum base metal alloy cathode catalysts have been developed with using 10% Pt/C as catalyst precursor (1) (2) (3) (4). However, the optimization of platinum loading amount on these alloy cathode catalysts has not yet been reported. This paper presents the high platinum loading amount carbon-supported Pt-Fe-Co alloy catalyst, which enables to construct the higher power density fuel cell systems with better cost performance compared with the conventional 10% Pt alloy/C cathode catalyst.

EXPERIMENTAL

A series of carbon-supported Pt-Fe-Co alloy (atomic ratio 50:25:25) catalysts with various platinum-loading amounts (10%, 20%, 30%, and 35% platinum by weight) were prepared with the two-step metal loading and alloying method described previously (2) (5). The common carbon carrier was a graphitized carbon black of BET surface area 110m^2/g. The characterization of Pt/C precursors and Pt-Fe-Co alloy/C catalysts were conducted with X-ray powder diffraction (XRD), carbon monoxide chemisorption metal surface area (CO MSA), and transmission electron microscope (TEM). The gas diffusion electrodes of 10% Pt/C anode catalyst and Pt-Fe-Co alloy/C cathode catalysts were prepared by the method of coating the catalyst-polytetrafluoroethylene (PTFE) mixture on the wet-proofed carbon paper. The catalyst loading amount on the electrode was kept constant as 5.0 mg catalyst per 1 cm^2 projected electrode area for all electrodes. The dry basis weight ratio of catalyst:PTFE was kept constant as 1:1. The electrochemical evaluation of these electrodes was conducted by the electrochemical metal surface area (EC.MSA), and air half cell. The air/H_2 single cell initial I-V performance and life performance (3,000-10,000 hours) were examined with a small-sized single cell (effective

electrode area 50cm2) using each of the cathode catalysts, 10%, 20%, 30%, and 35% Pt-Fe-Co/C, and the standard anode catalyst 10% Pt/C.

RESULTS AND DISCUSSION

1. Characterization of Pt/C precursors and Pt-Fe-Co alloy/C catalysts

   The characterization of Pt/C precursors showed that the platinum particles of them were finely divided and well dispersed on the carbon black carrier, i.e., XRD Pt crystallite size 20A even for the precursor of 35% Pt alloy/C. Alloying treatment of secondary-loaded Fe and Co with Pt of Pt/C precursor with increasing platinum loading amount from 10% to 35% induced the increase in sintering degree of platinum crystallites. The crystallite size growth, however, was still suppressed to lower than 56A even for the 35% Pt-Fe-Co alloy/C.

2. Electrochemical Evaluation of Pt-Fe-Co alloy/C Catalysts

   The air half cell oxygen reduction activity of 35% Pt-Fe-Co/C catalyst was increased by about three times as much as that of 10% Pt-Fe-Co/C. IR-free single cell voltage of 35% Pt-Fe-Co/C cathode at 200mA/Cm^2 was increased by 35mV compared with that of 10% Pt-Fe-Co/C. The data of single cell I-V performance, i.e., current density-cell terminal voltage (IR-involved) curves, shown in Fig. 1, suggest that the 20%, 30%, and 35% Pt-Fe-Co alloy/C cathode cells can generate 21%, 36%, and 39% more output power at 700mV (constant voltage basis), compared with that of 10% Pt alloy cell, i.e., W=1.21w, 1.36w, and 1.39w, respectively. The life performance of the series of alloy cathode cells didn't seem to depend on the platinum loading amount of the cathode catalysts. When unalloyed Pt/C catalyst was used as cathode, the single cell generated 41% lower power at 700mV than the corresponding Pt-Fe-Co alloy/C cathode cell. Moreover the decay rate of cell terminal voltage of unalloyed Pt/C cathode cell was 50% higher than the corresponding Pt-Fe-CO alloy/C cathode cell.

3. Calculation of Cost Performance

   Table 1 shows the calculation of cost performance of fuel cells using various platinum loading amount Pt-Fe-Co alloy/C as their cathode catalysts. The construction cost of fuel cell system might be expressed as a sum of the material cost of cathode catalyst (X) and the rest (Y), which does not depend on

the platinum loading amount of cathode catalyst. The catalyst costs of 20%, and 30% Pt alloy/C may be twice and three times more expensive than that of 10% alloy/C, i.e., X=2x and 3x, respectively. However, if the ratio of the cathode catalyst cost to the rest (R=x/y) for the base line 10% Pt alloy catalyst cell system is assumed to be 0.03, the cell construction cost per unit power output ((X+Y)/W) of 20%, 30%, and 35% Pt alloy cathode cell systems are 15%, 23%, and 23% lower than that of conventional 10% Pt alloy cathode cell system as shown in Table 1. When the cost ratio R increases from 0.03 to 0.20, the optimum platinum loading amount in Pt-Fe-Co alloy/C catalysts shifts from approximately 35% to approximately 20%.

CONCLUSION

1. The cost performance of PAFC system depends on the platinum loading amount of cathode catalyst.

2. The initial construction cost of PAFC per unit output power can be minimized with an optimum platinum loading amount in Pt-Fe-Co alloy cathode catalyst between 20% and 35%, when the ratio of cathode catalyst cost to the rest of total construction cost for 10% Pt alloy/C cathode PAFC system is not higher than 0.26.

3. The high platinum loading alloy cathode catalyst with high activity and improved stability enables to construct the high power density PAFC systems, in other words, the more compact PAFC systems.

REFERENCES

1. F. J. Luczk and D. A. Landsman, U.S. Patent 4,613,582 (1986)
2. T. Ito, S. Matsuzawa, and K. Kato, U.S. Patent 4,794,054 (1988)
3. F. J. Luczk and D. A. Landsman, U.S. Patent 4,806,515 (1989)
4. C. Z. Wan, U.S. Patent 4,822,699 (1989)
5. T. Ito, K. Kato, M. Kamiya, and H. Kirinuki, "Program and Abstracts of 1988 Fuel Cell Seminar, Long Beach, California, Oct., 1988", pp.160-163, Courtesy Associates, Inc., Washington D.C., 1988.

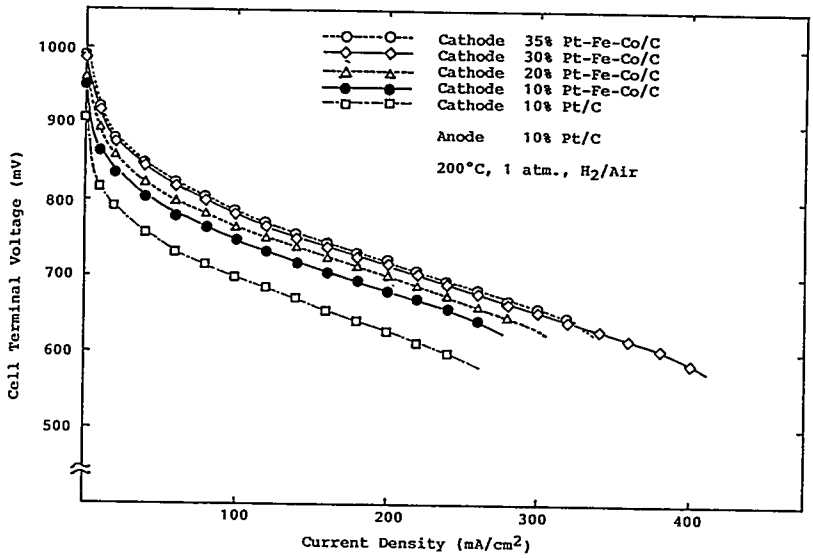

Fig. 1. Comparison of Single Cell Current Density-Voltage (I-V) Performance of 10% Pt/C and 10%, 20%, 30%, and 35% Pt-Fe-CO Alloy/C Cathodes.

Table 1. Calculation of Cost Performance of Fuel Cell Using High Platinum Loading Supported Alloy Cathode Catalysts

Catalyst	10% Pt-Fe-Co/C	20% Pt-Fe-Co/C	30% Pt-Fe-Co/C	35% Pt-Fe-Co/C
EC.MSA (m2/g Pt)	90	72	58	48
Single cell current density at 700mV (mA/cm^2)	165	200	225	230
Cell output power (W)	w	1.21w	1.36w	1.39w
Cell construction cost				
Cathode catalyst (X)	x	2x	3x	3.5x
The rest (Y)	y	y	y	y
Ratio of construction cost per unit output power ((X+Y)/W)	(x+y)/w	:(2x+y)/1.21w:	(3x+y)/1.36w:	(3.5x+y)/1.39w
R=x/y	R+1	1.65R+0.83 :	2.20R+0.73 :	2.51R+0.72
R $\longrightarrow$ 0	1.00 :	0.83 :	0.73 :	0.72
R=0.03	1.00 :	0.85 :	0.77 :	0.77
R=0.05	1.00 :	0.87 :	0.80 :	0.81
R=0.10	1.00 :	0.90 :	0.86 :	0.88
R=0.20	1.00 :	0.97 :	0.98 :	1.02

THE METHANOL PERMEABILITY ISSUE FOR THE DIRECT METHANOL AIR PEM FUEL CELL

Liu Jingsong
Dept. of Chemical Technology
Royal Institute of Technology
S-100 44 Stockholm, Sweden

Methanol has a high potential for replacing petroleum-derived fuels employed for terrestrial transportation applications. A fuel cell generator with a polymer electrolyte membrane (PEM) operating at ambient temperature and direct electroxidation of liquid methanol seems to be too good to be true. The direct methanol/air fuel cell with a PEM, however, may become commercial reality in the future. The PEM fuel cell is subject to considerable interest and R & D efforts particularly in Europe in these days.

The perfluorosulfonic acid (Nafion^R) membrane developed by Du Pont is a proven PEM material. However, methanol permeates through the membrane to the cathode, which results in an internal electric "short circuit" —— chemical oxidation rather than electrochemical oxidation (1). The permeation problem must either be surmounted or circumvented for a successful direct methanol PEM fuel cell concept to be realized.

In this work, Nafion^R 117 (equivalent weight 1100) was tested for methanol permeation at various swelling degrees. The membrane was installed between two compartments of the permeation cell. Aqueous methanol solution (0.001 mole cm^{-3}) was put into one compartment and deionized water in the other. Methanol concentrations in both compartments were monitored by Perkin-Elemer Model 8700 gas chromatography. Diffusion coefficients were calculated based on the one-dimensional diffusion equation. Results are shown in Figure 1. Figure 2 illustrates the relationship between ion conductivity and water content, i. e. the swelling degree (2). For comparison, another promising cadidate membrane —— Selemion CMV (provided by Asahi Glass, Japan), was tested in the same way. The diffusion coefficients of the as-received and treated with 1N H_2SO_4 Selemion membrane are 0.29 X 10^{-6} and 0.76 X 10^{-6} cm^2sec^{-1} respectively. In Figure 1, the mole ratio of water to sulfonic ion group is another way of expressing the swelling degree where

$$n_{H_2O}/n_{SO_3^-} = \frac{\text{water content percentage X 1100}}{18 \text{ X } 100}$$

with the membrane equivalent weight 1100.

Figure 2 shows that a high ion conductivity can be achieved only at a relatively high swelling degree. Unfortunately, a high swelling degree also increases the methanol transfer through the membrane.

The methanol permeability issue is thus connected with the fuel cell performance as well as efficiency. Here emphasis is put only on efficiency. The ratio of practical power density to theoretical power density is one way to express fuel cell efficiency. We consider only two factors which make the practical power density deviate from the theoretical value: the

membrane resistivity and methanol permeation through the membrane. The efficiency is given in Equation (1)

$$Eff = \frac{(V_o - jd/L)j}{V_o(j + D\Delta C\, nF/d)} \qquad (1)$$

where j —— current density of the fuel cell (A cm^{-2}),
d —— membrane thickness (0.022 cm for Nafion^R and 0.014 cm for Selemion),
L —— ion conductivity of the membrane, i. e. the reciprocal of the membrane resistivity ($ohm^{-1}cm^{-1}$),
V_o—— open circuit voltage of the cell, i. e. zero-load voltage extrapolated from the cell performance curve (assumed to be 0.8 V),
ΔC—— methanol concentration difference (0.001 mole cm^{-1}),
n —— number of electrons transfered in the reaction (6),
F ——Faraday constant (96485 coulomb/equiv.),
D —— methanol diffusion coefficient (cm^2 sec^{-1}).

In Equation (1), jd/L is the voltage drop due to the ohmic loss of the membrane, $D\Delta C\, nF/d$ is the equivalent leakage "current density" due to methanol permeation and $j + D\Delta C\, nF/d$ can be considered as the "total" current density which, according to Faraday's law, is proportional to the amount of methanol consumed per unit area of the membrane per unit time.

Figure 3 shows curves of the cell efficiency versus current density at two different swelling degrees. The efficiency reaches its maximum values of 74% at j=0.28 A cm^{-2} for swelling degree $n_{H_2O}/n_{SO_3^-}$ = 15 and 68% at j=0.40 A cm^{-2} for swelling degree $n_{H_2O}/n_{SO_3^-}$ = 20 respectively. In addition, for lower swelling degrees, the efficiency is higher at low current densities and lower at high current densities and vice versa.

As for Selemion CMV, though it exhibits a lower methanol diffusion coefficient, its ion conductivity is also much lower. (0.004-0.007 $ohm^{-1}cm^{-1}$ (3)). It can be calculated that the voltage drop due to the electrolyte resistance alone will dissipate the cell open circuit voltage at the load of 230 to 400 mA cm^{-2}.

Conclusions:

1. Methanol permeation is mainly a concentration gradient controlled transport process, which is governed by the diffusion equation though complicated interactions may be involved.

2. The apparent diffusion coefficient is approximately proportional to the swelling degree.

3. Considering only the electrolyte resistivity and the methanol permeation effects, there will always be a maximum efficiency achievable at certain current density. It seems that low swelling degree of membrane is suitable at low current

density and high swelling degree at high current density.

4. It seems that Selemion CMV would be a useful PEM only in fuel cells at low current densities.

References:

1. M. R. Verbrugge: "Methanol Diffusion in Perfluorinated Ion-exchange Membrane", J. Electrochem. Soc., 136, (1989) 417-423.
2. Richard S. Yeo: "Intrinsic Conductivity of the Perfluorosulfonic Acid Membranes and Its Application to the Solid Polymer Electrolyte", Proc. Symp. on Transport Processes in Electrochemical Systems. The Electrochemical Society Inc., Pemmington, NJ, 1982.
3. "Selemion Ion-exchange Membranes", Asahi Glass Brochure, July, 1984.

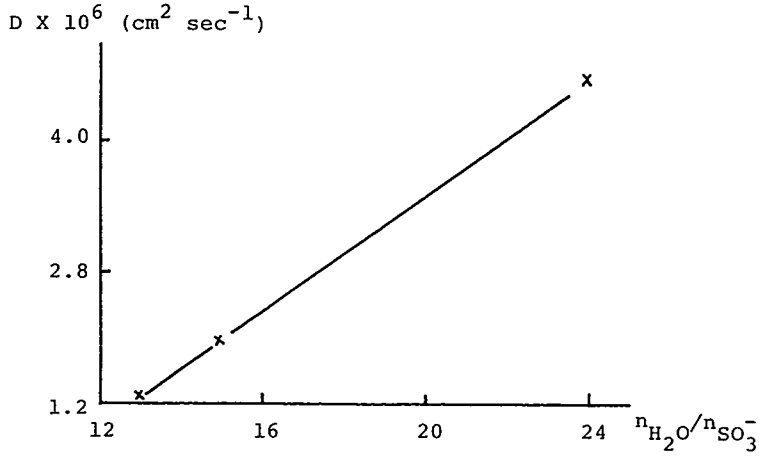

Fig. 1 Plot of Apparent Diffusion Coefficient to Swelling Degree for Nafion Membrance

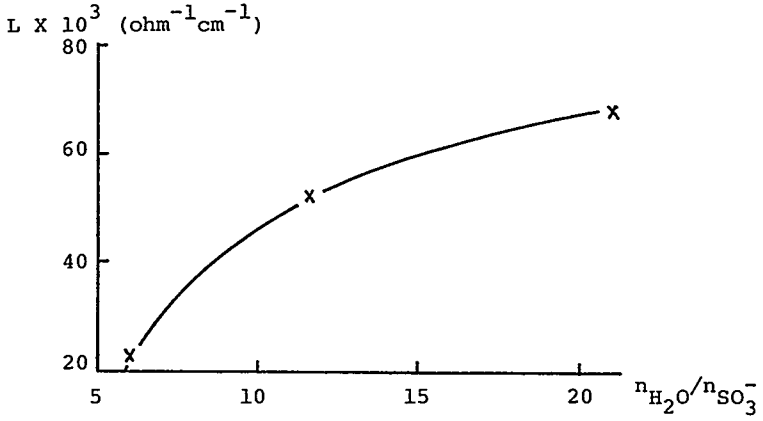

Fig. 2 Relationship between Ion Conductivity and Water Content for Nafion Membrane (Data from Ref. 5)

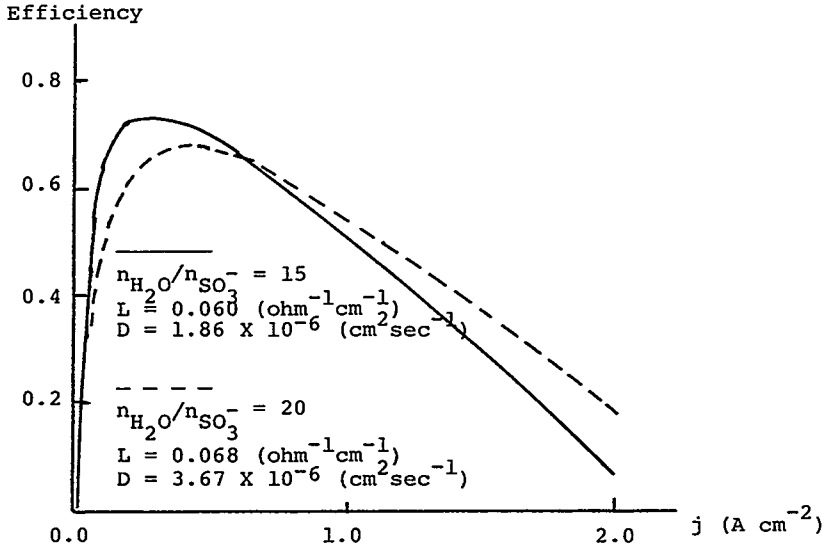

Fig. 3 Curves of Efficiency versus Current Density

PYROLYZED MACROCYCLES ON HIGH SURFACE AREA CARBONS FOR THE REDUCTION OF OXYGEN IN ALKALINE FUEL CELLS.

Y. Kiros and S. Schwartz
Department of Chemical Technology
Royal Institute of Technology
S-100 44 Stockholm, Sweden.

INTRODUCTION

Electrocatalysis of oxygen reduction by organic metal complexes, particularly the metalloporphyrins and phtalocyanines in alkaline, acidic and neutral electrolytes have been the subject of extensive study in the past(1-4). The metalloporphyrins, which are essential for life in nature, have major effects in the transport, storage and activation of oxygen as well as redox processes(5). These metal chelates have attracted much attention as potential catalysts in electrochemistry, especially in the reduction of oxygen in porous gas diffusion electrodes. These macrocycles, which can be either synthesized or naturally obtained as from crude oil products(6) or green plants(7) are now considered as main alternatives to the costly noble metal catalyst.

Metalloporphyrins in their original state are not very active and are also unstable in alkaline, acidic and neutral electrolytes. The poor activity and stability in these chemical environments have been overcome by heat treatment between 400-1000^{o}C in inert gases. At these temperatures profound changes in the porphyrin structure are expected to take place (8,9). The pyrolysis product of tetraphenylporphyrin with transition metals on high surface area carbons exhibits excellent catalytic properties in the reduction of oxygen when incorpoated into a porous teflon-bonded electrode.

The aim of this study is to assess and compare the electrochemical performance of some carbon materials promoted with catalysts in double-layered PTFE-bonded electrodes in alkaline solutions. The report is based on experimental evidence to substantiate the relationships between electrode performance of the catalyst on the one hand, and the physiochemical nature of the support material on the other.

EXPERIMENTAL

Double-layer teflon-bonded gas diffusion electrodes were prepared by the rolling method described by Schautz(10). The electrodes are composed of a nickel screen serving as a current collector and structural support for the electrode, the gas diffusion-layer with its hydrophobic structure as an oxygen/air supplying zone and an active(catalyst)-layer as a reaction zone.

Current-voltage characteristics of the electrodes were studied in 5M KOH and at 40^{o}C. The incoming air was scrubbed with a KOH solution. The electrode potentials were measured periodically vs. the Hg/HgO(5M KOH) reference electrode, attached with a Luggin capillary to the working electrode having an area of 10 cm^{2}. The counter electrode was a nickel wire mesh.

RESULTS AND DISCUSSIONS

SEM photograph of the 0.15mm thick active(catalyst)-layer composed of the activated carbon, catalyst(CoTPP) and PTFE is shown in Fig.1 and displays the aggregation of fine particles of the electrode. Fig.2a shows TEM images with well-defined particle structures of cobalt and carbon support. TEM in conjunction with EDS(Fig 2b) gives a characteristic feature of the morphology and structure of this layer. The image shows cobalt particles surrounded by carbon substrate, often having a rectangular shape, indicating a well-developed crystalline structure. The particle size of the cobalt ranges from 10-80 nm.

Fig.3 shows the electrochemical performance characteristics estimated from polarization measurements, both at 30 mA/cm^2 and 100 mA/cm^2, operated with oxygen and air as a function of the surface areas of the active-layer.The surface areas of the pyrolysis products of carbon blacks with CoTPP and of the active-layers were determined by the BET-method using nitrogen as the adsorbing gas at -196°C (Tab. 1). Poor current-voltage characteristics were exhibited by Flamruss, which had a carbon with catalyst loadings almost as twice as high as that of the Ketjenblack. Increasing the weight ratio of Vulcan XC-72 to Flamruss improved the performance linearly with the electrode surface areas, until it finally reached a maximum at which the electrode material was entirely substituted by Vulcan.The electrode activity then rose slightly with increased surface area of the carbon black support.

From a comparison of the results shown in Fig.3, it may be suggested that high surface area electrodes, due to their larger amount of exposed surface area and a pore structure with many micropores, have a pronounced effect on the overall activity of cathodic applications in fuel cells. In addition, current-voltage characterstics of some porous gas diffusion electrodes on Vulcan XC-72 promoted with CoTPP, FeTPP and Ag reduced from its oxides are presented in Fig.4. The aim of this comparison is to assess the catalytic activity of these catalysts and to find optimum conditions for further applications in oxygen reduction electrodes. As shown in the figure, the activity decreases in the order CoTPP > Ag > FeTPP. Among the catalysts studied, the electrode consisting of CoTPP has very good performance and can be loaded with high current densities as shown in Fig.5.

Table 1. Surface areas of the active-layers with CoTPP and Teflon.

carbon type	weight ratio(w/w)	BET-(mg/cm^2)	cat.loading (mg/cm^2)
Flamruss/Vulcan	1,0/0	24,3	2,24
Flamruss/Vulcan	1,5/1,0	52,2	1,90
Flamruss/Vulcan	1,0/4,0	80,5	1,84
Vulcan/Ketjenblack	1,0/0	94,7	1,78
Vulcan/Ketjenblack	1,0/1,0	174,3	1,71
Vulcan/Ketjenblack	0/1,0	397,6	1,64

The cathodic activity improvements encountered in this study for the reduction of oxygen in alkaline fuel cells are due to good utilization of the catalyst particles,augmented especially by high structure carbon blacks with high surface areas on the active-layer, and the diffusion processes of oxygen. Thus better preparation techniques of both catalyst and double-layered teflon-bonded electrodes are of prime concern in increasing the limiting current densities(11).

Acknowledgment The authors wish to express their gratitude to Professor O. Lindström for his helpful discussions. They also thank Mr. H. Gustafsson and Mr. R. Ömlin for their experimental assistance. Financial support from the Swedish National Board for Technical Development is gratefully acknowledged.

REFERENCES

1. H. Alt et al, J. of Catalysis 28, 8-19 (1973).
2. H. Jahnke et al, Fortschr. Chem. Forsch. 61, 133 (1976).
3. S. Gamburtsev et al, Elektrokhimiya 18,1602-1606 (1982).
4. E. Yeager, Eletrochimica Acta 29, 1527-1537 (1984).
5. D. Dolphin et al, Amer. Chem. Soc., 201 (1982).
6. K. A. Radyushkina et al, Elektrokhimiya 21, 1390-1393 (1985).
7. O. Lindström, Symposium Fuel Cells IV, San Francisco,CA , 5-10 Nov.1989.
8. K. Okabayashi, Chem. Letters, 1659-1662 (1982).
9. I. Iliev et al, Int. Soc. of Electrochem. 32nd meeting,Vol.1, Dubrovnik (1981).
10. M. Scautz, Doctoral dissertation at the Technical University,Graz, Austria (1984)
11. P. Björnbom, Electrochimica Acta 32, 115-119(1987).

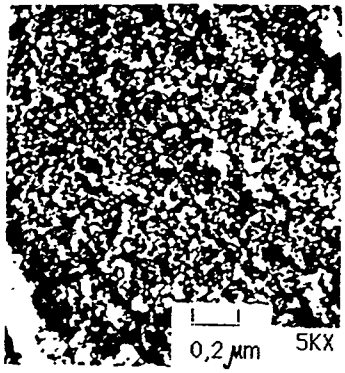

Fig. 1. SEM micrograph of the active- layer on Vulcan XC-72.

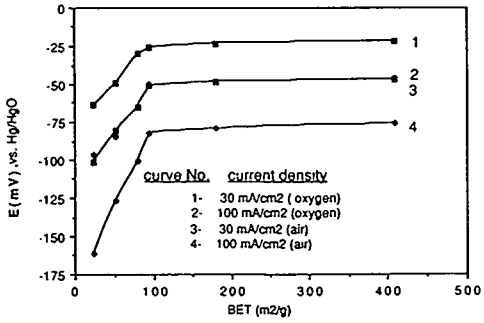

Fig. 3. Electrode performance based on the electrode surface areas.

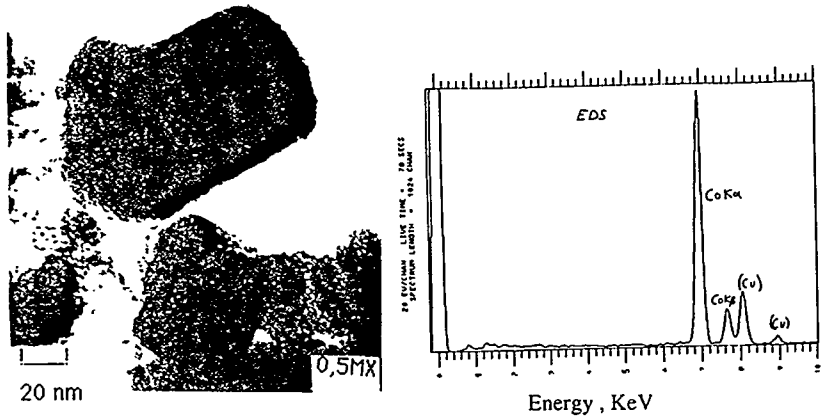

a) b)

Fig 2. Structural and morphological analyses by TEM(a) and EDS(b) of the active-layer on Vulcan XC-72.

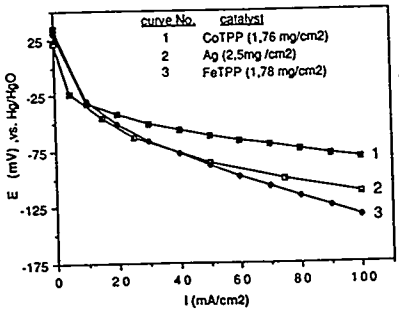

Fig. 4. Polarization curves of double-layer electrodes, supplied with air.

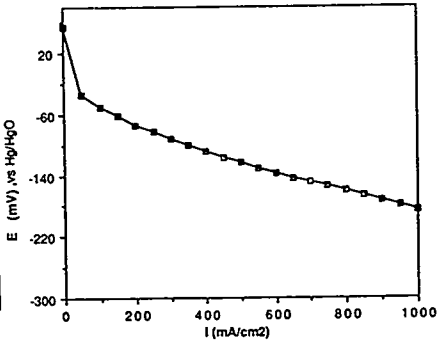

Fig. 5. Current-Voltage characteristics of a CoTPP promoted electrde operating with O_2

AFC CO-GENERATION SYSTEMS

T. Kivisaari, S. Thyberg, P. Björnbom and O. Lindstrom
Dept. of Chemical Technology, Royal Institute of Technology
S - 100 44 Stockholm, Sweden

The alkaline fuel cell generator (AFC) is neglected when it comes to terrestrial power due to the so called CO_2-syndrome. The CO_2 present in the reactants is taken up by the fuel cell electrolyte (KOH) [1]. The CO_2-syndrome, which has determined the priorities of the fuel cell community for too long, is due to the fact that it is considered too expensive to purify the air and hydrogen. Swedish workers, however, claim that this is not the case [2,3]. The removal of CO_2 is a common process in the CPI (chemical process industries) and is e.g. practised in ammonia plants all over the world.

Investment cost and efficiency for a 600 MW AFC co-generation power plant was evaluated. The plant is characterized by the following main features.

- The fuel processor, consisting of a catalytic steam reformer and high temperature shift reactor for the production of hydrogen from natural gas.
- Gas purification by pressure swing adsorption (PSA), for removing mainly carbon dioxide.
- Turbines for the reduction of the hydrogen pressure before entering the fuel cells.
- Alkaline fuel cells (AFC) for power production.
- Inverters for converting DC to AC.
- Heat exchangers for cooling the fuel cells and production of hot water for the district heating system.
- NaOH scrubbers for air purification.

All components of the power plant, except the AFC-generators, are commercially available.
The flowsheet for a 600 MW plant was developed and the investment costs were studied by conventional methods. The capital cost is compared with the cost of ammonia plants with the same production capacity of hydrogen. A state of art ammonia plant for natural gas is easily converted to an AFC power plant by substituting the ammonia reactors for AFC-generators and adding inverters.
NH_3 itself is an economic and convenient alternative fuel for small and medium size AFC power and co-generation plants.

Figure 1 shows the major blocks of the co-generation plant.

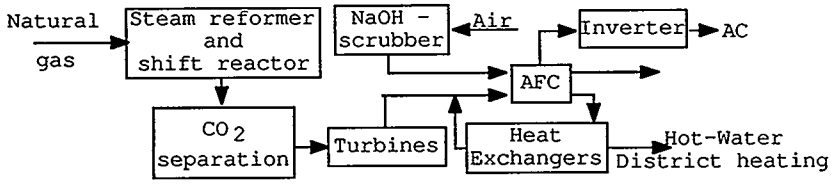

FIGURE 1. Block diagram of the power plant

The sulfur content of the natural gas is lowered below 0.1 ppm by absorption of H_2S in zinc oxide.

After mixing with steam the gas is passed to a catalytic steam reformer where the hydrocarbons are converted to carbon monoxide and hydrogen. Carbon monoxide then reacts with steam in the high temperature shift reactor to generate additional hydrogen in the shift reaction.

The hydrogen gas is purified by pressure swing adsorption (PSA). After expansion in turbines the purified hydrogen is passed to the anodes of the fuel cell generator. The purge gas from the PSA is used for heating the steam reformer.

The reactant air is passed through an alkaline scrubber for CO_2 removal and humidification.

Figure 2 compares the CO_2 handling of the AFC option with the CO_2 recycle necessary for economic MCFC power. The AFC scheme has to rely on external reforming, whereas MCFC schemes may also rely on direct internal reforming (DIR), which route is indicated in Figure 2. The same quantity of CO_2 has to be separated in the two competing flowsheets.

The fuel cell stacks are divided into modules containing seven individual cells each. Some data for the target stack is given in Table 1. The electrolyte between the electrodes is immobilized in a porous matrix, with a small bleed of electrolyte.
The electrode matrix assembly (EMA) consists of anode and cathode separated by the electrolyte matrix.

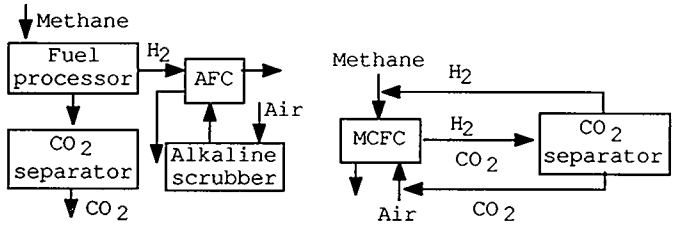

FIGURE 2. Comparision of CO_2 handling in AFC and MCFC

The matrix of chrysotile also allows some of the water produced at the anode to diffuse to the cathode side. The EMA's are electrical series connected by means of bipolar current collectors which also serve as a separator distributor assembly (SDA) thus providing pathways for the gases. The bi-polar design is considered since this is the most convenient for manufacture [4]. The two assemblies, EMA and SDA, are framed in molded polysulfone structures for containment and leak prevention

The module end plates (MEP) separating the modules at the same time act as contact cooling plates (CCP), which are cooled by a circulating cooling medium and gives cooling of the stack by physical contact in addition to the cooling provided by the external cooling/dehumidification of the recirculating hydrogen.

Fuel cell plants have to offer competitive economics, besides their enviromental merits to attract commercial utility interests. Combining the cost picture of modern ammonia plants with the properties of the target stack in Table 1, yields a favorable prognosis well below the present goals set for PAFC ($800/kW), MCFC ($600/kW) and SOFC ($500/kW). The efficiency of AFC plants is "second to none" due to the high inherent efficiency of the AFC-generator itself, and especially if combined with optimization of the complete system (fuel processor + fuel cells) by means of pinch technology.

TABLE 1

PROPERTIES OF THE TARGET FUEL CELL STACK (275 kW)

Number of cells in stack	259	(37x7)
Electrode area	5,000	[cm^2]
Cell voltage	0.850	[V]
Current density	2,500	[A/m^2]
Power rating	275	[kW]
Nominal weight	858	[kg]
Cost (incl. profit)	64	(US$/kW)

The calculations involved in the development of the flowsheet for the power plant were mostly carried out by means of the ASPEN PLUS ^{TM} flowsheeting program, provided under licence from Aspen Technology Inc.

References

[1]. K. Kinoshita, F. R. McLarnon and E. J. Cairns, "Fuel Cells Handbook" - U.S. Department of Energy, DOE/METC-88/6096, pp. 109, May 1988.

[2]. O. Lindström, "Fuel cell power plants" Chemtech, Vol. 17, pp. 553-559, Sept. 1988.

[3]. S. Thyberg, " Feasibility Studies of High Efficiency AFC Power Plants for Natural Gas" to be published in J. Electrochem. Soc., Vol. 137, No. 9, Sept. 1990.

[4]. K. Kordesch and J. C. T. Oliveira, "Fuel cells: The present state of the technology and future applications, with special consideration of the alkaline hydrogen/oxygen (air) systems" Int. J. Hydrogen Energy, Vol. 13, No. 7, pp. 411-425, 1988.

FUEL PROCESSORS FOR RURAL FUEL CELL POWER PLANTS

S Thyberg, Y Kiros, C Myrén, H Lindström, O Lindstrom
Dept of Chemical Technology, Royal Institute of Technology
S - 100 44 Stockholm, Sweden

The project "Stand alone fuel cell power plants for rural electrification" is a joint Indo-Swedish program between the Department of Chemical Technology at the Royal Institute of Technology (KTH) and three Indian institutes. The main Indian partner is the School of Energy Studies at the Punjab Agricultural University (PAU) in Ludhiana and the two others are the Tamil Nadu Agricultural University (TNAU) in Coimbatore and the Central Institute of Agricultural Engineering (CIAE) in Bhopal.

The three year project is financed by SAREC (the Swedish Agency for Research and Cooperation with Developing Countries), ICAR (the Indian Council of Agricultural Research) and the Indian universities. The work was initiated in 1989.

The task of the project is to develop a fuel cell power plant for rural Indian villages not connected to the electrical grid. The fuel will consist either of gasified biomass (producer gas) or of biogas from a digester or a combination of these fuels.

The work is focused on the fuel processors for conversion of the fuel gas to a hydrogen-rich gas to be fed to the fuel cell generator. Other parts of the plant i.e. the fuel cell generator, the inverter to convert DC to AC and the primary conversion of the biomass to fuel gas will also be studied, however. (Figure 1)

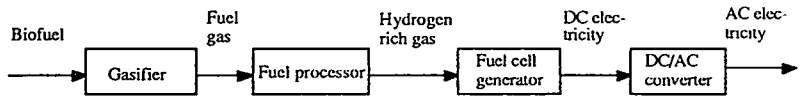

Figure 1. Scheme of biofuel fuel cell plant

The power plant should of cource be as efficient as possible but even more weight is given to simplicity and reliability. These units will be put up in isolated villages and cannot depend on frequent service or deliveries of chemicals.

Three fuel processor options are presently under evaluation.

Steam reforming is a common way to convert hydrocarbons to hydrogen. This process is well investigated and catalysts are commercially available. Calculations on a system with steam reforming and shift reactors indicate an efficiency around 40% (biogas LHV to DC). (Figure 2)

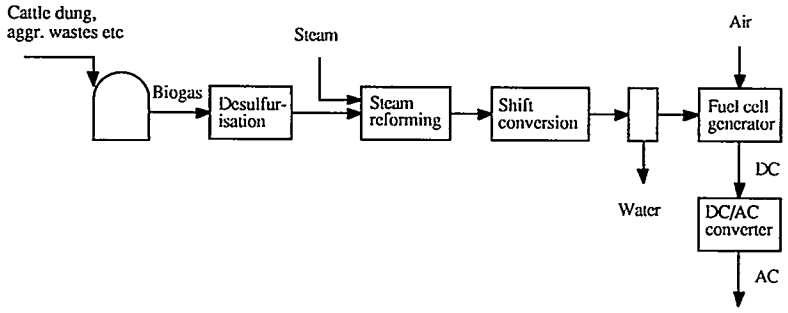

Figure 2. Steam reforming option.

A steam iron process may be used for conversion of reformed gas to hydrogen. This process consists of two steps. In the first step Fe_3O_4 is reduced to FeO and Fe with H_2 and CO. After the reduction the bed is oxidized with steam. The product gas consists of pure hydrogen wich makes it possible to use alkaline fuel cells (AFC), with high efficiency, for the electricity production. To rise the efficiency of this process it is possible to remove CO_2 from the reformed gas before it enters the iron oxide bed.

The third option is partial oxidation with air. Here the methane in the biogas reacts with oxygen in air to form hydrogen in a catalyst bed. There is no need for external heat supply since the oxidation of CO supplies the heat needed. The efficiency will be lower than for the two other processes due to the partial oxidation of CO.

At present experimental work at KTH is directed sulphur- and CO_2-removal from the fuel gases. A single tube reformer has been constructed and is used for catalysts testing.

To be competetive fuel cell plants have to show better economics than diesel engines and engine-generators. The purpose of Table 1 (page 4) is to give an idea about the break even costs for the fuel cell systems. The target for the R&D program may be set at half the break even figures to give a competetive scheme with an investment somewhat below the level of the diesel engine-generator set and a much lower fuel cost.

A combined system using biogas for the baseload and producer gas for the peaks will give flexible operation and looks very attractive. (Figure 3)

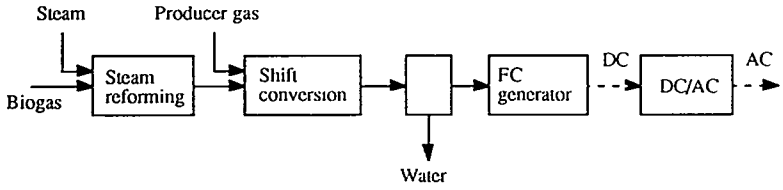

Figure 3. A combined biogas - producer gas fuel cell power plant.

	Diesel Engine-Generator	Wood Gasifier, Engine-Generator	Wood Gasifier Fuel Cell Plant	Biogas Generator Fuel Cell Plant
Investments (Rs/kW)	5,400	Gasifier 1,600 Engine-Gen 5,400 Total 7,000	Gasifier 1,160 FC Plant 8,000 Total 9,160	Digester 4,000 FC Plant 6,400 Total 10,400
Fuel consumption (per kWh)	300 ml diesel-oil	1.1 kg wood 75 ml diesel oil	0.8 kg wood	13 kg dung
Costs (Rs/kWh)			Gasifier FC Plant	Gasifier FC Plant
Fixed	0.59	0.77	0.26 0.88	0.37 0.70
Fuel	1.11	0.76	0.35 -	0.39 -
Labor	0.60	0.60	0.30 0.30	0.30 0.30
Maintenance	0.16	0.21	0.07 0.24	0.10 0.24
			0.98 1.42	1.16 1.24
Total cost	2.46	2.34	2.40	2.40

Table 1. Cost data for 10 kW power plants, 2000 h/year, with estimates of break even investments for fuel cell options. (15 Rs = 1 $)

Reference

- S Thyberg, O Lindström, A K Jain "Fuel cell electricity from biomass fuels" paper presented at the International Symposium on Application and Management of Energy in Agriculture - the Role of Biomass Fuels in New Delhi May 21-23, 1990.

PREPARATION AND MEASUREMENT OF AIR ELECTRODES FOR ALKALINE FUEL CELLS

Juhani Kivisaari
Dept. of Chemical Technology, Royal Institute of Technology
S-100 44 Stockholm, Sweden
and
Jaakko Lamminen, Markku J. Lampinen and Minna Viitanen
Dept. of Energy Engineering, Helsinki University of Technology
Otakaari 4, SF-02150 Espoo, Finland

Summary

The optimum structure and materials for the gas diffusion layer of air electrodes for alkaline fuel cells was studied. These electrodes contains carbon black, pretreated in different ways (e. g. boiling nitric acid, heat treatment in different atmospheres), and polytetrafluorethylene as a hydrophobic binder. The samples prepared were studied by different methods, e. g. air permeability, electrical conductivity and porosity. Heat-treated cobolt-tetra-methoxyphenylporphyrine was used as a catalyst in the active layer.

Introduction

To make it possible to use fuel cells for terrestrial applications it is necessary to improve the performance of the air electrode without using precious metal catalysts. One way to achieve this is to use macrocycles such as porphyrins found in the nature as catalysts [1, 2].
As important as an active catalyst is a good backing material for the gas diffusion layer so that the polarization due to diffusion resistance and ohmic resistance in the gas diffusion layer of the electrode remain small.
In this study several materials for the gas diffusion layer have been investigated. The aim of the study was to find an optimum material by means of air diffusivity and electrical conductivity.

Experimental

Materials

The materials used for the samples in this study were carbon black (Vulcan XC-72 and Black Pearls 2000, Cabot Corp.) and PTFE (Teflon resin 30N, Du Pont and Hostaflon TF2053, TF2071, TF9205, Hoescht AG) as a hydrophobic binder. Heat-treated CoTMPP (CoboltTetraMethoxyPhenylPorphyrine) on carbon black was used, as a catalyst.

Preparation of carbons

Many different types of treatment of the carbons are suggested in the literature e.g. boiling with nitric acid, heat treatment in different atmospheres [3, 4, 5, 6].

In this study samples of the carbons were treated in four different ways:

a) untreated,
carbon directly from the can. The only treatment before use was to grind the carbon in a coffee-mill in order to break down large lumps of carbon.

b) boiling with concentrated nitric acid,
the carbon was dispersed in concentrated nitric acid and boiled for 24 hours.

c) heat treatment at 850 and 1000 °C in nitrogen atmosphere,
the carbon was heat treated in nitrogen atmosphere for 30 minutes at 850 or 1000 °C.

d) heat treatment at 850 and 900 °C in carbondioxide atmosphere, the carbon was heat treated in carbondioxide atmosphere for 30 minutes at 850 or 900 °C.

Manufacture of electrodes

For the manufacture of electrodes several different methods are proposed, the main methods being: pressing [3, 4, 5], rolling [7], screen-printing [8] and spraying [9]. In this study the rolling technique was used for electrode manufacture. The preparation of the electrodes was carried out in two different way depending of the PTFE type used. When using PTFE as a water dispersion, the wet-method was used and when using PTFE as a powder, the dry-method was used.

A total of 30 samples, with duplicates was prepared. Variables which have been changed are: carbon type, treatment of the carbon, dry or wet method, spacer used or not, solvent used to make the dough. On top of the diffusion layer was a catalytic layer of the same type in all the samples.

Characterisation of electrodes

The following measurements were made to characterise the samples:

a) thickness
was measured with a micrometer.

b) weight
was measured with a laboratory balance.

c) porosity
was calculated by measuring the dimensions of the sample, and knowing the weight of the sample, the porosity could be calculated under the assumption that the density of the compact material in the sample is 1.9 g/cm^3.

d) air permeability
was measured with a sample with a diameter of 20 mm (area of measurement: 3.14 cm^2).

e) resistivity
was measured by a four-point method.

f) polarization curve
was measured with an electrode with an area of 10 cm^2 in an alkaline electrolyte (5 M KOH) and with air on the gas side. As a counter-electrode a stainless steel plate was used. The polarization was measured versus a mercury/mercuryoxide reference electrode.

h) transfer coefficients (Tafel parameters i_0 and α)
were measured according to the model in [10].

Characterisation of catalyst

Samples of cobolttetramethoxyphenylporphyrine and hydrogen-tetramethoxy-phenylporphyrine, on carbon black, both untreated and heat-treated at 700 °C were received from I. Iliev. These samples were studied by using ESCA, which is suitable for studying the chemical bonds of the electrode surface.The study was conducted to determine whether the bonding between the nitrogen and the metalatom were still present after the heat-treatment.

Results and discussion

It was found out that the best results in terms of conductivity was obtained with Black Pearls 2000, but the resulting dough was very sticky and hard to roll to an electrode sheet. The best samples in terms of air permeability were # 6, but it was very brittle. The best overall result was obtained with samples # 29 and 30. Rough calculations shows that a conductivity of 200 $1/\Omega m$ or more gives a polarization of 2-3 mV at 100 mA/cm^2. A similar calculation for air permeability indicates that a permeability of 0.87 ml/s is enough to give a polarization of less than 4 mV at 100 mA/cm^2. A complete table of the results will be displayed in the poster

The ESCA study of the catalyst shows that the peak showing the nitrogen to metal bond has disappeared after the heat-treatment of the porphyrine. A small shift in the binding energy of the carbon atoms can be seen. This implies some structural changes in the porphyrine structure during the treatment.

Acknowledgement

This work was financially supported by a grant from NEMO and a scholarship from the Nordic Ministry Council. The authors

acknowledge the assistance of and discussions with I. Iliev and A. K. Shukla.

References

[1]. O. Lindström, E. Björnbom, T. Kaimakis, "Low cost macrocycle black for air cathodes", Paper presented at American Institute of Chemical Engineers, 1989 Annual Meeting, Symposium Fuel Cells IV, November 5-10, 1989, San Francisco.

[2]. O. Lindström, "That incredible fuel cell", Chemtech, 17, (1988), 495.

[3]. S. Motoo, M. Watanabe, N. Furuya, "Gas Diffusion Electrode of High Performance", J. Electroanal. Chem., 160, (1984), 351-57.

[4]. M. Watanabe, K. Makita, H. Usami, S. Motoo, "New Preparation Method of a High Performance Gas Diffusion Electrode Working at 100 % Utilization of Catalyst Clusters and Analysis of the Reaction Layer", J. Electroanal. Chem., 197, (1986), 195-208.

[5]. M. Watanabe, M. Tozawa, S. Motoo, "A Gas Diffusion Electrode for Oxygen Reduction Working at 100 % Utilisation of Catalyst Clusters", J. Electroanal. Chem., 183, (1985), 391-94.

[6]. R. Manoharan, A. K. Shukla, "Oxygen-Reducing Porous Carbon Electrode for Electrochemical Power Sources with Alkaline Electrolytes", J. of Power Sources, 10, (1983), 333-341.

[7]. M. Schautz, "Herstellung von Elektroden für alkalische Wasserstoff-Luft-Brennstoffzellen und bau einer Batterie", Diss., Graz, (1985), 54-58.

[8]. B. J. Krätschmer, "Untersuchungen von Kohlenmateriale für Gasdiffusionselektroden", Diss., Graz, (1981), 15-22.

[9]. K. Kordesch, S. Jahangir, M. Schautz, "Engineering Concepts and Technical Performance of Oxygen-Reducing Electrodes for Batteries and Electrochemical Processes", Electrochimica Acta, 29, no. 11, (1984), 1589-1596.

[10]. M. Viitanen, M. J Lampinen, "A Mathematical Model and Optimization of the Structure for Porous Air Electrodes, accepted for publication in J. of Power Sources.

ELECTROCHEMICAL INVESTIGATION OF MICROAGGLOMERATES FROM FC-CATHODES

M. Bursell and P. Bjornbom
Deparment of Chemical Technology,
Royal Institute of Technology
S-100 44 Stockholm, SWEDEN

Introduction

An new method related to microelectrochemistry makes it possible to study electrochemically active agglomerates from from 5 micron and up (1). The technique is mainly based upon a device composed of a 7 micron (in diameter) carbon fibre attached to a x.y-z micromanipulator (sliding device) making it possible to contact the small agglomerates under investigation. The work is done under a stereomicroscope with large enlargment factor.

Compared to the traditional techniques in microelectrochemistry, eg metal wire in a glass capillary, this method has the advantage that it is possible also to study agglomerates from porous electrodes like lead dioxide, nickel hydroxide and gas diffusion electrodes. In this work we have continued the experiments described in a recent paper (1).

Experimental

Numerous of agglomerates were scratched from the active layer of a standard type of oxygen-electrode. This electrode was catalyzed with CoTPP on carbon, bonded with PTFE in the usual manner. The agglomerates were transferred to a piece of smooth separator cloth at the microscope-table soaked with 5 M potassium hydroxide. The capillary of an Hg/HgO reference-electrode was put into liquid-junction with the separator cloth. A carbon fibre 7 mm in diameter, 3 mm long, was glued with a conductive laquer on a metal wire attached to the micromanipulator with XYZ sliding-possiblilites The voltage drop over the carbon fibre caused by its own resistance was approximately 3 mV/µA. The carbon fibre was deactivated towards oxygen reduction with a paraffin coating, by a simple dip into molten paraffin. The activity of the tip of the carbon fibre itself was 0,01 µA at -200 mV vs Hg/HgO. With the aid of the microscope the agglomerate was then easily contacted by the tip of the carbon fibre. Different potentials were set up between the reference electrode, here also working as counter electrode, and the selected agglomerate with a simple potentiostat, voltage-divider, described earlier (1,). A sensitive µA-meter was connected in series with the electrode circuit.

Results and discussion

Fig. 1 shows the polarization curves for three different agglomerates of varying size. It is easily seen that the current by no means is proportional to the cube of the diameter of the agglomerates at a given potential. Obviously a smaller agglomerate works more effectively, in spite of the fact that even the largest agglomerate here must be concidered as very small too. In fig 2 the same data are expressed as polarization vs mA/mm^3. In the same figure the curve of the real electrode from which the agglomerates were scratched is plotted in the same way. There is a very big difference between the current generated per mm^3 in the electrode and in the individual agglomerate. The oxygen-reduction current of the 25 µm-agglomerate at -200 vs Hg/HgO is 250 A/g. This is surprising even considering that it is unlikely to get the same current contribution from all the agglomerates in an electrode. For example the agglomerates must suffer from the IR-drop in the pore electrolyte resulting in a lower current density per mm^3 towards the gas-side of the electrode. Yet the great differences measured and reported here are quite remarkable. Our work will continue and we are planning to improve this method to be able to work with smaller agglomerates with a size of around 1 µm. This work combined with our continuing theoretical model work (234) should hopefully result in a better theoretical understanding of the electrode processes and in more efficient electrodes.

Acknowledgements
This work was supported by the Swedish Energy Administeration
References:

1. M. Bursell and Pehr Björnbom, J. Electrochem. Soc. 137,115 (1990)
2. P.Björnbom, Electrochimica Acta,32,115 (1987)
3. P.Björnbom,J.Electrochem.Soc.133,1874 (1986)
4. P.Björnbom,M.Bursell, "Influence of Diffusion on Oxygen Electrodes", Paper presented at American Institute of Chemical Engineers, 1989 Annual Meeting, Symposium Fuel Cells IV, November 5-10, 1989 San Francisco

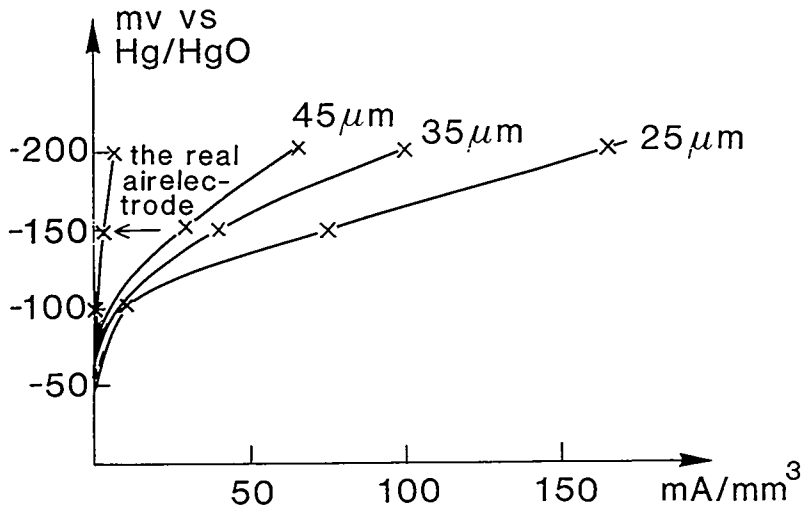

Fig. 1. Polarization curves for three different air electrode agglomerates.

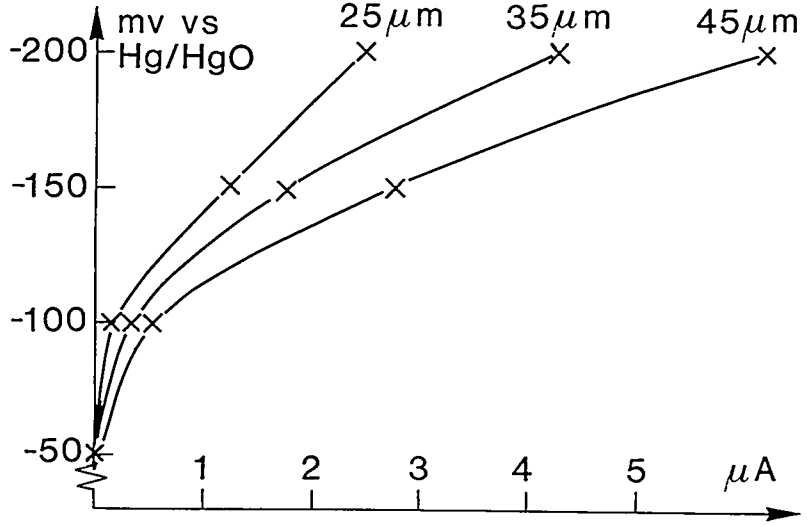

Fig. 2. Curves showing polarization vs current per volume for an air electrode and for agglomerates scratched from the same electrode.

Reducing Downtime Using POINTER™: An Intelligent Maintenance Aid

ARINC Research Corporation
2551 Riva Road
Annapolis, Maryland 21401 USA

Abstract

Reducing the downtime needed to troubleshoot and isolate faults in complex electromechanical systems can lead to improvements in both technician productivity and plant availability. In the early 1980s, ARINC Research Corporation developed the System Testability and Maintenance Program (STAMP®) to aid the process of designing in good testability for new systems and improving the testability of existing systems. Recently, STAMP was applied to major subsystems of an 11-MW prototype fuel-cell power plant under development by Tokyo Electric Power Company (TEPCO).

The Electric Power Research Institute (EPRI) recognized the need to incorporate more simplified operational and diagnostic procedures and improve troubleshooting techniques for the fuel-cell project. This led to the application of a microcomputer-based diagnostic tool developed by ARINC Research Corporation that can be used to improve the troubleshooting proficiency of TEPCO technicians. The Portable Interactive Troubleshooter (POINTER™) uses the STAMP methodology to develop an optimum sequence for isolating the cause of a system failure. The POINTER-based maintenance aid developed for the TEPCO plant is being used to fault-jsolate the cause of plant failures.

POINTER is not a rule-based expert system. Rather it is a shell, using STAMP output as an input, that is capable of modifying fault-isolation strategies depending on the outcome of various tests. These test strategies can be influenced with weighting factors such as test times, test cost, technician skill level, and component failure rates. Test times and failure rates are automatically updated by POINTER on the basis of actual experience.

Testability—A Design Attribute

Testability is a design-related property that becomes increasingly important with the evolution of more sophisticated system designs. To be cost-effective, any testability analysis should begin in the early design stages and continue into production.

The MIL–STD–2165 definition of testability is "a design characteristic that allows the status (operable, inoperable, or degraded) of an item to be determined and the isolation of faults within the item to be performed in a timely and efficient manner." Therefore, testability is a design-related property that can be defined by the location, accessibility, and the sophistication of tests and test points.

A system is said to have good testability if it confidently identifies faults (i.e., frequently and unambiguously identifying only failed parts with no removal of good items) in an efficient manner (i.e., limited resources such as time, money, manpower, and equipment). Because inherent testability is a design-related property, it can be optimized by incorporation at the very beginning of the design process. Although the sequence and manner in which testing is performed can improve the achieved testability of poorly designed (from a testability perspective) systems, such efforts rarely achieve the same results as with a design-for-testability approach. Some post-design efforts to improve testability, such as developing sophisticated automatic test equipment (ATE), may actually increase the total cost to support a system.

STAMP®—A Testability Analysis Tool

The System Testability and Maintenance Program (STAMP), a computer-based testability analysis tool developed by ARINC Research, evaluates system testability and develops fault-isolation strategies for improved system maintenance. STAMP analyzes the testability of already designed systems and assesses the inherent capability for isolating faults to one or more defined components using existing or defined tests and test points. STAMP assists in deciding where additional test points or special tests are needed to improve testability, whether or not redundant or excessive tests exist, and how to reconfigure or repartition a system design to reduce or eliminate failure ambiguities.

In addition to an optimized fault-isolation strategy, the result of a STAMP testability analysis provides more than 20 measures that reflect the inherent testability characteristics of a specific system or equipment. Some of these measures include the following:

- Isolation level
- Test uniqueness
- Excess tests
- Components not detected
- Operational isolation
- False-alarm tolerance

In addition to providing the measures of testability, STAMP analysis identifies component ambiguity groups,

redundant tests, multiple-failure groups that could cause false-failure indication, and feedback loops and their components. While not all data are of interest in each application, the information provided is sufficient to determine how to improve testability.

STAMP application to a number of systems and equipment has proved favorable, especially the design for testability (DFT) program on the B-2 bomber avionics systems. Under this program, STAMP was used to evaluate the advanced avionics designs focusing on more than 100 state-of-the-art systems. Before applying STAMP, more than 50% of the initial designs did not comply with the goals of isolation to one shop replaceable unit (SRU) 90% of the time, isolation to no more than two SRUs 95% of the time, and isolation to no more than three SRUs 100% of the time. Redesigns that met the goals were identified with the aid of a STAMP analysis.

The B-2 bomber DFT program is an excellent example of using STAMP as a design tool in the early stages of a system life cycle. STAMP also can be applied to fielded systems that are difficult to troubleshoot. Table 1 lists examples of how STAMP was used to analyze and improve the testability of three fielded systems. The UH-60 Blackhawk stability augmentation system (SAS) is a fielded system that was difficult to troubleshoot. Before applying STAMP, the normal fault-isolation time was 8 to 12 hours using 78 tests. STAMP was able to maximize the information provided by the existing tests and reduce the fault-isolation time to 1 to 2 hours using up to an average of 5 tests. Similar results were obtained on the AN/MSQ-103C TEAMPACK and the Mk 84 60- to 400-Hz static-frequency converter, where the average number of tests required to fault-isolate using existing technical manuals was reduced by 88% and 72%, respectively.

Table 1. Improvement of Testability of Fielded Systems

System	Average Number of Tests Required to Fault-Isolate: Using Existing Manuals	Using STAMP	Reduction (%)
UH-60 Blackhawk Stability Augmentation System (Army)	78	5	93
AN/MSQ-103C TEAMPACK (Army)	42	5	88
Mk 84 60- to 400-Hz Static-Frequency Converter (Navy)	81	23	72

STAMP can be used to automatically provide a fault-isolation table, or it can be used interactively. The interactive fault-isolation option allows the user to enter initial conditions such as known bad or known good tests, that may exist. On the basis of this information, STAMP will choose the first test in the sequence and present the appropriate test procedure. The user can then perform the test and enter the result as good or bad. Also, the user can override STAMP and choose another test or declare the test untestable. If the test is declared untestable, STAMP will then choose the next test. In this way, the fault-isolation sequence is produced interactively.

The interactive fault-isolation feature was originally incorporated in STAMP. This feature, along with the potential for substantial downtime reductions and improved technician proficiency, led to the development of POINTER as an intelligent interactive maintenance aid.

POINTER™—A Portable Maintenance Aid

ARINC Research recently introduced an intelligent portable maintenance aid that is based on STAMP interactive fault-isolation capabilities. This aid, called Portable Interactive Troubleshooter (POINTER), has some unique features that make it a dynamic tool. The most important feature of POINTER is its learning capabilities. The POINTER program uses a STAMP-generated dependency model as the knowledge base from which it computes an optimized test performance order. This optimization process can be influenced or weighted by component failure rates, test times, test costs, or any logically defined factor. The current version of POINTER can automatically capture failure rate and test-time information. A historical data base of these weighting factors will be automatically developed for an optimum test order on the basis of actual experience.

Do not confuse POINTER with a hardware product. POINTER is a shell that will take any STAMP model as input and provide a learning, logging, and teaching troubleshooting tool. It can be hosted on any 80386-based MS-DOS compatible computer with at least 3 megabytes of active memory and sufficient hard-disk storage for its application. POINTER also requires a 80387 math coprocessor.

POINTER is applicable to a wide variety of systems that include the following:

- Analog electronic
- Digital electronic
- Analog/digital hybrid
- Mechanical
- Hydraulic
- Electrohydraulic
- Electromechanical
- Pneumatic
- Electrochemical
- Fluid and process systems

All levels of analyses are applicable, from the highest system level to piece-parts found on printed circuit boards. Mixed level analyses can be performed with a particular subsystem of interest modeled in greater detail.

Testability Analysis of the TEPCO 11-MW Fuel Cell

For the past several years, the Tokyo Electric Power Company (TEPCO) has devoted considerable effort to the development of multimegawatt fuel-cell power plants for electric utility applications. Between 1982 and 1985, TEPCO demonstrated a 4.5-MW phosphoric acid fuel-cell pilot plant

supplied by International Fuel Cells (IFC). On the basis of the successful operational results of that project, an effort is now under way at TEPCO to demonstrate a larger, more efficient, improved 11-MW fuel-cell design. The primary objectives will be to verify performance of major components and the overall system, evaluate plant operational characteristics at various conditions, assess reliability and availability, and quantify environmental impact on emissions and noise.

Site preparation and civil works were initiated in January 1989 and completed in June 1989. Fabrication of major components and truck-transportable pallet assemblies was initiated in 1989, and the assemblies will be shipped to Japan by July 1990. System process and control tests will begin in April 1990 to confirm proper operation of all subsystems. Power generation, plant acceptance testing, and demonstration tests will be initiated in early 1991.

A lesson learned from the earlier 4.5-MW pilot-plant test program was that future designs should incorporate more simplified operational and diagnostic procedures and improve troubleshooting techniques to quickly isolate subsystem faults. Electric Power Research Institute (EPRI) initiated efforts to conduct STAMP testability analysis of the DC Module (a major subsystem of the 11-MW fuel-cell power plant design). The overall objective was to assess the DC Module testability and to optimize the selection and placement of test and test points such that each relevant component failure within the DC Module could be uniquely isolated in the event of a system shutdown.

Results of initial STAMP analysis indicated that only 10% of all failure events could be uniquely isolated using only system shutdowns as tests. A total of 54 ambiguity groups were identified, ranging in size from 2 to 41 failure events in a single group. ARINC Research, working with IFC engineers, added tests that use existing sensors in plant data loggers, new sensors, or test points. Testability improved significantly in the following areas:

- Approximately 67% of all possible component failure modes are uniquely isolatable.
- Approximately 95% of all possible component failure modes are contained in an ambiguity group of two or fewer.
- Approximately 99% of all possible failure modes are contained in an ambiguity group of three or fewer.

The testability analysis proceeded concurrently with the design process and eventually led to one of the first applications of POINTER.

Developing a POINTER Maintenance Aid for the Fuel-Cell DC Module

ARINC Research, in conjunction with IFC, developed one of the first applications of the POINTER system for EPRI. The POINTER system for the DC Module was completed in early 1990.

The DC Module of the TEPCO fuel-cell power plant will operate in several modes during the demonstration project. POINTER will help troubleshoot problems that may occur from the two primary operating modes, on-load and start-up. From the on-load condition, POINTER will have the capability to troubleshoot a plant shutdown or a return-to-standby (standby is a plant state that is doing everything but producing power). During start-up, POINTER will have the capability to troubleshoot a plant shutdown or a hold condition. (Holds are possible for certain start-up states wherein the plant maintains its present state, giving the operator the opportunity to correct any problems to avoid a complete shutdown.)

Figure 1 shows how POINTER was developed for the DC Module. Beginning with the system-specific design data, a functional dependency model was created and entered into STAMP.

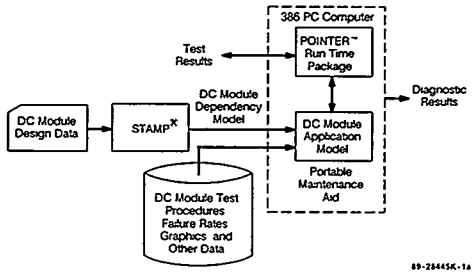

Figure 1. Application of the STAMP and POINTER System to Prototype TEPCO 11-MW DC Module

Upon completion of testability and fault-isolation analysis, the STAMP-compiled dependency model became the primary knowledge-base input for POINTER. Supporting data can be added, such as test and repair descriptions, graphics material that can be displayed at appropriate times during fault isolation or repair, and other material (e.g., test screens, menus, and fault-isolation weighting criteria). Other programs automatically can be executed independently from within POINTER (without user intervention). (There may be times when it is useful to access a library of information via a hypertext program.)

Although this discussion focuses on the development of a DC Module maintenance aid, a POINTER-based maintenance aid can be developed for virtually any application because of its modularized architecture.

POINTER Application Modules

There are several application modules that comprise the POINTER software shell. Figure 2 illustrates the functional flow among the POINTER application modules. Each of these modules has a number of commands and options that can be made accessible to the application. The commands and options in each module are tailored to the application. The modules are briefly described in the following sections.

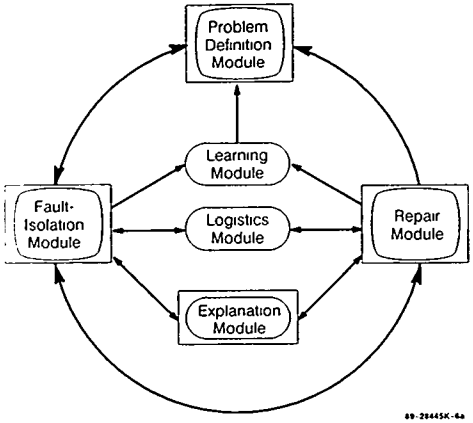

Figure 2. POINTER Process Functional Flow

The Problem Definition Module

Once the proper input files are created and processed, POINTER is ready for use. POINTER contains a number of layered menus in its problem definition module that allows a user to specify the knowledge base to be used and any specific known symptoms or conditions that exist before troubleshooting. Because of the layered-menu capability, POINTER can be used to troubleshoot several related or unrelated symptoms provided the STAMP-generated system model exists. Figure 3 is a sample menu of possible symptoms and conditions for a shutdown for the on-load condition of the TEPCO plant DC Module. Associated with each symptom and condition are the initiation of learning and logging files and fault-isolation criteria, such as the minimum time to fault-isolate on the basis of failure rates, test times, skill level, or a combination of two or more factors. By using POINTER, up to 999 different symptoms and conditions can be defined. Note that the user can choose an option of no existing symptoms and conditions.

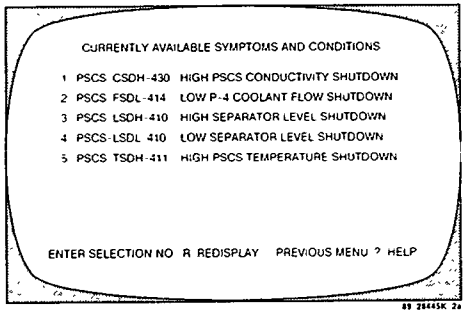

Figure 3. POINTER Provides Possible Symptoms and Conditions for Diagnosis

The Fault-Isolation Module

Once the symptom is entered, the first test that is based on the initial conditions is computed, and the test procedure is then presented. An example test within the fault-isolation module is shown in Figure 4. The top of the screen in Figure 4 provides information about the current problem, including the file name, the symptom or condition being fault-isolated, and whether or not learning is ON.

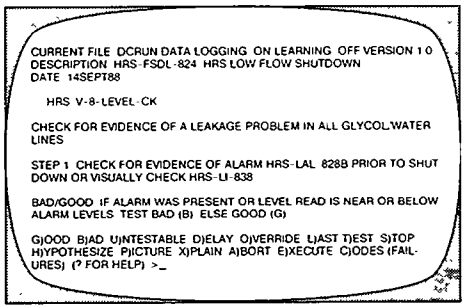

Figure 4. Sample Instructions and Instrument Designations Provided by POINTER for Each Test

The method of test order computation by POINTER previously described is based on the information theoretic algorithm used by STAMP. Shown at the bottom of the screen in Figure 4 are options available to the user during fault isolation. The available options can be tailored to any given situation and allow the user to interactively fault-isolate a failure. These options are described as follows:

- Good or Bad—The user can perform the test described and then enter the result, good (G) or bad (B). On the basis of these data, POINTER will then choose the next test or, if a test results in a fault isolation, present the bad component or group of components.
- Untestable—If a test cannot be performed (e.g., the information is not available or a sensor cannot be accessed), the user can declare the test untestable and the next best test will be chosen and presented. The consequence of declaring a particular test untestable is available using the explain option.
- Delay—The delay option is used to delay a test for any reason (e.g., this test requires three people, and only two are available for the next half hour). When the user enters D for delay, POINTER chooses another test, and fault isolation continues. With the delay option, POINTER can come back to the delayed test if it is needed, whereas with the untestable option previously described, POINTER does not return to the test.

- Override—The override option is used to choose a test that is different from the one selected by POINTER. This option permits an expert technician to use his or her knowledge of the symptom or condition in fault isolation. Once the test is chosen, POINTER then presents the appropriate procedure for the chosen test. Upon test completion, POINTER will choose the next best test on the basis of the outcome.

- Last Test—The last test option is a backup feature that enables the user to step back through previous tests. It may be used if a mistake was made on the previous test and the user wants to change the answer. With this option, the user can back up to the first test performed from anywhere within the test sequence.

- Stop—The stop option is available for situations in which it may be critical to quickly get the equipment back on line. A technician may have a fixed number of hours, or even minutes, to perform testing. If the fault has not be isolated in that period, the user can enter S for stop, and POINTER will present all components that still remain as the possible cause. The technician can then remove and replace each component until the system is functioning again.

- Hypothesize—The hypothesize option is another unique feature of POINTER that enables the user to tell the system which component might be causing the problem. Once the user enters the component name, POINTER redirects its test choice algorithm to choose the test sequence required for the most rapid check of the hypothesis. If the component chosen is not the one causing the problem, the system asks if fault isolation should continue. If the answer is yes, the next best test is chosen on the basis of the results of the last test performed.

- Picture—The picture option is available to view a graphic that is associated with the displayed test procedure. The graphic can show a schematic of the system under test or other information that would aid the user in performing the test. When the user enters a P for picture, the system reads in the graphic, and if one exists, displays it on the screen. When the user presses RETURN, the system returns to the test procedure. The picture can be viewed as many times as desired before a result (e.g., good, bad, untestable, or delay) is entered.

- Explain—The explain option provides information on a number of items that will assist the user in making decisions about how best to troubleshoot any given problem or symptom. The explain option is discussed in the section on the POINTER explanation module.

- Abort—The abort option is available to allow the user to completely exit a fault-isolation session and return to the problem definition module. In contrast to the stop option, abort does not provide a list of components that remain as possible causes of failure.

- Execute—The execute option appears only when a separately executable program is associated with a test. Such a program may actually execute the test and return the answer to POINTER. In some cases, a test chosen by POINTER may automatically execute without any further interaction with the user. Obviously, this requires appropriate additional test hardware.

- Codes (Failures)—Any independent program may be linked to POINTER and made available to the user at any point in the fault-isolation or repair module. The associated prompt is predefined. Other possible examples could be a CAD or hypertext interface.

- Help—The help option is available for each of the user options within POINTER and provides expanded descriptions of each of the options when chosen.

During the fault-isolation process, each test is timed, and the value is retained for learning purposes. At the end of repair, these values are used to update the learning file using an 11-point smoothing algorithm. In addition, each step in the diagnostic process is recorded in a log file for future use in logistic analyses.

The Repair Module

The repair module may be entered if the user has terminated fault isolation or if POINTER can go no further in isolating the fault. When the repair module is entered, the user is presented with the fault-isolation answer. The user may then choose to display a repair procedure, if one is available, or historical maintenance records relevant to the fault.

If the learning option has been chosen, POINTER asks for specific repair information—what was repaired and the operating hours associated with the repair. This information is placed into the log file, and new failure rates are computed for the learning file. Conflicts between actual repairs and isolations are stored in a file to be used in future extensions of learning.

The POINTER Explanation Module

The explanation module has the full power of the inference engine to provide information and analyses to the user. Upon selection of the explain option, a secondary menu is provided, which may include the following:

- Tests given or inferred good—Tests determined to be good are listed, and the option is provided to view the reasoning that determined the good outcome.

- Tests given or inferred bad—Tests determined to be bad are listed, and a reasoning option (as in tests given or inferred good) is available.

- Tests untestable or unavailable—Tests determined to be untestable or unavailable are listed, and a reasoning option (as in tests given or inferred good) is available. Also available is an analysis of any ambiguity groups resulting from declaring a test or tests untestable.

- Components, replaceable units, and multiple failures no longer being considered—Conclusions or answers eliminated from consideration are listed with an explanation of the reasoning.

- Tests that are unknown and available—Tests still available for performing are listed with or without any associated weighting factors (e.g., test time or skill level).
- Actively considered answers—Conclusions or answers are listed that have not been eliminated from consideration. The list comprises the ambiguity group that would exist if isolation were terminated.
- Why this test—This option provides an explanation of the test choice, including the value of any factors considered (e.g., failure rates or test times), compared with the range of values available and the differentiation ability of the test in terms of separating the conclusions.
- Consequences of not doing the test—An analysis of the consequences of declaring a test untestable may be performed with this option. The analysis includes efficiency changes, ambiguity groups, and related tests that are declared untestable.
- Hypothesis—The steps necessary are listed to verify a specific user-hypothesized answer on the basis of current information.

A number of analyses and explanations are available from the repair module. After isolation is achieved, these data are provided by the explanation module using the full power of the inference engine as follows:

- Verification steps—This feature provides the user with the minimum number of steps (with their expected outcome) necessary to verify the isolated failure. This is a good feature for quality maintenance.
- Inference trace—The user is able to step through the testing that was just completed and examine, at each step, a list of the components under consideration. This is a good feature for training because the user has to determine at what points certain conclusions are eliminated.
- Hidden-failure analysis—When this multiple-failure option is selected, it provides a list of failures whose presence cannot be identified with the current failure isolation. If any of the members of this list could be the root cause of the isolated failure (i.e., a failure of the hidden unit would cause the failure of the isolated unit), a maintenance problem can be avoided by repairing both failures.
- Failure combinations with identical symptoms—This is another multiple-failure analysis option that scans the knowledge base for combinations of failures that have identical symptoms. If one of these multiple failures exists, repair of the isolated components will not restore the system. The maintenance technician can then consider a multiple repair in a logical fashion.

The Learning Module

During the fault-isolation session, POINTER times the tests as they are performed. The test times are then recorded and combined with previously recorded test times to derive a new test time measure. This measure is used by POINTER to improve fault isolation when attempting to minimize the time required to fault-isolate.

In addition, POINTER records the repairs made to the system with the current number of hours of system operation. Failure rates are then recomputed on the basis of the repairs and operating hours, and the new failure rates are used by POINTER when attempting to isolate failures using failure probability.

The Logistics Module

In addition to recording test times and failure rates for improving fault-isolation performance, POINTER maintains two sets of files that can be used in logistic documentation. First, the learning file associated with each POINTER model can contain information on test times, skill level, failure rates, number of recorded failures, the most recent operating hours for each repair, and a link to a log file. The second set of files comprises log files.

Each fault-isolation session creates a log file containing information about that session. Each log file includes a description of the setup conditions for fault isolation, a record of the test sequence, a list of failures identified, any repair actions, and comments provided by the technician. The test sequence information includes the times to perform each test, all POINTER actions taken by the technician, and the test outcome. If learning takes place, POINTER includes information on test times and failure rates. Finally, each log file is linked to the previous log file associated with a repair of the same failure (if one exists).

The information provided in these files does not include the results of any logistic analyses. However, it does provide some of the data required for such analyses. In addition, other files can be used with a separate documentation system that records and analyzes logistic information.

Anticipated Benefits

On the basis of previous success in reducing fault-isolation time using STAMP (Table 1), there are several anticipated benefits using the POINTER-based maintenance aid. Some anticipated key benefits from using the POINTER-based maintenance aid for the TEPCO DC Module are as follows:

- More timely start-up of the DC Module because of an increase in ability to locate and fix problems
- More on-load operating hours because of reduced downtime to locate and fix problems
- An increase in troubleshooting capabilities for less experienced technicians
- An increase in training capabilities for TEPCO engineers on troubleshooting the DC Module
- An increase in the capability to automatically collect maintenance data
- Less wear and tear and induced failures because of reduced false removals

These benefits should result in decreased costs of running this first-time demonstration power plant, reduced plant downtime, and improved technician proficiency.

Summary

The testability of complex systems, such as power plant controls, is a critical design feature that affects plant availability. The STAMP model has been proved as an effective tool for designing good inherent testability into new systems and for improving the achievable testability of existing systems. STAMP analyses have resulted in reductions of more than 90% in required tests, as well as in the elimination of test ambiguities.

The interactive fault-isolation capability of STAMP is now incorporated in an intelligent, portable maintenance aid called POINTER. POINTER provides the field technician with a powerful tool for failure diagnosis and troubleshooting. When embedded into a plant control system, a POINTER-based maintenance aid can prove especially valuable for unmanned stations.

It is anticipated that any POINTER system will significantly contribute to the ability of maintenance personnel to respond to failures. The POINTER system developed for a fuel-cell plant is expected to reduce fault-diagnostic time and plant downtime, enable less-experienced personnel to perform complex troubleshooting, and improve technician training through the use of graphics, the explain option, and other features.

References

1. *Testability Program for Electronic Systems and Equipment*, MIL-STD-2165, January 26, 1985.
2. C. R. Unkle, et al., "A SMART Portable Troubleshooting Aid for Power Plant Controls," 1989 Conference on Power Plant Controls and Automation, Miami, Florida, February 1989.
3. C. R. Unkle and D. M. Rastler, "The Portable Interactive Troubleshooter (POINTER): An Intelligent Maintenance Aid for Complex Systems," *Proceedings 1989 Advanced Computer Technology for the Power Industry.*
4. J. W. Sheppard, W. R. Simpson, and C. R. Unkle, "POINTER—An Intelligent Maintenance Aid," *Proceedings 1989 AUTOTESTCON.*

Note: Presented at the 17TH Inter-Ram Conference for the Electric Power Industry.

FUEL CELL COGENERATION PLANT - A Technical and Economical Feasibility Study for a Petrochemical Plant in Finland

Nieminen J-P., Hiltunen J., Suhonen P.,Yao N.P.[1]
Neste Oy, P.O.B. 310, SF-06101, Porvoo, Finland
[1] Consultant

Neste Oy is a major oil, gas and chemical company in Finland. Within the company we have two oil refineries and several petrochemical plants, most of which are located in Porvoo, 50 km east of Helsinki.

At present heat and power demand of Neste Porvoo Works is about 550 MW heat and 150 MW electricity, much of which are produced on-site. A projected demand for the period 1992-1995 is about 700 MW heat and 180 MW electricity, which can still be met with present production capability as shown in Figure 1. However we are continuously assessing other alternatives to meet the future demand beyound the year 1995.

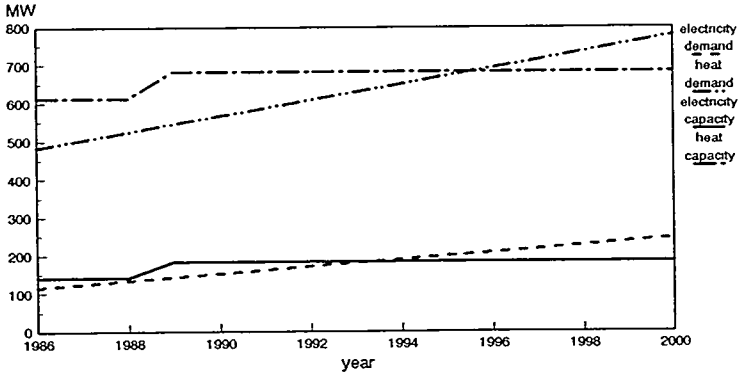

FIGURE 1 **Forecasted electricity and heat demands for Porvoo Works**

Since 1988 Neste Corporate Technology has been conducting a design and cost study of a 40 MW_e fuel cell cogeneration plant to meet the projected requirements. This paper presents the results of this assessment study.

Natural gas (NG) fueled MCFC and SOFC plants, both atmospheric (first subscript = a) and pressurized (first subscript = p), were considered in the total power plant design to provide about 40 MW_e and about 20 tn/h high pressure (100 bar) steam (second subscript = s) or low pressure (16 bar) steam (second subscript = p). The high pressure steam is used in a existing pack pressure steam turbine while the low pressure steam is used in chemical processes. Figure 2 shows the existing steam system of the Works. PAFC plant was initially considered, but the economics were unfavorable due to its lower operating temperature and insufficient usable heat. Advanced gas turbine with heat recovery boiler was used as a reference case.

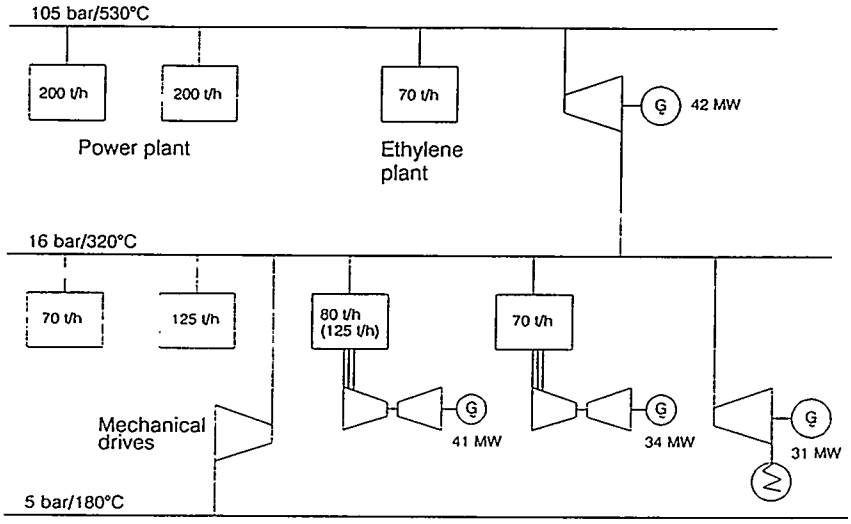

FIGURE 2 The existing process steam production scheme of Neste Porvoo Works

In Table 1 is shown performance figures of different alternatives in our application. Sizing was done so that in all cases we are producing about same proportion of electricity and heat we are using. The differences in figures are due to different use of exiting production facilities.

TABLE 1
Performance data summary of different cases

	GT	SOFCps	SOFCpp	MCFCas
Steam pressure, bar	106	106	16	106
Fuel cell pres. bar(a)	-	16	16	1
H_2-utilization	-	70	65	70
POWER PRODUCTION				
-fuel cell, MW_e (DC)	-	34.3	34.0	40.8
-gas turbine, MW_e	41.6	10.6	14.2	-
-steam turbine, MW_e	11.6	1.0	-	3.4
Total, MW_e	53.2	45.9	48.2	44.2
Efficiencies, % (HHV)				
-Fuel cell system, % (H_2)	-	46.2	42.9	45.0
-Electrical, % (NG)	26.2	55.2	53.1	40.8
-Total, % (NG)	71.9	68.5	75.0	74.7

Table 2 summarizes investment cost evaluations made for the three fuel cell alternatives compared with a gas turbine (GT). The most expensive case is MCFC, mainly because of huge expensive gas ducts (item 1.3) for recirculating the anode gas. Prices for fuel cell stacks are from literatures and other component prices are based on actual quotations from manufacturers.

Energy savings, in Table 2 , represent the cost savings for all fuels and possible purchased electricity for the Porvoo Works against a base case, where all needed electricity will be purchased at a price of 128.00 FIM/MWh (app. US 3.2 ¢/kWh).

TABLE 2
Investment costs, in MFIM*, for the pressurized SOFC and the atmospheric MCFC plants**

	GT	SOFCps	SOFCpp	MCFCas
MECHANICAL EQUIPMENT				
1.1 Steam boiler plant		12.4	10.0	15.3
1.2 Gas turbine plant		31.8	31.8	-
1.3 Ducts		2.2	2.2	50.0
1.4 Water treatment		0.5	0.2	0.5
1.5 Heat exchangers		0.1	0.1	2.4
1.6 Piping		2.0	0.8	2.4
1.7 Auxiliary devices		1.6	0.7	1.8
1.8 Automation		7.2	6.6	4.2
1.9 Electricity		2.8	2.0	2.5
1.10 Fuel cell stacks		55.0	57.9	93.6
1.11 FC el. & instr.		8.6	9.0	6.3
1.12 FC power conditioning		17.4	18.4	22.0
TOTAL		**141.6**	**139.6**	**201.0**
CONSTRUCTION WORK				
2.1 Power plant building		3.9	3.4	1.8
2.2 Excavation		0.4	0.4	0.4
2.3 FC building		-	-	3.5
2.4 FC control building		1.2	1.2	1.2
2.5 FC electr. building		1.5	1.5	1.5
TOTAL		**7.0**	**6.5**	**8.4**
INDIRECT EXPENSES				
3.1 Planning		8.9	8.8	12.6
3.2 General facilities		5.9	5.8	8.4
TOTAL		**14.8**	**14.6**	**21.0**
SPARE PARTS		**2.8**	**2.8**	**4.0**
INVESTMENT TOTAL	**122.0**	**166.2**	**163.5**	**234.4**
Specific cost, FIM/kW	2312	3567	3392	5303
Energy savings, MFIM/a	19.59	38.67	39.13	23.67

* Currency conversion factor: 1 MFIM = 0.25 M$
** Plant specifications are given in Table 1.

An economic and cash flow analysis has indicated that the pressurized SOFC was the most promising alternative. Total investment costs for the SOFC plant were estimated to be about 160 MFIM (app. US$ 40 M) and savings against purchased electricity were 40 MFIM/a (app. US$ 10 M/a). The internal rate of return (IRR) for the investment was 13.8 % and a pay back time of 6.2 years. This is to be compared to the reference case of gas turbine which has investment costs of 120 MFIM (app. US$ 30 M), fuel savings of 20 MFIM/a (app. US$ 5 M/a) giving an IRR of 5.4 % and a pay back time of 10.1 years. Table 3 compares the profitability figures for the four cases.

TABLE 3
Profitability of fuel cell and GT plants

	IRR (%)	Pay Back Period (years)
Gas turbine	5.4	10.1
MCFCas	-4.7	>15.0
SOFCpp	13.8	6.2
SOFCps	13.2	6.4

Sensitivity to the plant economics and the fuel cost was also analyzed. The results, in Figure 3, indicated that fuel cell power plant will become more favorable than gas turbine when the natural gas fuel price rises above the current level of 615 FIM/tn (app. US$ 3.8/MBTU).

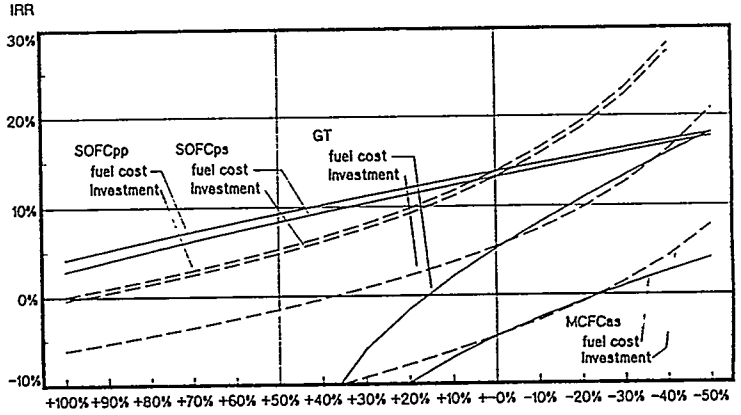

FIGURE 3 Sensitivity of IRR to investment and fuel cost changes for SOFCpp, SOFCps, MCFCas and GT

In our opinion, SOFC offers very likely an attractive alternative for chemical industry for on-site heat and power generation within next ten to fifteen years.

COMPARITIVE ANALYSIS OF POWER GENERATION TECHNOLOGIES

Richard Root Woods
Gas Research Institute
Chicago, Illinois

The power generation market is continually changing and evolving. Once dominated by regulated utilities operating as monopolies in a given territory, this marketplace is becoming more and more competitive. Independent power producers, industrial cogeneration, self-generators, demand side strategies, energy rate structures and increasing environmental regulations all factor into this marketplace's future. Fuel cells are the most efficient electric generation technology under development, but their market success is not based on this characteristic alone. Ultimately, the trade-offs between benefits and risks will determine which products are successful in the marketplace. By analyzing the characteristics of existing and emerging conventional technologies within the framework of various business strategies, fuel cell manufacturers can develop appropriate cost and performance goals for their products.

This analysis was directed at the competitiveness of gas-fueled technologies, but as a baseline for these comparisons, a coal-fueled integrated gasifier combined cycle was assumed. The net installed cost of this system was set at $1500/kW with a heat rate of 8800 Btu/kWh. With coal priced between $1.50 and 2.50/MMBtu, this power plant provided bus-bar cost of electricity (COE) between 5.3 and 6.2 ¢/kWh. The COE analysis also assumed a 65% capacity factor and regulated utility ownership which was modeled by a 12% annual capital charge rate (ACCR).

Several gas-fueled systems will compete with fuel cell technologies during the next century. Turbine-based technologies are the primary competition in the megawatt capacity ranges (10s to 100s of MW). Fundamentally, these are defined as simple cycle combustion turbines (CT), combined cycle power plants (CC) and steam injected gas turbines (SIGT). Figure 1 provides base case assumptions for cost and performance of these technologies and for an advanced fuel cell power plant. Using the baseline capacity factor (65%) and business criteria (ACCR at 12%), the COE for these gas-fueled systems are plotted as a function fuel price. As expected, the higher efficiency

technologies are preferred at higher fuel prices. In conclusion, gas-fueled systems (electric only) are competitive with coal-fueled power plants for baseloaded applications even with fuel prices between $4 and $6.5/MMBtu. The CC and MCFC are direct competitors for these opportunities.

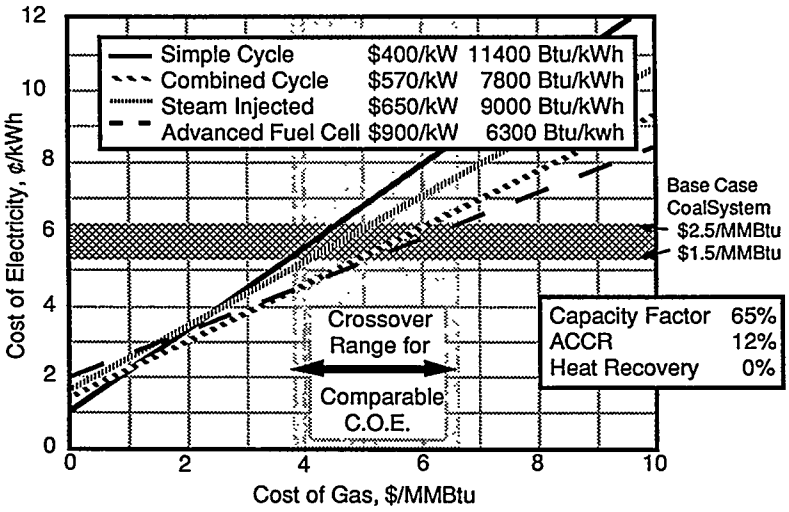

Figure 1 Competitiveness of Gas Technologies

This approach answers one set of questions with one set of assumptions, but what if the cost or performance characteristics change? What if the business criteria should represent an independent power producer and not a regulated utility? A better analysis tool is to conceptualize the variations that each parameter has on the competitiveness of each technology. Figure 2 provides this mechanism by identifying each technology according to its cost and performance and plotting lines of constant COE. The slope and position of the COE lines will change as the business, fuel, and operating parameters are modified. To illustrate this approach two sets of parallel lines are shown. The solid lines represent the baseloaded (65% capacity factor), utility ownership (12% ACCR), $5/MMBtu gas price comparison. The dashed lines represent a

similar case except the capacity factor is set at 20% to represent intermediate load applications.

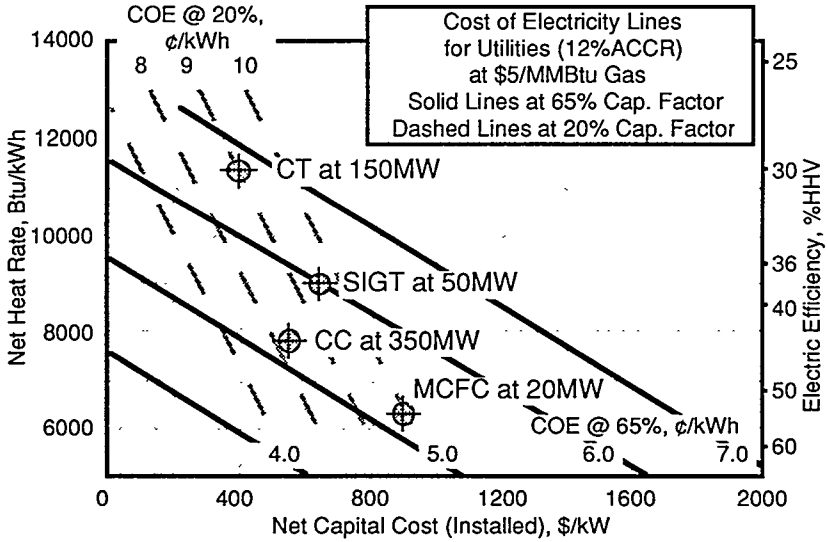

Figure 2 Performance and Cost Trade-off Analysis

The analysis indicates several aspects with regards to the competitiveness of the various gas-fueled technologies. The previous graphs illustrated that both the CC at 350MW and the molten carbonate fuel cell (MCFC) at 20MW are competitive for baseloaded applications. Also, these two systems are perferable to the less efficient CT at 150MW and SIGT at 50MW. If the application characteristics are lowered to intermediate capacity factors (20%), the lower cost characteristics of the CC makes it the technology of choice and the higher priced MCFC the least preferred technology. Adjustments in the capital cost or performance can be assessed directly without recalculating the economics. For example, if $50 to $75/kW is required for exhaust gas clean-up subsystems with the CC and CT power plants, the impact is apparent by simply shifting the cost of these two technologies to the left. The fuel cell system achieves this competitive position at a capacity ten times smaller than the CC, and therefore, additional cost benefits are realized by

the utility from transmission and distribution system savings. This impact is addressed by shifting the point to the right based on the value of these savings.

This technique can be used to conceptualize the effects of all the major factors or elements of an economic evaluation. These elements are identified as follows:

- Business criteria as represented by ACCR (12 to 16% for utility ownership; 14 to 20% for independent power producer ownership; and 18 to 30% for customer ownership scenarios);
- Fuel cost issues as represented by the price of gas in $/MMBtu;
- Application characteristics as represented by the capacity factor in percent;
- Performance as represented by net heat rate (HHV) in Btu per kWh; and
- Capital cost as represented by net installed cost (net cost through initial operation) in $ per kW.
- Non-fuel operating and maintenance (O&M) cost are minor cost elements in these gas-fueled systems and was assumed constant for all systems at $10/kW-yr and 0.026 ¢/kWh.

The technique is to envision the effect on the slope and position of the COE lines with changing values. First, the impact of capacity factor is illustrated in Figure 2. The COE lines at a fixed value and various capacity factors appear to rotate around a point where the net capital cost is zero (actual slightly less due to the fixed O&M cost). If the equipment is free, the COE is only a function of the heat rate, fuel price and O&M. The slope of a COE line approachs horizontal with increasing capacity factors and decreasing business criteria (ACCR). Increasing fuel prices will also cause the slope of the COE line to approach horizontal, but the fixed point for the rotation is at an imaginary point where the heat rate is equal to 0 Btu/kWh.

POLYMER ELECTROLYTE FUEL CELL RESEARCH

C. Derouin, R. Sherman, T. Springer, F. Uribe, J. Valerio, T. Zawodzinski,
M. Wilson, and S. Gottesfeld
The Electronics Research Group, Los Alamos National Laboratory
Los Alamos, NM 87545

We describe in this paper efforts in two areas of polymer electrolyte fuel cell (PEFC) research. The first is the optimization of the performance of such cells while minimizing the Pt loading, and the second is the modeling of characteristics of an operating cell based on experimentally derived parameters.

1. Lowering the Pt loading While Maintaining High Cell Performance

We have demonstrated previously (1) that high power densities can be achieved in PEFCs employing Pt loadings as low as 0.45 mg/cm^2 (typical loadings for phosphoric acid fuel cells). Such cells have been based on ionomer-impregnated gas-diffusion electrodes, hot-pressed onto an ionomeric membrane electrolyte. We report here on several advances in the optimization of such membrane-electrode assemblies.

(1a) Further reduction of the Pt loading by a factor of two with only marginal sacrifice of cell performance could be achieved by carefully "planarizing" the carbon powder underlying the Pt/C catalyst prior to the application of the latter. This approach helped to avoid loss of catalyst into gaps in the carbon cloth backing, and ensured intimate contact between the very thin (nominally 25 micron thick) catalyst layer and the membrane electrolyte. The performance achieved with only 0.225 mg/cm^2 on each electrode (0.175 mg/cm^2 as Pt/C and additional 0.05 mg/cm^2 as sputtered layer on the front surface of the catalyst) is shown in Figs. 1a and 1b.

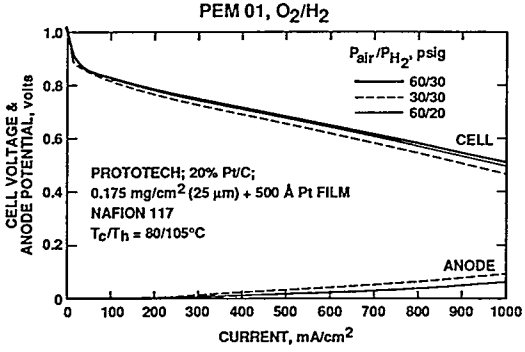

Fig. 1a

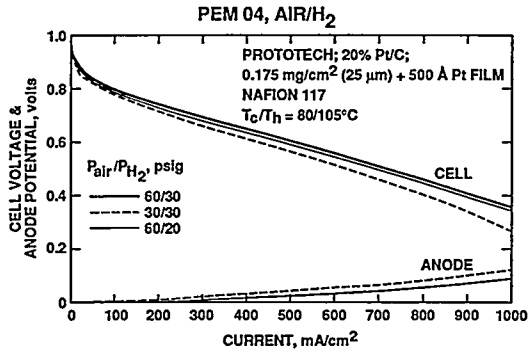

Fig. 1b

(1b) We have stressed before the significance of membrane thickness in achieving the best cell performance (1) . At this point our best performance on pressurized air and hydrogen has been achieved with 50 micron thick experimental Nafion® membranes. An example is given in Fig. 2, showing that currents in excess of 3A/cm^2 can be achieved with the Prototech air electrode employed operating on only 0.45 mg/cm^2 of Pt in the cathode.

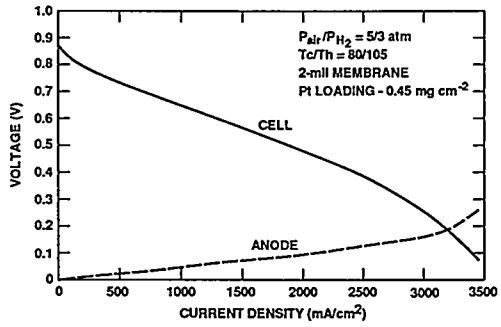

Fig. 2

Out of various experimental membranes we have tested some were supplied in larger quantities and allowed us to run tests of performance reproducibility. Table 1 shows results of tests of three different cells employing a perfluorosulfonate 125 micron thick membrane of EW=900, supplied by Chlorine Engineers (Japan), and designated by

the manufacturer as "Membrane C." The reproducibility of the performance from cell to cell is seen to be satisfactory, allowing at this point reliable analysis of cell polarization characteristics.

(1c) Analysis of cell characteristics has been routinely performed, employing measurements of the dependence of half cell potentials on current density, comparative performance of the cell on oxygen and on air and ac impedance measurements. Central conclusions from these measurements can be summarized in the following way: (a) In a well humidified cell ($T_{hum} > T_{cell}$) cathode losses due to gas transport limitations are more severe (particularly for operation on air) than any anode losses associated with local membrane dehydration. This is confirmed also by the cell modelling effort described below. Such cathode losses seem to be relieved by thinner membranes, the only reasonable explanation being effective removal of excess liquid water from cathode to anode across the membrane. (b) Impedance measurements of the fuel cell cathode under typical cell operating conditions reveal an increasing effective "Tafel slope" for the oxygen reduction process as the current density increases. A recent investigation of a model interface: smooth Pt microelectrode/recast ionomeric film, has revealed a similar behavior, suggesting a limiting (potential independent?) kinetic barrier. (c) The investigation of the model system described above reveals an apparent "catalyst utilization" in the oxygen reduction process of the order of 10% - 20%. This number is strongly influenced, however, by the electrochemical surface cleaning process which is applied in the study of the model system but not in an operating fuel cell.

(2) Polymer Electrolyte Fuel Cell Model based on Experimentally Derived Transport Parameters

We have recently developed a comprehensive model for a single PEFC which has the important advantage of being based on a complete set of membrane transport parameters measured by us for the full range of membrane hydration conditions (2) . The model treats the complete cell, including transport through electrode and the membrane as well as interfacial polarization. Results of model calculations for water flux and for membrane resistance and overall cell polarization at 80°C are shown in Fig. 3 for the case of Nafion® 1100. Figure 3 clearly demonstrates the (nonlinear) advantage of a thinner membrane in minimizing cell resistance losses at high currents, and shows that even for a Nafion® 1100 material such losses can be small at a current density as high as $2A/cm^2$. (This model does not consider at this point effects of liquid water on mass-transport limitations in the electrodes).

TABLE I

MEMRANE-C-BASED CELL VOLTAGES (UNCORRECTED) FOR THREE CELLS

Pt loading ----0.45 mg/cm^2

mA/cm^2	V.PEFC 76		V.PEFC 85		V.PEFC 86	
	O_2	AIR	O_2	AIR	O_2	AIR
500	0.77	0.72	0.75	0.70	0.75	0.70
1000	0.67	0.60	0.64	0.54	0.66	0.55
1500	0.57	0.42	0.53	0.33	0.55	0.30
2000	0.42		0.40		0.40	

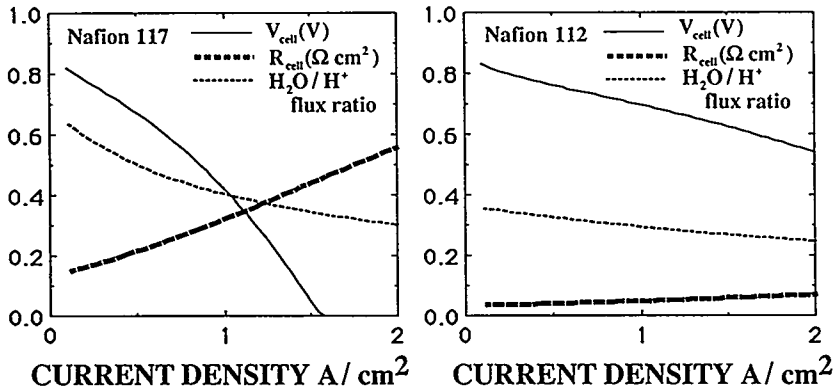

Fig. 3

References:
(1) S. Gottesfeld et al, Book of Abstracts of the 1988 Fuel Cell Seminar, p.206.
(2) T. Zawodzinski and S. Gottesfeld, see this book of abstracts.

THE TREATMENT OF CO POISONING IN LOW TEMPERATURE FUEL CELLS BY THE INJECTION OF OXYGEN OR AIR INTO THE ANODE FEED STREAM

by

M. T. Paffett, P. A. Pappin, J. Valerio, and S. Gottesfeld
Los Alamos National Laboratory

Methanol is the most likely transportable form of hydrogen considered for terrestrial transportation applications. Steam reforming of methanol results in a gas mixture of an approximate composition 75% H_2, 24% CO_2, 1% CO. In an acid fuel cell, such as the polymer electrolyte fuel cell (PEFC), the effect of CO_2 in an anode feed stream is a slight dilution of the H_2 reactant ,with only minor effects on anode performance. The presence of CO at the level of 1% in the anode feed stream is, on the other hand, intolerable for a fuel cell which operates at 80°C. At this temperature, the Pt anode electrocatalyst will be severely deactivated by adsorption of CO when CO is present in the gas at such a partial pressure. One method to lower the CO concentration (1) is to mix the reformate with ca 2% O_2 and then pass this gas mixture on a Pt/Al_2O_3 catalyst held at ca 150°C. This approach, named "preferential oxidation" (POX), significantly lowers the CO level in the gas mixture by the catalytic oxidation of CO to CO_2. Residual CO concentrations of 10 to 100 ppm have been reported following this treatment (2,3). Considering the reported residual levels of CO following the POX step, as well as any possible imperfections in the performance of the reformer/POX stage , we have investigated the effects of CO concentrations in the range of 10 to 100 ppm in the anode feed stream on the performance of the PEFC. Our investigation, previously described in Ref. 4, revealed that CO at the 100 ppm level in the anode feed stream, causes a severe loss of cell performance, that results from anode electrocatalyst poisoning. A possible solution for the problem was developed and demonstrated in single PEFC tests (4). We showed that bleeding O_2 at the 2% level into the CO-contaminated H_2 anode feed resulted in a complete recovery of the CO-free cell performance. This is demonstrated in Fig. 1, which shows both the loss of performance in the presence of 100 ppm CO in the anode feed stream and the complete recovery of performance following the addition of 2% O_2 to the anode feed stream.

Because all of these results (Fig. 1) were obtained under very low fuel utilization (i.e., very high stoichiometric flows of H_2), further tests of the "oxygen bleeding" approach were subsequently performed under conditions of high H_2 utilization. The fuel stoichiometry in these recent tests was in the range of 1.2 to 1.5. The anode gas exhaust was analyzed during such tests at several fuel flow

stoichiometries. Figure 2 shows that the degree of performance loss in the presence of a given level of CO in the H_2 feed stream is smaller as the fuel flow is lowered to 1.2 to 1.5 stoichiometry. The reason for this behavior is revealed by results of anode exhaust analysis described next.

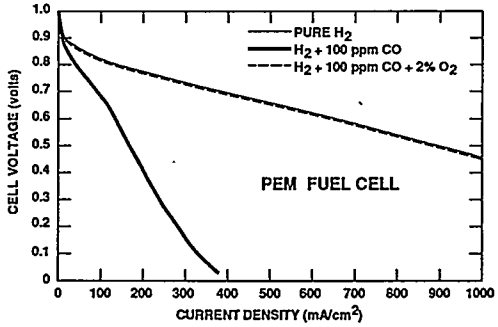

POWER LOSS BY POISONING AND POWER RESTORATION BY OXYGEN INJECTION

Fig. 1

The CO and CO_2 levels were determined by infrared (IR) spectrophotometry performed with a variable optical path-length IR (2.25 - 20.25 m) cell for gas analysis. The levels of the two gases were first determined for PEFCs operating on CO-contaminated anode feed streams without any intentional bleeding of O_2. The results are shown in Fig. 3. At high fuel flow rates, it is apparent that the level of CO in the anode exhaust is the same as that in the anode feed stream (100 ppm). However, at lower rates of fuel flow, the level of CO in the anode exhaust becomes smaller, and at flow rates close to fuel stoichiometry of 1 a large fraction of the CO has "disappeared" from the anode exhaust. This phenomenon is most probably caused by the access of low levels of O_2 to the anode catalyst, even when no O_2 is intentionally added to the anode feed stream. Penetration of small amounts of O_2 from the cathode compartment through the ionomeric membrane to the anode compartment (gas "crossover") is one possible explanation. This explanation is supported by the best apparent "CO tolerance" found in our tests of PEFCs with the thinnest (50 μm) membranes, for which the degree of gas crossover is relatively high.

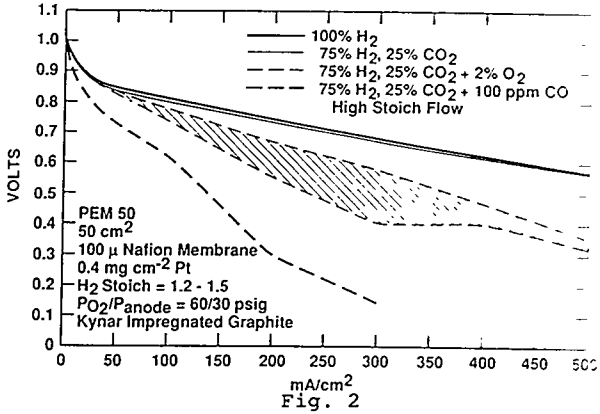

Fig. 2

For the whole range of fuel flows tested, the IR analysis of the anode exhaust showed that CO was completely eliminated at the exhaust by intentional injection of 2% O_2. This finding clearly demonstrates that CO at the 100 ppm level is completely oxidized as a result of this concentration of O_2 (2%) in the gas stream. In fact, this finding is fully expected from recent reports by Berlowitz *et al.* (5) on the rate of CO oxidation by O_2 at Pt catalysts at low temperatures, close to 80°C. The presence of H_2 and H_2O at the Pt anode electrocatalyst apparently does not significantly lower the rate of the catalytic oxidation of CO by O_2 at this temperature. (The H_2 could, in fact, enhance it). CO_2 levels found in the anode exhaust were somewhat higher than expected from the oxidation of CO. This was the case both in the presence and in the absence of intentional O_2 bleeding. The apparent reason for the higher concentrations of CO_2 is low level of gasification of carbon components in the gas diffusion electrode during cell operation (i.e., another source of CO_2 in the operating cell). The rate of the latter process has no real significance in terms of long term electrode material loss.

The significant lowering in CO concentration that occurred as a result of just passing the fuel stream through the anode chamber in an operating cell (Fig. 3), suggests that near a fuel stoichiometry of 1 the degree of intentional O_2 bleeding required for a complete recovery of cell performance could be significantly smaller than the 2% level we previously reported for high stoichiometric flows. Furthermore, the bleeding of air, rather than O_2, is a more realistic mode of operation in terrestrial transportation applications. Accordingly, we tested PEFCs operating on H_2 with 100 ppm CO at a stoichiometric flow close to 1, to determine the lowest level of air added to the anode feed stream to completely recover cell losses caused by catalyst CO poisoning. The result is shown in Fig. 4. Close to unit

stoichiometry, the cell performance is seen to be fully recovered (in the presence of 100 ppm CO in the fuel feed) when only 2% of air is added to the anode feed stream. (Figure 4 also shows that even smaller levels of air in the fuel stream are not sufficient for complete recovery). This result is quite encouraging because, at the last level of O_2 (0.4%) the loss of fuel caused by this mode of anode catalyst "cleansing" is negligible.

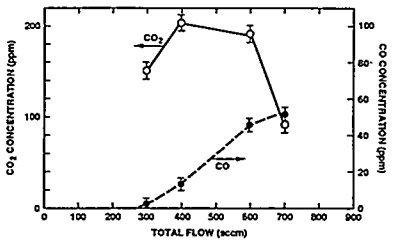

Fig. 3

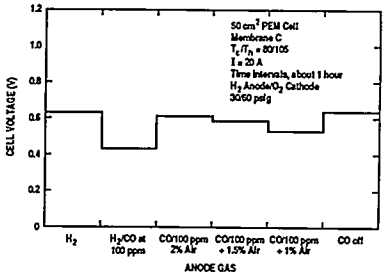

Fig. 4

In conclusion, from our single cell PEFC tests, we find that the bleeding of small amounts of air into the H_2 feed stream seems to be a very effective approach to the problem of anode catalyst poisoning by CO at the 100 to 500-ppm level. This technique seems to work particularly well under the most realistic conditions of fuel stoichiometric flows close to 1.

References

(1) J.C. Bonacci *et al.*, U.S. patent No. 4, 238, 468, Dec. 9 1980

(2) N.E. Vanderborgh, C.A. Spirio and J.R. Huff, Extended Abstract of the International Seminar on Fuel Cell Technology and Applications, The Hague, The Netherlands, October 1987, p.253.

(3) N.E. Vanderborgh, J. Guante, R.E. Dean and R.D. Sutton, Abstracts of The Fuel Cell Seminar, Long Beach CA., Oct. 1988, p. 52.

(4) a) S. Gottesfeld and J. Pafford, J. Electrochem Soc., 135, 2651 (1988); b) S. Gottesfeld, US. Patent No. 4,910,099 (March 20, 1990).

(5) P.J. Berlowitz, C.H.F. Peden and D.W. Goodman, J. Phys. Chem. 92, 5213 (1988).

MEASUREMENTS OF WATER TRANSPORT PROPERTIES AND IMAGING WATER PROFILES IN IONOMERIC MEMBRANES EMPLOYED IN POLYMER ELECTROLYTE FUEL CELLS

Thomas A Zawodzinski Jr., Michal Neeman, Laurel Sillerud, and Shimshon Gottesfeld
Los Alamos National Laboratory
Los Alamos, NM 87545

Introduction

Fuel cells employing hydrated Nafion® or other hydrated perfluorinated ionomeric materials as the electrolyte are promising candidates for electric vehicle applications. The polymer electrolyte provides room temperature start-up, elimination of many corrosion problems, and the potential for low resistance losses. Resistive losses within the fuel cell result in part from a decrease of membrane protonic conductivity following partial dehydration of the membrane. On the other hand, cathode flooding problems are caused by too much water in the system. Clearly, water management within the fuel cell involves achieving a compromise between the two extremes.

In order to fully understand water transport into and through the ionomeric material, information on a wide variety of membrane transport and water uptake characteristics is necessary. The dependence of membrane properties on water content of the membrane is a specific area of importance to fuel cells which has been inadequately probed. Spatial variations of water content within the polymeric electrolyte of a current-carrying fuel cell result from the drag of water with proton transport from anode to cathode, the production of water by the oxygen reduction reaction at the cathode, humidification differences of the inlet gas streams, and the "back-diffusion" of water from cathode to anode.

NMR Experiments: Diffusion Coefficients and Images

An important aspect of water diffusion measurements in ionomeric membranes is the dependence of the diffusion coefficient on the water content in the membrane. This dependence complicates the analysis of transport experiments performed under conditions of significant water concentration gradients because of the need to consider a distribution of local diffusion coefficients within the membrane. The simplest experiment which can be performed in such a system measures the intradiffusion coefficient, that is the translational thermal motion of water in the absence of a concentration gradient. Such measurements of intradiffusion coefficients can be made by NMR techniques applied to membranes of uniform water profile, with the water level in the membrane set by varying the equilibration conditions. We have employed several types of NMR experiments in studying water transport in PEFC membranes, including the pulsed

field-gradient spin echo (PGSE) method[1], a modification of the PGSE method in which slow diffusion is enhanced (SDE-PGSE), and an NMR diffusion-imaging technique.

The PGSE method, schematically shown in Figure 1a, employs a pair of field gradient pulses superimposed on a spin-echo sequence. Diffusion of molecules causes attenuation of the observed signal intensity. The diffusion coefficient is obtained from a fit of the observed intensity as a function of the gradient strength. The SDE-PGSE method is a slight modification of the PGSE technique, as shown in Figure 1b. Employing this pulse sequence with incremented values of the outer pair of gradient pulses results in increased attenuation of rapidly diffusing components. Diffusion coefficients obtained for Nafion 117 membranes of various water contents using either the PGSE or SDE-PGSE technique are shown in Table 1. The water content in the membrane was varied by equilibrating the membrane with water vapor above LiCl solutions of well known water activity.

TABLE 1
1H Intradiffusion Coefficients, 30°C

Water Content (H_2O/SO_3H)	D (x 10^6, cm^2/sec)
2	0.6 ± 0.06*(SDE**)
3	1.2 ± 0.08 (SDE)
4	2.1 ± 0.06 (SDE)
6	3.7 ± 0.15
9	4.4 ± 0.07
14	5.8 ± 0.21

*Errors reported here are the standard error of the non-linear least squares fit to experimental data.
**The label SDE indicates that this diffusion coefficient was determined using the SDE-PGSE technique.

We have used recently developed NMR diffusion imaging techniques[2] to obtain the diffusion coefficients of water in membranes immersed in liquid water as a function of temperature. This data is of importance because significantly higher water contents are obtained for membranes in contact with liquid water. Significantly higher values of D were obtained for water in immersed membranes.

In analyzing water fluxes within the membrane, it should be realized that diffusion occurs due to a gradient in chemical potential, while the flux due to diffusion is most often described in terms of concentration gradients. An effective, so-called "chemical" diffusion coefficient, which describes water motion in the presence of concentration

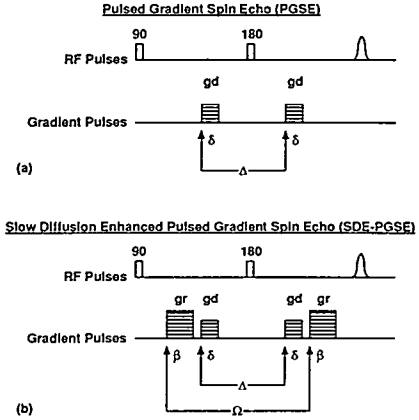

Figure 1
NMR Pulse Sequences for Diffusion Studies

gradients, can be defined as follows if the dependence of membrane water activity on membrane water content is known:

$$D_{chem} = \left(\frac{d\ln a}{d\ln C}\right) D^*$$

where D_{chem} is the "chemical diffusion coefficient", D* is the intradiffusion coefficient determined experimentally, a is the activity of the diffusing species, and C is the concentration of the diffusing species (i.e. the membrane water content). The chemical diffusion coefficients derived from our experimental data are shown in Table 2. It can be seen that the effective ("chemical") diffusion coefficient varies only slightly with water content in the membrane. This is caused by large variations of the activity coefficient of water at low water concentrations, providing additional "drive" for water transport and compensating for the big drop in the intradiffusion coefficients at low water contents as seen in Table 1.

Table 2
Chemical Diffusion Coefficients

Water Content (H2O/SO3H)	Dchem (x 106, cm2/sec)
2	1.3
3	4.2
4	2.3
6	2.0
9	1.7
14	1.5

The intradiffusion coefficients discussed above actually reflect the motion of all mobile ^1H nuclei in the samples studied. This means that proton (H^+) motion also contributes to the observed diffusion coefficients. The observed diffusion coefficient under these conditions reflects a population weighted average diffusion coefficient over the various ^1H environments. However, we maintain that the diffusion coefficients measured reflect the water motion since, at high water contents, water is in large excess over H^+, whereas at low water contents, the mobility of H^+ determined from conductivity approaches the overall observed diffusion coefficient from NMR, suggesting that all ^1H nuclei move together. This problem in interpretation will be made moot when we have the opportunity to measure diffusion coefficients by ^{17}O NMR, which will reflect only water molecule mobility.

NMR imaging experiments aiming at direct observation of water profiles within Nafion 117 membranes under a variety of hydration conditions are under way. Among the situations being probed are profiles of water in membranes drying uniformly (taken as a function of time), membranes only partly exposed to dry air, membranes separating dry air and liquid water, and a vertically suspended membrane with one end exposed to bulk liquid water. The imaging technique is very versatile in providing information relevant to a range of questions related to transport issues.

References

1) E. O. Stejskal, J. E. Tanner, J. Chem. Phys., 1965, **42**, 288.

2) M. Neeman, J. Freyer, L. Sillerud, accepted for publication, J. Mag. Res..

3) M. Neeman, K. Jarrett, L. Sillerud, J. Freyer, submitted for publication, Cancer Research.

4) H. J. V. Tyrell and K. R. Harris, Diffusion in Liquids, Butterworths, London, 1984.

CATALYTIC RECOMBINER FOR ELIMINATION OF FUEL CELL PURGE GASES

K. Ledjeff , J. Gieshoff, D. Schlegel
Fraunhofer-Institute for Solar Energy Systems, D-7800 Freiburg , FRG

I. Introduction

Fuel cell systems for use in submarines are under development in Germany since 1980. The work is performed under the industrial leadership of Howaldtswerke-Deutsche Werft AG (HDW), Ingenieurkontor Lübeck (IKL) and Ferrostaal (FS) /1/. The fuel cell modules have been delivered by Siemens /2/. IKL has been in charge of the overall design and has built up the equipment in a land test stand.

The fuel cell system is operated in the closed containment of the boat. It is necessary to process the off gases inside a special designed reactor, which must be capable to eliminate the hydrogen from the purge gases. Depending on the operational conditions the concentrations of hydrogen, oxygen and inert gases vary and explosive gas mixtures may be formed.

On the basis of the requirements specified by the fuel cell modules we have developed a novel type of catalytic reactor, which recombines even explosive hydrogen/oxygen mixtures in a controlled manner and forms water and heat.

II. Catalytic recombination of hydrogen

The reaction of hydrogen and oxygen can be catalysed by some metals of the platinum group. Platinum itself is a very active catalyst, so that the recombination reaction starts even at 0 °C. The capability of eliminating hydrogen of explosive mixtures is coupled to the necessity to limit the reaction temperature below the ignition temperature of 585 °C. The well known equation of Arrhenius shows a positive dependence of the reaction rate with the temperature:

$$r \sim \exp(-E_A/RT)$$

Thus, to avoid explosions the catalytic unit must be self-limiting and its principle arrangement is shown in Fig. 1.

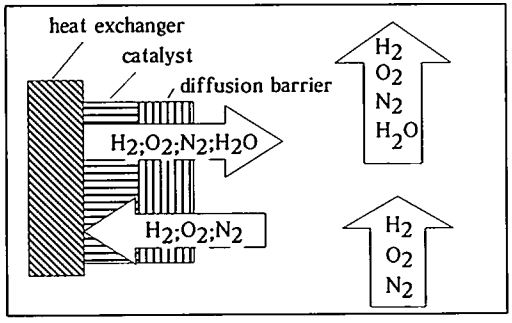

Fig. 1: Principle of the catalytic system

The catalyst structure and the diffusion barrier are very hydrophobic, fabric materials; the heat exchanger is formed as sheet metal made from copper, which is not attacked by the very pure water produced by the reaction.

The arrangement of the structure of the catalyst and of the diffusion barrier forces the reaction products to diffuse against the educts in a counterway. Thus the transport of the explosive H_2/O_2-mixture is hindered, a self-limiting effect is achieved and the temperature of the catalyst is limited to 250 °C, which is far below the ignition temperature /3,4/.

The reaction rate is proportional to the partial pressures of the gases. Water vapour being formed by the reaction decreases the partial pressures in that way, that the conversion rate decreases. In order to avoid this problem it is necessary to condensate the water vapour. This can be achieved by cooled surfaces positioned inside the reaction chamber.

The recombination rate depends on the oxygen concentration as well. High oxygen concentrations are of advantage, but the ratio of H_2 to O_2 must not be greater than 2 : 1.

III. Design of the reactor and experimental results

The purge gases leaving the fuel cell system are fed to the catalytic reactor. The recombiner used in this application consists of several single tube reactors. They are interconnected to build up a multi-stage reactor. Fig. 2 shows the arrangement schematically:

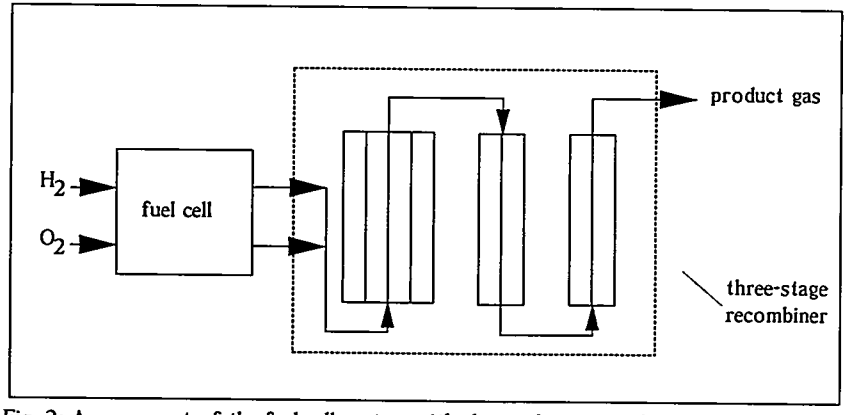

Fig. 2: Arrangement of the fuel cell system with the catalytic recombiner

The tubes are installed in a pressure vessel and various safety appliances are installed. By these measures no damage occurs in case of ignition.

The reactor was tested in combination with the fuel cells in a land test stand. Several start and stop cycles have been executed. The hydrogen concentration at the inlet of the

recombiner varied in the range of 6 to 40 vol%. At the exit of the recombiner the hydrogen concentrations have been reduced to numbers below 0,2 vol%. The temperatures in the reactor at the catalyst surface varied between 35 and 190 °C.

The same reactor was examined after a 700 h trial. No change in catalytic activity was observed, although the recombiner has not been stored under an inert gas atmosphere.

IV. Further improvements of the recombiner

In the next phase of the project the catalytic reactor had to be improved to gain higher rates and reduced volume. The optimization of the catalyst preparation and changes of the gas distribution system were necessary. The gas mixture used in the experiments was composed of 40 vol% H_2, 25 vol% O_2 and 35 vol% inert gases. Some experiments were made with a slightly higher partial pressure of oxygen (36,9 vol% H_2, 30,8 vol% O_2 and 32,3 vol% inert gas).

The catalytic activity is a function of the specific active surface of the catalyst. The preparation of the active coating is responsible for the pore size and distribution of the active material. The next figure shows some data to demonstrate this dependence.

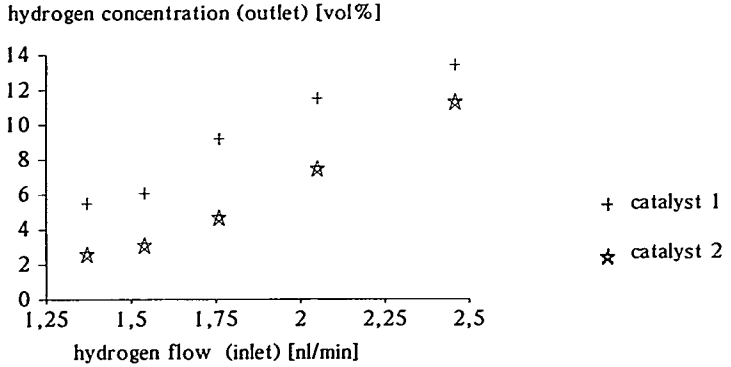

Fig. 3: Hydrogen concentration in the product gas as function of the preparation method (single tube reactor)

REM analysis indicates, that the sizes of the platinum particles of catalyst 2 are smaller than the particle sizes of the catalyst 1. So the active surface is enlarged.

Further improvements can be obtained by a careful design of the condensation areas.

The third measure to be taken for augmenting the turn over number is the increase in oxygen concentration. Fig. 4 shows the comparison of two different oxygen partial pressures for a two stage recombiner. Both stages are equipped with a special condensation zone.

A 1000 h trial has demonstrated a high and stable catalytic activity.

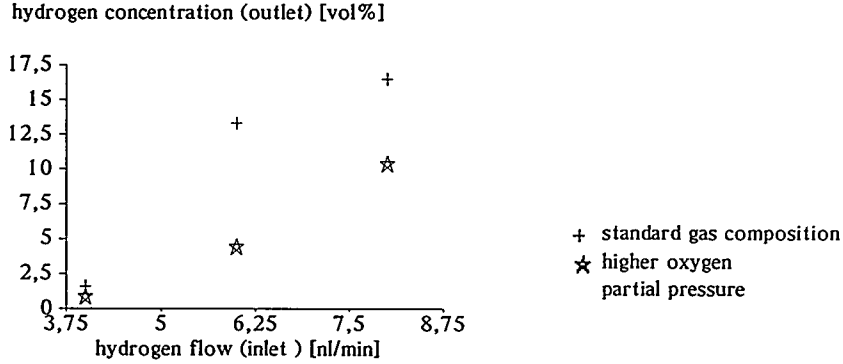

Fig. 4: Hydrogen concentration in the product gas as function of the input gas composition (two stage reactor)

V. Application of catalytic units in fuel cell systems

In our institute we study the incorporation of a hydrogen storage system in an energy self-sufficient solar house /5/. The main components are the electrolyser, the gas tanks, some units to produce heat and the fuel cell system. The fuel cells need pure feed gases, but the electrolyser produces hydrogen with a small amount of oxygen (~1 vol%) and vice versa. The catalytic technique discussed in this paper can be used to eliminate these impurities and recombiner are able to work as safety devices in the case of system failures.

References

/1/ Knaack,K; Sattler, G.: Comparison of different Hybrid Propulsion Systems. RINA Symposium, 1988, Vol II, Paper 30

/2/ Strasser, K:The Design of Alcaline Fuel Cells, The Grove Anniversary Fuel Cell Symposium, Sept. 1989, London

/3/ Ledjeff,K.: Elimination or Hydrogen or Oxygen from Explosive Mixtures by Catalytic Techniques ; Int. J. Hydrogen Energy,12, No.5 (1987),pp361-367

/4/ Ledjeff,K.: New Hydrogen Appliances; Proceedings of the8th World Hydrogen Energy Conference, Hawaii,1990

/5/ Ledjeff,K.;Heinzel,A.: Energy Storage System for Solar Houses; Proceedings of the 8th World Hydrogen Energy Conference, Hawaii,1990

PREPARATION AND CHARACTERIZATION OF GAS DIFFUSION ELECTRODES FOR ALKALINE FUEL CELLS

E. Gülzow, W. Schnurnberger
DLR-Institute for Technical Thermodynamics
Pfaffenwaldring 38-40
D-7000 Stuttgart 80
Tel 0049 711 6862-432
Fax 0049 711 6862-349

INTRODUCTION

Within the project HYSOLAR alkaline low temperature fuel cells are investigated at DLR, focussing on the preparation of PTFE-bonded gas diffusion electrodes, electrochemical characterization, surface analysis and in particular long term behaviour and degradation mechanisms.
The production of PTFE-bonded gas diffusion electrodes at DLR is based on principles developed by Prof. Winsel (VARTA Batterie AG and GH Kassel). Although the electrode production method can be extended to large scale production, fuel cells on a technical scale have not been developed so far at DLR. Thus results given here came out from half cell tests with small GDE (6 cm^2), punched out from electrode tapes about 10 cm in width.

THE CATALYST

The initial material for the production of the Raney-Nickel catalyst is i.e. a nickel-aluminum alloy containing 50% by weight of each metal /1/.
The powder is activated by adding cold KOH solution for dissolving the aluminum. Subsequently a copper salt solution is added for doping. After this procedure the solution process is continued at constant temperature of 80°C in order to remove further aluminum until a remainder of 5% is reached. Then the powder is washed and dried. During drying it is important to prevent the powder from burning in the presence of air because the catalyst contains 0.5 to 1.2 H-atoms per Ni-atom /2/. After reduced pressure controlled stepwise drying in air the catalyst is heated up to 400°C in nitrogen atmosphere and tempered for two hours at 400°C in nitrogen.

In a powder grinder the powder is mixed with PTFE using the reactive mixing process /3/. This means that the individual Raney- nickel granules are covered with PTFE and thus joined to each other. During mixing a dark brown mass is formed which is processed to electrodes using a calander.

THE ELECTRODE

The catalyst mass is thickened between two rollers turning in opposite directions and thus formed into a self-carrying strip. This catalyst strip is rolled onto a nickel-net to increase mechanical stability and for homogeneous backside current collection.

The electrode consists of single Raney-nickel granules surrounded by polytetrafluorethylen (PTFE) fibers and thus joined together. In each granule there is a PTFE-free pore system which is hydrophilic and guarantees electrolyte transport. Due to the PTFE filaments a hydrophobic pore system is linking together the individual catalyst particles through which the reaction gas can reach the inner volume the electrode.

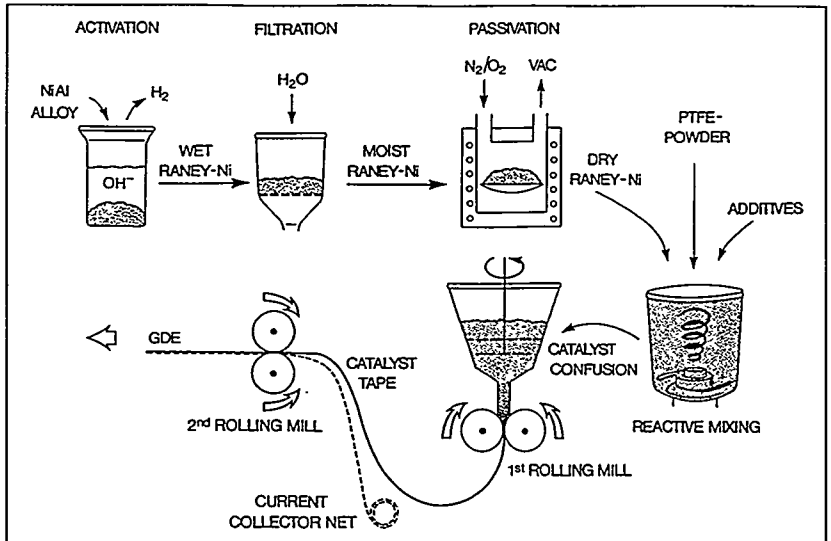

Figure 1. **Manufacturing program of PTFE-bonded gas diffusion electrodes with Raney-alloys**

The electrolyte exchange takes place at the contact points of the granules and the electrolyte bridge. For a typical pore radius of 5 nm in one granule 400 bar is expeted to be necessary in order to fill this with gas against the capillary pressure of the electrolyte.
Without hydrophobic PTFE threads the whole electrode would be flooded by electrolyte. It is to be assumed that the electrolyte is not only present in the fine pores but also parts of the outer surface of the granules are covered with an electrolyte film. It is not to be assumed that threads are stretched exactly over all catalyst pores thus preventing the flow of electrolyte from the fine catalyst pores into the gas pores. One must imagine that electrolyte film exists on the surface of each granule supplied by the hydrophilic pores inside the catalyst. Break through of the electrolyte into the gas compartment is limited by the PTFE threads.

In the contact area of the compressed granules the small gaps between the PTFE-fibers are bridged by the liquid thus forming a compending electrolyte-filled pore system. An overpressure of the electrolyte enhances this electrolyte bridge forming process.

ELECTROCHEMICAL CHARACTERISTICS

To investigate the degradation of anodes and cathodes a computer-controlled characteristic half cell test system has been installed, which allows to take galvanostatic I-V characteristics including IR-drop correction of each test and every point of the characteristic. With this equipment characteristics in depending on

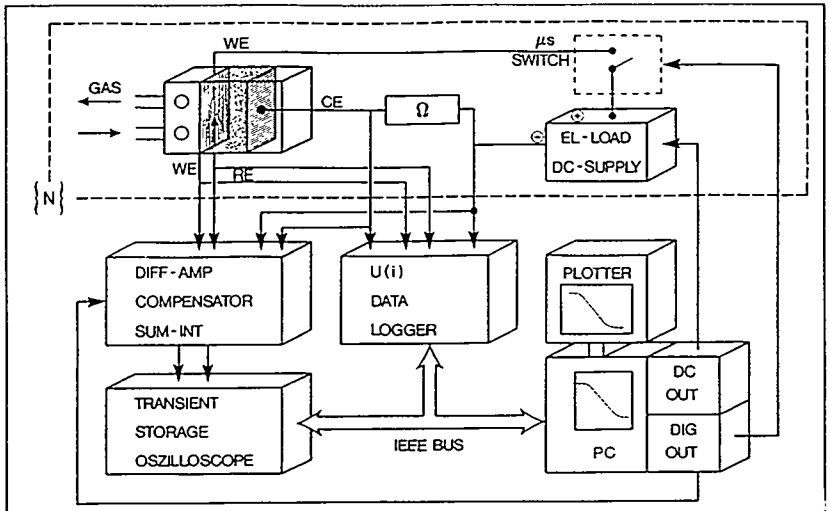

Figure 2. Fuel cell test setup for PC-assisted U(i) characterization of up to 9 cells including IR-compensation

testing time of the electrodes have been recorded. In our study measurements up to 1600 hours have been processed. It has been observed that hydrogen electrodes show an increase of overvoltage during the first 100 hours of operation, subsequently being constant for over 1000 hours. After 1000 hours the electrodes (being unstressed for several hours) again showed a small overvoltage.

X-RAY PHOTOELECTRON SPECTROSCOPY (XPS)

XPS measurements previous revealed the problem of decomposing PTFE at the electrodes due to highenergetic radiation and sputtering. Therefore decomposition of electrode surface layers has been investigated using supplemental SIMS. The results showed a unexpected thick layer of PTFE on the surface. According to this the free active surface is considerably smaller than we supposed to be for electrodes based on Raney metals. Aged electrodes (1600 hours constantly stressed up to 250 mA/cm²) exhibit a significant oxide growth. On the other hand this effect could not be observed with oxygen electrodes made of silver compounds. Common was only the decomposition or the shift of the PTFE-cover. However, the decomposition and chemical shift effects of PTFE coverage can be observed both for anodes and cathodes. With aging time the thickness of PTFE layers on the surfaces decreases significantly.

ENERGY DISPERSIVE X-RAY ANALYSIS (EDX)

EDX investigations prove that except for silicon no foreign substances out of the periphery cover the electrodes. The concentration of aluminum decreased on the electrodes made of Raney materials and a strong potassium peak occured, result-

ing from electrolyte which has not been completely washed out thus forming dry salt residues in the micropores.

BET-GASADSORPTION / MERCURY-POROSITY / PORE-DISTRIBUTION

The active surface and the pore distribution are determined with two different methods: N2-gasadsorption (BET) and mercury penetration. With these equipments we investigated the pore distribution relevant for fuel cell reaction and for transport mechanism. It has to be pointed out that the pore systems for gas transport and electrochemical reaction differ significantly in size. In the presence of PTFE exact pore size distribution is difficult to be determined. Therefore catalyst materials have been characterized before reactive mixing and rolling. After preparation of the Raney Catalyst, significant reduction of effective surface area has been observed. First experiments indicate, that the degradation process can be influenced by variation of the leaching and drying procedure.

SCANNING ELECTRON MICROSCOPY (SEM)

SEM pictures significantly show the coverage of the surface with PTFE. The organic binder is spun to threads during the "reactive mixing" process, partly spherical shaped PTFE can be seen. On the rolled particles large areas are thickly covered with PTFE.

SUMMARY

The PTFE-covered electrochemically active surface is smaller than assumed.

Degradation measurements revealed macroscopic variations on the electrodes.

EDX spectra indicate no significant differences in chemical composition of stressed and unstressed electrodes.

XPS investigations demonstrate a strong oxide layer on the surface of hydrogen electrodes, furthermore a decomposition of polytetrafluorethylen.

PTFE bonded Gas Diffusion Electrodes have been operated for more than 1600 hours at $\geq$ 100 mA/cm² (including short time stress up to 200 mA/cm²) without reduction of lifetime.

LITERATURE

[1] M. Jung, Kröger, "Verfahren zur Herstellung aktivierter Katalysatoren aus Raney-Nickel-Legierungen", DBP 1156769

[2] E. Justi, A. Winsel, "Kalte Verbrennung-Fuel Cells", Steiner Verlag, Wiesbaden, 1962

[3] H. Sauer, "Verfahren und Vorrichtung zur Herstellung einer kunststoffgebundenen Aktivkohleschicht für dünne Gasdiffusionselektroden", DBP 2941774 C 2, 1985

THE FUEL CELL BUS PROGRAM AND ITS APPLICATION TO TRANSIT MISSIONS

Samuel Romano
Georgetown University
Washington, DC

INTRODUCTION

The fuel cell powered bus offers all the environmental and energy advantages of a battery powered vehicle without the severe restrictions in distance traveled (range). The limitation in range, inherent in a battery powered vehicle, is not a problem for the fuel cell bus because the fuel cell uses liquid methanol which permits the same rapid refueling for extended range as an ordinary internal combustion engine (ICE) powered vehicle. This attractive advantage has prompted the U.S. Departments of Energy and Transportation program to sponsor a program to develop a fuel cell/battery power system for transit bus applications.

The power system for the fuel cell bus is a hybrid arrangement which is required to meet the severe cyclic power demands of the transit bus's stop and go operation. The inertia of the PAFC system, due primarily to fuel processing in the reformer, does not allow rapid changes in the output power level. In addition, the power density available with current PAFC technology cannot provide the peak power required by the propulsion system for hill climbing and rapid acceleration without excessive weight and size penalties. In this hybrid system the battery is used to provide the peak power required and the fuel cell provides the average power. Two PAFC systems have been evaluated for transportation use. An air cooled system and a liquid cooled system.

PHOSPHORIC ACID FUEL CELL CHARACTERISTICS

The schematic flow diagram for a liquid cooled phosphoric acid fuel cell system (L-PAFC) similar to that used in Phase I is shown in Figure 1[1]. This system utilizes the fuel cell stack waste heat via the circulating liquid coolant to vaporize the incoming fuel mixture of methanol and water. The reformer converts the vaporized fuel to H_2, CO_2 and H_2O and a small amount of CO. This gas mixture is fed to the fuel cell where 80 to 90% of the H_2 is oxidized electrochemically producing electron flow. The unused gas (spent fuel or tail gas), which is primarily hydrogen, is used to sustain the action in the reformer. The amount of tail gas made available for use in the reformer burner is a function of the amount of heat that is required to produce the flow of hydrogen required for the desired power output of the fuel cell. The use of the waste heat from the fuel cell stack as a preheater to vaporize the fuel used in the reformer, will reduce the amount of tail gas needed for the reformer burner and increase the fuel utilization in the fuel cell stack and hence the efficiency. In a thermodynamic analysis, Kumar (et al, ref 1) shows that the efficiency of the liquid cooled system peaks at 41.7% (HHV)

at a fuel utilization rate of approximately 90%. (The fuel utilization rate is the ratio of the reformed fuel utilized in the fuel cell stack and the amount produced in the reformer).

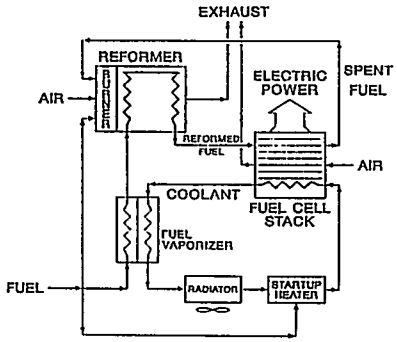

Figure 1

Liquid Cooled Phosphoric Acid Fuel Cell Subsystem

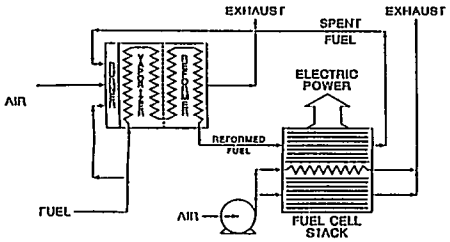

Figure 2

Air Cooled Phosphoric Acid Fuel Cell Subsystem

Figure 2 is the flow diagram for the air cooled phosphoric fuel cell system (A-PAFC). In this system the fuel mixture is vaporized in the reformer using the spent fuel from the fuel cell stack, rather than waste heat from the fuel cell. This means that more heat must be generated in the reformer burner of the air cooled system. Therefore the fuel utilization rate in the fuel cell stack will be lower than that of the L-PAFC since some of the fuel sent to the fuel cell stack must be reserved for use in the reformer burner. Kumar shows that for the A-PAFC system the efficiency is 31.2% at a fuel utilization rate of approximately 72%.

Figure 3 is a comparison of the net efficiency vs. the electrochemical fuel utilization in the L-PAFC and the A-PAFC based on a thermodynamic analysis by Kumar. This efficiency is defined as the net electrical power output divided by the higher heating value of the methanol used to generate that power. The improved heat transfer characteristic of liquid cooling also allows the fuel cell plates to be designed for higher current densities resulting in a smaller fuel cell stack for a given power output. The current density of the A-PAFC brassboard test system used in Phase I was on the order of 175 ma/cm^2 at 0.6 volts/cell. The current density of the L-PAFC brassboard test system was 240 ma/cm^2 at 0.62 volts/cell.

POWER SYSTEM LABORATORY TEST PROGRAM

The proof of feasibility of the technology was confirmed by analysis and testing of brassboard power systems in the laboratory. The two systems configurations shown in Figure 4 consisted of the complete fuel cell system, the battery and

interface controller and the variable load. These systems were designed to operate at one half the power of a full size test bus system to afford some savings in program costs. Both the L-PAFC and the A-PAFC brassboard test systems performed well during the Phase I program. And while a comparative analysis of the two systems is difficult due to the different test conditions at the contractor facilities and the different assumptions made for the auxiliary equipment power requirements, the test data supports the general trend of higher efficiency for the L-PAFC system.

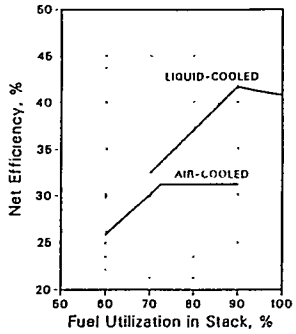

Figure 3

Variation of System Efficiency with Electrochemical Fuel Utilization for Two Phosphoric Acid Fuel Cell Systems

	L-PAFC	A-PAFC
● Fuel Cell		
- FC Power Rating (nom)	25 KW	30 KW
- FC Output Voltage	53 V	150 V
- Plate Current Density	240 ma/cm^2	175 ma/cm^2
- Plate Voltage	0.62 V	0.60 V
- Fuel Utilization Factor	75%	70%
● Battery Type	Pb-SO_4	NiCd
● Interface Control	Step-up Chopper	Current Limiter

Figure 4

Brassboard Test Configurations

The two brassboards test systems were operated below the optimal fuel utilization point. This produced a lower efficiency than would be possible if the systems were optimized. The L-PAFC was operated at a fuel utilization rate of about 75%. Figure 3 indicates that better performance is possible as we approach 90%. The A-PAFC brassboard operated near 70%, which is close to the point where the utilization factor and efficiency is maximum.

Two other differences were significant in the design of the two brassboards. First, the air cooled fuel cell system was mated to a nickel cadmium battery to form the hybrid system and the liquid cooled system was used with a lead acid battery to meet the total mission power requirements. The second difference was the method used to control the power sharing between the fuel cell and battery. The L-PAFC contractor used a step-up chopper at the output of the fuel cell to properly match the power sharing of the two power sources. This assured that the fuel cell voltage was always higher than that of the battery as it needed to be for charging and to protect the fuel cell. The A-PAFC contractor used a current limiter to keep the fuel cell voltage high enough to serve the same purpose. This technique must be evaluated over time to be assured that aging of the various components will not change the fuel cell battery voltage relationship.

The results of the breadboard tests show that both power systems worked well and are capable of higher operating efficiencies than the internal combustion engine operating on diesel fuel or methanol and offer significantly reduced emissions[2&3].

Having demonstrated the feasibility of the combined fuel cell/battery as a power source for transportation, there remains the demonstration or proof of concept of the technology. This will be accomplished in two steps . First by developing a full size system and installing it in a bus and then testing the bus system in a controlled operational environment. These steps are planned for the near future.

COMMERCIALIZATION PROCESS

The object of the program is to demonstrate the applicability of the fuel cell/battery powered bus to the transit mission. The feasibility of the concept has been demonstrated by the successful operation and test of the brassboards. The next phases will provide proof that the concept is workable and finally the system will be demonstrated in a small fleet of prototype in revenue service. The results of this demonstration will provide the data and experience the industry needs to make decisions on commercialization of the fuel cell powered bus.

Thus far the system has been configured to satisfy several transit routes for the small bus. A computer simulation program[4], has been developed to size the modular power system for any transit route and a variety of transit bus types.

The computer simulation program considers two sources of power for the bus and controls the output of each according to the control strategies established. The specific transit route structure for which the system is being sized is entered where stops and dwell times, grades, maximum allowable speed on each segment and passenger loads are set. The characteristics of each element are set and the program traverses the route and

records bus performance in terms of speed, time and distance travelled, power delivered by the fuel cell and battery, battery state of charge, and voltage, current and temperature of major components. The characteristics of these elements of the system are analyzed to assure they are in safe limits for each run and the combination of fuel cell size and battery size are varied to meet performance criteria. At the end of the run, which may be a series of traverses of the route, a summary is recorded. The summary includes: total distance traveled, total dwell time used, rate of energy consumption, total regenerative energy recovered, rate of methanol consumption and battery state of charge. The format and the input and output data for the computer simulation is shown in Figure 5.

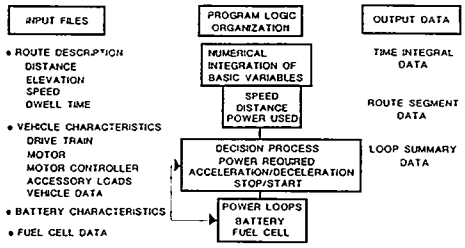

Figure 5

Computer Simulation

Using the simulation program, it is possible to configure the Fuel Cell/Battery Powered Transit Bus developed under this program to meet the operational requirements of most of the transit properties using diesel buses. This will allow transit operators to evaluate the fuel cell bus system for their specific needs and compare it to the diesel buses. The expected improvement in life cycle costs and the ability to meet all existing and future environmental requirements will be a strong factor in favor of selecting the fuel cell bus for transit use.

References

1. R. Kumar, M. Krumpelt, B. Misra "Fuel Cells for Vehicle Propulsion Applications: A Thermodynamic Systems Analysis, IECEC 1989, Washington, D.C. (August 6 - 11, 1989).

2. "Research Development and Demonstration of a Fuel Cell/Battery-Powered Bus System", Phase I Final Report, Booz-Allen & Hamilton, Bethesda, MD. (February 28, 1990).

3. "Research and Development of a Fuel Cell/Battery Powered Bus System", Phase I Final Report, Energy Research Corporation, Danbury, CT (February, 1990).

4. S. Romano, "Installing a Fuel Cell in a Transit Bus: SAE Technical Publication SP-817, Electric Vehicle Technology, & SAE TP 900178, Warrendale PA, (February, 1990).

ELECTROCHEMICAL ENERGY CONVERSION FOR STORAGE OF SOLAR ENERGY

K. Ledjeff, J. Ahn, D. Zylka, A. Heinzel
Fraunhofer-Institute for Solar Energy Systems,
Oltmannsstr. 22, 7800 Freiburg, Federal Republic of Germany

1. Introduction

The great environmental problems of our time are due to the consumption of fossil fuels. For the future, it is necessary to focus the research on energy saving techniques and the use of solar energy. Because of the fluctuation of solar irradiation an energy storage system is required for solar devices. For short term storage, batteries like the lead acid accumulator are suitable. But for long term storage, the generation of hydrogen as energy carrier by electrolysis is the better choice. The use of solar energy is at time restricted to stand alone houses or other consumers, where a connection to the grid is too expensive. These solar systems need small and compact storage devices with a long service life and a high efficiency. In the low power range, such systems are not commercially available. The solution of the technical problems and the system optimization for solar application are a challenge and require engineering work as well as basic research.

2. Concept of the hybride storage system

The energy storage system for a solar house which meets the need for electric energy and high temperature heat for cooking purposes for a 4 persons household consists of a lead acid battery and a small hydrogen system /1/. The first approach is the build-up with commercial components:

lead acid battery:	10 kWh, 85 % efficiency
alkaline pressure electrolyser:	800 W, 85 % efficiency
alkaline fuel cell:	600 W, 50 % efficiency
hydrogen storage:	4 m^3, 30 bar

Besides these components, a cooking stove using the technology of catalytic combustion of hydrogen has been developed.

2.1. Test of the storage system

The electrochemical characterization of the pressure electrolyser and the fuel cell nearly verified the data given by the supplier. But some problems are connected with these devices, especially for the household application:

- the creeping behaviour of alkaline electrolytes
- the alkaline dust in the electrolysis gases
- the sensitivity of the fuel cell towards standstill
- the necessity of purge processes in the fuel gas loops

Another very important feature is a low energy demand of the gas- and electrolyte management system, so technical improvement of the peripheral systems is required.

2.2. Development of polymer electrolyte devices

The substitution of the alkaline devices by membrane electrolyser and fuel cell is a promising goal /2/. The work concerning membrane technology includes membrane pretreatment, coating with electrocatalyst, cell construction and electrochemical characterization of the produced membrane/electrode composites. Presently, the Nafion^{R}117 membrane (DuPont De Nemours) serves as polymer electrolyte. Though membrane electrolysers are commercially available now, a special pressure electrolyser for solar application has been designed. First results with platinum as electrocatalyst and a pressure of 30 bar are obtained and will be improved according to the data received in lab scale cells by varying the oxygen electrode catalyst (Ru, Ir).

The development of membrane fuel cells is a matter of intensive research for example in the United States and in Canada /3,4/, they are still not available for commercial use at all. Therefore, membrane/electrode composites have been prepared for fuel cell application and have been electrochemically characterized by half cell measurements. The cell design, the improvement of the structure of the porous current collectors, gas temperature and humidity control are the main themes of the current work in order to realize a fuel cell system.

2.3. The reversible system

The development of a fuel cell which works as electrolyser as well is of special interest for the small hydrogen devices for solar application. Two possibilities for its realization have been examined:

- bifunctional hydrogen and oxygen electrodes
- bifunctional oxidation and reduction electrodes

The behaviour of Nafion^R/platinum composites towards the change of reaction from electrolysis to fuel cell operation is depicted in fig. 1 a-d.

The development of special designed catalysts for the four types of electrodes will show which system reaches a better storage efficiency. For platinum, the values at 100 mA/cm^2 are:

electrolysis:	U = 1,82 V
fuel cell operation:	U = 0,92 V

The voltage efficiency of the storage system is calculated to be 50,5% with these data. A decrease in oxygen evolution overpotential is possible with mixtures of noble metals or their oxides as catalyst. However, these catalysts are not suitable for oxygen reduction. The bifunctional oxidation

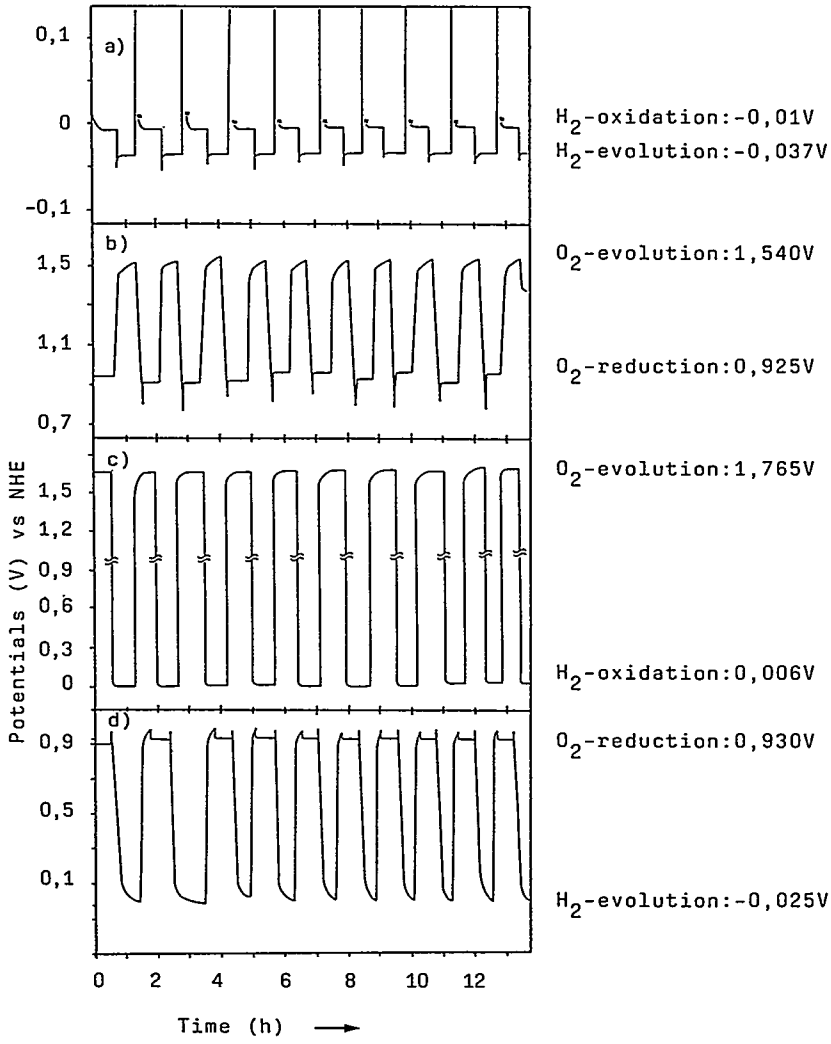

Fig. 1: Electrochemical characterization of bifunctional electrodes at platinum/Nafion^{R}117, a temperature 80°C, 2 bar gas pressure at a current density of 100 mA/cm^2. The reactions are:
a) H_2-oxidation and H_2-evolution
b) O_2-reduction and O_2-evolution
c) H_2-oxidation and O_2-evolution
d) O_2-reduction and H_2-evolution

electrode is supposed to be the solution of the problem. An overall storage efficiency of 60 % is realizable with optimized electrodes.

2.4. The methanol electrode

Though methanol as a fuel penetrates the membrane in a remarkable extent, it is attractive as energy reserve for solar systems. For the methanol electrode, modified platinum electrodes are required. The improvement achieved by additional deposition of Sn and Ru is shown in fig. 2.

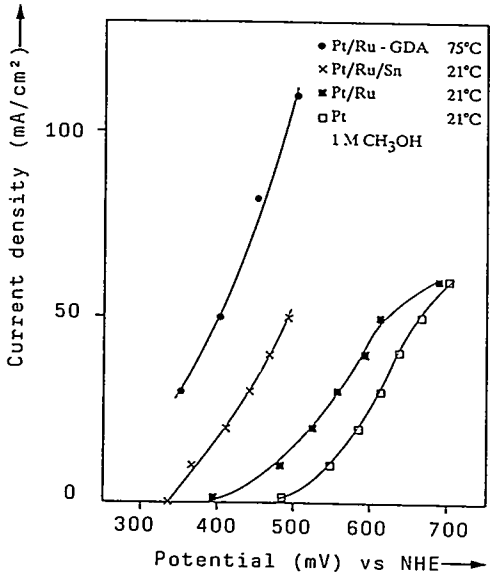

Fig. 2: Current/voltage characteristics of methanol oxidation at different electrocatalysts

3. Conclusion

A widespread use of solar generated electric energy will depend on the success of developing an economic storage system. Therefore, the main themes for the future work are:

- cell design for prototypes of technical cells
- process engineering for the use of the devices in solar applications

- selection of optimal catalysts for the differnt electrode reactions and bifunctional electrodes
- improvement of coating procedure by hot pressing, chemical, galvanic and plasma techniques

In 1992, a hybride storage system will be integrated into a solar house in Freiburg.

References:

/1/ K.Ledjeff, J.Ahn, D.Zylka, A.Heinzel
Ber.Bunsenges.Phys.Chem. 94(9) (1990), in press.

/2/ K.Ledjeff, A.Heinzel
Proc. 8th Worl Hydrogen Energy Conf. 1990, Hawaii

/3/ N.E.Vanderborg, J.Hedstrom, J.R.Huff
Proc.Europ.Space Power Conf., p.211, 1989, Madrid

/4/ K. Prater
J. Power Sources 29 (1990), 239

EFFECT OF DIFFERENT COOLANT AIR FLOW DIRECTIONS ON PHOSPHORIC ACID FUEL CELL PERFORMANCE

M. T. Le
Westinghouse Electric Corporation
Advanced Energy Systems Department
P. O. Box 10864
Pittsburgh, PA 15236
(412) 382-5138

I. ABSTRACT

A number of advantages have been identified in cooling a phosphoric acid fuel cell stack with air. One of the characteristics of the air-cooled system is that its cell performance is a function of temperature distribution. Since it is known that the cell temperature profile varies with changes in coolant flow rate and direction, this paper examines the effect of two different flow arrangements on the performance of full size fuel cells in a ten-cell phosphoric acid fuel cell stack. Performance was assessed at various operating conditions. The flow configurations studied were: 1) Co-current with process gas flow (coolant air entering at anode and cathode process gas inlet side) and 2) Countercurrent (coolant air entering at anode and cathode outlet side). The cell performance was found to be lower for the countercurrent flow but the relationships of the cell voltage and operating parameters remained unchanged. This finding was based on the results of the designed mapping tests which were conducted at rated pressure with air and Synthetic Reformer Gas (SRG) process gases. Controlled variables introduced were current, temperature, reactant (anode fuel and air) utilizations and coolant air inlet to outlet temperature difference in both coolant flow directions. The effects of variance of these operating parameters and their interactions on cell performance were empirically correlated and found to be consistent with predicted ten-cell stack performance. Empirical equations were developed for both flow arrangements to predict cell voltages as a function of the measurable parameters.

II. INTRODUCTION

Westinghouse has been involved in developing phosphoric acid fuel cell (PAFC) as an alternate source of energy for over a decade. The Westinghouse fuel cell uses air to remove heat generated during operation. The advantages of air cooling are its simplicity, reliability, and relatively low cost. In air-cooled system, the coolant flow and direction control cell temperature distribution, and affect cell voltage response. A full size ten-cell stack with baseline technology electrodes was used to examine the effect of different flow arrangements on the cell performance at various operating conditions. The two different

cooling flow configurations studied were: 1) Co-current and 2) countercurrent process gas flow with coolant air entering at process gas inlet and outlet side, respectively.

The relationships of operating variables and cell performance were also examined in both flow arrangements. A partial factoral mapping test was designed with five (5) operating variables. The thirty (30) test conditions were defined and conducted in both coolant flow directions. Theoretical and empirical data were developed for these cases and the resulting stack performance was compared to the values obtained from the previously tested baseline technology stacks (Ref. 1-3).

III. EXPERIMENTS AND METHOD OF ANALYZING DATA

Cell performance at rated conditions (310A, 374^{o}F, 70 psia) was compared when the stack was switched from one flow configuration to the other. During the test, there were a total of four (4) changes in the flow direction. Performance losses or gains were then recorded.

The mapping tests were performed to obtain the effect of major operating variables on the cell performance in both co-current and countercurrent flow direction. The corresponding results of measured cell voltages are listed in Tables 1 and 2. The tests were conducted at rated pressure, with air and Synthetic Reformer Gas (SRG mixture of 75% H_2, 24% CO_2, and 1% CO by mole) as cathode and anode gas, respectively. The controlled variables introduced were temperature (X_1), current (X_2), coolant inlet to outlet temperture different (coolant ΔT, X_3), air utilization (X_4), and hydrogen utilization (X_5).

Multiple regression analyses were performed to establish the cell performance characteristics in both flow arrangements. These results were then compared to the theoretical values which were calculated based on the Nerst equation, and also to the existing baseline data (Ref. 1, 2).

IV. DISCUSSION AND SUMMARY OF THE RESULTS

Of the two flow arrangements, the co-current flow gave better cell performance, and an average improvement of 4 mV was observed at rated conditions. However, the temperature distributions in the cell remained unchanged in the direction of the coolant flow for both flow arrangements. For the countercurrent flow, the hot spots in the cell were at the process gas inlet corners, while in the other flow mode, they were at the outlet corners. The former case could have an advantage of reduction in evaporation loss of electrolyte due to low temperatures of the process exit gas streams.

TABLE 1

RESULTS OF REGRESSION ANALYSIS - DEPENDENT VARIABLE, CELL VOLTAGE RESPONSE

Fitted Coefficients		Standard Err. of Fitted Coef.	t - Value
Fitted V = A	Constant Term	10.5	48.2
+B	X_1, Temp (^oF)	0.03	33.8
-C	X_2, Current (A)	0.01	-43.6
+D	X_3, Coolant ΔT (^oF)	0.04	2.5
-E	X_4, 0_2 Ut. (%)	0.04	-17.4
-F	X_5, H_2 Ut. (%)	0.03	-7.6

TABLE 2

Comparison of Measured and Predicted Parameter Effects

Parameters	Fitted			Predicted
	Co-current	Counter-current	Baseline Stack	
1) Temp. Effect ($mV/^oF$)	+1.58	+1.53	+1.1	1.48
2) Current Effect (mV/A)	-0.41	-0.40	-0.41	-0.37
3) Coolant ΔT Effect ($mV/^oC$)	+0.18	N/A	+0.09	N/A
4) Air Ut., (mV/%)	-0.52	-0.47	-0.37	-0.21
5) SRG Ut., (mV/%)	-0.18	-0.15	-0.05	-0.07

Unfortunately, this stack testing was not long enough to access acid retention rate of each flow mode.

Regression analysis of the mapping test results for both flow directions showed that the relationships of cell performance and operating variables were not affected by the coolant flow directions. All analyses were in agreement due to insignificant interaction effects, and there were no evidence other than the predicted effects of the controlled variables. This permits us to present the following empirical equation which could be used to predict cell performance in either flow configuration:

$$V = A + BX_1 - CX_2 + DX_3 - EX_4 - FX_5 \qquad (1)$$

where

A through F are derived constants

V = cell voltage in mV

X_1 = stack temp. in ^{o}F

X_2 = stack current in amps

X_3 = coolant ΔT in ^{o}F

X_4 = air utilization in %

X_5 = H_2 utilization in %

Comparison of cell voltage predictions determined from the above model with theoretical and previous test data showed excellent agreement as shown in Table 2. Based on these results, the decision was to remain with the co-current flow arrangement in the Westinghouse fuel cell stack design because of its performance advantage over that of the other flow mode.

ACKNOWLEDGMENT

This work was performed under Contract DE-AC21-82MC24223 that was funded by the U.S. Department of Energy, Office of Fossil Energy, Morgantown Energy Technology Center.

REFERENCES

1. M. Le, et al., "Effects of Operating Parameters on PAFC Stack Performance, presented at the 1988 IECEC Conference, July 31 - August 5, 1988 Denver, Colorado.

2. M. Le, et al., "Operating Characteristics of Fuel Cells in Multi-cell Stacks," presented at 1988 International Fuel Cell Conference, October 23-26, 1988, Long Beach, California.

CARBON DIOXIDE TOLERANT HYDROGEN AND METHANOL FUEL CELL WITH AN AQUEOUS CARBONATE ELECTROLYTE

Peter Kalal and Jiri K. Nor
ASTRIS INC.
2480 Dunwin Drive, Mississauga,
Ontario, Canada L5L 1J9

ABSTRACT

Astris Inc. conducts applied research and experimental development of alternative electrolytes and electrocatalyst systems leading to improved fuel cells with increased or full tolerance of carbon oxides, making them suitable to utilize

- hydrogen rich reformate gas as fuel (product of steam reforming of e.g. methanol)
- methanol as fuel directly
- CO_2-unscrubbed air as an oxidant.

The objective of the present work is to reach these goals using very little precious metals as catalyst or none at all. This can be achieved with fuel cells with alkali carbonate electrolyte.

INTRODUCTION

Astris has been active in the field of fuel cells since 1983. The alkaline technology was chosen because of its inherent ability to operate at ambient temperature and start instantly. Alkaline fuel cells also offer the highest electrochemical efficiency among the known fuel cell types.

Their main advantage, however, is their capability to work with a broad range of non-noble electrocatalysts, unlike their acidic and solid polymer counterparts, which depend solely on the platinum group metals as catalysts which, in turn, are sensitive to poisoning by carbon monoxide in the feed gases.

Against these significant advantages of alkaline fuel cells there is one drawback: they are sensitive to carbon dioxide in the air and fuel streams. Carbon dioxide has to be removed or kept at low level to prevent carbonation of the hydroxide electrolyte, which would result in reduced performance and life. Moreover, use of alkaline hydroxide electrolyte is impractical in the direct methanol fuel cell.

A possible solution of this dilemma - the desire to use alkaline electrolyte and CO_2 containing (or yielding, as with DMFC) gases is the use of aqueous alkali carbonate electrolyte.

THE AQUEOUS CARBONATE FUEL CELL

It was shown by Cairns and Macdonald (1) and by Cairns and Bartosik (2) as early as 1964, that highly concentrated solutions of cesium or rubidium carbonate support complete electrochemical oxidation of hydrocarbon fuels. These electrolytes are not affected by the reaction product CO_2 as the bicarbonates are unstable above about 120 C thus rejecting the CO_2 and maintaining the electrolyte invariance. The high solubility allows operation up to 200 C.

More recent work of Cairns et al.(3) and Striebel et al.(4) show that oxygen reduction rates in carbonate electrolytes are at least comparable to rates measured in KOH. Moreover, lower peroxide-ion production rates were observed in the lower-pH carbonates. However, significant polarization of the oxygen reduction in carbonate electrolytes was observed, due to an increase in the local pH of the electrolyte in the electrode pores.

According to recent work of Giner and Kosek (5, 6), this polarization can be overcome by addition of CO_2 to the oxidant stream resulting in decrease of the OH^- concentration, and current transport via CO_3^{2-} ions analogous to the molten carbonate fuel cell mechanism.

EXPERIMENTAL

During the experimental work both free flowing (circulating) and matrix test cells were employed. As the cells work at ambient pressure, maintenance of the proper electrolyte concentration is much more important than when operating at higher pressure, because of the delicate relationship between concentration and boiling point. The reaction gases were humidified at the appropriate temperatures, and flow checked by flowmeters. The methanol or methanol-water fuel mixture was fed at constant flow rate by a syringe pump through an evaporator. The cell can be heated up to 250 C with accuracy of +- 3 C.

The electrodes were typical PTFE bonded gas diffusion electrodes using nickel mesh as a current collector and a fluoropolymer membrane backing on the gas side prepared by Astris Inc. All were parallel tested in KOH with H_2/air and exceeded 3000 hours at 100 mA/cm^2.

Although it is intended to replace the precious metals in full, for the time being the anode still employs Pt as catalyst. The air cathode uses proprietary non noble catalyst deposited on Vulcan XC72.

RESULTS

The polarisation curves (Figure 1) show the performance of the aqueous carbonate fuel cell when a mixture of 50 % CH_3OH and 50 % H_2O vapour is used as the fuel gas and air or air-CO_2 mixture (80 : 20) as an oxidant gas. For comparison the polarisation curve of the H_2/air-CO_2 pair is shown. Both terminal and IR free (Kordesch-Marko interruptor method) voltages are shown.

Our results confirm the finding of Giner and Kosek (5, 6) that addition of CO_2 to the cathode gas stream results in an increase of the cell voltage. The measurements indicate that the addition affects mainly the magnitude of resistive losses, which agrees with the proposed current transport mechanism. Monitoring of the electrode potentials against the reference electrode shows that the effect is slightly more pronounced on the cathode.

CONCLUSION

The aqueous carbonate electrolyte supports oxidation of methanol and remains invariant due to CO_2 rejection. It was shown, that at least the cathode operates in this medium with non-noble catalyst. It is hoped that the present noble catalyst for anodic oxidation could also be replaced.

It was confirmed that CO_2 addition to the cathode results in better cell performance.

The optimal operating conditions are studied and it is possible that higher than atmospheric pressure will be used in the future, which will allow lower electrolyte concentration and thus also lower resistive losses. Higher operating pressure would also be beneficial to the electrode performance.

ACKNOWLEDGEMENTS

This work is in part supported by a grant from Canadian Department of Energy, Mines and Resources, under Contract No. 23216-8-9089/01-SQ, N.R. Beck, Research Advisor. Their contribution is gratefully acknowledged.

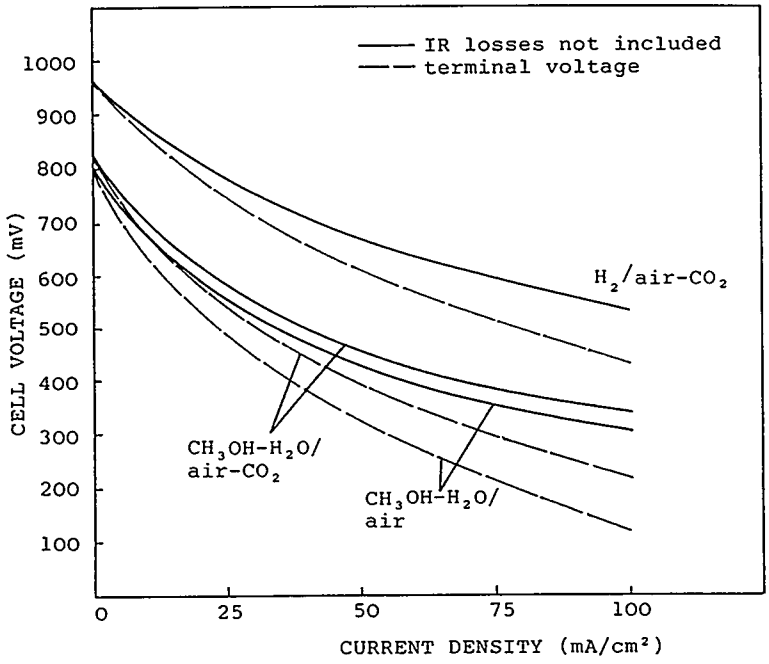

FIGURE 1: POLARISATION CURVES OF AN AQUEOUS CARBONATE FUEL CELL (CELL WITH CIRCULATING ELECTROLYTE)
T=145 C, electrolyte: Cs_2CO_3, 87.5 W/o solution

REFERENCES

1) Cairns, E.J. and Macdonald, D.I., Electrochem. Tech., 2, 65, (1964)
2) Cairns, E.J. and Bartosik, D.C., J. Electrochem. Soc., 111, 1205 (1964)
3) Striebel, K.A., McLarnon, F.R., Cairns, E.J., Lawrence Berkeley Laboratory Report No. LBL-24340 (1987)
4) Cairns, E.J., Striebel, K.A., McLarnon, F.R., in Extended Abstracts, Ninth Battery and Electrochemical Contractors' Conference, November 12-16, 1989, Alexandria, VA
5) Giner, J. and Kosek, J.A., Fuel Cell Seminar, Oct. 23-26, 1988, Long Beach, CA
6) Giner, J. and Kosek, I.A., in Proceedings of the Symposium on Fuel Cells, Nov. 6-7, 1989, San Francisco, CA

CORROSION SCREENING OF CANDIDATES FOR THE ALKALINE FUEL CELL CATHODE

Richard S. Baldwin, Joseph Singer and William L. Fielder
NASA Lewis Research Center
Cleveland, OH 44135

INTRODUCTION

The identification and development of new electrocatalysts and supports for the alkaline H_2-O_2 fuel cell oxygen cathode is anticipated to have significant impact upon the viability of utilizing these power sources for future space missions. In addition to exhibiting high electrocatalytic activity for oxygen reduction, viable electrocatalyst candidate materials must exhibit high resistance to chemical corrosion and must be electrochemically stable under O_2-reducing conditions.

Recently, several viable catalyst candidates for oxygen reduction have been identified and investigated to various levels. These candidate materials include noble metals of relatively high surface area and various mixed metal oxides representing perovskites, pyrochlores, spinels, and bronzes. Development programs for various candidates have been directed towards addressing such factors as increasing the surface area, optimizing the morphology and/or the composition, and investigating the effects of low-level dopants on performance.

Prior to extensive electrochemical performance testing of the catalyst materials in an oxygen cathode configuration, the candidates were subjected to a series of corrosion screening tests. These tests were designed to afford an initial assessment of the electrochemical stability of the candidates when subjected to potentials representative of oxygen reduction conditions in an alkaline fuel cell environment.

CORROSION SCREENING METHODS

Corrosion test electrodes were specially made to be more wettable than typical oxygen reduction performance electrodes. To fabricate a typical corrosion test electrode, the candidate powder was blended with PTFE at 10-15% by weight of catalyst and then applied to either a pure gold mesh or a gold-plated nickel mesh current collector. The electrode was then thermally processed at 275-300°C to try to achieve a suitable compromise between physical integrity and good electrolyte penetration.

Electrochemical corrosion testing was implemented in a floating electrode half-cell with the electrode suspended vertically in a 30-31% KOH solution at ambient temperature. Presaturated nitrogen gas was continuously passed into the cell to blanket the electrolyte and minimize oxygen contamination. Electrochemical measurements were performed with a PAR 173 potentiostat interfaced with an Apple computer, and a Hg/HgO reference electrode was employed in the alkaline media.

The electrochemical stability of the catalyst material was assessed from the results of several types of electrochemical measurements performed on the flooded electrode. To afford a measure of the resistance of the catalyst to electrochemical reduction at a fixed potential, the steady-state cathodic current was measured at constant potential within the practical limits of an operating fuel cell (e.g., 0.6 to 1.0 V versus RHE). The dependency of this corrosion current with time was also monitored. The gold current collector was found to exhibit a very low base level of steady-state cathodic current (<1.0 uA/cm^2).

Cyclic voltammetric sweeps were periodically performed over the voltage range of interest in order to monitor such stability-affecting factors as electrochemical oxidation or reduction processes, loss of electrochemical surface area, and catalyst poisoning. This monitoring was done prior to and after holding the electrode at fixed potentials (e.g., 0.6 and 1.0 V versus RHE) for at least 18 hours, and also after stressing the electrode by repeated cycling between voltage limits of interest at a relatively slow sweep rate (1 mV/sec).

CORROSION SCREENING RESULTS

IFC Orbiter O_2 electrode: The International Fuel Cells (IFC) Au-10%Pt Orbiter O_2 electrode represents the state-of-the-art cathode for oxygen reduction in the H_2-O_2 fuel cell with a lifetime of >4000 hours. Thus, comparisons of test electrode stabilities with those obtained for the IFC electrode are useful for a preliminary screening of the catalyst candidates. The IFC electrode was potentiostatically held at 0.6 V for about 24 hours. As illustrated in Figure 1, the cathodic current decreased rapidly during the first hour and then at a slower rate to a steady-state value of $<10^{-6}$ A/cm^2.

Alkaline-earth ruthenates: Perovskite ruthenates have exhibited electrocatalytic activity for oxygen reduction, and the alkaline-earth ruthenates of barium, calcium, and strontium, which had surface areas in the 2-10 m^2/g range, were screened for electrochemical stability. Steady-state corrosion currents at 0.6 V were very low for all three candidates; however, the rate of decay to the steady-state value was significantly faster for $BaRuO_3$. As indicated by cyclic voltammetry, both $BaRuO_3$ and $CaRuO_3$ appeared to be very stable after being held at fixed potentials of 0.6 and 1.0 V and after being subjected to 50 cycles between these voltage limits. No significant faradaic processes or loss of surface area were observed. $SrRuO_3$ appeared to be the least stable of the three candidates. Tentative results also indicated that if these ruthenates are driven to high potentials to initiate anodic oxidation, permanent material damage can occur. Higher surface area powders need to be synthesized for further testing and for practical applications.

Lithium-doped lanthanum nickelate: The effects of low-level lithium doping on the conductivity, stability, and electrochemical activity of perovskite-type lanthanum nickelate are presently being examined. Several new synthetic routes for the preparation of high surface area $LaNiO_3$:Li powders are being developed, and preliminary material characterization studies have yielded some interesting results. Microscopic analyses have indicated that the lithium is highly dispersed within the nickelate lattice, which consists of a network of fused particles containing La-rich and Ni-rich regions. Corrosion screening results of test electrodes fabricated from relatively low surface area powders indicate that reasonable stability may be evident under O_2-reducing conditions, but these results are presently inconclusive. Steady-state corrosion currents measured at 0.6 V were low; however, there were indications from the cyclic voltammograms that some loss of surface area was initially occurring when the electrodes were held at reducing potentials. Subsequent cycling and potentiostatic holding did not appear to adversely affect the material.

Ni-Co spinel: Corrosion current measurements have shown that PTFE-bonded $NiCo_2O_4$ spinel electrodes are unstable under O_2-reducing conditions. Steady-state cathodic corrosion currents of $>10^{-5}$ A/cm^2 were observed at 0.6 V. Cyclic voltammetry was also employed to examine the $NiCo_2O_4$ electrode electrochemistry between 0.5 and 1.0 V. As shown in Figure 2, the nonsymmetry of the voltammogram shows that the spinel decomposes irreversibly at these reducing potentials; also, this was clearly indicated by the plating out of Ni and Co on the counter electrode.

Pb-Ru pyrochlore: NASA-sponsored research has produced encouraging results with respect to the oxygen reduction performance of PTFE-bonded $Pb_2Ru_2O_{6.5}$ cathodes, and the long-term stability of this candidate needs to be assessed. Corrosion current measurements suggest that this pyrochlore is stable under O_2-reducing conditions; steady-state cathodic currents of $<10^{-6}$ A/cm^2 were observed at 0.6 V. Cyclic voltammetric analyses in the 0.6 to 1.0 V potential range were in agreement with this assumption. Voltammograms obtained at lower potentials suggested that irreversible reduction of this pyrochlore may occur below approximately 0.6 V versus RHE.

Na-Pt bronze: The PTFE-bonded $Na_{0.75}Pt_3O_4$ bronze electrode, which has been shown to exhibit reasonable electrochemical activity for both oxygen reduction and evolution, was shown by preliminary corrosion screening to be stable under O_2-reducing conditions. Additional corrosion screening was performed at ambient temperature by comparing cyclic voltammograms obtained both before and after a test electrode was held at a reducing potential of 0.6 V for approximately 300 hours under a nitrogen

atmosphere. The voltammograms, which are shown in Figure 3, were quite similar, thus, indicating that little or no change in the electrochemical surface area had occurred during the period under potentiostatic control.

SUMMARY

Although they are not unequivocal indicators of long-term electrochemical stability, potentiostatic testing and cyclic voltammetry are valuable screening methods to be combined with other observations for assessing the corrosion resistance of electrocatalyst candidates.

Preliminary screening results have indicated that desired stability may be exhibited by some alkaline-earth ruthenates and by lithiated lanthanum nickelate. More in-depth corrosion studies need to be performed on higher surface area samples of these materials.

Both the Pb-Ru pyrochlore and the Na-Pt bronze candidate materials appear to possess sufficient stability to warrant extensive long-term performance testing.

FIGURE 1. - CORROSION CURRENT WITH TIME FOR IFC ORBITER ELECTRODE (0.6 V; N2; 24 oC)

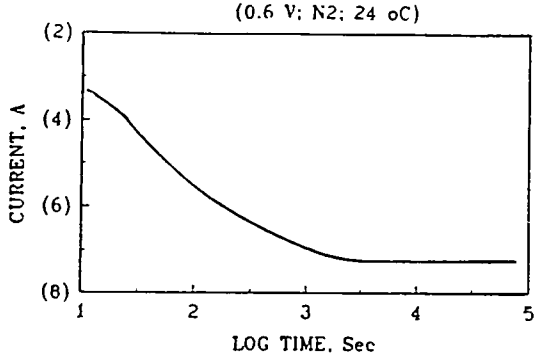

FIGURE 2. - CYCLIC VOLTAMMOGRAM FOR Ni-Co SPINEL ELECTRODE (1 mV/Sec; 80 oC; N2)

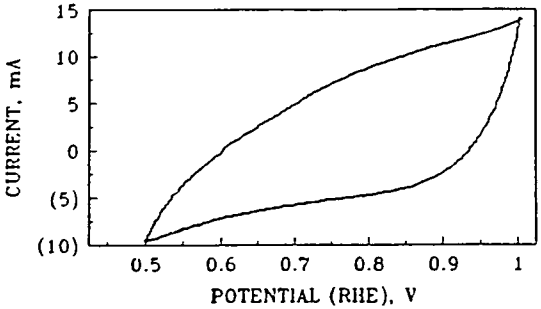

FIGURE 3. - CYCLIC VOLTAMMOGRAMS FOR Na-Pt BRONZE ELECTRODE BEFORE AND AFTER 0.6 V

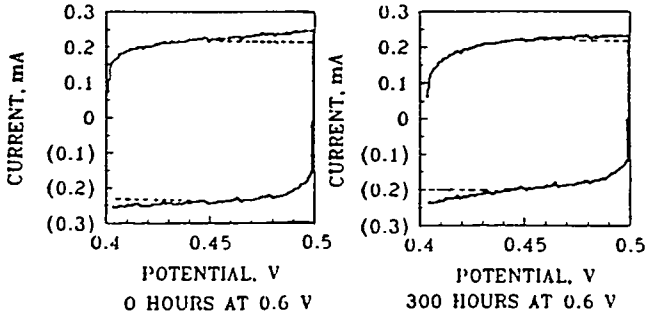

THE GRI ELECTROLYTE PROGRAM
TETRAFLUOROETHYLENE-1,2-BIS-PHOSPHONIC ACID

D. A. Scarpiello, Gas Research Institute, Chicago Ill;
D. J. Burton, Ranil Guneratne,
University of Iowa, Iowa City, Iowa;
K. J. Espinosa, D. L. Maricle*
International Fuel Cells, South Windsor Ct.

The objective of the GRI Electrolyte Program is to develop an alternative to phosphoric acid as a medium-temperature acid fuel cell electrolyte. The program has focused on fluorinated organic acids as candidates for improved performance. This is based on the higher O_2 solubility-diffusivity product, and lower cathodic anion adsorption observed for these materials than for phosphoric acid.

The GRI program has funded several university laboratories which collectively have synthesized many perfluorinated acids. These include, sulfonic acids, phosphonic acids, sulfonyl imides, and carbon acids. Initial electrochemical testing was done at Case Western Reserve University under GRI sponsorship. Several acids showed enhanced performance, but at temperatures below the 200°C phosphoric acid operating point. A minimum 177°C is required to avoid excessive anode polarization with reformed hydrocarbon fuels containing trace levels of carbon monoxide. Many of the perfluorinated acids proved unstable or volatile at temperatures at or above 177°C.

This paper reports test results on a new electrolyte, Tetrafluoroethylene-1, 2-bis-phosphonic acid, synthesized at the University of Iowa by Professor Burton and Ranil Guneratne. This acid was qualified at Case Western Reserve and run at International Fuel Cells in a subscale commercial fuel cell at temperatures ranging from 204 to 213°C. Analysis of the test data indicates the material survived for approximately 500 hours. This is a major improvement in high temperature stability for a fluorinated organic acid.

Evidence for the thermal stability of this material is provided by the TGA curve shown in Figure 1. This data was obtained on approximately 85 percent bis-phosphonic acid, in air in a platinum sample holder at a scan rate of 10°C/min. The initial weight loss at 100°C is loss of water. No significant additional weight loss is seen until the temperature reaches 300°C. This thermal stability contrasts sharply with the sulfonic acid analog which exhibits thermal decomposition slightly over 100°C in the presence of air and platinum in a similar experiment.

Based on this evidence and the performance enhancements reported by CWRU, 2 inches x 2 inches subscale cell testing was initiated at IFC. A summary of the test results is shown in Figure 2. The open squares display the performance (mV) vs time of a single cell filled with an initial concentration of 85 percent bisphosphonic acid (operating concentration unknown) running at 204°C, 200 ASF current density, 129°C anode dewpoint and 47°C cathode dewpoint. The solid curve labeled "E-Line" is a typical phosphoric acid cell life curve for the same type of electrodes run under the same conditions. The solid squares plotted against the right hand axis show the 200 ASF matrix iR loss vs time for the bis–phosphonic acid cell.

* Primary Author, 195 Governors Highway, South Windsor CT 06074, (203) 727-2278 FAX (203) 272-2319

International Fuel Cells
HP258

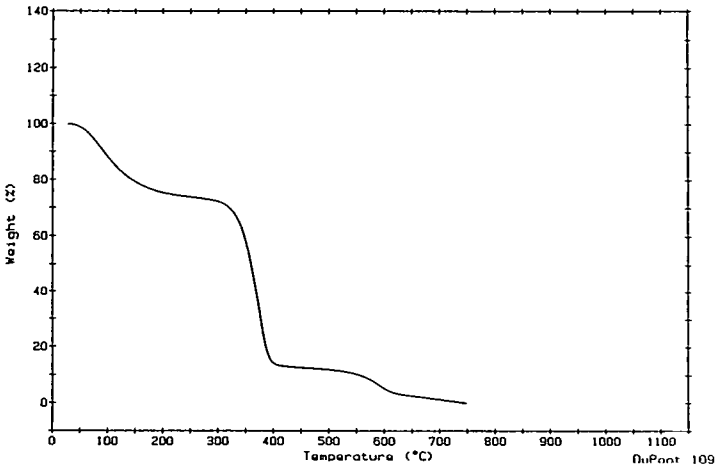

Figure 1. TGA Analysis of Bis-Phosphonic Acid

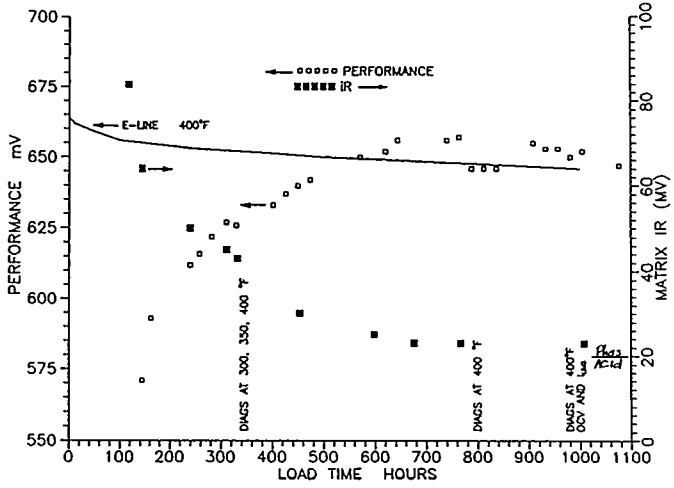

Figure 2. BIS-Phosphonic Acid Performance and iR vs Time
400°F, 200 ASF

International Fuel Cells
HP258

The fluorinated acid performance started well below the phosphoric acid norm, due primarily to an iR roughly 4 times typical. As the test proceeded the iR decreased causing the bis-phosphonic acid performance to peak above the phosphoric acid norm in the 600-1000 hour time period. The decrease in iR is attributable to conversion of the bis-phosphonic acid to phosphoric acid which is more conductive at the cell operating conditions.

Figure 3 shows the O_2 reduction activity expressed as mA of current at 0.9V per mg of cathode catalyst vs time for the bis-phosphonic acid cell. A decay of activity with time is seen. However, the initial O_2 reduction activity (61 mA/mg of cathode Pt) was higher than normal (50-55 mA/mg) for this type of cell running on phosphoric acid. The activity loss is presumably related to slow decomposition of the electrolyte.

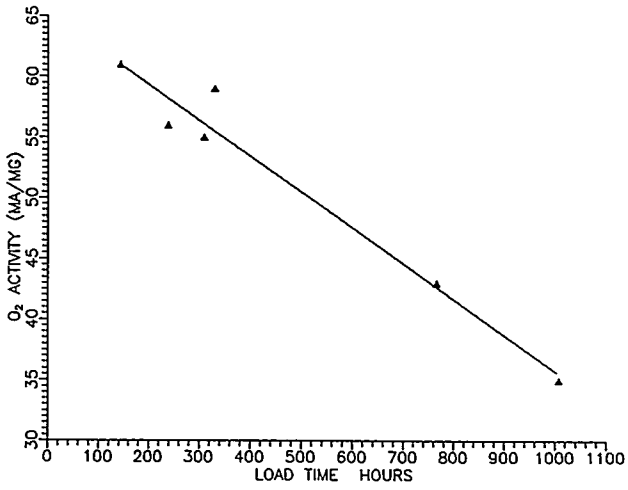

Figure 3. BIS-Phosphonic Acid - Activity vs Time 400°F

Other performance parameters attributed to the electrolyte were typical except for the Tafel slope. It was also high, possibly due to higher cathode internal ionic iR losses as a result of lower conductivity of the bis-phosphonic acid at cell operating conditions.

Post-test electrolyte analysis (NMR) conducted at the University of Iowa indicated conversion of the bis-phosphonic acid to a lower volume of phosphoric acid during the >1100 hours of cell operation. The decomposition may involve hydrolysis of the bis acid to H_3PO_4 and a volatile fluorinated fragment. The cell was ultimately terminated due to loss of electrolyte and resultant reactant gas crossover.

These results provide encouragement that organic acids can be developed to operate at practical fuel cell temperatures. Assuming that the iR increase is linearly related to the bis-phosphonic acid concentration, some material survived for approximately 500 hours at 200°C.

International Fuel Cells
HP258

This is the first time on this program that any organic acid has been operated in a commercial fuel cell, at conditions consistent with real fuel cell systems, long enough to assess its operational characteristics. At least one of the hoped for benefits of fluorinated acids, higher O_2 reduction activity appears to be real. The issues of conductivity and hydrolytic stability remain to be addressed.

Work continues to synthesize new and more stable fluorinated electrolytes by Professor Burton's group at Iowa and Professor Des Marteau's group at Clemson University. Further testing of the bis-phosphonic acid is under way at IFC to characterize the acid at 176°C to minimize decomposition and with electrodes optimized for the conditions and electrolyte properties. Testing at elevated pressures will be conducted to determine if higher water content will improve the conductivity.

Fluorinated sulfonyl imides from Des Marteau's group have shown performance enhancement when used as additives to H_3PO_4 in tests at Case Western Reserve University. These are also scheduled for evaluation at IFC.

FUEL CELL COMMERCIALIZATION THROUGH A PARTIAL ENERGY SERVICE

By David M. Moard
Southern California Gas Company

SoCalGas Company, after completing the research, development and demonstration programs for the Phosphoric Acid Fuel Cell, examined the alternatives for commercializing the equipment. In this review we included promotion, merchandising, a Partial Energy Service (P.E.S.) and a Total Energy Service. In analyzing each of these scenerios, it was necessary to examine what services would be available from the manufacturer and what services would need to be developed by either SoCalGas or other agencies. We determined a P.E.S. offered by SoCalGas was the best match between the manufacturer, SoCalGas and our customers.

In a P.E.S. business SoCalGas would purchase the fuel cell from the manufacturer, install the units on a customers property and maintain the fuel cell for the life of the equipment. The manufacturer is responsible for the fuel cell meeting specifications through out the warranty period, spare parts and technical support. The customer has no direct responsibility for the fuel cell or its operation, but must maintain the site and allow access for service.

The customers electrical and thermal energy requirements are augmented by the fuel cell. The fuel cell becomes the customers primary source for their electric and thermal needs. The electric utility grid and gas boiler meet additional energy requirements or backup needs when the fuel cell is down for maintenance. It is essential that the electrical and thermal energy from the fuel cell be used to the greatest extent possible to secure the economic benefits for the customer and SoCalGas in a P.E.S.

The customers economic benefits are derived by reducing their energy bill for the portion of electric and thermal requirements provided by the fuel cell. We feel between a 10 to 15 percent savings is the necessary incentive for a customer to be interested in having the unit on the property. The customer's savings are based upon the retail cost of electricity, that would have been provided by the utility grid, and the value of the thermal energy, as if supplied by a boiler. The customer essentially pays for 85 to 90 percent of what the building receives from the fuel cell. If, for example, the equipment produced 100 kilowatts and 100,000 BTUs an hour, the customer is billed for the equivalent of 85 kilowatts and 85,000 BTUs.

The actual mechanism for SoCalGas to collect our portion of the revenues will be through a gas bill, for the gas consumed by the fuel cell, and a facility or use fee for the equipment. The additional electricity and thermal requirements of the building are billed in the conventional manner. Since the retail value of the energy is the basis for fuel cell savings any changes in the rates for electricity or gas are automatically accounted for.

SoCalGas Company's portion of the revenues provide for the maintenance, spare parts, installation, overhead, purchase of the equipment plus profit. The equipment has an expected useful life of twenty years. A contract between SoCalGas and the customer will be in effect through out this period identifying the obligations of each party.

The P.E.S. is similar to third party ownership and operation that has been done on engine driven co-generation systems. It allows the customer to derive a savings without directly investing in the capital equipment. Since SoCalGas has supported the fuel cell development to this point, and is in the energy business, we feel it appropriate to become involved in a P.E.S. and this involvement is the key to the successful commecialization of the fuel cell.

DOC: DM_FCOPES
11/8/88

PAFC - APPROACH TO COMMERCIALIZATION

R. Anahara

Fuji Electric Co., Ltd.
1-12-1 Yurakucho Chiyoda-ku
Tokyo 100, Japan

1. Introduction:

Fuji Electric is committing substantial resources towards the commercialization of PAFC in 1993. We are focusing on three applications:

(i) On-site cogeneration uses (50-500kW)
(ii) Dispersed power plants for utilities (MW class)
(iii) Vehicular application (< 100kW)

The on-site cogeneration application is likely to be our first commercial products. We plan to construct a 5MW dispersed type power plant for the Japanese electric utility companies within the next few years. To this end, Fuji Electric has installed a semi-mass production facility with an annual capacity of 15MW per year for producing on-site power systems and stacks for dispersed power plant.

The cost barrier is a substantial one for commercialization. Market acceptance along with mass production is critical in cutting cost. Our developmental work in cogeneration has been strongly supported by three major gas companies in Japan and orders for numerous pre-commercial units have thus far been secured. We plan to supply fully commercializable products to our customers worldwide in 1993 after achieving manufacturing and operation goals.

2. On-site PAFCs:

The first 50kW engineering model developed for Tokyo Gas Company at the end of 1989 has the following characteristics:

(i) Packaged-type design
(ii) Grid connected and grid independent operation
(iii) Fully automatic push-button operation

Supported by satisfactory operation at Tokyo Gas Company, other companies have expressed interest in securing additional units. For example, Tokyo Gas, Osaka Gas and Toho Gas plan to have 9 sets of 50kW and 7 sets of 100kW by 1991. Kansai Electric Power Company (Kyoto/Osaka area) plans to have 16 sets of 50kW and this is part of a NEDO Project for the demonstration of new type of power generation system at Rokko Testing Station near Osaka. Included in the NEDO plan are: 1000kW (17 sets) of PAFCs, 600kW photovoltaic generating plants and 2 x 15kW wind power generators under grid connected conditions.

There are several other 50kW demonstration projects in Europe and Asia (see Table 1).

Table 1 Order List of 50kW On-site PAFC Plant (Trial units)

Item	Customers	Quantity	Delivery
1	Tokyo Gas	1	1989
2	NEDO, Kansai Electric Power (Rokko Island)	16	1990-1992
3	EGAT (Thailand) ODA Project	1	1991
4	Europe (Spain, Italy, Sweden)	4	1990-1992
5	Tokyo Gas	4	1990-1991
6	Osaka Gas	4	1990-1991
7	Toho Gas	1	1991
8	Tokyo, Osaka and Toho Gas	~50*	1991-1992
	Total	~81	1990-1992

*Option

The key specifications of 50kW is shown in Table 2.

Table 2 Key Specification of 50kW PAFC On-site Plant

Purpose	On-site Co-generation
Type	Water cooled PAFC
Output	50kW (Sending end)
Electrical efficiency	40% (LHV) (Sending End)
Total efficiency	80% (LHV) (65°C Hot water)
Construction	Packaged type (Indoor/Outdoor)
Fuel	Town gas (LNG) (13A) (100~250mmAq)
Working pressure	Atmosphere
Range of output	0 ~ 100%
Load response	±50% (instantaneous)
Start-up time	< 3 hours (cold start) < 1 hour (hot start)
Voltage distortion	< 5% total
Operation mode	Independent and/or Grid connected
NOx	< 20 ppm (O_2 : 7%)
Weight	< 5 ton
Foot-print	< 0.09 m^2/kw (L: 2.9m, W: 1.6m, H: 2.2m)

3. Dispersed PAFCs:

Based on the construction and operation experience of the 1MW plant under the Moonlight Project completed in 1989, Fuji plans to construct a 5MW plant suitable for electric utilities. The special feature of this 5MW plant is its compactness which is critical for urban installation. Fuji Electric plans to cooperate with Kansai Electric Power company in implementing this new development. The time for construction will be about 45 months after contract.

A number of developmental items have been initiated at Fuji Electric inclusive of large size electrodes (8000 cm^2), reformer and compact

design. The performance of the 8000 cm² electrode surpassed that of the 1MW plant demonstrated earlier (see Table 3).

Table 3 Comparison of Stack Performance between 1MW Plant (1986) and 5MW Plant (1992)

	1MW Plant (1986) Moonlight Project	5MW Plant (1992) Proposal
Stack Output (DC)	260kW	860kW
Cell voltage	0.7V	0.746V
Current density	200mA/cm²	300mA/cm²
Working conditions	4kg/cm² g, 190°C	6kg/cm² g, 200°C
Cell size (effective)	3600cm² class	8000cm² class
Electrode structure	Ribbed substrate	Ribbed substrate
Cooling method	Water cooling	Water cooling
Inner diameter of P V	φ1,700	φ2,300

Life test results of the stack under simulated conditions are quite satisfactory. Haldor Topsoe's "Heat Exchange Reformer" is being considered for this project. The 5MW unit requires further investigation in terms of compactness, dynamic response and operation characteristics.

4. Vehicular PAFCs:

Based on the developmental experience gained from our PAFC powered forklift truck program, Fuji Electric successfully completed Phase I of the Department of Energy (DOE) Fuel Cell/Battery Hybrid Bus Program. The DOE's program is divided into 4 phases from 1988 to 1996. Fuji Electric supplied a 25kW brassboard PAFC system and was successfully tested at Pentastar Electronic (Chrysler). The plant is methanol based with dielectric-liquid cooling.

Phase II of this important program, both from an energy-conservation and environmental emission perspectives, calls for several 50kW PAFC plants. Close cooperation between several U.S. companies inclusive of Booz Allen & Hamilton, bus manufacturers and components manufacturers will be required. Support from many sectors of the United States have been strong in particular the Southern California region.

5. Cost Reduction:

Cost reduction is undoubtedly the single most important issue for PAFC commercialization.

5.1 Technology considerations:

Three technology improvements areas have major impact on overall cost reduction: cell performance, reformer and inverter.

a. Cell performance:
Cell performance improvements lead to size reduction and cost reduction for the entire plant. This is achieved via achieving a power density of three times that of the 1986 technology of 80mW/cm². Current technology is at 160mW/cm² and future technology will be at 230mW/cm².

b. Reformer:
The second generation reformer has improved in both size, weight, volume and the amount of catalyst loading (see Table 4).

Table 4 Comparison of 50kW Reformer

Item	1st model (1988)	2nd model (1990)
Space	100%	59%
Weight	100%	37%
Volume	100%	52%
Catalyst	100%	24%

c. Inverter:
Similarly, the high frequency modulated IGBT inverter can achieve a size reduction of 1/5 and a weight reduction of 1/3.

All the improvements lead to reduced plant cost.

5.2 Standardization:

Cost reduction can further be achieved via design standardization and mass production. All stacks will be standardized to a 2000cm² and 8000cm² cell area.
Standardization in standard plant capacities is shown in Table 5.

Table 5 Fuji Electric's Series of Standard Plant Capacities

Application	Type	Output (kW)
On-site use (ambient pressure system)	FP-50 FP-100 FP-500	50 100 500
Dispersed station use (pressurized system)	FPD-5 FPD-20	5,000 20,000

Modular design general can be achieved at a slightly higher unit cost in comparison to large size system. However, this increased in cost can be offset by mass production of standard plants, short construction, etc..

6. Future Prospect:

Encouraged by the recent worldwide clean-air and energy conservation movements, the commercialization of fuel cell plants has taken to an even greater significance.
Reflecting such a global request, Japanese government has recently set up a long term introductory plan for fuel cell power plants (see Table 6.)

Table 6 New Energy Long Term Introductory Plan (by MITI)

Year	Target (MW)	Fuel Cell Plants	
		Total (MW)	For Electric Utility (MW) (%)
2000	~ 2,100	~ 2,000	~ 1,100 (0.5%)
2010	~13,000	~ 8,500	~ 5,700 (2%)

Substantial efforts not only from the developers but also from all circles are required to realize a 1100MW capacity for the electric utility by the year 2000. As a footnote, 1100MW is only about 0.5% of the total electric power plants in Japan.

The Japanese government is currently planning to accomplish this ambitious target by establishing new promotion organizations with national subsidiaries. We at Fuji Electric are exerting our best effort to contribute to this plan. To accelerate, comprehensive cooperation from all sectors is a must: government, potential customers, and manufacturers/suppliers.

TOSHIBA'S STRATEGY FOR FUEL CELL POWER PLANT COMMERCIALIZATION

Haruo Kawahara
Tetsushi Matsushita, Toshiro Terayama, and Nobumitsu Ishikawa
Fuel Cell Systems Division
Toshiba Corporation, Tokyo, Japan

General

The Advisory Committee for Energy - an advisory organization to Japanese Ministry of Trade and Industries-issued recently the policy guidance for the introduction of new energy towards 21st century.

In this guidance fuel cell power generation is projected to be 1900 MW (0.85% of total generation) and 8200 MW (3%) in the year 2000 and 2010 respectively.
With these Government policy guidance and strong customers enthusiasm, Toshiba, whose corporate identity is E&E (Energy & Electronics) and with the total 1989 sales of 22 billion dollars, identified the Fuel Cell as a promising energy business toward 21st century.
The fuel cell power generation will be introduced for small scale class (10's MW) in Japanese electric utility power generation mix (Large: Nuclear, Middle: Fossile) and also its promising market will be expected for cogeneration use below 1000 kW in urban area for its superiority in heat/electricity ratio and environmental characteristics, where gas companies are especially enthusiastic toward its development.

To accelerate fuel cell power plant commercialization, Toshiba is now actively working in each fuel cell field characterized and summarized as:

Type	Status	Use
PAFC	Commercialization Stage	o Electric Utility and On-Site
MCFC	Research and Development of Cell Stack and Plant	o Electric Utility
SOFC	Basic Research and Development of Cell Stack	o Mainly for On-Site

Toshiba's activities for phosphoric acid fuel cell (PAFC)

Toshiba has made technology developmental and commercialization efforts with his own original activities and international joint cooperation as their driving force in the following:

Own Original Activities

(Year)	(Activities)
1960	(o Started Development on AFC.)
1978	o Started Major Development Effort on PAFC
1981	o 35 kW PAFC Cell Stack Completed o 50 kW Reformer Completed
1982	o 50 kW Demo-Plant Construction completed
1984	o 100 kW PAFC Cell Stack Completed
1986	o Manufactured 260 kW PAFC Cell Stack and 1 MW Reformer for Moonlight 1 MW PAFC Fuel Cell Power Plant
1988	o Completed Moonlight 1 MW Project o Started Development and Commercialization Effort for On-Site Fuel Cell Power Plant

International Joint Cooperation

(Year)	(Activities)
1980-83	o Assisted Installation and Operation of TEPCO 4.5 MW PAFC Plant Manufactured by UTC
1985	o Established a Joint Venture Company, International Fuel Cells Corporation (IFC) by United Technologies Corporation (UTC) and Toshiba. o IFC and Toshiba started jointly the Engineering and Development of PC-23 (11 MW PAFC). Full Scale Verification Tests conducted for major equipments.
1987	o PC-23 Joint Development Completed. o IFC Restructure.
1988	o World Largest TEPCO Goi 11 MW PAFC Plant Ordered to TOSHIBA as Main Contractor and Manufacturer. (Cell Stacks Manufactured by IFC)
1990	o Investment to IFC to establish IFC's subsidiary ONSI for commercialization of On-Site fuel cell power plant under 1000 kW. o Completed Installation of and Started Test of Goi 11 MW Plant o Completed 1 m^2-Class Cell Stack Production Facility and Factory with support by IFC

Commercialization Effort

Toshiba is focussing commercialization effort on PAFC for electric utility and On-Site use.

For electric utility use, plant compactness targets have been settled as 0.08 m^2/kW footprint and 1.1 m^3/kW volume competitive with other power generation methods. To realize these targets and cost reduction described below, following improvement effort has been started:

- o Larger Stack Capacity (670 kW to 1MW class)
- o Transportability of Reformer (11 MW class)
- o Inverter Cooling and Larger Element
- o System Simplification
- o Better Mass-Manufacturing Technology

The cost reduction projection is expected as the Figure-1. In Japan, $2000/kW of the construction cost will be competitive taking into account superior characteristics and other credits of the fuel cell power plant. We are optimistic about the level of $1000/kW in the stage of full commercialization.

Figure-1

CONSTRUCTION COST PROJECTION
OF
10 MW CLASS ELECTRIC UTILITY PAFC POWER PLANT

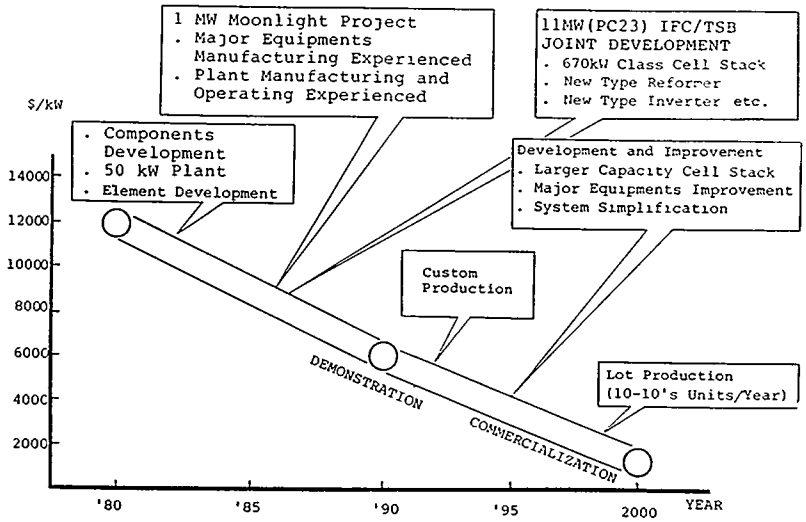

Also for On-Site use, Toshiba has now the working programs for 200 kW and 100 - 50 kW class development and commercialization activity for mainly Japan incorporating IFC/ONSI technology and experiences. Dlelivery of the initial lot for commercial use is scheduled in 1993. As the market requirement for on-site use will be improved much earlier than that for electric utility use, cost reduction will be accelerated. Cost projection of $1500/kW will be realized in the near future with the production level of several 100's units per year, although cost for initial lot will be much higher. We are also optimistic about the cost level of $1000/kW in the stage of full commercialization.

MCFC Development Activity

Toshiba initiated its technology development in 1980, participated in the Moonlight Project, and demonstrated 10 kW MCFC stack power generation in 1986.

After that, Toshiba has forced his own R&D program to establish technologies necessary to resolve basic difficulties of MCFC cell performance and life and to manufacture large size cell and stack, 100 kW with 1 m^2 cell class for example, as next stage.
Toshiba corporate R&D center, the design and research department of a heavy apparatus works, the works laboratory and the engineering department are sharing and integrating such MCFC development.

Toshiba believes significant progress has been achieved in the technical fields since we could obtain life projection of more than 15000 hours and manufacturing of 1 m^2 cell repeating elements became possible.

Toshiba and IFC have worked together to enhance the respective results of development and now start a very strong joint activities for a large cell stack development such as 100 kW class. This joint relationship will include some other participants and continue and strengthened to move towards next demonstrater stage in the near future.

Toshiba considers it will be after entering 21st century when its commercialization will be realized.

References

1. T. Iino, J.S. Caraceni, Y. Shiba, "CONSTRUCTION OF 11 MW PAFC POWER PLANT AT TEPCO GOI THERMAL POWER STATION", 1988 Fuel Cell Seminar.

2. T. Iino, J.S. Caraceni, Y. Shiba, N. Kato, K. Hayakawa, "PAC TEST OPERATION OF 11 MW PAFC POWER PLANT AT TEPCO GOI THERMAL POWER STATION", 1990 Fuel Cell Seminar.

3. T. Terayama, K. Murata, M. Yamamoto, M. Hori, M. Sasaki, "MCFC TECHNOLOGY IN TOSHIBA", 1990 Fuel Cell Seminar.

HIGH-TEMPERATURE FUEL CELL POWER SYSTEM STUDIES FOR SMALL AND MEDIUM SIZED POWER PLANTS

W. Drenckhahn
Siemens AG KWU, D-8520 Erlangen, Germany

W. Schramm
Linde AG, D-8023 Höllriegelskreuth, Germany

1. Introduction

Since 1988 Siemens is also engaged in the development of high temperature fuel cells. During a two years preparation phase the developments of MCFC as well as SOFC have been carried out in the research laboratories and system studies for small and medium sized power plants were performed by the power generation group of Siemens in collaboration with Linde AG, Germany. Goal of this preparation phase was to decide which of the high temperature fuel cells should be developed by Siemens. The result of the development work, market and system studies was that Siemens will now develop SOFC in a flat plate design with metal separator plate. This paper will present the results of the power plant system studies based on MCFC respectively SOFC as electrochemical energy converter and with natural gas as fuel.

The first application of high temperature fuel cells is expected in the decentralized energy supply in the power range of about 1 MW. In a second step industrial power plants in the power range of 30 - 50 MW will become applicable.

2. MCFC Power Plants

Our first investigations checked the power plants with external reforming units containing the preheating of natural gas up to 400 °C, desulphurization and blending with additional steam as well as further temperature increase before entering the reforming unit itself.

The syngas produced is cooled down to about 600 °C to enter the cell and reach the anode in order to oxidize electrochemically the main part of H_2 and CO. From the product gas leaving the cell, water is removed by cooling and carbon dioxide is washed out. The conditioned product stream passes a compressor before entering a pressure swing adsorption unit to separate the hydrogen. A minor amount of hydrogen produced serves the hydrodesulphurization, the major part ist recycled to the anode. Inert gas fractions associated with natural gas are directed to the reformer furnace.

The cathode section is supplied with compressed and preheated gas containing air and carbondioxide removed in the wash unit. This gas stream is added into the cathode cycle stream.

This cycle is to keep the cell temperature under control. After leaving the cooling cycle the air/CO_2 gas mixture passes a turbine and another cooling section.

To keep any trouble of carbon deposition out of the cell system you have to make sure that the external reforming operates with a high steam/carbon ratio and at low process pressure. These precautions only lead to an electrical efficiency of about 47 %.

Internal reforming provides the reaction of the natural gas/steam mixture on the catalyst integrated in the anode section. There is no need for any further reforming unit. Thus the endothermal reforming step keeps the energy equilibrium with the exothermal oxidation process. At steam/carbon ratios of 2.5 this low loss heat transfer makes electrical efficiencies of 60 % achievable.

In the case of small, decentralized combined heat and power plants the energy supply of an administration building with an electric energy demand of 1.5 MW was investigated for MCFC with internal reforming. Because of the small power range it is not possible to use the waste heat for additional electric power generation in this case. Therefore an electric efficiency of 48 % can be reached, the total efficiency (electricity plus heat) as about 80 %.

Cost analysis in comparison with existing gas or fuel oil fired cogeneration plants show that the investment cost for a MCFC plant are not allowed to exceed 1000 $/kW.

3. SOFC Power Plants

The SOFC process operates at temperatures around 900 °C. The external and internal processes using MCFC are very much alike. At such temperatures carbon deposition is not a problem. Thus the steam/carbon ratio of 2.5 and a total pressure of 8 bar are advisable operation conditions. This leads to even higher efficiencies in the overall process.

The above mentioned supply of an administration building was also investigated for the SOFC (Fig. 1). Fuel is again natural gas internally reformed in the fuel cell. The exergy of the anode waste gas is used for the generation of steam necessary for the internal reforming. Oxidant is air which is also used as coolant for the fuel cell. The hot waste gases are used as heating media of the building. In the opposite case of cooling the building it would also be possible to use the waste heat in an absorption cooling process. In the investigated combined heat- and power plant the electric efficiency is 50 % and the total efficiency 83 %.

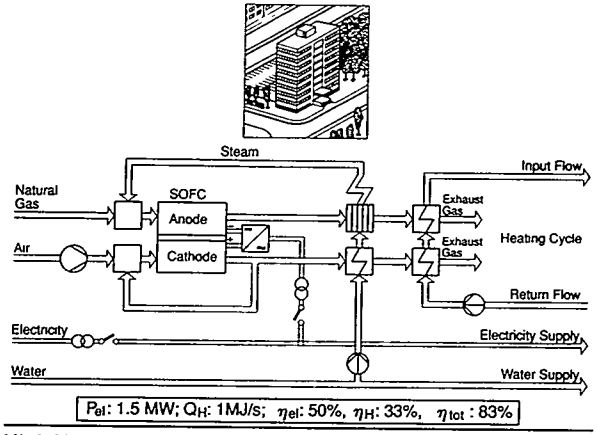

High Temperature Fuel Cell (SOFC) for Electricity and Heat Supply to an Administration Building Fig.1

In larger plants, suitable for industrial application e. g. 40 MW, (Fig. 2) the exergy can be additionally used for electric power generation. In this example a bottoming cycle consisting of a gas expansion and steam turbine is supplied by the heat of the exhaust gas. The total electric efficiency is then 68 % which is very encouraging for the development of the solid oxide fuel cell.

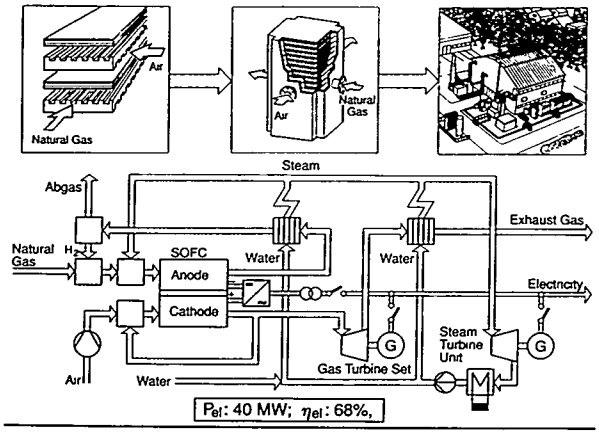

High Temperature Fuel Cell Power Station for Industrial Application (Maximum Electricity Generation) Fig.2

Economic analysis lead to the result that allowable investment cost of a SOFC plant have to be about 1000 $/kW to be competetive with state of the art fossil fuel fired power plants.

4. Summary

Our power system studies for small and medium sized plants using MCFC resp. SOFC as energy converter with natural gas as fuel show that in the case of MCFC with external reforming electric efficiencies can be reached which are in the same order as already realized combined cycle power plants of the GUD type. On the other hand MCFC with internal reforming can be attractive for power plant application. The situation for SOFC, however, seems to be more attractive. Because of their high operation temperature the waste heat can be used in a bottoming cycle more efficient.

As Table 1 explains electrical efficiencies of 63 % for systems applying SOFC plus external reforming and 69 % using internal reforming are within reach. This result is very encouraging for the further SOFC development and can help to solve some of our environmental problems.

Fuel	Natural Gas			
Cell Type	MCFC		SOFC	
Reforming	external	internal	external	internal
Oxidation with	Air			
Pressure Range	< 5 bar	8 bar	8 - 12 bar	
Maximum Operation Temperature	690°C		950°C	
Cell Efficiency	80 %	80 %	80 %	80 %
System Efficiency	47 %	60 %	63 %	68 %

Electrical Efficiency of Different HT - FC Plants Tab. 1

RESULTS FROM APPA'S "NOTICE OF MARKET OPPORTUNITY FOR FUEL CELLS" (NOMO): A NEW COMMERCIALIZATION PARTNERSHIP

M.K. Bergman
Instar Community Systems, Inc.
Hamilton, MT 59840

R.W. Claussen
Alabama Municipal Electric Authority
Montgomery, AL 36103

D.M. Rastler
Electric Power Research Institute
Palo Alto, CA 94303

Over the next several decades, electric utilities in the United States will be looking for generation options that are efficient, cost-effective and smaller-scale, and that can meet stringent environmental standards for siting near growing electrical loads. Dispersed fuel cell power plants offer potentially unparalleled advantages over other generation technologies in meeting these requirements. Results from recent studies conservatively estimate a near-term market for fuel cells of 12,000 to 14,000 MW over a fifteen-year period, with public power utilities as a "likely early market" (1).

The NOMO

In response to these factors, the American Public Power Association (APPA) issued its "Notice of Market Opportunity for Fuel Cells" (NOMO) in October 1988 (2). The NOMO invited responses from fuel cell developers worldwide to begin a process of discussions and collaborations to help catalyze the commercial availability of megawatt-scale fuel cells by the mid-1990s. The initiative was intended to break the "commercialization conundrum" of costs as a function of volume that had stymied fuel cell development efforts of the past. The NOMO was also intended to communicate buyers' requirements so as to achieve maximum market acceptance.

Five detailed responses to the NOMO were received from leading fuel cell developers in the United States, Japan, and Europe. Phosphoric acid, molten carbonate and solid oxide fuel cell technologies were each proposed. The responses were evaluated by a twelve-member Review Team comprised of managers from leading public power systems. The Review Team was seeking a mutually beneficial partnership with one or more fuel cell developers that could lead to a product that met the mature unit cost and performance goals as outlined in the NOMO. The Review Team's evaluation was based upon criteria relating to cost, reliability, risk, technical readiness, incentives for early participants and the developer's commitment to commercialization.

The Review Team's evaluation of responses in 1989 resulted in the selection and endorsement of Energy Research Corporation of Danbury, CT. ERC has been developing advanced molten carbonate fuel cells for more than 10 years and has received support from the U.S. DOE, the Electric Power Research Institute, and Pacific Gas and Electric Co., among others.

ERC's Product Design

ERC's proposed product offering is a 2-MW (1.77 MWe net) power plant. ERC's design promises exceptionally high efficiency (5700 Btu/kWh - 6300 Btu/kWh [LHV], depending on the type of system design); high reliability; extremely low emissions; and small footprint and height allowing for siting within urban service areas and for distribution-related applications. A 2-MW plant easily fits within the area of a standard size tennis court. The plant can also operate over a wide power range (25% to 125% of rating), offering additional benefits due to operational flexibility and capacity credits in pooling arrangements.

Characteristics of the market entry (also called "early production units", or EPUs) and demonstration units and the commercial units are presented elsewhere at this seminar (3). A unique feature of ERC's design over earlier fuel cell concepts is the use of internal reforming of the natural gas fuel. This eliminates the need for an external fuel processing system and translates into significantly lower investment costs and higher reliability than earlier fuel cell designs.

ERC has made significant technical progress during the last three years in developing molten carbonate fuel cells that use the internal fuel reforming concept. ERC's next major technical milestone is verification and durability testing of a full-scale 100-kW stack (~300 cells) and operation of a completely integrated 100-kW MCFC system. These steps are currently underway with results due in 1991-92.

Principles for Commercialization

The NOMO Review Team, in collaboration with ERC, developed a set of detailed Principles for the introduction of this new power generation option to the electric utility market. The Principles define ERC's Commercialization Plan, ERC and buyer obligations, technical and financial risk protections, financial incentives and benefits for early participation, and the conditions necessary for proceeding to each subsequent step in the program. These Principles form the basis for negotiating formal purchase contracts between individual buyers and ERC.

ERC's commercialization program requires several 2-MW demonstration units at ~$16 million (1990 $) each, followed by ~50 EPUs (100 MW total) at a target price of ~$1500/kW (~$3.0 million each, installed). As specifically contained

in the Principles negotiated with ERC, the first set of early buyers is expected to host one of the early demonstrations, and to order 40 MW of EPUs.

Financial commitments by ERC have already been made towards constructing a 2-MW/yr pilot production facility that will manufacture and assemble MCFC components for the demonstration units. Construction of the early demonstration units begins in mid-1993. Based on success in the demonstration units and utility commitments for 100 MW of early production units, a commercial scale fuel cell manufacturing facility (~400 MW/yr) will be constructed. Operation of commercial MCFC power plants would begin in 1997. A solicitation period through 1994 is defined in which the necessary 100 MW of early commitments needs to be secured.

The Principles attempt to balance technical and financial risks and incentives for both developer and the utility participants. Before a 2-MW demonstration unit is built, the manufacturer is required to achieve specified technology milestones and have letters of intent for EPUs. MCFC stack performance, endurance and manufacturability as well as technical success in 100-kW integrated systems and 2-MW systems must be thoroughly demonstrated for the program to proceed. EPU orders require no financial commitments for several years and are contingent upon the prototype demonstration plant successfully achieving specified operational criteria. EPU orders become "firm" commitments and require payment of a deposit when the manufacturer offers these units at agreed upon target price and performance and operational warranties, and commits to build the commercial fuel cell manufacturing facility to support these orders.

Other risk management measures include: technical and cost review by the utility participants and EPRI of ERC's design, manufacturing and construction efforts; use of proven design techniques such as failure mode and effects analysis, through performing UNIRAM and STAMP analysis to assess reliability and fault isolation and maintenance; and documentation of demonstration plant experiences using a site "engineer-of-record."

The demonstration unit and the EPUs are being offered at prices higher than their intrinsic value. The Principles address this issue by including financial incentives to early buyers in the form of royalties. For the demonstration unit, priced at $16 million excluding site and utilities, royalties equal to two times this capital investment will be paid to the host utility and its participants. For the EPUs, the royalties equal two times the capital cost premium paid over commercial unit price, but only for the first 40 MW of orders. Royalties are indexed to account for the effects of inflation. The equivalent cost of these first 20 2-MW units is thus about $750 to $950/kW, on a present worth basis, depending on order of installation. Other incentives for early participation include "most favored nation" status with

respect to future pricing, priority access to replacement fuel cell stacks, and the ability to influence the product design for utility market needs and applications.

Current Status

A Fuel Cell Commercialization Group (FCCG) representing potential buyers was formed in June 1990 to meet those buyers' obligations that are part of the negotiated Principles. The FCCG has as its mission the early commercialization of ERC's carbonate fuel cell power plant. The objectives of the FCCG are to promote this opportunity to potential buyers and to coordinate the information flow among the FCCG members. As one of its first activities, the FCCG is translating the Principles negotiated with ERC into a model contract.

The FCCG currently has 18 members, including investor-owned electric and gas utilities, rural electric cooperatives and public power systems. Any potential buyer of ERC's EPUs or a participant in an ERC demonstration unit in North America is eligible to become a member of the FCCG. The FCCG is governed by a fifteen-member Board of Directors and is supported by a small professional staff. EPRI provides technical support.

The City of Santa Clara, California, is investigating becoming the demonstration host. Six additional major financial participants have formed a Steering Committee under Santa Clara's chairmanship. The FCCG has endorsed Santa Clara as the potential host. Additional utilities have indicated potential financial support. A project development plan has been drafted and contract development efforts in preparation for demo negotiations with ERC have begun.

The FCCG has already secured tentative commitments for nearly the entire 40 MW EPU requirement, and efforts on the Santa Clara demonstration are well underway. Thus, the momentum is growing in support of this initiative. However, information development, contract negotiations, and further utility commitments and financial support are still required if this program is to go forward.

References

1. EPRI, "The Market for Fuel Cell Power Plants Within Municipally Owned Utilities," EPRI Report GS-6692, January 1990.

2. APPA, "Notice of Market Opportunity for Fuel Cells," issued by the American Public Power Association, October 1988.

3. H.C. Maru, "Natural Gas/Direct Fuel Cell Power Plants: Development and Commercialization Activities," presented at the 1990 Fuel Cell Seminar, November 1990.

POTENTIAL FOR USE OF FUEL CELL POWER PLANTS IN TRANSIT BUSES

Thomas J. Ross
Phoenix Transit System
Phoenix, Arizona

Several attempts have been made to introduce alternate bus propulsion power plants. During the last twenty years battery powered buses, gas turbine powered buses, and steam powered buses have all been developed.

These programs were carried out as part of an overall plan to improve bus transit service. The Urban Mass Transportation Administration defined the basic criteria a transit bus should meet as the basis for the Transbus Program. (1) These were:

1. Speed of transit.
2. Passenger comfort and convenience.
3. Environmental compatibility.
4. Maintenance and reliability.
5. Safety.
6. Economy of capital and operating costs.
7. Accessibility.

Each of the previous programs to utilize alternate power plants met some, but not all of the criteria. In the early 70's the Electrobus was developed. This was a 20 passenger bus powered by electric motors. The bus used lead acid batteries. A total of 20 buses were manufactured. They had a low floor (22") and a one step entry. The vehicle was unaffected by altitude and had excellent gradability. However, with a 35 mile range, no heat or air conditioning, and a 25 mph top speed the market for this vehicle was limited. (2)

Several attempts were made to use steam power in a transit bus. The California Steam Bus Project was carried out from 1969 to 1972. Three buses were produced and operated by AC Transit, San Francisco Munci, and SCRTD. The vehicles were found to have performance equivalent to a diesel bus. Emissions were significantly lower. Fuel economy was much worse then the diesel buses (approximately 1/3). Reliability of the units was a problem. The program was discontinued in 1972. (3)

Gas turbine power plants were used to power both transit buses and inter city buses. Greyhound accumulated 1.3 million miles on their buses during the 70's. The experience was positive in several areas. The buses were quieter, smoother and more powerful then the diesels. Brake life was greater than on the standard diesel coach. Economy of operation was the deciding factor in halting the program. Poor fuel economy (15-20 % less) reliability and durability problems killed this program. (4)

These programs failed to produce a viable alternative to the diesel engine because they did not meet the performance of the standard diesel bus. While todays diesel bus is not significantly different then the standard bus of 20 years ago, no better alternative is on the market. An electric bus does have the potential to displace the standard transit bus. Simply meeting the 1978 Transbus standards would meet this goal.

First of all, the average speed of bus service relates directly to cost of operation and passenger mode choice. If a maximum acceleration of .2g is used instead of .1g, urban service average speeds are increased by about 14%. (5) If the bus body design incorporates a low floor and a wide double stream (in/out) front door passenger loading times are greatly decreased. This is a benefit to both the operator and the passenger. The fuel cell battery combination easily meets the environmental compatibility criteria making it possible to utilize buses in neighborhoods where diesel powered vehicles are unacceptable.

Maintenance and reliability problems can easily stop any project. This technology transfer issue will require careful handling. The use of stationary fuel cell power plants in transit operations may be the best first step to introduce this product.

Safety of operation applies to more then fuel cell operation. Because traffic accidents and passenger accidents are a major concern, any design features which improve driver accident avoidance, vehicle accessibility and vehicle body integrity are positive attributes.

Producing a fuel cell powered bus at a cost equal to a diesel bus is difficult. The life cycle cost is the only appropriate level of comparison.

Vehicle accessibility is a fundamental factor in choosing which bus to purchase and operate. If a low floor bus body is provided then use of a simple ramp for wheelchair accessibility becomes practical.

Previous bus alternate power plant experiments have been performed. They have all failed to capture a segment of the market for differing reasons. The lesson learned from these programs is just meeting a few of the Transbus criteria is not enough. Fuel cell/battery powered electric buses must take advantage of current technology to produce a bus which utilizes this power plants unique characteristics to offset its disadvantages.

1. Booz, Allen, & Hamilton, Inc. Transbus Program. (The final report on the Transbus program by Booz, Allen & Hamilton to the Department of Transportation). June 1978.

2. Borisoff, B. "Electrobus - Review of 9000 Miles of City Transit Demonstrations". Society of Automotive Engineers, SAE 740170. 1974.

3. Renner, Roy. "Reviewing the California Steam Bus Project". Society of Automotive Engineers, SAE 730218. 1973.

4. Flanigan, Eugene E. and Nigro, Daniel N. "Field Experience with the Detroit Diesel Allison 404/505 Industrial Gas Turbine Engines". Society of Automotive Engineers, SAE 790129. 1979.

5. Booz, Allen & Hamilton Inc. Transit Bus Propulsion Systems Propulsion Requirements. (This document was the third in a series of four reports on propulsion systems prepared for the Department of Transportation). January 1978.

SOFC TECHNOLOGY STATUS AT WESTINGHOUSE

E. R. Ray
Manager, Agency Programs
Advanced Energy Conversion Department
Westinghouse Electric Corporation
1310 Beulah Road
Pittsburgh, PA 15235
(Telephone Number: 412/256-2125)
(Telecopy Number: 412/256-1348)

This paper discusses advancements made in the development of the Westinghouse tubular solid oxide fuel cells which demonstrate improved performance, reduced rate of degradation and increased life as well as the design, construction, and test of cell bundles and generator modules. Single cell tests have now exceeded two years of continuous operation and generator tests approaching 6,000 hours have been achieved utilizing desulfurized pipeline natural gas as the fuel.

Discussion also centers on work currently being conducted by Westinghouse to design, fabricate and test a 20 kWe tubular solid oxide fuel cell (SOFC) generator. The unit, called the Multi-Kilowatt Generator (MKG), will be largely self-supporting and will be fueled with natural gas. Additional objectives of this program are to identify design requirements for 20 MWe and larger coal-fueled electric power plants, to establish a reference design for commercial coal-fueled plants, and to formulate technology development goals.

BACKGROUND

Westinghouse, for nearly three decades, has been developing the materials and establishing the processes that will be necessary to commercialize the tubular Solid Oxide Fuel Cell technology. The development was intensified in 1980 when the current contract initiated a joint program between Westinghouse and the U.S. Department of Energy, Morgantown Energy Technology Center. This continuing program is focusing on developing the technology for tubular SOFC cells and generator modules. The program has focused on the use of coal-derived fuel gas for large scale electrical power production; however, due to their high operating temperatures, solid oxide fuel cell generators are good candidates for cogeneration applications.

PROJECT DESCRIPTION

Development of the tubular solid oxide fuel cell technology is being supported by the Westinghouse Electric Corporation, the United States Department of Energy (DOE), and the Gas Research Institute (GRI). The cost sharing contract between Westinghouse and DOE is currently administered by the Morgantown Energy Technology Center (METC). Analysis and conceptual design of natural gas fueled SOFC cogeneration systems have been funded through GRI by a Japanese consortium composed of the New Energy and Industrial Development Organization (NEDO), Tokyo Gas, Osaka Gas and Toho Gas. Funding for the evaluation of the Westinghouse SOFC technology for utility applications is being supplied through the Electric Power Research Institute (EPRI) by a Japanese consortium composed of the New Energy and Industrial Technology Development Organization, the Tohoku Electric Power Company, the Chubu Electric Power Company, the Chugoku Electric Power Company, the Kyushu Electric Power Company and the Electric Power Development Corporation.

The potential to reform natural gas on the cell surface coupled with inherent modularity and simplicity of system configuration makes the SOFC a candidate for use in smaller on-site power plants as well. Because of the high operating temperature, there exists the concurrent potential for the cogeneration of usefully applied thermal energy in addition to electricity.

In the latter part of 1986, Westinghouse signed a contract with the Gas Research Institute to develop SOFC technology specifically for use with natural gas and directed toward applications in the commercial and industrial cogeneration market (20 kWe to 2 MWe). The primary objective of the GRI contract was the development of an SOFC generator that can consume natural gas directly - without the need for a separate fuel processing system. A 3 kW generator was designed, fabricated and successfully tested at Westinghouse as part of the GRI program. The GRI program was expanded in mid 1987 to include the study of applications and markets, and the development of conceptual designs and cost estimates for on-site cogeneration applications in the power range from 20 kWe to several megawatts. This effort was sponsored by a consortium of gas utilities in Japan (Tokyo Gas, Osaka Gas, Toho Gas) in cooperation with the Japanese New Energy and Industrial Development Organization (NEDO).

In 1989/90, the GRI program was further expanded to study alternate means of introducing fuel gas into the SOFC generator. Combined with the concept of spent fuel recycling, Westinghouse is continuing to develop distributed reforming under sponsorship from both the U.S. DOE and GRI.

The U.S. DOE program and the GRI program, along with EPRI/NEDO and several utility sponsored programs, are integral parts of the Westinghouse Commercialization Plan for the tubular SOFC technology.

PROGRAM ACCOMPLISHMENTS

Significant developments and accomplishments have occurred throughout the tubular SOFC program. Important technical milestones achieved include:

- Invention of practical cell and generator module configurations.
- Demonstration of stable performance and lifetime in excess of 8,700 hours for a three cell stack.
- Fabrication and operation for 2,000 hours of a 400 watt, 24 cell module.
- Demonstration that hundreds of tubular solid oxide fuel cells can be fabricated with consistent and reproducible performance.
- Continuous operation of a 3 kWe tubular SOFC system for over six months at a customer's test site.
- Demonstration of stable performance and lifetime in excess of 5,300 hours for a 3 kWe generator module, operating directly on non-humidified desulfurized natural gas.
- Demonstration of stable performance and life times in excess of two years in continuous single cell tests.
- Design and construction of a dedicated cell, module and generator fabrication facility with the capacity to produce 10,000 cells per year.
- Successful 5,000 hour and ongoing multi-cell (36 cells) bundle tests of 50 cm. long cells produced at the Pre-Pilot Manufacturing Facility (PPMF).
- Significant improvements in cell performance and life and marked reduction in cell degradation.

- Design and initiation of construction of a 20 kWe tubular solid oxide fuel cell generator module with completion and test planned in 1990.

- Development of a conceptual design for a 250 MWe tubular SOFC power plant fueled with coal-derived fuel gas.

- Development of a conceptual design for a 300 MW LNG/ tubular SOFC-Steam Turbine power plant, for electric utility applications in Japan.

Table 1 below summarizes the major accomplishments of the past and the current commitments:

THE PRE-PILOT MANUFACTURING FACILITY

A major programmatic milestone in the Westinghouse SOFC development program occurred in the latter part of 1986 when Westinghouse corporate management approved the construction of a Pre-Pilot Manufacturing Facility (PPMF). This 30,000 square foot facility is located near Pittsburgh (Monroeville) and has the capacity to produce 10,000 solid oxide fuel cells per year.

SOFC generator module production began in 1989 at the PPMF and represents the transfer of SOFC technology from the laboratory to a manufacturing environment. The PPMF will enable Westinghouse to put in place the processes and quality control programs that will be required to commercialize the technology during 1990's.

Table 1. Summary of Westinghouse Program Accomplishments and Commitments.

Event	Achieved	Committed
Cell-13 Watt, 20 cm Length	1981	
3-Cell Life Test	1983-4	
Cell-20 Watt, 30 cm Length	1985	
24 Cell Bundle Test (2,000 Hrs.)	1985	
5 kWe Generator (500 Hrs.)	1986	
Cell-24 Watt, 36 cm Length (9,200 Hrs.)	1986-7	
Cell-24 Watt, 36 cm Length, Natural Gas (2,200 Hrs.)	1987	
Cell-33 Watt, 36 cm Length (9,400 Hrs.)	1987-8	
Cell-33 Watt, 36 cm Length (18,000 Hrs.)	1990	
36 Cell, 50 cm Length Bundle Test, PPMF Produced Cells (2,500 Hrs. and Continuing)	1990	
SYSTEM EXPERIMENTAL UNITS:		
TVA 400 Watt (1,760 Hrs.)	1986-7	
Osaka Gas 3 kWe (3,000 Hrs., 2,600 Hrs. +)	1987-8	
Tokyo Gas 3 kWe (4,900 Hrs.)	1987-8	
36 Cell Bundle Test, Natural Gas Fuel (1,800 Hrs.)	1988	
Pre-Pilot Manufacturing Facility Construction	1988	
Pre-Pilot Manufacturing Facility Operation	1989	
GRI Natural Gas Fueled 3 kWe Generator (5,500 Hrs.)	1990	
Multi-kW Generator (DOE 20 kWe)		1990

FUTURE ACTIVITIES

The existing contract between Westinghouse and the Department of Energy is scheduled to end in December, 1990 following completion of the Multi-Kilowatt Generator. Westinghouse has presented a proposal to DOE to continue the tubular solid oxide fuel cell technology and generator development to the point that it represents an acceptable risk for Westinghouse to commercialize solid oxide power generation technology. The proposed 5 year program includes considerable financial contributions from Westinghouse, from domestic and foreign utilities, and from other agencies, in addition to the U.S. Department of Energy.

PLANAR SOFC DEVELOPMENT AT THE NETHERLANDS ENERGY RESEARCH FOUNDATION ECN

J.P.P. Huijsmans, E.J. Siewers and S.B. van der Molen
ECN, P.O. Box 1, 1755 ZG Petten, The Netherlands

INTRODUCTION

Within the framework of the CEC fuel cell R&D programme, ECN is developing planar type SOFC technology in two cooperative projects: one with the University of Twente (The Netherlands) and one with Siemens AG (Germany). The first project started in 1989 (1) and aims at the reduction of cell operating temperature. Final goal of the project is the development of a supported air-electrode (ECN) on which a thin layer of Y_2O_3-stabilized ZrO_2 (YSZ) will be deposited by (E)CVD (Univ. of Twente). The project with Siemens AG started recently and aims at the development of a 1 kW SOFC stack with metal separator plates. ECN's contribution concerns ceramic-component development and -testing. Final goal of the project is a 1 kW cell test in 1993 by Siemens. Sub-contractors in this project are GEC Alsthom Engineering Research Centre and Imperial College, both from UK.

SOFC MATERIALS DEVELOPMENT

Cathode development

Batch-wise and continuous processes have been investigated for the fabrication of $La_{1-x}Sr_xMnO_3$ cathode powders (LSM with x=0.15, 0.30 or 0.50), i.e. oxide-mix, liquid-mix, citrate pyrolysis (2), co-precipitation, spray-drying and spray-roasting. The reason was: 1/ to get experience with the power processing and 2/ to obtain a wide spectrum of powder morphologies available. For our current investigations we favour the citrate pyrolysis technique and we have systematically investigated powder properties. Calcination temperatures are in the order of 850 - 1000°C.

Pellets were pressed at 150 MPa and electronic conductivity was determined as a function of density and Sr-content using a four-probe technique (3). Results are shown in Fig. 1. Variation in density was obtained by sintering different batches of pellets in air between 1000 and 1300°C. From Fig. 1 it is concluded that for $d/d_{th} < 0.30$, the electronic conductivity is very low, irrespective of the Sr-content. We have also measured electronic conductivity of tape cast, thin (30 µm) layers of 15LSM. Conductivity is 23 S/cm, which implies that the sintered structure has a porosity of about 60% (Fig. 1). A minimum electronic conductivity for SOFC cathode material, which is often referred to in the literature (e.g. 4) is 100 S/cm. From this number and the data in Fig. 1 it follows that a cathode structure of e.g. 15LSM can have a maximum porosity of 30%. However, electronic conductivity of LSM is high compared to the ionic conductivity of YSZ (0.01-0.02 S/cm) (5). Therefore, in a flat plate design ohmic losses of the cathode can be neglected and the observed conductivity of tape cast LSM layers is considered to be sufficient.

An important observation, which resulted from the sintering experiments, is, that an increasing Sr-content has a

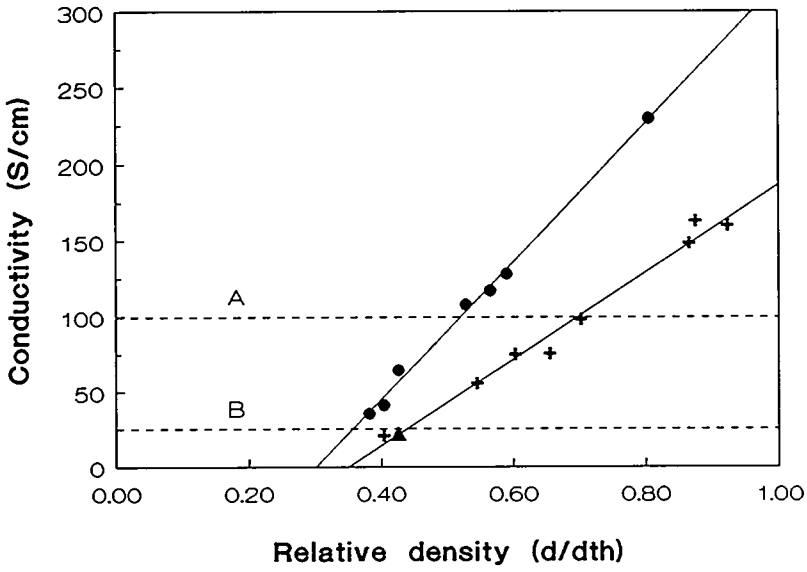

Fig. 1. Electronic conductivity of pressed pellets of LSM powder as a function of porosity, i.e. (1- d/d_{th})*100%, in which d=observed density, d_{th}=theoretical density. + = 15LSM; • = 50LSM; ▲ = tape cast 15LSM. A = required minimum conductivity LSM from literature (4). B = estimated required conductivity for flat plate concept.

negative effect on the densification behaviour, i.e. higher sintering temperatures are needed for 50LSM to obtain a similar density compared to a sintering treatment for 15LSM. This was also observed for LSM samples made by tape casting. In conclusion it is stated that a sintering temperature of 1100°C for a tape cast 15LSM citrate powder is sufficient to obtain a strong, porous micro-structure.

Anode development

For the fabrication of Ni-zirconia cermets commercially obtained NiO powder was attrition milled, yielding an average agglomerate size of 2 µm. In addition, this powder was mixed with 8YSZ from Tosoh by ball milling, to obtain cermets with Ni-contents between 30 and 70 vol.%. The mixed powders were pressed to pellets and fired in air at 1300°C. In addition, NiO was reduced to metallic Ni at 1000°C. After reduction the open porosity ranged from 29 to 43 % for respectively 40 to 70 vol% Ni. Electronic conductivity of the cermets was determined in a reducing atmosphere (H2) with the four-probe device mentioned above (3). Fig. 2 shows conductivities as a function of vol% Ni. Below 40 vol% Ni no electronic conductivity could be detected,

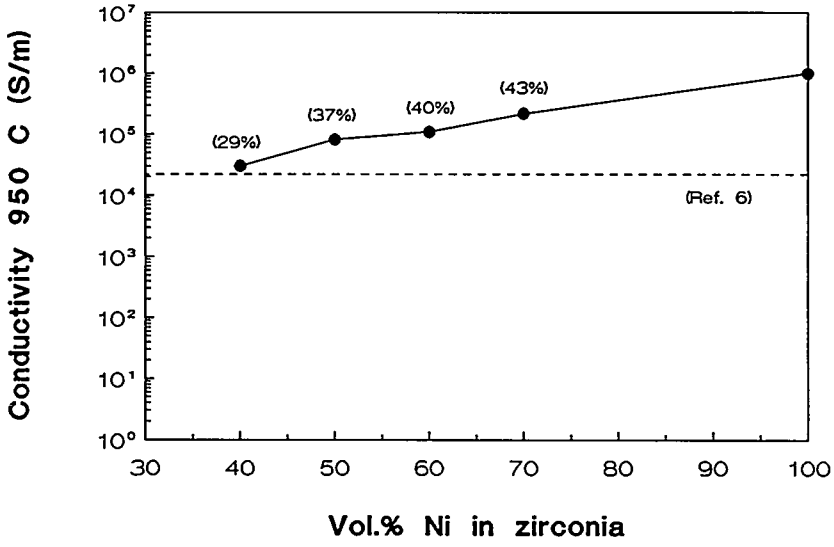

Fig. 2. Electronic conductivity of Ni-8YSZ cermets as function of vol% Ni in zirconia. Stippled line is required minimum value (6). Figures between brackets are measured porosities after reduction. For comparison conductivity of pure nickel (porosity 16%) is also given.

whereas between 40- and 70 vol%, the observed electronic conductivity is better than the required minimum value of 120 S/cm (6).

SOFC CELL DEVELOPMENT

Ceramic composite development

Presently, tape casting is used by ECN to manufacture SOFC ceramic composits. First, the YSZ electrolyte is tape cast, densified by firing in air at 1500°C and characterized. Experiments were carried out with zirconia powders from different suppliers. On the moment we fabricate flat, sintered electrolyte foils up to 5x5 cm2, which are $\geq$97% dense. Sintering shrinkage (25%) of these foils is controlled by careful binder burn-out and by the use of very smooth carrier materials. We are able to fabricate sintered thicknesses from 150 down to 100 µm.

The sintered electrolyte is coated with electrode structures in a two-step tape casting process, using a masking technique which centers the electrodes on both sides. Along the edges the electrolyte is not coated because of sealing purposes. Firing of the electrolyte/electrode composite occurs in air at

temperatures that ensure bonding to the electrolyte but prevent degradation of the micro-structure or the formation of deleterious reaction products on the interfaces. Sintering temperatures are 1300°C for the anode and 1100°C for the cathode respectively and R&D is going on to combine the sintering steps of the two electrodes. Reduction of the anode occurs during cell operation.

Cell testing

Testing of the ceramic materials is carried out in smale cells with an electrode area of 3 cm^2. On the moment we have concentrated on testing electrolyte/cathode composites in terms of micro-structure degradation and reactivity between the two components during cell operation. Post test analyses of small cells, which had been operated for more than 800 hrs, did not show degradation or chemical reaction. Similar experiments are carried out now with three layer composites.

In addition, cell testing is foreseen in bench cells with an electrode area of 5 x 5 cm2 and 10 x 10 cm2. Thickness of the electrolyte will be in the order of 150 - 100 µm. For these tests a metal separator plate will be developed. The required metal composition, i.e. a high temperature alloy with coefficient of thermal expansion close to YSZ, will be developed by Siemens (5). Materials for sealing the cell along metal/electrolyte contacts will be developed by GEC. For ECN the manifold design will be based on our MCFC separator plate, and fabrication methods for the plates will be rather simple, e.g. machining. For the gas distribution the active area of the separator plate will be corrugated. However, ECN will investigate the possibility of coarsely porous, electrode support structures for gas distribution in a thin catalytically active electrode layer.

ACKNOWLEDGEMENTS

Financial support from the CEC (Non-nucelar Energy R and D Programme: contracts EN3E-0173-NL and JOUE-048-C) is gratefully acknowledged.

REFERENCES

1. J.P.P. Huijsmans, S.B. van der Molen and E.J. Siewers, "Membrane-based thin layer SOFC components". In "Euro-Ceramics" , eds. G. de With et al., Vol. 3, Elsevier Science Publ. Ltd, London, pp. 3.626-3.630, 1989.
2. L.G.J. de Haart and K.J. de Vries, Final Report CEC proj. EN3E-0167-E/EN3E-168-P, July 1989.
3. L. Plomp, A. Booy, J.A.M. van Roosmalen and E.H.P. Cordfunke, "A four-probe ac apparatus for the high-resolution conductivity measurement of ceramic oxides at high temperatures", Rev. Sci. Instrum., Vol. 61, No. 7, pp. 1949-1953, 1990.
4. B.C.H. Steele, "Ceramic electrochemical reactors (CER) - Current status and applications", pp. 59, Ceramionics, Surrey, 1987.
5. W. Wersing, E. Ivers-Tiffee, M. Schiessl and H. Greiner, "New planar solid oxide fuel cell with metallic bipolar plate", Proc. Intern. Sym. Soli oxide fuel cell, Nagoya/Japan, pp. 21-26, Nov. 1989.
6. T.E. Easler, B.K. Flandermeyer, T.D. Claar, D.E. Busch, R.J. Fousek, J.J. Picciolo and R.B. Poeppel, "Electrode development for monolithic fuel cells", Abstract of 1986 Fuel Cell Seminar, Tucson, Arizona, Oct. 1986.

TONEN TEST OF PLANAR SOFC

T. Hoshina, T. Yoshida, S. Sakurada
Tonen Corporation
1-3-1, Nishi-tsurugaoka Ohi-machi,
Iruma-gun, Saitama 354, JAPAN

Introduction

The research on planar SOFC in Tonen Corporation started in 1987, and has been continued industriously as one of the answer to a cleaner environment. Partially stabilized zirconia (PSZ) which is doped 3 mol% yttria has been used as solid oxide electrolyte. Conductivity of PSZ is lower than that of fully stabilized zirconia (FSZ) at 1000°C. However PSZ possesses high strength and high toughness despite the fact that FSZ is brittle. The ability of SOFC using PSZ and features of stacked cells are summarized below.

Single cell with 0.5 cm^2 electrode area

Fig.1 shows the structure of single cell with 0.5 cm^2 electrode area. The main object of this examination was feasibility study to use PSZ as electrolyte of SOFC. The PSZ consists of 85 mol% tetragonal phase and 15 mol% cubic phase. In general, the PSZ plate has 25 mm in diameter with thickness of 0.2 mm, and is spread with anode slurry on one side and with cathode slurry on the other side. The slurries contain electrode powder, some binder and some solvent. Hydrogen and oxygen are used as fuel and oxidant, respectively. Gas seals are obtained by glass rings which soften at operating temperature. The cell is operated at 1000°C. Pt wires and meshes are used as current collector.

Extremely large power density of over 500 mW/cm^2 has been obtained(1). The effect of alumina additions on the electrical properties of yttria doped zirconia(2) or of Pt additions on the resistance of $La_{0.9}Sr_{0.1}MnO_3$ cathode(3) has also been tested by this structure.

Single cell with 25 cm^2 electrolyte area

Several configurations of single cell with 25 cm^2 electrolyte area have been tested in Tonen Corporation. Most suitable structure in the state of the art is shown in fig.2. The cylindrical manifold made of high purity alumina is cut to fit separators. The separators have about 2 mm thick and are made of alloy which has resistance to heat. The thermal expansion of the separator differs from that of PSZ, therefore glass seal was applied to Tonen's cell. Glass is softened at 1000°C and seals the clearance between separator and PSZ or manifold. Fuel and oxidant are supplied through pipes, respectively, and exhausted from opposite side ones. The cell

has 18 cm^2 active area.

The open circuit voltage was about 1.2 V. It indicates that glass keeps enough tight to seal gases. The power obtained by this assembly was about 3.5 W at typical conditions. The maximum power was over 5 W using 0.1 mm thick zirconia plate. Life test revealed that the cell power decreased slightly during continuous operation.

Ten cells stack with 100 cm^2 electrolyte area

Ten cells stack with 100 cm^2 electrolyte area each has a similar structure to the single cell with 25 cm^2 electrolyte area, shown in fig.3. Both electrodes on the PSZ plate have thickness of 0.1~0.3 mm. The stack is fabricated to pile up separators and unit cells alternately. This easiness about fabrication of stack is one of advantages of planar SOFC.

The I-V curve shown in fig.4 was measured immediately after the stack started. After two hours from the I-V measurement, the maximum power of 194 W was obtained in the condition that fuel utilization was 30% and oxidant utilization was 15%. Each cells performances were measured independently. Difference among them were under 10%.

Conclusion

1. The results of single cell tests showed the advantages of planar SOFC in regard to power density and fabricatability.
2. The 200 W class planar SOFC was substantiated, and volumetric power density was about 0.7 kW/l .
3. It seems that the glass used as sealant is very important key material for planar SOFC.

References

1. T. Yoshida et al, "Properties of Partially Stabilized Zirconia Fuel Cell," J. Electrochem. Soc., Vol. 136, No. 9, pp 2604-2606, 1989.
2. F. Ishizaki et al, "Effect of Alumina Additions on the Electrical Properties of Yttria-Doped Zirconia," - Proceedings of the first international symposium on Solid Oxide Fuel Cells, p 3-14, Dec. 1989.
3. A. Tsunoda et al, "Effect of Pt Additions on the Resistance of $La_{0.9}Sr_{0.1}MnO_3$ Cathode," - Proceedings of the first international symposium on Solid Oxide Fuel Cells, p 204-213, Dec. 1989.

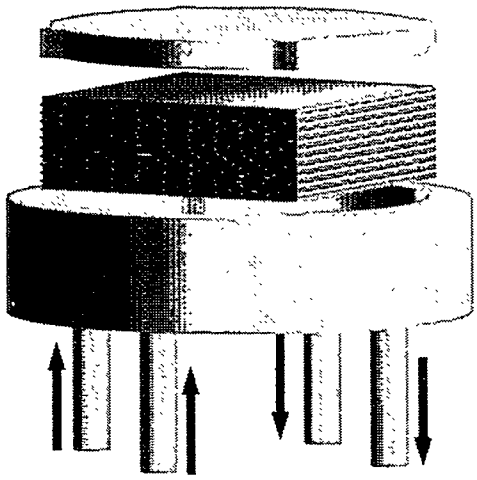

fig.3 Ten cells stack with 100 cm^2 electrolyte area

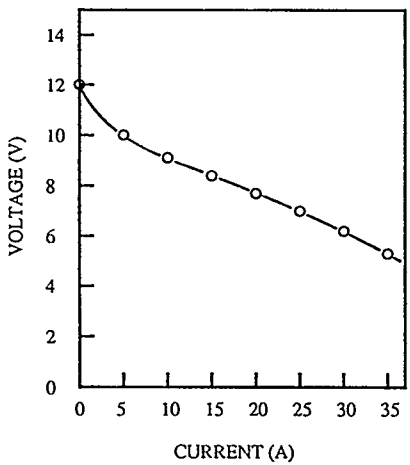

fig.4 I-V curve of ten cells stack

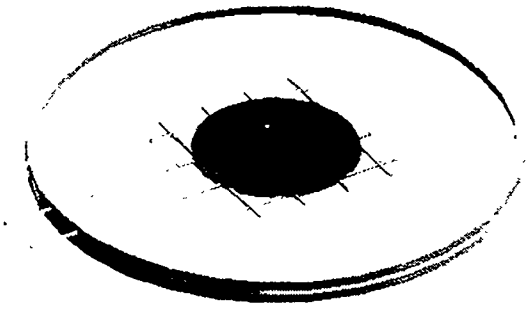

fig.1 Single cell with 0.5 cm^2 electrode area

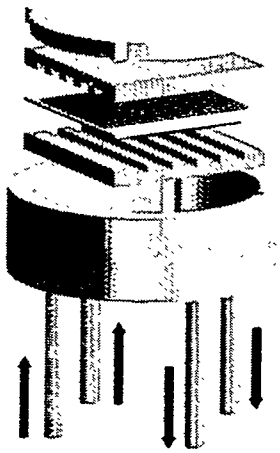

fig.2 Single cell with 25 cm^2 electrolyte area

DEVELOPMENT OF MOLB TYPE SOLID OXIDE FUEL CELL

T. Inoue, H. Yoshida and Y. Esaki
Electric Power Research & Development Center
Chubu Electric Power Company, Inc. Nagoya, Japan
H.Miyamoto and M.Ishibashi H.Haneda and K.Takenobu
Takasago R&D Center Kobe Shipyard and Machinery Works
Mitsubishi Heavy Industries, LTD., Japan
Hiroyasu Iwahara
Nagoya University, Nagoya, Japan

1. INTRODUCTION

Fuel cell development is accelerated in recent years primarily due to its high efficiency, silent operation and minimal enviromental effect. Especially solid oxide fuel cell (SOFC) is receiving much more attention due to various excellent characteristics. Among several types of SOFC, MOLB ≠(Mono-block layer built) type SOFC will provide the following advantages, which promise a large scale power plant;

1) suitable for mass production 2) able to obtain higher power density

2. OUTLINE OF MOLB TYPE SOFC

2.1 HISTORY OF THE RESEARCH AND DEVELOPMENT

Mitsubishi Heavy Industries, Ltd. (MHI) started fundamental study on SOFC since 1984 first for tubular cell, under the guidance of Electro Technical Laboratory, Tsukuba Japan. At 1986, 500W module test with exhaust fuel reburner was carried out successfully without any external electric heat in its Kobe shipyard and Machinery Works. Through this study, fundamental properties on SOFC were obtained. Since the end of 1986, studies started on MOLB type SOFC. And the generation tests by MOLB type SOFC was succeeded in 1988. Chubu Electric Power Company, Inc.(CEPCO) paid attention to the advantage of MOLB type SOFC and commenced the evaluation generation testing at its laboratory in 1989. In 1990, MHI and CEPCO finaly agreed to jointly develop and evaluate it. The study involves development of cell components, evaluation test of MOLB stack and MOLB module and feasibility study of 10 kW class SOFC. Each company evaluates the results with different standpoint as an user and as a manufacturer. Professor Hiroyasu Iwahara of Nagoya university has given the appropriate theoretical advise throughout its development since 1986. Present goal of module generation test is 1 kW class test in 1991.

2.2 STRUCTURE OF MOLB TYPE SOFC

As shown in Fig.1, the cell consists of electrolyte (Yttria Stabilized Zirconia; YSZ), anode (Ni/YSZ cermet), cathode ($La_{1-x}Sr_xMnO_3$;LSM) and interconnecter ($La\ Mg_x\ Cr_{1-x}O_3$; LMC). Two kinds of sealing are now adopted, one is called as fixed type, where flat YSZ bars are adhered with cell and interconnecter, the other is called as slide type, where special packing material enables cell to slide from interconnecter. The MOLB type SOFC is optimized through calculating distributions of flow, current density, temperature, and thermal stress, using the recent advanced three dimensional computing technology.

≠ MOLB is a trademark and it is under registration in several countries such as United States, European Communities, Australia besides Japan.

2.3 ULTIMATE PERFORMANCE TARGET OF MOLB TYPE SOFC

Gas diffusion characteristics in SOFC elements, especially the transport phenomena in cell electrodes and gaseous leakage through solid oxide electrolyte, have been studied by a simulation model shown in Table 1 and Fig.2. The model which provides concentration profiles at the interface between electrode and electrolyte can predict cell performance through evaluating concentration polarization in SOFC. And this mathematical model includes a contact model at the electrode-electrolyte interface; degree of sintering. Detailed discussion are described in Reference (1). Using this mathematical model ultimate performance target of the structure for MOLB type SOFC was compared with the values of tubular types of SOFC, where MOLB type SOFC attains superiority over them.

3. CELL AND STACK PERFORMANCE

Fundamental studies using ϕ23mm single cell improved cell performance rapidly. Figure 3 shows an example of cell V-I characteristics, which has 2 A/cm^2 of short circuit current (Imax). Here, temperature, fuel gas constituents, oxdizing gas constituents are 1000℃, 50% H_2 mixed with 50% N_2 and 100% air respectively. Figure 4 illustrates three V-I characteristics for MOLB stacks (fixed type) which had □60mm in dimensions, 16cm^2 in effective area, and two, nine, and ten cells respectively. Other operating conditions were the same as that of single cells. These stacks showed 590, 384 and 344 mA/cm^2 of short circuit current density. Figure 5 shows 650 hour continuous generation test data for the □60mm stack having two cells. Open circuit voltage showed no deterioration, whereas short circuit current decreased 20% after 650 hour. Figure 6 shows test apparatus. Now stack size is enlarged and □75mm×2 cells and □150mm×10 cells stacks (Figure 7) are under test.

4. SYSTEM DESIGN FOR LARGE CAPACITY SOFC

The conceptual design works on 10 kW SOFC was carried out (Figure 8). A MW class SOFC system will be expected to offer 60 ~ 65% efficiency (on HHV). More detailed studies on a MW class SOFC system and 300 MW class SOFC system feasibility study will be carried by March 1991 (Figure 9).

5. CONCLUSION

1) Newly proposed SOFC, named MOLB type, shows great possibility for large scale power plant; because of easier manufacturing and higher performance.
2) Chubu Electric Power Co.Inc. and Mitsubishi Heavy Industries, Ltd. started collaboration work since May 1990 for the development of MOLB type SOFC.
3) MOLB stacks of □60mm, having two to ten cells, showed excellent performance. Now scale up to □150mm is under test.
4) System design for large capacity SOFC are performed.

REFERENCE

1. H.Miyamoto, M.Ishibashi, H.Nakatani, N.Tomita and H.Iwahara, "Gas Diffusion in SOFC Elements", Proc.Int. Symp. SOFC, 1989.

Fig.1 MOLB type SOFC structure

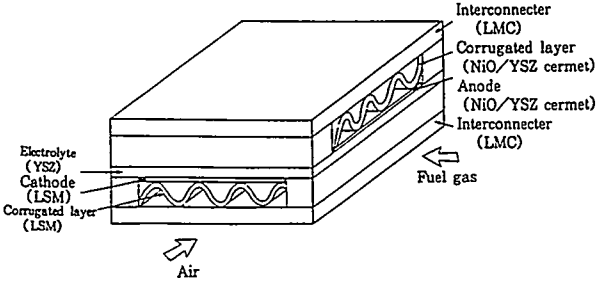

Table 1 Phenomena in SOFC and modeling

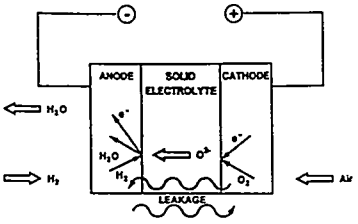

		Anode	Electrolyte	Cathode
Mass transfer	Phenomena	Diffusion of H_2 and H_2O	Molecular Transport of gases	Diffusion of O_2 and N_2
	Equations	Fick's law		
Charge transfer	Phenomena	Electron transfer	Diffusion and Migration of O^{2-}	Electron transfer
	Equations	Maxwell eq.	Nernst-Planck eq.	Maxwell eq.

Fig.2 Modeling of interface

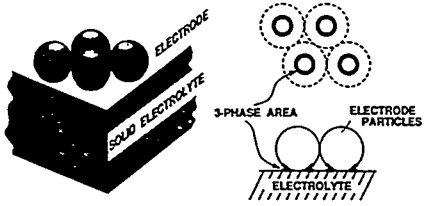

Fig.3 ϕ23mm cell test (5/1989)

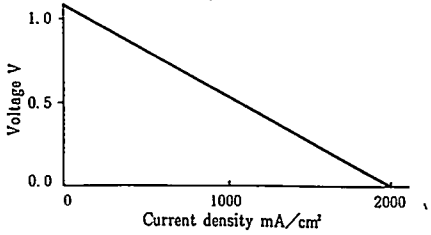

Fig.4 □60mm MOLB type stack test

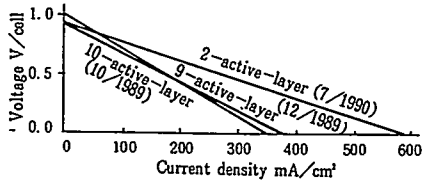

Fig.5 □60mm×2-active-layer MOLB type stack (Fixed type)
650-Hour Continuous Generation Test
(7/1990)

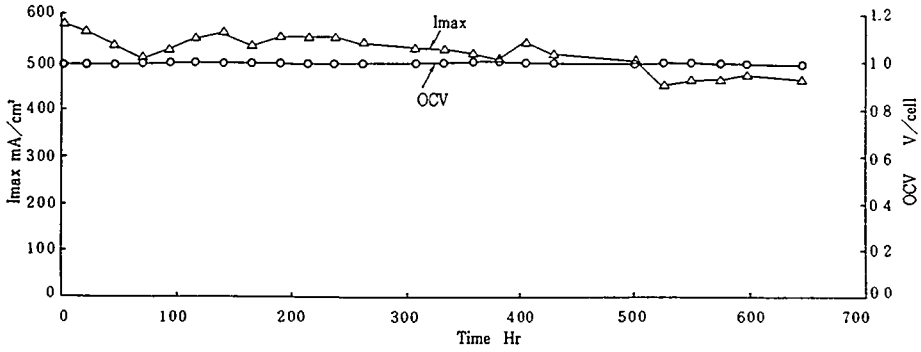

Fig.6 Stack performance test module

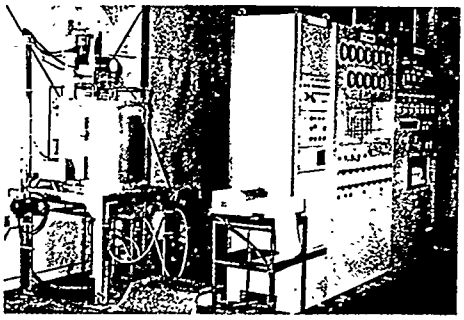

Fig.7 □150mm×10-active-layer MOLB type stack
(7/1990)

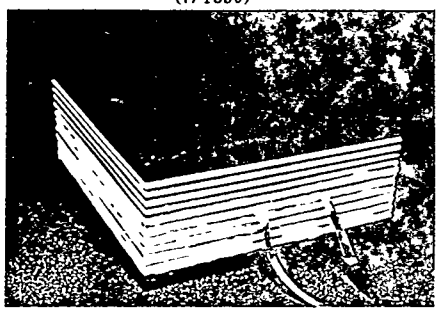

Fig.8 MOLB type SOFC 10kW class generator module

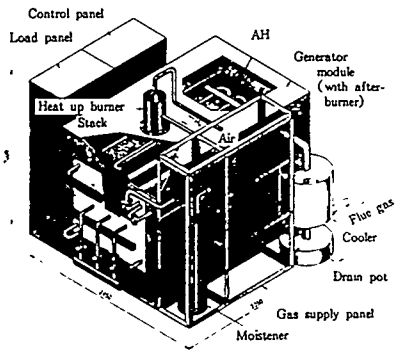

Fig.9 MOLB type SOFC 300MW class power plant

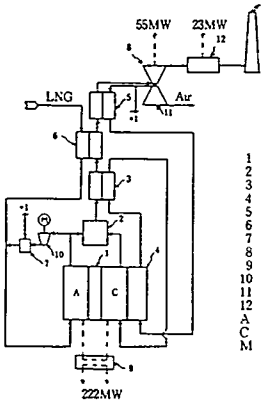

1 SOFC
2 Exhaust fuel reburner
3 High temp AH
4 AH at cell
5 Low temp AH
6 Fuel gas heater
7 GR combustor
8 Gas turbine
9 Inverter
10 GR compressor
11 Air compressor
12 Flue gas boiler
A Anode
C Cathode
M Motor

MONOLITHIC SOLID OXIDE FUEL CELL TECHNOLOGICAL STATUS

Nguyen Q. Minh, Timothy R. Armstrong, James V. Guiheen, Craig R. Horne, Felix S. Liu, Dawne M. Moffatt, Thomas L. Stillwagon, and James J. Van Ackeren

Allied-Signal Aerospace Company, AiResearch Los Angeles Division
2525 West 190th Street
Torrance, California 90504-6099

INTRODUCTION

The monolithic solid oxide fuel cell (MSOFC) is an all-ceramic structure in which cell components are fabricated in a compact, corrugated array. Small cell size, self-supporting corrugated structure, and thin components are the key characteristics of the MSOFC design. The MSOFC offers excellent prospects for a variety of applications, ranging from multimegawatt electric utilities to kilowatt-sized aerospace power systems. The feasibility of the MSOFC has been demonstrated on a small laboratory scale. In the past few years, considerable research and development have been carried out to extend the MSOFC from proof of concept toward technology demonstration. The major efforts have been focused on developing suitable materials and fabrication methodologies, defining material and process quality assurance requirements, and demonstrating cell performance under specified conditions. Other work on the MSOFC includes stack performance modeling and stress analysis. The status of MSOFC stack fabrication and material research and development is briefly discussed in this extended abstract.

STACK FABRICATION

Recent MSOFC fabrication has been concentrated on making crossflow stacks. A fabrication sequence based on tape calendering is used to produce the fuel cell structure. A schematic diagram of the tape calendering method is shown in Figure 1. Basically, tape calendering is a forming process in which ceramic powder and organic binder are dispersively mixed to form a plastic mass and then rolled into thin

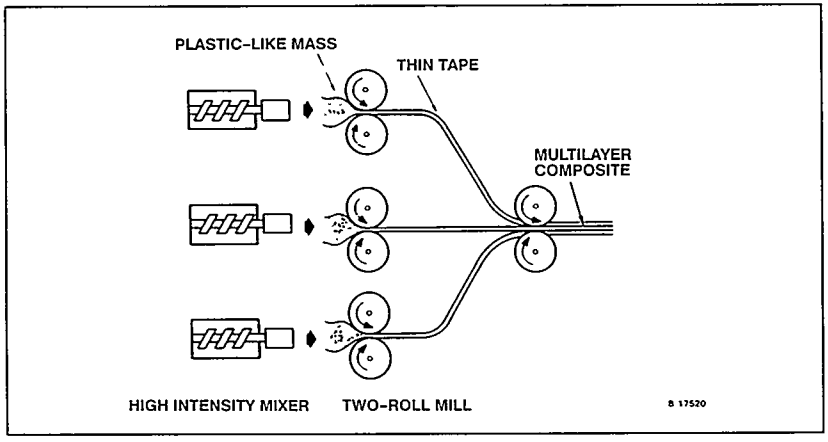

Figure 1. Schematic Diagram of Tape Calendering

tape using a two-roll mill. The process is being developed and optimized to allow cofiring of various cell components into the sintered MSOFC structure. The development of the tape calendering process for the MSOFC includes the following: (1) tailoring starting powder characteristics (particle size and particle size distribution, surface area, morphology) to impart the required properties, (2) defining ceramic powder/organic binder formulations to have the desired formability and sinterability, and (3) optimizing mixing and rolling conditions to foster defect-free tapes with a minimum amount of particle agglomeration. The objective is to match the thermal behavior (firing shrinkage and thermal expansion) of cell components during firing and, at the same time, to achieve the desired stability, porosity/density, and mechanical properties for all the layers. Firing methodologies are also being developed to sinter the green bodies without structural defects.

Crossflow MSOFC stacks have been formed with calendered tapes. Figure 2 shows the cross-section of a green stack, cut perpendicular to the anode corrugations. As can be seen from the figure, the uniformity of the components and the bonding between the layers are excellent. To date, crossflow stacks of several sizes have been produced. Examples of sintered stacks are shown in Figures 3 and 4. Figure 3 is a photograph of a sintered two-cell stack. A photograph of a sintered eight-cell stack and a sintered ten-cell stack is shown in Figure 4. In general, the stacks show well-defined corrugations, open passages, and no visible cracking.

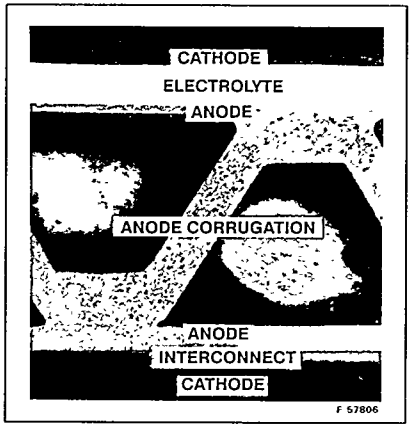

Figure 2. Polished Cross-Section of a Green, Crossflow Stack

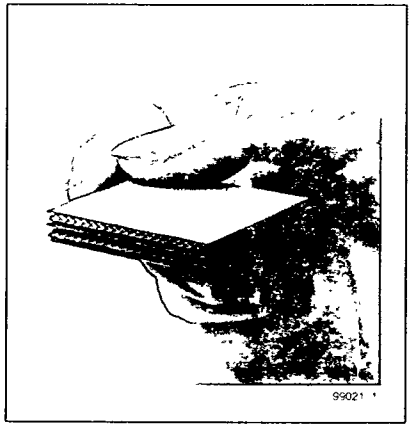

Figure 3. Two-Cell Stack

MATERIAL RESEARCH AND DEVELOPMENT

Another major technical effort on the monolithic fuel cell is development of suitable materials for the unique MSOFC structure and environment. Several issues are being addressed: interconnect sinterability, material stability and performance, and material quality control.

Interconnect sinterability: Highly reactive starting powder, various dopants, and sintering aids are the approaches being pursued to densify the lanthanum chromite interconnect at temperatures below 1400°C in oxidizing atmospheres. These ap-

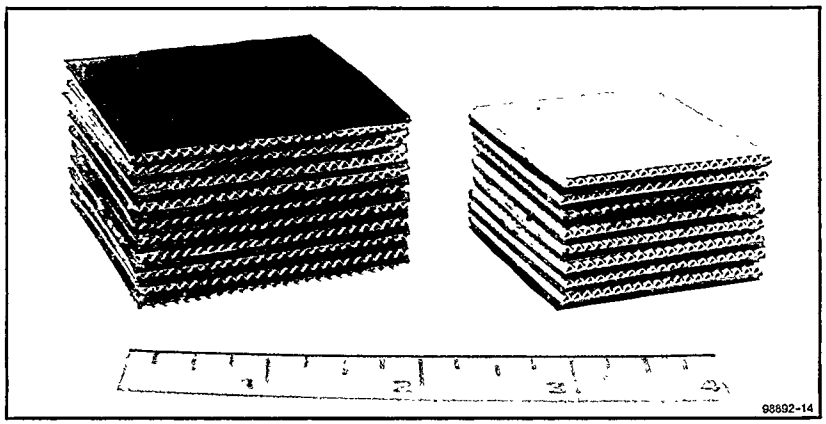

Figure 4. Sintered Eight-Cell and Ten-Cell Crossflow MSOFC Stacks

proaches have been found to be effective in enhancing interconnect sinterability. However, the current difficulty is the problem of elemental migration from the interconnect material to other parts of the fuel cell during sintering, preventing interconnect densification and also causing chemical and morphological changes in the electrode layers.

Material stability and performance: Studies on long-term cathode stability and effects of sulfur on anode performance have been initiated. Electrodes and electrode/electrolyte interfaces have been modified to reduce interfacial resistances. Modifications to interfacial characteristics such as porosity, morphology, bonding, and active material distribution have significantly improved interfacial resistances.

Material quality control: Quality control of starting materials is critical in the fabrication of the MSOFC. The material quality control effort is thus concentrated on the development of material specifications. Baseline specifications have been developed for all the materials required to produce the fuel cell structure. The material specifications document characteristics, composition, and quality requirements for each of the starting materials. The material specifications define material requirements and limits to ensure reliable and reproducible fabrication of the MSOFC.

ACKNOWLEDGMENTS

The work is supported by the Department of Energy/Morgantown Energy Technology Center and Allied-Signal.

Planar Solid-Oxide Fuel Cell Design, Characterization, and Investigation

Meilin Liu, Ashok Khandkar, and Mark Timper

Ceramatec, Inc.
2425 South 900 West
Salt Lake City, Utah 84119

1. Introduction

The operation of a fuel cell, in general, involves mass transfer and charge transfer processes near or across the electrode/electrolyte interfaces. Accordingly, the overall response of a cell under certain perturbation typically reflects the complexity of the processes in the system and thus, it is very difficult, if not impossible, to extrapolate useful information about each individual process. Reliable characterization of each individual process is crucially important to the identification of the limiting factor to the performance of a cell and hence to the effective improvement of cell performance. Recently, experimental isolation in performance of each individual cell component, anode, cathode, electrolyte, current collector, and interconnect materials, has been successfully accomplished in our laboratory through unique test cell design, proper positioning of reference electrodes, together with appropriate electrochemical techniques, such as 4-probe impedance spectroscopy, current-interruption methods, potential sweep techniques, and galvanostatic testing. A number of fundamental studies of solid oxide fuel cells, based on several specially designed test cells, is being actively conducted at Ceramatec. These studies include electrode kinetics and electrocatalysis of oxygen reduction, hydrogen oxidation, and oxidation of methane; transport properties of electrolyte materials; stability and electrical properties of interconnect materials, and the behavior of current collector materials. The purpose of this paper is to present (i) cell design for isolation in performance of each cell component, (ii) appropriate techniques to characterize various individual processes, (iii) error analysis, (iv) illustrative characterization of electrode kinetics, transport properties, as well as the behavior of interconnect materials for multi-layer stacking, and (v) characteristic performance of planar solid oxide fuel cells.

2. Experimental

Tape-cast yttria-stablized zirconia (YSZ, 8 mole % Y_2O_3) were used as electrolyte throughout the study. The electrode materials evaluated in this study include modified $La_{(1-x)}Sr_xMnO_3$ and $La_{(1-x)}Sr_xCoO_3$ for oxygen reduction and nickel-based (NiO/ZrO_2) electrodes for fuel oxidation. Slurry of electrode materials were screen printed on electrolyte discs and subsequently fired at high temperatures (1150-1350°C). Electrochemical cells designed for this investigation include regular fuel cells ($O_2/YSZ/H_2$), oxygen concentration cells ($O_2/YSZ/O_2$), and cells incorporating interconnect materials.

Performance isolation of each cell component was accomplished using 4-probe impedance spectroscopy. Ohmic drop across a single interface was validated using current-interruption techniques. In addition, the potential decay in a current-interruption experiment also provide valuable information about electrode kinetics (1). Potential (or current) sweep or step methods were further used to confirm the current-interruption and impedance measurements. I-V characteristics of fuel cells were determined using galvanostatic, potentiostatic, as well as load testing methods.

Solartron 1255 (frequency response analyzer) and 1286 (electrochemical interface) impedance analysis system, interfaced with an IBM PC/386, were used to measure the impedance of cells or interfaces in the frequency range from 10 mHz to 1 MHz. Tektronix 50MHz storage oscilloscope was used to record the potential response in current-interruption measurement.

3. Results and Discussion

Cell Design: Shown in Figure 1 is one of the cell configuration used routinely to separate the performance of the electrolyte, the anode-electrolyte interface, and the cathode-electrolyte interface. Similar cell configuration was also used to isolate the performance of the interconnect materials, the anode-interconnect interface, cathode-interconnect interface, and the bonding materials between two cell components. While perturbation input signals were applied to a whole cell, the response was monitored only across a single interface with the appropriate positioning of two reference electrodes. Thus, the response (impedance, overpotential, etc.) observed is only dependant on a single interface rather than on the overall cell and the complication associated with multi-interface or multi-time-constant processes was effectively minimized or eliminated. Accordingly, the interpretation of experimental results is dramatically simplified.

Performance Isolation of Cell Components: Some typical impedance spectra of a Ni/YSZ/LSM cell at 1000^{o}C are shown in Figure 2. Spectrum (a) clearly indicates that there are two or more processes involved, each having different time constants. Difficulties associated with the interpretation of this spectrum include determining how many processes contribute to the total impedance as well as identifying which process correspond to which specific part of the spectrum. The electrochemical processes accountable for the total impedance include oxygen reduction at the cathode-electrolyte interface, hydrogen oxidation at the anode-electrolyte interface, as well as conduction of $O^{=}$ across the grain boundaries or through the grains of the electrolyte. In addition, the electrode reactions, oxygen reduction or hydrogen oxidation, could involve more than one step; each step having its own characteristic time constants. Perhaps the most confusing part of impedance interpretation is the overlapping of processes when their constants are barely separated. However, with 2 additional reference electrodes, the impedance of the interface between anode and electrolyte as well as the interface between cathode and electrolyte was obtained, as shown in Figure 2 (b) and (c). The interpretation of these impedance spectra is straight forward.

The charge transfer resistance for oxygen reduction and for hydrogen oxidation can be accurately determined. The ohmic drops across these interfaces can be estimated as well.

Error Analysis: Experimental error brought about by inappropriate cell design and characterization techniques often has considerable impact on data interpretation. For instance, investigation of electrode kinetics using large-amplitude controlled-current or controlled-potential techniques typically introduce error due to mass transport limitations or ohmic drop across the working electrode and the reference electrode (2). Effect of mass transport on kinetics can be eliminated effectively by perturbation techniques, as such impedance spectroscopy, whereas the ohmic polarization has to be compensated accordingly. The IR compensation usually involves the determination of ohmic resistance of an interface using impedance spectroscopy or current-interruption technique. Shown in Figure 3 is a typical potential response after a steady current was interrupted. Ohmic drop of the system can be unambiguously determined.

Cell geometry as well as properties of electrode or current collector materials, electronic conductivity in particular, dramatically influences the uniformity of potential and current distribution in the system. In general, non-uniform distribution will complicate experimental observation and hence interpretation. Detailed analysis, including mathematical modeling, of cell geometry and materials properties on potential distribution in solid-oxide fuel cells will be addressed in a subsequent communication.

Electrode Kinetics and Transport Properties: Impedance spectroscopy was extensively used for kinetic investigations. The charge transfer resistance determined from Nyquist and Bode plots were used to estimate the exchange current densities or rate constant. Alternatively, linear and Tafel polarization measurements at a single interface, as shown in Figure 4, directly give the exchange current densities. Analysis of this data indicated that the exchange current densities determined from impedance spectroscopy closely match the values determined from polarization measurements. In addition, transport properties, such as conductivity and ionic or electronic transport number, of electrolytes and interconnect materials were also accurately determined by several techniques.

Identification of limiting factors to cell performance: Shown in Figure 5 is a summary of the performance of each cell component and the overall cell. The total potential loss was split into 3 parts, the potential drop across the electrolyte (IR drop), the anodic overpotential (across the anode-electrolyte interface), and the cathodic overpotential (across the cathode-electrolyte interface). For this specific cell, ohmic drop across the electrolyte clearly contribute most to the overall polarization loss at high operating current (above 500 mA). In this case, improvement in electrolyte conductivity will most effectively improve the overall cell performance. At low operating current (below 100 mA), however, each component has similar contribution to the overall polarization loss. Therefore, the succecessful separation in performance

of each cell component clearly identifies the rate limiting factor for a specific cell or a process and hence provide valuable information for most effective improvement of cell performance.

4. Conclusions

Performance isolation of each cell component has been successfully demonstrated using suitable testing cell design and appropriate characterization techniques. This approach is particularly useful in investigation of fundamental processes in a solid-oxide fuel cell system, including electrode kinetics and transport processes. In addition, the identification of the rate limiting factor to a specific cell further furnishes valuable information on effective improvement of cell performance.

Acknowledgment

This work was supported by Gas Research Institute under contract number GRI 5086-294-1292.

References

(1) A. J. Bard and L. R. Faulkner, "Electrochemical Methods, Fundamentals and Applications", Wiley, N.Y., 1980.

(2) M. Liu and A. Khandkar, *Abs. No. 746, Electrochem. Soc. Fall Meeting, 1990.*

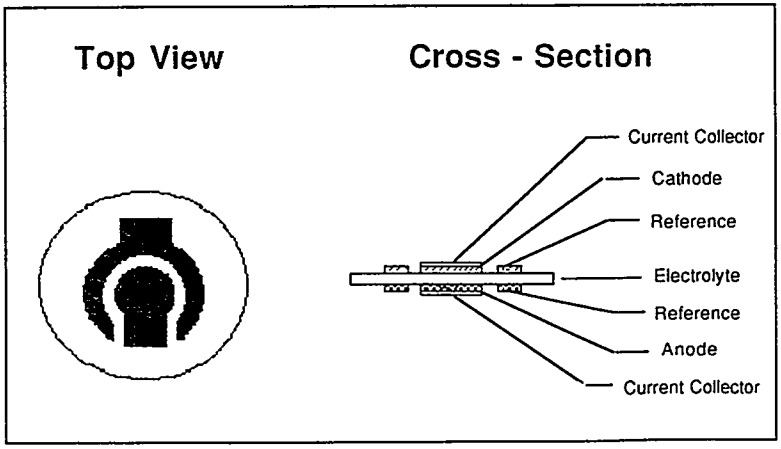

Figure 1 A schematic view of a test cell used for performance isolation of each cell component.

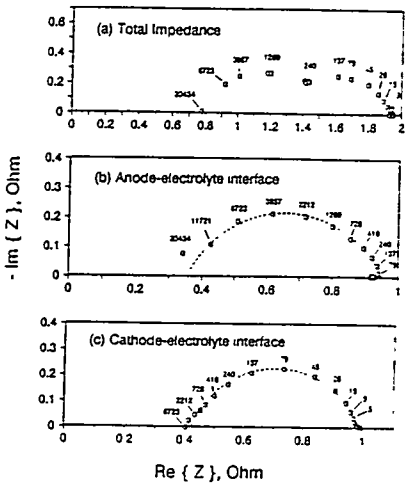

Figure 2 Impedance spectra of a cell (H_2 with 3% H_2O, Ni/YSZ/LSM, air) at 1000°C: (a) the total impedance of the cell, (b) the impedance of the anode-electrolyte interface, and (c) the impedance of the cathode-electrolyte interface. The numbers by the data points represent frequency in Hertz. The working electrode area was 2.5 cm^2.

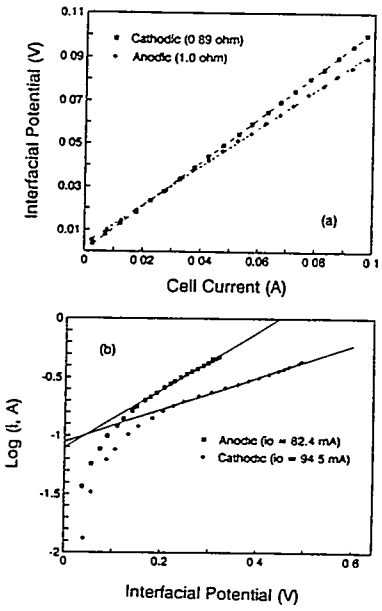

Figure 4 Linear (a) and Tafel (b) polarization measurements of the two interfaces of the same cell as described in Figure 2.

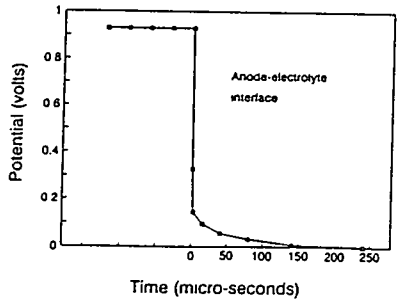

Figure 3 Potential response in a current-interruption measurement at anode-electrolyte interface of the cell as described in Figure 2.

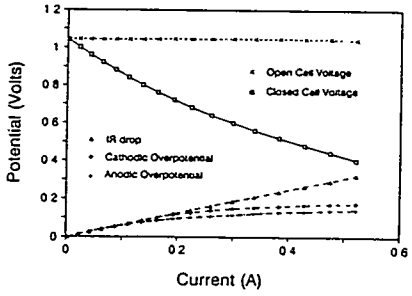

Figure 5 Current-potential characteristics of the cell as described in Figure 2.

NOTES

NOTES

NOTES